To the Graduate Council:

I am submitting herewith a dissertation written by Peter Senn, entitled "The Effects of Nuclear Motion in the Photoelectron Spectra of Diatomic Molecules." I have examined the final copy of this dissertation for form and content and recommend that it be accepted in partial fulfillment of the requirements for the degree of Doctor of Philosophy, with a major in Chemistry.

J. E. Bloor

J. E. Bloor, Major Professor

We have read this dissertation
and recommend its acceptance:

Jerry Kovac

Harold C. Schweinler

William H. Fletcher

Accepted for the Council:

L. Evans Roth

Vice Chancellor
Graduate Studies and Research

Thesis
C1
1983
S47
c.2

THE EFFECTS OF NUCLEAR MOTION IN THE PHOTOELECTRON SPECTRA OF DIATOMIC MOLECULES

A Dissertation

Presented for the

Doctor of Philosophy

Degree

The University of Tennessee, Knoxville

Peter Senn

March 1983

3065950

This work is dedicated to the many individuals who have contributed unselfishly towards its successful completion

There are some for whom the night holds no terrors; on the contrary, for them it is the day with its hordes of martyred slaves to time that is haunted. And of all these night figures - criminals, insomniacs, whores, alcoholics, the inconsolable, the dreamers and lovers - Janis was the Queen. At home in bars as anywhere, she always looked better as the evening progressed, like a night-blooming flower.

David Dalton in "Janis,"
part three: "The Caterpillar on the leaf."

ACKNOWLEDGEMENTS

The author has been granted financial assistance by the University of Tennessee at Knoxville in the form of teaching assistantships from the time he entered Graduate School until recently. This work was made possible also through a generous allocation of resources by the Computing Center of the University of Tennessee at Knoxville.

The author also wishes to express gratitude to James Davenport whose expertise has been very helpful. Appreciation is extended to the many researchers who corresponded with the author while this work was in progress. Special thanks are due to Yukikazu Itikawa and Isao Shimamura, and also to John Schendel who assisted in proofreading this text.

Finally, the author is most grateful to Ron Sherrod who spent a great deal of effort introducing him to the use of the Xα computer program. Special thanks are due to Professor Frederick A. Grimm who acted as the author's research advisor.

ABSTRACT

Different methods for the computation of rovibronic cross sections and angular distributions of photoelectrons have been evaluated for the photoionization of diatomic molecules.

The methods considered were: (i) the Franck-Condon approximation, (ii) the r-centroid approximation, and, (iii) explicit integration over the nuclear coordinates.

In each of the methods, the effect of the rotational motion on the vibrational wave functions could be taken into account. The effects of vibration-rotation interaction were noticeable for H_2, HD, and D_2, but negligible for N_2 and CO.

The rotational structures of the vibronic bands in a vibronic progression are similar, unless a shape resonance is present.

The r-centroid method represents an improvement over the Franck-Condon approximation, in the absence of shape resonances. If a shape resonance is present, the Franck-Condon and the r-centroid approximations break down; i.e., the r-centroid approximation will no longer represent an improvement over the Franck-Condon approximation.

The SW-Xα model has been used to represent the electronic wave functions involved in the photoionizations.

TABLE OF CONTENTS

CHAPTER PAGE

VOLUME I

INTRODUCTION 1

1. VIBRATIONAL MOTION IN THE HARMONIC OSCILLATOR APPROXIMATION 2

2. THE DUSCHINSKY EFFECT FOR TWO MIXING MODES 13

3. THE CALCULATION OF WEIGHTED FRANCK-CONDON FACTORS IN THE HARMONIC APPROXIMATION 19

4. THE TRANSITION MOMENT FUNCTION FROM EXPERIMENTAL INTENSITIES 26

5. THE MORSE OSCILLATOR 70

6. THE PERTURBED MORSE OSCILLATOR 91

7. THE PÖSCHL-TELLER OSCILLATOR 101

8. PHENOMENA IN PHOTOELECTRON SPECTROSCOPY AND THEIR THEORETICAL INTERPRETATION 106

A. The Photoelectric Effect 106

B. The Xα Method 117

C. The Computation of Partial Photoionization Cross Sections from SW-Xα Wave Functions 151

D. Resonances in Photoionization Spectra 169

9. DYNAMICAL SYMMETRY BREAKING IN PHOTOIONIZATIONS FROM INNER SHELLS 216

VOLUME II

10. THE EFFECTS OF NUCLEAR MOTION IN THE PHOTOELECTRON SPECTRA OF DIATOMIC MOLECULES 232

CHAPTER PAGE

A. Theory 232

B. Results 299

1. The Photoionization of H_2, HD, and D_2 299

2. The $3\sigma_g$ Photoionization of N_2 334

3. The $1\pi_u$ Photoionization of N_2 352

4. The $2\sigma_u$ Photoionization of N_2 359

5. The 5σ Photoionization of Carbon Monoxide . . . 382

6. The Photoionization of the 1π Level of Carbon Monoxide 395

7. The Photoionization of the 4σ Level of Carbon Monoxide 413

8. Vibrationally Averaged Cross Sections and β Values 425

C. Summary and Discussion 439

11. AN OUTLOOK ON POLYATOMIC MOLECULES 444

LIST OF REFERENCES 456

APPENDICES 494

APPENDIX 1. HARMONIC FRANCK-CONDON FACTORS 495

APPENDIX 2. GEOMETRY OF THE EXCITED STATE FROM EXPERIMENTAL TRANSITION PROBABILITIES . . . 498

APPENDIX 3. EXCITED STATE GEOMETRY FOR TWO MODES WITH DUSCHINSKY MIXING 502

APPENDIX 4. TRANSITION MOMENT WEIGHTED FRANCK-CONDON FACTORS OF TWO DISPLACED ONE-DIMENSIONAL HARMONIC OSCILLATORS 508

CHAPTER PAGE

APPENDIX 5. GEOMETRY OF THE EXCITED STATE FROM EXPERIMENTAL TRANSITION PROBABILITIES WITH VIBRONIC COUPLING TERMS INCLUDED 514

APPENDIX 6. CALCULATION OF THE TRANSITION MOMENT FUNCTION FROM EXPERIMENTAL VIBRONIC TRANSITION PROBABILITIES 519

APPENDIX 7. WEIGHTED FRANCK-CONDON FACTORS BETWEEN MORSE OSCILLATORS 544

APPENDIX 8. THE PÖSCHL-TELLER OSCILLATOR 552

APPENDIX 9. THE USE OF REAL SPHERICAL HARMONICS 558

VITA 566

LIST OF TABLES

TABLE		PAGE
4-1.	THE TRANSITION MOMENT FUNCTION OF THE FIRST POSITIVE SYSTEM OF N_2 COMPUTED IN THE HARMONIC OSCILLATOR APPROXIMATION. I. FIXED POPULATION FACTORS	44
4-2.	THE TRANSITION MOMENT FUNCTION OF THE FIRST POSITIVE SYSTEM OF N_2 COMPUTED IN THE HARMONIC OSCILLATOR APPROXIMATION. II. VARIABLE POPULATION FACTORS	58
4-3.	RELATIVE POPULATION FACTORS IN THE FIRST POSITIVE SYSTEM OF N_2	64
5-1.	A COMPARISON OF COMPUTED VIBRATION-ROTATION INTERACTION CONSTANTS	75
5-2.	EXPECTATION VALUES OF THE FIRST POSITIVE SYSTEM OF N_2 COMPUTED IN THE MORSE OSCILLATOR APPROXIMATION	79
5-3.	THE TRANSITION MOMENT FUNCTION OF THE FIRST POSITIVE SYSTEM OF N_2 COMPUTED IN THE MORSE OSCILLATOR APPROXIMATION	82
5-4.	THE ROTATIONAL DEPENDENCE OF FRANCK-CONDON FACTORS . . .	88
8-1.	SPHERE RADII AND SLATER EXCHANGE PARAMETERS	137
8-2.	VERTICAL IONIZATION POTENTIALS OF H_2	138
8-3.	ENERGY EIGENVALUES OF THE CONVERGED Xα POTENTIALS FOR TRANSITION STATES OF N_2	141
8-4.	ENERGY EIGENVALUES OF THE CONVERGED Xα POTENTIALS FOR TRANSITION STATES OF CO	142

TABLE PAGE

8-5. COMPUTED SPECTROSCOPIC CONSTANTS 147

8-6. ℓ-TYPE POPULATION ANALYSIS OF THE BOUND STATES OF N_2 AT DIFFERENT INTERNUCLEAR DISTANCES 150

8-7. ℓ-TYPE POPULATION ANALYSIS OF THE BOUND STATES OF CO AT DIFFERENT INTERNUCLEAR DISTANCES 154

8-8. ATOMIC PHOTOIONIZATION CROSS SECTIONS OF HELIUM AND SILICON 162

8-9. PHOTOIONIZATION CROSS SECTIONS AND ASYMMETRY PARAMETERS OF THE SILICON ATOM 163

8-10. PHOTOIONIZATION CROSS SECTIONS AND ASYMMETRY PARAMETERS OF THE SILICON ATOM FROM THE Xα POTENTIAL OF THE NEUTRAL ATOM 164

8-11. CROSS SECTIONS AND BETA VALUES OF H_2 167

8-12. COMPARISON OF CROSS SECTIONS 170

8-13. COMPARISON OF PHOTOIONIZATION CROSS SECTIONS OF H_2 . . 171

8-14. CHANNEL CONTRIBUTIONS TO THE CROSS SECTIONS AND ASYMMETRY PARAMETERS FOR $N_2(X^1\Sigma_g^+) \rightarrow N_2^+(X^2\Sigma_g^+) + e^-$ AT $r_{NN}=1.6a_o$ 190

8-15. CHANNEL CONTRIBUTIONS TO THE CROSS SECTIONS AND ASYMMETRY PARAMETERS FOR $N_2(X^1\Sigma_g^+) \rightarrow N_2^+(X^2\Sigma_g^+) + e^-$ AT $r_{NN}=2.35a_o$ 191

8-16. CHANNEL CONTRIBUTIONS TO THE CROSS SECTIONS AND ASYMMETRY PARAMETERS FOR $N_2(X^1\Sigma_g^+) \rightarrow N_2^+(X^2\Sigma_g^+) + e^-$ AT $r_{NN}=3.1a_o$ 192

TABLE PAGE

8-17. CHANNEL CONTRIBUTIONS TO THE CROSS SECTIONS AND ASYMMETRY PARAMETERS FOR $N_2(X^1\Sigma_g^+) \rightarrow N_2^+(A^2\Pi_{ui}) + e^-$ AT $r_{NN}=1.6a_o$ 193

8-18. CHANNEL CONTRIBUTIONS TO THE CROSS SECTIONS AND ASYMMETRY PARAMETERS FOR $N_2(X^1\Sigma_g^+) \rightarrow N_2^+(A^2\Pi_{ui}) + e^-$ AT $r_{NN}=2.5a_o$ 194

8-19. CHANNEL CONTRIBUTIONS TO THE CROSS SECTIONS AND ASYMMETRY PARAMETERS FOR $N_2(X^1\Sigma_g^+) \rightarrow N_2^+(A^2\Pi_{ui}) + e^-$ AT $r_{NN}=3.6a_o$ 195

8-20. CHANNEL CONTRIBUTIONS TO THE CROSS SECTIONS AND ASYMMETRY PARAMETERS FOR $N_2(X^1\Sigma_g^+) \rightarrow N_2^+(B^2\Sigma_u^+) + e^-$ AT $r_{NN}=1.6a_o$ 196

8-21. CHANNEL CONTRIBUTIONS TO THE CROSS SECTIONS AND ASYMMETRY PARAMETERS FOR $N_2(X^1\Sigma_g^+) \rightarrow N_2^+(B^2\Sigma_u^+) + e^-$ AT $r_{NN}=2.35a_o$ 197

8-22. CHANNEL CONTRIBUTIONS TO THE CROSS SECTIONS AND ASYMMETRY PARAMETERS FOR $N_2(X^1\Sigma_g^+) \rightarrow N_2^+(B^2\Sigma^+) + e^-$ AT $r_{NN}=3.1a_o$ 198

8-23. CHANNEL CONTRIBUTIONS TO THE CROSS SECTIONS AND ASYMMETRY PARAMETERS FOR $CO(X^1\Sigma^+) \rightarrow CO^+(X^2\Sigma^+) + e^-$ AT $r_{CO}=1.6a_o$ 199

8-24. CHANNEL CONTRIBUTIONS TO THE CROSS SECTIONS AND ASYMMETRY PARAMETERS FOR $CO(X^1\Sigma^+) \rightarrow CO^+(X^2\Sigma^+) + e^-$ AT $r_{CO}=2.35a_o$ 200

TABLE PAGE

8-25. CHANNEL CONTRIBUTIONS TO THE CROSS SECTIONS AND ASYMMETRY PARAMETERS FOR $CO(X^1\Sigma^+) \rightarrow CO^+(X^2\Sigma^+) + e^-$ AT $r_{CO}=3.1a_o$ 201

8-26. CHANNEL CONTRIBUTIONS TO THE CROSS SECTIONS AND ASYMMETRY PARAMETERS FOR $CO(X^1\Sigma^+) \rightarrow CO^+(A^2\Pi_i) + e^-$ AT $r_{CO}=1.6a_o$ 202

8-27. CHANNEL CONTRIBUTIONS TO THE CROSS SECTIONS AND ASYMMETRY PARAMETERS FOR $CO(X^1\Sigma^+) \rightarrow CO^+(A^2\Pi_i) + e^-$ AT $r_{CO}=2.5a_o$ 203

8-28. CHANNEL CONTRIBUTIONS TO THE CROSS SECTIONS AND ASYMMETRY PARAMETERS FOR $CO(X^1\Sigma^+) \rightarrow CO^+(A^2\Pi_i) + e^-$ AT $r_{CO}=3.6a_o$ 204

8-29. CHANNEL CONTRIBUTIONS TO THE CROSS SECTIONS AND ASYMMETRY PARAMETERS FOR $CO(X^1\Sigma^+) \rightarrow CO^+(B^2\Sigma^+) + e^-$ AT $r_{CO}=1.6a_o$ 205

8-30. CHANNEL CONTRIBUTIONS TO THE CROSS SECTIONS AND ASYMMETRY PARAMETERS FOR $CO(X^1\Sigma^+) \rightarrow CO^+(B^2\Sigma^+) + e^-$ AT $r_{CO}=2.35a_o$ 206

8-31. CHANNEL CONTRIBUTIONS TO THE CROSS SECTIONS AND ASYMMETRY PARAMETERS FOR $CO(X^1\Sigma^+) \rightarrow CO^+(B^2\Sigma^+) + e^-$ AT $r_{CO}=3.1a_o$ 207

8-32. THE EFFECT OF THE "BASIS SET" ON CROSS SECTIONS AND ASYMMETRY PARAMETERS OF CARBON MONOXIDE AT $r_{CO}=1.6a_o$ . . 209

TABLE PAGE

8-33. THE EFFECT OF THE "BASIS SET" ON CROSS SECTIONS AND ASYMMETRY PARAMETERS OF CARBON MONOXIDE AT $r_{CO}=2.13a_o$ 210

8-34. THE EFFECT OF THE "BASIS SET" ON CROSS SECTIONS AND ASYMMETRY PARAMETERS OF CARBON MONOXIDE AT $r_{CO}=3.1a_o$ . . 211

8-35. THE EFFECT OF THE "BASIS SET" ON CROSS SECTIONS AND ASYMMETRY PARAMETERS OF CARBON MONOXIDE 212

9-1. PHOTOIONIZATION OF THE $1\sigma_g$ LEVEL IN MOLECULAR NITROGEN. ($D_{\infty h}$ SYMMETRY) 223

9-2. PHOTOIONIZATION OF THE $1\sigma_u$ LEVEL IN MOLECULAR NITROGEN. ($D_{\infty h}$ SYMMETRY) 225

9-3. PHOTOIONIZATION OF THE N1s LEVEL IN MOLECULAR NITROGEN. (BROKEN SYMMETRY) 228

9-4. CROSS SECTIONS AND ASYMMETRY PARAMETERS FOR THE CORE LEVEL PHOTOIONIZATION OF N_2 230

10-1. STORAGE OF 3-j AND 6-j SYMBOLS 237

10-2. CONVERGENCE TEST FOR THE HYDROGEN MOLECULE 253

10-3. TESTING FOR NOISE 255

10-4. SAMPLING OF PHOTOELECTRON ENERGIES 259

10-5. LEAST SQUARES APPROXIMATION OF THE DIPOLE MOMENT AMPLITUDES 260

10-6. SPECTROSCOPIC CONSTANTS OF DIATOMIC MOLECULES 262

10-7. FRANCK-CONDON AMPLITUDES AND R-CENTROIDS FOR THE PHOTOIONIZATION OF H_2, HD, AND D_2 263

TABLE		PAGE
10-8.	"COMBINED" CLASSICAL REGIONS, FRANCK-CONDON FACTORS, AND R-CENTROIDS IN THE MORSE OSCILLATOR APPROXIMATION . .	264
10-9.	NUCLEAR STATISTICS IN HOMONUCLEAR DIATOMIC MOLECULES . .	270
10-10.	LEAST SQUARES APPROXIMATIONS OF THE COMPUTED DIPOLE MOMENT AMPLITUDES OF HYDROGEN	290
10-11.	COMPARISON OF CROSS SECTIONS AND BETA VALUES OBTAINED FROM DIFFERENT LEAST SQUARES APPROXIMATIONS	296
10-12.	COMPARISON OF CROSS SECTIONS AND BETA VALUES OF CARBON MONOXIDE OBTAINED WITH DIFFERENT "BASES"	298
10-13.	CROSS SECTIONS AND BETA VALUES FOR PHOTOIONIZATIONS INVOLVING INDIVIDUAL VIBRATIONAL-ROTATIONAL LEVELS OF H_2 AND H_2^+	300
10-14.	CROSS SECTIONS AND BETA VALUES FOR PHOTOIONIZATIONS INVOLVING INDIVIDUAL VIBRATIONAL-ROTATIONAL LEVELS OF HD AND HD^+	302
10-15.	CROSS SECTIONS AND BETA VALUES FOR PHOTOIONIZATIONS INVOLVING INDIVIDUAL VIBRATIONAL-ROTATIONAL LEVELS OF D_2 AND D_2^+	304
10-16.	VIBRONIC CROSS SECTIONS AND BETA VALUES OF H_2 AT T=300K	308
10-17.	VIBRONIC CROSS SECTIONS AND BETA VALUES OF HD AT T=300K	309
10-18.	VIBRONIC CROSS SECTIONS AND BETA VALUES OF D_2 AT T=300K	310

TABLE PAGE

10-19. THE VIBRONIC CROSS SECTIONS OF THE ROTATIONAL LEVELS OF H_2 312

10-20. BETA VALUES OF THE ROTATIONAL LEVELS OF H_2 FOR DIFFERENT VIBRATIONAL STATES OF H_2^+ 314

10-21. THE VIBRONIC CROSS SECTIONS OF THE ROTATIONAL LEVELS OF HD 316

10-22. BETA VALUES OF THE ROTATIONAL LEVELS OF HD FOR DIFFERENT VIBRATIONAL STATES OF HD^+ 318

10-23. THE VIBRONIC CROSS SECTIONS OF THE ROTATIONAL LEVELS OF D_2 320

10-24. BETA VALUES OF THE ROTATIONAL LEVELS OF D_2 FOR DIFFERENT VIBRATIONAL STATES OF D_2^+ 322

10-25. THE TOTAL CROSS SECTIONS AND THE AVERAGE BETA VALUES OF H_2 AT DIFFERENT TEMPERATURES 327

10-26. THE TOTAL CROSS SECTIONS AND THE AVERAGE BETA VALUES OF HD AT DIFFERENT TEMPERATURES 328

10-27. THE TOTAL CROSS SECTIONS AND THE AVERAGE BETA VALUES OF D_2 AT DIFFERENT TEMPERATURES 329

10-28. THE TOTAL CROSS SECTIONS AND THE AVERAGE BETA VALUES OF THE ROTATIONAL LEVELS OF H_2 330

10-29. THE TOTAL CROSS SECTIONS AND THE AVERAGE BETA VALUES OF THE ROTATIONAL LEVELS OF HD 331

10-30. THE TOTAL CROSS SECTIONS AND THE AVERAGE BETA VALUES OF THE ROTATIONAL LEVELS OF D_2 332

TABLE PAGE

10-31. PHOTOIONIZATION CROSS SECTIONS AND BETA VALUES OF N_2. $N_2(X^1\Sigma_g^+) \rightarrow N_2^+(X^2\Sigma_g^+) + e^-$ 335

10-32. SCALED PHOTOIONIZATION CROSS SECTIONS FOR $N_2(X^1\Sigma_g^+) \rightarrow N_2^+(X^2\Sigma_g^+) + e^-$ ($h\nu$=21.2 eV) 336

10-33. BETA VALUES FOR $N_2(X^1\Sigma_g^+) \rightarrow N_2^+(X^2\Sigma_g^+) + e^-$ ($h\nu$=21.2 eV) . 337

10-34. RELATIVE INTENSITIES AND AVERAGE BETA VALUES OF THE BRANCHES IN THE PHOTOIONIZATION OF THE $3\sigma_g$ LEVEL OF N_2 FOR v_f=0 340

10-35. RELATIVE INTENSITIES AND AVERAGE BETA VALUES OF THE BRANCHES IN THE PHOTOIONIZATION OF THE $3\sigma_g$ LEVEL OF N_2 FOR v_f=1 341

10-36. RELATIVE INTENSITIES AND AVERAGE BETA VALUES OF THE BRANCHES IN THE PHOTOIONIZATION OF THE $3\sigma_g$ LEVEL OF N_2 FOR v_f=2 342

10-37. VIBRONIC INTENSITIES AND BETA VALUES FOR THE PHOTOIONIZATION OF THE $3\sigma_g$ LEVEL OF N_2 AT DIFFERENT ROTATIONAL TEMPERATURES 343

10-38. PHOTOIONIZATION CROSS SECTIONS AND BETA VALUES OF N_2. $N_2(X^1\Sigma_g^+) \rightarrow N_2^+(A^2\Pi_{ui}) + e^-$ 353

10-39. SCALED PHOTOIONIZATION CROSS SECTIONS FOR $N_2(X^1\Sigma_g^+) \rightarrow N_2^+(A^2\Pi_{ui}) + e^-$ ($h\nu$=21.2 eV) 354

10-40. BETA VALUES FOR $N_2(X^1\Sigma_g^+) \rightarrow N_2^+(A^2\Pi_{ui}) + e^-$ ($h\nu$=21.2 eV) . 355

10-41. VIBRONIC INTENSITIES FOR THE PHOTOIONIZATION OF THE $1\pi_u$ LEVEL OF N_2 AT DIFFERENT TEMPERATURES 357

TABLE PAGE

10-42. AVERAGE BETA VALUES FOR THE PHOTOIONIZATION OF THE $1\pi_u$ LEVEL OF N_2 FOR DIFFERENT VIBRONIC BANDS AND AT DIFFERENT ROTATIONAL TEMPERATURES 358

10-43. RELATIVE INTENSITIES AND AVERAGE BETA VALUES OF THE BRANCHES IN THE PHOTOIONIZATION OF THE $1\pi_u$ LEVEL OF N_2 FOR v_f=0 360

10-44. RELATIVE INTENSITIES AND AVERAGE BETA VALUES OF THE BRANCHES IN THE PHOTOIONIZATION OF THE $1\pi_u$ LEVEL OF N_2 FOR v_f=4 361

10-45. RELATIVE INTENSITIES AND AVERAGE BETA VALUES OF THE BRANCHES IN THE PHOTOIONIZATION OF THE $1\pi_u$ LEVEL OF N_2 FOR v_f=8 363

10-46. PHOTOIONIZATION CROSS SECTIONS AND BETA VALUES OF N_2. $N_2(X^1\Sigma_g^+) \rightarrow N_2^+(B^2\Sigma_u^+) + e^-$ 369

10-47. SCALED PHOTOIONIZATION CROSS SECTIONS FOR $N_2(X^1\Sigma_g^+) \rightarrow N_2^+(B^2\Sigma_u^+) + e^-$ ($h\nu$=21.2 eV) 370

10-48. BETA VALUES FOR $N_2(X^1\Sigma_g^+) \rightarrow N_2^+(X^2\Sigma_u^+) + e^-$ ($h\nu$=21.2 eV) . 371

10-49. VIBRONIC INTENSITIES AND BETA VALUES FOR THE PHOTOIONIZATION OF THE $2\sigma_u$ LEVEL OF N_2 AT DIFFERENT TEMPERATURES 372

10-50. RELATIVE INTENSITIES AND AVERAGE BETA VALUES OF THE BRANCHES IN THE PHOTOIONIZATION OF THE $2\sigma_u$ LEVEL OF N_2 FOR v_f=0 374

TABLE PAGE

10-51. RELATIVE INTENSITIES AND AVERAGE BETA VALUES OF THE BRANCHES IN THE PHOTOIONIZATION OF THE $2\sigma_u$ LEVEL OF N_2 FOR v_f=1 375

10-52. RELATIVE INTENSITIES AND AVERAGE BETA VALUES OF THE BRANCHES IN THE PHOTOIONIZATION OF THE $2\sigma_u$ LEVEL OF N_2 FOR v_f=2 376

10-53. PHOTOIONIZATION CROSS SECTIONS AND BETA VALUES OF CARBON MONOXIDE. $CO(X^1\Sigma^+) \rightarrow CO^+(X^2\Sigma^+) + e^-$ 383

10-54. SCALED PHOTOIONIZATION CROSS SECTIONS FOR $CO(X^1\Sigma^+) \rightarrow CO^+(X^2\Sigma^+) + e^-$ ($h\nu$=21.2 eV) 384

10-55. BETA VALUES FOR $CO(X^1\Sigma^+) \rightarrow CO^+(X^2\Sigma^+) + e^-$ ($h\nu$=21.2 eV) . 385

10-56. RELATIVE INTENSITIES AND AVERAGE BETA VALUES OF THE BRANCHES IN THE PHOTOIONIZATION OF THE 5σ LEVEL OF CO FOR v_f=0 386

10-57. RELATIVE INTENSITIES AND AVERAGE BETA VALUES OF THE BRANCHES IN THE PHOTOIONIZATION OF THE 5σ LEVEL OF CO FOR v_f=1 387

10-58. RELATIVE INTENSITIES AND AVERAGE BETA VALUES OF THE BRANCHES IN THE PHOTOIONIZATION OF THE 5σ LEVEL OF CO FOR v_f=2 388

10-59. VIBRONIC INTENSITIES AND BETA VALUES FOR THE PHOTOIONIZATION OF THE 5σ LEVEL OF CO AT DIFFERENT ROTATIONAL TEMPERATURES 396

TABLE PAGE

10-60. PHOTOIONIZATION CROSS SECTIONS AND BETA VALUES OF CARBON MONOXIDE. $CO(X^1\Sigma^+) \rightarrow CO^+(A^2\Pi_i) + e^-$ 397

10-61. VIBRONIC INTENSITIES FOR THE PHOTOIONIZATION OF THE 1π LEVEL OF CO AT DIFFERENT ROTATIONAL TEMPERATURES . . 398

10-62. AVERAGE BETA VALUES FOR THE PHOTOIONIZATION OF THE 1π LEVEL OF CO FOR DIFFERENT VIBRONIC BANDS AND AT DIFFERENT ROTATIONAL TEMPERATURES. 399

10-63. SCALED PHOTOIONIZATION CROSS SECTIONS FOR $CO(X^1\Sigma^+) \rightarrow CO^+(A^2\Pi_i) + e^-$ ($h\nu$=21.2 eV) 401

10-64. BETA VALUES FOR $CO(X^1\Sigma^+) \rightarrow CO^+(A^2\Pi_i) + e^-$ ($h\nu$=21.2 eV) . 402

10-65. RELATIVE INTENSITIES AND AVERAGE BETA VALUES OF THE BRANCHES IN THE PHOTOIONIZATION OF THE 1π LEVEL OF CO FOR v_f=0 403

10-66. RELATIVE INTENSITIES AND AVERAGE BETA VALUES OF THE BRANCHES IN THE PHOTOIONIZATION OF THE 1π LEVEL OF CO FOR v_f=4 404

10-67. RELATIVE INTENSITIES AND AVERAGE BETA VALUES OF THE BRANCHES IN THE PHOTOIONIZATION OF THE 1π LEVEL OF CO FOR v_f=8 405

10-68. RELATIVE INTENSITIES AND AVERAGE BETA VALUES OF THE BRANCHES IN THE PHOTOIONIZATION OF THE 1π LEVEL OF CO FOR v_f=12 406

10-69. PHOTOIONIZATION CROSS SECTIONS AND BETA VALUES OF CARBON MONOXIDE. $CO(X^1\Sigma^+) \rightarrow CO^+(B^2\Sigma^+) + e^-$ 414

TABLE PAGE

10-70. VIBRONIC INTENSITIES AND BETA VALUES FOR THE PHOTOIONIZATION OF THE 4σ LEVEL OF CO AT DIFFERENT ROTATIONAL TEMPERATURES 416

10-71. SCALED PHOTOIONIZATION CROSS SECTIONS FOR $CO(X^1\Sigma^+) \rightarrow CO^+(B^2\Sigma^+) + e^-$ ($h\nu$=21.2 eV) 417

10-72. BETA VALUES FOR $CO(X^1\Sigma^+) \rightarrow CO^+(B^2\Sigma^+) + e^-$ ($h\nu$=21.2 eV) . 418

10-73. RELATIVE INTENSITIES AND AVERAGE BETA VALUES OF THE BRANCHES IN THE PHOTOIONIZATION OF THE 4σ LEVEL OF CO FOR v_f=0 419

10-74. RELATIVE INTENSITIES AND AVERAGE BETA VALUES OF THE BRANCHES IN THE PHOTOIONIZATION OF THE 4σ LEVEL OF CO FOR v_f=1 420

10-75. RELATIVE INTENSITIES AND AVERAGE BETA VALUES OF THE BRANCHES IN THE PHOTOIONIZATION OF THE 4σ LEVEL OF CO FOR v_f=2 421

10-76. RELATIVE INTENSITIES AND AVERAGE BETA VALUES OF THE BRANCHES IN THE PHOTOIONIZATION OF THE 4σ LEVEL OF CO FOR v_f=3 422

10-77. RELATIVE INTENSITIES AND AVERAGE BETA VALUES OF THE BRANCHES IN THE PHOTOIONIZATION OF THE 4σ LEVEL OF CO FOR v_f=4 423

10-78. VIBRATIONALLY AVERAGED CROSS SECTIONS AND BETA VALUES OF H_2 431

10-79. VIBRATIONALLY AVERAGED CROSS SECTIONS AND BETA VALUES OF HD 432

TABLE PAGE

10-80. VIBRATIONALLY AVERAGED CROSS SECTIONS AND BETA VALUES OF D_2 433

10-81. VIBRATIONALLY AVERAGED CROSS SECTIONS AND BETA VALUES OF N_2 435

10-82. VIBRATIONALLY AVERAGED CROSS SECTIONS AND BETA VALUES OF CO 436

LIST OF FIGURES

FIGURE PAGE

4-1. Contour plots of the roots of the Franck-Condon amplitudes and of the r-centroids for displaced harmonic oscillators 29

4-2. Comparison of the function $M(q)=\exp(-1.14q)$ and $M(\bar{q})$ . . 31

4-3. Plot of residues 46

4-4. The transition moment function of the first positive system of N_2. I. The transition moment function computed in the harmonic oscillator approximation with fixed population factors 49

4-5. The transition moment function of the first positive system of N_2. II. The transition moment function computed in the harmonic oscillator approximation with variable population factors 65

4-6. The r-centroids of the first positive system of N_2 obtained in the harmonic oscillator approximation versus the r-centroids from the Morse oscillator approximation 67

5-1. The transition moment function of the first positive system of N_2. III. The transition moment function computed in the Morse oscillator approximation 86

8-1. The Xα potential of the transition state for the ionization of the 3s level of the silicon atom 120

FIGURE PAGE

8-2. The radial wave functions of the 3s and 3p orbital of silicon computed from the Xα transition state potentials for the removal of an electron from these levels 121

8-3. MO diagram of N_2 123

8-4. MO diagram of N_2 showing the united atom limit, (the silicon atom) 152

8-5. MO diagram of CO showing the united atom limit, (the silicon atom) 153

8-6. Cross sections and β values of the $(3\sigma_g)^{-1}$ photoionization of N_2 at three different internuclear separations 179

8-7. Cross sections and β values of the $(1\pi_u)^{-1}$ photoionization of N_2 at three different internuclear separations 181

8-8. Cross sections and β values of the $(2\sigma_u)^{-1}$ photoionization of N_2 at three different internuclear separations 183

8-9. Cross sections and β values of the $(5\sigma)^{-1}$ photoionization of CO at three different internuclear separations 184

8-10. Cross sections and β values of the $(1\pi)^{-1}$ photoionization of CO at three different internuclear separations 186

FIGURE PAGE

8-11. Cross sections and β values of the $(4\sigma)^{-1}$ photoionization of CO at three different internuclear separations 188

9-1. Buridan's ass 218

9-2. The cross sections and β values of the $(1\sigma_g)^{-1}$ photoionization of N_2. (Using $D_{\infty h}$ symmetry) 224

9-3. The cross sections and β values of the $(1\sigma_u)^{-1}$ photoionization of N_2. (Using $D_{\infty h}$ symmetry) 226

9-4. The cross sections and values of the K-shell photoionization of N_2 obtained with the broken symmetry, $(C_{\infty v})$, solution 229

10-1. The r_{NN}-dependence of the channel contributions to the cross sections, the β values, and the orbital energies in the $(3\sigma_g)^{-1}$ photoionization of N_2 for E_e=0.37 Ryd . . 240

10-2. The r_{NN}-dependence of the channel contributions to the cross sections, the β values, and the orbital energies in the $(2\sigma_u)^{-1}$ photoionization of N_2 for E_e=0.14 Ryd . . 241

10-3. The r_{NN}-dependence of the channel contributions to the cross sections, the β values, and the orbital energies in the $(1\pi_u)^{-1}$ photoionization of N_2 for E_e=0.19 Ryd . . 242

10-4. The r_{CO}-dependence of the channel contributions to the cross sections, the β values, and the orbital energies in the $(5\sigma)^{-1}$ photoionization of CO for E_e=0.49 Ryd . . 243

FIGURE PAGE

10-5. The r_{CO}-dependence of the channel contributions to the cross sections, the β values, and the orbital energies in the $(4\sigma)^{-1}$ photoionization of CO for E_e=0.05 Ryd . . 244

10-6. The r_{CO}-dependence of the channel contributions to the cross sections, the β values, and the orbital energies in the $(1\pi)^{-1}$ photoionization of CO for E_e=0.17 Ryd . . 245

10-7. The real part of the dipole moment amplitude of a partial wave with ℓ=1 and λ=μ=0 for the photoionization of H_2 as a function of the internuclear separation . . 249

10-8. The real part of the dipole moment amplitude of a partial wave with ℓ=λ=μ=1 for the photoionization of H_2 as a function of the internuclear separation 250

10-9. The rotational distribution of CO at T_{rot}=300K 268

10-10. The cross sections of the branches in the $(3\sigma_g)^{-1}$ photoionization of N_2, expressed in % of the vibronic cross sections and their average β values 339

10-11. The isotropic component of the vibronic band with v_f=0 and its individual branches in the $(3\sigma_g)^{-1}$ photoionization of N_2 at T=300K 347

10-12. The anisotropic component of the vibronic band with v_f=0 and its individual branches in the $(3\sigma_g)^{-1}$ photoionization of N_2 at T=300K 348

10-13. Vibronic band contours in the $(3\sigma_g)^{-1}$ photoionization of N_2 at different temperatures 349

FIGURE PAGE

10-14. Contours of the anisotropic component of the vibronic bands in the $(3\sigma_g)^{-1}$ photoionization of N_2 at different temperatures 350

10-15. The cross sections of the branches in the $(1\pi_u)^{-1}$ photoionization of N_2, expressed in % of the vibronic cross sections, and their average β values 363

10-16. The isotropic component of the vibronic band with v_f=0 and its individual branches in the $(1\pi_u)^{-1}$ photoionization of N_2 at T=300K 364

10-17. The anisotropic component of the vibronic band with v_f=0 and its individual branches in the $(1\pi_u)^{-1}$ photoionization of N_2 at T=300K 365

10-18. Vibronic band contours in the $(1\pi_u)^{-1}$ photoionization of N_2 at different temperatures 366

10-19. Contours of the anisotropic component of three vibronic bands in the $(1\pi_u)^{-1}$ photoionization of N_2 at different temperatures 367

10-20. The cross sections of the branches in the $(2\sigma_u)^{-1}$ photoionization of N_2, expressed in % of the vibronic cross sections, and their average β values 377

10-21. The isotropic component of the vibronic band with v_f=0 and its individual branches in the $(2\sigma_u)^{-1}$ photoionization of N_2 at T=300K 378

FIGURE PAGE

10-22. The anisotropic component of the vibronic band with v_f=0 and its individual branches in the $(2\sigma_u)^{-1}$ photoionization of N_2 at T=300K 379

10-23. Vibronic band contours in the $(2\sigma_u)^{-1}$ photoionization of N_2 at different temperatures 380

10-24. Contours of the anisotropic component of the vibronic bands in the $(2\sigma_u)^{-1}$ photoionization of N_2 at different temperatures 381

10-25. The cross sections of the branches in the $(5\sigma)^{-1}$ photoionization of CO, expressed in % of the vibronic cross sections, and their average β values 389

10-26. The isotropic component of the vibronic band with v_f=0 and its individual branches in the $(5\sigma)^{-1}$ photoionization of CO at T=300K 390

10-27. The anisotropic component of the vibronic band with v_f=0 and its individual branches in the $(5\sigma)^{-1}$ photoionization of CO at T=300K 391

10-28. Vibronic band contours in the $(5\sigma)^{-1}$ photoionization of CO at different temperatures 392

10-29. Contours of the anisotropic component of the vibronic bands in the $(5\sigma)^{-1}$ photoionization of CO at different temperatures 393

10-30. The cross sections of the branches in the $(1\pi)^{-1}$ photoionization of CO, expressed in % of the vibronic cross sections, and their average β values 407

FIGURE PAGE

10-31. The isotropic component of the vibronic band with v_f=0 and its individual branches in the $(1\pi)^{-1}$ photoionization of CO at T=300K 409

10-32. The anisotropic component of the vibronic band with v_f=0 and its individual branches in the $(1\pi)^{-1}$ photoionization of CO at T=300K 410

10-33. Vibronic band contours in the $(1\pi)^{-1}$ photoionization of CO at different temperatures 411

10-34. Contours of the anisotropic component of three vibronic bands in the $(1\pi)^{-1}$ photoionization of CO at different temperatures 412

10-35. The cross sections of the branches in the $(4\sigma)^{-1}$ photoionization of CO, expressed in % of the vibronic cross sections, and their average β values 424

10-36. The isotropic component of the vibronic band with v_f=0 and its individual branches in the $(4\sigma)^{-1}$ photoionization of CO at T=300K 426

10-37. The anisotropic component of the vibronic band with v_f=0 and its individual branches in the $(4\sigma)^{-1}$ photoionization of CO at T=300K 427

10-38. Vibronic band contours in the $(4\sigma)^{-1}$ photoionization of CO at different temperatures 428

10-39. Contours of the anisotropic component of three vibronic bands in the $(4\sigma)^{-1}$ photoionization of CO at different temperatures 429

VOLUME I

INTRODUCTION

In many electronic spectra, vibrational and even rotational structure can be observed.

The first seven chapters in this text deal with quantum mechanical models for vibrational motion in molecules, and with the computation of the transition moment function from the experimental intensities in bound-bound electronic spectra.

The eighth, ninth, and tenth chapters deal with the computation of rovibronic cross sections and angular distributions of photoelectrons in the photoionization of diatomic molecules.

In the last chapter, a model for anharmonic vibrational motion in polyatomic molecules is presented.

The conventions by Herzberg[1,2] were followed regarding the spectroscopic notations, unless stated otherwise, and the mathematical notation by Abramowitz and Stegun[3] was used throughout.

The main objective of this work consists of determining if there are observable effects of rotational motion in the photoelectron spectra of diatomic molecules. Since a limited number of experimental work in photoelectron spectroscopy shows sufficient resolution to show effects of rotational motion, the present investigation will concentrate mainly on the identification of important side effects such as vibration-rotation interaction. The vibrational motion will be considered in the Franck-Condon and the r-centroid approximation, and also through explicit integration over the vibrational coordinate.

CHAPTER 1

VIBRATIONAL MOTION IN THE HARMONIC OSCILLATOR APPROXIMATION

Throughout this chapter we assume that the Born-Oppenheimer approximation is valid. In addition, we assume that the vibrational Hamiltonian can be expressed as a sum of one-dimensional operators

$$\hat{\mathcal{H}}_{vib} = \sum_{i=1}^{s} \hat{h}_i (q_i) \tag{1-1}$$

where the qs are the normal mode coordinates of a molecule with n atoms, and s=3n-6 for a non-linear molecule and s=3n-5 for a linear molecule. We can then perform a separation of variables on the corresponding Schrödinger equation, i.e.,

$$\hat{\mathcal{H}}_{vib} \psi_{vib} = E_{vib} \psi_{vib} \tag{1-2}$$

can be decomposed into a set of equations

$$\hat{h}_i \chi_i (q_i) = \epsilon_i \chi_i (q_i) \tag{1-3}$$

where

$$\Sigma_i \hat{h}_i = \hat{\mathcal{H}}_{vib} \tag{1-4}$$

and

$$\Sigma_i \epsilon_i = E_{vib} \tag{1-5}$$

and the wave function of nuclear vibration can then be expressed as a product,

$$\psi_{vib} = \Pi_i \chi_i (q_i) \tag{1-6}$$

Let us assume that the potentials in the normal mode coordinates are harmonic. The vibrational wave functions become

$$\chi_i (q_i) = N_{v_i} H_{v_i} (\alpha_i q_i) \exp(-(1/2)\alpha_i^2 q_i^2) \tag{1-7}$$

where the Hs are Hermite polynomials and the normalization factors N_{v_i} are

$$N_{v_i} = (\alpha_i/(\pi^{1/2} 2^{(v_i)} (v_i)!))^{1/2} \tag{1-8}$$

and $\alpha_i^2 = 4\pi^2 c\omega_i/h$, where ω is in cm^{-1}.

A more detailed treatment along the lines followed here can be found in one of Herzberg's books.[1,2] However, the expression for α given by Herzberg seems to be incorrect.[4]

In the present chapter, the concept of normal mode coordinates and the harmonic oscillator model is used to find the excited state geometry from the initial state geometry and intensities of the vibronic transitions. We assume initially that the relative intensities of these transitions are governed by Franck-Condon factors.

The transition moment associated with a vibronic transition is[5]

$$M = \int\int \psi_{el}' \psi_{vib}' M(\vec{x},\vec{q}) \psi_{el}'' \psi_{vib}'' d\vec{x}\, d\vec{q} \tag{1-9}$$

where $\vec{x}$ represents the electronic coordinates. Designating the integral over $\vec{x}$ by R_e, we may write

$$M = \int R_e (\vec{q}) \psi_{vib}' \psi_{vib}'' d\vec{q} \tag{1-10}$$

If the region of sizable overlap between the vibrational wave

functions is small, one can assume

$$R_e\ (q) \sim R_e\ (q_{eq}) = \text{const.} \tag{1-11}$$

To insure that the above holds, we restrict ourselves to cases where either $v' = 0$ and/or $v'' = 0$. If we express the total vibrational wave function as a product, as shown in (1-6), and assuming $R_e = \text{const.}$,

$$M = R_e \prod_i \int (\chi_i'(q_i') \chi_i''(q_i'')) dq_i' \tag{1-12}$$

where we have chosen to perform the integration over the final state normal mode coordinates. The normal mode coordinates of the initial state must, therefore, be expanded in terms of the ones of the excited state. Duschinsky has shown that the necessary transformation is of the form[6]

$$q_i'' = \Sigma_k a_{ik} q_k' - \delta_i \tag{1-13}$$

where the matrix a_{ik} is orthonormal, in which case the Duschinsky transformation in (1-13) represents a rotation and a translation in q-space.[7] We will discuss this transformation extensively in the next chapter. The elements a_{ik} between initial and final state coordinates are zero if their symmetry is different. In other words, the matrix a_{ik} is subblocked into matrices of smaller size if the normal mode coordinate frames have symmetries. We assume here that a_{ik} is a diagonal matrix, i.e., $a_{ik} = \delta_{ik} b_i$, and we will call this the "parallel frame approximation". This approximation was used by Coon et al.[8]

For 1×1 subblocks of the a_{ik} matrix, the parallel frame approximation holds, in a trivial sense. For example, Yersin et al., who wanted

to find the change in the metal-ligand bond length from intensity measurements in single crystal polarized luminescence spectra had to analyze only the A_1 breathing mode of the tetrahedral complexes $PtCl_4^{2-}$ and $PtBr_4^{2-}$ to obtain the desired information.[9] However, the displacements calculated by Yersin et al. are too small by a factor of $2^{-1/2}$. (They seem to have used Herzberg's formula for α.)

The overlap integrals between two displaced harmonic oscillators can be expressed analytically.[10-13] Large tables of such Franck-Condon factors have been prepared in a form suitable for extracting δ from observed intensity ratios.[14] These tables apply to the case $v'' = 0$ and/or $v' = 0$ only. The integrals for this case can be written as

$$\langle \chi_n' | \chi_o'' \rangle = N_o N_n \langle \exp(-(1/2)\,\alpha_1^2 (q-\delta)^2) | H_n(\alpha_2 q)\, \exp(-(1/2)\,\alpha_2^2 q^2) \rangle \qquad (1\text{-}14)$$

where $n = v'$. This gives

$$\langle \chi_n' | \chi_o'' \rangle^2 = (\alpha_1\alpha_2/n!)\, \exp(-\alpha_1^2\alpha_2^2\delta^2/(\alpha_1^2 + \alpha_2^2))\, ((1/2)(\alpha_1^2-\alpha_2^2)/(\alpha_1^2 + \alpha_2^2))^n (2/(\alpha_1^2 + \alpha_2^2))\, [H_n(\alpha_1^2\alpha_2\delta/(\alpha_1^4-\alpha_2^4)^{1/2})]^2 \qquad (1\text{-}15)$$

Using the notation

$$S_{kj} = (\text{intensity } k \leftarrow 0)/(\text{intensity } j \leftarrow 0) \qquad (1\text{-}16)$$

gives for the intensity ratio

$$H_j(x)[(2/K)^{k-j}(k!/j!)S_{kj}]^{1/2} \pm H_k(x) = 0$$

where $$K = (\omega_1-\omega_2)/(\omega_1 + \omega_2)$$

and $$x = \alpha_1\delta[\omega_1\omega_2/(\omega_1^2-\omega_2^2)]^{1/2} \qquad (1\text{-}17)$$

When trying to find δ using the above relation, one would have to locate the roots of a N-th degree polynomial of x where N = max (k,j). S_{kj} can mean a calculated or an experimental quantity. In the above case, S_{kj} would refer to the observed intensity ratio.

In some cases, x is an imaginary quantity. In this case, K is negative and it can be shown that (1-17) involves finding the roots of a real function. In the cases where max (k,j) ≤ 2, the roots of this function can readily be expressed analytically.

Defining

$$A_{kj} = \pm \{(2/K)^{k-j}(k!/j!)S_{kj}\}^{1/2} \qquad (1\text{-}18)$$

we obtain

$$x = (1/2)A_{10} \qquad (1\text{-}19)$$

$$x = (1/2)[A_{20} + 2u]^{1/2} \qquad (1\text{-}20)$$

$$x = [(1/2)(3u\pm[(A_{40}/4) + 6]^{1/2})]^{1/2} \qquad (1\text{-}21)$$

$$x = (A_{21}/4)\pm[(A_{21}/4)^2 + (1/2)u]^{1/2} \qquad (1\text{-}22)$$

$$x = (1/2)[A_{31} + 6u]^{1/2} \qquad (1\text{-}23)$$

$$x = [(1/2)(5u\pm[10 + (A_{51}/4)]^{1/2})]^{1/2} \qquad (1\text{-}24)$$

$$x = (1/2)[6u + (1/2)A_{42}\pm[24 + 4uA_{42} + ((1/2)A_{42})^2]^{1/2}]^{1/2} \qquad (1\text{-}25)$$

$$x = (1/2)[10u + (1/2)A_{53} \pm [40 + 4uA_{53} + ((1/2)A_{53})^2]^{1/2}]^{1/2} \quad (1\text{-}26)$$

where

$$u = \begin{cases} 1 \text{ if } K \geq 0 \\ -1 \text{ if } K < 0 \end{cases} \quad (1\text{-}27)$$

From three intensity measurements one can find the vibrational frequency and the displacement of the upper state. For example, the relation

$$K = S_{10} \pm (2S_{20})^{1/2} \quad (1\text{-}28)$$

and

$$\alpha_1 \delta = [2S_{10}/(1-K^2)]^{1/2} \quad (1\text{-}29)$$

can be derived. It is possible to find several additional pairs of formulae of the above type. For example,

$$K = (S_{10}/3) \pm [(2/3)(S_{30}/S_{10})]^{1/2}$$

$$\alpha_1 \delta = [2S_{10}/(1-K^2)]^{1/2} \quad (1\text{-}30)$$

It can readily be seen that, in the above formulae, ambiguities arise due to the "±" signs. In cases where complex quantities arise, these can be rejected as "physically meaningless solutions". The ambiguities can be resolved by taking several intensity ratios to compute displacements.

A computer program has been written which computes possible dislocations between vibronic frames from an observed intensity ratio. The program simply locates the real roots of F(x), where

$$F(x) = A_{kj} H_j(x) \pm H_k(x) = 0 \quad (1\text{-}31)$$

The program searches in a specified interval for sign changes. Roots discovered in this search are being located by the Newton-Raphson method. This requires the computation of Hermite polynomials of real or complex arguments. The Hermite polynomials and their derivatives are being calculated by a recursion formula. The recursion formula for the derivatives was obtained from the one of the Hermite polynomials by differentiation. If k and j are both odd numbers, F will have a physically meaningless root at x = 0. The program and input instructions for its use are shown in Appendix 2.

Let us apply the above considerations to two practical examples. Gardner and Samson reported the following relative intensities for the photoionization of nitrogen using a He(I) source:[15]

$$N_2(X^1\Sigma_q^+) \xrightarrow{h\nu} N_2^+(A^2\Pi_u)$$

$$v' = v'' = 0 \quad : \text{rel. intensity} = 87.1$$

$$v' = 1,\ v'' = 0: \text{rel. intensity} = 100.0 \tag{1-32}$$

According to (1-19),

$$\alpha_1\delta = (1/2)(\omega_1 + \omega_2)[2/(0.871\ \omega_1\omega_2)]^{1/2} \tag{1-33}$$

Using in (1-33) ω_es given by Huber and Herzberg, we obtain[16]

$$\alpha_1\delta = 1.524 \tag{1-34}$$

Using physical constants published by Abromowitz and Stegun to compute α gives[3]

$$\alpha_i = 1.336467(10^{19}(\omega_i/(g\ cm))^{1/2}$$

$$= 0.172219(\omega_i(cm)/(a.m.u.))^{1/2}\ \text{Å}^{-1} \qquad (1\text{-}35)$$

In (1-34), α_1 refers to the initial (doubly primed) state. This gives $\delta = 2.348(10^{-21})g^{1/2}cm$. The reduced mass of $^{14}N_2$ is $1.163(10^{-23})g$. Converting δ from normal mode coordinates to Cartesian coordinates gives $\Delta r_e = 0.069$Å, which compares favorably with $\Delta r_e = 0.077$Å from the book of Huber and Herzberg.[16] The percent error for Δr_e is of the same magnitude as the one for the experimental Franck-Condon factors by Gardner and Samson.[17]

Since the harmonic potential has an axis of symmetry, we do not know if the internuclear distance would expand or shrink by Δr_e. In the one-dimensional case, one can, in general, guess which of the two cases would be in effect if the nature of the electronic transition is known, i.e., the orbitals involved. However, if the a_{ki} matrix is larger than 1x1, i.e., if the excited state structure is obtained through displacements along several normal mode coordinates, several structures would be consistent with the observed intensity distribution. If n normal mode coordinate displacements are possible in a transition 2^n excited state structures would be consistent with the observed spectrum. In many cases, some of the vibrations are not being observably activated in the transition, and one takes $\delta = 0$ along the corresponding normal mode coordinates. This cuts down considerably on the number of structures to be considered, in many cases. For example, Hollas and Sutherley found that ν_2 was not activated in the photoionization of dicyanogen to $(C_2N_2)^+\ \tilde{X}^2\Pi_g$ and in the photoionization

to $(C_2N_2)^+ \tilde{}^1\Sigma_g^+$.[18] They therefore assumed that the dislocation along the corresponding normal mode coordinate is zero. There is one additional criterion pertaining to the "true" structure of the excited state. It is based on the general rule that if ω_i' is smaller than ω_i'', the excited state equilibrium structure should be "expanded" along the corresponding normal mode coordinate. The opposite would be the case, if $\omega_i' > \omega_i''$.[19]

As a second one-dimensional example, let us look at the observed relative intensities of the $\alpha(C^3\Delta\text{-}X'^3\Delta)$ band system of the ZrO molecule. The spectrum of this molecule is of considerable importance in distinguishing M and S stars.[20] In some cases, the observed vibronic transitions are not sufficiently resolved to obtain a reasonable estimate for ω_e'. The relative vibronic intensities obtained through a deconvolution process might be more accurate. Let us assume that, for the above transition, we know $\omega_e' = 819.93\ cm^{-1}$ and the following intensities have been observed by Gallas et al.:[21]

$$\begin{aligned} v' = v'' = 0 \quad &: \quad \text{Int} = 0.8450 \\ v' = 1,\ v'' = 0: \quad &\text{Int} = 0.3234 \\ v' = 2,\ v'' = 0: \quad &\text{Int} = 0.0662 \end{aligned} \tag{1-36}$$

According to (1-28),

$$K = 0.3831 \pm 0.3958 \tag{1-37}$$

If we take the plus sign in (1-37), the change in ω_e'' would be unreasonable. We take $K = -0.0128$, which gives $\omega_e'' = 799\ cm^{-1}$.

Using (1-29), we obtain $\alpha_1\delta = 0.875$. Together with the above ω_e'' in (1-35), this gives

$$\delta = 2.32(10^{-21})g^{1/2}cm \tag{1-38}$$

Taking the masses of the most abundant isotopes to calculate the reduced mass of ZrO gives $\Delta r_e = 0.049\text{Å}$. The actual shift of r_e, according to Schoonveld and Sundram, is[22]

$$\Delta r_{e,exp} = 0.047\text{Å} \tag{1-39}$$

which compares favorably with the calculated value. However, experimentally we find $\omega_e'' = 937.36\ cm^{-1}$, according to the same authors. In general, it is to be expected that Franck-Condon factors would be too insensitive towards changes in ω_e as to prove useful in finding this spectroscopic constant.

If $\delta = 0$, only transitions with $\Delta v = 0,2,4,...$ are allowed. In this manner, a bending vibration of a molecule which is linear in both the initial and the final state could be activated. According to (1-17),

$$S_{20} = (1/2)[(\zeta_{12} - 1)/(\zeta_{12} + 1)]^2 \tag{1-40}$$

where $\zeta_{12} = \omega_e''/\omega_e'$. The calculated intensity ratios S_{20} for various ζ_{12}s would be

ζ_{12}	S_{20}	ζ_{12}	S_{20}
1	0		
1.02	0.00005	0.98	0.00005
1.05	0.0003	0.95	0.0003
1.1	0.001	0.9	0.001
1.15	0.002	0.8	0.006
1.2	0.004	0.6	0.031
1.5	0.020	0.5	0.056
2	0.056		

(1-41)

The above data imply that vibronic transitions induced by a change in ω_e in a manner described above would be observed only if ω_e' and ω_e'' differ considerably.

CHAPTER 2

THE DUSCHINSKY EFFECT FOR TWO MIXING MODES

Duschinsky has shown that the normal mode coordinate frames of a molecule in two distinct electronic states are interconnected through the transformation[6]

$$q_i'' = \Sigma_i \ \ell_{ij} \ q_{ij}' - \delta_i \tag{2-1}$$

Let us treat the case where two modes mix according to (2-1):

$$q_1'' = \ell_{11} \ q_1' + \ell_{12} \ q_2' - \delta_1$$

$$q_2'' = \ell_{21} \ q_1' + \ell_{22} \ q_2' - \delta_2 \tag{2-2}$$

We assume that initially both normal modes have v = 0, i.e. $v_1'' = v_2'' = 0$. The Franck-Condon integral becomes

$$\langle v_1' v_2' | 00 \rangle = N_o^2 N_n N_m \iint \exp(-(1/2)[\alpha_1^2(\ell_{11}x_1 + \ell_{12}x_2 - \delta_1)^2 + \alpha_2^2(\ell_{21}x_1 + \ell_{22}x_2 - \delta_2)^2 + (\beta_1 x_1)^2 + (\beta_2 x_2)^2])$$

$$H_m(\beta_1 x_1) H_n(\beta_2 x_2) dx_1 dx_2 \tag{2-3}$$

where $m = v_1'$ and $n = v_2'$, and the integrations are from $-\infty$ to $+\infty$. We can perform one of the integrations readily, using a table of integrals.[23]

$$\langle v_1' v_2' | 00 \rangle = [2\pi(1-\beta_1^2/a^2)^m]^{1/2} \ S_2^{-1} \ \exp(-S_o)$$

$$\int_{-\infty}^{\infty} \exp(-z^2 + 2(S_1/S_2)z) H_n(\beta_2 z/S_2)$$

$$H_m((\kappa z/S_2) - \eta) dz \tag{2-4}$$

where the following substitutions have been made:

$$a^2 = \alpha_1^2 \ell_{11}^2 + \alpha_2^2 \ell_{21}^2 + \beta_1^2$$

$$b_1 = (\delta_1 \ell_{11} \alpha_1^2 + \delta_2 \ell_{21} \alpha_2^2)/a$$

$$b_2 = (\alpha_1^2 \ell_{11} \ell_{12} + \alpha_2^2 \ell_{21} \ell_{22})/a$$

$$b_3 = [a^2 - 2\beta_1^2]^{1/2}$$

$$2S_o = \alpha_1^2 \delta_1^2 + \alpha_2^2 \delta_2^2 - b_1^2$$

$$2S_1 = \alpha_1^2 \delta_1 \ell_{12} + \alpha_2^2 \delta_2 \ell_{22} - b_1 b_2$$

$$2S_2 = \alpha_1^2 \ell_{12}^2 + \alpha_2^2 \ell_{22}^2 + \beta_2^2 - b_2^2$$

$$\kappa = -(\beta_1/\beta_2)(b_2/b_3)$$

$$\eta = -\beta_1 b_1/b_3 \qquad (2\text{-}5)$$

No analytical expression could be found in literature for the above integral. We want to express the second Hermite polynomial in (2-4) as a Hermite polynomial expansion:

$$H_m(\kappa x - \eta) = \sum_{k=0}^{m} a_k H_k(x) \qquad (2\text{-}6)$$

The differential equation satisfied by the "shifted" Hermite polymial is

$$\{\frac{d^2}{dx^2} - 2\kappa(\kappa x - \eta)\frac{d}{dx} + 2\kappa^2 m\} H_m(\kappa x - \eta) = 0 \qquad (2\text{-}7)$$

Substituting the Hermite polynomial expansion in (2-6) into (2-7) and making use of recursion formulae for the Hermite polymials gives

$$\Sigma_k a_k \{ \kappa^2(m-k)H_k(x) + 2k\kappa\eta H_{k-1}(x)$$

$$+ 2k(k-1)(1-\kappa^2)H_{k-2}(x)\} = 0 \qquad (2\text{-}8)$$

Collecting equal terms in the above expression yields a recursion formula for the expansion coefficients:

$$(m-k+1)\kappa^2 a_{k-1} + 2k\kappa\eta a_k + 2k(k+1)(1-\kappa^2)a_{k+1} = 0 \qquad (2\text{-}9)$$

From (2-6), by inspection,

$$a_m = \kappa^m \qquad (2\text{-}10)$$

and from this, using the recursion formula in (2-9),

$$a_{m-1} = -2m\eta\kappa^{m-1} \qquad (2\text{-}11)$$

The remaining expansion coefficients can be obtained from a_m and a_{m-1} by downward recursion, using (2-9). In some cases, κ and η are both imaginary quantities. However, κ^2 and the product $\kappa\eta$ in (2-9) will always be real. Substituting the Hermite polynomial expansion into (2-4) yields a sum of integrals which can be expressed analytically.[24] The normalization factors for the harmonic oscillator eigenfunctions were given in (1-8). We obtain for the two-dimensional Franck-Condon factor

$$\langle v_1' v_2' | 00\rangle^2 = [\alpha_1\alpha_2\beta_1\beta_2/(2^{n+m-1}n!m!)]$$

$$(1-2\beta_1^2/a^2)^m \{(aS_2)^{-1} \exp((S_1/S_2)^2 - S_o)$$

$$\sum_{k=0}^{m} a_k \sum_{j=0}^{s} 2^j (j)! \binom{k}{j}\binom{n}{j}(1-\beta_2^2/S_2^2)^{(1/2)(k+n)-j} \qquad (2\text{-}12)$$

$$H_{k+n-2j}[(S_1\beta_2/S_2^2)/(1-\beta_2^2/S_2^2)^{1/2}]\}^2$$

where s = min (k,n). The two-dimensional Franck-Condon factors fulfill the following sum rules:

$$\sum_{v_1'=0}^{\infty}\sum_{v_2'=0}^{\infty}\langle v_1'v_2'|v_1''v_2''\rangle^2 = \sum_{v_1''=0}^{\infty}\sum_{v_2''=0}^{\infty}\langle v_1'v_2'|v_1''v_2''\rangle^2 = 1 \qquad (2\text{-}13)$$

The first one of these two rules was used to verify (2-12).

The following steps are necessary to work an actual example:

(i) Use the parallel frame approximation to find a first approximation to δ_1 and δ_2.

(ii) Compute the Duschinsky matrix.

(iii) Adjust the two dislocations of the frames such that the calculated and experimental Franck-Condon factors are in best agreement according to some chosen criteria.

From the knowledge of the geometry of the excited state, one can construct more exact normal mode coordinates of this state. One can then compute an improved Duschinsky matrix and continue with (iii) until a self-consistent excited state structure is computed. Coon et al. describe such a strategy in their paper.[8]

A computer program was written which computes the dislocations δ_1 and δ_2 for a given Duschinsky matrix from two distinct ratios of intensities. We require

$$G_1(\delta_1,\delta_2)=(\mathrm{Int}_1/\mathrm{Int}_2)\langle v_1'v_2'|00\rangle_2^2-\langle v_1'v_2'|00\rangle_1^2 = 0$$

$$G_2(\delta_1,\delta_2)=(\mathrm{Int}_3/\mathrm{Int}_4)\langle v_1'v_2'|00\rangle_4^2-\langle v_1'v_2'|00\rangle_3^2 = 0 \qquad (2\text{-}14)$$

where Int_{1-4} are the observed Franck-Condon factors. Two of these may be the same as long as a ratio of the type $\mathrm{Int}_k/\mathrm{Int}_k$ does not result. Let us substitute $x = \delta_1$ and $y = \delta_2$. The Newton-Raphson iterations can then be formulated as

$$x_{k+1} = x_k - [\mathrm{Jac}(G_1,G_2)]^{-1} \det \begin{pmatrix} G_1 & \frac{\partial G_1}{\partial y} \\ G_2 & \frac{\partial G_2}{\partial y} \end{pmatrix} \tag{2-15}$$

$$y_{k+1} = y_k - [\mathrm{Jac}(G_1,G_2)]^{-1} \det \begin{pmatrix} \frac{\partial G_1}{\partial x} & G_1 \\ \frac{\partial G_2}{\partial x} & G_2 \end{pmatrix} \tag{2-16}$$

The Jacobian is

$$\mathrm{Jac}(G_1,G_2) = \det \begin{pmatrix} \frac{\partial G_1}{\partial x} & \frac{\partial G_1}{\partial y} \\ \frac{\partial G_2}{\partial x} & \frac{\partial G_2}{\partial y} \end{pmatrix} \tag{2-17}$$

The partial derivatives are computed by the program numerically.

Some work has been done on the bent molecule SO_2, where the two totally symmetric modes mix, using the intensities published by Coon et al.[8] It turned out that the Newton-Raphson search converged properly. There was some doubt, however, whether the Duschinsky matrix was constructed correctly. At any rate, this work was not considered worth being included here.

The procedure outlined here should be appropriate for the mixing of two modes of the same symmetry. However, the present approach of dealing with the Duschinsky effect will become rather difficult when dealing with more than two mixing modes and removing the restriction $v_1'' = v_2'' = 0$. Faulkner and Richardson managed to find a coordinate transform of the ground and excited state normal mode frames which effectively removes any Duschinsky mixing.[25] They did some work, as well, involving contact transformation perturbation theory. Since the present approach is completely outclassed by the work of Faulkner and

Richardson, it seemed advisable to discontinue fundamental research on this subject.

The work done so far would constitute a theoretical basis for finding the excited state geometries for linear-linear transitions in the photoelectron spectrum of N_2O, where the stretching vibrations have some Duschinsky mixing. Recently, Dehmer et al., reported high-resolution photoelectron spectra of this molecule.[26]

CHAPTER 3

THE CALCULATION OF WEIGHTED FRANCK-CONDON FACTORS IN THE HARMONIC APPROXIMATION

The normal mode coordinate dependence of the transition moment is usually expressed in a power series expansion

$$M(q) = M_o + M_1 q + M_2 q^2 + \ldots\ldots \tag{3-1}$$

We choose here an expansion of a slightly more general type:

$$M(q) = \exp(-(1/2)(\alpha_o q)^2) \sum_{k=0}^{K} \mathscr{M}_k q^k \tag{3-2}$$

(3-1) is a special case of this expansion with $\alpha_o = 0$.

Let us take $v' = n$ and $v'' = m$. The weighted Franck-Condon factors in the harmonic approximation are

$$\begin{aligned} \langle n|M|m\rangle^2 = N_m^2 N_n^2 [\int_{-\infty}^{\infty} & \exp(-(1/2)(\alpha_o^2 + \alpha_1^2 + \alpha_2^2) q^2 \\ & + \delta\alpha_1^2 q - (1/2)\delta^2 \alpha_1^2) \sum_{k=0}^{K} \mathscr{M}_k q^k H_m(\alpha_1(q-\delta)) \\ & H_n(\alpha_2 q)\, dq]^2 = N_m^2 N_n^2 [\int_{-\infty}^{\infty} Fo(q)\, dq]^2 \end{aligned} \tag{3-3}$$

Let us introduce a new variable $z = \beta_1 q - \beta_o$.

Then,

$$\langle n|M|m\rangle^2 = [\int_{-\infty}^{\infty} Fo(z)\, dz]^2 / \beta_1^2 \tag{3-4}$$

and we take β_o and β_1 such that

$$\begin{aligned} 2\beta_1^2 &= \alpha_o^2 + \alpha_1^2 + \alpha_2^2 \\ 2\beta_o\beta_1 &= \alpha_1^2 \delta = \alpha_1 D, \text{ where } D = \alpha_1 \delta \end{aligned} \tag{3-5}$$

This gives, in (3-3),

$$\langle n|M|m\rangle^2 = N_n^2 N_m^2 (\beta_1^{-2} \exp(2\beta_o^2 - D^2))$$
$$[\int_{-\infty}^{\infty} e^{-z^2} \Sigma_k \mathscr{H}_k (\gamma_o + \gamma_1 z)^k H_m(S_1 z + d_1) H_n(S_2 z + d_2) dz]^2 \qquad (3\text{-}6)$$

where the following substitutions have been made:

$$\gamma_1 = \beta_1^{-1} \qquad S_1 = \alpha_1\gamma_1 \qquad d_1 = \alpha_1\beta_o\gamma_1 - D$$
$$\gamma_o = \beta_o/\beta_1 \qquad S_2 = \alpha_2\gamma_1 \qquad d_2 = \alpha_2\beta_o\gamma_1 \qquad (3\text{-}7)$$

The integration in (3-6) cannot readily be performed. If we could express the three factors in (3-6) in terms of Hermite polynomial expansions, integrals of the following type would arise:

$$Fs(k,n,m) = \int_{-\infty}^{\infty} e^{-z^2} H_k(z) H_n(z) H_m(z) dz \qquad (3\text{-}8)$$

This integral could be located in a table of integrals:[27]

$$Fs(k,n,m) = \begin{cases} \pi^{1/2} 2^s k!n!m!/[(s-k)!(s-n)!(s-m)!], \\ \quad \text{if } k+m+n \text{ is even and} \\ \quad k+n \geq m \text{ and } m+n \geq k \text{ and } k+m \geq n. \\ \quad 0 \text{ otherwise} \end{cases} \qquad (3\text{-}9)$$

where $2s = k+m+n$. Let us expand the terms in the power series expansion in (3-6) in terms of Hermite polynomials. It can readily be shown that

$$\{(\gamma_o + \gamma_1 z)\frac{d}{dz} - k\gamma_1\}(\gamma_o + \gamma_1 z)^k = 0 \qquad (3\text{-}10)$$

If a Hermite polynomial expansion is substituted into the above equation, we obtain

$$\Sigma_{j_1} a_{j_1} \{\gamma_1(j_1-k)H_{j_1}(z) + 2\gamma_o j_1 H_{j_1-1}(z)$$

$$+ 2\gamma_1 j_1(j_1-1)H_{j_1-2}(z)\} = 0 \qquad (3\text{-}11)$$

Collecting equal terms in the above equation, and demanding that their coefficients vanish, gives rise to a three-term recursion formula among the expansion coefficients:

$$a_{j_1-2} = 2((j_1-1)/(k-j_1+2))\{j_1 a_{j_1} + \beta_\odot a_{j_1-1}\} \qquad (3\text{-}12)$$

where $\beta_\odot = \gamma_o/\gamma_1$ has been substituted. The expansion coefficients are most readily obtained through downward recursion with

$$a_k = ((1/2)\gamma_1)^k \text{ and } a_{k-1} = \gamma_o k((1/2)\gamma_1)^{k-1} \qquad (3\text{-}13)$$

In the previous chapter expansions of the type

$$H_m(S_1 z + d_1) = \sum_{j_2=0}^{m} b_{j_2} H_{j_2}(z) \qquad (3\text{-}14)$$

have been defined in terms of a three-term recursion formula among the expansion coefficients

$$(m-j_2+1)S_1^2 b_{j_2-1} - 2j_2 S_1 d_1 b_{j_2} + 2j_2(j_2+1)(1-S_1^2)b_{j_2+1} = 0 \qquad (3\text{-}15)$$

together with the starting values for downward recursion

$$b_m = S_1^m \text{ and } b_{m-1} = 2md_1 S_1^{m-1} \qquad (3\text{-}16)$$

The last required Hermite polynomial expansion is

$$H_n(S_2 z + d_2) = \sum_{j_3=0}^{n} C_{j_3} H_{j_3}(z) \qquad (3\text{-}17)$$

It can be defined in an analogous manner

$$(n-j_3+1)S_2{}^2C_{j_3-1} - 2j\ S_2d_2C_{j_3} + 2j_3(j_3+1)(1-S_2{}^2)C_{j_3+1} = 0$$

$$\text{with} \quad C_n = S_2{}^n \quad \text{and} \quad C_{n-1} = 2nd_2S_2{}^{n-1} \tag{3-18}$$

Using the three expansions, we obtain integrals of the type shown in (3-9) exclusively:

$$\langle n|m\rangle^2 = (N_nN_m/\beta_1)^2 \exp(2\beta_o^2 - D^2)$$

$$\left[\sum_{k=0}^{K} \mathscr{K}_k \sum_{j_1=0}^{k} a_{j_1} \sum_{j_2=0}^{m} b_{j_2} \sum_{j_3=0}^{n} C_{j_3} Fs(j_1,j_2,j_3)\right]^2 \tag{3-19}$$

This general formula is also applicable to the calculation of vibronic intensities for transitions allowed through Herzberg-Teller coupling, i.e., $\mathscr{K}_o = 0$. It is suitable, as well, for the computation of r - centroids.

Since this expression for the calculation of weighted harmonic Franck-Condon factors is so versatile in terms of its potential application, a large scale investigation into the number of significant figures obtained for these Franck-Condon factors was undertaken. For the unwary, the finite sums in (3-19) don't seem very suspicious. However, the expansion terms do not all have the same sign. In many cases, such alternating series are rather ill-conditioned. One can readily estimate the number of significant figures for a sum, simply by finding the term with maximum magnitude and comparing it with the actual value of the sum. IBM software uses approximately 16 decimal digits to represent double precision quantities. A pessimistic estimate for the number of significant decimal figures of a sum obtained in this manner becomes

$$\text{No. sig. figures} = 15 - \log\left(|\text{term}|_{max}/|\text{sum}|\right) \tag{3-20}$$

The investigation covered all cases with

$$D = 0,1, \ldots\ldots ,5$$

$$\alpha_o = 0,(1/2)$$

$$2\alpha_1 = 1,2,3$$

$$2\alpha_2 = 1,2,3$$

$$m,n = 0,1, \ldots\ldots ,15$$

and $K = 0,1,2,3$; with $\mathscr{K}_k = \delta_{k,K}$. (3-21)

The resulting number of significant figures estimated according to (3-20) were printed in large tables. This generated approximately 100,000 numbers. Visual examination of the tables indicated that for large D, and m and n both large, one can end up with as little as seven significant figures for the sum. This, however, is more than enough accuracy required for most applications. The range covered for the various parameters in (3-21) should also cover the range these parameters cover in most applications. Significant figures are lost in the neighborhood of roots of the sum, due to near-cancellation of relatively large terms. This is not a problem in our case, whatsoever.

Based on the above findings, one can conclude that the algorithm developed in this chapter for the calculation of weighted Franck-Condon factors fortunately is not ill-conditioned, in most cases of interest, as long as double precision accuracy is used throughout.

From the theory of orthogonal sets:[28]

$$\sum_{n=0}^{\infty} \langle n|M|m\rangle^2 = \langle m|M^2|m\rangle \qquad (3\text{-}22)$$

$$\sum_{m=0}^{\infty} \langle n|M|m\rangle^2 = \langle n|M^2|n\rangle \qquad (3\text{-}23)$$

These relationships were used to make sure that no mistakes had sneaked into the mathematical derivation or the programming of the formula.

For the B-X transition of molecular iodine Herzberg gives the following spectroscopic constants:[1]

$$\text{X:}\quad \omega_e'' = 214.57\ \text{cm}^{-1},\ r_e'' = 2.666\text{Å}$$

$$\text{B:}\quad \omega_e' = 128.0\ \text{cm}^{-1},\ r_e' = 3.016\text{Å} \qquad (3\text{-}24)$$

Let us assume that we wish to compute the r-centroid of the transition $(v' = 0)B \leftarrow (v'' = 0)X$ of I_2. An r-centroid can be considered an "average geometry" of a transition. We will discuss r-centroids in the next chapter extensively. The average geometry of the transition considered corresponds simply to an average internuclear distance. According to Fraser,[29]

$$\bar{r} = \langle\chi'|r|\chi''\rangle/\langle\chi'|\chi''\rangle \qquad (3\text{-}25)$$

We define the normal mode coordinate of a diatomic molecule as $q = q' = \mu^{1/2}(r-r_e')$. This gives, in (3-25),

$$\bar{r} = r_e' + [\mu^{-1/2}\langle\chi'|q|\chi''\rangle/\langle\chi'|\chi''\rangle] \qquad (3\text{-}26)$$

where μ is the reduced mass. Using the spectroscopic constants in (3-24) in (1-35) we obtain

$$\alpha'' = 2.5227\ ((\text{a.m.u.})\text{Å}^2)^{-1/2}$$

$$\alpha' = 1.948\quad\ "\qquad (3\text{-}27)$$

And the dimensionless displacement parameter is

$$D = (r_e'' - r_e')\mu^{1/2}\alpha'' \tag{3-28}$$

Using the mass of the most abundant iodine isotope to find the reduced mass, we obtain D = -7.021. The r-centroid according to (3-26) becomes then

$$\bar{r} = [3.016 + 0.12554(-0.000171596/0.000098435)]\text{Å} = 2.797\text{Å} \tag{3-29}$$

According to Joel Tellinghuisen, $\bar{r} = 2.827$Å.[30] Sixteen r-centroids with $v', v'' \leq 3$ were computed. They were consistently too small, by 0.028 to 0.033Å, when compared with Tellinghuisen's values, which were obtained from an RKR calculation. It will become apparent in the next chapter that this discrepancy is caused by the neglect of anharmonicities.

A computer program has been written in FORTRAN which computes the possible dislocation parameters D from given intensities of a pair of vibronic transitions.

CHAPTER 4

THE TRANSITION MOMENT FUNCTION FROM EXPERIMENTAL INTENSITIES

The emission intensity of a vibronic transition can be calculated[31]

$$I_{v'v''} = (\text{const.})\ N_{v'} S_{v'v''} / \lambda^4_{v'v''} \tag{4-1}$$

where $N_{v'}$ is the population of the v' vibrational sublevel. The band strength $S_{v'v''}$ is the major component of several spectroscopic quantities, which are:

(i) Einstein A and B coefficients[32-34]

(ii) oscillator strength

(iii) linear absorption coefficient

(iv) mass absorption coefficient

(v) extinction coefficient.

We direct our attention to the quantity $S_{v'v''}$. Assuming separability of electronic and nuclear motion,

$$S_{v'v''} = \langle v' | M | v'' \rangle^2 \tag{4-2}$$

where M is the transition moment function. For a diatomic molecule, M is a function of the internuclear separation. We will use normal coordinates in general, with the singly primed normal mode coordinates taken as the frame of reference. In a diatomic molecule this becomes simply

$$q = \mu^{1/2}(r - r_e') \tag{4-3}$$

In the Franck-Condon approximation, one takes

$$M(q) \sim M(q_{eq}) = \text{const.} \tag{4-4}$$

where q_{eq}, in general, denotes the equilibrium geometry of the initial state. If the transition moment function is not dependent on q, we can write

$$S_{v'v''} = [M(q_{eq})]^2 \langle v' | v'' \rangle^2 \tag{4-5}$$

According to Fraser, for a given vibronic transition a better approximation is[29]

$$S_{v'v''} = (M(\bar{r}))^2 \langle v' | v'' \rangle^2 \tag{4-6}$$

where $\bar{r}$ is something like an average geometry of the transition

$$\bar{r} = \langle v' | r | v'' \rangle / \langle v' | v'' \rangle \tag{4-7}$$

commonly referred to as r-centroid. According to the above, the coordinate dependence of the transition moment can be obtained from the observed band strengths

$$M(\bar{r}) = \pm S_{v'v''}^{1/2} / \langle v' | v'' \rangle \tag{4-8}$$

where, in this case, $S_{v'v''}$ would represent the experimental transition probability for $v' \leftarrow v''$.

The validity of the r-centroid approximation has been proven by Smith within the confines of a semiclassical theory.[35] Recently, Yazykova and Butyrska reported on their efforts to justify the r-centroid approximation on rigorous mathematical grounds.[36] They succeeded in showing that the r-centroid approximation has a quasi-classical nature. They didn't seem to be aware of Smith's work on this subject.

It is well-known that the r-centroid approximation may break down, and a correction term has been introduced by Halevi.[37,38] It turns out that r-centroids mean different things to different people. In general, the quantity $\bar{r}$ in (4-7) is called an r-centroid. As mentioned previously, $\bar{r}$ approximates the "average geometry" of a transition. Some people consider the "average geometry" the actual r-centroid and $\bar{r}$ an approximation thereof. In our notation, $\bar{r}$ as defined in (4-7) is called an r-centroid.

A breakdown of the r-centroid approximation can easily be visualized. Assume that the Franck-Condon overlap in the denominator in (4-7) becomes zero. Then if $\langle v' | r | v'' \rangle$ is not zero as well, the transition moment in (4-8) has to be taken as

$$M(\bar{r}) \sim M(+\infty) \text{ or } M(\bar{r}) \sim M(-\infty) \tag{4-9}$$

depending on the direction from which the singularity is approached. Figure 4-1 consists of a graph of the roots of $\langle v' | v'' \rangle$ and $\langle v' | q | v'' \rangle$ for the one-dimensional harmonic oscillator and for the special case $v'' = 5$ and $v' = 6$. Figure 4-1 illustrates that the roots of the numerator and of the denominator in (4-7) do not coincide, in general. Quantitative insight into situations where the r-centroid approximation fails has been claimed by Nicholls for model wave function products represented by a train of finite length of rectangular pulses of varying amplitude.[39] The transition moment of the $X^1\Sigma^+$-$A^1\Sigma^+$ system of LiH has a maximum at $r_{LiH} \sim 7a_o$, where a_o is Bohr's radius. Kate Docken found that the correct shape of the transition moment was reproduced only by the transitions with relatively large Franck-Condon overlap,

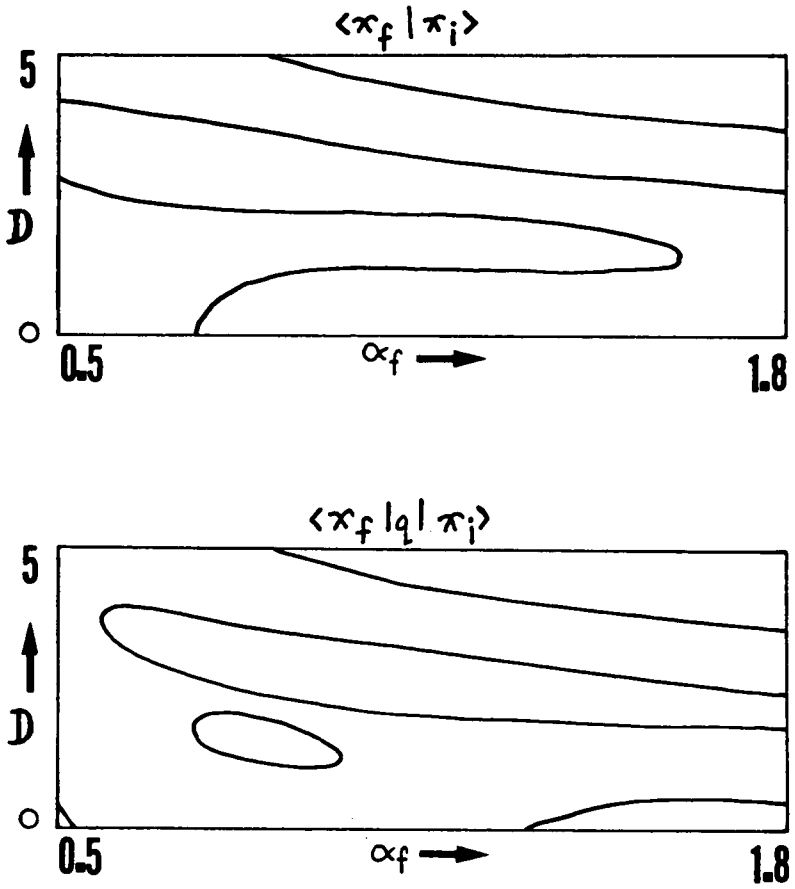


Fig. 4-1. Contour plots of the roots of the Franck-Condon amplitudes and of the r-centroids for displaced harmonic oscillators.

indicating that the r-centroid approximation didn't work too well in this case.[40]

In Figure (4-2) the quantity

$$\langle v' \left| M(q) \right| v'' \rangle / \langle v' \left| v'' \right\rangle \tag{4-10}$$

has been plotted against $\bar{q}$ for the vibronic progressions

$$v'' = 0, \quad v' = 0,1, \ldots, 10$$

$$v'' = 6, \quad v' = 0,1, \ldots, 10 \tag{4-11}$$

using $M(q) = \exp(-1.14q)$.

The exponential was expressed as a power series

$$\exp(-1.14q) = \Sigma_k \mathscr{M}_k q^k \tag{4-12}$$

where

$$\mathscr{M}_k = (-1)^k (1.14)^k / k! \tag{4-13}$$

According to (4-8) the points should be located on a curve $M(\bar{q})$. The points indicated by arrows are points on the M(q) curve. Actually, the $M(\bar{q})$ curve, which, according to Fraser, should approximate the M(q) curve, is not a real curve but rather a set of discrete points. Francke *et al.* insist that one carefully distinguish between the $M(\bar{q})$ and the M(q) curve.[41]

Nicholls and Jarmain established empirically the following approximation:[42,43]

$$[\langle v' \left| r \right| v'' \rangle / \langle v' \left| v'' \right\rangle]^n \sim \langle v' \left| r^n \right| v'' \rangle / \langle v' \left| v'' \right\rangle \tag{4-14}$$

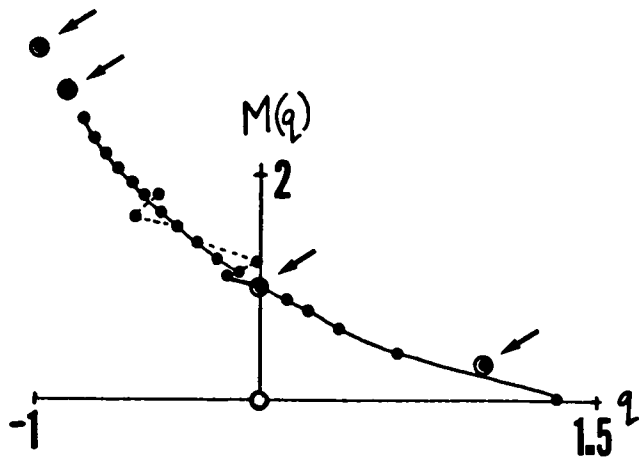


Fig. 4-2. Comparison of the function M(q) = exp(-1.14q) and M($\bar{q}$).

Using (4-14), one can take

$$\langle v'|M|v''\rangle = \langle v'|\Sigma_k \mathscr{M}_k q^k|v''\rangle \sim \Sigma_k \mathscr{M}_k (\bar{q}_{v'v''})^k \qquad (4\text{-}15)$$

Nicholls thereafter published extensively on topics involving the r-centroid approximation.[44-48]

The present author believes that using the r-centroid approximation beyond linear dependence gives unreliable results. If in (4-14) for a diatomic molecule one takes r as the internuclear distance the approximation by Nicholls and Jarmain holds in a trivial sense. Taking, instead of the internuclear separation, a variable r' centered at r_e',

$$r' = r - r_e' \qquad (4\text{-}16)$$

(4-14) becomes

$$\langle v'|(r' + r_e')^n|v''\rangle / \langle v'|v''\rangle$$

$$\sim [\langle v'|r' + r_e'|v''\rangle / \langle v'|v''\rangle]^n \qquad (4\text{-}17)$$

The vibrational overlap does not extend far beyond r_e' and r_e'', if r_e' and r_e'' are not very different. In other words,

$$r' + r_e' \sim r_e' \quad \text{or} \quad r' \sim 0 \qquad (4\text{-}18)$$

In this case, (4-17) holds trivially, i.e.

$$\langle v'|(r_e')^n|v''\rangle / \langle v'|v''\rangle = [\langle v'|r_e'|v''\rangle / \langle v'|v''\rangle]^n \qquad (4\text{-}19)$$

However, if the variable for the r-centroid is centered near r_e' or r_e'', the empirical relation of Nicholls and Jarmain does not hold well for such a variable, i.e.,

$$\langle v'|q^n|v''\rangle/\langle v'|v''\rangle \overset{?}{\sim} [\langle v'|q|v''\rangle/\langle v'|v''\rangle]^n \qquad (4\text{-}20)$$

is a valid assumption only if you are willing to stretch your imagination considerably. That this is the case at least for the first positive system of N_2 will be shown with a Morse oscillator model. Since the relation by Nicholls and Jarmain can be made questionable simply by changing the variable, we must draw the previously stated conclusion that the r-centroid approximation does not give reliable normal mode coordinate dependence of the transition moment beyond a linear dependence.

The advantage of the r-centroid approximation is that some research group can calculate the potential energy curves involved in a transition, and from these compute the expectation values $\langle v'|v''\rangle$ and $\langle v'|q|v''\rangle$, by some fancy method, and publish their findings. Based on these published data, another group, equipped for intensity measurements, can make use of the r-centroids in finding $M(\bar{q})$. According to previous statements, the q-dependence of the transition moment beyond

$$M(\bar{q}) = C_o + C_1 q \qquad (4\text{-}21)$$

cannot be reliably extracted from the given information. In the present work, an attempt was made to drop the r-centroid approximation altogether.

Let us assume that the transition moment function can be expanded in normal mode coordinates in terms of some suitable basis set $\mathcal{H}_o$, $\mathcal{H}_1$, ... :

$$M(q) = \mathcal{N}_o \mathcal{H}_o(q) + \mathcal{N}_1 \mathcal{H}_1(q) + ... \qquad (4\text{-}22)$$

The square root of the transition probability $v' \leftarrow v''$ becomes

$$\langle v' | M | v'' \rangle = \Sigma_k \mathcal{A}_k \langle v' | \mathcal{M}_k | v'' \rangle \tag{4-23}$$

One can then formulate for a series of transitions

$$n \leftarrow m \tag{4-24}$$

a weighted least squares scheme

$$\begin{pmatrix} Sn_{00} & Sn_{01} & \cdots \\ Sn_{10} & Sn_{11} & \cdots \\ \vdots & \vdots & \end{pmatrix} \begin{pmatrix} \mathcal{A}_0 \\ \mathcal{A}_1 \\ \vdots \end{pmatrix} = \begin{pmatrix} Sa_0 \\ Sa_1 \\ \vdots \end{pmatrix} \tag{4-25}$$

where

$$Sa_j = \Sigma_n \Sigma_m W_{nm} \langle n | \mathcal{M}_j | m \rangle \Phi_{nm} Int_{nm}^{1/2} \tag{4-26}$$

and

$$Sn_{kj} = Sn_{jk} = \Sigma_n \Sigma_m \langle n | \mathcal{M}_k | m \rangle \langle n | \mathcal{M}_j | m \rangle \tag{4-27}$$

and $Int_{nm}^{1/2}$ is the magnitude of the "experimental" weighted Franck-Condon overlap (WFCO) for $n \leftarrow m$, obtained by taking the positive square root of the experimental transition probability. "Weighted" Franck-Condon amplitudes simply mean $\langle v' | M | v'' \rangle$ with $M(q) \neq 1$, i.e., the transition moment function is being considered a weighting function. The Φs are quantities which are either +1 or -1, depending on the sign of the corresponding WFCOs. The W_{nm}s are weighting factors. Since the Φs

are not determined at this point, one is dealing with potentially $2^{(\#\text{ of transitions}-1)}$ distinct linear systems in (4-25), and of course, a corresponding number of distinct solutions. We are therefore faced with the problem of finding the signs of the experimental WFCOs. These signs depend on the conventions used for the mathematical representation of the wave functions. One can, for example, follow the convention that the wave function is positive for large q.[49] Sileo and Cool evaluated the dipole moment function of HF and DF from vibrational spectra.[50] They determined the expansion coefficients as non-linear parameters. Their least-squares functional was obtained by comparing the intensities with the squares of the WFCOs, thus eliminating the question of signs. They end up with a quadratic system with multiple solutions. In other words, they generated a non-linear system with the same ambiguities as the one they started out with.

One can "guess" the signs of the WFCOs recursively using the formulae published by Ansbacher.[11] For

$$\langle v'|v''\rangle = N_{v''}N_{v'}\int_{-\infty}^{\infty} H_{v''}(\alpha_2(q-\delta))H_{v'}(\alpha_1 q)$$
$$\exp(-(1/2)(\alpha_1^2 q^2 + \alpha_2^2(q-\delta)^2))dq \qquad (4\text{-}28)$$

the following two recursion formulae apply:

$$(2aD_A)\langle n|m\rangle + (a^2+1)[2(n+1)]^{1/2}\langle n+1|m\rangle$$
$$+ (2n)^{1/2}(a^2-1)\langle n-1|m\rangle = 2a(2m)^{1/2}\langle n|m-1\rangle \qquad (4\text{-}29)$$

and

$$(2D_A)\langle n|m\rangle + 2a(2n)^{1/2}\langle n-1|m\rangle +$$

$$(2m)^{1/2}(a^2-1)\langle n|m-1\rangle = (a^2+1)[2(m+1)]^{1/2}\langle n|m+1\rangle \quad (4\text{-}30)$$

where the following substitutions have been made:

$$n = v', \; m = v''$$

$$a = \alpha_1/\alpha_2 = (\omega_e'/\omega_e'')^{1/2}$$

$$D_A = \alpha_1\delta \quad (4\text{-}31)$$

and for $v' = v'' = 0$,

$$\langle 0|0\rangle = [2a/(a^2+1)]^{1/2}\exp(-(1/2)\alpha_1{}^2\delta^2/(a^2+1)) \quad (4\text{-}32)$$

The actual procedure to choose the signs of the WFCOs in the harmonic approximation is especially simple if $v'\leftarrow 0$ transitions are considered, and $\omega' \leq \omega''$. The recursion formula in (4-29) becomes for $m=0$

$$\langle n+1|0\rangle = [n^{1/2}(1-a^2)\langle n-1|0\rangle - 2^{1/2}aD_A\langle n|0\rangle]/[(n+1)^{1/2}(1+a^2)] \quad (4\text{-}33)$$

Inspection of the above recursion formula gives

$$\mathrm{sgn}(\langle n|0\rangle) = (-1)^n \text{ for } a^2 = \omega_e'/\omega_e'' \leq 1 \quad (4\text{-}34)$$

For example, for the photoionization of oxygen

$$O_2(X^3\Sigma_g^-) \xrightarrow{h\nu} O_2^+(a^4\Pi) + e^- \quad (4\text{-}35)$$

we have[1]

$$a^2 = 1035.69/1580.361 = 0.655<1 \quad (4\text{-}36)$$

and we can obtain the WFCOs from the experimental transition probabilities by simply taking

$$\langle v' | 0 \rangle = (-1)^{v'} \left| \mathrm{Int}(v' \leftarrow 0) \right|^{1/2} \tag{4-37}$$

If a>1 an appropriate choice of signs requires more elaborate procedures. The photoionization of oxygen

$$O_2(X^3\Sigma_g^-) \xrightarrow{h\nu} O_2^+(X^2\Pi_g) + e^- \tag{4-38}$$

gives[1]

$$a^2 = 1876.4/1580.361 = 1.187 > 1 \tag{4-39}$$

This is an appropriate example to illustrate the use of the recursion formula to find the signs of the WFCOs. We take, arbitrarily,

$$\mathrm{sgn}(\langle 0 | 0 \rangle) = 1 \tag{4-40}$$

Then, using the recursion formula (4-33), we can readily see that

$$\mathrm{sgn}(\langle 1 | 0 \rangle) = -1 \tag{4-41}$$

The signs so far are independent of the magnitude of the overlap. Subsequently, the recursion formula will be used in a manner such that we mimick an interpolation rather than an extrapolation. We write (4-33) as follows:

$$\langle n | 0 \rangle = [(1-a^2) n^{1/2} \langle n-1 | 0 \rangle - (1+a^2)(n+1)^{1/2} \langle n+1 | 0 \rangle] / (2^{1/2} a D_A) \tag{4-42}$$

For the photoionization in (4-38),[1]

$$\delta = ((1.207398 - 1.1227)\text{Å}) \mu^{1/2} = 0.240\text{Å}(\text{a.m.u.})^{1/2} \tag{4-43}$$

Using the mass of the most abundant oxygen isotope to compute the reduced mass, we obtain

$$D_A = 1.79 \tag{4-44}$$

According to (4-40) and (4-41), we have

$$\langle 0|0\rangle = u(\mathrm{Int}(0\leftarrow 0))^{1/2}$$

$$\langle 1|0\rangle = u(\mathrm{Int}(1\leftarrow 0))^{1/2} \tag{4-45}$$

where u is a scaling factor.

Using vibronic intensities published by Gardner and Samson in (4-45) gives[15]

$$\langle 0|0\rangle = u(54.9)^{1/2} = 7.41u$$

$$\langle 1|0\rangle = u(100)^{1/2} = -10u \tag{4-46}$$

From the data of Gardner and Samson

$$\langle 2|0\rangle^2 = u^2(81.3) \tag{4-47}$$

Let us assume that the sign of $\langle 2|0\rangle$ is positive. Then, taking n = 1 in the recursion formula shown in (4-42) gives

$$\langle 1|0\rangle \overset{?}{\sim} -[2^{1/2}(2.19)(9.02) + (0.187)(7.41)]u/2.75 = -10.7u \tag{4-48}$$

whereas, if we take the negative sign for $\langle 2|0\rangle$ we obtain

$$\langle 1|0\rangle \overset{?}{\sim} 9.65u \tag{4-49}$$

The value calculated using the plus sign for $\langle 2|0\rangle$ is obviously much

closer to the value obtained in (4-46) for $\langle 1|0\rangle$. We therefore take

$$\langle 2|0\rangle = 9.02u \tag{4-50}$$

From the data of Gardner and Samson

$$\langle 3|0\rangle^2 = (31.5)u^2 \tag{4-51}$$

Assuming $\langle 3|0\rangle$ to be positive and taking n = 2 in the recursion formula gives

$$\langle 2|0\rangle \overset{?}{\sim} -6.78u \tag{4-52}$$

whereas, if we take $\langle 3|0\rangle$ negative we would obtain

$$\langle 2|0\rangle \overset{?}{\sim} 8.70u \tag{4-53}$$

Obviously, the second choice of sign for $\langle 3|0\rangle$ gives a value for $\langle 2|0\rangle$ which is closest to the accepted value in (4-50). The signs of the Franck-Condon amplitudes of the remaining observed transitions in the vibronic progression can be determined in an analogous manner. Using the above procedure, doubtful cases might arise if one or more transitions in a vibronic progression are very weak or missing altogether. It might appear that the process of assigning signs to the experimental Franck-Condon amplitudes is a very tedious one. However, for machine computations, the situation is not very worrysome. For this purpose, a so-called "self-consistent signs" (SCS) procedure was developed. The term "self-consistent" implies some iterative process. The initial signs of the experimental WFCOs are assigned such that they are the same as the signs of the expectation values corresponding to the

dominant term in the expansion of the transition moment

$$\mathcal{M}_{nm} = \mathrm{sgn}(\langle n|\mathcal{M}_j|m\rangle) \tag{4-54}$$

Of course this requires that we know in advance what the dominant term in the expansion of the transition moment function is. In most cases $\mathcal{M}_o = 1$ is the dominant term in the expansion. Even if $\mathcal{M}_o = 1$ is not included in the basis set, taking the signs of the experimental WFCOs the same as the signs of the computed overlap integrals has to be considered a suitable initial guess in many cases.

In the r-centroid approximation the signs of the experimental WFCOs are always taken the same as the overlap integrals. This can be seen from

$$C_o(\bar{r})^0 + C_1\bar{r} = C_o + C_1\frac{\langle v'|r|v''\rangle}{\langle v'|v''\rangle} \stackrel{?}{=} |\mathrm{Int}^{1/2}(v'\leftarrow v'')/\langle v'|v''\rangle| \tag{4-55}$$

where the quantity on the right-hand side of the above equation seems to be understood as being positive in all the publications that have been read by the present author. This is indicated by taking the absolute value on the right-hand side. However, it can be shown that this assumption is not necessarily correct. Let us assume a linear dependence of the transition moment on q. For simplicity, we take $v' = v'' = 0$ and $\alpha' = \alpha'' = 1$. Taking the transition moment as

$$M(q) = 1 - C_1 q \tag{4-56}$$

we obtain

$$\langle 0|0\rangle = \exp(-(1/4)\delta^2) \tag{4-57}$$

and

$$\langle 0|M|0\rangle = (1-(1/2)\delta C_1 - C_1)\langle 0|0\rangle \qquad (4\text{-}58)$$

Whereas the quantity in (4-57) is always positive, $\langle 0|M|0\rangle$ can be negative for large C_1 and δ. If one was to replace $\text{Int}^{1/2}$ by $\langle 0|M|0\rangle$ in (4-55) with M as shown in (4-56), the right-hand side would not necessarily be equal to the left-hand side in the resulting equation if the absolute sign is kept on the right-hand side. This means that with the conventions in current literature one will not necessarily be able to reproduce an analytic expression for M, even if it is of the same form as the model the analysis is based upon. This shortcoming is not inherent in the r-centroid approximation. The SCS iterations proposed here should take care of this problem. Even though the current sign conventions are mathematically incorrect, one finds in practice that for the small dependence of M on q the SCS iterations are terminated with the original assignment of signs, or the sign changes performed change the linear parameters of the model very little. At least this turned out to be the case for the first positive system of molecular nitrogen.

Although it is quite obvious what is meant by SCS iterations, let us have a closer look at the actual strategy implemented in the algorithm. With the initial assignment of signs made, a set of linear parameters is calculated according to the least squares scheme presented in (4-25). A comparison of signs between experimental and calculated WFCOs is made, i.e., the signs are brought in agreement according to

$$\mathcal{N}_{nm} = \text{sgn}(\langle n|\Sigma_k \mathcal{A}_k \mathcal{W}_k|m\rangle) \qquad (4\text{-}59)$$

If no signs have been switched in the above process, the calculation is considered "converged". Otherwise, a new set of linear parameters is being calculated using the updated WFCOs. This is done until all signs of the experimental WFCOs agree with the computed ones. Since we have no continuous measure of convergence in these iterations, it is conceivable that at the end of this process some signs keep on flipping indefinitely in an oscillatory manner. In this case, one would have to take the case with the "best" fit to the observed spectrum, based on some criteria for the goodness of the fit. In all the calculations done in the study of the first positive system of nitrogen, there was no indication of an oscillatory behaviour of the "rate of convergence".

If the transitions are allowed via Herzberg-Teller coupling, i.e.,

$$M(q) = \mathscr{N}_k \, \mathscr{M}_k(q) + \mathscr{N}_{k+1} \, \mathscr{M}_{k+1}(q) + \ldots, \; k>0 \qquad (4\text{-}60)$$

the initial assignment of signs, of course, is done taking $j = k > 0$ in (4-54). This will be a good starting point as long as the first term is dominant in the expansion in (4-60).

The assignment of signs is the only non-trivial task in this whole procedure. Once this problem is solved, one is dealing with a simple linear least squares problem.

In the present case, the harmonic oscillator approximation has been used and the chosen basis set for the transition moment is

$$\mathscr{M}_k(q) = q^k \exp(-(1/2)\alpha_o^2 q^2) \qquad (4\text{-}61)$$

A computer program has been written and tested extensively using

intensity measurements on the first positive system of N_2 by Turner and Nicholls.[51] This system ($B^3\Pi_g \rightarrow A^3\Sigma_u^+$) is an important component of the spectrum of the aurora.[52] These data were fitted using simply a polynomial for M, i.e., $\alpha_o = 0$

$$M(q) = \mathcal{M}_o + \mathcal{M}_1 q + \mathcal{M}_2 q^2 + \ldots\ldots \tag{4-62}$$

The necessary spectroscopic constants were taken from an earlier publication by Jarmain and Nicholls, which are the same as the ones given by Herzberg.[1,53] Notice that in these calculations the sign of δ is relevant. In our case,

$$D = \alpha''\delta = \alpha''\mu^{1/2}(r_e''-r_e') = +1.4 \tag{4-63}$$

The transition probabilities used were derived from data in Table II, p 476 and Table III, p 478, given by Turner and Nicholls.[51] Thirty-eight transitions could be treated in this manner. The computer output generated for a linear form of the transition moment function is shown in Table 4-1. A measure of the error of the calculated spectrum would be

$$SEE = \{\Sigma_n\Sigma_m W_{nm}(\langle n|M|m\rangle - \mathcal{M}_{nm}Int_{nm}^{1/2})^2/(\Sigma_n\Sigma_m W_{nm}-1)\}^{1/2} \tag{4-64}$$

This quantity is called "standard error of estimate" throughout this chapter. In the example presented in Table 4-1, all weighting factors have been set to 1.

In a one-dimensional least squares analysis, the "goodness" of the fit can often be visualized by graphing the differences between experimental and calculated data as a function of the variable. Based on

TABLE 4-1

THE TRANSITION MOMENT FUNCTION OF THE FIRST POSITIVE SYSTEM OF N_2 COMPUTED IN THE HARMONIC OSCILLATOR APPROXIMATION. I. FIXED POPULATION FACTORS

MOLECULAR NITROGEN : THE NORMAL MODE COORDINATE DEPENDENCE OF THE TRANSITION MOMENT OF THE FIRST POSITIVE SYSTEM.
BASED ON INTENSITIES MEASURED BY R.G. TURNER AND R.W. NICHOLLS, CAN.J.PHYS., 32(1954)PP.468-474, CAN.J.PHYS., 32(1954)PP.475-479.

ALPHA" = 6.5813205 ALPHA' = 7.1716637

ITERATION NO. 1. THE DIMENSIONLESS PARAMETER C = 1.40535
THE EXPONENTIAL FACTOR OF THE TRANSITION MOMENT : EXP(0.0 *Q*Q)
THE LINEAR COEFFICIENTS ARE :
IA(0) = 0.839723 IA(1) = -0.738834

STANDARD ERROR OF ESTIMATE = 0.09335

NO.	V'	V"	EXP. FRANCK-CONDON AMP.	CALC. FRANCK-CONDON AMP.	DIFFERENCE	WEIGHTING FACTOR
1	0	0	0.5830952	0.4482566	-0.1348386	1.0000000
2	0	1	-0.5302525	-0.5260009	0.0042516	1.0000000
3	0	2	0.4620433	0.4064518	-0.0555915	1.0000000
4	1	0	0.4160793	0.3976213	-0.0184580	1.0000000
5	1	2	-0.3369829	-0.3739395	-0.0369566	1.0000000
6	1	3	0.3870566	0.4871559	0.1000993	1.0000000
7	1	4	-0.4385668	-0.3716284	0.0669384	1.0000000
8	2	0	0.2517812	0.2731970	0.0214158	1.0000000
9	2	1	0.3499303	0.2335589	-0.1163713	1.0000000
10	2	2	-0.2252237	-0.2364238	-0.0112001	1.0000000
11	2	4	0.3209947	0.4534604	0.1324658	1.0000000
12	2	5	-0.3727130	-0.4570232	-0.0843101	1.0000000
13	3	0	0.1106854	0.1638864	0.0532011	1.0000000
14	3	1	0.3313753	0.2734389	-0.0579364	1.0000000
15	3	3	-0.3037448	-0.2843006	0.0194442	1.0000000
16	4	1	0.1552095	0.2167601	0.0615507	1.0000000
17	4	2	0.3056590	0.1944175	-0.1112414	1.0000000
18	4	4	-0.2608561	-0.2383366	0.0225194	1.0000000
19	5	1	0.0680271	0.1431497	0.0751226	1.0000000
20	5	2	0.2121732	0.2147879	0.0026147	1.0000000
21	5	3	0.2801058	0.0898701	-0.1902357	1.0000000
22	6	1	0.0225662	0.0843225	0.0617563	1.0000000
23	6	2	0.0961881	0.1717371	0.0755490	1.0000000
24	6	3	0.2539513	0.1752034	-0.0787478	1.0000000
25	6	5	-0.1877603	-0.2050349	-0.0172747	1.0000000

TABLE 4-1 (CONTINUED)

26	7	2	0.0339882	0.1158251	0.0818369	1.0000000
27	7	3	0.1206720	0.1750927	0.0544207	1.0000000
28	7	4	0.2593260	0.1148623	-0.1444637	1.0000000
29	7	6	-0.2150203	-0.1868505	0.0281698	1.0000000
30	8	3	0.3500432	0.1359767	0.0859336	1.0000000
31	8	4	0.1464555	0.1569120	0.0104565	1.0000000
32	8	5	0.2508277	0.0480875	-0.2027403	1.0000000
33	9	4	0.0581827	0.1428232	0.0846405	1.0000000
34	9	5	0.1631922	0.1231367	-0.0400554	1.0000000
35	9	6	-0.2302361	-0.0143382	0.2158979	1.0000000
36	10	5	0.0643690	0.1366599	0.0722909	1.0000000
37	10	6	0.1680777	0.0803723	-0.0877054	1.0000000
38	10	7	-0.1950603	-0.0652899	0.1297704	1.0000000

THE FINAL TRANSITION MOMENT : EXP(0.0 *Q*Q)
THE LINEAR COEFFICIENTS ARE :
0.839723*(Q**(0)) - 0.738834*(Q**(1))

R-CENTROID ANALYSIS OF RESIDUES :

(0.09762,	-0.23050)	(0.00657,	-0.00675)	(-0.09896,	-0.12485)	(0.20574,	-0.03192)	(0.00401,	0.08270)
(-0.09033,	0.18626)	(-0.21213,	-0.17948)	(0.29547,	0.04865)	(0.20618,	-0.34249)	(0.16002,	0.03418)
(-0.09664,	0.26400)	(-0.19928,	0.18207)	(0.37705,	0.18716)	(0.30390,	-0.13335)	(0.15892,	-0.04940)
(0.39572,	0.15752)	(0.30762,	-0.35043)	(0.15956,	-0.06820)	(0.45922,	0.26262)	(0.39343,	0.00668)
(0.29546,	-1.31542)	(0.52693,	0.32987)	(0.46765,	0.21741)	(0.39933,	-0.24482)	(0.27797,	0.05345)
(0.53540,	0.31382)	(0.47550,	0.15180)	(0.40048,	-0.68399)	(0.28076,	-0.09532)	(0.54359,	0.27687)
(0.48241,	0.03221)	(0.37744,	-2.36461)	(0.55142,	0.25620)	(0.48747,	-0.15600)	(0.57102,	-6.29160)

THE QUANTITIES ABOVE ARE (<V'|Q|V">/<V'|V">,DIFFERENCE/<V'|V">)

<V'|Q|V">

< 0|Q| 0> = 0.05701	< 0|Q| 1> = -0.00414	< 0|Q| 2> = -0.04406	< 1|Q| 0> = 0.11895	< 1|Q| 2> = -0.09179	
< 1|Q| 3> = -0.04854	< 1|Q| 4> = 0.07911	< 2|Q| 0> = 0.13050	< 2|Q| 1> = 0.07006	< 2|Q| 2> = -0.05244	
< 2|Q| 4> = -0.04347	< 2|Q| 5> = 0.09228	< 3|Q| 0> = 0.11012	< 3|Q| 1> = 0.13508	< 3|Q| 3> = -0.06255	
< 4|Q| 1> = 0.15071	< 4|Q| 2> = 0.09765	< 4|Q| 4> = -0.05269	< 5|Q| 1> = 0.13136	< 5|Q| 2> = 0.15391	
< 5|Q| 3> = 0.04273	< 6|Q| 1> = 0.09865	< 6|Q| 2> = 0.16251	< 6|Q| 3> = 0.12845	< 6|Q| 5> = -0.08985	
< 7|Q| 2> = 0.13962	< 7|Q| 3> = 0.17047	< 7|Q| 4> = 0.08458	< 7|Q| 6> = -0.08297	< 8|Q| 3> = 0.16872	
< 8|Q| 4> = 0.15662	< 8|Q| 5> = 0.03236	< 9|Q| 4> = 0.18217	< 9|Q| 5> = 0.12517	< 9|Q| 6> = -0.01959	
<10|Q| 5> = 0.17865	<10|Q| 6> = 0.08178	<10|Q| 7> = -0.06464			

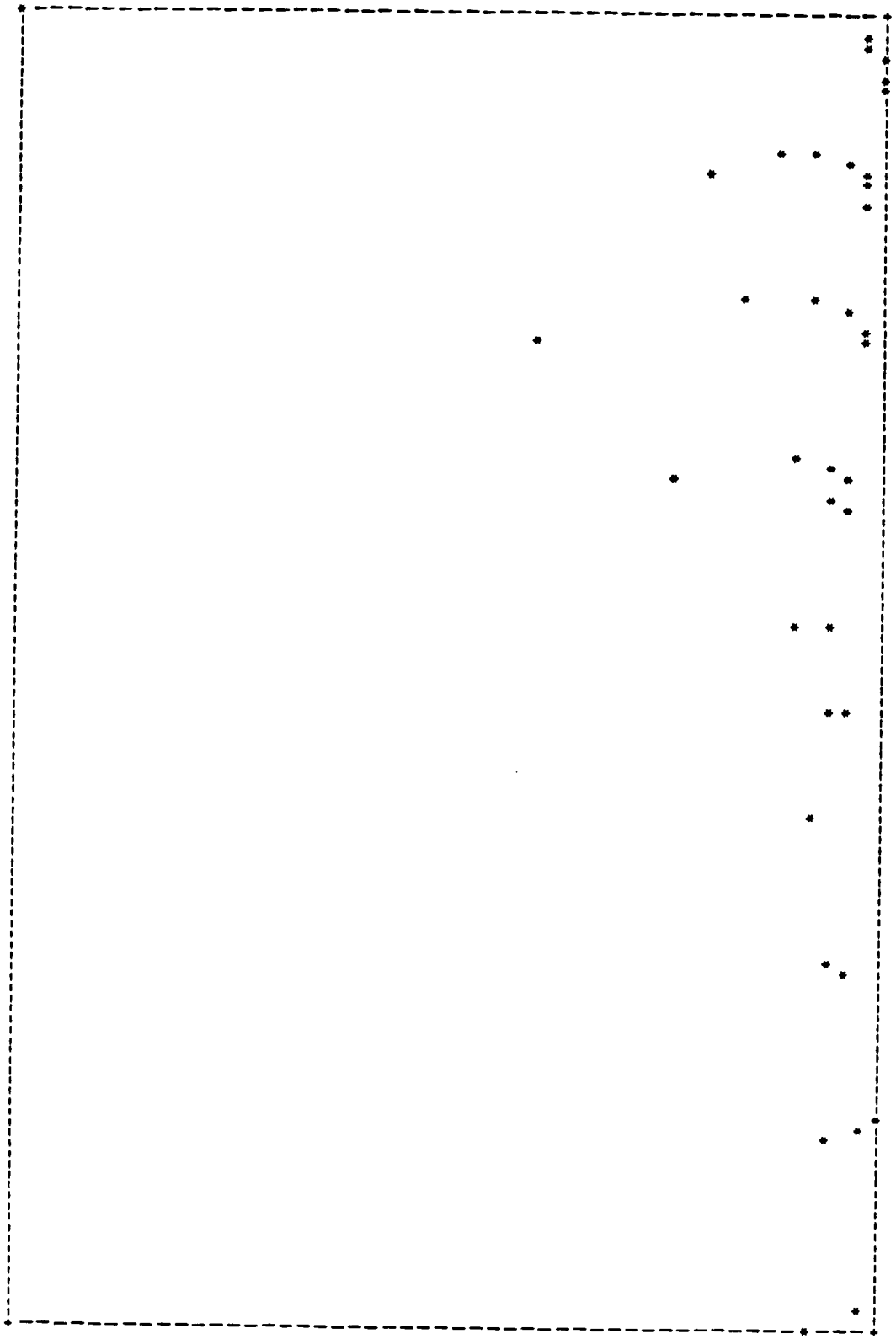


Fig. 4-3. Plot of residues.

patterns in this graph one can determine to a certain extent if the information contained in the given data base has been fully extracted by the model. Within the r-centroid approximation we are dealing with a one-dimensional least squares fit. For this reason, the r-centroid approximation is being invoked for the analysis of residues. Of course, we will again encounter near-breakdowns of the r-centroid approximation which might be misleading. In the case of the residue analysis, this is not a very serious problem, because this whole business is merely of qualitative nature anyway. The graph in Figure 4-3 consists of $[\nu_{nm} Int_{nm}^{1/2} - \langle n|M|m\rangle]/\langle n|m\rangle$ graphed vs. $\langle q\rangle/\langle 1\rangle$. The FORTRAN program which has been written to do these calculations is listed in Appendix 6, together with input instructions. This program is capable of computing the required expectation values in the harmonic oscillator approximation only. However, it can be operated in a manner in which the expectation values are entered via some input device. Because of this feature, the program can operate within any kind of approximation for the vibrational wavefunction as long as the necessary expectation values can be supplied. Later, the algorithm will be applied to the first positive system of N_2, using the Morse oscillator as a model. In this connection, the criticism voiced here regarding the approximation (4-14) by Jarmain and Nicholls will be justified on a quantitative basis.

Turner and Nicholls included 38 transitions in their calculations. With the harmonic model, two of these transitions gave rise to disproportionately large discrepancies between calculated and experimental intensities. For this reason, the two transitions

$$\begin{array}{c} v' \rightarrow v'' \\ 8 \rightarrow 5 \\ 9 \rightarrow 6 \end{array} \qquad (4\text{-}65)$$

were eliminated from the data set. The computer output contains a calculation with all of the 38 transitions still included.

With the 36 remaining transitions the following transition moments have been calculated:

K	M	SEE	
0	0.696	0.105	
1	$0.839-0.762q$	0.082	
2	$0.877-0.175q-1.653q^2$	0.077	
3	$0.951-0.251q-4.664q^2 + 5.677q^3$	0.074	
4	$0.950-0.221q-4.640q^2 + 5.131q^3 + 0.719q^4$	0.073	
5	$0.987 + 0.191q-8.832q^2 + 1.437q^3 + 47.674q^4-51.184q^5$	0.071	(4-66)

The SEE does not significantly decrease by including quadratic and higher terms in the expansion. This leads us to conclude that the linear dependence of the transition moment is adequate for the given data

$$M(q) \sim 0.839-0.762q \qquad (4\text{-}67)$$

Turner and Nicholls find the following expression:

$$M(\bar{q}) \sim 0.95 \exp(-1.14\bar{q}) \qquad (4\text{-}68)$$

In Figure 4-4, the various approximations for the transition moment function given in (4-66) have been plotted. The curves are

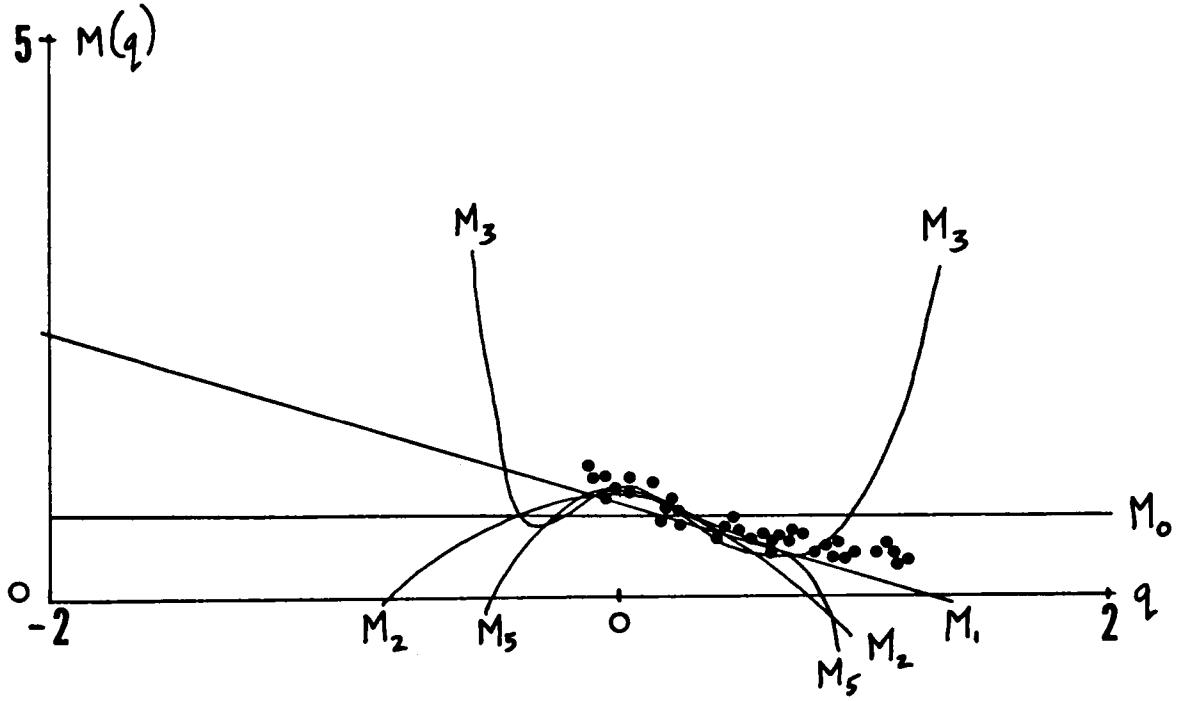


Fig. 4-4. The transition moment function of the first positive system of N_2. I. The transition moment function computed in the harmonic oscillator approximation with fixed population factors.

labelled using K as a subscript of M. Since M_4 practically coincides with M_3, it was omitted from this graph. On the same graph, the data in the r-centroid approximation published by Turner and Nicholls are indicated as points. These data reach to considerably larger q than would be suggested by the range where the analytical curves M_1, M_2, ... M_5 nearly coincide. This is probably due to the harmonic approximation used here, which does not take into account the asymmetry of the potential energy curve of diatomic molecules.

Yeager and McKoy computed the transition moment of the first positive system of N_2 quantum mechanically in the higher random phase approximation as[54]

$$M(q) \propto 1-0.370q + 0.057q^2 \tag{4-69}$$

and in the Tamm-Dancoff approximation[54]

$$M(q) \propto 1-0.402q-0.029q^2 \tag{4-70}$$

Francke et al. gave the $M(\bar{q})$ curve as[41]

$$M(\bar{q}) \propto 1-1.000\bar{q} + 0.408(\bar{q})^2 \tag{4-71}$$

which is in reasonable agreement with the M(q) function computed in this work.

In measured intensities the population factors $N_{v'}$ are included. Turner and Nicholls extracted the relative populations by matching $M(\bar{q})$ curve segments from the various vibronic progressions. Cunio and Jansson included the population factors in a least squares scheme using the r-centroid approximation.[55] One can include the population factors

equally well in our least squares scheme. Let us denote the experimentally observed intensities with $Bi_{v',v''}$ as follows:

$$Bi_{v',v''} = (\text{const.})\ 10^{2}_{v',v''}\ N_{v'}\ \text{Int}(v' \rightarrow v'') \tag{4-72}$$

The sum of squared error terms is then

$$\delta_{LS} = \Sigma_{v'}\Sigma_{v''} W_{v',v''} (Gs_{v'}\ Bi^{1/2}_{v',v''} - \Sigma_{k}\ \mathcal{R}_{k} \langle v' | \mathcal{M}_{k} | v'' \rangle)^{2} \tag{4-73}$$

where, according to (4-72),

$$Gs_{v'} \propto N_{v'}^{-1/2} \tag{4-74}$$

The conditions that δ_{LS} be a minimum are

$$\frac{\partial \delta_{LS}}{\partial \mathcal{R}_{o}} = \ldots\ldots\ldots = \frac{\partial \delta_{LS}}{\partial \mathcal{R}_{K}} = 0 \tag{4-75}$$

and

$$\frac{\partial \delta_{LS}}{\partial Gs_{v'_{o}}} = \ldots\ldots\ldots = \frac{\partial \delta_{LS}}{\partial Gs_{v'_{J}}} = 0 \tag{4-76}$$

where J + 1 is the number of vibronic progessions in the observed spectrum and K + 1 is the number of terms in the expansion of the transition moment function.

(4-75) and (4-76) give $\delta_{LS} = 0$, i.e.

δ_{LS} is a minimum if all linear coefficients in (4-73) are zero. To find a non-trivial solution, one has to introduce a constraint in the minimization. The most natural constraint is one of having a spectrum of some fixed total intensity, i.e.,

$$\Sigma_{v'}\Sigma_{v''} Gs^{2}_{v'} Bi_{v',v''} = I_{tot} = \text{const.} \tag{4-77}$$

This constraint, however, would give rise to a nasty nonlinear problem, which would be solved most readily by some non-linear optimization technique. (4-75) and (4-76) define a homogeneous linear system

$$\begin{pmatrix} Sn_{00} & \cdots & Sn_{0K} & Su_{00} & \cdots & Su_{0J} \\ \vdots & & \vdots & \vdots & & \vdots \\ Sn_{K0} & \cdots & Sn_{KK} & Su_{K0} & \cdots & Su_{KJ} \\ Su_{00} & \cdots & Su_{K0} & Se_0 & & 0 \\ \vdots & & \vdots & & \ddots & \\ Su_{0J} & \cdots & Su_{KJ} & 0 & & Se_J \end{pmatrix} \begin{pmatrix} \mathcal{H}_0 \\ \vdots \\ \mathcal{H}_K \\ Gs_{v'_0} \\ \vdots \\ Gs_{v'_J} \end{pmatrix} = \begin{pmatrix} 0 \\ \vdots \\ 0 \end{pmatrix} \tag{4-78}$$

where Sn has been defined previously and

$$Su_{kv'_j} = -\Sigma_{v''} W_{v'_j v''} \langle v'_j | \mathcal{H}_k | v'' \rangle Bi^{1/2}_{v'_j v''} \tag{4-79}$$

$$Se_{v'_j} = \Sigma_{v''} W_{v'_j v''} Bi_{v'_j v''} \tag{4-80}$$

The Ws are again weighting factors. Cunio and Jansson introduced the constraint $Gs_{v'_o} = 1$, and eliminated the equation in (4-78) corresponding to the condition

$$\frac{\partial \delta_{LS}}{\partial Gs_{v'_o}} = 0 \tag{4-81}$$

such that (4-78) becomes a non-homogeneous system of K + J + 1 equations and the same number of unknowns. However, one can single out any of the vibronic progressions in making it the dependent variable in the above manner. The corresponding linear systems and their solutions will depend on this choice. The computer program was designed to handle any constraint $Gs_{v'_j} = 1$ or $\mathcal{H}_k = 1$. In the calculations

with the population factors included, the raw data published by Turner and Nicholls, i.e., the experimental transition probabilities, were used. Initially Turner and Nicholls had measured the intensities of 52 transitions. From these, they eliminated 14 because of erratic behavior of these data, probably due to near-breakdowns of the r-centroid approximation. In the present study all 52 transitions were included in the calculation.

In these calculations, the SEE is no longer an appropriate measure of the fit between calculated and experimental spectra. The quantity introduced to express the quality of the fit was

$$RE = \{\Sigma_n \Sigma_m W_{nm}(\langle n|M|m\rangle - Gs_n\, 10_{nm} Int_{nm}^{1/2})^2 / \Sigma_n \Sigma_m Gs_n^2 Int_{nm}\}^{1/2} (100\%) \quad (4\text{-}82)$$

which is called the "relative error" in this text. In the limit where the model fits the experimental data exactly, the choice of the dependent variable is irrelevant. By making comparison between solutions computed for two or more distinct dependent variables, one can obtain a qualitative idea about the "goodness" of the fit. For example, in linear regressions we can denote any one of the two variables as the dependent variable, i.e.,

$$y = a_x + b_x x \quad (4\text{-}83)$$

or

$$x = a_y + b_y y \quad (4\text{-}84)$$

The correlation coefficient

$$r_{xy} = (b_x b_y)^{1/2} \quad (4\text{-}85)$$

in this case often serves as a measure of the agreement of the data with a linear model.[56] If Gs of the first vibronic progression with v' = 0 is taken unity, one obtains

K	M(q)	I_{tot}	RE(%)
0	0.77	4.68	52.6
1	1.18-1.67q	6.18	34.1
2	$1.34-0.40q-4.07q^2$	6.40	27.8
3	$1.45-0.96q-9.71q^2 + 12.21q^3$	5.78	26.5

(4-86)

Judging from the decrease in the relative error with increasing K, a quadratic form of M(q) seems appropriate.

Let us take Gs of the vibronic progression with v'=1 as the dependent variable. This gives

K	M(q)	I_{tot}	RE(%)
0	1.63	21.14	52.7
1	1.67-2.41q	12.32	33.9
2	$1.68-0.77q-4.45q^2$	10.20	28.0
3	$1.72-1.24q-9.31q^2 + 11.10q^3$	8.81	26.6

(4-87)

and taking Gs of the vibronic progression with v'=2 as the dependent variable, we obtain

K	M(q)	I_{tot}	RE(%)
0	1.63	21.32	53.3
1	1.67-2.35q	12.43	34.5
2	$1.68-0.81q-4.25q^2$	10.32	28.6
3	$1.70-1.00q-6.58q^2 + 5.13q^3$	9.57	27.7

(4-88)

Finally, using the constraint $\mathscr{H}_o = 1$ gives

K	M(q)	I_{tot}	RE(%)
0	1.63	12.51	46.9
1	1.67-2.40q	9.89	32.1
2	$1.68-0.50q-5.19q^2$	8.61	26.8
3	$1.74-1.19q-12.28q^2 + 16.01q^3$	7.10	26.2

(4-89)

where I_{tot} is the total intensity of the spectrum calculated from the computed Gs' and the experimental transition probabilities. The above expressions refer to the situation where the linear coefficients have been "normalized" by scaling them such that $Gs_o = 1$ was obtained. Perhaps a normalization such that the total intensity becomes unity would be more appropriate. This can be achieved by multiplying M(q) through by $I_{tot}^{-1/2}$.

The relative error and the disagreement between solutions for different dependent variables can be decreased by the following procedure:

(i) Take the computed linear coefficients and use them in the equation which was dropped from the homogeneous linear system in (4-78), i.e., revoke the assumption that the chosen linear parameter is fixed.

(ii) Introduce the computed linear parameter in the solution instead of taking it unity as originally assumed.

This concept was realized in the computer program only for the cases where the intensities of an arbitrarily chosen vibronic progression are taken as the dependent variable, i.e., cases where the constraint $Gs_{v'_j} = 1$ had been in effect originally. Then

$$Gs_{v'_j} = (-Se_j^{-1})(Su_{oj} \ldots\ldots\ldots Su_{Kj}) \begin{pmatrix} \mathscr{R}_o \\ \vdots \\ \mathscr{R}_K \end{pmatrix} \qquad (4\text{-}90)$$

If the intensities of a vibronic progression constitute the dependent variable, and the "correction" in (4-90) is not made, a disproporionate amount of error is concentrated in the corresponding vibronic progression. Let us look at the distribution of sums of error terms among the vibronic progressions using the quadratic approximation for M, i.e., $M(q) = \mathscr{R}_o + \mathscr{R}_1 q + \mathscr{R}_2 q^2$:

v'	0	1	2	3	4	5	6	7	8	9	10	11	12
$Gs_o=1$	24	10	17	25	4	4	10	4	0	0	1	1	1
$Gs_1=1$	4	31	17	26	4	4	10	4	0	0	0	1	0
$Gs_2=1$	4	8	42	25	4	4	9	3	0	0	0	1	0

(4-91)

where the quantities in (4-91) are expressed in percent

$$\% \text{ error} = (100\%)\Big(\sum_{v'=v'_j} W_{v'v''}(Gs_{v'}\, 10_{v'v''}\, Int^{1/2}_{v'v''} - \langle v'|M|v''\rangle)^2\Big)/(\Sigma_{v'}\Sigma_{v''}W_{v'v''}Gs^2_{v'}\, Int_{v'v''}) \qquad (4\text{-}92)$$

If the correction in (4-90) is being used, the error is distributed among the vibronic progressions a bit more evenly. Again, referring to the quadratic approximation for M,

v'	0	1	2	3	4	5	6	7	8	9	10	11	12
Gs_o=1	5	12	21	31	5	5	13	5	0	0	1	1	1
Gs_1=1	5	11	22	33	5	5	12	5	0	0	0	1	0
Gs_2=1	5	11	22	33	5	5	12	5	1	0	0	1	0

(4-93)

Notice that the distribution of the error becomes essentially the same for any choice of the dependent variable if (4-90) is being used. In this case, the remaining discrepancies are probably due almost exclusively to the harmonic approximation. This conclusion is based on the rationale that discrepancies due to different choices of the dependent variable are due to the model used here, and residual errors in the case of agreement are inherent in the approximations made, mostly in respect to the vibrational wave functions.

Only the scaling factors for the transition moments may change by applying the correction in (4-90). For this reason, only the total intensities of the spectra and the relative errors for the computations, with (4-90) included, are being supplied. (See Table 4-2). It is believed that including (4-90) enhances considerably the reliability of the relative population factors extracted from the observed spectrum.

TABLE 4-2

THE TRANSITION MOMENT FUNCTION OF THE FIRST POSITIVE SYSTEM OF N_2 COMPUTED IN THE HARMONIC OSCILLATOR APPROXIMATION. II. VARIABLE POPULATION FACTORS

MOLECULAR NITROGEN : THE NORMAL MODE COORDINATE DEPENDENCE OF THE TRANSITION MOMENT OF THE FIRST POSITIVE SYSTEM.
BASED ON INTENSITIES MEASURED BY R.G. TURNER AND R.W. NICHOLLS, CAN.J.PHYS., 32(1954)PP.468-474, CAN.J.PHYS., 32(1954)PP.475-479.

ALPHA" = 6.5813205 ALPHA' = 7.1716637

THE INITIAL SIGNS OF THE EXPERIMENTAL FRANCK-CONDON AMPLITUDES WERE TAKEN SUCH THAT SGN(<V'|M(Q)|V">) = SGN(<V'|Q**(0)|V">).

NO.	NO. OF ENERGY LEVEL	V'	V"	FRANCK-CONDON FACTOR	WEIGHTING FACTOR
1	1	0	0	1.00000000	1.00000000
2	1	0	1	0.82800000	1.00000000
3	1	0	2	0.62500000	1.00000000
4	2	1	0	0.66300000	1.00000000
5	2	1	2	0.43400000	1.00000000
6	2	1	3	0.57000000	1.00000000
7	2	1	4	0.73600000	1.00000000
8	3	2	0	0.21600000	1.00000000
9	3	2	1	0.41900000	1.00000000
10	3	2	2	0.17300000	1.00000000
11	3	2	3	0.15000000	1.00000000
12	3	2	4	0.35100000	1.00000000
13	3	2	5	0.47700000	1.00000000
14	4	3	0	0.02640000	1.00000000
15	4	3	1	0.23500000	1.00000000
16	4	3	2	0.13700000	1.00000000
17	4	3	3	0.19700000	1.00000000
18	4	3	4	0.13300000	1.00000000
19	4	3	5	0.22700000	1.00000000
20	4	3	6	0.47900000	1.00000000
21	5	4	1	0.05940000	1.00000000
22	5	4	2	0.23100000	1.00000000
23	5	4	3	0.03890000	1.00000000
24	5	4	4	0.16700000	1.00000000
25	6	5	1	0.00869000	1.00000000
26	6	5	2	0.08520000	1.00000000
27	6	5	3	0.14700000	1.00000000

TABLE 4-2 (CONTINUED)

28	6	5	5	0.10800000	1.00000000
29	7	6	1	0.00105000	1.00000000
30	7	6	2	0.01260000	1.00000000
31	7	6	3	0.08850000	1.00000000
32	7	6	4	0.08490000	1.00000000
33	7	6	5	0.04660000	1.00000000
34	8	7	2	0.00135000	1.00000000
35	8	7	3	0.01700000	1.00000000
36	8	7	4	0.07780000	1.00000000
37	8	7	5	0.03560000	1.00000000
38	8	7	6	0.05370000	1.00000000
39	9	8	3	0.00230000	1.00000000
40	9	8	4	0.02050000	1.00000000
41	9	8	5	0.06000000	1.00000000
42	10	9	4	0.00299000	1.00000000
43	10	9	5	0.02240000	1.00000000
44	10	9	6	0.04480000	1.00000000
45	11	10	5	0.00305000	1.00000000
46	11	10	6	0.02090000	1.00000000
47	11	10	7	0.02840000	1.00000000
48	12	11	6	0.00330000	1.00000000
49	12	11	7	0.02020000	1.00000000
50	12	11	8	0.01680000	1.00000000
51	13	12	7	0.00370000	1.00000000
52	13	12	8	0.01580000	1.00000000

```
  1 GAUSS-SEIDEL ITERATION

THE INTENSITIES OF THE VIBRONIC PROGRESSION NO. 3 CONSTITUTE THE DEPENDENT VARIABLE


ITERATION NO.  1 :     THE DIMENSIONLESS PARAMETER OF DISPLACEMENT  D = ALPHA**DELTA =  1.40535
THE EXPONENTIAL FACTOR OF THE TRANSITION MOMENT  :     EXP(  0.0  *Q*Q)
THE LINEAR COEFFICIENTS ARE  :
IA( 0) =    1.674144        IA( 1) =   -0.859798        IA( 2) =   -3.985387

THE SIGNS OF THE FOLLOWING FRANCK-CONDON AMPLITUDES HAVE BEEN CHANGED  :
 45  48  49  51
STANDARD ERROR OF ESTIMATE =     0.11263

  1 GAUSS-SEIDEL ITERATION

THE INTENSITIES OF THE VIBRONIC PROGRESSION NO. 3 CONSTITUTE THE DEPENDENT VARIABLE


ITERATION NO.  2 :     THE DIMENSIONLESS PARAMETER OF DISPLACEMENT  D = ALPHA**DELTA =  1.40535
THE EXPONENTIAL FACTOR OF THE TRANSITION MOMENT  :     EXP(  0.0  *Q*Q)
```

TABLE 4-2 (CONTINUED)

THE LINEAR COEFFICIENTS ARE :
IA(0) = 1.675249 IA(1) = -0.813268 IA(2) = -4.207924

THE SIGNS OF THE FOLLOWING FRANCK-CONDON AMPLITUDES HAVE BEEN CHANGED :
42
STANDARD ERROR OF ESTIMATE = 0.11151

1 GAUSS-SEIDEL ITERATION

THE INTENSITIES OF THE VIBRONIC PROGRESSION NO. 3 CONSTITUTE THE DEPENDENT VARIABLE

ITERATION NO. 3 : THE DIMENSIONLESS PARAMETER OF DISPLACEMENT D = ALPHA**DELTA = 1.40535
THE EXPONENTIAL FACTOR OF THE TRANSITION MOMENT : EXP(0.0 *Q*Q)
THE LINEAR COEFFICIENTS ARE :
IA(0) = 1.675500 IA(1) = -0.808421 IA(2) = -4.247005

STANDARD ERROR OF ESTIMATE = 0.11135

NO.	V'	V''	EXP. FRANCK-CONDON AMP.	CALC. FRANCK-CONDON AMP.	DIFFERENCE	WEIGHTING FACTOR
1	0	0	1.0000000	0.8825492	-0.1174508	1.0000000
2	0	1	-0.9099451	-1.0461108	-0.1361657	1.0000000
3	0	2	0.7905694	0.7824076	-0.0081618	1.0000000
4	1	0	0.7904451	0.7714199	-0.0190252	1.0000000
5	1	2	-0.6395284	-0.6978095	-0.0582811	1.0000000
6	1	3	0.7329129	0.9129418	0.1800289	1.0000000
7	1	4	-0.8328252	-0.6476968	0.1851284	1.0000000
8	2	0	0.4753580	0.4816794	0.0063214	1.0000000
9	2	1	0.6620654	0.4234220	-0.2386434	1.0000000
10	2	2	-0.4254191	-0.5104020	-0.0849830	1.0000000
11	2	3	-0.3961316	-0.2390764	0.1570552	1.0000000
12	2	4	0.6059649	0.8140717	0.2081068	1.0000000
13	2	5	-0.7064039	-0.7841900	-0.0777861	1.0000000
14	3	0	0.1632306	0.2388150	0.0755844	1.0000000
15	3	1	0.4870052	0.4584924	-0.0285127	1.0000000
16	3	2	0.3718433	0.0477714	-0.3240719	1.0000000
17	3	3	-0.4458952	-0.5762093	-0.1303142	1.0000000
18	3	4	0.3663747	0.1427268	-0.2236479	1.0000000
19	3	5	0.4786439	0.5941033	0.1154594	1.0000000
20	3	6	-0.6952923	-0.8256269	-0.1303346	1.0000000
21	4	1	0.2192574	0.2967199	0.0774625	1.0000000
22	4	2	0.4323814	0.3032620	-0.1291194	1.0000000
23	4	3	-0.1774336	-0.2163002	-0.0388666	1.0000000
24	4	4	-0.3676371	-0.4545390	-0.0869020	1.0000000
25	5	1	0.0590504	0.1307802	0.0717298	1.0000000

TABLE 4-2 (CONTINUED)

26	5	2	0.1848983	0.2729163	0.0880180	1.0000000
27	5	3	0.2428688	0.1188377	-0.1240310	1.0000000
28	5	5	-0.2081732	-0.2543522	-0.0461790	1.0000000
29	6	1	0.0233660	0.0250934	0.0017274	1.0000000
30	6	2	0.0809423	0.1383092	0.0573669	1.0000000
31	6	3	0.2145170	0.2024141	-0.0121029	1.0000000
32	6	4	-0.2101087	-0.0408047	0.1693040	1.0000000
33	6	5	-0.1556622	-0.3707737	-0.2151116	1.0000000
34	7	2	0.0297681	0.0195579	-0.0102102	1.0000000
35	7	3	0.1056352	0.1207220	0.0150868	1.0000000
36	7	4	0.2259821	0.1148560	-0.1111261	1.0000000
37	7	5	-0.1528654	-0.1518375	0.0010279	1.0000000
38	7	6	-0.1877463	-0.3154712	-0.1277250	1.0000000
39	8	3	0.0119657	0.0046476	-0.0073182	1.0000000
40	8	4	0.0357234	0.0883298	0.0526064	1.0000000
41	8	5	0.0611154	0.0317986	-0.0293168	1.0000000
42	9	4	-0.0122128	-0.0153174	-0.0031046	1.0000000
43	9	5	0.0334275	0.0515406	0.0181131	1.0000000
44	9	6	-0.0472737	-0.0336638	0.0136099	1.0000000
45	10	5	-0.0183833	-0.0350858	-0.0167025	1.0000000
46	10	6	0.0481224	0.0187866	-0.0293357	1.0000000
47	10	7	-0.0560961	-0.0757883	-0.0196922	1.0000000
48	11	6	-0.0224166	-0.0497535	-0.0273369	1.0000000
49	11	7	-0.0554612	-0.0044093	0.0510519	1.0000000
50	11	8	-0.0505788	-0.0944430	-0.0438643	1.0000000
51	12	7	-0.0166599	-0.0556327	-0.0389728	1.0000000
52	12	8	-0.0344270	-0.0155674	0.0188597	1.0000000

IN THE ABOVE TABLE THE "EXPERIMENTAL" FRANCK-CONDON AMPLITUDES ARE THE EXPERIMENTAL TRANSITION PROBABILITIES DIVIDED BY THE CALCULATED RELATIVE POPULATION FACTORS

DISTRIBUTION OF THE SUMS OF ERROR TERMS AMONG THE VIBRONIC PROGRESSIONS

NO.	1	2	3	4	5	6	7	8	9	10	11	12	13
%	5	11	22	33	5	5	12	5	1	0	0	1	0

DISTRIBUTION OF INTENSITIES AMONG THE VIBRONIC PROGRESSIONS (USING THE CALCULATED POPULATION FACTORS)

NO.	1	2	3	4	5	6	7	8	9	10	11	12	13
%	28	26	21	16	5	2	1	1	0	0	0	0	0

TABLE 4-2 (CONTINUED)

TOTAL INTENSITY OF THE SPECTRUM : 8.840566
RELATIVE ERROR : 26.7447 %

THE FINAL TRANSITION MOMENT : EXP(0.0 *Q*Q)
THE LINEAR COEFFICIENTS ARE :
1.000000*(Q**(0)) - 0.482495*(Q**(1)) - 2.534769*(Q**(2))

RELATIVE POPULATION OF THE ENERGY LEVELS :

NO. 1	1.00000	NO. 2	1.06113	NO. 3	0.95590	NO. 4	0.99083
NO. 5	1.23560	NO. 6	2.49215	NO. 7	1.92318	NO. 8	1.52346
NO. 9	16.06384	NO. 10	20.04653	NO. 11	9.02511	NO. 12	6.56708
NO. 13	13.33084						

R-CENTROID ANALYSIS OF RESIDUES :

(0.09762, -0.20112)	(0.00657, 0.21612)	(-0.09896, -0.01833)	(0.20574, -0.03291)	(0.00401, 0.13042)
(-0.09033, 0.33498)	(-0.21213, -0.49639)	(0.29647, 0.01436)	(0.20618, -0.70235)	(0.16002, 0.25934)
(-0.04214, -0.85729)	(-0.08664, 0.41475)	(-0.19928, 0.16798)	(0.37705, 0.25880)	(0.30390, -0.06415)
(0.11478, -5.60427)	(0.15892, 0.33108)	(0.41189, -4.47640)	(-0.09278, 0.29357)	(-0.18922, 0.25893)
(0.38572, 0.19825)	(0.30762, -0.40675)	(0.28844, 0.24514)	(0.15956, 0.26319)	(0.45922, 0.25076)
(0.39343, 0.22499)	(0.29546, -0.85764)	(0.14983, 0.22727)	(0.52693, 0.00923)	(0.46765, 0.16508)
(0.39933, -0.03763)	(0.58727, -7.41452)	(0.27797, 0.66552)	(0.53540, -0.03915)	(0.47550, 0.04208)
(0.40048, -0.52615)	(0.38647, -0.00658)	(0.28076, 0.43221)	(0.54359, -0.02358)	(0.48241, 0.16203)
(0.37744, -0.34193)	(0.55142, -0.00940)	(0.48747, 0.07054)	(0.57102, -0.39661)	(0.55873, -0.05218)
(0.48774, -0.17497)	(0.48017, 0.14627)	(0.56518, -0.09667)	(0.46415, 0.72806)	(0.47564, 0.21221)
(0.57000, -0.17384)	(0.68144, -0.76685)			

THE QUANTITIES ABOVE ARE (<V'|Q|V">/<V'|V">,DIFFERENCE/<V'|V">)

The relative population factors of Turner and Nicholls have been extracted from their data and are shown in Table 4-3.

If only one term is included in the expansion of the transition moment, including (4-90) makes the approximation independent of the choice of the dependent variable. This is based on observations made with the present computations. A mathematical explanation for this effect could not be found. According to (4-86)-(4-89), the "best" fit should be obtained taking K = 2 and the constraint $Gs_1 = 1$ or $Gs_2 = 1$. In the computation shown in Table 4-2, the latter constraint was used, together with (4-90). The relative population factors computed there are presented in Table 4-3, together with the ones found by Turner and Nicholls. These data seem to indicate that the harmonic oscillator approximation loses its validity beyond $v', v'' \geq 4$. In Figure 4-5, the transition moment functions for various approximations

$$M_k(q) = \mathcal{M}_o + \mathcal{M}_1 q + ... + \mathcal{M}_k q^k \qquad (4\text{-}94)$$

have been graphed. The transition moment functions M_K have been scaled there such that in all cases the total intensity of the spectrum is the same. The graphed transition moment functions had been computed using the constraint $Gs_2 = 1$ and making use of (4-90).

The transition moment functions computed within the harmonic oscillator approximation reproduces correctly the general shape of the transition moment functions computed by other investigators. The present work seems to indicate that the computed transition moment functions are rather sensitive to the approximations made for the wave functions.

TABLE 4-3

RELATIVE POPULATION FACTORS IN THE FIRST POSITIVE SYSTEM OF N_2

(a) Obtained in the present work from experimental oscillator strengths reported by Turner and Nicholls,[51] using the harmonic oscillator model.

(b) The same as in (a), but using the Morse oscillator model. (See Chapter 5!)

(c) Obtained from data reported by Turner and Nicholls.[51] (They used the Morse oscillator model and the r-centroid approximation.)

v'	a	b	c
0	1	1	1
1	1.06	1.09	1.30
2	0.96	1.28	1.16
3	0.99	1.59	0.73
4	1.24	1.17	0.84
5	2.49	1.21	0.64
6	1.92	0.90	0.70
7	1.52	0.75	0.40
8	16.06	0.63	0.31
9	20.05	0.53	0.30
10	9.03	0.40	0.25
11	6.57	0.31	
12	13.33	0.18	

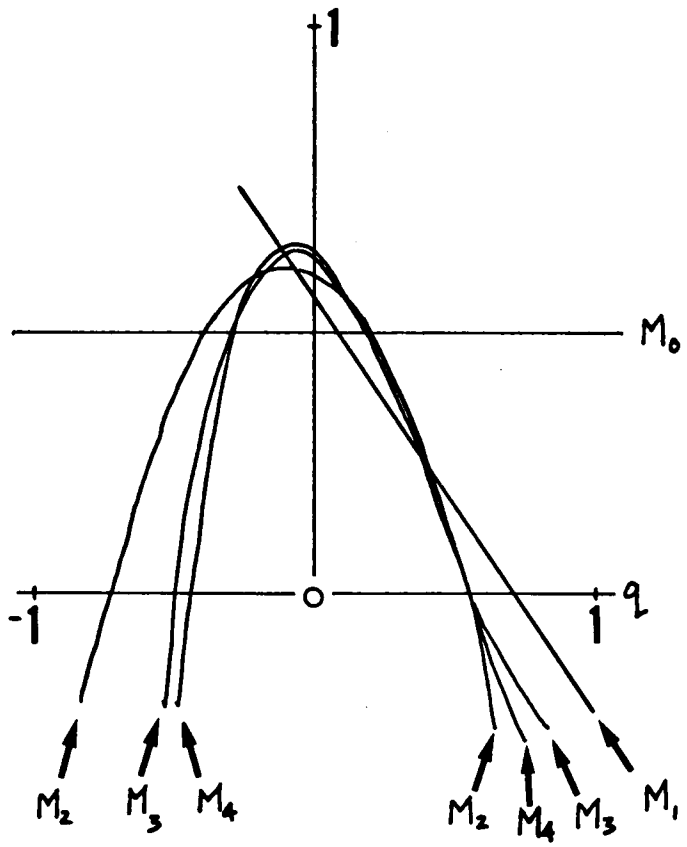


Fig. 4-5. The transition moment function of the first positive system of N_2. II. The transition moment function computed in the harmonic oscillator approximation with variable population factors.

Within the r-centroid formalism we have the possibility of an improvement, if the r-centroids from a superior approximation are known. In Figure 4-6 (p 67), the expectation values $\langle v'|q|v''\rangle/\langle v'|v''\rangle$ in the harmonic oscillator approximation have been plotted against the ones in the Morse oscillator approximation for the 38 transitions treated by Turner and Nicholls. We can express $\bar{q}_{harm}$ in terms of $\bar{q}_{Morse}$:

$$\bar{q}_{harm} = f(\bar{q}_{Morse}) \tag{4-95}$$

Let us assume that a "distorted" normal mode coordinate is all that's wrong with M(q) found in the harmonic approximation. Let us furthermore assume that the Morse oscillator approximation is pretty close to the "truth", i.e.,

$$\bar{q}_{actual} \sim \bar{q}_{Morse} \tag{4-96}$$

We can take

$$M(q) \sim M(\bar{q}_{actual}) \sim \tilde{M}(f(\bar{q}_{Morse})) \tag{4-97}$$

where $\tilde{M}$ is the expression of the transition moment in the harmonic oscillator approximation.

This Janus-faced attempt of reintroducing the r-centroid approximation after it has been abandoned is not very satisfactory. The $\bar{q}_{Morse}$ needed to prepare Figure 4-6 (p 67) were taken from the data of Turner and Nicholls, who based their treatment on the Morse oscillator approximation. The formula used was

$$\bar{q}_{Morse} = \mu^{1/2}(\bar{r}_{Morse} - r_e') \tag{4-98}$$

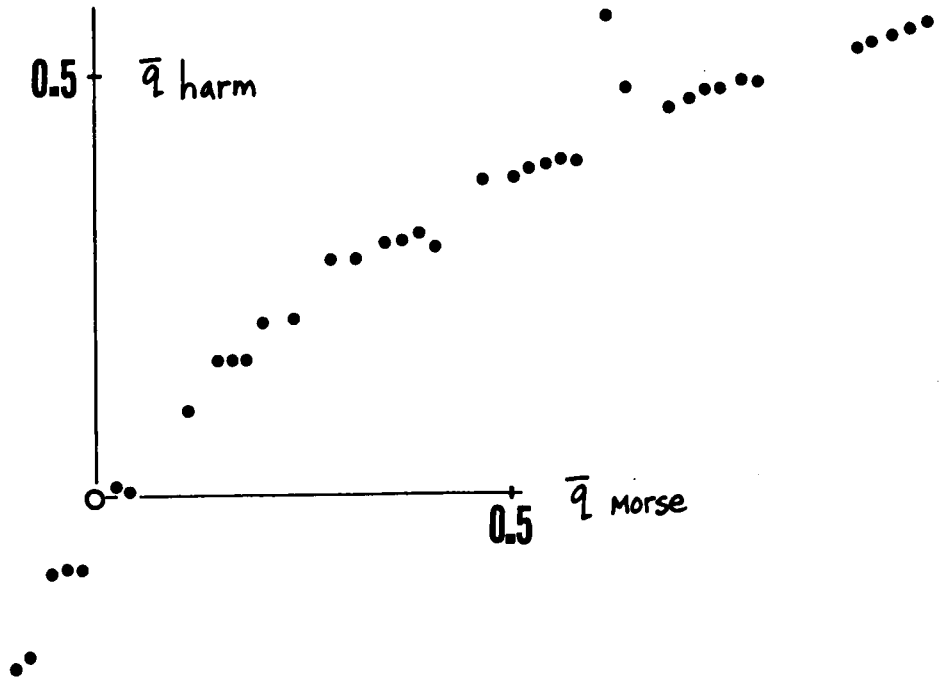


Fig. 4-6. The r-centroids of the first positive system of N_2 obtained in the harmonic oscillator approximation versus the r-centroids from the Morse oscillator approximation.

Even though we are not really interested in making any use of the above mapping procedure, we can still gain some insight into the mathematical principles at work in these approximations. One can formulate a hypothetical mapping process analogous to the one shown in (4-95) and (4-97) for a chosen vibrational model:

$$\bar{q}_{model} = f(\bar{q}_{actual}) \tag{4-99}$$

and

$$M(q) \sim \tilde{M}(f(\bar{q}_{actual})) \tag{4-100}$$

where $\tilde{M}$ is the expression for the transition moment function obtained with the model. The implications of (4-99) and (4-100) are that one can obtain a perfectly good fit to the observed spectrum with an inferior model; with the resulting M(q) greatly distorted, however, if

$$f(x) \sim x \tag{4-101}$$

is not the case. In other words, the computed transition moment function may look alright, i.e., different M_Ks may practically coincide in the region $r \in (r_e', r_e'')$, even if an inferior vibrational model has been used. Likewise, the RE does not necessarily indicate whether the vibrational model used is adequate.

Using a linear dependence in (4-95) gives

$$\bar{q}_{harm} = 0.003 + 0.637\ \bar{q}_{Morse} \tag{4-102}$$

where the two points which do not fit the general trend in Figure 4-6 (p 67) have been left out when computing (4-102). The corrected

transition moment in the quadratic approximation becomes

$$M(q) \sim 0.563-0.178q-0.580q^2 \qquad (4-103)$$

If the dislocation of the vibronic frames is not known, one can treat δ simply as a non-linear parameter in the model. The program is set up to compute the least squares fit for a series of geometries which are "equidistant" along the normal mode coordinate. The program is therefore equipped to perform tasks which previous, more specialized programs were designed to do.

In many cases, anomalous vibronic intensities are experimentally observed which have their origin in some kind of intensity-borrowing mechanisms or nonradiative processes. In work based on the r-centroid approximation, it would have been difficult to establish the presence of such interactions, because there is always the possibility of a breakdown of the r-centroid approximation. Using the input option for the expectation values, one can run the program also in the r-centroid approximation in the form used by Cunio and Jansson.

The scheme used here also allows for a certain amount of flexibility. For example, for bound-continuum transitions, i.e., photofragmentations the upper states have no definite quantum numbers. In this case, the sums in (4-78) would become integrals over the kinetic energy of the fragments. It has been shown by Hazi and Taylor that this vibration Hamiltonian, having a continuous spectrum, can be treated by a finite series of square-integrable functions.[57] A number of calculations have been reported for vibronic bound-continuum transitions; the most recent one apparently by Römelt and Runau.[58]

CHAPTER 5

THE MORSE OSCILLATOR

The radial Schrödinger equation of nuclear motion of a diatomic molecule can be written

$$\{-\frac{\hbar^2}{2\mu} r^{-2} \frac{d}{dr}\left(r^2 \frac{d}{dr}\right) + Qr^{-2} + V(r)-\varepsilon\}\Phi(r) = 0 \qquad (5\text{-}1)$$

where $Q = (1/2)[J(J+1)-\Lambda^2]\,\hbar^2/\mu$.

The term with the first derivative can be removed from (5-1) by the transformation

$$\Phi(r) = r^{-1}\,\psi(r) \qquad (5\text{-}2)$$

We assume that V(r) is a Morse potential:

$$V(r) = A + D(1-\exp(-\beta\rho))^2 \qquad (5\text{-}3)$$

where $\rho = r-r_e$. ψ satisfies the following differential equation:

$$\{-\left(\frac{\hbar^2}{2\mu}\right)\frac{d^2}{dr^2} + Qr^{-2} + V(r)-\varepsilon\}\psi(r) = 0 \qquad (5\text{-}4)$$

If in (5-4) the variable ρ is substituted for r, one obtains

$$\{-\left(\frac{\hbar^2}{2\mu}\right)\frac{d^2}{d\rho^2} + V_{eff}(\rho)-\varepsilon\}\psi(\rho) = 0 \qquad (5\text{-}5)$$

where

$$V_{eff}(\rho) = V(r) + Q(\rho + r_e)^{-2} \qquad (5\text{-}6)$$

The rotational term can be approximated in a truncated expansion of exponentials:

$$Q(\rho + r_e)^{-2} \sim f(\rho) = \alpha_o + \alpha_1 e^{-\beta\rho} + \alpha_2 e^{-2\beta\rho} \tag{5-7}$$

The following criteria can be used for the above approximation:

$$f^{(k)}(\rho) = \left\{\left(\frac{d}{d\rho}\right)^k [Q(\rho+r_e)^{-2}]\right\}_{\rho=0 \text{ or } r=r_e} \tag{5-8}$$

and the following two distinct cases arise:

(i) $\alpha_o = 0$ and $k = 0,1$

which gives

$$\alpha_1 = 2U(1-q_o)$$

$$\alpha_2 = -U(1-2q_o)$$

where $q_o = (\beta r_e)^{-1}$ and $U = Q/r_e^2$ (5-9)

(ii) $k = 0,1,2$ which gives

$$\alpha_o = U(1-3q_o + 3q_o^2)$$

$$\alpha_1 = 2U(2q_o-3q_o^2)$$

$$\alpha_2 = U(3q_o^2-q_o) \tag{5-10}$$

The effective potential is approximated at this point as

$$V_{eff}(\rho) \sim (\alpha_o + A + D) + (\alpha_1-2D)x + (\alpha_2 + D)x^2 \tag{5-11}$$

where the following substitution has been made:

$$x = e^{-\beta\rho} \tag{5-12}$$

The approximation in (ii) is identical with the one obtained by Pekeris by a slightly different approach.[59] It might appear that (ii), being a higher order approximation, would be better. This is certainly true for the lowest rotational states in most cases. However, in (i)

the constraint $\alpha_o = 0$ assures that the dissociation limit for all rotational states is the same. Allowing $\alpha_o \neq 0$ might introduce considerable errors for rotationally highly excited states and for shallow potentials with a limited number of bound rotational sublevels. Substituting (5-12) into (5-5) gives

$$\{\left(x\frac{d}{dx}\right)^2 - \gamma[\alpha_o + A + D - \varepsilon + (\alpha_1 - 2D)x + (\alpha_2 + D)x^2]\}\psi(x) = 0 \qquad (5\text{-}13)$$

where $\gamma = 2\mu/(\hbar\beta)^2$. The additional substitutions

$$\begin{aligned} \psi(x) &= (z^a \exp(-z))^{1/2} \; R(z) \\ a^2 &= 4\gamma(\alpha_o + A + D - \varepsilon) \\ z &= 2bx \\ b^2 &= \gamma(\alpha_2 + D) \end{aligned} \qquad (5\text{-}14)$$

transform (5-13) into a confluent hypergeometric differential equation

$$\{z\frac{d^2}{dz^2} + [a+1-z]\frac{d}{dz} - (1/2)(a+1+\sigma)\}R(z) = 0 \qquad (5\text{-}15)$$

where $\delta = \gamma(\alpha_1 - 2D)/b$. It can be shown that the physically meaningful solutions of (5-15) are its polynomial solutions. In the present case we are dealing with associated Laguerre polynomials. The polynomial solutions are obtained if

$$-(1/2)(a+1+\sigma) = v = 0,1,2,.... \qquad (5\text{-}16)$$

which corresponds to a quantization of the energy. The wave functions are

$$\psi_{v,J}(r) = (\beta/N_v)^{1/2}(z^a e^{-z})^{1/2} L_v^{(a)}(z) \qquad (5\text{-}17)$$

It can be shown that the normalization constant is[60,61]

$$N_v = \Gamma(a+1+v)/(a\Gamma(v+1)) \tag{5-18}$$

Notice that Morse originally used the notation L^a_{n+a} for what in the current notation would be $(-1)^a\Gamma(n+a+1)L_n^{(a)}$. From (5-14), (5-15), and (5-16) we obtain

$$(\alpha_o + A + D-\varepsilon)^{1/2} = -\gamma^{1/2}\{(v + (1/2)) + (1/2)\gamma^{1/2}\,((\alpha_1-2D)/(\alpha_2 + D)^{1/2})\} \tag{5-19}$$

We substitute $\alpha_1 = Qs_1$ and $\alpha_2 = Qs_2$ where Q has been defined in (5-1). A truncated power series expansion of the second term in (5-19)

$$(Qs_1-2D)/(Qs_2 + D)^{1/2} \sim D^{-1/2}\{Q(s_1 + s_2)-2D - (1/2)(Q^2s_2/D)(s_1 + (3/2)s_2)\} \tag{5-20}$$

substituted into (5-19), and taking the squares on both sides of (5-19), gives a polynomial expression in (v + 1/2) and Q for the energy:

$$\varepsilon = \alpha_o + A-(4\gamma)^{-1}\{4(v + (1/2))^2- 4(\gamma/D)^{1/2}[2D-Qb_1 + (1/2)Q^2b_2](v + (1/2)) -(\gamma/D)[4DQb_1-Q^2(s_1 + 2s_2)^2 + Q^3b_1b_2 -Q^4(b_2/2)^2]\} \tag{5-21}$$

where $b_1 = s_1 + s_2$, and $b_2 = (s_2/D)(s_1 + (3/2)s_2)$ has been substituted. According to (5-21), we can write for the spectroscopic constants

$$\omega_e = (\beta/(\pi c))(D/(2\mu))^{1/2} \tag{5-22}$$

$$\omega_e x_e = (\gamma hc)^{-1} \tag{5-23}$$

$$B_e = \begin{cases} \hbar/(4\pi\mu r_e^2 c) = \hbar(4\pi I_e c) & \text{if } \alpha_o = 0 \\ ((3\hbar)/(4\pi\beta\mu r_e^3 c))(1-q_o) & \text{if } \alpha_o \neq 0 \end{cases} \tag{5-24}$$

$$D_e = -\hbar^3 q_o^2/(8\pi I_e^2 Dc) \tag{5-25}$$

$$\alpha_e = \begin{cases} \hbar/(4\pi I_e(\gamma D)^{1/2} c) & \text{if } \alpha_o = 0 \\ ((3\hbar)/(4\pi q_o I_e(\gamma D)^{1/2} c)(1-q_o) & \text{if } \alpha_o \neq 0 \end{cases} \tag{5-26}$$

where $I_e = \mu r_e^2$ has been substituted. Notice that B_e comes out inversely proportional to I_e only if we assume $\alpha_o = 0$. On the other hand, the vibration-rotation interaction term α_e, in general, is better approximated if the constraint $\alpha_o = 0$ is dropped. In Table 5-1, the α_es are presented for a list of transitions published by Steele et al.[62] It can readily be seen that the agreement between experimental and calculated α_es is better for (ii), i.e., if $\alpha_o \neq 0$. The weighted Franck-Condon factors were computed numerically by a Simpson integration. The "weighting factor" is of the same type as the one used in the harmonic oscillator approximation

$$\langle v'J' | \exp(-(1/2)\beta_o\rho^2) \Sigma_k \mathcal{R}_k \rho^k | v''J'' \rangle \tag{5-27}$$

where ρ is centered at the singly primed state, i.e., $\rho = \rho' = r - r_e'$. The associated Laguerre polynomials were initially computed using a Horner's scheme given by Abramowitz and Stegun:[3]

$$L_n^{(\alpha)}(x) = \binom{n+\alpha}{n} a_o(x)$$

where a_o is obtained through downward recursion

TABLE 5-1

A COMPARISON OF COMPUTED VIBRATION-ROTATION INTERACTION CONSTANTS

	$\alpha_{e,exp}(cm^{-1})$	$\alpha_{e,calc} / \alpha_{e,exp}$ (i)	(ii)
H_2 $X^1\Sigma_g^+$	3.0177	1.106	0.684
I_2 $X^1\Sigma_g^+$	0.0001208	1.765	0.984
N_2 $X^1\Sigma_g^+$	0.0171	1.406	0.989
N_2 $A^3\Sigma_u^+$	0.01798	1.534	1.008
N_2 $a^1\Pi_g$	0.0183	1.444	0.975
N_2 $B^3\Pi_g$	0.01794	1.598	1.057
O_2 $X^3\Sigma_g^-$	0.01579	1.399	0.950
O_2 $B^3\Sigma_u^-$	0.011	1.702	1.111
O_2 $A^3\Sigma_u^+$	0.0165	1.911	1.138
CO $X^1\Sigma^+$	0.0175	1.353	0.957
CO $d^3\Delta$	0.0171	1.016	0.739
CO $A^1\Pi$	0.02229	1.646	1.048
CO $e^3\Sigma^-$	0.0179	1.239	0.860
CO $a'^3\Sigma^+$	0.01872	1.286	0.877
NO $X^2\Pi_{1/2}$	0.0174	1.418	0.963
NO $B^2\Pi$	0.0121	1.362	0.967
OH $X^2\Pi_i$	0.708	1.180	0.884
OH $A^2\Sigma^+$	0.7868	1.569	1.121
HF $X^1\Sigma^+$	0.7888	1.138	0.853

$$a_{m-1}(x) = 1-((n-m+1)/(m(\alpha+m)))xa_m(x) \qquad (5\text{-}28)$$

with $a_n(x) = 1$. It turned out that this method is not very accurate for large n, and the associated Laguerre polynomials were computed using their well-known recursion formula:

$$(n+1)L_{n+1}^{(\alpha)}(x) = (2n+\alpha+1-x)L_n^{(\alpha)}(x)-(n+\alpha)L_{n-1}^{(\alpha)}(x) \qquad (5\text{-}29)$$

For large n, the associated Laguerre polynomials show the following asymptotic behaviour:[3]

$$L_n^{(\alpha-1)}(z) \sim \Gamma((1/2)\alpha+n+(1/4))(e^z z^{1/2-\alpha}/\pi)^{1/2}$$

$$\binom{n+\alpha}{n}\cos((2\alpha z+4nz)^{1/2}-((1/2)\alpha+n-(1/4))\pi) \qquad (5\text{-}30)$$

Based on this asymptotic behaviour, the numerical integration is expected to be more stable if the roots of the integrand are made to be more evenly distributed, by using the following variable for the integration:

$$y = z^{1/2} \qquad (5\text{-}31)$$

with

$$dz = 2ydy \quad \text{and} \quad 0 \leq y < \infty \qquad (5\text{-}32)$$

In practice, one will have to decide, in addition, which of the two Morse potentials is being used to determine y if the βs of the two Morse potentials differ. The variable for the eigenfunctions of the other Morse potential becomes, then, a non-integer power of y.

The above integration limits are impractical. One has to figure out a way to determine appropriate limits of integration. For this reason, we determine the classical regions of a Morse oscillator. The classical turning points are given by the equation

$$D-(((1/2)a)^2/\gamma) = D(1-\exp(-\beta\rho))^2 \tag{5-33}$$

which gives

$$R_{min,max} = \{\ell n[1/(1\pm(1-(((1/2)a)^2/(\gamma D)))^{1/2})]\} + r_e \tag{5-34}$$

where the rotational term in the potential was neglected. The limits in the numerical integrations are then taken from the union of the classical regions of the two Morse oscillators, i.e., $\min(R'_{min}, R''_{min}) \leq r \leq \max(R'_{max}, R''_{max})$, extended to the right and to the left by some suitable increments. The resulting limits of integration are then mapped onto the x-axis.

We need to know, also, the number of integration intervals required to compute Franck-Condon factors to a desired degree of accuracy. The answer to this question has been found empirically. Extensive test calculations have shown that

$$\text{number of partitions} = 50 + (1/2)(v_1 + v_2)^2 \tag{5-35}$$

in general gives Franck-Condon factors with at least five significant digits after the decimal point. The accuracy of the weighted Franck-Condon factors was tested with the sum rules:[28]

$$\sum_{v'=0}^{\infty} \langle v'|M|v''\rangle^2 = \langle v''|M^2|v''\rangle$$

$$\sum_{v''=0}^{\infty} \langle v'|M|v''\rangle^2 = \langle v'|M^2|v'\rangle \tag{5-36}$$

The computer program which computes the weighted Franck-Condon factors of Morse oscillator is shown in Appendix 7, together with input instructions. Let us apply the Morse oscillator model to the problem of finding the experimental transition moment. In Table 5-2 (p 79), the expectation values for the 52 observed transitions in the first positive system of molecular nitrogen are shown. The Franck-Condon factors shown are the same as the ones computed by Jarmain and Nicholls, who used the Morse oscillator model as well.[53] The quantities ρ' and q' in Table 5-2 (p 79) are

$$\rho' = r - r_e' \qquad q' = \mu^{1/2}\rho' \tag{5-37}$$

In Table 5-2, the bars indicate the following operations:

$$\overline{\rho'} = \langle v'|\rho'|v''\rangle / \langle v'|v''\rangle \tag{5-38}$$

$$\overline{(\rho')^k} = \langle v'|(\rho')^k|v''\rangle / \langle v'|v''\rangle \tag{5-39}$$

According to current conventions in the use of the r-centroid approximation we should have

$$\overline{(\rho')^k} \sim (\overline{\rho'})^k \quad , \quad k > 1 \tag{5-40}$$

i.e., in Table 5-2, the ratios should be close to unity. This is the case to a certain degree, but it seems that (5-40) is a rather poor approximation for low quantum numbers and $k > 2$. Notice that we have decent agreement between the data and (5-40) for large vibrational quantum numbers and small k. It has been mentioned previously that the r-centroid approximation has a quasi-classical nature.[35,36] For large quantum numbers the correspondence principle is in effect.[63]

TABLE 5-2

EXPECTATION VALUES OF THE FIRST POSITIVE SYSTEM OF N_2 COMPUTED IN THE MORSE OSCILLATOR APPROXIMATION

v'	v''	$\langle 1 \rangle$	$\langle q' \rangle$	$\langle (q')^2 \rangle$	$\langle (q')^3 \rangle$	$\langle (q')^4 \rangle$	$\langle (q')^5 \rangle$
0	0	0.58	0.068	0.0142	0.00320	0.000856	0.0002471
0	1	-0.57	-0.015	-0.0008	0.00106	0.000465	0.0002032
0	2	0.44	-0.024	-0.0019	-0.00100	-0.000086	0.0000072
1	0	0.64	0.144	0.0332	0.00910	0.002678	0.0008649
1	2	-0.32	-0.019	-0.0099	-0.00060	0.000227	0.0003348
1	3	0.42	-0.013	0.0026	-0.00176	-0.000395	-0.0001534
1	4	-0.38	0.040	-0.0021	0.00150	-0.000126	-0.0000327
2	0	0.44	0.154	0.0484	0.01546	0.005286	0.0018971
2	1	0.46	0.118	0.0407	0.01639	0.006558	0.0027579
2	2	-0.34	-0.045	0.0021	0.00372	0.003017	0.0017173
2	3	-0.03	-0.009	-0.0138	-0.00271	-0.000772	0.0001363
2	4	0.28	0.000	0.0081	-0.00142	-0.000457	-0.0003904
2	5	-0.36	0.029	-0.0046	0.00250	0.000036	0.0000829
3	0	0.22	0.109	0.0463	0.01843	0.007339	0.0030040
3	1	0.55	0.203	0.0750	0.03020	0.012926	0.0057113
3	2	0.20	0.061	0.0356	0.01979	0.010246	0.0054078
3	3	-0.40	-0.066	-0.0112	-0.00077	0.002251	0.0020598
3	4	0.18	0.008	-0.0116	-0.00396	-0.002060	-0.0004409
3	5	0.10	0.007	0.0120	-0.00012	-0.000059	-0.0005338
3	6	-0.26	0.013	-0.0076	0.00278	0.000187	0.0003065
4	1	0.36	0.184	0.0859	0.03934	0.018473	0.0089210
4	2	0.52	0.208	0.0903	0.04395	0.022424	0.0117271
4	3	-0.04	-0.001	0.0214	0.01831	0.012485	0.0081719
4	4	-0.34	-0.067	-0.0220	-0.00644	0.000005	0.0015742
5	1	0.17	0.110	0.0660	0.03665	0.019770	0.0106651
5	2	0.46	0.244	0.1239	0.06407	0.034409	0.0189945
5	3	0.43	0.183	0.0936	0.05433	0.032383	0.0196378
5	5	-0.21	-0.050	-0.0273	-0.01165	-0.003300	0.0000831
6	1	0.05	0.047	0.0356	0.02459	0.015832	0.0098180
6	2	0.25	0.171	0.1084	0.06532	0.038971	0.0234519
6	3	0.51	0.284	0.1570	0.09059	0.054657	0.0338656
6	4	0.29	0.136	0.0855	0.05951	0.041247	0.0287216
6	5	-0.32	-0.097	-0.0194	0.00221	0.009358	0.0108662
7	2	0.09	0.081	0.0648	0.04737	0.032869	0.0222535
7	3	0.33	0.233	0.1559	0.10132	0.066127	0.0437688
7	4	0.52	0.303	0.1822	0.11664	0.078196	0.0537650
7	5	0.14	0.077	0.0673	0.05837	0.047478	0.0379091
7	6	-0.36	-0.120	-0.0387	-0.01001	0.003481	0.0093434
8	3	0.14	0.124	0.1025	0.07918	0.058850	0.0430926
8	4	0.40	0.292	0.2059	0.14376	0.101821	0.0734099
8	5	0.49	0.302	0.1977	0.13991	0.103575	0.0784494
9	4	0.18	0.173	0.1485	0.12089	0.095788	0.0753280
9	5	0.45	0.345	0.2561	0.19134	0.146200	0.1140134
9	6	0.44	0.282	0.2021	0.15823	0.128991	0.1071567
10	5	0.24	0.226	0.2023	0.17312	0.145664	0.1223568
10	6	0.49	0.388	0.3038	0.24237	0.198934	0.1669462
10	7	0.36	0.246	0.1949	0.16968	0.152399	0.1385889
11	6	0.29	0.283	0.2628	0.23618	0.210361	0.1879424
11	7	0.51	0.421	0.3467	0.29489	0.259197	0.2331852
11	8	0.27	0.197	0.1763	0.17267	0.171615	0.1709218
12	7	0.34	0.342	0.3291	0.31007	0.291606	0.2761612
12	8	0.52	0.441	0.3827	0.34672	0.325653	0.3131999

TABLE 5-2 (CONTINUED)

v'	v''	$\overline{s'}$	$\overline{(s')^2}/(\overline{s'})^2$	$\overline{(s')^3}/(\overline{s'})^3$	$\overline{(s')^4}/(\overline{s'})^4$	$\overline{(s')^5}/(\overline{s'})^5$
0	0	0.1175	1.78	3.39	7.73	19.01
0	1	0.0265	1.93	-99.92	-1648.01	-27120.13
0	2	-0.0542	-1.47	14.36	-22.91	-35.17
1	0	0.2257	1.02	1.24	1.62	2.32
1	2	0.0590	8.82	9.04	-58.34	-1459.96
1	3	-0.0298	6.98	157.86	-1187.26	15454.90
1	4	-0.1048	0.50	3.42	2.74	-6.81
2	0	0.3468	0.91	0.83	0.82	0.85
2	1	0.2559	1.35	2.12	3.32	5.45
2	2	0.1330	-0.35	-4.71	-28.70	-122.82
2	3	0.2685	5.50	4.02	4.27	-2.81
2	4	0.0014	15059.11	-1902944.18	-438884738.23	-269360197609.31
2	5	-0.0805	1.97	13.44	-2.43	68.72
3	0	0.4846	0.88	0.72	0.59	0.50
3	1	0.3711	1.00	1.08	1.25	1.48
3	2	0.3105	1.88	3.36	5.60	9.52
3	3	0.1648	1.03	0.43	-7.58	-42.08
3	4	0.0424	-35.80	-288.52	-3536.10	-17831.78
3	5	0.0734	23.37	-3.06	-21.38	-2621.88
3	6	-0.0512	11.04	78.95	-103.73	3325.00
4	1	0.5075	0.92	0.83	0.77	0.73
4	2	0.3980	1.09	1.33	1.71	2.24
4	3	0.0269	-697.71	-22255.03	-564453.50	-13746425.64
4	4	0.1976	1.67	2.47	-0.01	-15.49
5	1	0.6680	0.90	0.74	0.60	0.49
5	2	0.5315	0.96	0.93	0.94	0.98
5	3	0.4295	1.19	1.61	2.24	3.16
5	5	0.2439	2.23	3.89	4.52	-0.47
6	1	0.8619	0.89	0.71	0.53	0.38
6	2	0.6912	0.92	0.80	0.69	0.60
6	3	0.5566	0.99	1.03	1.12	1.24
6	4	0.4716	1.33	1.97	2.89	4.27
6	5	0.2998	0.67	-0.25	-3.59	-13.90
7	2	0.8855	0.90	0.74	0.58	0.44
7	3	0.7152	0.93	0.85	0.77	0.72
7	4	0.5834	1.03	1.13	1.30	1.53
7	5	0.5559	1.57	2.45	3.59	5.15
7	6	0.3338	0.97	0.75	-0.78	-6.27
8	3	0.9096	0.91	0.77	0.63	0.51
8	4	0.7400	0.95	0.90	0.86	0.84
8	5	0.6124	1.07	1.23	1.49	1.84
9	4	0.9343	0.92	0.80	0.68	0.57
9	5	0.7657	0.97	0.95	0.94	0.96
9	6	0.6448	1.11	1.35	1.70	2.19
10	5	0.9596	0.93	0.83	0.73	0.64
10	6	0.7925	0.99	0.99	1.03	1.09
10	7	0.6829	1.16	1.48	1.94	2.59
11	6	0.9857	0.94	0.86	0.78	0.70
11	7	0.8205	1.00	1.04	1.12	1.22
11	8	0.7324	1.22	1.64	2.22	3.02
12	7	1.0125	0.95	0.89	0.82	0.77
12	8	0.8500	1.02	1.09	1.20	1.36

Therefore the r-centroid, being quasi-classical in nature, is expected to work well for large quantum numbers, which turned out to be the case. The reduced mass of N_2 was taken here as 7.0015 a.m.u., which is slightly different from the value used by Jarmain and Nicholls (7.00377 a.m.u.).[53] Least squares calculations, as described in the previous chapter, were performed using different dependent variables. The choice of the dependent variable affected the outcome insignificantly if the additional relation (4-90) was included. This is in agreement with previous findings. If the intensities of the third vibronic progression are being declared the dependent variable, the following is obtained:

$$
\begin{aligned}
M_o(q) &= 0.389 && \text{RE} = 28.1\% \\
M_1(q) &= 0.607-0.684q && \text{RE} = 21.7\% \\
M_2(q) &= 0.615-1.124q + 0.713q^2 && \text{RE} = 18.5\% \\
M_3(q) &= 0.610-1.305q + 1.652q^2-0.928q^3 && \text{RE} = 18.5\% \\
M_4(q) &= 0.536-1.185q + 3.940q^2-8.329q^3 + 5.599q^4 && \text{RE} = 17.1\% \qquad (5\text{-}41)
\end{aligned}
$$

Judging from the relative error, the information in the data seems to be exhaustively extracted by the quadratic model. The computer output for M_2 in (5-41) is shown in Table 5-3. The transition moment functions in (5-41) have been graphed in Figure 5-1. The broken line, labelled M_x, represents the curve obtained from the quadratic dependence of M in the harmonic oscillator approximation and applying the transformations in (4-95), (4-96), and (4-97). The function obtained through this transformation is shown in (4-103). The transition moment obtained in this manner has not been normalized using the total

TABLE 5-3

THE TRANSITION MOMENT FUNCTION OF THE FIRST POSITIVE SYSTEM OF N_2 COMPUTED IN THE MORSE OSCILLATOR APPROXIMATION

MOLECULAR NITROGEN : THE NORMAL MODE COORDINATE DEPENDENCE OF THE TRANSITION MOMENT OF THE FIRST POSITIVE SYSTEM.
BASED ON INTENSITIES MEASURED BY R.G. TURNER AND R.W. NICHOLLS,
CAN.J.PHYS., 32(1954)PP.468-474, CAN.J.PHYS., 32(1954)PP.475-479.

ALPHA" = 6.5813205 ALPHA' = 7.1716637

NO.	NO. OF ENERGY LEVEL	V'	V"	FRANCK-CONDON FACTOR	WEIGHTING FACTOR
1	1	0	0	1.00000000	1.00000000
2	1	0	1	0.82800000	1.00000000
3	1	0	2	0.62500000	1.00000000
4	2	1	0	0.66300000	1.00000000
5	2	1	2	0.43400000	1.00000000
6	2	1	3	0.57000000	1.00000000
7	2	1	4	0.73600000	1.00000000
8	3	2	0	0.21600000	1.00000000
9	3	2	1	0.41900000	1.00000000
10	3	2	2	0.17300000	1.00000000
11	3	2	3	0.15000000	1.00000000
12	3	2	4	0.35100000	1.00000000
13	3	2	5	0.47700000	1.00000000
14	4	3	0	0.02640000	1.00000000
15	4	3	1	0.23500000	1.00000000
16	4	3	2	0.13700000	1.00000000
17	4	3	3	0.19700000	1.00000000
18	4	3	4	0.13300000	1.00000000
19	4	3	5	0.22700000	1.00000000
20	4	3	6	0.47900000	1.00000000
21	5	4	1	0.05940000	1.00000000
22	5	4	2	0.23100000	1.00000000
23	5	4	3	0.03890000	1.00000000
24	5	4	4	0.16700000	1.00000000
25	6	5	1	0.00869000	1.00000000
26	6	5	2	0.08520000	1.00000000
27	6	5	3	0.14700000	1.00000000
28	6	5	5	0.10800000	1.00000000
29	7	6	1	0.00105000	1.00000000
30	7	6	2	0.01260000	1.00000000
31	7	6	3	0.08850000	1.00000000
32	7	6	4	0.08490000	1.00000000

TABLE 5-3 (CONTINUED)

33	7	6	5	0.04660000	1.00000000
34	8	7	2	0.00135000	1.00000000
35	8	7	3	0.01700000	1.00000000
36	8	7	4	0.07780000	1.00000000
37	8	7	5	0.03560000	1.00000000
38	8	7	6	0.05370000	1.00000000
39	9	8	3	0.00230000	1.00000000
40	9	8	4	0.02050000	1.00000000
41	9	8	5	0.06000000	1.00000000
42	10	9	4	0.00299000	1.00000000
43	10	9	5	0.02240000	1.00000000
44	10	9	6	0.04480000	1.00000000
45	11	10	5	0.00305000	1.00000000
46	11	10	6	0.02090000	1.00000000
47	11	10	7	0.02840000	1.00000000
48	12	11	6	0.00330000	1.00000000
49	12	11	7	0.02020000	1.00000000
50	12	11	8	0.01680000	1.00000000
51	13	12	7	0.00370000	1.00000000
52	13	12	8	0.01580000	1.00000000

THE INITIAL SIGNS OF THE EXPERIMANTAL FRANCK-CONDON AMPLITUDES WERE
TAKEN SUCH THAT SGN(<V'|M(Q)|V">) = SGN(EXPECTATION VALUE NO. 1).

1 GAUSS-SEIDEL ITERATION

THE INTENSITIES OF THE VIBRONIC PROGRESSION NO. 3 CONSTITUTE THE DEPENDENT VARIABLE

ITERATION NO. 1 : THE DIMENSIONLESS PARAMETER OF DISPLACEMENT D = ALPHA**DELTA = 1.40535
THE EXPONENTIAL FACTOR OF THE TRANSITION MOMENT : EXP(0.0 *Q*Q)
THE LINEAR COEFFICIENTS ARE :
IA(0) = 1.824608 IA(1) = -3.337571 IA(2) = 2.117605

STANDARD ERROR OF ESTIMATE = 0.07693

NO.	V'	V"	EXP. FRANCK-CONDON AMP.	CALC. FRANCK-CONDON AMP.	DIFFERENCE	WEIGHTING FACTOR
1	0	0	1.0000000	0.8633246	-0.1366754	1.0000000
2	0	1	-0.9099451	-0.9910629	-0.0811179	1.0000000
3	0	2	0.7905694	0.8700850	0.0795156	1.0000000
4	1	0	0.7804674	0.7533301	-0.0271373	1.0000000
5	1	2	-0.6314557	-0.5439222	0.0875335	1.0000000
6	1	3	0.7236615	0.8178312	0.0941697	1.0000000

TABLE 5-3 (CONTINUED)

7	1	4	-0.8223126	-0.8324137	-0.0101011	1.0000000
8	2	0	0.4107730	0.3989412	-0.0118318	1.0000000
9	2	1	0.5721133	0.5331012	-0.0390121	1.0000000
10	2	2	-0.3676191	-0.4600690	-0.0924498	1.0000000
11	2	3	-0.3423109	-0.0615642	0.2807466	1.0000000
12	2	4	0.5236349	0.5231092	-0.0005257	1.0000000
13	2	5	-0.6104277	-0.7571627	-0.1467350	1.0000000
14	3	0	0.1289939	0.1443292	0.0153354	1.0000000
15	3	1	0.3848585	0.4790577	0.0941992	1.0000000
16	3	2	0.2938512	0.2305371	-0.0633141	1.0000000
17	3	3	-0.3523711	-0.5372548	-0.1848837	1.0000000
18	3	4	0.2895296	0.2776405	-0.0118891	1.0000000
19	3	5	0.3782510	0.1758591	-0.2023918	1.0000000
20	3	6	-0.5494585	-0.5407642	0.0086943	1.0000000
21	4	1	0.2248486	0.2293771	0.0045285	1.0000000
22	4	2	0.4434075	0.4508094	0.0074019	1.0000000
23	4	3	-0.1819583	-0.0282976	0.1536607	1.0000000
24	4	4	-0.3770121	-0.4397675	-0.0627554	1.0000000
25	5	1	0.0848796	0.0728533	-0.0120263	1.0000000
26	5	2	0.2657743	0.2858025	0.0200282	1.0000000
27	5	3	0.3491017	0.3646833	0.0155816	1.0000000
28	5	5	-0.2992300	-0.2666739	0.0325561	1.0000000
29	6	1	0.0342336	0.0185025	-0.0157311	1.0000000
30	6	2	0.1185886	0.1099199	-0.0086687	1.0000000
31	6	3	0.3142891	0.3155002	0.0012111	1.0000000
32	6	4	0.3078304	0.2533723	-0.0544581	1.0000000
33	6	5	-0.2280608	-0.3067669	-0.0787061	1.0000000
34	7	2	0.0424784	0.0331585	-0.0093200	1.0000000
35	7	3	0.1507391	0.1465444	-0.0041947	1.0000000
36	7	4	0.3224714	0.3221793	-0.0002921	1.0000000
37	7	5	0.2181356	0.1383391	-0.0797964	1.0000000
38	7	6	-0.2679098	-0.3370705	-0.0691607	1.0000000
39	8	3	0.0605087	0.0520825	-0.0084263	1.0000000
40	8	4	0.1806472	0.1812330	0.0005859	1.0000000
41	8	5	0.3090508	0.3103581	0.0013073	1.0000000
42	9	4	0.0749717	0.0754019	0.0004302	1.0000000
43	9	5	0.2052039	0.2130165	0.0078126	1.0000000
44	9	6	0.2902021	0.2845666	-0.0056355	1.0000000
45	10	5	0.0870612	0.1031978	0.0161366	1.0000000
46	10	6	0.2279018	0.2412762	0.0133744	1.0000000
47	10	7	0.2656646	0.2489032	-0.0167614	1.0000000
48	11	6	0.1031176	0.1354927	0.0323751	1.0000000
49	11	7	0.2551240	0.2655984	0.0104744	1.0000000
50	11	8	0.2326646	0.2068303	-0.0258343	1.0000000
51	12	7	0.1446882	0.1722315	0.0275433	1.0000000
52	12	8	0.2989929	0.2856642	-0.0133287	1.0000000

IN THE ABOVE TABLE THE "EXPERIMENTAL" FRANCK-CONDON AMPLITUDES ARE THE EXPERIMENTAL TRANSITION PROBABILITIES DIVIDED BY THE CALCULATED RELATIVE POPULATION FACTORS

TABLE 5-3 (CONTINUED)

DISTRIBUTION OF THE SUMS OF ERROR TERMS AMONG THE VIBRONIC PROGRESSIONS

NO.	1	2	3	4	5	6	7	8	9	10	11	12	13
%	10	6	37	29	9	1	3	4	0	0	0	1	0

DISTRIBUTION OF INTENSITIES AMONG THE VIBRONIC PROGRESSIONS
(USING THE CALCULATED POPULATION FACTORS)

NO.	1	2	3	4	5	6	7	8	9	10	11	12	13
%	28	25	16	10	5	3	3	3	1	1	1	1	1

TOTAL INTENSITY OF THE SPECTRUM : 8.814368
RELATIVE ERROR : 18.5055 %

THE FINAL TRANSITION MOMENT : EXP(0.0 *Q*Q)
THE LINEAR COEFFICIENTS ARE :
1.000000*(Q**(0)) - 1.829199*(Q**(1)) + 1.160581*(Q**(2))

RELATIVE POPULATION OF THE ENERGY LEVELS :

NO. 1	1.00000	NO. 2	1.08844	NO. 3	1.28012	NO. 4	1.58659
NO. 5	1.17491	NO. 6	1.20618	NO. 7	0.89595	NO. 8	0.74816
NO. 9	0.62819	NO. 10	0.53196	NO. 11	0.40239	NO. 12	0.31035
NO. 13	0.17674						

R-CENTROID ANALYSIS OF RESIDUES :

(0.11745, -0.23501)	(0.02653, 0.14233)	(-0.05422, 0.18245)	(0.22568, -0.04257)	(0.05898, -0.27241)
(-0.02980, 0.22306)	(-0.10476, 0.02653)	(0.34677, -0.02663)	(0.25593, -0.08471)	(0.13297, 0.27482)
(0.26849, -8.06430)	(0.00139, -0.00189)	(-0.08048, 0.41090)	(0.48465, 0.06850)	(0.37114, 0.17236)
(0.31053, -0.32174)	(0.16478, 0.45892)	(0.04244, -0.06622)	(0.07345, -2.12508)	(-0.05116, -0.03307)
(0.50755, 0.01248)	(0.39802, 0.01414)	(0.02688, -3.62523)	(0.19759, 0.18593)	(0.66798, -0.07283)
(0.53145, 0.04364)	(0.42946, 0.03664)	(0.24385, -0.15762)	(0.86194, -0.29099)	(0.69123, -0.03497)
(0.55660, 0.00237)	(0.47161, -0.18890)	(0.29983, 0.24406)	(0.88547, -0.10135)	(0.71521, -0.01286)
(0.58338, -0.00056)	(0.55588, -0.57591)	(0.33385, 0.19253)	(0.90956, -0.06186)	(0.74000, 0.00148)
(0.61241, 0.00265)	(0.93425, 0.00233)	(0.76570, 0.01735)	(0.64487, -0.01286)	(0.95960, 0.06840)
(0.79246, 0.02729)	(0.68292, -0.04649)	(0.98565, 0.11265)	(0.82047, 0.02043)	(0.73237, -0.09620)
(1.01246, 0.08161)	(0.84998, -0.02571)			

THE QUANTITIES ABOVE ARE (<V'|Q|V">/<V'|V">,DIFFERENCE/<V'|V">)

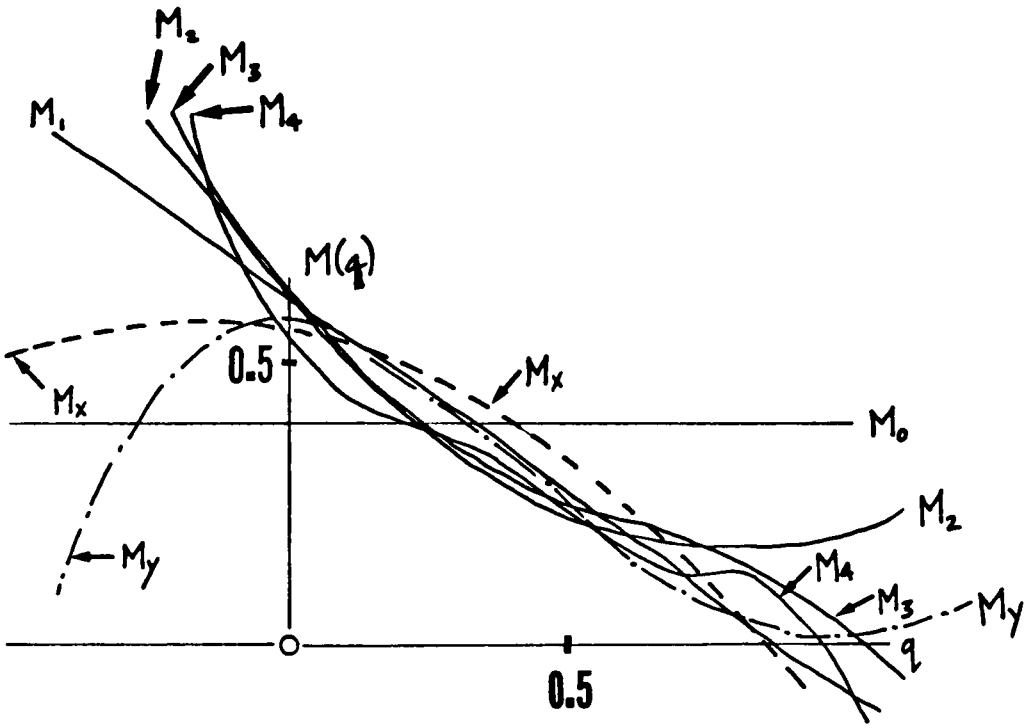


Fig. 5-1. The transition moment function of the first positive system of N_2. III. The transition moment function computed in the Morse oscillator approximation.

intensity. The transformed transition moment function seems to be in reasonable agreement with M_o, M_1, M_2, M_3, and M_4, except that its convexity is definitely incorrect. One should be able to cure this deficiency by using a more accurate description for $\bar{q}_{harm} = f(\bar{q}_{Morse})$ than the linear dependence in (4-103). If a quadratic dependence is assumed in (4-99), we obtain

$$\bar{q}_{harm} = -0.06 + 1.20\ \bar{q}_{Morse} - 0.61(\bar{q}_{Morse})^2 \qquad (5\text{-}42)$$

The transformed transition moment becomes, then,

$$M(q) \sim 0.575 - 0.111q - 2.00q^2 + 2.08q^3 - 0.52q^4 \qquad (5\text{-}43)$$

The transition moment function above is shown in Figure 5-1 (p 86) as a broken line labelled M_y. M_y seems to be in fairly good agreement with the other transition moment functions in Figure 5-1 (p 86).

The Morse oscillator model used here can take into account the rotational dependence of the Franck-Condon factors. Extensive studies dealing with diatomic molecules of astrophysical interest have been done.[64,65] These studies used the model used here with $\alpha_o \neq 0$, and with a modification due to Schumaker.[66] Schumaker takes into account the dependence of the internuclear distance on the rotational quantum number. This change could readily be incorporated in our algorithm. Based on (5-1), one might suspect a quadratic dependence of the Franck-Condon factors on the rotational quantum number J. Extensive calculations have been done on the rotational dependence of Franck-Condon factors for the photoionization of molecular nitrogen. The data in Table 5-4 refer to

TABLE 5-4

THE ROTATIONAL DEPENDENCE OF FRANCK-CONDON FACTORS

	$\alpha_o = 0$		$\alpha_o \neq 0$	
$J''=J'-2$	$Fc_{J'J''}$	$\Delta_J \cdot 10^4$	$Fc_{J'J''}$	$\Delta_J \cdot 10^4$
0	0.8860		0.8860	
5	0.8853	-7	0.8853	-7
10	0.8846	-7	0.8845	-8
15	0.8838	-8	0.8837	-8
20	0.8829	-9	0.8828	-9
25	0.8819	-10	0.8817	-11
30	0.8808	-11	0.8806	-11
35	0.8797	-11	0.8794	-12
$J''=J'+2$	$Fc_{J'J''}$	$\Delta_J \cdot 10^4$	$Fc_{J'J''}$	$\Delta_J \cdot 10^4$
0	0.8864		0.8864	
5	0.8870	6	0.8869	5
10	0.8875	5	0.8874	5
15	0.8880	5	0.8879	5
20	0.8884	4	0.8882	3
25	0.8887	3	0.8884	2
30	0.8890	3	0.8886	2
35	0.8891	1	0.8887	1

$$(v''=0)\,{}^{14}N_2X\,{}^1\Sigma_g^+ \xrightarrow{h\nu} (v'=0)\,{}^{14}N_2^+X\,{}^2\Sigma_g^+ + e^- \qquad (5\text{-}44)$$

where the O and S branches have been considered. The Franck-Condon factors have been abbreviated Fc with J as a subscript. From the column of differences, one can conclude that the dependence of Fc on the rotational quantum number is indeed roughly quadratic as indicated by the change in $\Delta_{J'}$,

$$\Delta_{J'} = Fc_{J'} - Fc_{J'-5} \qquad (5\text{-}45)$$

which seems to depend linearly on J. The above investigation is just of an empirical nature. The present findings will be used in the second-last chapter to represent the rotational dependence of the Franck-Condon factors in a suitable mathematical form. According to Table 5-4 (p 88), the rotational dependence of the Franck-Condon factors for $\alpha_o = 0$ and $\alpha_o \neq 0$ are almost the same for the photoionization in (5-44).

For diatomic molecules, one can construct a Morse potential basically in two ways:

(i) Take $\beta = (2\mu hc\omega_e x_e)^{1/2}/\hbar$

and $D = 2\mu(\omega_e \pi c/\beta)^2 \qquad (5\text{-}46)$

(ii) Take D = depth of the well from the experimental dissociation energy and zero point energy, and

$\beta = (\omega_e \pi c)(2\mu/D)^{1/2} \qquad (5\text{-}47)$

One will have to decide which of the two choices would be appropriate for some situation of interest. The second method is preferable in

situations where the long-range behaviour of the wave function is critical, as would be the case for collision-induced transitions.[67] In most cases, (i) is the proper approach to determine the parameters of the Morse potential. A practical example would be the theoretical interpretation by Rahn et al. of the observation of the optical Stark effect on vibrational and rotational transitions, based on the Morse oscillator model.[68]

CHAPTER 6

THE PERTURBED MORSE OSCILLATOR

In the previous chapter, the rotational term has been partially included in the Morse potential. The Taylor series used to represent this term was truncated to three terms. In this chapter we will look at the possibility of including the higher order terms as perturbations which will be treated to first order.[69] We want to take the perturbations in a form where the magnitude of this perturbation is as small as possible in the neighbourhood of $\rho = 0$. This is the case for

$$V_k(\rho) = (2b(1-\exp(-\beta\rho)))^k \tag{6-1}$$

which in the neighbourhood $\rho = 0$ or, equivalently, $r = r_e$ becomes

$$V_k(\rho) \sim (-1)^k(2b\beta\rho)^k \quad \text{for } \rho \sim 0 \tag{6-2}$$

where b has been defined in (5-14).

A perturbed Morse oscillator of a different form was investigated extensively by Huffaker and Dwivedi.[70-73] They derived a power series expansion in terms of the vibrational quantum number for the expectation values $\langle v_1|(1-(2b/z))^k|v_2\rangle$, where z denotes the same variable as in the previous chapter.[74] A Morse oscillator with a perturbation of the type chosen by Huffaker and Dwivedi does no longer have a finite dissociation limit. This is not the case with the type of perturbations considered here. In the last chapter, it was mentioned that the normalization factors for the Morse oscillator eigenfunctions have been expressed in terms of simple gamma functions. It turns out that

using this form of the normalization factor, the expectation values for (6-1) become simply polynomials of order k of the vibrational quantum number v. Let us briefly demonstrate the method used to compute the expectation values. The expectation value for k = 1 is found easily. Instead of computing

$$\langle v|(2b-z)^k|v\rangle \tag{6-3}$$

as shown in (6-1), we derive formulae for

$$\langle v|z^k|v\rangle \tag{6-4}$$

where z has been defined in (5-14). The expectation values of interest, shown in (6-3), can, of course, easily be expressed in terms of the ones in (6-4). The integral for k = 1,

$$\langle v|z|v\rangle = N_v^{-1}\int_0^\infty z^a e^{-z}[L_v^{(a)}(z)]^2 dz \tag{6-5}$$

is well-known.[75]

$$\int_o^\infty e^{-z} z^a L_n^{(a)}(z) L_m^{(a)}(z) dz = \delta_{nm}\Gamma(a+n+1)/n! \tag{6-6}$$

Substituting this into (6-5) gives

$$\langle v|z|v\rangle = a = -2(v+(1/2)) - (\alpha_1-2D)(\gamma/(\alpha_2+D))^{1/2} \tag{6-7}$$

where γ has been defined in the previous chapter. The expectation values for the cases k > 1 can be obtained through repeated application of the recursion formula for the associated Laguerre polynomials:

$$(n+1)L_{n+1}^{(a)}(z) = [(2n+a+1)-z]L_n^{(a)}(z)-(n+a)L_{n-1}^{(a)}(z) \tag{6-8}$$

Substituting this into $\langle v|z^2|v\rangle$ gives

$$\langle v|z^2|v\rangle = a(a+2(v+(1/2))) \tag{6-9}$$

Repeated application of (6-8) gives

$$z^2 L_v^{(a)}(z) = \ldots\ldots\ldots + [6v(v+a+1) + (a+1)_2] L_v^{(a)}(z) + \ldots\ldots \tag{6-10}$$

$$z^3 L_v^{(a)}(z) = \ldots\ldots\ldots + [6[5v(v+av+a)+a^2(2v+1)+1] + 20v^3 + 11(2v+a)+a^3] L_v^{(a)}(z) + \ldots\ldots\ldots \tag{6-11}$$

where the terms which, according to (6-6), vanish, were indicated by strings of dots in the above formulae. We obtain, then,

$$\langle v|z^3|v\rangle = 6av(v+a+1) + (a)_3 \tag{6-12}$$

In (6-10), and in the above equation, Pochhammer's symbol has been used.[3] From (6-11) and (6-6) we obtain

$$\langle v|z^4|v\rangle = a[6[5v(v+av+a)+a^2(2v+1)+1] + 20v^3 + 11(2v+a)+a^3] \tag{6-13}$$

It was later discovered that Pekeris had computed these first-order perturbations previously, using a Laplace transform technique.[59] The formula in (6-13) is different from the one given by Pekeris. The formula in (6-13) reproduces results computed numerically, whereas Pekeris' doesn't.

Examination of the above recursion process indicates that we have to expect, in general, a k-th order polynomial in v for an expectation value $\langle v|z^k|v\rangle$. The case with k = 2 is an exception to this rule, due to unfortunate cancellation of the coefficient of the highest

power in v. This fact can readily be verified by substituting (6-7) into (6-9).

After this work had been completed, Requena et al. published expressions for the energy levels of the perturbed Morse oscillator of the type treated here.[76] They used the hypervirial and Hellmann-Feynmann theorems to obtain perturbation expansions for the expectation values of the kind shown in (6-1).

Huffaker and Dwivedi used the expressions obtained for the perturbations to find, among other things,

(i) Potential energy curves of extended accuracy

(ii) Improved wave functions and Franck-Condon factors

(iii) Expressions for higher order spectroscopic parameters in terms of anharmonicities.

These findings are obtained typically by comparing expressions for the energy levels of the model with the standard power series expansion for the energy levels of diatomics used by spectroscopists. Since we have managed to express the first order correction exactly and as a truncated power series, it might at first appear that we are doing better than Huffaker and Dwivedi. However, these authors, through Taylor series expansion techniques, express perturbations to arbitrarily high order as polynomials in v. When making comparisons between the spectroscopic expression and the expression from the model to find the expansion coefficients of the perturbation, these authors can include high orders of perturbations, whereas, in our case, only the first order perturbation gives mathematically suitable expressions. Huffaker and Dwivedi reported convergence problems if the term

$(1-(2b/z))^3$ was included, i.e., they started their expansion with $(1-(2b/z))^4$. This leads us to suspect that their method might, in fact, be inferior to the one shown here. Experimentalists say that an experiment is worth more than a thousand speculations. So far, comparisons between the present model and the one of Huffaker and Dwivedi did not progress past the stage of wild speculations. It would be very interesting to redo some of the work on diatomics by Huffaker and Dwivedi. The real interest lies, however, with polyatomic molecules, where we will have a chance to obtain first order wave functions with the vibrational interaction included via perturbation theory. As previously mentioned, the expectation values required for higher order perturbations and perturbed wave functions are no longer simple polynomial expressions. The integrals are of the form $\langle v_1|z^k|v_2\rangle$. Gradshteyn and Ryzhik express a related integral in terms of a generalized hypergeometric series of several variables.[77] After a number of substitutions one obtains

$$\langle v_1|z^k|v_2\rangle = [a_1a_2v_1!v_2!\Gamma(a_1+v_1+1)\Gamma(a_2+v_2+1)]^{1/2}$$
$$\sum_{m=0}^{v_1}\sum_{n=0}^{v_2}(-1)^{m+n}\,\Gamma((1/2)(a_1+a_2)+m+n+k)$$
$$[\Gamma(v_1-m+1)\Gamma(v_2-n+1)\Gamma(a_1+m+1)\Gamma(a_2+n+1)m!n!] \qquad (6\text{-}14)$$

Since (6-14) is a finite series, one is not very suspicious at first regarding its numerical stability. A test revealed, nevertheless, that (6-14) is not suitable for machine computations unless v_1 and v_2 are both small. The Morse oscillator program has been designed to compute eigenvalues of the type shown in (6-14). It is recommended that this

program be used to compute the eigenvalues $\langle v_1|z^k|v_2\rangle$, rather than (6-14).

Before demonstrating an application, let us present the higher order terms in the expansion of the rotational term. Let us take a truncated power series expansion:

$$Q(\rho+r_e)^{-2} \sim \kappa_o + \kappa_1 e^{-\beta\rho} + \kappa_2 e^{-2\beta\rho} + \kappa_3 e^{-3\beta\rho} \tag{6-15}$$

A Taylor series expansion technique, as the one shown in (5-8), gives

$$\begin{aligned}
\kappa_o &= S[1-(11/3)q_o + 6q_o^2-4q_o^3] \\
\kappa_1 &= Sq_o[12q_o^2-15q_o + 6] \\
-\kappa_2 &= Sq_o[12q_o^2-12q_o + 3] \\
\kappa_3 &= Sq_o[4q_o^2-3q_o + (2/3)]
\end{aligned} \tag{6-16}$$

where $S = Q/r_e^2$. If we place again the restriction $\kappa_o = 0$, we obtain

$$\begin{aligned}
\kappa_1 &= S[3q_o^2-5q_o + 3] \\
\kappa_2 &= -S[6q_o^2-8q_o + 3] \\
\kappa_3 &= S[3q_o^2-3q_o + 1]
\end{aligned} \tag{6-17}$$

where Q and q_o have the same meaning as in the previous chapter. An expansion with a fourth term included gives

$$\begin{aligned}
\kappa_o &= S[5q_o^4-10q_o^3 + (35/4)q_o^2-(25/6)q_o + 1] \\
\kappa_1 &= -Sq_o[20q_o^3-36q_o^2 + 26q_o-8] \\
\kappa_2 &= Sq_o[30q_o^3-48q_o^2 + (57/2)q_o-6] \\
\kappa_3 &= -Sq_o[20q_o^3-28q_o^2 + 14q_o-(8/3)] \\
\kappa_4 &= Sq_o[5q_o^3-6q_o^2 + (11/4)q_o-(1/2)]
\end{aligned} \tag{6-18}$$

If we place again the restriction $\kappa_o = 0$, we obtain

$$\begin{aligned}
\kappa_1 &= -S[4q_o^3 - 9q_o^2 + (26/3)q_o - 4] \\
\kappa_2 &= S[12q_o^3 - 24q_o^2 + 19q_o - 6] \\
\kappa_3 &= -S[12q_o^3 - 21q_o^2 + 14q_o - 4] \\
\kappa_4 &= S[4q_o^3 - 6q_o^2 + (11/3)q_o - 1]
\end{aligned} \tag{6-19}$$

Let us now demonstrate the use of the above theories. We take the case where the anharmonicities x_e and y_e of a diatomic molecule are known. We want to express the internuclear potential of this molecule as

$$V(\rho) = D(1-e^{-\beta\rho})^2 + D_3(1-e^{-\beta\rho})^3 + \kappa_o + \kappa_1 e^{-\beta\rho} + \kappa_2 e^{-2\beta\rho} + \kappa_3 e^{-3\beta\rho} \tag{6-20}$$

where the last four terms are an expansion of the rotational term in the potential. Using the formalism of the previous chapter, we can take the unperturbed solution as corresponding to the potential

$$V(\rho) = D(1-e^{-\beta\rho})^2 + \alpha_o + \alpha_1 e^{-\beta\rho} + \alpha_2 e^{-2\beta\rho} \tag{6-21}$$

where

$$\begin{aligned}
\alpha_o &= \kappa_o + \kappa_3 \\
\alpha_1 &= \kappa_1 - 3\kappa_3 \\
\alpha_2 &= \kappa_2 + 3\kappa_3
\end{aligned} \tag{6-22}$$

and the perturbation becomes

$$V_{pert}(\rho) = (D_3 - \kappa_3)(1-e^{\beta\rho})^3 \tag{6-23}$$

Near $\rho = 0$, this perturbation asymptotically approaches $(\beta\rho)^3$.

According to (6-7), (6-9), and (6-12), the first order energy correction is

$$\begin{aligned}\langle v|V_{pert}|v\rangle &= (D_3-\kappa_3)[1-3a/(2b)) \\ &+ (3a/(4b^2))(a + 2(v + (1/2))) \\ &- (a/(8b^3))[6v(a+v+1) + (a+1)_2]] \end{aligned} \tag{6-24}$$

To express the J-dependent term in a and b, we use a truncated power series expansion:

$$\begin{aligned}&(Qs_1-2D)^n(Qs_2 + D)^{-m} \sim (-1)^n 2^{n-2} D^{n-m} \\ &\{4-2(s_1 n + 2s_2 m)X + [((1/2)s_1 n+s_2 m)[s_1(n-1) + 2s_2(m+1)] \\ &-s_1 s_2(n-m)]X^2\}\end{aligned} \tag{6-25}$$

where $X = Q/D$ and $\alpha_1 = Qs_1$, $\alpha_2 = Qs_2$.

The perturbation becomes, then,

$$\begin{aligned}&\langle v|V_{pert}|v\rangle \sim (D_3-\kappa_3)\{8-6(s_1+2s_2)X \\ &+ 3((1/2)s_1^2 + 4s_1 s_2 + 6s_2^2)X^2 + (X_o/8)[1-w_1 X+w_2 X^2] \\ &+ (v+(1/2))X_o^{1/2}[3[2-w_1 X + (3/4)w_2 X^2] + (X_o/32)[4- \\ &6s_2 X + (15/2)s_2^2 X^2]]-(3/2)X_o(v+(1/2))^2[1-w_1 X+w_2 X^2] \\ &- ((1/2)X_o^{1/2})^3(v+(1/2))^3[4-6s_2 X + (15/2)s_2^2 X^2]\}\end{aligned} \tag{6-26}$$

where $w_1 = (1/2)s_1 + 2s_2$, $w_2 = s_2(s_1 + 3s_2)$, and $X_o = (\gamma D)^{-1}$. The above relation is exact if $X = 0$. First, we would like to know what potential energy function, according to the above procedure, has energy levels

$$\varepsilon_v = \text{const.} + \omega_e[(v+(1/2))-x_e(v+(1/2))^2 + y_e(v+(1/2))^3] \qquad (6\text{-}27)$$

to first order. We take $J = \kappa_3 = 0$ in (5-21) and (6-26):

$$\varepsilon_v^{(o)} + \langle v|V_{pert}|v\rangle = \text{const.} + (v+(1/2))X_o^{1/2}[2D + D_3[6+(X_o/8)]]-(v+(1/2))^2X_o[D+(3/2)D_3] - \tfrac{1}{2}(v+(1/2))^3D_3X_o^{3/2} \qquad (6\text{-}28)$$

Equating the coefficients in the above expression with the spectroscopic constants in (6-27), one obtains a quadratic expression for $X_o^{1/2}$. The sign for the physically meaningful solution is taken such that the result reduces to the unperturbed Morse oscillator solution if $y_e = 0$:

$$X_o^{1/2} = [2x_e + [4x_e^2-6y_e(4+y_e)]^{1/2}/[2+(1/2)y_e] \qquad (6\text{-}29)$$

The above quantity should be a real number. Using (6-29), the remaining two parameters of the potential can be readily evaluated using any pair from the equations below:

$$\begin{aligned} \omega_e &= X_o^{1/2}[2D + D_3(6+(X_o/8))] \\ \omega_e x_e &= X_o[D + (3/2)D_3] \\ \omega_e y_e &= -\tfrac{1}{2} X_o^{3/2}D_3 \end{aligned} \qquad (6\text{-}30)$$

The dissociation limit is the sum of the coefficients D and D_3:

$$\text{diss. en.} = D + D_3 = (\omega_e x_e/X_o) + (\omega_e y_e/X_o^{3/2}) \qquad (6\text{-}31)$$

One can use the above relation, as well, to find the parameters of the potential, i.e., one can construct a potential with a proper

dissociation limit. The situation is similar to the one described in (5-46) and (5-47).

Let us assume that we wish to find the vibration-rotation interaction α_e from the spectroscopic constants ω_e, $\omega_e x_e$, and $\omega_e y_e$. According to (5-21) and (6-26),

$$\alpha_e[J(J+1)-\Lambda^2] = X_o^{1/2}\{\alpha_1+\alpha_2 + (3D_3/D)[(1/2)\alpha_1 + 2\alpha_2 + (\alpha_2 X_o/32)] + \kappa_3(6 + (X_o/8))\} \qquad (6\text{-}32)$$

The αs are defined in (6-22). The κs can be taken either from formula (6-16) or from (6-17). One can see that we have a number of options at our disposal. Some of these options may be better than others. In some cases $X_o^{1/2}$ may turn out to be a complex number if it is defined according to (6-29), in which case the procedure is not applicable.

The formulae with D_4, i.e., including z_e, have not been worked out here. This would require procedures similar to the ones shown here. One could end up in this approximation with nonlinear equations which would have to be solved by an appropriate method.

CHAPTER 7

THE PÖSCHL-TELLER OSCILLATOR

There are extensive accounts in the literature of efforts to find Schrödinger equations with analytical solutions. Presently, insights into the nature of strong interactions have stirred renewed interest in various types of potentials.[78,79] A number of potentials are known which simulate reasonably well bound potential energy curves of diatomic molecules.[62,80-82] Beyond the simple harmonic oscillator, only the Morse oscillator seems to enjoy popularity, even though its quantum mechanical treatment is not straightforward.[83] The motive for using the Morse oscillator model is based simply on the fact that its energy levels are mathematically in a form analogous to a truncated power series used by spectroscopists:

$$E_v = T_e + (v+(1/2))\omega_e - (v+(1/2))^2\omega_e x_e \qquad (7\text{-}1)$$

It would be useful to have a model with an expression for the energy levels as the one in (7-1), but based on a symmetric potential. This model would be applicable, for example, to the bending vibration of linear molecules. It turns out that such a model has been known for a long time. It is the modified Pöschl-Teller potential as described, among others, by Flügge.[84] The treatment shown here differs from the one by Flügge. Flügge considered the potential of interest as a special case. The eigenfunctions appear, therefore, as hypergeometric functions which do not reveal readily the expected parity of the eigenfunctions of a symmetric potential.

In the Schrödinger equation

$$\{-\frac{\hbar^2}{2\mu}\frac{d^2}{dx^2} + V(x)-E_n\}\psi_n(x) = 0 \tag{7-2}$$

with

$$V(x) = -((1/2)C_o/\mu)(\hbar\alpha/\cosh(\alpha x))^2 \tag{7-3}$$

we make the substitutions

$$t = \tanh(\alpha x) \tag{7-4}$$

and

$$\psi_n(t) = (1-t^2)^{\beta}\chi_n(t), \text{ where } \beta^2 = -(1/2)\mu E_n/(\hbar\alpha)^2 \tag{7-5}$$

This gives

$$\{(1-t^2)\frac{d^2}{dt^2} - 2t(2\beta+1)\frac{d}{dt} - 2\beta(2\beta+1) + C_o\}\chi_n(t) = 0 \tag{7-6}$$

A power series expansion of χ,

$$\chi_n(t) = \Sigma_k g_k t^k \tag{7-7}$$

is defined by the following recursion relation among its expansion coefficients

$$g_{k+2} = g_k[k(k+2)^{-1} + (2\beta(2k+2\beta+1)-C_o)(k^2+3k+2)^{-1}] \tag{7-8}$$

In (7-6), we have a hypergeometric differential equation. Based on linear transformation formulae valid for hypergeometric functions, one reaches the conclusion that, in order to satisfy the infinity condition for bound states, the hypergeometric series must terminate with a finite number of terms:

$k_{max} = 0,2,4,\ldots,$ n for states with even parity, i.e., even n

$k_{max} = 1,3,5,\ldots,$ n for states with odd parity. (7-9)

This is the case if the energy eigenvalues are

$$E_n = -[\hbar\alpha((C_o+(1/4))^{1/2}-(n+(1/2)))]^2/(2\mu) \tag{7-10}$$

For $C_o>0$ the energy eigenvalue spectrum is finite:

$$0\leq n\leq (C_o+(1/4))^{1/2}-(1/2) = a_o-(1/2) \tag{7-11}$$

The quantity a_o defined above will be referred to later.

The physically meaningful solutions can be expressed in ultraspherical polynomials:

$$\psi_n(x) = N_n^{-1/2}(\cosh(\alpha x))^{1/2-a}C_n^{(a)}(\tanh(\alpha x)) \tag{7-12}$$

where $a = a_o-n$, and N_n is the normalization factor of the n-th state. The normalization integral of ψ_n becomes[85]

$$N_n = \alpha^{-1}\int_{-1}^{1}(1-t^2)^{a-3/2}[C_n^{(a)}(t)]^2dt$$

$$= [\pi 4^{1-a}\Gamma(2a+n)]/[\alpha n!(2a-1)[\Gamma(a)]^2] \tag{7-13}$$

The ultraspherical polynomials can be generated by the following recursion relation:[3]

$$(n+1)C_{n+1}^{(a)}(x) = 2(n+a)xC_n^{(a)}(x)-(2a+n-1)C_{n-1}^{(a)}(x) \tag{7-14}$$

with $C_o^{(a)} = 1$ and $C_1^{(a)} = 2ax$. For the n-th bound state, the classically allowed region is

$$\alpha|x|\leq \operatorname{arccosh}(C_o^{1/2}/[a_o-(n+(1/2))]) \tag{7-15}$$

If the bottom of the well is taken as the point of reference for the energy levels, we obtain

$$E_n + C_o = ((\hbar\alpha)^2/(2\mu))[(-1/4) + 2a_o(n+(1/2))-(n+(1/2))^2] \qquad (7\text{-}16)$$

If a_o is large, i.e., for a deep potential well, the second term in (7-16) dominates for the lowest few states. In this case the hyperbolic potential appears as nearly harmonic.

It can be shown that

$$\langle\psi_n|\cosh^{-2}(\alpha x)|\psi_n\rangle = (a_o-n-(1/2))/a_o \qquad (7\text{-}17)$$

Using this, we obtain

$$\langle\psi_n|V|\psi_n\rangle = (1/2)(\hbar\alpha)^2(C_o/a_o)(a_o-(n+(1/2)))/\mu \qquad (7\text{-}18)$$

From this, based on the fact that $E_n = \langle V\rangle_{nn} + \langle T\rangle_{nn}$, we obtain

$$\langle\psi_n|T|\psi_n\rangle = (1/2)(\hbar\alpha)^2[(n+(1/2))^2-a_o(n+(1/2)) + (1/4)(1-((n+(1/2))/a_o))]/\mu \qquad (7\text{-}19)$$

where T, of course, represents the kinetic energy term. Potential and kinetic energy are not related in terms of a simple proportionality for this potential. All one can say is that they both become zero in the limit $(n+1/2)\rightarrow a_o$.

A computer program was written which computes the expectation values

$$\langle\psi_n|\Sigma_k b_k \tanh^k(\gamma x)|\psi_m\rangle \qquad (7\text{-}20)$$

and

$$\langle\psi_n|\Sigma_k b_k x^k \exp(-(1/2)\gamma x^2)|\psi_m\rangle \qquad (7\text{-}21)$$

with $k \geq 1$. This program together with input instructions is shown in Appendix 8. It can be shown that

$$\langle\psi_n|\tanh^2(\alpha x)|\psi_n\rangle = (n+(1/2))/a_o \qquad (7\text{-}22)$$

and

$$\langle\psi_n|\tanh^4(\alpha x)|\psi_n\rangle = [3(a_o-1) +$$

$$n(6a_o-7) + 3n^2(2a_o-1)-2n^3]/[4a_o(a_o^2-1)] \qquad (7\text{-}23)$$

and that, in general, an expectation value $\langle\tanh^{2k}(\alpha x)\rangle_{nn}$ gives a (2k-1)-th order polynomial in n. We will make use of this fact in the last chapter.

CHAPTER 8

PHENOMENA IN PHOTOELECTRON SPECTROSCOPY AND THEIR THEORETICAL INTERPRETATION

A. THE PHOTOELECTRIC EFFECT

In 1887 Hertz observed that ultra-violet light of an electric spark falling upon the negative electrode of a spark gap will facilitate an electric discharge.[86] Later the photoelectric effect played a prominent role in developments which revolutionized physics.[87] Inspired by the observation of the photoelectric effect, Einstein postulated the existence of light quanta.[88-90] Einstein apparently coined the word "photon."[91] It was not until much later that the photoelectric effect was exploited as a tool for spectroscopic measurements.[92]

Initially it was thought that photoelectron spectra would be relatively easy to interpret due to the fact that interpretation in terms of molecular orbitals requires that we identify the initial orbital of the electron only. However, photoelectron spectra show so-called satellites which appear as transitions in excess of the expected "one peak per orbital" situation.[93]

In nature photoionization takes place whenever we have an interaction of matter with high energy radiation. For radiation of very high frequency photoionization takes place mainly through the Compton effect,[94] which represents essentially an inelastic collision of a photon with an electron. Photoionization is an important process in plasmas. Plasmas represent a state of matter. A collection of Rydberg

atoms will undergo a phase transition, a so-called Mott transition, at a critical density beyond which it exists in the plasma state.[95] Most of the matter in the universe is believed to be in the plasma state.[96] A quantitative knowledge of photoionization process is therefore needed for plasma physics and related areas such as nuclear fusion, study of the upper atmosphere and astrophysics in general.[97] The fact that the upper atmosphere, the so-called ionosphere, is ionized is of great importance for radio communications.[98-99] By the ionosphere/earth wave guide transmission mode, radio communications over very long distances are possible.[99] Radio signals generated in the ionosphere by sunspot activity can have adverse effects on radio communications.[100]

The ionosphere blocks low frequency signals from outer space and therefore limits astronomical observations at ground level.[101] The bulk of solar radiation is emitted in the visible and in the infrared portion of the spectrum. The energy output of the sun is nearly constant, but the small portion of energy emitted as high energy radiation changes with sun spot activity and is therefore far more variable.[102] Even though the energy input in terms of ionizing radiation may be small and confined to the outermost layers of the atmosphere, it may appreciably influence the weather at ground level by changing the electrical conductivity of the atmosphere.[103] Ambient electric fields in the atmosphere may be important in controlling cloud electrification and rainfall.[103] The problem of long-term weather changes is compounded by manmade emissions into the atmosphere.[104] The ions created by photoionizations in the upper atmosphere will eventually combine with

oppositely charged particles. This "recombination" can proceed over a large number of steps giving rise to a rich chemistry in the upper atmosphere.[105-107] Ozone, which is considered an important component of the atmosphere, attenuating harmful solar UV radiation,[108] can be formed from molecular oxygen by the action of ionizing radiation.[109] Photoionization, in a sense, may be one driving force in the ozone cycle.

Photoionization in the atmosphere has also recently attracted widespread attention in connection with nuclear explosions. In the sixties, at least seven operating civilian and an unknown number of military satellites were put out of service by high-altitude nuclear tests.[110] The damage results from electrical pulses generated by a burst of ionizing radiation.[110] These pulses are generated mainly through the Compton effect. Recently it has been pointed out that the "atomic flash" may require much more hardening of the power grid and of electrical devices in general, if the nuclear device is detonated above the atmosphere. In this case the electromagnetic pulse originates from a carpet of shortlived artificial plasma in the uppermost layers of the atmosphere.[111,112]

Since the ionosphere affects everyday life at ground level, there have been a giant number of investigations of the ionosphere of the earth and other planets in the solar system.[112-114] The ionosphere can be studied by natural phenomena such as nightglow[115] and whistlers,[116] or by the release of artificial plasma clouds, such as barium vapor, from sounding rockets.[117,118] Probably the most extensive investigation of photoionization in the atmosphere was conducted by a series of

spacecraft which were essentially "flying photoelectron spectrometers."[119] Actually the photon source and the sample were not part of these "spectrometers." The photon source in this case was the sun and the sample was the surrounding and underlying atmosphere. The spacecraft were stationed on orbits with elliptical shapes such that a large range of altitudes was sampled. Below 300 km altitude photoelectrons are produced and lost locally, whereas the photoelectrons detected above 300 km have mostly escaped from lower altitudes.[119] The photoelectron spectra recorded by these spacecraft show some prominent peaks between 22 and 27 eV from photoionization of atomic oxygen and N_2 by the intense He II (30.4nm) flux.[119]

Besides planets, comets also have an ionosphere. Since comets do not have magnetic fields to deflect the solar wind, their ionosphere is maintained by both photon and particle emissions by the sun.[120] Several ionic species, such as N_2^+ and CO^+, have been identified spectroscopically in comets.[121]

The interest in photoionization, insofar as astronomy is concerned, is connected with the emission of high energy radiation by many different types of sources. Since the high energy radiation represents a useful tool for plasma diagnostics, the observation of high-energy photon emissions is expected to enhance considerably our insight in the makeups and the dynamics of unusual astrophysical objects.[122,123]

Many x-ray sources show periodic changes in their brightness. These periodic changes can be caused by the rotation of an object around its axis, or by binary systems such that the astronomer has different views on the object as it revolves.[124-126]

When radio astronomy was discovered by Karl Jansky, it quickly led to the discovery of pulsars, supernova remnants, and interstellar molecules.[127,128] Since x-ray astronomy, similar to radio astronomy, has opened the door to a different "invisible universe," one might wonder if some new exotic astrophysical objects wait to be discovered. The recent advances in x-ray optics and the capability of performing astronomical observations outside earth's atmosphere have not led to such discoveries so far. However, it is hoped that observations of high energy photons will help to discover the products of gravitational collapses, predicted by general relativity and known as black holes.[129] Black holes have frequently been suspected to be part of astrophysical objects with extremely high energy output.[130,131] The system Cygnus X-1 has especially been suspected of containing a black hole.[132] The name "black hole" comes from the fact that no photons can escape the gravitational field of a black hole. Actually, Hawking has shown that due to quantum gravitational effects a black hole can emit particles like photons and neutrinos.[133] However, there is little chance to observe emissions from a black hole against the cosmic background radiation, and so the efforts are directed towards finding black holes by indirect observation. There are two possibilities considered for indirect observation of black holes. The first possibility has to do with the fact that black holes can act as gravitational lenses.[134] Gravitational lenses have recently been discovered in connection with quasars,[135,136] which has led some people to believe that quasars may be images formed by the action of gravitational lenses rather than a unique type of astrophysical objects.[137,138] However, the observation

of gravitational lens does not reveal too much about the lens itself, which means that its observation would be conclusive only in conjunction with additional observations. The second method for indirect observation of black holes is possible for black holes in binary systems, where the black hole essentially sucks in the solar wind of the companion star.[139] As the mass captured by the gravitational field of the black hole spirals inward, it heats up by frictional forces and thermal x-rays are emitted. X-rays produced outside the Schwarzschild sphere of the black hole can reach an outside observer. Such "x-ray binaries" have been observed, but in all cases they could involve a white dwarf or a neutron star instead of a black hole.[140,141] Black holes are rather interesting from a theoretical point of view beyond proving or disproving certain aspects of general relativity. If primordial black holes have played a part in the development of the early universe, the matter-antimatter asymmetry of the universe can be explained within the confines of established theories.[142,143] Based on the time symmetry of general relativity, the existence of the opposite of black holes, namely white holes, has been predicted.[141] However, time-reversal symmetry was recently discovered to break down on the level of subatomic physics.[144]

As previously indicated, photoionization plays an important role in the thermal balance and in the selfabsorption of astrophysical objects. The observed brightness of astrophysical objects is also affected by interstellar and intergalactic dust on the path of the radiation. Low energy radiation is only affected in small regions of the spectrum by interstellar and intergalactic atoms and molecules.

However, Compton scattering and photoionization of interstellar and intergalactic molecules can affect considerably the observed brightness of a source of high energy radiation.[145-147] The dominant opacity of interstellar gas below 91 nm is provided by photoionization of atomic hydrogen.[147] The understanding of photoionization of interstellar and intergalactic matter is therefore necessary for measuring the absolute luminosity of distant sources of high energy radiation.

It follows from the above that molecular clouds close to high energy radiation sources are photoionized to a considerable extent.[148] The photoionization of the interstellar medium is at equilibrium with recombination processes which often involve steps with radiative decays, thus providing valuable information about molecular clouds.[149] Molecular ions are expected to play an important role in chemical processes taking place in the interstellar medium.[150]

Ionization in intense radiation fields such as laser beams can also proceed through the absorption of several photons. In this discussion we have so far come across three types of ionization by electromagnetic radiation

$$M+h\nu \rightarrow M^{+}+e^{-} \qquad \text{photoionization}$$

$$M+h\nu \rightarrow M^{+}+h\nu'+e^{-} \qquad \text{Compton scattering}$$

$$M+h\nu+h\nu'+ \ldots\ldots \rightarrow M^{+}+e^{-} \qquad \text{multiphoton ionization}$$

We can also have emission of more than one electron

$$M+h\nu \rightarrow M^{n+}+ne^{-},\ n>1$$

If n=2, we are dealing with double photoionization by a single photon, which has been observed experimentally.[151,152] No reports could be located in literature about observations of double ionization through the Compton effect or through the absorption of more than one photon. Double photoionizations are rather interesting from a theoretical point of view because they are completely determined by electron correlation.[151] The resulting doubly charged ions are frequently strongly fragmentated.[152]

Photoelectrons can be emitted from surfaces. As stated previously, the discovery of the photoelectric effect was made on surface emission of electrons caused by UV irradiation.[86,87] The emission of photoelectrons from surfaces has proven an irreplaceable tool for the study of surfaces.[153,154] Microscopes have been built which operate through the photoelectric effect, and allow examination of the sample using energy selected photoelectrons.[155] The detection of light by photomultiplier tubes is based on the emission of electrons from surfaces by photons.[156] Other technical applications of the photoelectric effect are in conjunction with gas chromatography and mass spectroscopy. In gas chromatographs the signal can be generated by measuring the ionization caused by a photon source.[157] In mass spectra a photon source can be used for the ionization of the sample.[158-160] Hudgens et al.[161] observed that stereoisomers which give identical fragmentation patterns with electron impact can give distinguishable fragmentation patterns with multiphoton ionization. Resonance enhanced multiphoton ionization can be used for isotope separations.[162] Multiphoton ionization can also be done in transparent liquids.[163] This requires that

the rate of recombination in the liquid is not excessively large. The photoelectrons can of course not be energy analyzed in this case unless the emission is from the surface of the liquid.[164]

The photoionization process may in principle degrade the efficiency of some high-energy lasers. This is due to the fact that rather than undergoing stimulated radiative decay an excited molecule may also undergo photoionization.[165] The rate of photoionization in lasing systems are predictably low, but the problem has been given less thought in connection with laser candidates which fail to show the expected lasing.

High energy lasers are of interest in connection with photoionization in two ways. On one hand, high energy lasers, especially tunable high energy lasers, would be practically ideal photon sources for photoelectron spectrometers. On the other hand, the photoionization process itself is an attractive pumping mechanism for high energy lasers. The pumping action is through an x-ray source which ionizes the sample creating ions with inner shell vacancies. Lasing is then possible if the recombination mechanism of the ions with the electrons involves a suitable radiative decay step.[166-168] The possibility of tunable high energy lasers operating through radiative autoionization has been investigated by Nicolaides and Komninos.[169]

There have been rumors of an operating x-ray laser pumped by a nuclear explosion.[170] This laser, according to Robinson,[171] may find application as a laser weapon in space warfare, but obviously it is of little practical importance, except for the fact that it would demonstrate lasing at high energies.

Photoelectron spectroscopy has developed rapidly in recent years. The achievement of the ultimate analytical sensitivity, single atom detection, by resonance enhanced multiphoton ionization, demonstrates how far this field has progressed.[172-174] Recent developments in photoelectron spectroscopy are based mainly on coincidence techniques. The ions created in the photoionization are mostly in excited states, and they can decay radiatively[175] and through fragmentation.[176] In fragmentation processes, we can be dealing simply with dissociative photoionization if the ion is in a nonbonding state, or, predissociation. Rapid internal conversion processes can preceed predissociation.[177] With coincidence measurements one can follow the fate of state selected ions, be it fluorescence or fragmentation, including the half life times of these processes.[178] Detection of ion fragmentation is of interest in respect to the electronic structure of the parent molecule, since it gives information about the bonding power of the electrons before their removal.[179] Ion fragmentations frequently proceed through several competing channels. For example, in the photoionization of CS_2, besides CS_2^+ also CS^+, S_2^+, S^+, and C^+ are observed.[177] The fluorescence following photoionization has an anisotropic angular distribution and is also polarized.[180-182]

The photoelectrons themselves are spin polarized,[183-184] where the spin polarization has an anisotropic angular distribution.[185] Spin polarization of photoelectrons is caused by spin-orbit interaction, regardless of whether it arises using unpolarized radiation or through a spin transfer from the photon to the electron. In atoms, the continuum wave function consists of a limited number of partial waves. By

measuring the spin polarization of the photoelectron, one often has sufficient information to compute the partial wave amplitudes.[186] It becomes evident that the measurement of spin polarization of the photoelectrons increases the amount of information about the photoionization process. This led Kessler[187] to pose the question: "What is the perfect photoionization experiment?" where "perfect" refers to the amount of information extracted.

The photoionization of negatively charged ions is known as photodetachment.[188] Photodetachment represents a useful process for measuring electron affinities.[188] It has been shown that the main source of the opacity of the atmosphere of the sun at red and infrared wavelengths originates from the continuum absorption of H^-, through photodetachment.[188,189] Photodetachment is a useful tool for the spectroscopic investigation of radicals, many of which are intermediates in chemical reactions. Radicals are often minor components among "debris" from "violent" reactions which have been performed to produce them. Their spectroscopic investigation is therefore complicated by the presence of vast quantities of side products. Negatively charged reaction products can be introduced into ion traps in a mass selective fashion.[190,191] Recently Engelking *et al.*[190] studied CH_2^- by photodetachment with a laser. This produced the famous methylene radical in its ground and some excited states.[190] CH_2 has also been studied through electron capture by CH_2^+.[192] In photodetachments from diatomic negative ions Breyer *et al.*[193] resolved rotational branches.

The inverse photoionization process, radiative electron attachment, has been observed experimentally, but has attracted little attention.[194]

B. THE Xα METHOD

The Xα method aims to solve the Fock equation

$$\hat{F}\psi_i = \lambda_i\psi_i \tag{8-1}$$

directly by using an approximate potential in the Fock operator $\hat{F}$, which is composed of a kinetic energy term $\hat{T}$, a coulomb potential $\hat{V}_C$, and an exchange potential $\hat{V}_E$

$$\hat{F} = \hat{T} + \hat{V}_C + \hat{V}_E \tag{8-2}$$

The coulomb potential energy is due to the interaction of the nuclei with the electron density ρ, which is given by

$$\rho(1) = \Sigma_i n_i \psi_i^*(1)\psi_i(1) \tag{8-3}$$

where n_i is the occupation number of the i-th spin orbital. The electron density and the exchange term can be divided into two components of opposite spin. The Xα method approximates the exchange term by

$$\hat{V}_E\uparrow(1) = -3\alpha[3\rho\uparrow(1)/(8\pi)]^{(1/3)} \tag{8-4}$$

with an analogous expression for the "spin-down" component.

The Fock equations can be solved with the usual LCAO method, or, by the scattered wave method. The scattered wave method is vastly superior in terms of computational efficiency and has therefore been used more widely than the LCAO method. The Xα method itself[195-197] and both methods of solution, the LCAO[198,199] and the scattered wave method,[196] have been described and discussed in great detail in the literature. Sambe and Felton[200,201] developed a semiempirical LCAO-Xα method. Additional semiempirical methods have been developed in connection with the LCAO formalism, such as pseudopotential[202] and

model potential[203] methods. In the semiempirical method by Sambe and Felton, a superposition of atomic electron densities is used. Their calculations deal only with the difference between this electron density and the molecular electron density.[204]

The total Xα energy can be changed by changing α, (in (8-4)), from $-\infty$ to $+\infty$. Since Slater's exchange parameter, α, is an empirical factor in the exchange potential, the variational principle obviously doesn't apply to the Xα method. For an ideal electron gas, Slater's exchange parameter would have to be 2/3. Schwarz looked at the effect the choice of α has in calculations of atoms. He chose two criteria for the choice of α, and he compared the resulting pairs of values obtained for each atom.[205] The values were very close throughout for both criteria, which were:

a. The α for which the statistical total Xα energy = configuration averaged HF energy.

b. Computing the kinetic and potential energy from the Xα orbitals and adjusting α such that the virial theorem is satisfied.

Gopinatham et al.[206] did an investigation similar to the one by Schwarz and concluded that in spin-unrestricted calculations electrons of opposite spin should have different α values. It is a well-known fact that in spin-unrestricted Xα calculations the singlet-triplet splittings are consistently too large. Since these splittings are small they might be sensitive to the choice of α.

Kmetko determined the values α for the atoms by using α as a nonlinear parameter in a variational scheme.[207]

In the LCAO-Xα method the choice of α applies for the whole system, but in the scattered wave method, where the space is partitioned into different regions, one can assign to each region an appropriate value of α.

A wide variety of expressions have been proposed for the exchange potential shown in (8-4). These different approximations for the exchange potential have been surveyed by Rennert.[208] Das developed a formalism for the exchange of a relativistic electron gas with quantum electrodynamical effects included.[209]

The Xα method can be regarded as a modification of the Thomas-Fermi-Dirac (TFD) method which removes all major errors in that method.[210] The TFD method can be applied successfully only to atoms because it does not give rise to bound molecules.[211]

The Xα method, and the related TFD method give for atoms in their ground state electron densities which fall off continuously with increasing radius. The Xα potential and the 3s and 3p radial wave functions are shown for silicon in Figure 8-1 and Figure 8-2. In contrast to this monotone decrease of the electron density, the Hartree-Fock (HF) method gives electron densities which show local maxima.[212,213] It is widely believed that these local maxima mirror the shell structure of the atoms.[202] This is a misconception, however. According to Weinstein et al., in atoms in their ground state, shell structure does not manifest itself as local maxima in the one-electron density.[214] This striking difference in the one-electron densities therefore seems to indicate that, as far as atoms are concerned, the Xα method is more realistic than the HF method.

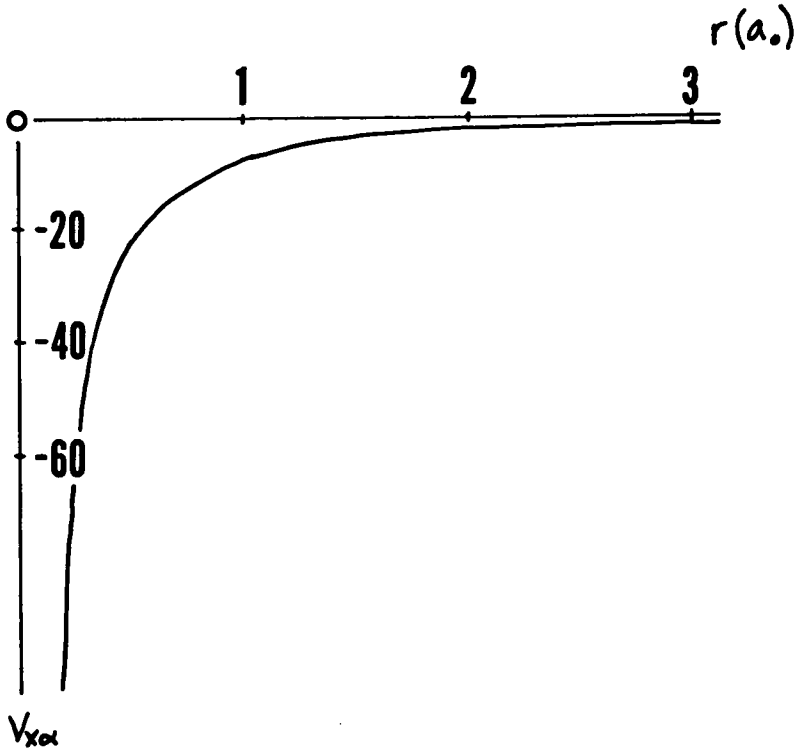


Fig. 8-1. The Xα potential of the transition state for the ionization of the 3s level of the silicon atom.

The Xα potential is expressed in Rydbergs.

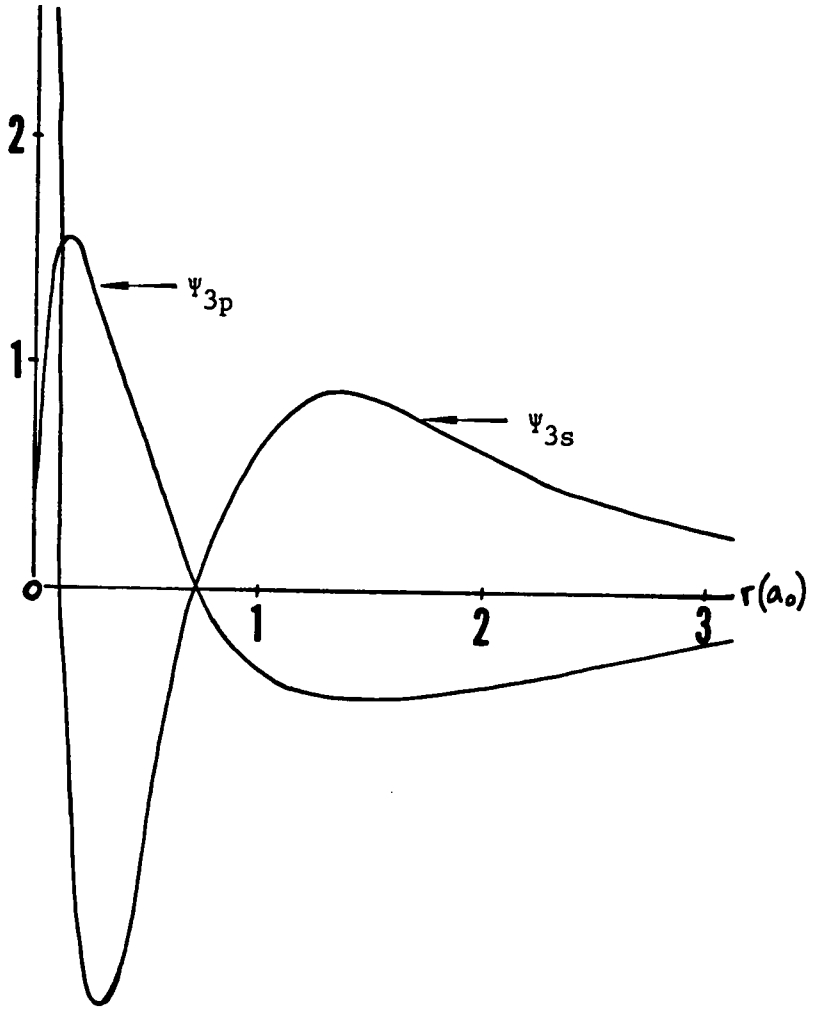


Fig. 8-2. The radial wave functions of the 3s and 3p orbital of silicon computed from the Xα transition state potentials for the removal of an electron from these levels.

The wave functions have been normalized such that $\int(r\Psi)^2 dr = 1$. For the 3s wave function we have $\Psi(0) = 14.04$.

The Xα method also outperforms the HF method in some aspects of *ab initio* calculations on molecules. Alti *et al.* treated twelve small molecules with HF, MS-Xα, and the LCAO-Xα method.[215] They found that the Xα method gives orders of ionization potentials which are in better agreement with experiment in general than the ones computed with the HF method. A smaller such investigation was carried out for CO by Mintmire and Sabin.[216]

The HF theory can give ionization potentials through Koopmans' theorem,[217] or through the ΔSCF method, in which two separate SCF calculations are performed and the ionization potential then becomes the relatively small difference of two large numbers.[218] The main factors which are being ignored when using Koopmans' theorem are the relaxation energy and electron correlation.[218]

The breakdown of Koopmans' theorem correlates closely with the appearance of strong satellite bands in photoelectron spectra.[219] In N_2 Koopmans' theorem breaks down.[220] In the homonuclear diatomic molecules B_2, C_2, and N_2, the molecular orbitals derived from the 2p levels are as shown in the MO diagram of N_2 in Figure 8-3. However, in O_2 and F_2, where the 2s-2p energy difference is large, the 2p derived π and π^* levels are sandwiched in between the 2p derived σ and σ^* level.[221] N_2 can therefore be regarded as the dividing line between these two types of MO diagrams. However, for F_2, which is at the other end of the series, the HF method fails again, both on the Koopmans' theorem and on the ΔSCF level.[215] Besides the ordering of energy levels, there is one additional major difference between the HF and the Xα method. Unlike the single-determinantal HF method, the Xα

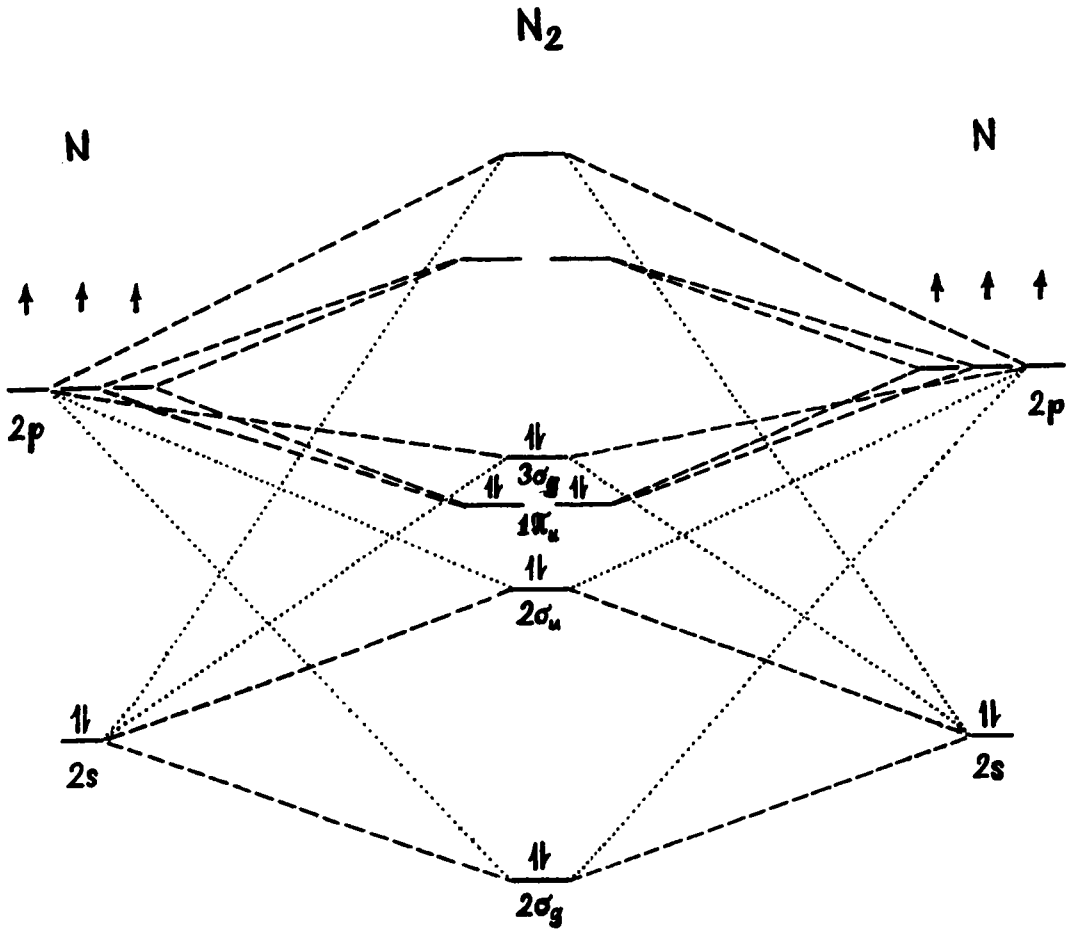


Fig. 8-3. MO diagram of N_2.

method gives the dissociation products from some kind of fragmentation process usually in their correct electronic states.[222] The reasons for obtaining incorrect dissociation products usually have something to do with avoided crossings and with incorrect representations of long-range interactions. Spin-spin magnetic coupling terms contribute considerably to long-range forces.[223] The different treatment of the electron spins in the two methods may therefore be responsible for the different dissociation limits obtained with the HF and the Xα method. It has indeed been reported by Danese,[224] and by Niemczyk and Melius,[225] that appropriate spin-unrestricted calculations have to be done in order to obtain the correct dissociation limits. This is expected to apply in all cases where spin segregation takes place at the dissociation limit.

The avoided crossings are caused by configuration interaction in general. For diatomic molecules, the non-crossing rule applies which states that potential energy curves of states of the same symmetry are not allowed to cross.[226,227] Teller has shown that the noncrossing rule does not apply to polyatomic molecules.[228,229] Katriel and Davidson[230] pointed out that, almost half a century after the work by Teller, references are made to the "noncrossing rule" for polyatomic molecules. The intersections of potential energy surfaces in polyatomic molecules, which can be classified by their geometry, often represent the pathways of reactive collisions.[231] In some cases the noncrossing of potential energy curves of diatomic molecules gives rise to double minimum potential energy curves. Such a case for H_2 has been studied extensively, spectroscopically and through ab initio

calculations.[232,233] Very small perturbations become important in the region of close approach of energy surfaces of the same symmetry.[227] Thus it is found that, for the double-minimum state of H_2, nonadiabatic corrections become important near the region of avoided crossing.[232,233] The nonadiabatic behavior near avoided crossings can be rationalized based on the fact that extensive reorganization of the electronic structure takes place when the system passes through this region, such that electronic and nuclear motions are coupled. The $A^1\Pi$ potential energy curve of CO has a maximum which is of considerable interest for the study of the electronic spectra of CO.[234,235]

As previously stated, a method which never fails to give the correct dissociation limits must reproduce avoided crossings in diatomic potential energy surfaces and also give the correct long range interaction. It is believed that the better performance of the Xα method, in giving proper dissociation products, is connected with the long-range forces which are dominated by spin correlations. It is a well-known fact that the HF theory includes spin correlations for electrons of the same spin, whereas the Hartree-Fock-Slater Hamiltonian treats the spin correlations of electrons of opposite spin as well.[236] If, in addition, the success of the Xα method in giving the correct dissociation limit was attributed to its ability to reproduce avoided corssings, one would in fact state that the Xα method behaves like a method with configuration interaction included. In avoided crossings we have one dominant configuration on the left hand side and a different dominant configuratiuon on the right hand side of the region of avoided crossing. In the region with dominant configurations, a

single determinantal HF description is adequate. In the region of the avoided crossing, the electronic wave function can contain sizable contributions from several configurations, and a configuration interaction method is needed for its proper description.[232,233] There have been multi-configuration HF studies of avoided crossings,[237] but the behavior of the Xα method in this respect is unknown. Since the Xα method is a HF type of approximation, one expects to obtain actual crossings, as in the single determinantal HF method. However, some people have suggested that the Xα method does contain features of a configuration interaction method.[238-240] Especially Salahub et al. seem to be obsessed with this idea. They recently published a paper entitled: "Is there correlation in Xα?"[240]

Salahub et al.[239] have referred to the Hohenberg-Kohn-Sham density functional theory[241-243] in connection with their speculations. The Hohenberg-Kohn theorem is an important part of the density functional theory. It states that the diagonal part of the ground state density matrix completely describes the system.[243] This has led many people to believe that the Hohenberg-Kohn theorem-in principle-allows for a one-particle formalism to completely describe the ground state of a many-particle system, (including correlation energy!).[243] This has led to many unsuccessful efforts to disprove the Hohenberg-Kohn theorem.[243] However, Kryachko[244] pointed out that the Hohenberg-Kohn theorem has been misunderstood. Apparently, the construction of a one-particle formalism for a many-particle system has to be separated into two steps:

Step 1: Construct the exact diagonal part of the density of a many-particle system using a one-particle formalism.

Step 2: From the exact diagonal part of the density matrix of a many-particle system, find the gound state energy using a one-particle formalism.

The Hohenberg-Kohn theorem applies only to the second step. Kryachko states:

> "The construction of a functional of one-particle density only to find the exact ground-state energy is impossible."

It should be pointed out that Salahub et. al. do not claim that the Xα method is such an "exact" one-particle formalism for many-particle systems. They are much less specific, stating that the Xα method has "some configuration interaction included," and, as far as an explanation is concerned, they simply state that these things are presently incompletely understood.[239] Mintmire and Sabin[216] pointed out that, simply by citing numbers and level orderings, efforts to show that there are correlation terms in the Xα functional will convince nobody, simply because the Xα method is too different from the HF method to be viewed as "beyond HF." The Xα formalism does not contain any easily recognizable features for dealing with electron correlation. According to Löwdin, the correlation energy is the difference between the exact (many-body) energy of the system and the energy from the best one-particle description of the system.[245] It is a well-known fact that the HF theory provides the best one-particle description of a many-body system from an energy point of view.[240,246] There are

several ways to deal with electron correlation.[247] One can deal with correlation terms with a single determinantal method by using correlated coordinates.

It has previously been mentioned that the Xα method has never been used to study avoided crossings in diatomic molecules. Of course, there would be two possible outcomes for such an investigation. The more likely one of the two would be that the Xα method would behave analogous to the single determinantal HF method. The unexpected outcome would be one where avoided crossings show up. If this should turn out to be the case, one would have to evaluate the implications regarding the Xα method. Would it prove that there is "correlation" in Xα, or, would it be an idle effort comparable to an attempt of wanting to prove the four-colour map theorem,[248] by colouring the map of England with four pencils of different colours? The objection by Mintmire and Sabin [216] of comparing "apples with oranges" should definitely not be dismissed lightly in connection with such an effort.

In connection with correlation energies, it is of considerable interest that the Xα method predicts stable anions - such as H^-, Cl^-, and O^- - to be unstable.[249] Using the HF method, the solutions for such anions such as N^- and O^- collapse to the atomic solution plus a free electron.[250] In the HF method, these instabilities are due to the omission of correlation terms.[250]

Many-body effects manifest themselves in the photoelectron spectra of most molecules, mainly in the form of satellites, which often borrow intensity from more than one orbital.[251] Many-body effects have been treated theoretically by:

(i) Configuration interaction[252]

(ii) Green's functions[93,253-255]

(iii) Third-order Raleigh-Schrödinger perturbation with[256] and without Feynmann diagrams.[257-259]

The Green's function method has mostly been used with ab initio computations. This method can be used also with any kind of wave functions. It has been used with semiempirical methods, such as CNDO[260] and INDO.[261,262] Levin[263] has developed a scattering formalism with many-body effects included.

Koopmans' theorem does not apply to the Xα method. Instead, Slater's transition state[264-268] is being used. The transition state corresponds to placing the electrons which undergo transitions "half" in the initial state and "halfway" in the final state. Actually this represents an approximation of the original transition state concept corresponding to a truncation of a power series expansion of the total Xα energy.[267] The energy of a transition, in which the occupation numbers of the molecular orbitals change from n_1'', n_2'',..... to n_1', n_2'..... respectively, is given by:

$$\Delta E = \Sigma_i (n_i' - n_i'') \varepsilon_i^{TS}$$

where the ε^{TS}s denote the Xα eigenvalues of the "transition state," defined by the occupancies $(n_1' + n_1'')/2$, $(n_2' + n_2'')/2$,.....[269] The concept of the transition state has been applied to:

(i) Ionization potentials and electron affinities[270-273]

(ii) Electronegativities[274]

(iii) Two-electron x-ray transition energies[275]

(iv) Shake up transition energies.[276]

Williams et al.[277] have explored the possibility of using fractions of completion of the transition other than 1/2. There have also been efforts to incorporate the transition state concept in HF theory,[278,279] and using it for the computation of dissociation energies.[280] The transition state density used for the computation of dissociation energies is the average of the density of the parent species, and the superimposed densities of the fragments.[280]

The main effect of the transition state is to correct for the self energy of the electron in the Hartree-Fock-Slater potential.[281] Gopinathan showed that the relaxation energy in atoms is roughly proportional to the self energy of the ionizing electron. He also showed that, from computed self energies of the electrons, all the ionization potentials could be extracted from a single Xα calculation of the neutral atom.[281]

Using the HF method to compute excited states, one often encounters serious complications. If the excited state is not the lowest state of a given symmetry, the state has to be orthogonalized to a reference state to prevent collapse into a lower-lying state of the same symmetry in the SCF iterations.[282] This problem exists in Xα calculations, but it does not require orthogonalization to a reference state. Entire series of Rydberg states have been computed with spin-restricted and spin-unrestricted Xα calculations without any trouble

reported.[239] There are many SCF algorithms in existence.[283] The wave function is a function of the electron density, $\psi(\rho)$, and, the electron density is a function of the wave function, $\rho(\psi)$, as shown in (8-3). The SCF iterations can be performed by an algorithm which has a certain similarity with the fixed point iterations used to solve nonlinear equations

$$\rho_{i+1} = (1-\alpha_1)\rho_i + \alpha_1\rho(\psi(\rho_i)) \qquad (8\text{-}5)$$

where α_1 is the "mixing parameter" and the subscript of ρ refers to the number of the iteration. In some cases two or more levels of the same symmetry can become nearly degenerate. Such situations can be troublesome. De Alti *et al.*[215] have reported that, for particular choices of sphere radii, in some cases levels were missing. Since in their case, a single state was absent, this problem cannot be dismissed as simply being accidental or connected with shortcomings in the computational procedure. Case and Yang addressed the problem of "missing states" in Xα, but not in detail.[284]

Once the states have all been located, the SCF iterations can still give rise to "jumps." In many cases, this problem can be solved by reducing the mixing parameter at the expense of a reduction of the rate of convergence.

Relativistic corrections often affect computed ionization potentials noticeably. The most readily observable relativistic effects in molecular spectra arise from the interaction of the electron spin with electrical orbital motion and nuclear motion.[285] There have been numerous reports in literature of relativistic Xα formalisms.[286-292] Gagarin and Kovtun[292] treated only the core levels relativistically.

"Core levels" stands for an approximation in multiple scattering calculations, where the wave function of the "core levels" are confined to the atomic sphere; ψ_i=0 outside this sphere. Besides relativistic effects, magnetic terms and quantum electrodynamical corrections could - in principle - be included.[293] However, such minor effects are beyond the expected accuracy of most computations.

In the standard scattered wave Xα method, the "muffin-tin" approximation is used in general. In the muffin-tin approximation, the space is partitioned into spherical regions around the atoms in the molecule or solid and a spherically shaped intersphere region which encloses the "atomic" spheres. The region outside this intersphere region is called the outer sphere region. The potential is spherically symmetric in the atomic spheres and in the outer sphere region. In the intersphere region, the potential is constant. The multiple scattering wave functions are not shaped like this, which means that averaging procedures have to be used to compute the potential from them. Oliveira and Maffeo[294] have pointed out that because of this no true self-consistency can be achieved with the multiple scattering Xα method.

There have been many efforts to drop the muffin-tin approximation altogether, or to partition the space more realistically. The different approaches are listed below:

(i) Introducing dummy spheres, mainly to reduce the space taken up by the intersphere region.[295]

(ii) Using overlapping spheres.[296-298]

(iii) Using truncated spheres,[238,299-301] or the more general cellular method.[452]

(iv) Using arbitrarily shaped boundaries.[302-304]

(v) Perturbation theory.[305,306]

(vi) Numerical calculations on diatomic molecules using prolate spheroidal coordinates.[453]

The following LCAO methods of solution have been reported in literature:

(i) Linear combination of muffin-tin orbitals.[454,455]

(ii) LCAO using Gaussian-type orbitals.[456-458]

(iii) Discrete variational method using Slater-type orbitals.[459-462]

(iv) Discrete variational method using numerical Hartree-Fock-Slater orbitals.[463]

In some cases, Xα potentials are modified artifically. Two important such modifications are:

(i) The "Latter tail," which is used as asymptotic form of the molecular potential of neutral and positively charged species.[307] The asymptotic form of such a potential is coulombic.

(ii) The "Watson sphere," which is used for negatively charged ions to simulate a cloud of positive charge surrounding the anion.[308]

When doing calculations with the muffin-tin approximation, one has to choose the sphere radii. If touching spheres are used, the geometry is often sufficient to determine the radii. Such an example is benzene where we have two different atomic radii, and also two different bond lengths. The bond radii are then determined by the

requirement that the spheres touch the spheres of the "bonded" atoms. One could also imagine molecules with rings where the number of bonds is larger than the number of "different" atoms, where different means here having a different environment. The case where the number of "different" bonds is smaller than the number of "different" atoms is much more common. In this case, additional criteria are needed. In these cases, one often assumes that a pair of atoms "share" the bond length in the ratio of the covalent or ionic radii, whichever is more appropriate.[309] Even if overlapping spheres are being used, a model with touching spheres is usually taken as the starting point. A popular procedure takes a touching sphere model where all its radii, (except the outer sphere radius), are multiplied by a uniform scaling factor (usually 1.3).[215,239] Another popular method consists of charge counting, i.e. finding a sphere enclosing a given integrated charge density.[299] The criterion by Norman[310] is also widely used for the choice of the sphere radii. The Xα method fulfills the quantum mechanical virial theorem only for a particular choice of α, even if the muffin-tin approximation is circumvented. The quantum mechanical virial theorem for a system with coulombic interactions is[311]:

$$\text{potential energy} = -2(\text{kinetic energy}) \qquad (8\text{-}6)$$

Norman explored a scheme where the sphere radii were adjusted such that the virial theorem is satisfied.[310] Garritz et al.[301] proposed that the sphere radii should be chosen such that the interstitial charge is minimized. They studied extensively some possible schemes for space partitioning in multiple scattering calculations. Among other things, they looked into the possibility of shortening the radius

of the outer sphere such that small segments of the atomic spheres overlap with the outer sphere region. Although the intersphere region can be reduced considerably, if the atomic regions penetrate beyond the outer sphere, the outer sphere is usually taken such that it is of minimum size while tangent to the atomic spheres, even in calculations with overlapping atomic spheres.

Although "reasonable" changes of Slater's exchange parameters and of the sphere radii do not cause the energy levels to change drastically,[298] the curvatures of the potential energy surface and the equilibrium geometry are strongly affected by the choice of these empirical parameters, especially the sphere radii.[312-314]

The previously mentioned ability of the Xα method to give dissociation products in their correct electronic states, together with the possibility of computing excited states economically and without much fuss with the scattered wave (SW) method of solution would make the SW-Xα method an attractive tool for the computation of potential energy surfaces. Although the SW-Xα method is unable to give spectroscopic constants and equilibrium geometries with reasonable accuracy, the general shape of the potential energy surfaces should be correct in most cases. Such qualitative results are quite valuable for some purposes such as identifying laser candidates. The SW-Xα method has indeed been used extensively to compute potential energy curves of diatomic molecules,[315-318] especially by Konowalow et al.[316-318] Konowalow et al. use touching spheres, and they adjust Slater's exchange parameter α such that, in homonuclear diatomic molecules, the experimental equilibrium internuclear distance is obtained.

The present author proposed a strategy of obtaining potential energy surfaces of excited states by mapping them pointwise onto the potential energy surface of the ground state, using energies obtained with Slater's transition state.[319] Barrow, Sambe, and Felton[320] later did actual computations with this method, using their semiempirical LCAO-Xα method. Since the muffin-tin approximation evidently gives rise to poor agreement between experimental and computed spectroscopic constants, it would be interesting to see if the transition state could in a sense neutralize its detrimental effects. The transition states of H_2, N_2 and CO had to be computed at several internuclear separations for this work, and it was felt that the computed transition energies might as well be put to good use.

The Xα parameters used in these calculations are shown in Table 8-1. The exchange parameters α were taken from Schwarz.[205] In carbon monoxide, the exchange parameter α for the constant potential and the outer sphere region was taken as the average of the carbon and the oxygen values. The sphere radii were chosen to have the ratio of the covalent radii of C and O.[321]

Several SCF-SW-Xα programs have been written.[284,322-324] One of these programs is available through the "National Resource for Computation in Chemistry."[284] The program used here was originally written by Johnson and Smith,[322,323] and later modified extensively by Liberman and Batra.[325] The "Latter tail"[307] option was used in the Xα calculations. Overlapping spheres and touching spheres were used for H_2. When taking overlapping spheres, the radii of the atomic spheres were kept constant at 1.1 Bohr (Table 8-2). The ionization energy is the

TABLE 8-1

SPHERE RADII AND SLATER EXCHANGE PARAMETERS

	Sphere Radii	α
He	$r_{He} = 1.6a_o$, $r_{out} = 1.601a_o$	$\alpha_{He} = \alpha_{out} = 0.77298$
H_2	$r_H = (1/2)r_{HH}$ or $r_H = 1.1a_o$	$\alpha_H = \alpha_{out} = 0.97804$
Si	$r_{Si} = 2.373a_o$, $r_{out} = 2.374a_o$	$\alpha_{Si} = \alpha_{out} = 0.72751$
N_2	$r_N = (1/2)r_{NN}$	$\alpha_N = \alpha_{out} = 0.751$
CO	$r_C = (1.15/2.13)r_{CO}$ $r_O = (0.98/2.13)r_{CO}$	$\alpha_C = 0.75928$, $\alpha_O = 0.74447$ $\alpha_{out} = (\alpha_C+\alpha_O)/2 = 0.75188$

TABLE 8-2

VERTICAL IONIZATION POTENTIALS OF H_2

	$-\varepsilon$(Ryd)		
$r_{HH}(a_o)$	Touching spheres $r_H = (1/2)\ r_{HH}$	Overlapping spheres $r_H = 1.1\ a_o$	$\varepsilon_{tot}(H_2^+) - \varepsilon_{tot}(H_2)$
0.8	1.743		1.431
1.0	1.629		1.346
1.2	1.556		1.272
1.3	1.495	1.646	1.239
1.4	1.457	1.505	1.209
1.5	1.420	1.468	1.181
1.6	1.388	1.426	1.155
1.8	1.331	1.352	1.110
2.0	1.279	1.290	1.071
2.2	1.237	1.237	1.039
3.0	1.107	1.075	0.959

difference between the total energy of the ion and the parent species. The total energies of H_2 and H_2^+ have been computed with relatively great accuracy.[326,327]

The ionization energies computed with SW-Xα, at different internuclear separations, are shown in Table 8-2. When using touching spheres, the SCF iterations failed to converge when the sphere boundaries approached the origin of the neighboring sphere. One can readily see that the calculation with overlapping spheres does not reproduce too well the dependence of the ionization potential on the internuclear separation. It is expected that the same applies to other molecular properties.

The difference between the computed and the "exact" vertical ionization potentials[326,327] decreases from 0.31 Rydbergs, at small internuclear separation, gradually to 0.15 Rydberegs at the largest internuclear separation. At the dissociation limit, the correlation energy, according to Löwdin,[245] is -7.7 eV; at the united atom limit the correlation energy, (exact energy - HF limit), is roughly -1.1 eV.[328]

The HF method gives large correlation energies at the dissociation limit. Evidently, the Xα method picks up some of this correlation energy in a systematic manner. One would expect that this property of the Xα method does not disappear without a trace at equilibrium geometries.

It would be interesting (and expensive!) to see how calculations, where the potential energy curves are obtained in terms of the total Xα energy, would compare with potential energy curves obtained through the mapping procedure. Notice that at the dissociation limit of H_2, we

would take Slater's exchange parameter as α_H, whereas near the united atom limit α_{He} seems a more appropriate choice.

The reason why an improvement was expected in some cases from the mapping procedure has to do with the constant potential in the intersphere region. The neutral molecule H_2 is expected to have a considerable amount of charge in this region. In the transition state, half an electron is removed and most of the charge is "sucked" into the atomic spheres. In optical transitions, one half of each of the electrons undergoing the transition is in the initial orbital and the other half is in the final orbital. It would be unlikely that a large amount of charge from both the initial and the final orbital is simultaneously located in the intersphere region. These qualitative arguments led the author to believe that there is something to be gained from the mapping procedure in terms of "neutralizing" the errors introduced by the muffin-tin approximation. Of course, Barrow et al.[320] have already applied the mapping procedure, but since they did not use the muffin-tin approximation they did not answer the question which inspired the author to propose this procedure.

The transition state energies, for the ionization of N_2 and CO to the three lowest levels of N_2^+ and CO^+ are shown in Table 8-3 and in Table 8-4. At $r_{CO} = 2.05\ a_o$ the SCF iterations for the transition state of the ionization of the 5σ orbital did not converge.

Recently, configuration interactions have been published for N_2^+ by Collins et al.,[329] and for 25 bound states of CO^+ by Honjou and Sasaki.[330] Singh and Rai[331] published potential energy curves of N_2^+ and CO^+ obtained from spectroscopic data using the RKR method. In both

TABLE 8-3

ENERGY EIGENVALUES OF THE CONVERGED Xα POTENTIALS FOR TRANSITION STATES OF N_2

X: $N_2(X^1\Sigma_g^+) \rightarrow N_2^+(X^2\Sigma_g^+) + e^-$

A: $N_2(X^1\Sigma_g^+) \rightarrow N_2^+(A^2\Pi_{ui}) + e^-$

B: $N_2(X^1\Sigma_g^+) \rightarrow N_2^+(B^2\Sigma_u^+) + e^-$

$r_{NN}(a_o)$	X(Ryd)	A(Ryd)	B(Ryd)
1.6	-0.9606	-1.7156	-1.1211
1.75	-1.0000	-1.5685	-1.1999
1.9	-1.0318	-1.4525	-1.2767
2.05	-1.0578	-1.3604	-1.3481
2.08	-1.0622	-1.3447	-1.3615
2.2	-1.0781	-1.2867	-1.4122
2.35	-1.0932	-1.2275	-1.4693
2.5	-1.1023	-1.1790	-1.5187
2.7	-1.1059	-1.1271	-1.5739
2.9	-1.1014	-1.0857	-1.6175
3.1	-1.0911	-1.0524	-1.6512
3.3		-1.0245	
3.6		-0.9899	

TABLE 8-4

ENERGY EIGENVALUES OF THE CONVERGED Xα POTENTIALS FOR TRANSITION STATES OF CO

X: $CO(X^1\Sigma^+) \rightarrow CO^+(X^2\Sigma^+) + e^-$

A: $CO(X^1\Sigma^+) \rightarrow CO^+(A^2\Pi_i) + e^-$

B: $CO(X^1\Sigma^+) \rightarrow CO^+(B^2\Sigma^+) + e^-$

$r_{CO}(a_o)$	X(Ryd)	A(Ryd)	B(Ryd)
1.6	-0.8885	-1.7511	-1.2172
1.75	-0.9092	-1.6141	-1.3045
1.9	-0.9324	-1.5038	-1.3636
2.05		-1.4122	-1.3993
2.13	-0.9711	-1.3697	-1.4111
2.2	-0.9831	-1.3356	-1.4187
2.35	-1.0074	-1.2706	-1.4291
2.5	-1.0282	-1.2156	-1.4361
2.7	-1.0458	-1.1541	-1.4462
2.9	-1.0560	-1.1038	-1.4602
3.1	-1.0548	-1.0623	-1.4753
3.3		-1.0279	
3.6		-0.9860	

of these ions the lowest Σ state and the lowest Π state cross. In the paper by Singh and Rai[331] the potential energy curve of the lowest Σ state of N_2^+ stops short of the point of intersection with the Π state. For CO^+, the point of intersection is located at $r_{CO} \sim 1.48$ Å. The transition state energies computed with Xα coincide near $r_{CO} = 1.7$ Å (Table 8-4).

The transition state energies computed for the ionization of N_2 and CO were used to compute spectroscopic constants of the ions in the different states, from the spectroscopic constants of the parent molecules. The idea is simple. Let us assume that we have the potential energy curve V"(r) of the parent molecule. The potential energy curves of the ions are given by I.P.(r), the vertical ionization potentials at different internuclear separations.

$$V'(r) = V''(r) + I.P.(r) \tag{8-7}$$

Let us take harmonic potentials for V' and V"

$$V'(r)=T_e+(1/2)k'(r-r_e')^2 \quad \text{and} \quad V''(r)=(1/2)k''(r-r_e'')^2 \tag{8-8}$$

We approximate I.P.(r) in a least squares sense by

$$I.P.(r)=c_0+c_1(r-r_e'')+c_2(r-r_e'')^2 \tag{8-9}$$

The singly primed spectroscopic constants can then be expressed in terms of the doubly primed spectroscopic constants and the coefficients in the above equation:

$$k'=2c_2+k''$$

$$r_e'=r_e''-(c_1/k')$$

$$T_e=c_0-(1/2)k'(r_e'-r_e'')^2 \qquad (8\text{-}10)$$

Morse potentials were also used to represent V' and V". When using the Morse potential, the spectroscopic constants have to be computed by a nonlinear least squares calculation. In this case, there is the danger of computing a set of parameters which corresponds to a local minimum rather than the global minimum. The minimization consisted simply of a pedestrian search. Several sets of "reasonable" starting values gave identical results in all cases.

One could expand the Morse potentials in power series, such that a linear system has to be solved in the least squares analysis.

$$V''(r)=D''(1-\exp(-\beta''(r-r_e'')))^2$$

$$\sim b_2(r-r_e'')^2 + b_3(r-r_e'')^3 \qquad (8\text{-}11)$$

$$V'(r)=T_e+D'(1-\exp(-\beta'(r-r_e')))^2$$

$$\sim c_0 + c_2(r-r_e')^2 + c_3(r-r_e')^3 \qquad (8\text{-}12)$$

We simply use a Taylor series expansion for the Morse potential in which case:

$$b_2=(\beta'')^2D'' \qquad b_3=-(\beta'')^3D''$$

$$c_0=T_e \qquad c_2=(\beta')^2D' \qquad c_3=-(\beta')^3D' \qquad (8\text{-}13)$$

Let us approximate the vertical ionization potentials by a power series

$$I.P.(r)=d_o+d_1(r-r_e'') + d_2(r-r_e'')^2 + d_3(r-r_e'')^3 \qquad (8\text{-}14)$$

This gives

$$r_e'=r_e''-[[b_2+d_2\pm((b_2+d_2))^2-3c_3d_1)^{(1/2)}]/(3c_3)]$$

$$T_e=c_0=d_0-c_2(r_e'-r_e'')^2 + c_3(r_e'-r_e'')^3$$

$$\beta' = -c_3/c_2$$

$$D' = c_2^3/c_3^2 \qquad (8\text{-}15)$$

where

$$c_3=b_3+d_3 \quad \text{and} \quad c_2=b_2+d_2+3c_3(r_e'-r_e'') \qquad (8\text{-}16)$$

An ambiguity of signs arises for the expression for r_e'. This also affects T_e and the signs of β' and D'. If we take the plus sign in (8-15), β' and D' will both be negative, clearly an unacceptable outcome, leading us to conclude that the minus sign gives the physically meaningful solution. In some cases, the argument of the square root is negative, as was the case for the $A^2\Pi_i$ state of CO^+.

The power series expansion of the Morse potential should give rise to computed spectroscopic constants which are close to the ones obtained with the nonlinear least squares approximation. The problem with obtaining a complex number for r_e' has already been mentioned. The Taylor series are valid only in the neighbourhood of the expansion centers. If the expansion centers (r_e' and r_e'') are far apart, the approximation breaks down. We conclude that it is unsafe to replace

the Morse potentials with a truncated power series for the present purpose.

For the Morse approximation (nonlinear least squares) the difference between computed and experimental r_e ranges from 0.027 a_o to 0.132 a_o in magnitude (Table 8-5). Gunnarsson et al.[332] did Xα calculations with non-muffin-tin corrections. They could compute r_e to an accuracy of 0.1-0.2 a_o, and the harmonic constants to an accuracy of 100-200 cm^{-1}. The harmonic constants computed here differ by several hundred wave numbers from the experimental harmonic constants. However, the harmonic constants computed with the different approximations differ widely among themselves, which is not the case for r_e. It is to be expected that the agreement with experiment could be improved by using more accurate potential energy curves. In large scale CI computations, equilibrium internuclear separations and harmonic constants can be obtained with considerably greater accuracy. The computed values for r_e are expected to deviate from the experimental values by not more than 0.08 a_o, and the harmonic constants by no more than 30 cm^{-1}. Although such impressive agreement could not be obtained here, the results appear to be as accurate as the ones where corrections were made for the muffin-tin approximation. Since the mapping procedure requires the same effort as any point-by-point computation of potential surfaces, its application can be recommended based on encouraging, but somewhat inconclusive results obtained here.

Many computations of one-electron properties from MS-Xα wave functions have been reported.[334-343] Recently Cook and Karplus presented two-electron properties obtained from MS-Xα wave functions.[344]

TABLE 8-5

COMPUTED SPECTROSCOPIC CONSTANTS

The Anharmonic Approximations Refer to:

(a) Using a Power Series
(b) From a Nonlinear Least Squares Fit

"Adiabatic" Ionization Potentials (Ryd)

Molecule	Ion State	Harm.	Anharm. (a)	Anharm. (b)	Exp.
N_2	X	1.056	1.058	1.059	1.145
N_2	A	1.326	1.295	1.303	1.228
N_2	B	1.323	1.328	1.328	1.377
CO	X	0.972	0.967	0.969	1.030
CO	A	1.333		1.315	1.219
CO	B	1.390	1.407	1.405	1.448

$r_e(a_o)$

Molecule	Ion State	Harm.	Anharm. (a)	Anharm. (b)	Exp.
N_2	X	2.019	2.025	2.021	2.110
N_2	A	2.236	2.337	2.271	2.220
N_2	B	1.910	1.946	1.946	2.030
CO	X	2.069	2.071	2.066	2.107
CO	A	2.321		2.381	2.350
CO	B	2.035	2.062	2.077	2.209

TABLE 8-5 (CONTINUED)

$\omega_e (cm^{-1})$

Molecule	Ion State	Harm.	Anharm. (a)	Anharm. (b)	Exp.
N_2	X	2261	2475	2482	2207
N_2	A	2518	1000	1831	1904
N_2	B	2237	2793	2902	2420
CO	X	2114	2395	2397	2214
CO	A	2331		1549	1562
CO	B	2026	2160	2004	1734

$\omega_e x_e (cm^{-1})$

Molecule	Ion State	Anharm. (a)	Anharm. (b)	Exp.
N_2	X	12	17	16
N_2	A	495	15	15
N_2	B	7	14	23
CO	X	10	15	15
CO	A		15	14
CO	B	10	11	28

According to Green's theorem,[345] the integration in the intersphere region can be converted to surface integrals over its boundaries. In the case of touching spheres, all boundaries have a spherical shape and the integrals are straightforward to compute. If the spheres overlap, the integrals become much more difficult to evaluate. Case and Karplus[335] circumvented this difficulty by simply redistributing the intersphere electronic charge among the basis functions centered at the individual atomic spheres. Thereafter the integration over the intersphere region is not needed. Roche et al.[346] used overlapping spheres for the computation of photoionization cross sections and β values. They did not report any details about the integration over the intersphere region.

SW-Xα wave functions can be characterized by their ℓ-type population in the various spherical regions. These ℓ-type populations refer to the orbital being ionized indicated by the states of the ions, (N_2^+ and CO^+), and computed for the transition states of the ionizations.

At the united atom limit, the $3\sigma_g$ orbital of N_2 becomes the 3s level of the silicon atom.

The ℓ-type population in the outer sphere shows indeed an increase in s-character towards smaller internuclear distances (Table 8-6). The $2\sigma_u$ level of N_2 shows an expected increase in p-character towards small r_{NN}. The state B of N_2^+, which results from the ionization of the $2\sigma_u$ level of N_2, is not represented too well by a single determinantal wave function. It mixes strongly with the state C of N_2^+, which has the dominant configuration:[347,348]

$$C^2\Sigma_u^+: \ldots\ldots (2\sigma_u)^2(3\sigma_g)^1(1\pi_u)^3(1\pi_g)^1 \qquad (8\text{-}17)$$

TABLE 8-6

ℓ-TYPE POPULATION ANALYSIS OF THE BOUND STATES OF N_2 AT DIFFERENT INTERNUCLEAR DISTANCES

State of the ion	$r_{NN}(a_o)$	Outer sphere						Nitrogen atomic sphere			
		ρ_{out}	%s	%p	%d	%f	%g	ρ_N	%s	%p	%d
X	1.6	0.52	74		25		1	0.17	1	98	1
X	2.35	0.25	51		46		3	0.30	8	92	0
X	3.1	0.11	32		62		6	0.38	5	95	0
A	1.6	0.31		98		2		0.12		99	1
A	2.5	0.14		92		8		0.25		100	0
A	3.6	0.04		78		22		0.37		100	0
B	1.6	0.58		99		1		0.11	68	32	0
B	2.35	0.23		96		4		0.27	85	15	0
B	3.1	0.08		91		9		0.39	95	4	0

$\rho_{inter\text{-}sphere} = 1-\rho_{out}-2\rho_N$.

The ℓ-type population analyses of the orbitals of CO in their transition states are consistent with the united atom limits shown in Figure 8-5.

The MO diagram constructed for N_2, as shown in Figure 8-4, was obtained from ab initio calculations by Mulliken.[349] In Tables 8-6 and 8-7, ρ denotes the integrated charge density in the various regions.

Frequently the virial ratio V/2T is examined to judge the quality of ab initio computations. For molecules, the actual virial theorem has a term which contains the gradient of the potential energy surface.[350] Far from the equilibrium geometry this term becomes important. This makes it impossible to follow the "quality" of the wave functions through different internuclear separations using the virial theorem.

It has been mentioned that the use of overlapping spheres gives rise to unreliable geometry-dependence of the vertical ionization potentials. It will be shown later that the results obtained, with overlapping spheres, for the differential cross sections are also discouraging. It should be pointed out that overlapping spheres could be used in a number of ways. In this work the sphere radii were kept constant at $r_{HH} = 1.1\ a_o$. It may be that other schemes of choosing sphere radii will give more reliable results.

C. THE COMPUTATION OF PARTIAL PHOTOIONIZATION CROSS SECTIONS FROM SW-Xα WAVE FUNCTIONS

According to Yang's theorems,[351] the angular distribution of photoelectrons emitted from a randomly oriented sample by polarized dipole radiation is given by the expression[352]

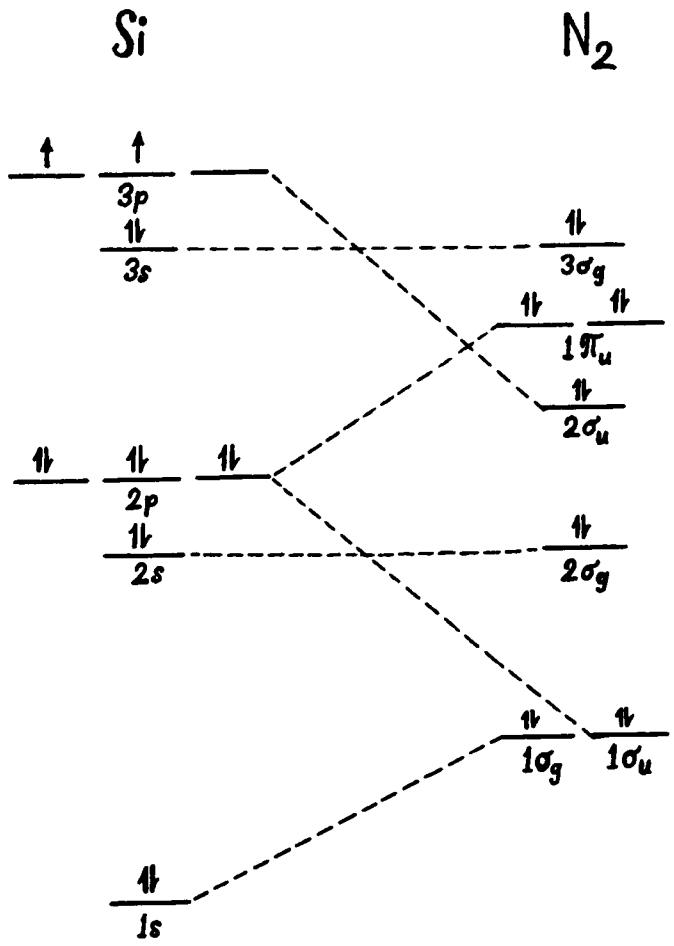


Fig. 8-4. MO diagram of N_2 showing the united atom limit, (the silicon atom).

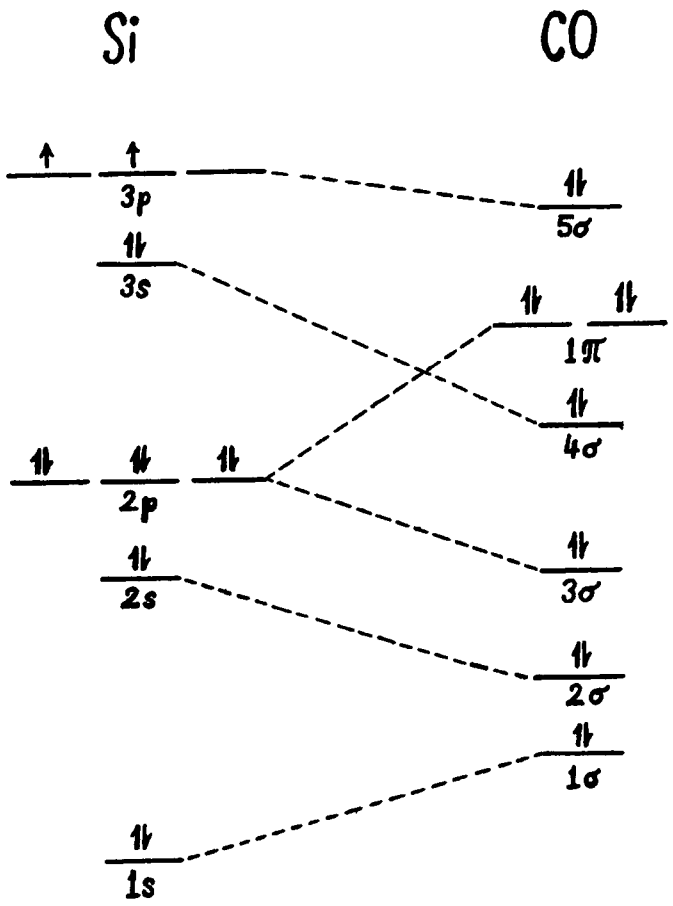


Fig. 8-5. MO diagram of CO showing the united atom limit, (the silicon atom).

TABLE 8-7

ℓ-TYPE POPULATION ANALYSIS OF THE BOUND STATES OF CO AT DIFFERENT INTERNUCLEAR DISTANCES

State of the ion	$r_{CO}(a_o)$	Outer sphere						Carbon atomic sphere				Oxygen Atomic Sphere			
		ρ_{out}	%s	%p	%d	%f	%g	ρ_C	%s	%p	%d	ρ_O	%s	%p	%d
X	1.6	0.62	62	26	9	0	0	0.16	16	82	2	0.08	11	88	0
X	2.35	0.31	57	16	26	0	1	0.34	36	63	1	0.18	0	100	0
X	3.1	0.12	38	3	54	0	5	0.36	22	77	1	0.39	1	99	0
A	1.6	0.29		95	3	2	0	0.07		97	3	0.19		100	0
A	2.5	0.12		82	8	9	1	0.09		98	2	0.44		100	0
A	3.6	0.04		67	10	21	2	0.11		99	1	0.64		100	0
B	1.6	0.47	6	75	18	2	1	0.05	80	19	1	0.28	21	79	0
B	2.35	0.19	0	79	14	6	1	0.21	95	5	0	0.36	27	73	0
B	3.1	0.08	13	79	0	8	0	0.57	100	0	0	0.16	38	61	1

$$\rho_{\text{inter-sphere}} = 1-(\rho_{out} + \rho_C + \rho_O)$$

$$\frac{d\sigma(h\nu)}{d\Omega} = (4\pi)^{-1}\sigma_{tot}(h\nu)\ [1 + \beta P_2(\cos\Phi)] \qquad (8\text{-}18)$$

where Φ is the angle between the direction of polarization and the direction of the outgoing photoelectron. If unpolarized radiation is used, the partial cross sections are

$$\frac{d\sigma(h\nu)}{d\Omega} = (4\pi)^{-1}\sigma_{tot}(h\nu)\ [1-(1/2)\beta P_2(\cos\Theta)] \qquad (8\text{-}19)$$

where Θ is now the angle between the incident photon beam and the direction of the ejected photoelectron. P_2 represents a Legendre polynomial.[3]

Parzynski[353] published an expression for the angular photoelectron distributions due to elliptically (and circularly) polarized radiation.

According to Ritchie,[354] circularly polarized radiation gives different distributions for the enantiomers of optically active molecules. (Circularly polarized radiation can be used for asymmetric synthesis.[355])

Small variations of the wave function change the energy only in second order.[356] Oscillator strengths are computed with a lower accuracy than the energy.[357,358] For this reason computed oscillator strengths are a sensitive probe of the accuracy of the wave functions used to compute them. In photoionizations the wave function representing the photoelectron is a continuum wave function. Photoionization cross sections and angular distributions of the photoelectrons will be greatly influenced by the representation chosen for this wave function of the photoelectron.

For the photoionization of one-electron systems, such as the hydrogen atom and the hydrogen molecular ion, H_2^+, the initial and the final wave function of the electron can in principle be computed to any degree of accuracy. For hydrogenic atoms, calculations have been published for common photoionization[359,360] and photoionization in electric[361] and magnetic fields.[362] Cross sections for multiphoton ionizations of atomic hydrogen have been published in several papers.[363-365]

In the hydrogen molecular ion, there are effects of nuclear motion. This system has been treated to various degrees of approximation.[366-370]

Computations on more complex systems require that drastic approximations be made in several respects. The wave function of the photoelectron can be expressed as a plane-wave[371,372] or an orthogonalized plane-wave.[372-375] The plane-wave approiximation has shortcomings, expecially at threshold.[372]

To find a suitable representation for the wave function of electrons in the continuum, Dill et al.[376-380] developed the continuum multiple scattering model.

The electromagnetic field of radiation is represented by the oscillating electric and magnetic vectors F and H, which are perpendicular to each other. They are equal in magnitude if F is measured in electrostatic units and H in electromagnetic units. According to Maxwell's equations, the energy density of the radiation field is:

$$\rho(\omega)d\omega = (\overline{F^2} + \overline{H^2})/(8\pi) = \overline{F^2}/(4\pi) \qquad (8\text{-}20)$$

The interaction of the electromagnetic field with the electron will be almost completely due to its electric field; the contribution from its magnetic field is negligible in general. This is because the force exerted by an electric field on a particle of charge e is eF, whereas the force excerted an it by the magnetic field is eH(v/c), where v is the velocity of the particle. The influence of the magnetic field is important only for relativistic electrons.

The electric component of the radiation field can be expressed in a multipole expansion, but in practice only the dipole operator is used in most cases to represent the radiation field. For the photoionization of H_2, terms from electric and magnetic multipoles have been computed.[381] The electric dipole gave the dominant contribution to the cross sections. Different mathematical representations are possible for the multipole moments.[382] For the dipole moment operator, three expressions can be used[383] which can be interconverted by commutation relations:[384]

(i) the dipole length operator $\hat{D}$

(ii) the velocity operator $\hat{P}$

(iii) the acceleration operator $\hat{A}$

If the wave functions used are exact, any choice of the dipole moment operator will yield identical results. According to Seaton,[383] the dipole length and the velocity operator give results of comparable accuracy when using approximate wave functions, whereas the acceleration operator frequently gives inferior results. Several papers have been published where the results obtained from the dipole length and the dipole velocity representation have been compared.[385-387] Thiel[387]

made a comparative study involving different continuum wave functions and different dipole moment operators.

The SW-Xα method has been used by a number of authors to compute optical intensities[388] and photoionization cross sections, including the angular distribution of the photoelectrons.[346,376-380,380-392] When computing cross sections with the HF method, one has to integrate over the coordinates of each particle in its initial and final orbital. According to Slater,[266] when using the transition state, one obtains very good values for the transition probability by integrating only over the coordinates of the electrons which undergo transitions. Slater states that this is suggested by Bohr's correspondence principle.[266] (It is not quite clear how the correspondence principle could have led to Slater's conclusion.)

When the continuum wave function is being expressed as a partial wave expansion, the cross sections are obtained by summation of the contributions from the different partial waves. For the cross sections, there are no cross terms between different partial waves. Dill and Dehmer[394] have proposed a "partial wave analysis," where the contributions of the sets of partial waves with the same ℓ are compared. Partial waves with the same ℓ experience identical centrifugal "barriers," which give rise to shape resonances.

In the computation of the β values, the partial waves mix and we have diagonal and off-diagonal terms in the summation, both of which have intrachannel and interchannel contributions. However, a small portion of the partial waves contribute the lion share to the sum. Based on this, Thiel[395] performed a "partial wave analysis" of the β values computed for linear molecules.

As previously mentioned, photoelectron spectra often contain a large number of satellites, especially in the intervalence region. Most of these satellites are not compatible with a single-particle picture for photoionization.[93,396-401] Shakeup transitions in photoelectron spectra can be reproduced by SW-Xα calculations, as long as they are compatible with a one-particle picture of photoionization.[402-407]

At high energies, the cross sections and β values of inner shell orbitals are almost identical with the corresponding cross sections and β values of isolated atoms. There exist various schemes which obtain molecular cross sections as weighted sums of atomic cross sections plus multi-center interference effects.[408-411] Near threshold, subtle features of the molecular potential become important. Grimm et al.[412,413] pointed out that the β values of inner shells of bound atoms differ considerably from the β values of isolated atoms near threshold. In photoelectron spectra, one can often observe bands which are split by spin-orbit interaction.[414] Very strong Jahn-Teller coupling can also give rise to multiple-peaked structure of the band shape.[415] Photoelectron peaks arising from spin-orbit splitting or Jahn-Teller splitting of the same initial orbital have nearly the same β values.[416] This makes it possible, in some cases, to resolve overlying bands in photoelectron spectra by detecting shifts in the angular distribution parameter β.[417]

The recently developed dynamical theory for the computation of photoionization cross sections is somewhat related to the methods which compute molecular cross sections from atomic cross sections and

multicenter interference effects.[418,419] The dynamical theory includes the independent atom approximation in the lowest order.

Cross sections and β values have been computed by the author for H_2, N_2, and CO at different internuclear separations and at their united atom limits, namely the helium and the silicon atom. Atomic s orbitals have β=2, regardless of the energy of the photon if relativistic effects are ignored.[420] In addition, the angular distribution is affected by the transfer of linear momentum from the photon to the electron.[92] This effect is noticeable only at high energies of the photon and is neglected in this work.

The computer program used to compute the cross sections was originally written by James Davenport,[422] and has later been fused by Sherrod and Grimm[709] with the Xα program written by Johnson and Smith.[322,323]

Davenport assumes that the continuum wave functions asymptotically approach coulomb wave functions corresponding to a coulombic long-range potential. The effective charge of the coulomb potential was taken such that it simulates the charge of the ionized species, (Z_{eff} = 1). The coulombic long-range behaviour was put in effect through the Latter "tail."[307]

The computed ionization potential of the transition state of helium was 27.28 eV, and its experimental I.P. was observed at 24.59 eV.[423] The orbital energies of the neutral silicon atom were -1782.8 eV, -140.8 eV, -98,3 eV, -11.67 eV and -5.27 eV for the 1s, 2s, 2p, 3s, and 3p orbitals respectively. The ionization potentials obtained from the transition states were 1855.4 eV, 152.4 eV, 110.8 eV, 14.70 eV, and 7.36 eV. The first I.P. of Si has been observed at 8.15 eV.[424]

Davenport uses the acceleration operator to compute the dipole moment amplitudes. It has previously been stated that this operator often gives inferior results. However, in the acceleration operator, the gradient of the molecular potential occurs as a factor. Since the intersphere region has a constant potential, it should give no contribution to the dipole moment amplitudes. This probably simplifies things. In addition, the potential - and therefore the wave function in the intersphere region - is not too realistic. Therefore, the acceleration operator, which vanishes in this region, might in fact give better results than the other two dipole moment operators.

The photoionization cross sections of helium have served as a test case for all sorts of theories for the computation of photoionization cross sections,[425] some with autoionization included.[426] Although the calculated I.P. of He does not agree too well with the experimental value, the photoionization cross sections shown in Table 8 agree with the experimental cross sections within experimental accuracy.[425] The cross sections in are given in megabarns (Mb), where 1 Mb = 10^{-18} cm^2. In Table 8, the cross sections for the photoionization of the s orbitals of silicon are also listed. The cross sections and β values for the photoionization of the p orbitals of silicon have been computed from the Xα potential of the neutral molecule, and from the transition state potentials, (Tables 8-9 and 8-10). The results obtained with the transition states were compared with the ones obtained by Manson,[420] using the Hartree-Slater central field method. Besides Manson, a number of authors have published computed photoionization cross sections for atoms.[411]

TABLE 8-8

ATOMIC PHOTOIONIZATION CROSS SECTIONS OF HELIUM AND SILICON

	σ(Mb)			
E_e(Ryd)	He(1s)	Si(1s)	Si(2s)	Si(3s)
0.01	7.32	17.15	0.469	0.034
0.02	7.26	12.95	0.470	0.040
0.05	7.11	9.74	0.473	0.060
0.075	6.98	9.00	0.476	0.078
0.1	6.86	8.68	0.478	0.097
0.15	6.61	8.47	0.482	0.136
0.2	6.37	8.44	0.485	0.175
0.3	5.92	8.41	0.491	0.247
0.4	5.50	8.24	0.495	0.310
0.5	5.11	7.91	0.498	0.361
0.75	4.27	6.64	0.500	0.443
1.0	3.59	5.13	0.497	0.475
1.5	2.59	2.52	0.482	0.463
2.0	1.92	0.94	0.464	0.417
3.0	1.13	0.00	0.434	0.322
4.0	0.72	0.18	0.408	0.251
5.0	0.48	0.37	0.389	0.199

TABLE 8-9

PHOTOIONIZATION CROSS SECTIONS AND ASYMMETRY PARAMETERS OF THE SILICON ATOM

E_e(Ryd)	σ_{2p}(Mb)	σ_{3p}(Mb)[a]	σ_{3p}(Mb)[b]	β_{2p}	β_{3p}^{a}	β_{3p}^{b}
0.01	5.23	125.45		0.93	0.94	
0.02	5.32	119.06		0.84	1.03	
0.05	5.55	100.92		0.67	1.22	
0.075	5.67	87.29		0.58	1.34	
0.1	5.74	75.15	27.28	0.51	1.43	1.21
0.15	5.79	55.30		0.42	1.58	
0.2	5.77	40.57	18.29	0.38	1.69	1.48
0.3	5.63	22.08	11.24	0.35	1.85	1.65
0.4	5.50	12.36	6.73	0.36	1.93	1.78
0.5	5.40	7.15	4.00	0.39	1.93	1.86
0.75	5.28	2.20	1.14	0.49	1.41	1.79
1.0	5.27	1.05	0.41	0.60	0.23	1.01
1.5	5.24	0.92	0.24	0.78	-0.14	-0.25
2.0	5.07	1.07	0.29	0.92	0.49	0.33
3.0	4.50	1.05		1.11	1.08	
4.0	3.97	0.88		1.22	1.31	
5.0	3.47	0.70		1.30	1.44	

[a]This work.

[b]S. T. Manson, J. Electron Spectrosc. Relat. Phenom. 2(5), (1973) 482-484.

TABLE 8-10

PHOTOIONIZATION CROSS SECTIONS AND ASYMMETRY PARAMETERS OF THE SILICON ATOM FROM THE Xα POTENTIAL OF THE NEUTRAL ATOM

E_e(Ryd)	σ_{2p}(Mb)	β_{2p}	σ_{3p}(Mb)	β_{3p}
0.01	1.44	1.17	112.87	0.75
0.02	1.50	1.03	107.54	0.83
0.05	1.69	0.75	93.17	0.96
0.075	1.85	0.60	82.79	1.08
0.1	2.02	0.49	73.64	1.16
0.15	2.37	0.35	58.38	1.29
0.2	2.72	0.27	46.35	1.40
0.3	3.41	0.20	29.15	1.57
0.4	4.02	0.21	18.17	1.70
0.5	4.51	0.25	11.21	1.80
0.75	5.21	0.37	3.27	1.88
1.0	5.40	0.50	1.04	1.36
1.5	5.27	0.71	0.47	-0.27
2.0	5.06	0.86	0.61	0.31
3.0	4.68	1.06	0.74	1.01
4.0	4.22	1.19	0.68	1.29
5.0	3.70	1.28	0.56	1.42

Silicon is of importance from the point of view of astrophysics because the spectra of Si and Si^+ contribute significantly to the opacity of Ap stars.[429]

N_2 and CO are isoelectronic. If one writes a Lewis dot structure for CO the oxygen has a formal plus charge:

$$: \bar{C} :: \overset{+}{O} : \qquad (8\text{-}21)$$

However, in metal carbonyls, the CO group attaches with the carbon atom to the metal.[430] It turns out that the dipole moment of CO changes sign very close to $r_{CO} = r_e$.[431,432] In solid CO, the carbon and the oxygen end of this molecule can interchange positions in the lattice. This randomness contributes considerably to the entropy of solid carbon monoxide.[433]

In metal carbonyls, the CO ligands stabilize low oxidation states of the metal.[434] This and other properties of metal carbonyls are explained by backbonding. While it is generally felt that backbonding is essential for a realistic description of the electronic structure of metal carbonyl compounds[435] and CO chemisorption on metals,[436] Johnson and Wahlgren[437] stated that the Xα method shows no backbonding in metal carbonyls, and that the backbonding concept is of very limited usefulness. Later Larsson and Braga[438] flatly rejected these findings by Johnson and Wahlgren, noting that Xα calculations predict a strong back-donation effect for $Ni(CO)_4$. It appears that this controversy is far from over. Recently, Davenport[439] mentioned in a paper that the Xα method does not show any back-donation for metal carbonyls.

The chemisorption of CO on metal surfaces is of considerable commercial interest. Coal or lignite derived CO can be converted to marketable chemicals,[440] mainly via the Fischer-Tropsch[441] reaction, which is a heterogeneous hydrogenation of CO. The Fischer-Tropsch reaction, which is reversible, has also been considered for storage and transport of energy.[442] The CO molecule bonds strongly to metal surfaces.

Dittrich et al.[443] measured energies of desorption of CO as 83, 133, 116, and 67 kJ/mol for Fe, Co, Ni, and FeCo alloy respectively. CO can polymerize on surfaces to give $(CO)_n^{m-}$, where n = 2,3,....,6 and m = 0,1,...,4.[444] From surface enhanced Raman studies of CO on Ni(100), it was concluded that linear and bridged structures exist in an equilibrium which depends on the temperature and on the degree of coverage.[445] The vibrational spectra of some absorbed molecules can depend on the degree of coverage, due to coupling of vibrational modes.[446] There have been attempts to determine the bonding configuration of absorbed species through angular resolved photoemission.[447] Due to the above mentioned complications, such measurements are not expected to give reliable results in general. Recently, photon-stimulated desorption has attracted a lot of attention as a probe for geometries of absorbed molecules.[448,449] The desorption is caused by coulombic repulsions resulting from emissions of Auger electrons.[449]

The photoionization cross sections and β values for H_2 are listed for five internuclear separations in Table 8-11. The subscripts x and y refer to the $\sigma\rightarrow\pi^+$ and the $\sigma\rightarrow\pi^-$ channels respectively; the subscript z refers to the $\sigma\rightarrow\sigma$ channel. This notation applies throughout this text. The energies have been sampled in the range which covers the

TABLE 8-11

CROSS SECTIONS AND BETA VALUES OF H_2

(a) Using touching spheres ($r_H = (1/2)\ r_{HH}$)
(b) Using overlapping spheres ($r_H = 1.1\ a_o$)

$\sigma_x = \sigma_y$ (Mb)

E_e(Ryd)	$r_{HH} = 1.2\ a_o$		$r_{HH} = 1.4\ a_o$		$r_{HH} = 1.6\ a_o$		$r_{HH} = 1.8\ a_o$		$r_{HH} = 2\ a_o$	
	a	b	a	b	a	b	a	b	a	b
0.25	2.46	0.22	2.37	2.41	2.24	2.45	2.13	2.27	2.02	2.10
0.28125	2.34	0.22	2.23	2.32	2.10	2.32	1.99	2.14	1.89	1.97
0.3125	2.22	0.22	2.11	2.23	1.98	2.20	1.87	2.01	1.77	1.85
0.34375	2.11	0.22	1.99	2.15	1.86	2.09	1.75	1.90	1.65	1.73
0.375	2.01	0.22	1.88	2.07	1.75	1.98	1.65	1.79	1.55	1.63
0.40625	1.91	0.22	1.78	2.00	1.65	1.89	1.55	1.69	1.45	1.53
0.4375	1.82	0.22	1.69	2.00	1.56	1.80	1.46	1.60	1.37	1.44
0.46875	1.74	0.22	1.60	1.86	1.47	1.71	1.37	1.52	1.29	1.36

σ_z (Mb)

E_e(Ryd)	$r_{HH} = 1.2\ a_o$		$r_{HH} = 1.4\ a_o$		$r_{HH} = 1.6\ a_o$		$r_{HH} = 1.8\ a_o$		$r_{HH} = 2\ a_o$	
	a	b	a	b	a	b	a	b	a	b
0.25	1.78	2.50	0.98	1.02	0.42	0.32	0.12	0.09	0.02	0.01
0.28125	1.65	2.25	0.89	0.94	0.37	0.29	0.10	0.07	0.01	0.01
0.3125	1.53	2.03	0.81	0.86	0.33	0.26	0.09	0.06	0.01	0.01
0.34375	1.42	1.84	0.74	0.79	0.29	0.23	0.07	0.05	0.01	0.01
0.375	1.31	1.67	0.68	0.73	0.26	0.21	0.06	0.05	0.01	0.01
0.40625	1.22	1.53	0.62	0.68	0.23	0.18	0.05	0.04	0.01	0.01
0.4375	1.14	1.39	0.57	0.62	0.21	0.17	0.05	0.03	0.01	0.01
0.46875	1.06	1.28	0.52	0.58	0.19	0.15	0.04	0.03	0.01	0.01

TABLE 8-11 (CONTINUED)

β

E (Ryd)	$r_{HH} = 1.2\ a_o$		$r_{HH} = 1.4\ a_o$		$r_{HH} = 1.6\ a_o$		$r_{HH} = 1.8\ a_o$		$r_{HH} = 2\ a_o$	
e	a	b	a	b	a	b	a	b	a	b
0.25	1.90	1.27	1.81	1.68	1.68	1.60	1.55	1.52	1.45	1.44
0.28125	1.90	1.30	1.81	1.69	1.68	1.61	1.56	1.52	1.45	1.44
0.3125	1.90	1.32	1.81	1.69	1.68	1.61	1.56	1.53	1.45	1.45
0.34375	1.90	1.35	1.81	1.69	1.68	1.61	1.56	1.53	1.45	1.45
0.375	1.90	1.37	1.81	1.69	1.68	1.61	1.56	1.53	1.45	1.45
0.40625	1.89	1.38	1.81	1.70	1.68	1.62	1.55	1.53	1.45	1.45
0.4375	1.89	1.40	1.81	1.70	1.68	1.62	1.55	1.54	1.45	1.45
0.46875	1.89	1.41	1.80	1.70	1.68	1.62	1.55	1.54	1.45	1.45

energy of the photoelectrons (E_e) for the vibronic transitions in the photoionization of H_2 by the 58.4 nm radiation. The energies are expressed in Rydbergs throughout. (1 Ryd = 13.605 eV). The results from touching and overlapping spheres, (taking r_{HH} = const. = 1.1 a_o), are compared in Table 8-11. At small internuclear separations, the results from overlapping spheres look somewhat suspicious. In Table 8-12, some of the cross sections obtained here have been compared with the ones obtained by Itikawa[450] for H_2. The conversion formula to obtain Itikawa's cross sections in megabarns is shown in Table 8-12. In Table 8-13, the channel contributions to the cross sections, at the photoelectron energies for different vibrational quantum numbers of the ion, are compared with the ones published by Itikawa.[450] The results shown in Table 8-12 and in Table 8-13 were obtained using touching spheres, and by linear interpolation along the E_e-axis.

According to Tai and Flannery,[451] the cross section of H_2 has a maximum in its r_{HH} - dependence below E_e=0.5 Ryd. In contrast to N_2 and CO, there are no sharp features in the E_e - dependence of the cross sections of H_2.

The occurrence of relativistic effects in the photoionization of s sublevels from atoms has been discussed by Manson and Starace.[575]

D. RESONANCES IN PHOTOIONIZATION SPECTRA

Vibrational branching ratios in photoelectron spectra are, in most cases, well represented by Franck-Condon factors between the vibrational ground state and the ionic state wave function. In cases where deviations do occur, they are usually attributed to many-electron interactions with autoionizing states.[464] However, some of these

TABLE 8-12

COMPARISON OF CROSS SECTIONS

(a) Cross sections reported by Itikawa
(b) Present work using touching spheres

E_e(eV)	r_{HH}=1.2 a_o		r_{HH}=1.6 a_o		r_{HH}=2.0 a_o	
	a	b	a	b	a	b
5.79	5.15	4.88	4.52	3.41	4.02	2.81
4.39	6.45	5.86	5.85	4.20	5.30	3.47
3.50	7.47	6.61	6.95	4.82	6.36	4.00

The cross sections are expressed in megabarns (Mb).

Itikawa's cross sections were converted to Mb taking

$$\sigma = 1226\ (\text{Å}/\lambda)(4M_x^2 + M_z^2)$$

$$\lambda = 584.3\text{Å}$$

TABLE 8-13

COMPARISON OF PHOTOIONIZATION CROSS SECTIONS OF H_2

$\sigma_x=\sigma_y$(Mb)

v_f	E_e^a(eV)	$r_{HH}=1.2a_o$		$r_{HH}=1.6a_o$		$r_{HH}=2.0a_o$	
		SW-Xα	Itikawa	SW-Xα	Itikawa	SW-Xα	Itikawa
0	5.79	1.85	1.93	1.59	1.99	1.40	1.97
6	4.39	2.18	2.36	1.94	2.51	1.73	2.56
12	3.50	2.43	2.69	2.21	2.93	1.99	3.04

σ_z(Mb)

v_f	E_e^a(eV)	$r_{HH}=1.2a_o$		$r_{HH}=1.6a_o$		$r_{HH}=2.0a_o$	
		SW-Xα	Itikawa	SW-Xα	Itikawa	SW-Xα	Itikawa
0	5.79	1.17	1.30	0.22	0.55	0.01	0.09
6	4.39	1.49	1.73	0.32	0.83	0.01	0.18
12	3.50	1.75	2.08	0.41	1.08	0.02	0.28

[a]The electron energies correspond to the vibrational states v' of H_2^+ formed by He(I) photons.

resonances can arise at the one-electron level. In this case the non-Franck-Condon behaviour is caused by shape resonances.[465-470] These shape resonances arise from centrifugal barrier effects in high-ℓ components of the final state wave functions.[378,472] These resonances are a few electrovolts above threshold in most cases.[473]

Since they can be understood in one-electron terms, any theoretical scheme describing photoionization should at least qualitatively reproduce observed shape resonances.

The shape resonances of N_2, CO, and O_2 have been particularly well studied.

Autoionization processes in atoms are resonably well understood.[474] Rhemus and Berry[426] searched for a mechanistic interpretation of autoionization by electron correlation. Autoionization can also be induced through nonadiabatic coupling. In fact, Rydberg levels below the first ionization limit can autoionize if they have sufficient energy of nuclear motion.[475] H_2 would be a simple enough molecule for the theoretical investigation of autoionization.

There is indeed evidence of preionization in the ultrahigh resolution absorption spectrum of H_2.[476] Autoionization can be caused by configuration interaction or by nonadiabatic coupling.[477] In hydrogen, autoionization is observed near threshold and it is apparently caused mostly by nonadiabatic effects.[477-479] The preionization of O_2 appears to be, by far, the most extensively studied case of configuration interaction-induced preionization.[480,481] Notice that, in a strict sense, the term autoionization applies to atoms only. For molecules, the term preionization should be used.

In N_2, the Hopfield series, which converges to the B state of N_2^+, can autoionize to the lower lying X and A states of N_2^+.[538] Wendin[482] suggested that the peak around 23 eV photon energy in the $3\sigma_g$ partial cross section, which cannot be described in terms of single excitations, is caused by double excitation having the configuration $....3\sigma_g\ 1\pi_u\ 1\pi_g^2$. Although the Rydberg states of N_2 and CO have been investigated extensively,[483-487] little is known about their participation in autoionization processes. Gardner and Samson[15] measured the vibrational cross section distributions of N_2 and CO, (and O_2), with more than 20 different line sources. Near threshold, they observed dramatic deviations of the vibrational branching ratios from a Franck-Condon distribution. Besides autoionization, Rydberg states can undergo other deexcitation processes, especially nonradiative processes.[488] In some cases, autoionization represents just one channel of several competing deexcitation processes.[489] The most dramatic demonstrations of such competing channels can be found by the comparison of absorption and emission spectra, where transitions for predissociating levels can be observed in the absorption spectra, but are absent or very weak in the fluorescence spectra.[490]

Rydberg levels can also undergo deexcitation by dissociative ionization and, of course, also through fluorescence and inelastic collisions. In addition, the electronic energy of the excited molecule can be converted into vibration/rotation energy.[491]

Predissociation could also precede autoionization. One such sequence is:

$$AB \xrightarrow{h\nu} A^+ + (B^-)^* \rightarrow A^+ + B + e^- \qquad (8\text{-}22)$$

A number of authors have done photoionization experiments with N_2 and CO in which fragmentation yields resulting in ionic fragments such as N^+, C^+, and O^+, together with the formation of doubly charged ions, were measured.[492-494] According to Wight et al.[492] the ionization efficiency for nitrogen is essentially 1 beyond 4 eV above threshold of the first ionization potential. In carbon monoxide, the ionization efficiency shows a sharp drop roughly at 3 eV above threshold of the first ionization potential. The ionization efficiency of CO reaches values close to 1 approximately 6 eV above the first ionization potential. It appears that near threshold of the first ionization potential, the superexcited states can decay by processes other than preionization. Any model which attempts to simulate the decay modes for superexcited states near threshold of the first ionization potential has to deal with several competing channels. The problem is expected to be more serious in "large" molecules. In this case, competing channels may affect photoionization cross sections farther from threshold. Predissociation is expected to contribute the lion's share of the deexcitations which do not result in the formation of ions. "Large" molecules are actually expected to fragmentate at a slower rate than small molecules because the fragments frequently have to execute complicated motions in order to uncouple. However, the internal conversion steps which lead to fragmentation of such a large molecule are "efficient" modes for the dissipation of the energy into a large number of different modes. The point of view taken here is that, once the conversion to energy of nuclear motion has begun, the molecule is unlikely to return to a state from which it is likely to ionize. The reason for

the greater efficiency of the conversion steps in "large" molecules has to do with the greater number of possible pathways, or, equivalently, the greater density of states. The rapid redistribution of energy by intramolecular conversions has "unfortunate" consequences for the laser chemistry of "large" molecules. Laser induced cleavages of specific bonds are only possible in the cases where the cleavage is accomplished before extensive redistribution of the added energy has taken place.

N_2O is a triatomic molecule which, according to the above, should have ionization efficiencies which increase more gradually beyond the lowest ionization potential. For N_2O, the increase, according to Hitchcock et al.,[495] is from 0 to 0.3, 0.63, 0.72, 0.77, 0.80, 0.87, 0.94, and 0.98 at 1, 2, 3, ..., 7 eV above the lowest ionization potential. There is definitely some indication that with increasing "size" of the molecule predissociation becomes more important. One might wonder why there is no drop in the ionization efficiency at the second and higher ionization potentials, because we have Rydberg series converging to all the ionization potentials. It may be that, at the lowest ionization potential internal conversion processes use up some of the electronic energy such that the system from the point of view of its electronic energy falls below its ionization threshold with little chance of ever accumulating, at a later time, sufficient electronic energy to undergo an ionization process.

Atoms do not show any shape resonances in photoionization experiments. They do, however, show shape resonances in electron scattering experiments.[496] In photoionization experiments, atomic cross sections show minima at certain photon energies. These so-called

Cooper minima are not due to any sort of resonance effect. They arise when dipole matrix elements go through zero as they change signs as a function of energy.[497] According to Luke and Phillips,[498,499] the complex photoionization amplitudes of atoms, in the neighbourhood of an isolated autoionization resonance, describe to a close approximation a circle in the complex plane.

Fano[500] has shown that any state coupled to a continuum should give rise to a characteristic line profile in transitions involving such states. Such line shapes have been observed for predissociation[501,502] and autoionization[478,504] processes.

Autoionizing states can be viewed as structures in the continuum. Structures in the continuum may be created artifically with magnetic fields or with laser radiation. Laser-induced continuum structures behave much as autoionizing resonances, but can be tuned in position and width.[505]

Many autoionizing states are expected to have unresolved fine structure. The limitations due to natural line widths can be overcome with spectroscopic techniques which are based on interference of states.[506] In the case of autoionization, quantum beats may provide useful information about intramolecular couplings and about bound-continuum coupling.[507-509]

A systematic investigation of resonances requires a tunable source of high energy radiation. The ideal such source would be a tunable high energy laser. Since no such lasers are operating at the present time, synchrotrons have turned out to be the closest thing to such a source of radiation.[510-512] Free-electron lasers, which operate

on a principle somewhat related to synchrotron radiation, have been expected to become sources of high energy radiation.[513-517]

Resonances in photoionizations show up as resonance structures in the angular distribution. It may be that changes in β serve as more sensitive indicators of the presence of autoionization than the corresponding energy dependence of the total cross section.[518] Very little is known about the effects photoionization resonances have on the polarization of photoelectrons.[519]

From experiment the $3\sigma_g$-photoionization is known to have a resonance at 28.1 eV energy of the photon.[387] The 5σ-photoionization of CO has a resonance at 23.6 eV, and the 4σ-photoionization shows a resonance at 32.2 eV.[387] One would expect to find a shape resonance in acetylene in analogy with the photoelectron spectra of N_2 and CO, which are isoelectronic with acetylene. Such a shape resonance has not yet been unambiguously confirmed for acetylene.[520] For the present work, dipole moment amplitudes for the photoionization of H_2, N_2, and CO were needed at different internuclear distances over a limited range of photoelectron energies. In some cases, the range of the energies has been extended in order to have comprehensive studies at different geometries. The β values of N_2 for v_f=0 and v_f=1 differ considerably at low energies.[521] Xα-SW computation of cross sections and β values of N_2 and CO at their respective equilibrium internuclear separations have been done by several authors.[346,390,522-524] The results obtained by the different authors differ only slightly. The cross sections differ from the experimental results, in general, near threshold and the computed cross sections for the photoionization of

the π orbitals of N_2 and CO fall off too rapidly.[524] The computed β values agree well with the experimental values determined by Marr et al.,[526] with the exception of the $2\sigma_u$ photoionization of N_2 and the 4σ photoionization of CO.[390] The results computed here for N_2 and CO are shown in Figure 8-6 to Figure 8-11 and listed in Table 8-14 to Table 8-31. From these data, it becomes readily apparent that vibrational averaging is required near threshold, with the possible exception of the photoionization of the π levels of N_2 and CO, where a single-geometry calculations might be adequate. Especially for the photoionization of the σ levels of CO the need for vibrational averaging at threshold is indicated by the present data. The discrepancy between the experimental and the computed β values does not seem to be resolvable by vibrational averaging for the photoionization of the $2\sigma_u$ level of N_2, according to the data graphed in Figure 8-8.

In the SW method, the wave functions are expanded in partial waves. In these expansions, ℓ ranges - in principle - from 0 to infinity. In practice, such expansions have to be truncated to a manageable number of terms. The maximum ℓ for the partial wave expansion is given by the maximum of ℓ at the different sites. Let us represent the basis for the molecule ABCD .... by

$$(\ell_A^i, \ell_B^i, \ell_C^i, \ldots, \ell_{OS}^i; \ell_A^f, \ell_B^f, \ell_C^f, \ldots, \ell_{OS}^f) \qquad (8\text{-}23)$$

where the superscripts denote the initial and the final state, and the subscript "OS" denotes the outer sphere. The quantities ℓ denote the maximum values of the azimutal quantum number at the different sites.

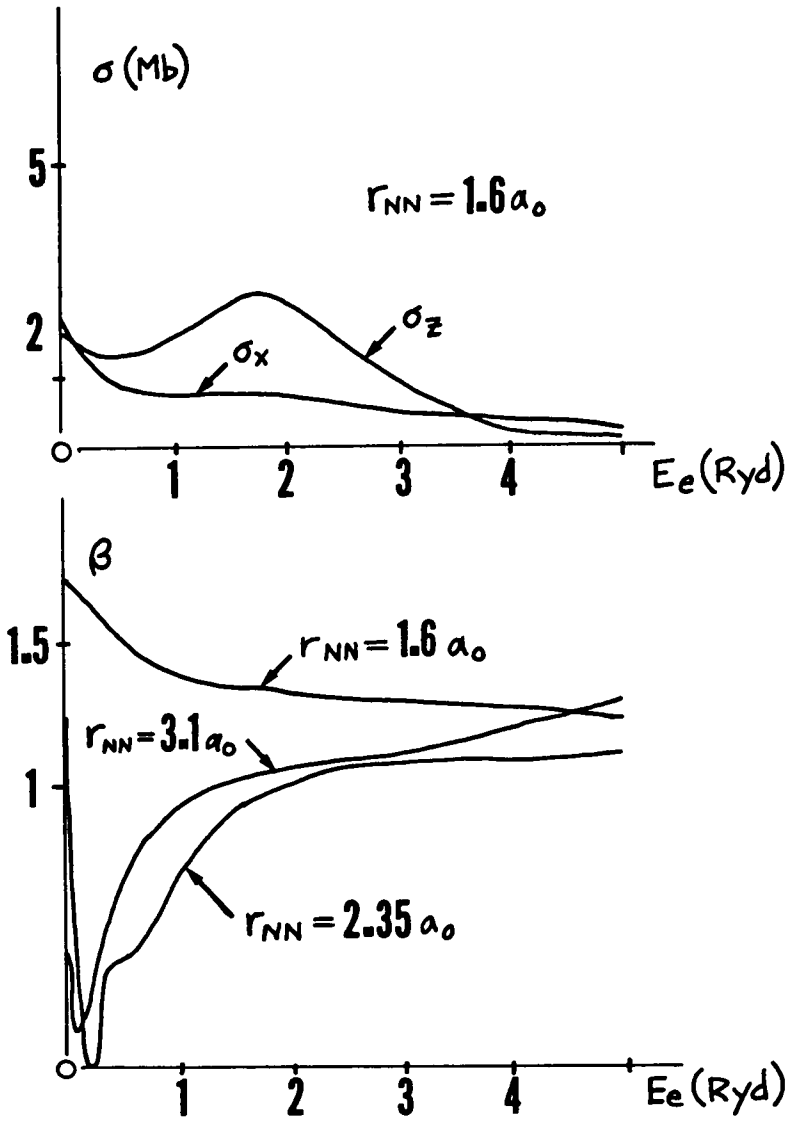


Fig. 8-6. Cross sections and β values of the $(3\sigma_g)^{-1}$ photoionization of N_2 at three different internuclear separations.

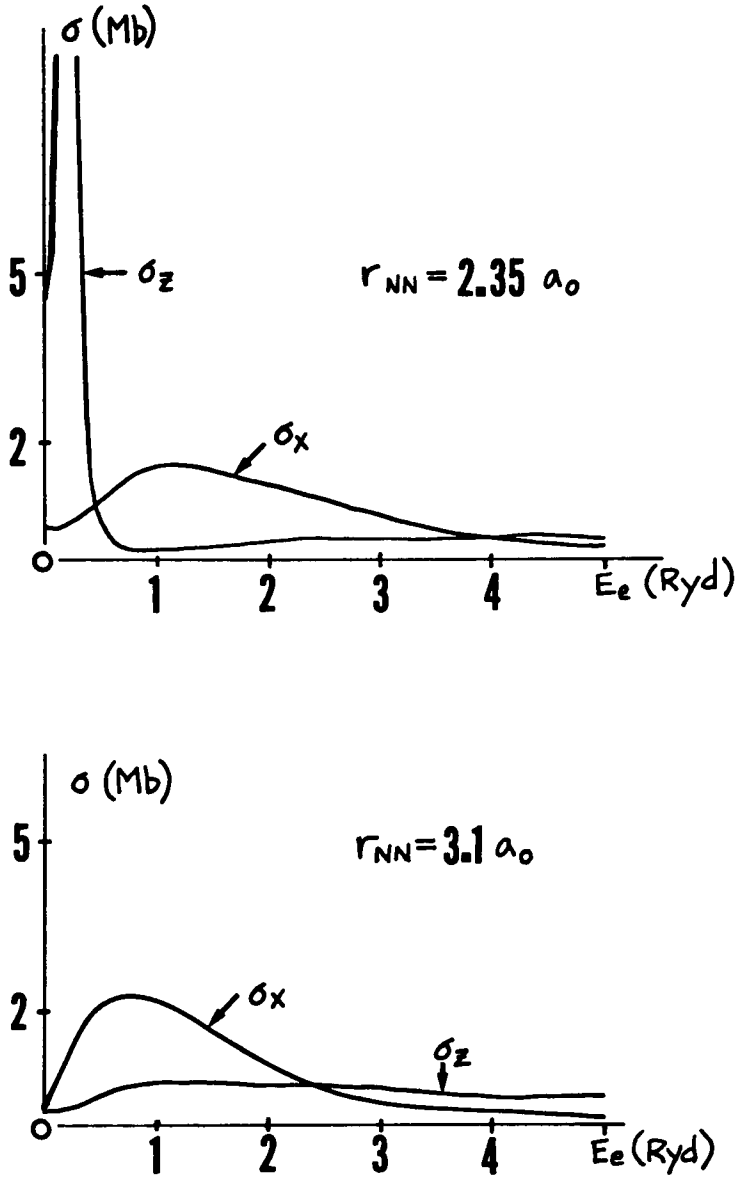


Fig. 8-6. (Continued).

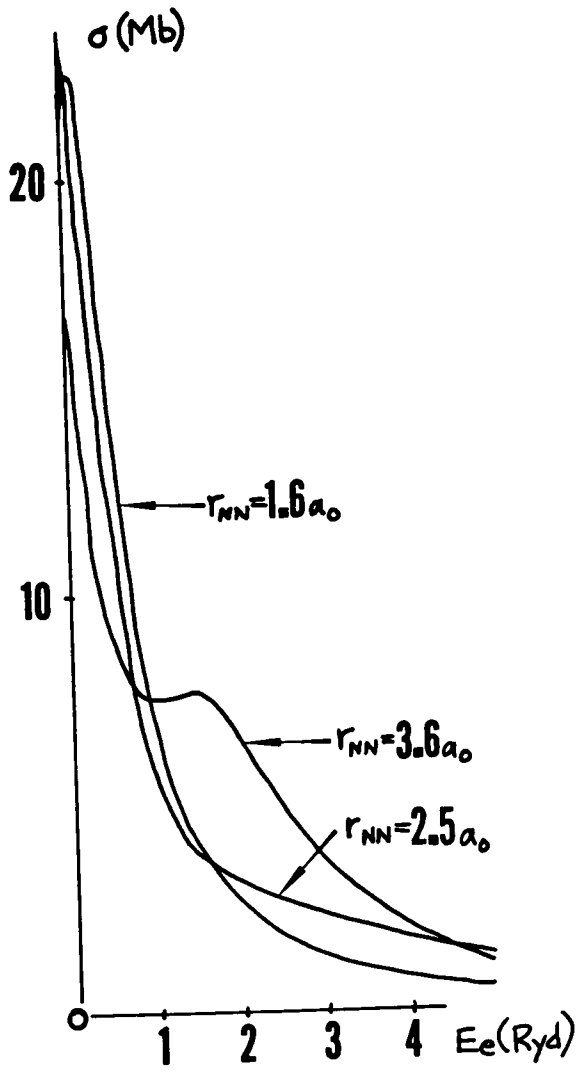


Fig. 8-7. Cross section and β values of the $(1\pi_u)^{-1}$ photoionization of N_2 at three different internuclear separations.

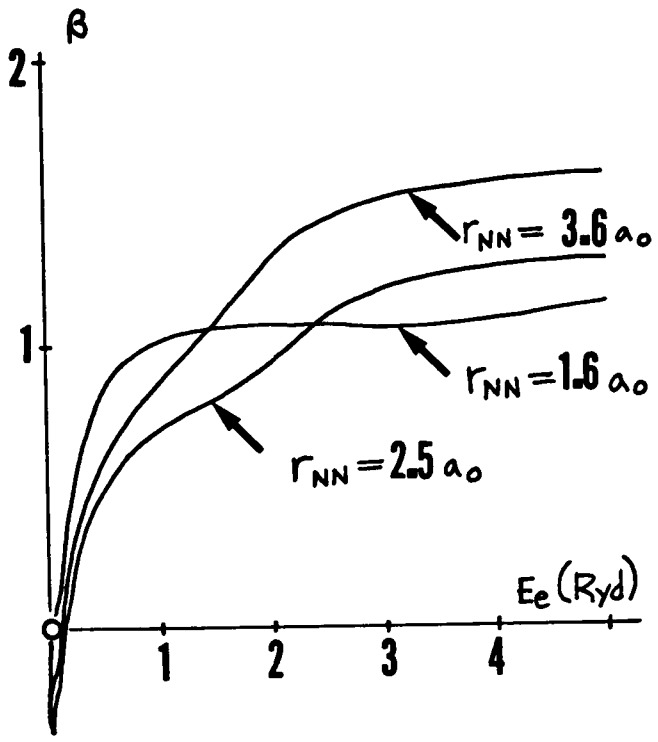


Fig. 8-7. (Continued).

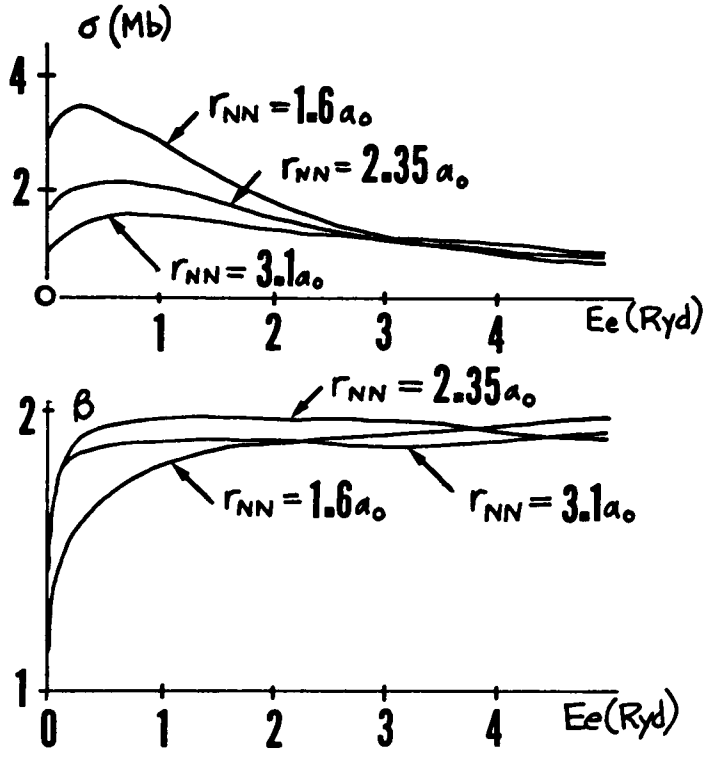


Fig. 8-8. Cross sections and β values of the $(2\sigma_u)^{-1}$ photoionization of N_2 at three different internuclear separations.

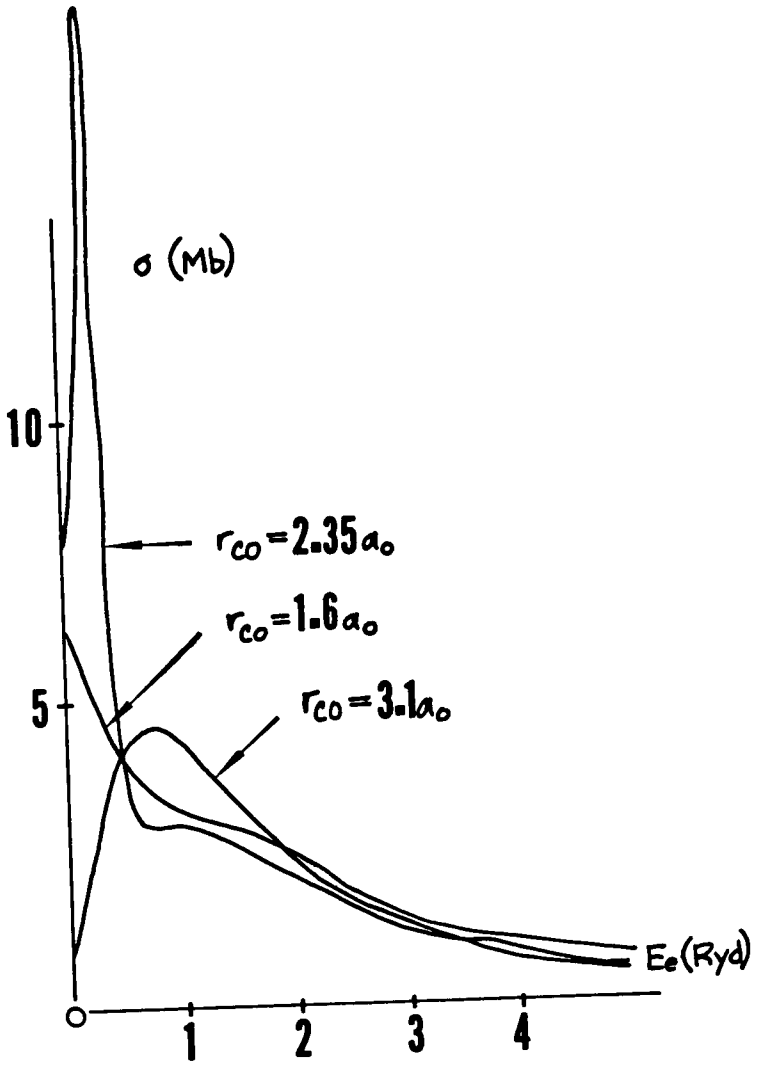


Fig. 8-9. Cross sections and β values of the $(5\sigma)^{-1}$ photoionization of CO at three different internuclear separations.

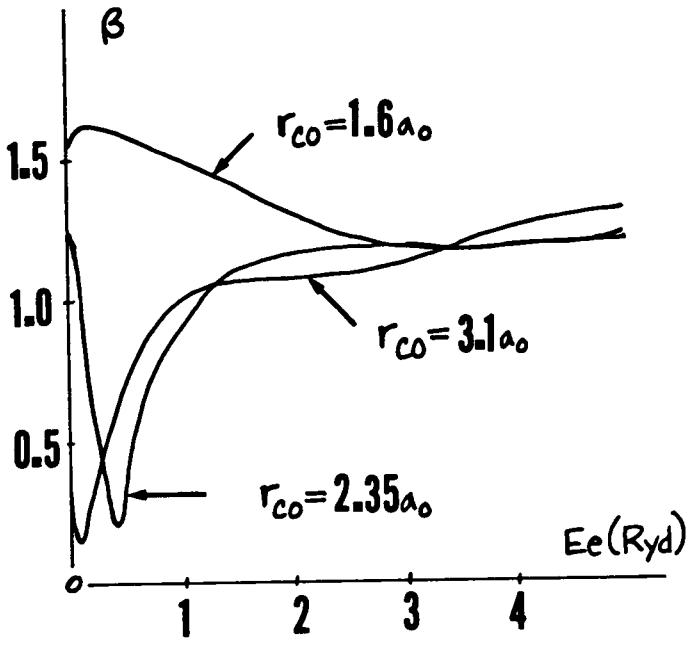


Fig. 8-9. (Continued)

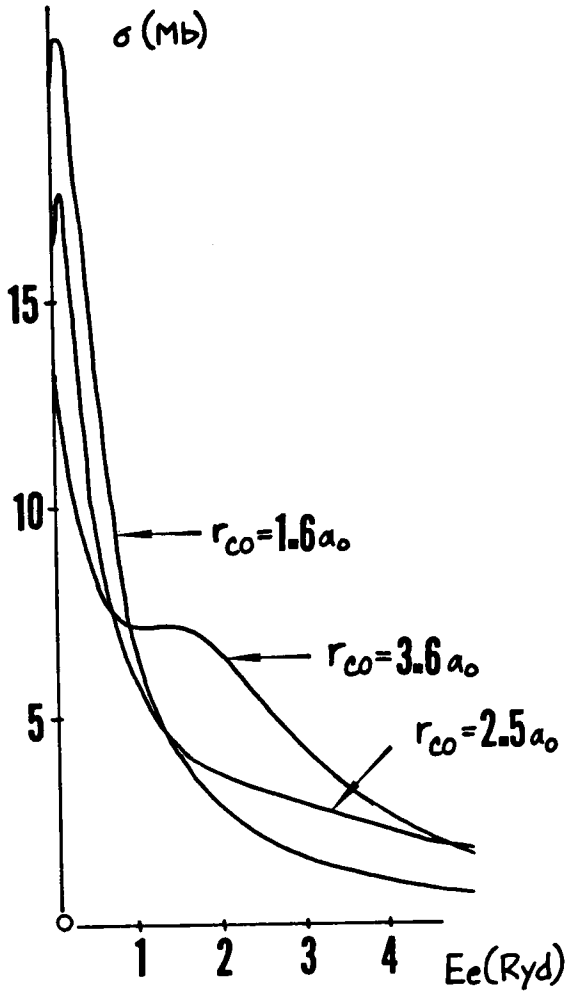


Fig. 8-10. Cross sections and β values of the $(1\pi)^{-1}$ photoionization of CO at three different internuclear separations.

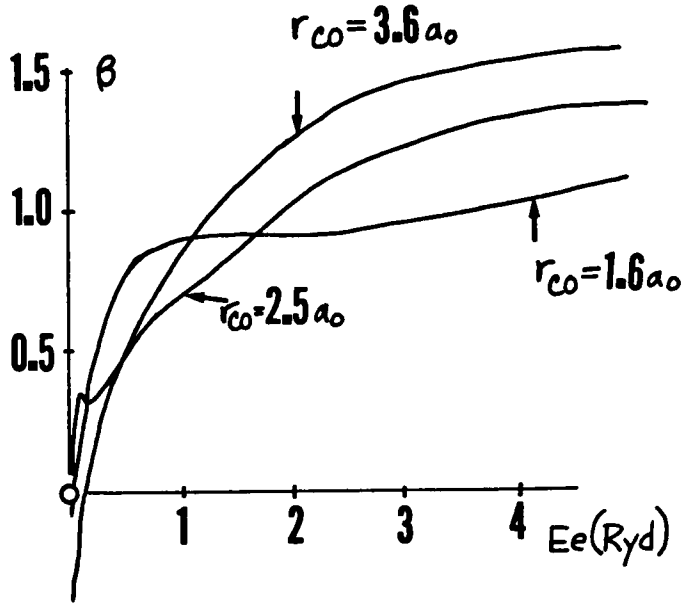


Fig. 8-10. (Continued)

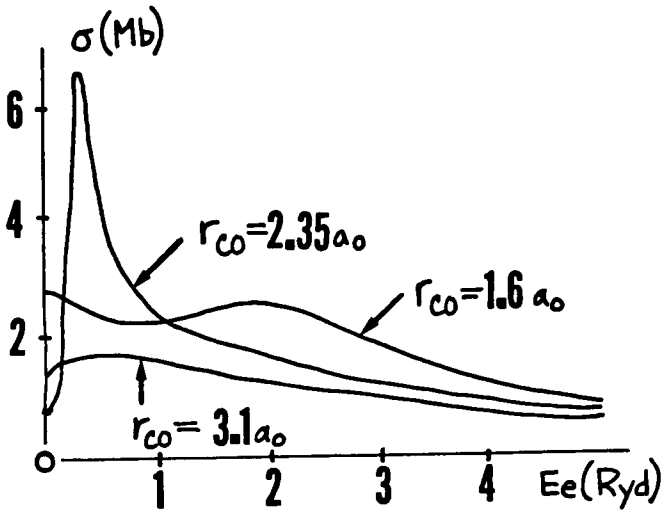


Fig. 8-11. Cross sections and β values of the $(4\sigma)^{-1}$ photoionization of CO at three different internuclear separations.

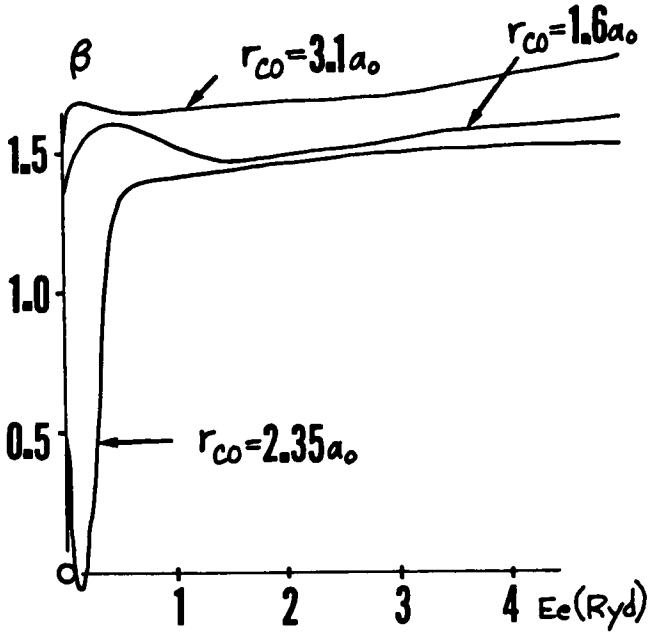


Fig. 8-11. (Continued)

TABLE 8-14

CHANNEL CONTRIBUTIONS TO THE CROSS SECTIONS AND ASYMMETRY PARAMETERS FOR $N_2(X^1\Sigma_g^+) \rightarrow N_2^+(X^2\Sigma_g^+) + e^-$ AT $r_{NN} = 1.6\ a_o$

	σ(Mb)		
E_e(Ryd)	$3\sigma_g \rightarrow k\sigma_u$	$3\sigma_g \rightarrow k\pi_u$	β
0.005	2.03	4.55	1.75
0.01	2.02	4.51	1.75
0.015	2.01	4.46	1.74
0.025	1.99	4.38	1.73
0.05	1.94	4.17	1.72
0.075	1.90	3.98	1.70
0.1	1.86	3.80	1.69
0.15	1.79	3.48	1.67
0.2	1.73	3.20	1.65
0.25	1.69	2.96	1.63
0.3	1.65	2.76	1.61
0.35	1.63	2.58	1.59
0.4	1.61	2.42	1.56
0.5	1.59	2.18	1.52
0.6	1.61	2.01	1.49
0.8	1.72	1.83	1.43
1.0	1.91	1.78	1.39
1.3	2.29	1.80	1.36
1.6	2.60	1.82	1.35
1.9	2.62	1.78	1.34
2.2	2.30	1.66	1.32
2.5	1.80	1.52	1.31
3.0	1.03	1.28	1.28
3.5	0.56	1.06	1.27
4.0	0.31	0.88	1.26
4.5	0.18	0.74	1.25
5.0	0.11	0.62	1.23

TABLE 8-15

CHANNEL CONTRIBUTIONS TO THE CROSS SECTIONS AND ASYMMETRY PARAMETERS FOR $N_2(X^1\Sigma_g^+) \rightarrow N_2^+(X^2\Sigma_g^+) + e^-$ AT $r_{NN} = 2.35\ a_o$

	σ(Mb)		
E_e(Ryd)	$3\sigma_g \rightarrow k\sigma_u$	$3\sigma_g \rightarrow k\pi_u$	β
0.005	4.32	1.10	1.24
0.01	4.42	1.09	1.14
0.015	4.54	1.08	1.07
0.025	4.79	1.07	0.94
0.05	5.63	1.05	0.68
0.075	6.91	1.05	0.48
0.1	8.96	1.05	0.31
0.15	19.25	1.08	0.08
0.2	56.22	1.15	0.00
0.25	30.32	1.25	0.06
0.3	8.11	1.39	0.19
0.35	3.22	1.54	0.31
0.4	1.64	1.72	0.37
0.5	0.66	2.11	0.38
0.6	0.37	2.49	0.41
0.8	0.22	3.09	0.55
1.0	0.20	3.39	0.68
1.3	0.23	3.36	0.84
1.6	0.27	3.04	0.93
1.9	0.31	2.64	0.99
2.2	0.33	2.22	1.03
2.5	0.34	1.90	1.05
3.0	0.34	1.42	1.07
3.5	0.33	1.06	1.08
4.0	0.31	0.79	1.08
4.5	0.30	0.59	1.09
5.0	0.29	0.45	1.11

TABLE 8-16

CHANNEL CONTRIBUTIONS TO THE CROSS SECTIONS AND ASYMMETRY PARAMETERS FOR $N_2(X^1\Sigma_g^+) \rightarrow N_2^+(X^2\Sigma_g^+) + e^-$ AT $r_{NN} = 3.1\ a_o$

	σ(Mb)		
E_e(Ryd)	$3\sigma_g \rightarrow k\sigma_u$	$3\sigma_g \rightarrow k\pi_u$	β
0.005	0.19	0.54	0.58
0.01	0.20	0.57	0.46
0.015	0.20	0.61	0.38
0.025	0.21	0.68	0.28
0.05	0.22	0.86	0.16
0.075	0.24	1.06	0.13
0.1	0.26	1.27	0.13
0.15	0.30	1.71	0.19
0.2	0.33	2.15	0.27
0.25	0.37	2.58	0.36
0.3	0.41	2.98	0.43
0.35	0.45	3.35	0.50
0.4	0.49	3.67	0.56
0.5	0.56	4.15	0.66
0.6	0.62	4.46	0.74
0.8	0.71	4.62	0.86
1.0	0.76	4.40	0.93
1.3	0.78	3.76	0.99
1.6	0.76	3.04	1.02
1.9	0.73	2.38	1.04
2.2	0.70	1.84	1.05
2.5	0.67	1.42	1.07
3.0	0.63	0.95	1.11
3.5	0.58	0.69	1.16
4.0	0.51	0.53	1.21
4.5	0.45	0.43	1.25
5.0	0.38	0.36	1.29

TABLE 8-17

CHANNEL CONTRIBUTIONS TO THE CROSS SECTIONS AND ASYMMETRY PARAMETERS FOR $N_2(X^1\Sigma_g^+) \rightarrow N_2^+(A^2\Pi_{ui}) + e^-$ AT $r_{NN} = 1.6\ a_o$

	σ(Mb)			
E_e(Ryd)	$1\pi_u \rightarrow k\sigma_g$	$1\pi_u \rightarrow k\pi_g$	$1\pi_u \rightarrow k\delta_g$	β
0.005	3.56	0.65	15.98	-0.15
0.01	3.56	0.64	16.20	-0.12
0.015	3.56	0.63	16.41	-0.09
0.025	3.56	0.60	16.80	-0.04
0.05	3.56	0.55	17.62	0.07
0.075	3.54	0.49	18.22	0.16
0.1	3.51	0.45	18.60	0.25
0.15	3.42	0.36	18.80	0.38
0.2	3.30	0.29	18.38	0.49
0.25	3.17	0.23	17.57	0.58
0.3	3.03	0.18	16.52	0.66
0.35	2.88	0.15	15.38	0.72
0.4	2.73	0.11	14.23	0.77
0.5	2.45	0.07	12.06	0.85
0.6	2.18	0.04	10.22	0.91
0.8	1.74	0.01	7.45	0.98
1.0	1.39	0.00	5.60	1.02
1.3	1.02	0.01	3.85	1.05
1.6	0.76	0.03	2.78	1.06
1.9	0.58	0.04	2.08	1.06
2.2	0.45	0.05	1.61	1.05
2.5	0.36	0.06	1.27	1.05
3.0	0.25	0.07	0.90	1.05
3.5	0.19	0.08	0.66	1.06
4.0	0.14	0.08	0.51	1.07
4.5	0.11	0.08	0.41	1.10
5.0	0.09	0.08	0.34	1.13

TABLE 8-18

CHANNEL CONTRIBUTIONS TO THE CROSS SECTIONS AND ASYMMETRY PARAMETERS FOR $N_2(X^1\Sigma_g^+) \rightarrow N_2^+(A^2\Pi_{ui}) + e^-$ AT $r_{NN} = 2.5\ a_o$

	σ(Mb)			
E_e(Ryd)	$1\pi_u \rightarrow k\sigma_g$	$1\pi_u \rightarrow k\pi_g$	$1\pi_u \rightarrow k\delta_g$	β
0.005	4.35	0.35	17.84	-0.37
0.01	4.28	0.36	17.91	-0.36
0.015	4.23	0.36	17.96	-0.35
0.025	4.11	0.37	18.04	-0.33
0.05	3.84	0.39	18.09	-0.25
0.075	3.59	0.40	17.97	-0.17
0.1	3.36	0.42	17.69	-0.10
0.15	2.96	0.44	16.83	0.03
0.2	2.61	0.46	15.72	0.14
0.25	2.32	0.47	14.51	0.23
0.3	2.08	0.48	13.31	0.30
0.35	1.86	0.49	12.16	0.36
0.4	1.68	0.49	11.10	0.41
0.5	1.38	0.50	9.26	0.49
0.6	1.15	0.49	7.79	0.55
0.8	0.85	0.47	5.70	0.63
1.0	0.66	0.45	4.38	0.69
1.3	0.50	0.43	3.20	0.76
1.6	0.43	0.43	2.55	0.84
1.9	0.41	0.46	2.16	0.93
2.2	0.40	0.49	1.89	1.01
2.5	0.40	0.53	1.69	1.09
3.0	0.39	0.57	1.42	1.18
3.5	0.35	0.58	1.18	1.23
4.0	0.30	0.56	0.98	1.26
4.5	0.24	0.52	0.81	1.27
5.0	0.18	0.47	0.67	1.27

TABLE 8-19

CHANNEL CONTRIBUTIONS TO THE CROSS SECTIONS AND ASYMMETRY PARAMETERS FOR $N_2(X^1\Sigma_g^+) \rightarrow N_2^+(A^2\Pi_{ui}) + e^-$ AT $r_{NN} = 3.6\ a_o$

	σ(Mb)			
E_e(Ryd)	$1\pi_u \rightarrow k\sigma_g$	$1\pi_u \rightarrow k\pi_g$	$1\pi_u \rightarrow k\delta_g$	β
0.005	2.91	0.88	13.26	-0.34
0.01	2.87	0.89	13.24	-0.33
0.015	2.83	0.89	13.22	-0.31
0.025	2.75	0.89	13.16	-0.27
0.05	2.56	0.90	12.94	-0.17
0.075	2.39	0.90	12.65	-0.08
0.1	2.24	0.89	12.32	-0.01
0.15	1.98	0.88	11.57	0.13
0.2	1.77	0.87	10.79	0.23
0.25	1.60	0.85	10.04	0.31
0.3	1.45	0.83	9.34	0.38
0.35	1.34	0.82	8.71	0.44
0.4	1.24	0.81	8.15	0.49
0.5	1.10	0.81	7.23	0.57
0.6	1.02	0.84	6.54	0.64
0.8	0.97	0.97	5.66	0.75
1.0	1.04	1.19	5.19	0.86
1.3	1.27	1.60	4.76	0.99
1.6	1.43	1.92	4.31	1.12
1.9	1.20	2.06	3.75	1.25
2.2	0.83	2.00	3.15	1.37
2.5	0.59	1.81	2.62	1.44
3.0	0.37	1.37	1.93	1.51
3.5	0.27	0.95	1.46	1.55
4.0	0.22	0.65	1.12	1.57
4.5	0.19	0.45	0.87	1.58
5.0	0.16	0.32	0.68	1.59

TABLE 8-20

CHANNEL CONTRIBUTIONS TO THE CROSS SECTIONS AND ASYMMETRY PARAMETERS FOR $N_2(X^1\Sigma_g^+) \rightarrow N_2^+(B^2\Sigma_u^+) + e^-$ AT $r_{NN} = 1.6\ a_o$

	σ(Mb)		
E_e(Ryd)	$2\sigma_u \rightarrow k\sigma_g$	$2\sigma_u \rightarrow k\pi_g$	β
0.005	2.83	0.07	1.06
0.01	2.85	0.08	1.11
0.015	2.86	0.08	1.15
0.025	2.89	0.10	1.20
0.05	2.95	0.13	1.30
0.075	2.99	0.17	1.37
0.1	3.01	0.21	1.42
0.15	3.02	0.29	1.49
0.2	2.99	0.38	1.55
0.25	2.94	0.45	1.59
0.3	2.86	0.52	1.63
0.35	2.77	0.59	1.66
0.4	2.68	0.65	1.68
0.5	2.47	0.76	1.72
0.6	2.28	0.84	1.75
0.8	1.92	0.96	1.80
1.0	1.62	1.01	1.83
1.3	1.27	1.03	1.86
1.6	1.02	0.99	1.88
1.9	0.83	0.93	1.90
2.2	0.69	0.86	1.91
2.5	0.58	0.79	1.92
3.0	0.44	0.68	1.94
3.5	0.35	0.59	1.94
4.0	0.29	0.51	1.95
4.5	0.24	0.45	1.95
5.0	0.20	0.39	1.95

TABLE 8-21

CHANNEL CONTRIBUTIONS TO THE CROSS SECTIONS AND ASYMMETRY PARAMETERS FOR $N_2(X^1\Sigma_g^+) \rightarrow N_2^+(B^2\Sigma_u^+) + e^-$ AT $r_{NN} = 2.35\ a_o$

	σ(Mb)		
E_e(Ryd)	$2\sigma_u \rightarrow k\sigma_g$	$2\sigma_u \rightarrow k\pi_g$	β
0.005	1.09	0.51	1.29
0.01	1.09	0.52	1.37
0.015	1.09	0.53	1.43
0.025	1.10	0.54	1.51
0.05	1.10	0.59	1.64
0.075	1.11	0.63	1.71
0.1	1.11	0.66	1.76
0.15	1.11	0.73	1.82
0.2	1.10	0.80	1.85
0.25	1.08	0.86	1.88
0.3	1.06	0.91	1.89
0.35	1.04	0.95	1.91
0.4	1.02	0.99	1.92
0.5	0.98	1.06	1.93
0.6	0.94	1.11	1.94
0.8	0.85	1.16	1.95
1.0	0.77	1.16	1.96
1.3	0.68	1.12	1.97
1.6	0.60	1.04	1.97
1.9	0.53	0.95	1.97
2.2	0.48	0.87	1.97
2.5	0.43	0.79	1.97
3.0	0.37	0.69	1.97
3.5	0.32	0.61	1.95
4.0	0.27	0.54	1.94
4.5	0.24	0.48	1.92
5.0	0.21	0.42	1.90

TABLE 8-22

CHANNEL CONTRIBUTIONS TO THE CROSS SECTIONS AND ASYMMETRY PARAMETERS FOR $N_2(X^1\Sigma_g^+) \rightarrow N_2^+(B^2\Sigma_u^+) + e^-$ AT $r_{NN} = 3.1\ a_o$

	σ(Mb)		
E_e(Ryd)	$2\sigma_u \rightarrow k\sigma_g$	$2\sigma_u \rightarrow k\pi_g$	β
0.005	0.39	0.46	1.33
0.01	0.40	0.47	1.41
0.015	0.40	0.48	1.46
0.025	0.40	0.49	1.53
0.05	0.42	0.53	1.64
0.075	0.43	0.56	1.71
0.1	0.44	0.59	1.75
0.15	0.45	0.65	1.80
0.2	0.46	0.71	1.83
0.25	0.47	0.76	1.85
0.3	0.48	0.80	1.86
0.35	0.49	0.84	1.87
0.4	0.49	0.87	1.88
0.5	0.49	0.92	1.88
0.6	0.49	0.95	1.89
0.8	0.49	0.97	1.89
1.0	0.47	0.96	1.89
1.3	0.45	0.91	1.90
1.6	0.43	0.85	1.90
1.9	0.41	0.80	1.90
2.2	0.40	0.74	1.88
2.5	0.40	0.69	1.87
3.0	0.41	0.62	1.86
3.5	0.40	0.56	1.88
4.0	0.37	0.52	1.90
4.5	0.33	0.48	1.91
5.0	0.29	0.45	1.92

TABLE 8-23

CHANNEL CONTRIBUTIONS TO THE CROSS SECTIONS AND ASYMMETRY PARAMETERS FOR $CO(X^1\Sigma^+) \rightarrow CO^+(X^2\Sigma^+) + e^-$ AT $r_{CO} = 1.6\ a_o$

	σ(Mb)		
E_e(Ryd)	$5\sigma \rightarrow k\sigma$	$5\sigma \rightarrow k\pi$	β
0.005	3.87	3.03	1.56
0.01	3.85	3.02	1.57
0.015	3.83	3.00	1.58
0.025	3.79	2.97	1.59
0.05	3.68	2.90	1.61
0.075	3.58	2.83	1.62
0.1	3.47	2.77	1.62
0.15	3.27	2.64	1.62
0.2	3.08	2.53	1.62
0.25	2.91	2.42	1.62
0.3	2.75	2.33	1.61
0.35	2.62	2.25	1.61
0.4	2.49	2.17	1.60
0.5	2.27	2.05	1.59
0.6	2.11	1.95	1.57
0.8	1.88	1.83	1.54
1.0	1.76	1.75	1.50
1.3	1.65	1.67	1.45
1.6	1.54	1.57	1.39
1.9	1.36	1.44	1.33
2.2	1.12	1.30	1.28
2.5	0.88	1.16	1.24
3.0	0.49	0.95	1.24
3.5	0.32	0.78	1.19
4.0	0.20	0.65	1.19
4.5	0.13	0.54	1.19
5.0	0.09	0.45	1.20

TABLE 8-24

CHANNEL CONTRIBUTIONS TO THE CROSS SECTIONS AND ASYMMETRY PARAMETERS FOR $CO(X^1\Sigma^+) \rightarrow CO^+(X^2\Sigma^+) + e^-$ AT $r_{CO} = 2.35\ a_o$

	σ(Mb)		
E_e(Ryd)	$5\sigma \rightarrow k\sigma$	$5\sigma \rightarrow k\pi$	β
0.005	6.28	1.84	1.25
0.01	6.34	1.83	1.24
0.015	6.41	1.82	1.24
0.025	6.55	1.81	1.22
0.05	6.98	1.79	1.16
0.075	7.53	1.77	1.08
0.1	8.25	1.77	1.01
0.15	10.32	1.77	0.85
0.2	13.35	1.79	0.68
0.25	16.04	1.84	0.51
0.3	14.59	1.91	0.36
0.35	9.51	2.00	0.24
0.4	5.40	2.10	0.18
0.5	1.92	2.32	0.26
0.6	0.89	2.54	0.45
0.8	0.37	2.86	0.73
1.0	0.27	2.98	0.89
1.3	0.26	2.83	1.03
1.6	0.27	2.50	1.11
1.9	0.29	2.14	1.16
2.2	0.30	1.80	1.18
2.5	0.30	1.51	1.19
3.0	0.29	1.13	1.19
3.5	0.27	0.84	1.19
4.0	0.26	0.63	1.19
4.5	0.25	0.48	1.19
5.0	0.24	0.38	1.21

TABLE 8-25

CHANNEL CONTRIBUTIONS TO THE CROSS SECTIONS AND ASYMMETRY PARAMETERS FOR $CO(X^1\Sigma^+) \rightarrow CO^+(X^2\Sigma^+) + e^-$ AT $r_{CO} = 3.1\ a_o$

	σ(Mb)		
E_e(Ryd)	$5\sigma \rightarrow k\sigma$	$5\sigma \rightarrow k\pi$	β
0.005	0.30	0.68	0.37
0.01	0.30	0.71	0.31
0.015	0.31	0.74	0.26
0.025	0.31	0.81	0.20
0.05	0.31	0.98	0.15
0.075	0.32	1.16	0.15
0.1	0.33	1.35	0.17
0.15	0.35	1.76	0.25
0.2	0.38	2.17	0.34
0.25	0.40	2.58	0.42
0.3	0.43	2.95	0.50
0.35	0.46	3.28	0.57
0.4	0.49	3.57	0.63
0.5	0.55	4.00	0.73
0.6	0.60	4.25	0.81
0.8	0.68	4.33	0.93
1.0	0.72	4.06	1.00
1.3	0.72	3.40	1.06
1.6	0.70	2.71	1.09
1.9	0.67	2.12	1.09
2.2	0.66	1.65	1.10
2.5	0.67	1.31	1.11
3.0	0.68	0.93	1.14
3.5	0.66	0.72	1.19
4.0	0.58	0.59	1.24
4.5	0.50	0.50	1.28
5.0	0.41	0.42	1.31

TABLE 8-26

CHANNEL CONTRIBUTIONS TO THE CROSS SECTIONS AND ASYMMETRY PARAMETERS FOR $CO(X^1\Sigma^+) \rightarrow CO^+(A^2\Pi_i) + e^-$ AT $r_{CO} = 1.6\ a_o$

	σ(Mb)			
E_e(Ryd)	$1\pi \rightarrow k\sigma$	$1\pi \rightarrow k\pi$	$1\pi \rightarrow k\delta$	β
0.005	3.19	1.59	14.63	-0.08
0.01	3.19	1.56	14.83	-0.06
0.015	3.19	1.54	15.02	-0.03
0.025	3.19	1.49	15.37	0.01
0.05	3.18	1.39	16.12	0.10
0.075	3.15	1.29	16.67	0.18
0.1	3.12	1.20	17.02	0.25
0.15	3.03	1.05	17.20	0.37
0.2	2.92	0.92	16.83	0.47
0.25	2.79	0.82	16.10	0.55
0.3	2.66	0.73	15.17	0.61
0.35	2.52	0.65	14.15	0.67
0.4	2.39	0.58	13.11	0.71
0.5	2.13	0.47	11.18	0.78
0.6	1.89	0.39	9.52	0.83
0.8	1.49	0.28	7.03	0.88
1.0	1.19	0.22	5.36	0.90
1.3	0.88	0.17	3.77	0.91
1.6	0.68	0.16	2.79	0.90
1.9	0.55	0.15	2.15	0.90
2.2	0.47	0.15	1.71	0.91
2.5	0.40	0.15	1.38	0.92
3.0	0.31	0.15	1.02	0.95
3.5	0.24	0.15	0.78	0.98
4.0	0.18	0.14	0.62	1.02
4.5	0.15	0.14	0.52	1.06
5.0	0.12	0.14	0.44	1.11

TABLE 8-27

CHANNEL CONTRIBUTIONS TO THE CROSS SECTIONS AND ASYMMETRY PARAMETERS FOR $CO(X^1\Sigma^+) \rightarrow CO^+(A^2\Pi_i) + e^-$ AT $r_{CO} = 2.5\ a_o$

	σ(Mb)			
E_e(Ryd)	$1\pi \rightarrow k\sigma$	$1\pi \rightarrow k\pi$	$1\pi \rightarrow k\delta$	β
0.005	1.44	0.41	14.53	0.02
0.01	1.37	0.40	14.57	0.04
0.015	1.30	0.40	14.62	0.06
0.025	1.21	0.40	14.69	0.11
0.05	1.25	0.39	14.73	0.24
0.075	1.77	0.39	14.62	0.32
0.1	2.57	0.39	14.40	0.35
0.15	3.51	0.39	13.70	0.32
0.2	3.43	0.40	12.81	0.32
0.25	3.06	0.41	11.86	0.35
0.3	2.69	0.43	10.91	0.39
0.35	2.37	0.46	10.02	0.43
0.4	2.10	0.49	9.20	0.46
0.5	1.68	0.56	7.80	0.52
0.6	1.38	0.63	6.69	0.57
0.8	0.99	0.73	5.15	0.64
1.0	0.76	0.78	4.19	0.70
1.3	0.57	0.79	3.30	0.80
1.6	0.48	0.77	2.76	0.89
1.9	0.44	0.75	2.40	0.99
2.2	0.42	0.75	2.15	1.07
2.5	0.41	0.76	1.95	1.14
3.0	0.39	0.75	1.68	1.23
3.5	0.36	0.73	1.45	1.29
4.0	0.32	0.68	1.25	1.32
4.5	0.27	0.63	1.08	1.34
5.0	0.23	0.56	0.92	1.35

TABLE 8-28

CHANNEL CONTRIBUTIONS TO THE CROSS SECTIONS AND ASYMMETRY PARAMETERS FOR $CO(X^1\Sigma^+) \rightarrow CO^+(A^2\Pi_i) + e^-$ AT $r_{CO} = 3.6\ a_o$

	σ(Mb)			
E_e(Ryd)	$1\pi \rightarrow k\sigma$	$1\pi \rightarrow k\pi$	$1\pi \rightarrow k\delta$	β
0.005	2.83	0.69	10.66	-0.40
0.01	2.79	0.70	10.64	-0.38
0.015	2.76	0.71	10.61	-0.36
0.025	2.69	0.73	10.56	-0.32
0.05	2.53	0.76	10.37	-0.23
0.075	2.38	0.80	10.13	-0.14
0.1	2.25	0.84	9.86	-0.07
0.15	2.02	0.90	9.27	0.06
0.2	1.83	0.96	8.67	0.16
0.25	1.67	1.01	8.11	0.24
0.3	1.53	1.05	7.60	0.31
0.35	1.42	1.09	7.16	0.36
0.4	1.32	1.12	6.76	0.41
0.5	1.17	1.16	6.13	0.50
0.6	1.07	1.19	5.67	0.58
0.8	0.98	1.27	5.07	0.71
1.0	0.99	1.40	4.73	0.83
1.3	1.11	1.66	4.41	0.98
1.6	1.20	1.88	4.08	1.12
1.9	1.08	1.97	3.70	1.24
2.2	0.86	1.92	3.28	1.34
2.5	0.68	1.78	2.89	1.40
3.0	0.48	1.44	2.31	1.46
3.5	0.37	1.09	1.85	1.50
4.0	0.30	0.80	1.47	1.52
4.5	0.25	0.60	1.17	1.54
5.0	0.22	0.46	0.93	1.54

TABLE 8-29

CHANNEL CONTRIBUTIONS TO THE CROSS SECTIONS AND ASYMMETRY PARAMETERS FOR $CO(X^1\Sigma^+) \rightarrow CO^+(B^2\Sigma^+) + e^-$ AT $r_{CO} = 1.6\ a_o$

	σ(Mb)		
E_e(Ryd)	$4\sigma \rightarrow k\sigma$	$4\sigma \rightarrow k\pi$	β
0.005	1.52	1.41	1.30
0.01	1.53	1.40	1.33
0.015	1.54	1.38	1.34
0.025	1.56	1.36	1.37
0.05	1.61	1.30	1.42
0.075	1.64	1.26	1.45
0.1	1.66	1.21	1.48
0.15	1.69	1.15	1.52
0.2	1.70	1.09	1.55
0.25	1.69	1.05	1.57
0.3	1.67	1.02	1.58
0.35	1.64	1.00	1.59
0.5	1.53	0.97	1.60
0.6	1.47	0.96	1.59
0.8	1.37	0.99	1.55
1.0	1.34	1.04	1.51
1.3	1.39	1.12	1.47
1.6	1.48	1.17	1.46
1.9	1.53	1.17	1.47
2.2	1.47	1.13	1.49
2.5	1.33	1.07	1.51
3.0	1.04	0.95	1.55
3.5	0.77	0.83	1.57
4.0	0.57	0.73	1.59
4.5	0.43	0.64	1.60
5.0	0.34	0.57	1.60

TABLE 8-30

CHANNEL CONTRIBUTIONS TO THE CROSS SECTIONS AND ASYMMETRY PARAMETERS FOR $CO(X^1\Sigma^+) \rightarrow CO^+(B^2\Sigma^+) + e^-$ AT $r_{CO} = 2.35\ a_o$

	σ(Mb)		
E_e(Ryd)	$4\sigma \rightarrow k\sigma$	$4\sigma \rightarrow k\pi$	β
0.005	0.56	0.27	0.71
0.01	0.57	0.27	0.63
0.015	0.58	0.28	0.57
0.025	0.59	0.29	0.47
0.05	0.66	0.32	0.25
0.075	0.76	0.36	0.07
0.1	0.92	0.39	-0.04
0.15	1.52	0.47	-0.08
0.2	2.78	0.55	0.10
0.25	4.77	0.63	0.42
0.3	6.04	0.72	0.73
0.35	5.54	0.81	0.98
0.4	4.45	0.90	1.15
0.5	2.90	1.07	1.32
0.6	2.12	1.23	1.37
0.8	1.40	1.45	1.39
1.0	1.06	1.55	1.40
1.3	0.79	1.54	1.42
1.6	0.64	1.43	1.45
1.9	0.55	1.30	1.47
2.2	0.48	1.18	1.48
2.5	0.43	1.07	1.49
3.0	0.38	0.92	1.49
3.5	0.33	0.81	1.50
4.0	0.29	0.70	1.50
4.5	0.26	0.61	1.50
5.0	0.23	0.53	1.50

TABLE 8-31

CHANNEL CONTRIBUTIONS TO THE CROSS SECTIONS AND ASYMMETRY PARAMETERS FOR $CO(X^1\Sigma^+) \rightarrow CO^+(B^2\Sigma^+) + e^-$ AT $r_{CO} = 3.1\ a_o$

	σ(Mb)		
E_e(Ryd)	$4\sigma \rightarrow k\sigma$	$4\sigma \rightarrow k\pi$	β
0.005	0.60	0.81	1.51
0.01	0.60	0.82	1.56
0.015	0.60	0.83	1.58
0.025	0.61	0.85	1.62
0.05	0.61	0.89	1.66
0.075	0.61	0.94	1.68
0.1	0.61	0.98	1.68
0.15	0.61	1.05	1.68
0.2	0.61	1.11	1.67
0.25	0.60	1.16	1.66
0.3	0.60	1.20	1.65
0.35	0.59	1.23	1.64
0.4	0.58	1.25	1.64
0.5	0.57	1.28	1.64
0.6	0.55	1.28	1.64
0.8	0.52	1.25	1.64
1.0	0.49	1.19	1.65
1.3	0.44	1.10	1.67
1.6	0.41	1.02	1.67
1.9	0.38	0.95	1.68
2.2	0.35	0.89	1.68
2.5	0.33	0.82	1.69
3.0	0.31	0.69	1.72
3.5	0.30	0.59	1.76
4.0	0.27	0.51	1.78
4.5	0.25	0.44	1.80
5.0	0.23	0.40	1.82

Roche et al.[346] have determined that at higher energies ℓ^{f}_{OS} is by far the most critical parameter. They reported that in the high-energy region, above about 500 eV, reasonable convergence was not yet assured by taking $\ell^{f}_{OS} = 10$. If the basis taken here was too small, the computations for the higher rotational branches in the upcoming chapter would be very inaccurate. A preliminary investigation similar to the one conducted by Roche et. al.[346] was done in order to have some general idea about the minimum basis required for the present purpose, namely the computation of vibronic intensities and β values of N_2 and CO with He(I) radiation. The results for three different bases used for carbon monoxide are shown in Tables 8-32, 8-33, and 8-34. In agreement with the findings by Roche et al.,[346] the data in Tables 8-32, 8-33, and 8-34 imply that the maximum ℓ in the outer sphere should be higher than in the atomic spheres. It appears that Roche et. al.[346] use a different basis for the initial and final state. In this work, for the computation of cross sections and β values, the same basis was used for the initial and the final wave function. However, tests were conducted, again on CO, to determine if there was any difference between the two approaches. The basis for the initial state was taken as the same as the one used in the SCF interactions to obtain the transition state potentials. In this case, the cross sections at small internuclear distances apparently can differ by as much as 3 % (Table 8-35). It may seem more appropriate to use as the initial wave function in the same form as it has been used in the SCF iterations simply because the function with the expanded basis is not a converged SCF solution. Another way of looking at this could be that the wave

TABLE 8-32

THE EFFECT OF THE "BASIS SET" ON CROSS SECTIONS AND ASYMMETRY PARAMETERS OF CARBON MONOXIDE AT $r_{CO} = 1.6\ a_o$

State of the ion	$\max(\ell_{out})$	$\max(\ell_C) = \max(\ell_O)$	E_e(Ryd)	σ(Mb)	β
X	5	3	0.55	4.176	1.580
X	7	3	0.55	4.175	1.579
X	7	5	0.55	4.183	1.580
A	5	3	0.25	19.721	0.549
A	7	3	0.25	19.722	0.549
A	7	5	0.25	19.711	0.549
B	5	3	0.10	2.889	1.477
B	7	3	0.10	2.891	1.477
B	7	5	0.10	2.877	1.478

TABLE 8-33

THE EFFECT OF THE "BASIS SET" ON CROSS SECTIONS AND ASYMMETRY PARAMETERS OF CARBON MONOXIDE AT $r_{CO} = 2.13\ a_o$

State of the ion	$\max(\ell_{out})$	$\max(\ell_C) = \max(\ell_O)$	E_e(Ryd)	σ(Mb)	β
X	5	3	0.55	9.351	0.8889
X	7	3	0.55	9.361	0.8878
X	7	5	0.55	9.415	0.8871
A	5	3	0.25	14.138	0.2851
A	7	3	0.25	14.140	0.2848
A	7	5	0.25	14.121	0.2850
B	5	3	0.10	1.176	1.0385
B	7	3	0.10	1.177	1.0397
B	7	5	0.10	1.174	1.0330

TABLE 8-34

THE EFFECT OF THE "BASIS SET" ON CROSS SECTIONS AND ASYMMETRY PARAMETERS OF CARBON MONOXIDE AT $r_{CO} = 3.1\ a_o$

State of the ion	$\max(\ell_{out})$	$\max(\ell_C) = \max(\ell_O)$	E_e(Ryd)	σ(Mb)	β
X	5	3	0.55	4.737	0.777
X	7	3	0.55	4.731	0.777
X	7	5	0.55	4.727	0.776
A	5	3	0.25	12.180	0.222
A	7	3	0.25	12.177	0.222
A	7	5	0.25	12.159	0.222
B	5	3	0.10	1.588	1.681
B	7	3	0.10	1.588	1.681
B	7	5	0.10	1.589	1.682

TABLE 8-35

THE EFFECT OF THE "BASIS SET" ON CROSS SECTIONS AND ASYMMETRY PARAMETERS OF CARBON MONOXIDE

Initial State: $\max(\ell_{out}) = 4$ and $\max(\ell_C) = \max(\ell_O) = 2$

Final States: $\max(\ell_{out}) = 7$ and $\max(\ell_C) = \max(\ell_O) = 5$

State of the ion	$r_{CO}(a_o)$	E_e(Ryd)	σ(Mb)	β
X	1.6	0.55	4.149	1.592
X	3.1	0.55	4.857	0.765
A	1.6	0.25	19.921	0.544
A	3.1	0.25	12.335	0.221
B	1.6	0.10	2.972	1.477
B	3.1	0.10	1.582	1.672

function with the expanded basis, after the spherical averaging procedure, has not a significantly different electron density, but, reproduces some minute details of the true eigenfunction, which the original bound state wave function was unable to describe properly.

There is some indication that, at smaller internuclear distances, the basis required for acceptable convergence is larger than at large internuclear separations. This is an unexpected outcome, because the selection rule for photoionization at the united atom limit is:

$$\ell_{\text{continuum}} = \left|\ell_{\text{initial}} \pm 1\right|$$

where, in the united atom limit, the molecular orbitals of CO, (and N_2), become either 2s or 2p orbitals, such that according to the above selection rule the maximum ℓ in the outer sphere at the united atom limit does not have to be larger than 2.

According to the convergence tests done here, the smallest basis used here would have been adequate. It was felt, however, that the rotational motion effects considered in a later chapter might require a larger basis, and the largest basis used in the tests was used for the computation of the dipole moment amplitudes. Let us summarize the procedures followed in the computation of these quantities.

(i) Touching spheres were used for all geometries

(ii) The Latter tail was used in the SCF interations, and for the computation of dipole moment amplitudes. In Rydberg units:

$$V_{\text{out}}(r) = \min[V_{X\alpha}(r), -2Z/r]$$

where Z = 1

(iii) The basis used to represent the initial level was different in the SCF iterations and the computation of the dipole moment amplitudes. The basis used in the SCF iterations was:

$$\ell_{H} \leq 1 \quad \text{and} \quad \ell_{out} \leq 4 \quad \text{for } H_2$$

and

$$\ell_{atom} \leq 2 \quad \text{and} \quad \ell_{out} \leq 4 \quad \text{for } N_2 \text{ and CO.}$$

In the computation of the dipole moment amplitudes, (cross sections and beta values), the bases were the same for the initial level and the continuum wave function:

$$\ell_{H} \leq 3 \quad \text{and} \quad \ell_{out} \leq 5 \quad \text{for } H_2$$

and

$$\ell_{atom} \leq 5 \quad \text{and} \quad \ell_{out} \leq 7 \quad \text{for } N_2 \text{ and CO.}$$

In the homologues of N_2 and CO, we observe a reversal in the binding energies of the outermost molecular orbitals relative to the ordering observed in N_2 and CO. The molecular ion PN^+ has a Σ ground state,[527,528] whereas P_2^+ has a Π ground state.[16,527] As_2^+ seems to have, again, a Σ ground state,[529] whereas Bi_2^+ has a Π ground state.[530] In the homologues of CO, the level with the lowest ionization potential is a σ level in CS,[531] SiO,[532] and GeO,[533] but a π level in GeS,[533,534] SnSe,[533] SnTe,[533,534] and PbTe.[534] The third "one-electron" ionization potential is from a σ orbital in all the homologues whose photoelectron spectra have been recorded. This transition is inbedded in a large number of satellites in the higher homologues of N_2 and CO.[533] The related molecular ion BF^+ appears to have a Σ ground state.[536,537]

Dyke et al.[535] have reported Xα calculations on CO and some of its homologues.[535] No measurements of β values and hν-dependent cross sections of the homologues of N_2 and CO could be located in the literature.

CHAPTER 9

DYNAMICAL SYMMETRY BREAKING IN PHOTOIONIZATIONS FROM INNER SHELLS

When a core level is photoionized in a molecule with several equivalent atoms, the resulting hole may be localized on a particular one of the two or more equivalent centers. This means that the ion with the core hole will have a lowered symmetry. The basic principle underlying this "symmetry breaking" problem is that, in certain situations, there have to be an integral number of particles located in widely separated fragments of the system. For example, when N_2^+ is dissociated into N and N^+, one of the thirteen electrons in the molecular ion will have to "choose" among the two equivalent centers. The X state and the B state of N_2^+ dissociates into $N(^4S^0)$ and $N^+(^3P)$.[539]

In the case of N_2^+, symmetry breaking at the dissociation limit is indicated by common sense. However, molecules can dissociate into fragments which do not conserve the symmetry of the original system in situations where this wouldn't be so obvious. For example, the B state of H_2 dissociates into H(1s) and H(2p).[540]

In quantum mechanical treatments of such situations, one can deal with this complication by removing symmetry constraints, as recently done for O_2^+ by Ruttnik and Lenthe.[541]

Since we plan to compute photoionization parameters and β values at different internuclear separations for N_2, we should give the possibility of symmetry breaking some thought. However, it is believed that the largest internuclear distances considered here are too small to show noticeable effects for valence levels. For the core ionization of

N_2, the situation is different. It will be shown later in this chapter that, for the K-shell photoionization of N_2, at $r_e = 2.08\ a_o$, symmetry breaking lowers the height of the σ-resonance by approximately 8 %, and shifts the β-resonance.

First, let us look at the quantum mechanical description of the symmetry breaking process. Frequently an alert and devoted student of quantum mechanics will question the validity of a theory which lets H_2^+ dissociate into two fragments each containing one half of the electron. In many cases, such objections are dismissed by pointing out to the student that in a time-dependent description of this system the electron will "tunnel" between the widely separated nuclei, and, over an infinite period of time, will spend equal time at both nuclei. It can be shown, however, that, for sufficiently large internuclear separation, a solution with a lowered symmetry will become energetically more favorable. If the problem is being solved in a variational sense, then, according to Moiseyev et al.,[542] symmetry adapted and broken symmetry extrema can be located. These extrema are physically meaningless with the exception of the global minimum which may or may not be a solution with broken symmetry. These authors also pointed out the analogy of the symmetry breaking concept to Buridan's ass' dilemma. Buridan's ass is starving in indecision between two equidistant bales of hay of equal size, as shown in Figure 9-1. The invention of this scenario has been attributed to and named after the French philosopher Jean Buridan. Actually, "Buridan's ass" can't be found anywhere in Buridan's writings,[543] but a major concern of Buridan was man's freedom of choice.[544]

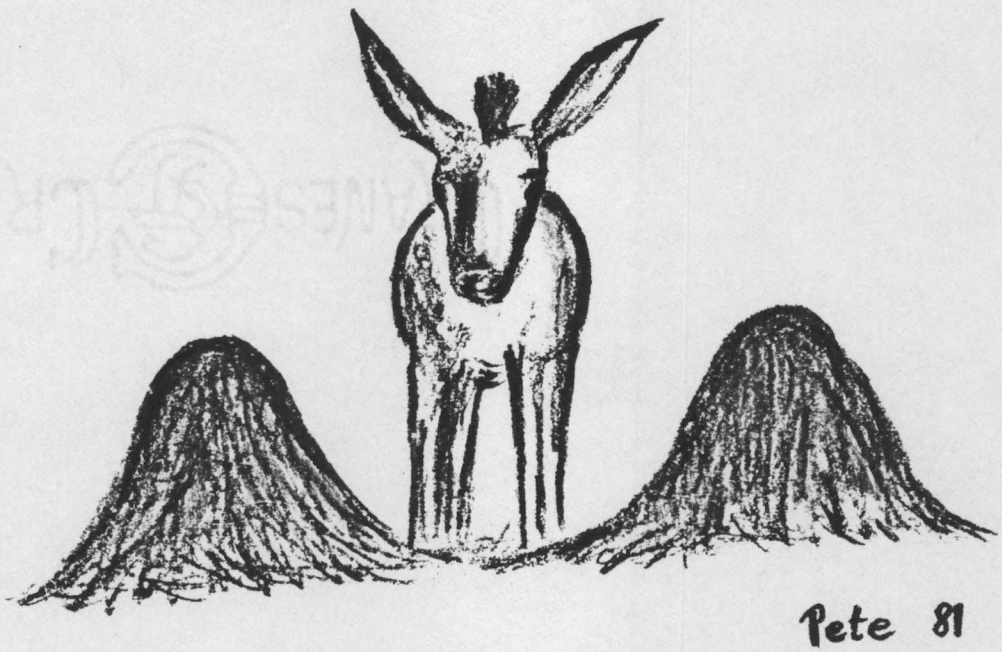


Fig. 9-1. Buridan's ass.

The distinction of "classical" and "nonclassical" structures of some organic molecules has its roots in symmetry breaking.[545] Symmetry breaking can also be observed in the solid state. In crystals with a degenerate energy spectrum, symmetry breaking can arise through autolocalization of exitons.[546] Symmetry breaking is also of interest to relativity theory. Fischer et al.[547] remarked that the space solution of Einstein's equation has an unexpected complexity near a spacetime with symmetries.

In the Born-Oppenheimer approximation, symmetry breaking occurs at a certain critical geometry; i.e., symmetry breaking affects the wave functions representing nuclear motion but not vice versa. It may well be that participation of nuclear motion in the symmetry breaking process has to be considered in some cases. Imagine a molecule vibrating through the "critical" geometry. Every time the molecule passes through the "critical" point, it changes from a symmetry adapted to a broken symmetry electronic structure. This implies an extensive reorganization of the electronic structure with each vibration, such that the situation becomes similar to avoided crossings. It has been indicated that such situations give rise to abnormally large nonadiabatic coupling terms. These situations have a certain resemblance to forced oscillations. In forced oscillations we have a phase lag. In the present case, the vibrational motion represents the driving force, and the "oscillations" of the electronic structure may lag behind. As a consequence the force field is different for an "approach from the left" from the one for an "approach from the right side."

Due to this "phase lag," symmetric molecules with isotopic substitutions can have slightly distorted charge distributions. HD is expected to have a minute dipole moment.[560]

Symmetry breaking can have a considerable effect on ionization energies. For example, Broer and Nieuwpoort[548] found that the O1s ionization energy in CrO_4^{2-} is computed as 551 eV if T_d orbital symmetry is used in HF calculations. If the orbital symmetry was lowered to C_{3v}, the ionization energy decreased to 533 eV in close agreement with the experimental value of 530 eV.

Ågren et al.[549,550] have shown that symmetry adapted solutions gave bond lengths of diatomic molecules with a K hole in poor agreement with experiment.

If the life time of a vacancy in the inner shell is of the same order of magnitude as the time required for the electron to leave, the description of the system as having a localized core hole is still not adequate. The random phase approximation with exchange gives a valid description in all cases.[551]

Using the discrete variational Xα method a symmetry breaking process in a rare gas compound was investigated by Gutsev and Smoljar.[552]

Another application of the Xα method to symmetry breaking was apparently involved in the computation of Auger spectra by Dunlap et al.[553]

Xα calculations were performed for the K-shell ionization of N_2, with a localized core hole, by Dill et al.[554] They used the energy-dependent Hara exchange.[555]

In the present work, the core level ionization of N_2 was computed. The transition state potential was obtained in three steps.

First step: A standard SCF calculation of N_2, (with 1/2 electron removed), using $D_{\infty h}$ symmetry. (The converged potential was used for the computation of cross sections and β values in the $D_{\infty h}$ symmetry).

Second step: The $X\alpha$ potential was converted to $C_{\infty v}$ symmetry by introducing two atomic spheres of nitrogen which initially were identical, (but no longer defined as equivalent).

The "symmetry decks" of $D_{\infty h}$ symmetry were replaced with "symmetry decks" of $C_{\infty v}$ symmetry.

Using the "core" option, the electron was being removed from one particular nitrogen atom by placing two electrons in the 1s level of one nitrogen while placing 3/2 electrons into the 1s level of the other nitrogen atom. What is obtained, at this point, is a "forced" breakage of symmetry, similar to hiding one of the bales of hay from Buridan's ass' view.

Third step: The forced nature of the broken symmetry solution is unsatisfactory. In this step we no longer use the "core" option, and a new set of SCF iterations is performed.

In the last step, strange things were happening. In the very first iteration, the potential was diagnosed as "converged." If the SCF iterations were restarted, unacceptable results were obtained. For example, taking $\ell_N \leq 2$, the resulting core level showed almost 100% d character and the ionization potential seemed to converge near 477 eV. If instead $\ell_N \leq 1$ was taken, the resulting core levels showed almost pure p character. These absurd outcomes could be avoided only if for

the core level $\ell_N = 0$ was specified. On the outer sphere, $\ell \leq 1$ was specified. The following ionization energies were obtained:

First step: 408 eV

Second step: 420 eV

Third step: 420 eV. (9-1)

The change in the ionization potential from the second to the third step was only about 0.03 eV. From the ionization potentials listed in (9-1), it is readily apparent that, after dropping the "core" option, the system does not return to the original solution with $D_{\infty h}$ symmetry.

Since the Xα method does not rest on a variational principle, it is not possible to tell for sure if what has been obtained is a physically meaningful solution. Actually, a comparison between the experimental ionization potential and the computed ionization potentials seems to favor the symmetry adapted solution, which reproduces the experimental value of 410 eV[16] fairly well. As previously mentioned, Ågren et al.[549,550] have shown that a localized treatment of the core hole in N_2 gives improved agreement with experiment.

In Tables 9-1 and 9-2, the cross sections and β values from the computations with $D_{\infty h}$ symmetry are shown. The total cross section of the core level is the sum of the cross sections of the "gerade" and "ungerade" state:

$$\sigma_{1s} = \sigma_g + \sigma_u \tag{9-2}$$

For the β values the weighted average has to be taken:

$$\beta_{1s} = (\sigma_g \beta_g + \sigma_u \beta_u)/(\sigma_g + \sigma_u) \tag{9-3}$$

TABLE 9-1

PHOTOIONIZATION OF THE $1\sigma_g$ LEVEL IN MOLECULAR NITROGEN. ($D_{\infty h}$ SYMMETRY)

	σ(Mb)		
E_e(Ryd)	$1\sigma_g \rightarrow k\sigma_u$	$1\sigma_g \rightarrow k\pi_u$	β
0.01	0.01	0.55	1.57
0.1	0.02	0.58	
0.2	0.05	0.60	1.17
0.3	0.15	0.62	0.88
0.35	0.26	0.63	0.70
0.4	0.46	0.63	0.52
0.45	0.88	0.63	0.38
0.5	1.72	0.63	0.32
0.55	3.05	0.63	0.37
0.6	3.81	0.62	0.51
0.65	3.17	0.62	0.68
0.7	2.28	0.61	0.83
0.75	1.65	0.60	0.96
0.8	1.26	0.59	1.07
0.9	0.95	0.57	1.21
1.1	0.52	0.52	1.38
1.5	0.33	0.45	1.58
2.0	0.25	0.38	1.73
3.0	0.19	0.33	1.85
5.0	0.13	0.29	
10.0	0.08	0.23	1.88
15.0	0.06	0.17	
25.0	0.07	0.10	1.94
35.0	0.03	0.07	
45.0	0.02	0.05	
60.0	0.01	0.03	

These data have been graphed in Fig. 9-2 (p 224).

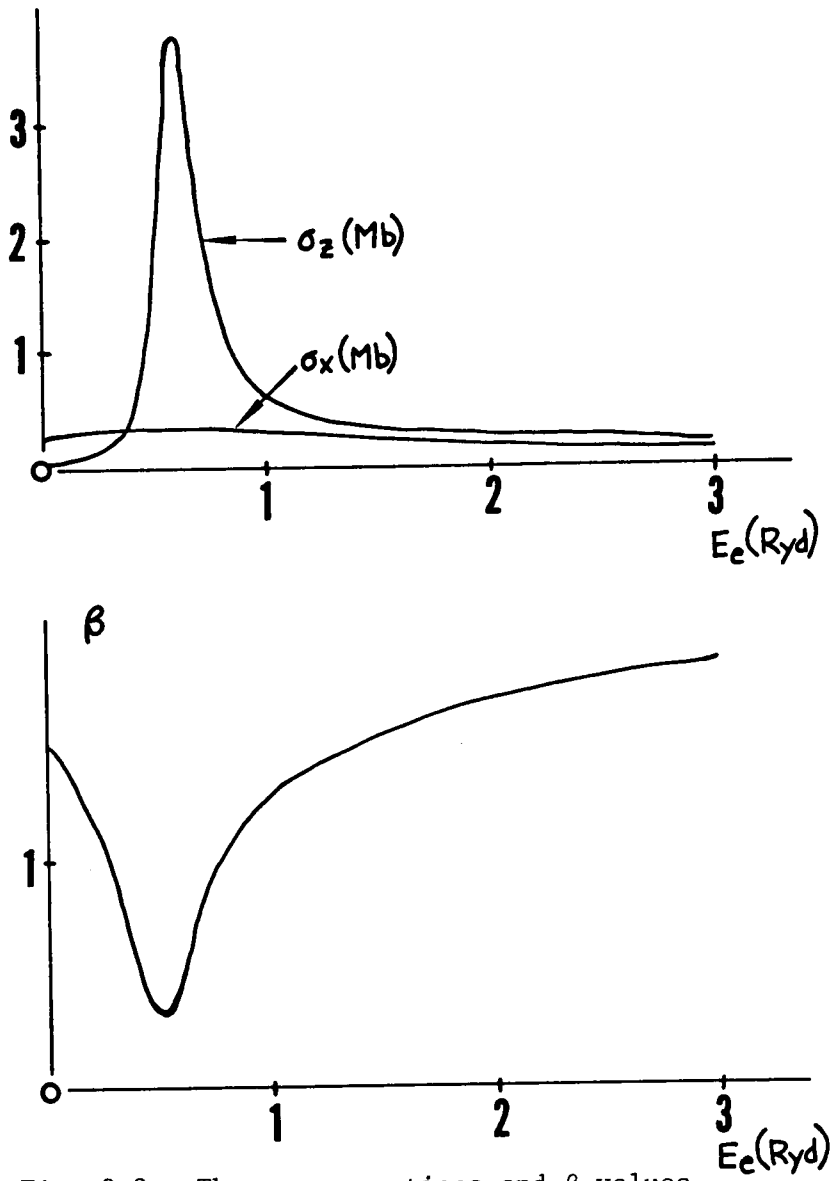


Fig. 9-2. The cross sections and β values of the $(1\sigma_g)^{-1}$ photoionization of N_2. (Using $D_{\infty h}$ symmetry).

TABLE 9-2

PHOTOIONIZATION OF THE $1\sigma_u$ LEVEL IN MOLECULAR NITROGEN. ($D_{\infty h}$ SYMMETRY)

	σ(Mb)		
E_e(Ryd)	$1\sigma_u \rightarrow k\sigma_g$	$1\sigma_u \rightarrow k\pi_g$	β
0.01	0.08	0.26	0.53
0.1	0.09	0.30	0.91
0.2	0.10	0.33	1.13
0.3	0.10	0.36	1.27
0.35	0.10	0.37	1.32
0.4	0.11	0.37	
0.45	0.11	0.38	
0.5	0.11	0.39	
0.55	0.11	0.39	1.45
0.6	0.11	0.40	1.48
0.65	0.11	0.40	1.50
0.7	0.11	0.40	1.52
0.75	0.11	0.41	1.53
0.8	0.11	0.41	1.55
0.9	0.11	0.41	1.58
1.1	0.11	0.42	1.61
1.5	0.11	0.41	1.66
2.0	0.10	0.39	
3.0	0.09	0.33	1.74
5.0	0.10	0.26	
10.0	0.15	0.18	1.84
15.0	0.11	0.14	1.90
25.0	0.04	0.11	1.91
35.0	0.03	0.07	1.91
45.0	0.03	0.05	
60.0	0.01	0.03	

These data have been graphed in Fig. 9-3 (p 226).

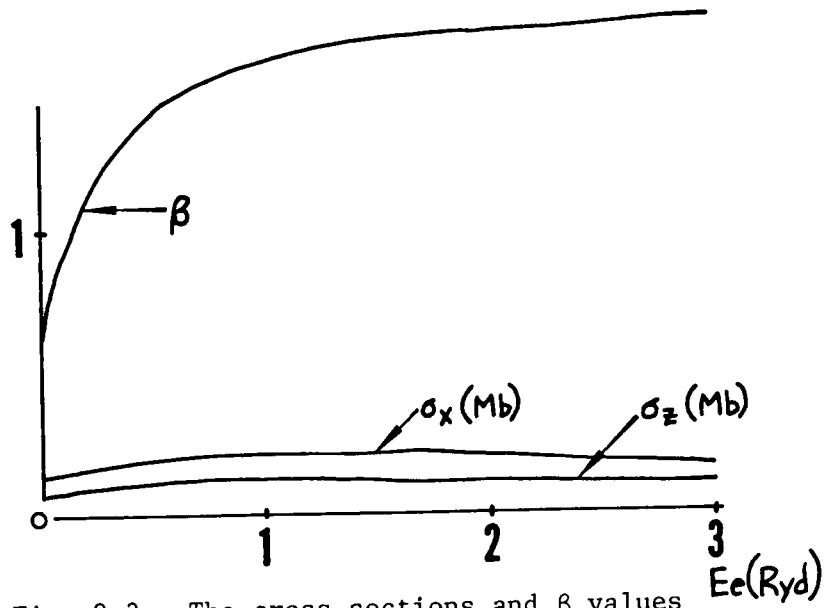


Fig. 9-3. The cross sections and β values of the $(1\sigma_u)^{-1}$ photoionization of N_2. (Using $D_{\infty h}$ symmetry).

The β values were not computed in all cases.

The broken symmetry solution could not be determined properly at E_e = 3 Ryd, apparently because the Ramsauer factor becomes zero in this region of E_e. In the computation of the cross sections and beta values, the wave function of the initial orbital was the same as the one used in the SCF iterations, in contrast to the usual procedure outlined in the last section of the previous chapter.

In the broken symmetry solution, the ion can have a localized hole at any of the previously equivalent centers. For this reason, the cross sections for the broken symmetry solution of N_2 were multiplied by a factor of 2 to obtain the overall cross sections.

The results obtained for the broken symmetry solution are tabulated in Table 9-3 and graphed in Figure 9-4.

Table 9-4 lists the overall cross sections and β values for the two different symmetries. In the cases where the computation of the β values was omitted, the missing values were obtained through a linear interpolation procedure.

In the present investigation, it has been found that the height of the σ-resonance was noticeably lower for the broken symmetry solution, but the location of its maximum remains the same as for the delocalized core hole solution. Dill et al.,[554] who used the Hara exchange, found just the opposite. In their case, the resonance was shifted, but had practically the same height in both cases. Davenport[422] obtained the resonance at approximately 1.2 Ryd, whereas the present calculation gave a resonance at 0.6 Ryd in slightly better agreement with the experimental feature attributed to this resonance,

TABLE 9-3

PHOTOIONIZATION OF THE N1s LEVEL IN MOLECULAR NITROGEN.
(BROKEN SYMMETRY)

	σ(Mb)		
E_e(Ryd)	$1\sigma \rightarrow k\sigma$	$1\sigma \rightarrow k\pi$	β
0.01	0.05	0.38	1.18
0.1	0.07	0.42	1.24
0.2	0.09	0.45	1.23
0.3	0.14	0.47	1.14
0.35	0.20	0.48	1.05
0.4	0.30	0.48	0.92
0.45	0.49	0.49	0.77
0.5	0.85	0.49	0.63
0.55	1.43	0.49	0.57
0.6	1.81	0.49	0.61
0.65	1.58	0.49	0.73
0.7	1.16	0.49	0.87
0.75	0.85	0.49	1.00
0.8	0.66	0.48	1.11
0.9	0.45	0.47	1.26
1.1	0.30	0.45	1.43
1.5	0.21	0.41	1.60
2.0	0.17	0.37	1.71
5.0	0.11	0.27	
10.0	0.11	0.21	1.86
15.0	0.09	0.18	
25.0	0.05	0.10	1.92
35.0	0.03	0.07	
45.0	0.02	0.05	
60.0	0.02	0.03	

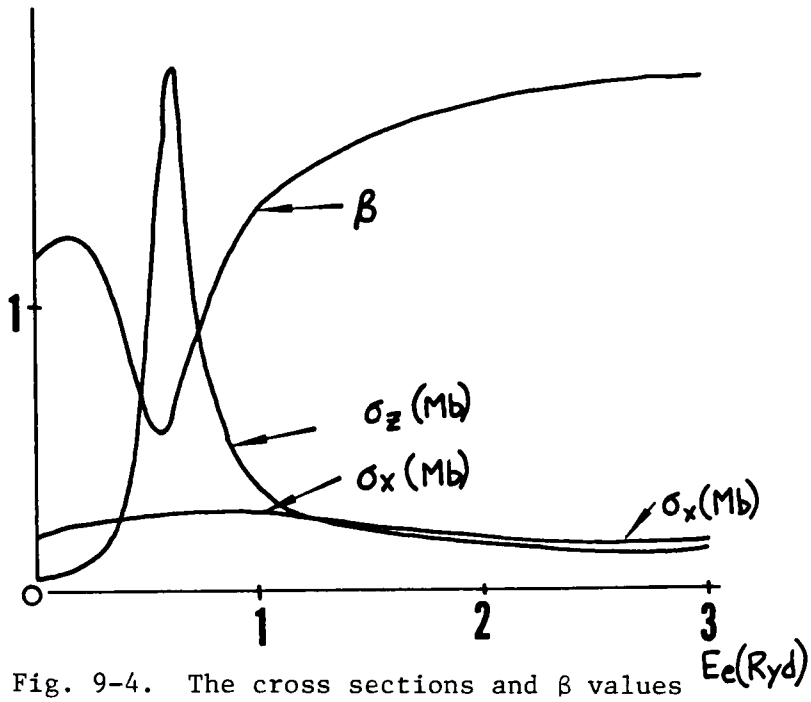


Fig. 9-4. The cross sections and β values of the K-shell photoionization of N_2 obtained with the broken symmetry, ($C_{\infty v}$), solution.

TABLE 9-4

CROSS SECTIONS AND ASYMMETRY PARAMETERS FOR THE CORE LEVEL PHOTOIONIZATION OF N_2

E_e(Ryd)	σ(Mb)		β	
	$D_{\infty h}$	$C_{\infty v}$	$D_{\infty h}$	$C_{\infty v}$
0.01	0.90	0.86	1.18	1.18
0.1	0.99	0.98	(1.19)	1.24
0.2	1.08	1.08	1.15	1.23
0.3	1.23	1.22	1.03	1.14
0.35	1.36	1.36	0.91	1.05
0.4	1.57	1.56	(0.77)	0.92
0.45	2.00	1.96	(0.63)	0.77
0.5	2.85	2.68	(0.51)	0.63
0.55	4.18	3.84	0.50	0.57
0.6	4.94	4.60	0.61	0.61
0.65	4.30	4.14	0.78	0.73
0.7	3.40	3.30	0.93	0.87
0.75	2.77	2.68	1.07	1.00
0.8	2.37	2.28	1.18	1.11
0.9	2.04	1.84	1.30	1.26
1.1	1.57	1.50	1.46	1.43
1.5	1.30	1.24	1.61	1.60
2.0	1.12	1.08	(1.71)	1.71
3.0	0.94		1.80	
5.0	0.78	0.76	(1.82)	
10.0	0.64	0.64	1.86	1.86
15.0	0.48	0.54	(1.90)	
25.0	0.32	0.30	1.93	1.92

The entries with brackets were computed with interpolated β-values.

located 0.8 Ryd above threshold.[378] The discrepancy between the two calculations must be due to the fact that Davenport did not include the Latter tail in the SCF iterations. The vast difference between the results from two different calculations with slightly different procedures is somewhat disturbing.

However, it is a well-known fact that the location of shape resonances depends strongly on parameters which affect the orbital energies very little. For example, Stephens, Dill, and Dehmer,[556] in some cases, adjusted Slater's exchange parameter to "tune" the computed resonance onto the reported experimental maximum attributed to the resonance.

Ågren et. al.[549,550] found it necessary to treat the core hole of N_2 localized when computing band contours from vibronic bands. Whether vibrational motion imparts added significance to symmetry breaking is not certain at the present time, but the possibility can by no means be dismissed, since symmetry breaking is absent in the united atom limit, but "complete" as $r_{NN} \to \infty$. Also, the possibility of strong nonadiabatic effects, arising from symmetry breaking, has been discussed earlier in this chapter.

Recently, Noodleman et al.[557] investigated symmetry breaking using an LCAO-Xα method. They also worked out criteria to be used in assessing whether the symmetry adapted or the broken symmetry solution is the physically meaningful solution. It should be pointed out that, even for variational schemes, the "lowest energy" criterion may not be conclusive in some cases. Cox et al.[558] found that the correlation energies computed for the symmetry adapted and the broken symmetry solution may differ considerably.

VOLUME II

CHAPTER 10

THE EFFECTS OF NUCLEAR MOTION IN THE PHOTOELECTRON SPECTRA OF DIATOMIC MOLECULES

A. THEORY

In the photoionization process, the angular momentum of a rotating molecule couples with that of the photoelectron. For this reason, photoionization cross sections and β values from the same vibronic level, but involving different rotational states, can differ greatly.

Itikawa,[561-563] and Ritchie and Tambe[564] have published expressions for the cross sections and β values for individual rovibronic transitions of diatomic molecules.

The notation by Itikawa is being used here. Itikawa gave the following expression for the partial cross section to an individual rovibronic level:

$$\frac{d\sigma}{d\vec{k}}(\gamma_i v_i J_i \Lambda_i \rightarrow \gamma_f v_f J_f \Lambda_f) = W(E_{ph}, \varepsilon_i, E_e) \sum_{L=0,2} (2L+1) \begin{pmatrix} 1 & 1 & L \\ 0 & 0 & 0 \end{pmatrix} P_L(\cos\theta_k)$$

$$\sum_{\ell=0}^{\infty} \sum_{\bar{\ell}=|\ell-L|}^{\ell+L} [(2\ell+1)(2\bar{\ell}+1)]^{1/2} \begin{pmatrix} \ell & \bar{\ell} & L \\ 0 & 0 & 0 \end{pmatrix} (2J_f+1) \sum_j (-1)^j (2j+1) \begin{Bmatrix} 1 & 1 & L \\ \ell & \bar{\ell} & j \end{Bmatrix}$$

$$\begin{pmatrix} J_f & J_i & J \\ -\Lambda_f & \Lambda_i & \Delta\Lambda \end{pmatrix}^2 \sum_{\lambda=-\ell}^{\ell} \sum_{\mu=-1}^{1} (-1)^{\mu} \begin{pmatrix} \ell & 1 & j \\ -\lambda & \mu & -\Delta\Lambda \end{pmatrix} \langle\langle E_e \ell\lambda \gamma_f v_f J_f \Lambda_f | \hat{a}^{(\mu)} | \gamma_i v_i J_i \Lambda_i \rangle\rangle$$

$$\sum_{\bar{\lambda}=-\bar{\ell}}^{\bar{\ell}} \sum_{\bar{\mu}=-1}^{1} (-1)^{\bar{\mu}} \begin{pmatrix} \bar{\ell} & 1 & j \\ -\bar{\lambda} & \bar{\mu} & -\Delta\Lambda \end{pmatrix} \langle\langle E_e \bar{\ell}\bar{\lambda} \gamma_f v_f J_f \Lambda_f | \hat{a}^{(\bar{\mu})} | \gamma_i v_i J_i \Lambda_i \rangle\rangle^* \qquad (10\text{-}1)$$

where it has been assumed that the continuum wave function has been expanded in partial waves, (ℓ,λ). The summation limits for j are

$$\max(\left|1-\ell\right|,\left|1-\bar{\ell}\right|,\left|J_i-J_f\right|)\leq j \leq \min(1+\ell,1+\bar{\ell},J_i+J_f) \qquad (10\text{-}2)$$

θ_k specifies the direction of the ejected electron relative to the polarization direction of the incident light; P_L is the common Legendre polynomial of order L.[3] The formula in (10-1) is of the same form as (8-18) and (8-19).

The following notation has been used:

(i) γ_i represents the electronic wave function of the initial diatomic molecule, AB, and γ_f represents the electronic wave function of the molecular ion, AB^+.

(ii) Λ is the component of the resultant orbital angular momentum along the molecular axis.[565]

(iii) The notation used here for J differs from the one used by Herzberg.[1] In this text, J denotes the absolute value of the total angular momentum for the case of electron spin zero or loosely coupled.[566] (Herzberg used the symbol K for this quantity).

The electronic states of diatomic molecules are represented by:[1]

$$^{2S+1}\Gamma_{\left|\Lambda\right|+\Sigma} \qquad (10\text{-}3)$$

where

$$\Gamma = \Sigma, \Pi, \Delta, \ldots . \qquad (10\text{-}4)$$

if

$$\left|\Lambda\right| = 0,1,2, \ldots . \qquad (10\text{-}5)$$

respectively. Σ is the component of S along the internuclear axis. It can take on the values:

$$\Sigma = S, S-1, \ldots ., -S \qquad (10\text{-}6)$$

For the Π states we have components of spin doublets, F_1 and F_2 whose energies can be expressed as:[1]

$$F_1(J)=B_v[(J+1)^2-\Lambda^2-(1/2)[4(J+1)^2+Y(Y-4)\Lambda^2]^{1/2}]-D_v(J+1/2)^4$$

$$F_2(J)=B_v[J^2-\Lambda^2+(1/2)[4J^2+Y(Y-4)\Lambda^2]^{1/2}]-D_v(J+1/2)^4 \qquad (10\text{-}7)$$

where $Y = A/B_v$; A is the spin-orbit coupling constant. Although the model by Itikawa does not treat spin-orbit interactions, the cross sections and β values were computed for both components, which differ slightly in E_e. L-S coupling predicts equal intensity for the pairs of spin-orbit split peaks, but spin-orbit interaction causes their intensities to differ slightly.[567] In this work, the cross sections for such pairs differ only in intensity because of the energy dependence of the cross sections, other effects being ignored. The spin-orbit coupling constant of the A state of N_2^+ is 81.5 cm^{-1},[568] and 117.5 cm^{-1} for the A state of CO^+.[569] The effects of Λ doubling are negligible.[570]

The 3-j and 6-j symbols in (10-1) have been used in the notation by Edmonds.[571] They were computed with analytic expressions given by Edmonds, with the exception of the 3-j symbols containing J_i and J_f. Since the rotational quantum numbers can be rather large, the summation given by Edmonds is not suitable for machine computations, partly because it gives rise to overflow and underflow. In this case, the 3-j symbol was evaluated through recursion, as recommended by Schulten and Gordon.[583] The recursion formula given by these authors for the 3-j symbol

$$\begin{pmatrix} j_1 & j_2 & j_3 \\ m_1 & m_2 & m_3 \end{pmatrix} \tag{10-8}$$

gives rise to an undetermined term of "zero divided by zero" if $j_3=j_1-j_2=m_3=0$. This case arises, for example, in the Q-branches of all $\Sigma-\Sigma$ transitions. This complication, which occurs in the upward recursion formula, can be eliminated by substituting in the "0/0" term $x=j_3=m_3$ and taking the limit of the ratio for $x\to 0$. Values obtained for the 3-j symbols computed in these cases were compared with values which had been published,[577] or computed with the analytic expression by Edmonds.

In (10-1), we have a factor W(.....). By comparing the expression given by Itikawa[561] for the total cross section, using the dipole length operator, with the expression given by Davenport,[422] one obtains

$$W(E_{ph}, \varepsilon_i, E_e) = (4/3)(4\pi)^{-1}(\alpha k/E_{ph})(E_e+\varepsilon_i)^{-2} \tag{10-9}$$

where E_{ph} is the energy of the photon and E_e is the energy of the electron. Davenport computes the energy of the photon from the experimental or computed ionization potential, ε_i, using the energy conservation principle. In this work, the energy conservation principle includes the energy of nuclear motion

$$E_e=E_{ph}-\varepsilon_i-\Delta E_{nucl} \tag{10-10}$$

(Notice that here ε_i is a positive number, whereas in Davenport's program it would be a negative number). In this text, ε_i represents the energy difference between the bottom of the potential energy curve

of the parent molecule and the bottom of the potential energy curve of the molecular ion. This definition of ε_i is analogous to the definition of T_e in bound-bound electronic transitions. ΔE_{nucl} is the difference of the energy of nuclear motion in the initial state and the final state, i.e. $\Delta E_{nucl}=E_{vibrot}(v_f,J_f)-E_{vibrot}(v_i,J_i)$.

In (10-9), α is the fine structure constant and k is the magnitude of the wave vector $\vec{k}$ of the photoemitted electron. Using atomic units, (with energies in Rydbergs), we have $k^2=E_e$.

The transitions $\Lambda_i \rightarrow \Lambda_f$ and $-\Lambda_i \rightarrow -\Lambda_f$ are equivalent. They give the same results in (10-1). Due to permutation relations among 3-j symbols,[571] the third 3-j symbol remains unaffected by such a substitution. In the fourth and fifth 3-j symbol, the nonzero dipole moment amplitudes would have opposite signs for λ and μ, and a factor of

$$(-1)^{\ell+\bar{\ell}+2(j+1)} \qquad (10\text{-}11)$$

would arise from those two 3-j symbols. It can be shown that the second 3-j symbol in (10-1) is zero unless the sum of ℓ and $\bar{\ell}$ is even,[571] in which case the factor in (10-11) is unity.

The computation of the 3-j and 6-j symbols is very time consuming. In general, one computes a giant number of cross sections and β values for different rotational and vibrational transitions, and for the photoionization of the same orbital. This allows us to avoid recomputing these quantities by storing them. In Table 10-1, storage schemes are shown, which result essentially in close packing of the nonzero 3-j and 6-j symbols. In the third 3-j symbol, which was computed by recursion, all the 3-j symbols for the range of j, shown in

TABLE 10-1

STORAGE OF 3-J AND 6-J SYMBOLS

Symbol	Storage location	Restriction(s) Used	Amount of Storage[a]
$\begin{pmatrix} \ell & \bar{\ell} & L=0 \\ 0 & 0 & 0 \end{pmatrix}$	$\ell + 1$	$\bar{\ell} = \ell$	$\ell_{max}+1$
$\begin{pmatrix} \ell & \bar{\ell} & L=2 \\ 0 & 0 & 0 \end{pmatrix}$	$2+(7\ell-\bar{\ell})/2$	$\bar{\ell}=\lvert\ell-2\rvert,\ell,\ell+2$	$3(\ell_{max}+1)$
$\begin{pmatrix} \ell & 1 & j \\ -\lambda & \mu & -\Delta K \end{pmatrix}$	$2+\mu+3(4\ell-j+1)$	$j=\lvert\ell-1\rvert,\ell,\ell+1$ $\mu= -1,0,1$ $\lambda=\mu-\Delta K$	$9(\ell_{max}+1)$
$\begin{Bmatrix} 1 & 1 & L=0 \\ \ell & \bar{\ell} & j \end{Bmatrix}$	$4\ell-j+2$	$\ell=\bar{\ell}$ $j=\lvert\ell-1\rvert,\ell,\ell+1$	$3(\ell_{max}+1)$
$\begin{Bmatrix} 1 & 1 & L=2 \\ \ell & \bar{\ell} & j \end{Bmatrix}$	$3-j+(13\ell-\bar{\ell})/2$	$\bar{\ell}=\lvert\ell-2\rvert,\ell,\ell+2$ $j\geq\max(\lvert\ell-1\rvert,\lvert\bar{\ell}-1\rvert)$ $j\leq\min(\ell+1,\bar{\ell}+1)$	$5(\ell_{max}+1)$

[a]It is assumed here that for the 3-j and 6-j symbols containing L, different arrays are used for storage if L=0 and L=2.

(10-2), were evaluated in one step, and stored in an array for later use. The 3-j symbols, in which all three projection quantum numbers are 0, can be computed with a simplified expression.[571]

In the computation of photoionization cross sections, we do not have a simple transition moment function. Guyon and Nenner[480] have formulated the computation of photoionization cross sections in terms of a transition moment function (TMF), which depends on the normal mode coordinate(s) and on E_e

$$\sigma(v_i, v_f) \propto \left| \langle \chi_f \left| M(\vec{q}, E_e) \right| \chi_i \rangle \right|^2 \qquad (10\text{-}12)$$

However, the TMF, M, in (10-12) is obtained through a Stieltjes imaging process.[640] Due to this additional step, most people have chosen to compute vibronic cross sections by integrating the dipole moment amplitudes over the normal mode coordinates. When computing M, one could follow a procedure similar to the one outlined in Chapter 4 for optical spectra, where the TMF can be computed from the observed intensities. A comparison of such an "experimental" TMF with a computed TMF will reveal the geometries where the theory used disagrees with experiment. This would be interesting in connection with resonances. Shape resonances often cut across the $q\text{-}E_e$ plane as ridges which are not parallel to the q-axis, i.e. the maximum of the resonance depends highly on the geometry of the molecule.[574] In optical spectra, the TMF affects the dynamics of the interaction of molecules with radiation fields.[576] For example, the particularly shaped dipole moment function of the molecule HF affects the performance of the HF

chemical laser.[50] In photoelectron spectra, shape resonances can affect the total cross sections and the vibronic branching ratios far from the location of the resonance determined with a calculation at a fixed geometry. In Figure 10-1, Figure 10-2, ..., and Figure 10-6, the dependence of the channel contributions to the cross sections, and the β values, on the internuclear separation is shown for N_2 and CO. Especially for the photoionization of the $3\sigma_g$ level of N_2, the cross sections and β values of the higher members of the vibronic progression with $v_i=0$ should be affected by the presence of a shape resonance although the resonance is not evident at the equilibrium internuclear separation of N_2 at the fixed energy E_e, which was used to prepare Figure 10-1, (E_e=0.37 Ryd).

The TMF could not be obtained reliably from a single vibronic progression, even if the number of the observed transitions is large. This is indicated by the fact that in the harmonic approximation, the energy E_e changes linearly with v_f, and the r-centroids also change linearly with v_f to a good approximation.[578] For this reason, the two variables in the photoelectron TMF are highly correlated, at least in the r-centroid approximation. The situation encountered here, according to Blass,[579] is an "accidental" rather than an "essential" linear dependence because it can be removed by enlarging the data set, in this case by adding additional vibronic progressions, (hot bands).

The problem can be overcome also by removing the dependence of the TMF on E_e, by taking the spectrum at a fixed E_e. Photoelectron spectra obtained at fixed E_e, by sweeping E_{ph}, have been recorded by Eland.[580] A special case of such a technique is threshold

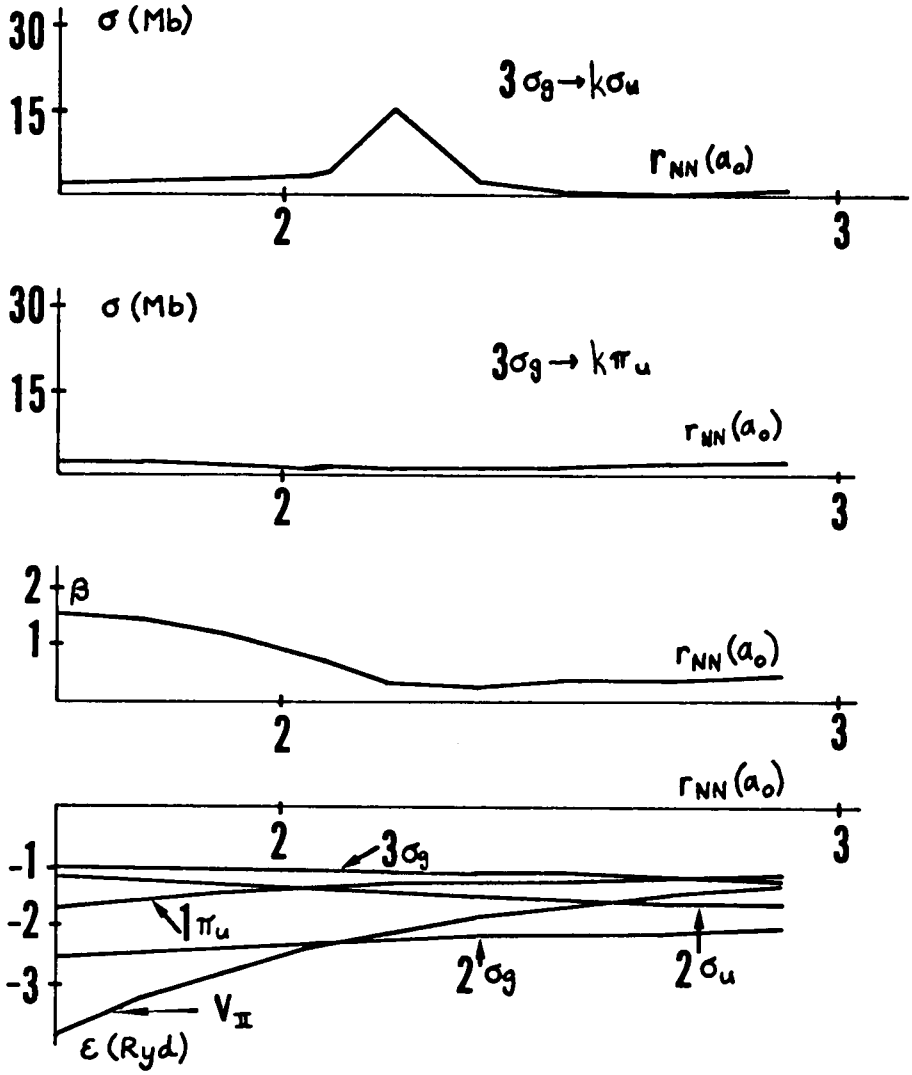


Fig. 10-1. The r_{NN}- dependence of the channel contributions to the cross sections, the β values, and the orbital energies in the $(3\sigma_g)^{-1}$ photoionization of N_2 for E_e= 0.37 Ryd.

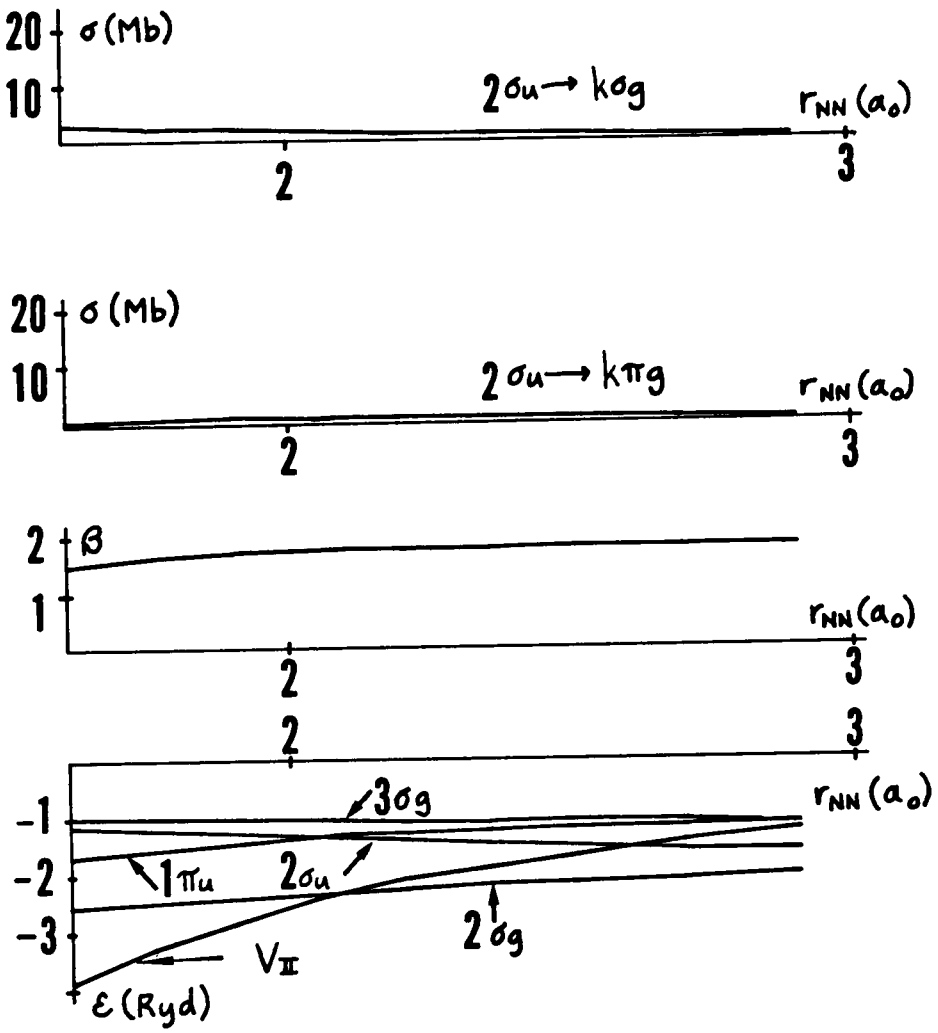


Fig. 10-2. The r_{NN}-dependence of the channel contributions to the cross sections, the β values, and the orbital energies in the $(2\sigma_u)^{-1}$ photoionization of N_2 for E_e = 0.14 Ryd.

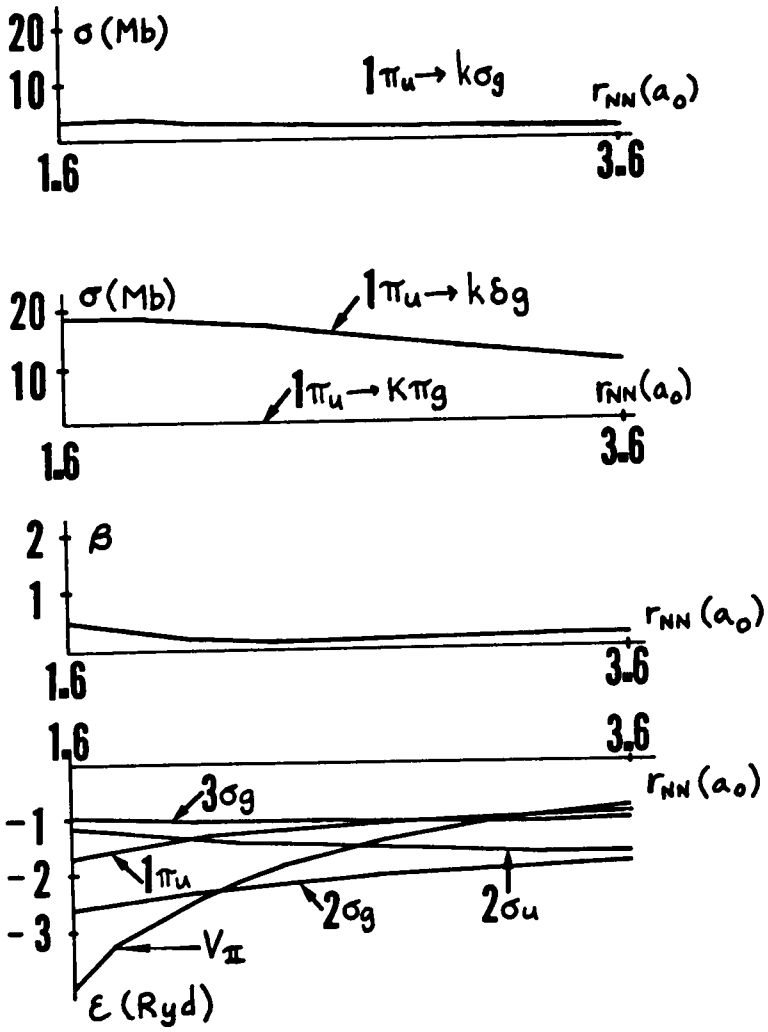


Fig. 10-3. The r_{NN}- dependence of the channel contributions to the cross sections, the β values, and the orbital energies in the $(1\pi_u)^{-1}$ photoionization of N_2 for E_e= 0.19 Ryd.

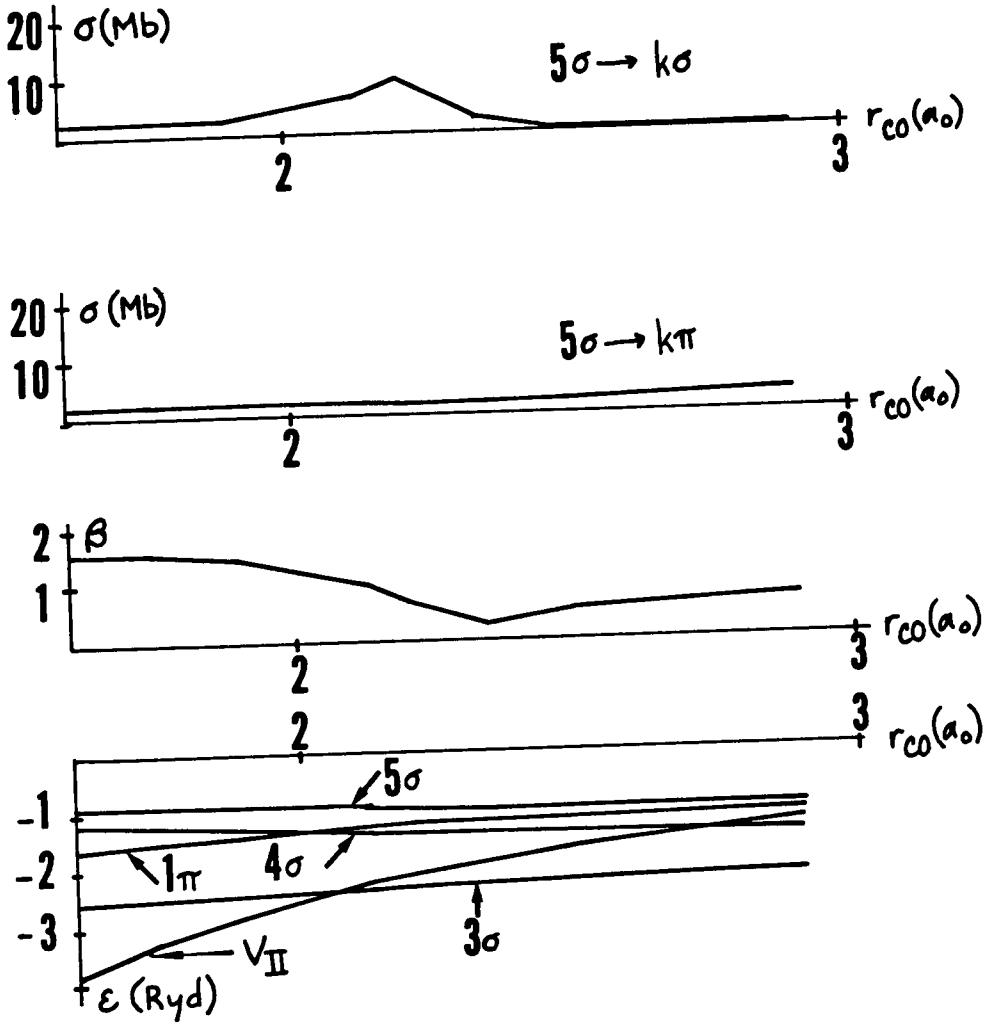


Fig. 10-4. The r_{CO} - dependence of the channel contributions to the cross sections, the β values, and the orbital energies in the $(5\sigma)^{-1}$ photoionization of CO for E_e= 0.49 Ryd.

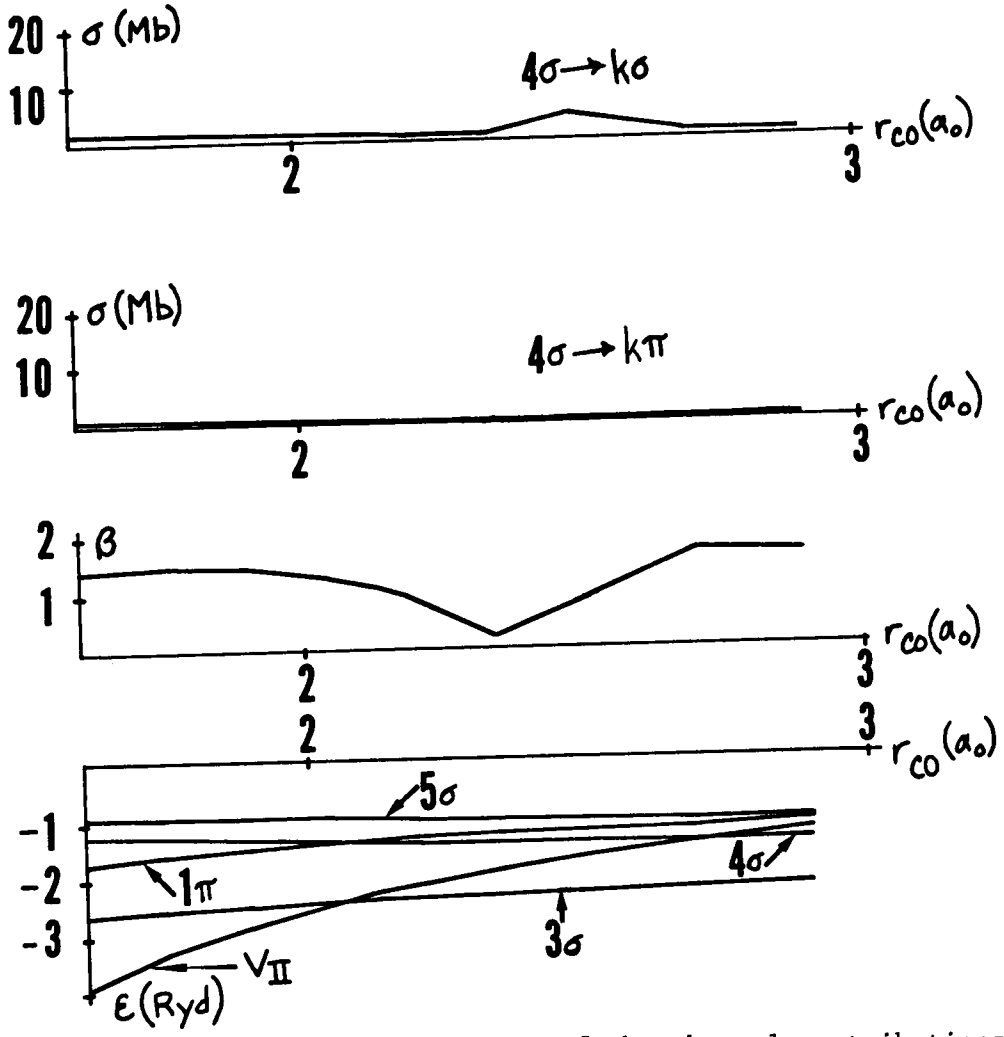


Fig. 10-5. The r_{CO}- dependence of the channel contributions to the cross sections, the β values, and the orbital energies in the $(4\sigma)^{-1}$ photoionization of CO for E_e= 0.05 Ryd.

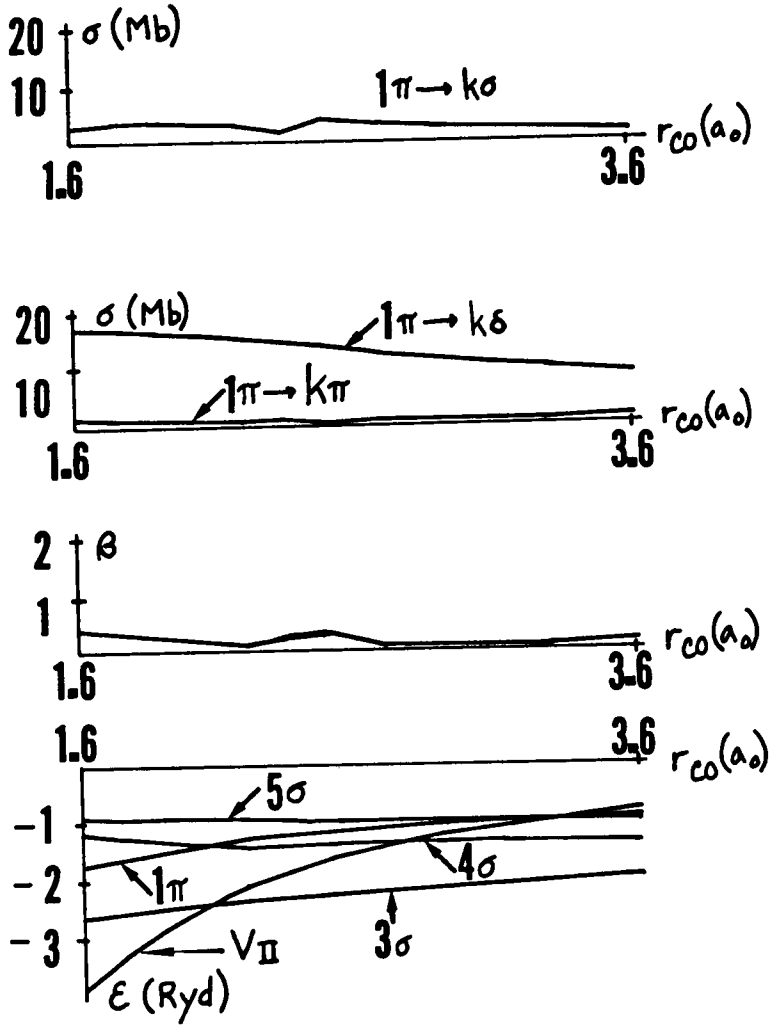


Fig. 10-6. The r_{CO}- dependence of the channel contributions to the cross sections, the β values, and the orbital energies in the $(1\pi)^{-1}$ photoionization of CO for E_e= 0.17 Ryd.

photoelectron spectroscopy, which gives spectra with extremely high resolution if the width of E_{ph} is small.[581]

In (10-1), the quantities

$$\langle\langle \ldots\ldots \left| \hat{a}^{(\mu)} \right| \ldots\ldots \rangle\rangle \qquad (10\text{-}13)$$

will be referred to as the "dipole moment amplitudes of the partial waves," (DMAPWs). Actually, the quantities in (10-13) represent individual components μ of the DMAPWs. The interaction with the radiation field can be represented by the operator[422]

$$\vec{A}\cdot\nabla V=(4\pi/3)\left[\sum_{\mu} Y^{*}_{1\mu}(\vec{A})Y_{1\mu}(\vec{r})\right]\frac{\partial V}{\partial r} \qquad (10\text{-}14)$$

where $\mu = -1,0,1$. In (10-13), the integration is over the coordinates of the electrons and the nuclei. Since, in this work, the acceleration operator is used, the operator in (10-13) is represented by "$\hat{a}$." The integration over the electronic and nuclear coordinates for each rovibronic transition is impractical. For this reason, an alternate approach was tried. Let us assume that we can express the DMAPWs analytically in terms of q and E_e, for example with an expansion of the form

$$\text{DMAPW}\sim A\left(q,E_e;\beta_o^2\right)=\Sigma_n\Sigma_m c_{nm} q^n\left(E_e-E_{ref}\right)^m \exp\left(-\beta_o^2 q^2/2\right) \qquad (10\text{-}15)$$

Then, we need expectation values

$$S_n\left(v_i,J_i;v_f,J_f;\beta_o^2\right)=\langle\chi_f\left|q^n\exp\left(-\beta_o^2 q^2/2\right)\right|\chi_i\rangle \qquad (10\text{-}16)$$

in which case the DMAPWs can be expressed as

$$DMAPW \sim \Sigma_n \Sigma_m c_{nm} S_n(v_i, J_i; v_f, J_f; \beta_o^2)(E_e - E_{ref})^m \qquad (10\text{-}17)$$

The expectation values S and the expansion coefficients can then be stored in the program which computes (10-1).

In the computation of the expectation values in (10-16), the influence of the rotational motion can be taken into account by its effect on the vibrational wave functions. In diatomic molecules, we have only one rotational quantum number. We can use a power series expansion to simulate the rotational dependence of the expression in (10-16)

$$S_n(....) \sim g_{00}^{(v_i, v_f; n)} + g_{10}^{(v_i, v_f; n)} J_f + g_{01}^{(v_i, v_f; n)} J_i + g_{20}^{(v_i, v_f; n)} J_f^2 + g_{02}^{(v_i, v_f; n)} J_i^2 + g_{11}^{(v_i, v_f; n)} J_i J_f + \ldots\ldots \qquad (10\text{-}18)$$

where the approximation would have to be made for each n, v_i, and v_f to be used. In this work, the approximation in (10-18) was done by a non-weighted least squares fit of data with an appropriate range of J_i and J_f. The details of these procedures have been described by the present author and Crosby.[582] The number of terms used was the same as the number of terms shown in (10-18), in all cases in which the effects of vibration-rotation interaction were included. In the cases where the expectation values in (10-18) have been computed with more than one term, the computation is said to have "vibration-rotation interaction included." The effect of the rotation on the vibrational wave functions was included in the same way as in Pekeris' original work.[59]

The DMAPWs are complex quantities. Consequently, the expansion coefficients in (10-15) will be complex numbers. Their real and their imaginary parts were obtained by separate least squares fits of the real parts, and of the imaginary parts of the computed DMAPWs.

The least squares fits of the DMAPWs are not straightforward. The problem is illustrated in Figure 10-7 and in Figure 10-8. Although the cross sections in the absence of resonances change in a monotonous fashion, the real and the imaginary parts of the DMAPWs undergo wild oscillations. Actually, the DMAPWs of H_2, shown in Figure 10-7 and in Figure 10-8, are relatively well behaved. Nevertheless, the problems associated with the least squares fit of the DMAPWs are plainly visible in Figure 10-7 and in Figure 10-8. Due to the oscillatory behaviour of the DMAPWs, high powers of q have to be included in the least squares fit. This has the following undesirable effects:

a. Outside the range of sampled values of q, the approximation shoots up or down. This unrealistic behaviour leads to nonsensical results, because the tails of the wave functions extend into this region.

b. The approximation can buckle if the sample points are widely separated.

The dependence of the DMAPWs on E_e is not oscillatory over the energy range of vibronic progressions, at least not in the examples presented here. The problem in "a" can be dealt with by modifying the behaviour of the approximation outside the sampled range of q. Such a modification can be achieved by using a different set of functions in the least squares approximation. Piecewise definition of the functions

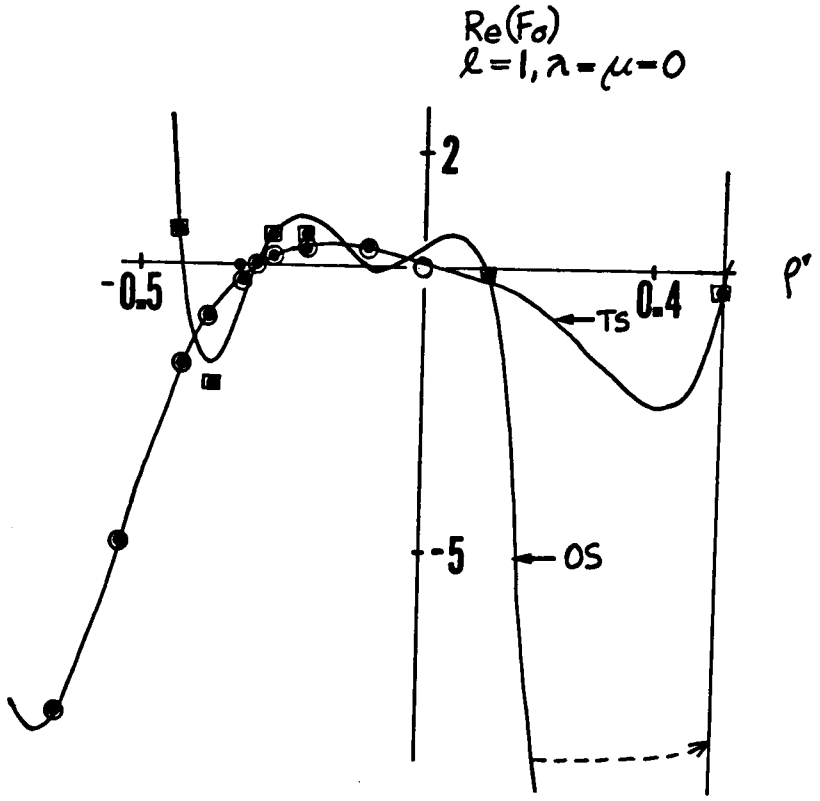


Fig. 10-7. The real part of the dipole moment amplitude of a partial wave with $\ell=1$ and $\lambda=\mu=0$ for the photoionization of H_2 as a function of the internuclear separation.

The internuclear separation is expressed in ρ', where $\rho' = r_{HH}-r'_e$. E_e is fixed at $E_e = 0.375$ Ryd.
Computed results are shown for results obtained with touching spheres (TS) and overlapping spheres (OS). The data obtained with TS are shown as circles and the data obtained with OS are shown as squares. The solid lines are least squares approximations of the data.

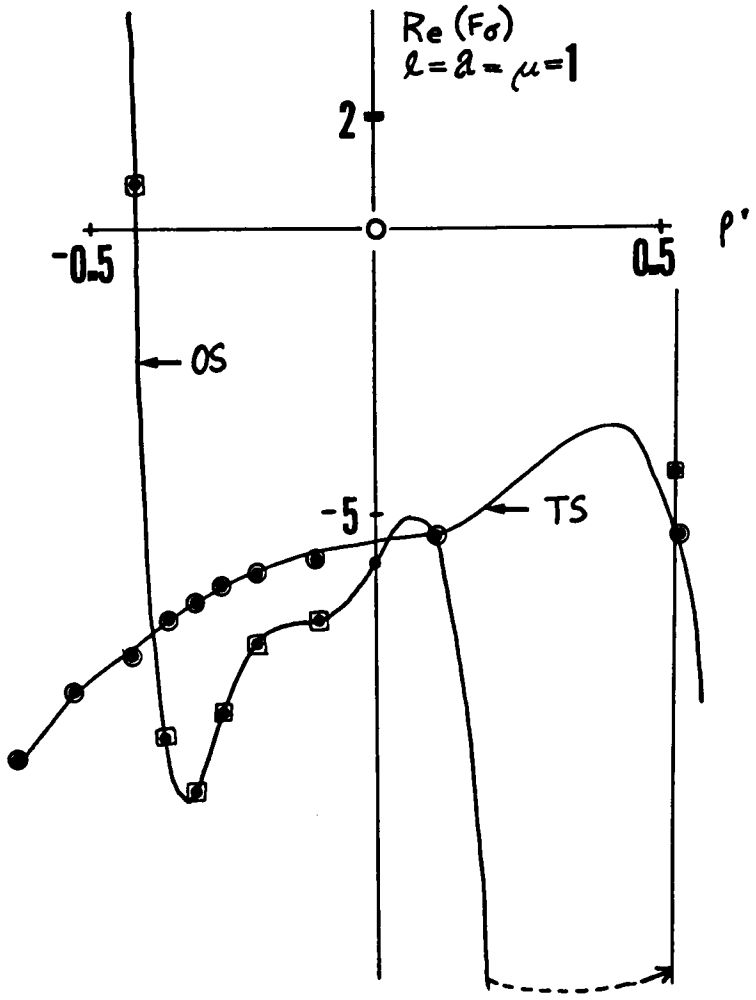


Fig. 10-8. The real part of the dipole moment amplitude of a partial wave with $\ell=\lambda=\mu=1$ for the photoionization of H_2 as a function of the internuclear separation.

E_e is fixed at E_e = 0.375 Ryd. For an explanation of the labels see Fig. 10-7 on the preceding page.

can be very useful in such a situation. Let us assume that the range of q where DMAPWs were sampled was

$$q_{min} \leq q \leq q_{max} \tag{10-19}$$

Then we redefine S_n as

$$S_n(.....)=\langle \chi_f | f_n(\beta_o^2;q) | \chi_i \rangle \tag{10-20}$$

where the functions f_n in this work were defined as

$$f_n(\beta_o^2;q)=s^n \exp(-\beta_o^2 s^2/2) \tag{10-21}$$

where

$$s=\begin{cases} q_{max} & \text{if } q>q_{max} \\ q_{min} & \text{if } q<q_{min} \\ q & \text{if } q_{min} \leq q \leq q_{max} \end{cases} \tag{10-22}$$

This modification will not affect the least squares approximation of the DMAPWs, as shown in (10-15), because, inside the range of q where samples were taken, we have s=q. It will affect, however, the computation of the expectation values S_n in (10-10). Since these expectation values are computed by numerical integration, only minor changes are required in going from (10-16) to (10-21). The functions approximating the DMAPWs will then be completely flat outside the range of q shown in (10-19). The present approximation reduces to the Franck-Condon approximation if $q_{min}=q_{max}$, i.e., if only one geometry was used.

When investigating the problem of "buckling," the initial concern is the accuracy of the original data. If these data show a considerable scatter, the problem will be complicated by this fact. The most plausible sources of inaccuracies in the computation of DMAPWs are:

(i) The mesh points of the Numerov integration for the computation of the wave function could change abruptly in their total number, and in the pattern of their placement at different geometries, causing discontinuities of the computed DMAPWs.

(ii) The SCF iterations, which appear converged in respect to the orbital energies, may not be adequately converged in respect to the DMAPWs.

In Table 10-2, two DMAPWs of H_2 at $r_{HH}=r_e$ are shown for transition state potentials which had converged to different extents. The development of the DMAPWs with each iteration parallels the development of the ionization potential and also of the total cross section and the β value. The convergence test, whose outcome is presented in Table 10-2, shows that the DMAPWs are properly converged at the accepted selfconsistency of the potential. This test gives information about a particular case only. Nevertheless, one can assume that adopted standards of selfconsistency are adequate in most cases. The DMAPWs in the column headings are simply identified by the corresponding partial wave and the component of the radiation field:

$$F_\sigma(\ell,\lambda;\mu) \qquad (10\text{-}23)$$

A common technique used to test the noise level in a function consists in the examination of a tiny segment of the function. In

TABLE 10-2

CONVERGENCE TESTS FOR THE HYDROGEN MOLECULE

j	ε_α(Ryd)	ε(Ryd)	σ(Mb)	β	$F_\sigma(1,1;-1) = F_\sigma(1,-1;1)$	$F_\sigma(1,0;0)$
1	0.0073	-1.4547	5.7214	1.8094	-8.0487-8.0403i	-0.8270-7.2913i
2	0.0044	-1.4557	5.7190	1.8093	-8.0469-8.0478i	-0.8226-7.2912i
3	0.0027	-1.4563	5.7179	1.8092	-8.0461-8.0519i	-0.8201-7.2913i
4	0.0016	-1.4566	5.7168	1.8092	-8.0456-8.0539i	-0.8187-7.2912i
5	0.0010	-1.4568	5.7169	1.8092	-8.0454-8.0556i	-0.8178-7.2913i
6	0.0006	-1.4569	5.7168	1.8092	-8.0454-8.0562i	-0.8176-7.2915i
7	0.0003	-1.4570	5.7165	1.8092	-8.0453-8.0569i	-0.8171-7.2915i
8	0.0002	-1.4570	5.7162	1.8092	-8.0452-8.0568i	-0.8171-7.2915i
9	0.0001	-1.4570	5.7168	1.8092	-8.0453-8.0574i	-0.8171-7.2917i
10	0.0001	-1.4571	5.7165	1.8092	-8.0454-8.0574i	-0.8172-7.2917i

E_e is 0.25 Ryd.

j is the number of the Xα SCF iteration.

ε_α is a measure of convergence in the Xα program (EPSILON).

Table 10-3, a test is shown for the photoionization of the 1π level of CO. DMAPWs were computed from converged transition state potentials, which differed in r_{CO} in increments of $0.0125a_o$. The differences between "neighbouring" DMAPWs show that they don't change smoothly with r_{CO}. However, the noise appears to be well below 1% of the values of the DMAPWs.

The buckling of the approximation has been solved by substituting sets of linearly interpolated points. The initial data were computed on a rectangular grid where, for each geometry, the same set of energies (E_e) was used. The linearly interpolated points were inserted for each energy such that they were equidistant in the intervals between neighbouring points. In the present work, five points were inserted per interval between neighbouring sample points. The insertion can be formulated mathematically as follows:

Assume computations have been done at K different geometries, which are along the normal mode coordinate in "increasing order" at q_1, q_2, q_3, ... Let d_n denote

$$d_n=(q_{n+1}-q_n)/(N+1) \qquad (10-24)$$

where N is the number of points inserted per interval. The inserted points are then at

$$q_i + jd_i,\ j=1,2,.....,\ N \text{ and } i=1,2,....,\ K-1 \qquad (10-25)$$

Using the inserted points, a weighted least squares approximation was done. In this modified least squares scheme, the original data

TABLE 10-3

TESTING FOR NOISE

$(CO(X^1\Sigma^+) \rightarrow CO^+(A^2\Pi_i) + e^-)$

	$r_{CO}(a_o)$	$F_\sigma(\lambda,m;\mu)$	Differences
	2.125	-2.7772-2.9602i	
			0.0124+0.0213i
ℓ=0	2.1275	-2.7648-2.9389i	
			0.0089+0.0227i
λ=0	2.13	-2.7559-2.9162i	
			0.0143+0.0233i
μ=1	2.1325	-2.7416-2.8929i	
			0.0095+0.0237i
	2.135	-2.7321-2.8692i	
	2.125	1.6471+0.9663i	
			-0.0080-0.0006i
ℓ=1	2.1275	1.6391+0.9657i	
			-0.0067-0.0013i
λ=0	2.13	1.6324+0.9644i	
			-0.0088-0.0003i
μ=1	2.1325	1.6236+0.9641i	
			-0.0070-0.0015i
	2.135	1.6166+0.9626i	
	2.125	1.7990-0.8881i	
			-0.0106+0.0065i
ℓ=1	2.1275	1.7884-0.8816i	
			-0.0107+0.0057i
λ=1	2.13	1.7777-0.8759i	
			-0.0107+0.0074i
μ=0	2.1325	1.7670-0.8685i	
			-0.0110+0.0054i
	2.135	1.7560-0.8631i	

E_e = 0.3435 Ryd.

were given a uniform weighting factor of $1-\eta$, and the inserted points were given the uniform weighting factor of

$$\eta((\text{number of original points})/(\text{number of inserted points})) \quad (10\text{-}26)$$

Since the weighting factors should be nonnegative, we require

$$0 \leq \eta \leq 1 \quad (10\text{-}27)$$

The quantity η will be referred to as "damping parameter." With this weighting scheme, one would expect that the original and the inserted data would be equally well approximated by taking a damping parameter of one half. However, with such a high damping parameter, the inserted points are better approximated, probably because the original data points are located in the edges of the connected line segments. The approximation tends to "smooth" these edges.

We need now a measure of the "goodness" of the approximation. One such measure is the "standard error of estimate" (SEE). Let us represent the data sampled at the coordinates $\vec{x}_1$, $\vec{x}_2$, ... by y_1, y_2, ..., and the least squares approximation by $F(\vec{x})$. The SEE is defined here as

$$\text{SEE}=[[\Sigma_i(y_i-F(\vec{x}_i))^2]/(\text{number of points}-1)]^{1/2} \quad (10\text{-}28)$$

A more useful measure of the "goodness" of the approximation is the "relative error" (R.E.)

$$\text{R.E.}=(100\%)\text{SEE}/[\max(y_1,y_2, \ldots.)-\min(y_1,y_2, \ldots.)] \quad (10\text{-}29)$$

which takes into account the range of y in the original data.

Least squares approximations have been done for the fixed geometries of the initial states of H_2, N_2, and CO. For the least squares approximation at a fixed geometry, the interpolation procedure is not used, of course. These least squares approximations are relatively straightforward and they will not be discussed further.

In the least squares approximation, the dipole moment amplitudes of the different partial waves are all expanded with the same set of terms, i.e., the same set of terms is used in (10-15) for all of the partial waves. It turns out that the DMAPWs with low quantum numbers ℓ require the greatest number of terms for an acceptable approximation. Among the DMAPWs which are hardest to approximate, the number of terms needed is usually comparable. The DMAPWs with high quantum numbers ℓ are then approximated with an excessive number of terms. The buckling problem is the most serious for the DMAPWs with low quantum numbers ℓ. The buckling problem is caused by the large number of terms needed for their approximation.

The least squares approximations were done in two steps. In the first step, an initial least squares approximation was done with just one term, and thereafter terms were added in a systematic fashion. The terms giving rise to a negligible decrease in the average SEE were later dropped. To the first term, the terms with n+m=1, then n+m=2, etc., were added, one after the other, until the maximum R.E. among all the needed least squares approximations had decreased to 1-3%.

The second step involves the inserted points. This step is omitted if the data set originates from a computation at a single geometry.

In this step, the inserted points are given increasing weight by increasing the damping parameter. The relative error is computed for the original points and the inserted points separately. (The relative error for the inserted points is abbreviated R.P.E.). The damping parameter is increased until the maximum R.E. computed for the inserted points has decreased to two or three times the maximum R.E. computed for the original sample points.

The geometries at which computations were done are shown in Table 8-2 for H_2, in Table 8-3 for N_2, and in Table 8-4 for CO. The energies of the photoelectron, E_e, were sampled in constant increments such that the range of E_e for the first vibronic progression in the corresponding 58.4 nm photoelectron spectra was covered. The range of E_e and the increment of E_e is shown for N_2 and CO in Table 10-4. The sampled energies for H_2 were: E_e=0.25 Ryd + j(0.03125 Ryd), where j=0,1,...,7.

The least squares approximations for N_2 and CO are summarized in Table 10-5. One can see there that the relative error at the original sample points rises to as much as 10% after the "debuckling" procedure. If this should translate into corresponding uncertainties in the computation of the cross sections and β values, it will be very difficult to make meaningful comparisons between vibronic levels, and to discuss with confidence minor effects such as the rotational temperature of the sample, and vibration-rotation interaction.

However, it will be shown later that, although the dipole moment amplitudes of individual partial waves are not too well approximated, the quantities in (10-1) are very well approximated. No plausible explanation could be found for this phenomenon, but an extensive series

TABLE 10-4

SAMPLING OF PHOTOELECTRON ENERGIES

Molecule	State of the ion	$\min(E_e)$	$\max(E_e)$	ΔE_e	No. of energies
N_2	X	0.33	0.45	0.02	7
N_2	A	0.15	0.37	0.02	12
N_2	B	0.10	0.22	0.02	7
CO	X	0.45	0.57	0.02	7
CO	A	0.13	0.37	0.02	13
CO	B	0.02	0.15	0.01	14

The energies are in Rydbergs.

TABLE 10-5

LEAST SQUARES APPROXIMATION OF THE DIPOLE MOMENT AMPLITUDES

(Five points have been inserted per interval)

Molecule	State of the ion	Number of terms	max (n)	max (m)	$R.E._{ave}$(%)	$R.E._{max}$(%)	$R.P.E._{ave}$(%)	$R.P.E._{max}$(%)	η
N_2	X	40	10	3	2.35	10.18	4.33	17.99	0.07
N_2	A	33	9	4	2.24	3.66	4.24	6.94	0.09
N_2	B	21	6	3	0.16	0.49	0.23	0.96	0.30
CO	X	28	9	2	1.89	8.67	3.72	16.49	0.05
CO	A	48	12	4	1.15	6.70	2.13	12.82	0.05
CO	B	44	10	5	2.07	4.65	5.37	9.72	0.15

of tests, not all of which are documented in this text, led to the above conclusion.

Let us first describe the different types of approximations used for the vibrational motion:

FR: This is the abbreviation used for computations based on the Franck-Condon principle. The least squares approximation in (10-15) was done for DMAPWs computed at the equilibrium geometry of the ground state only, and in (10-15) all terms had n=0.

RC: This is the abbreviation used for the r-centroid method. This is essentially, again, a computation at a fixed geometry analogous to FR. However, the technique used was slightly different than for computations in the Franck-Condon approximation, (see below).

RD: The method "RD" involves integration over the nuclear coordinates in the Herzberg-Teller approximation, i.e. max(n)>0 in (10-17).

The wave functions representing nuclear motion were the eigenfunctions of Morse potentials obtained from the set of spectroscopic constants shown in Table 10-6. From these, the r-centroids shown in Table 10-7 and in Table 10-8 were computed. In Table 10-8, the combined classical regions of the initial and final vibronic levels are shown for N_2 and CO, (see (5-34) and the text between (5-34) and (5-35)).

The subscripts "vr" refer to the treatment of vibration-rotation interaction. If the effects of vibration-rotation interaction were

TABLE 10-6

SPECTROSCOPIC CONSTANTS OF DIATOMIC MOLECULES[a]
(ACCORDING TO HUBER AND HERZBERG, REF. 16)

Molecule	State	T_e	ω_e	$\omega_e x_e$	r_e(Å)	B_e	α_e	$10^6 D_e$
H_2	$X^1\Sigma_g^+$		4401.21	121.336	0.74144	60.8530	3.0622	47100
H_2^+	$X^2\Sigma_g^+$		2321.7	66.2	1.052	30.21	1.685	18000
HD^+	$X^1\Sigma_g^+$		3813.15	91.65	0.74142	45.655	1.986	26050
HD	$X^2\Sigma_g^+$		2010.9[c]	49.7[c]	1.057[b]	22.452[b]	1.00[b]	11000[b]
D_2	$X^1\Sigma_g^+$		3115.50	61.82	0.74152	30.4436	1.0786	11410
D_2^+	$X^2\Sigma_g^+$		1642.4[c]	33.1[c]	1.0559	15.016	0.560	5300
N_2	$X^1\Sigma_g^+$		2358.57	14.324	1.09769	1.99824	0.01732	[5.76]
N_2^+	$X^2\Sigma_g^+$		2207.00	16.10	1.11642	[1.93176]	0.01881	[6.10]
N_2^+	$A^2\Pi_{ui}$	9166.9	1903.70	15.02	1.1749	1.7444	0.01883	5.6
N_2^+	$B^2\Sigma_u^+$	25461.5	2419.84	23.189	1.0742	2.07456	0.024	[6.17]
CO	$X^1\Sigma^+$		2169.81	13.288	1.12832	1.93128	0.01750	6.12
CO^+	$X^2\Sigma^+$		2214.24	15.164	1.11514	1.97720	0.01896	6.35
CO^+	$A^2\Pi_i$	20733.3	1562.06	13.532	1.24377	1.58940	0.01942	6.6
CO^+	$B^2\Sigma^+$	45876.7	1734.18	27.927	1.16877	1.79992	0.03025	7.75

[a]The spectroscopic constants are in wavenumbers (cm^{-1}). The quantities in square brackets refer to the vibrational ground state. Some of the entries have been truncated.

[b]These entries have been labelled "uncertain data" by Huber and Herzberg.

[c]These entries have been computed from the ones of H_2^+ using formulas for the isotope effect.

TABLE 10-7

FRANCK-CONDON AMPLITUDES AND R-CENTROIDS FOR THE PHOTOIONIZATION OF H_2, HD, AND D_2

	FRANCK-CONDON AMPLITUDES			R-CENTROIDS (Å)		
v_f	H_2	HD	D_2	H_2	HD	D_2
0	0.318	0.256	0.192	0.893	0.892	0.887
1	-0.428	-0.375	-0.311	0.844	0.850	0.853
2	0.444	0.419	0.379	0.800	0.812	0.821
3	-0.408	-0.410	-0.399	0.759	0.776	0.791
4	0.350	0.371	0.384	0.722	0.744	0.763
5	-0.288	-0.320	-0.349	0.688	0.713	0.736
6	0.231	0.267	0.304	0.656	0.685	0.711
7	-0.183	-0.218	-0.258	0.627	0.658	0.687
8	0.144	0.176	0.214	0.599	0.633	0.665
9	-0.113	-0.141	-0.175	0.574	0.610	0.643
10	0.089	0.113	0.142	0.551	0.588	0.622
11	-0.071	-0.091	-0.115	0.531	0.568	0.602
12	0.056	0.073	0.092	0.513	0.549	0.583
13		-0.059	-0.074		0.532	0.565
14		0.048	0.060		0.517	0.548
15		-0.039	-0.049		0.504	0.532
16			0.040			0.517
17			-0.032			0.503
18			0.027			0.491

TABLE 10-8

"COMBINED" CLASSICAL REGIONS, FRANCK-CONDON FACTORS, AND R-CENTROIDS IN THE MORSE OSCILLATOR APPROXIMATION

$(v''=0)\ N_2(X^1\Sigma_g^+) \rightarrow (v')N_2^+(X^2\Sigma_g^+) + e^-$

v'	r_{min}(Å)	r_{max}(Å)	$\langle v' \vert 0 \rangle^2$	$\bar{r}_{v'v''}$(Å)
0	1.055	1.166	0.917	1.111
1	1.043	1.207	0.078	1.004
2	1.025	1.237	0.005	0.903

$(v''=0)\ N_2(X^1\Sigma_g^+) \rightarrow (v')N_2^+(A^2\Pi_{ui}) + e^-$

v'	r_{min}(Å)	r_{max}(Å)	$\langle v' \vert 0 \rangle^2$	$\bar{r}_{v'v''}$(Å)
0	1.055	1.229	0.264	1.138
1	1.055	1.273	0.319	1.112
2	1.055	1.305	0.220	1.088
3	1.055	1.334	0.115	1.065
4	1.049	1.360	0.051	1.043
5	1.038	1.385	0.020	1.022
6	1.029	1.408	0.008	1.003
7	1.020	1.431	0.003	0.984
8	1.013	1.453	0.001	0.967

$(v''=0)\ N_2(X^1\Sigma_g^+) \rightarrow (v')N_2^+(B^2\Sigma_u^+) + e^-$

v'	r_{min}(Å)	r_{max}(Å)	$\langle v' \vert 0 \rangle^2$	$\bar{r}_{v'v''}$(Å)
0	1.033	1.146	0.883	1.090
1	1.005	1.162	0.115	1.182
2	0.988	1.192	0.002	1.376

TABLE 10-8 (CONTINUED)

(v"=0) $CO(X^1\Sigma^+)$ → (v') $CO^+(X^2\Sigma^+)$ + e^-				
v'	r_{min}(Å)	r_{max}(Å)	$\langle v' \mid 0 \rangle^2$	$\bar{r}_{v'v"}$(Å)
0	1.071	1.179	0.963	1.126
1	1.041	1.206	0.036	1.302
2	1.022	1.236	0.0001	1.810

(v"=0) $CO(X^1\Sigma^+)$ → (v') $CO^+(A^2\Pi_i)$ + e^-				
v'	r_{min}(Å)	r_{max}(Å)	$\langle v' \mid 0 \rangle^2$	$\bar{r}_{v'v"}$
0	1.083	1.304	0.079	1.185
1	1.083	1.353	0.176	1.166
2	1.083	1.390	0.215	1.148
3	1.083	1.423	0.192	1.130
4	1.083	1.453	0.141	1.113
5	1.083	1.480	0.090	1.097
6	1.082	1.507	0.052	1.081
7	1.073	1.533	0.028	1.066
8	1.065	1.559	0.014	1.051
9	1.057	1.584	0.007	1.037
10	1.050	1.609	0.003	1.023
11	1.044	1.633	0.002	1.010
12	1.038	1.658	0.001	0.997

(v"=0) $CO(X^1\Sigma^+)$ → (v') $CO^+(B^2\Sigma^+)$ + e^-				
v'	r_{min}(Å)	r_{max}(Å)	$\langle v' \mid 0 \rangle^2$	$\bar{r}_{v'v"}$
0	1.083	1.227	0.689	1.152
1	1.083	1.278	0.248	1.102
2	1.070	1.317	0.052	1.047
3	1.056	1.352	0.009	0.990
4	1.045	1.386	0.001	0.938

ignored, by using only $g_{00}^{(v_i,v_f;n)}$ in (10-18), the subscript "vr" is omitted. In the methods where vibration-rotation interaction was taken into account, the six terms shown explicitly in (10-18) were used in the least squares approximation.

In the r-centroid approximation, (method RC and RC_{vr}), the expansion terms in (10-15) were obtained from a least squares approximation used for the RD method, by specifying:

$$A(q,E_e;\beta_o^2)=A(\bar{q}_{v_i v_f},E_e;\beta_o^2); \qquad (10\text{-}30)$$

otherwise the number of geometries to be considered would have been excessively large. In (10-30), the r-centroids are represented by $\bar{q}$.

These r-centroids depend also on J_i and J_f. This would affect the expansion coefficients c in (10-17). Although no tests have been performed to determine the effects of the J-dependence of the r-centroids, it is believed that the resulting effects are smaller than effects of vibration-rotation interaction arising from the J-dependence of the expectation values in (10-16). In a sense, the vibration-rotation interaction is not taken fully into account in the RC_{vr} approximation because the J-dependence of the r-centroids is ignored.

The reduced masses were for $^{14}N_2$ and $^{12}C^{16}O$, i.e., not for a natural mixture of isotopes. The weights of the isotopes were taken from the CRC handbook.[584] The reduced masses of H_2, HD, D_2, N_2, and CO were 0.50433 a.m.u., 0.67207 a.m.u., 1.007 a.m.u., 7.0015 a.m.u., and 6.8562 a.m.u. respectively.

The ionization potentials used in (10-9) were obtained for N_2 and CO from the first adiabatic ionization potentials given by Huber and Herzberg,[16] and from the spectroscopic constants given in Table 10-6. (The higher ionization potentials were obtained by using the corresponding values of T_e for N_2^+ and CO^+). The ionization potentials of H_2 were computed from a high-resolution spectrum near threshold of H_2 by Åsbrink[585] for the transition

$$(v=J=0)H_2 \rightarrow (v=5,J=0)H_2^+ + e^- \qquad (10\text{-}31)$$

in which the ionization potential is 134139.5 cm^{-1}. With the spectroscopic constants shown in Table 10-6, the adiabatic ionization potentials of H_2, HD, and D_2 were computed as 15.438 eV, 15.455 eV, and 15.475 eV respectively.

The approximation shown in (10-21) and (10-22) was used in all cases. The quantities q_{min} and q_{max} are the limits of the interval in which "geometries" were sampled along the normal mode coordinate. In the present case, this refers simply to the internuclear separations.

It is assumed here that the populations of the initial rotational states are given by a Boltzmann distribution:

$$N_J/N_0=(g_J/g_0)(2J+1)\exp(-(E_{rot,J}-E_{rot,0})hc/(kT)) \qquad (10\text{-}32)$$

where g_0 and g_J are terms which arise through coupling between nuclear spin and the rotation of the molecule.[1] The rotational distribution of CO at T=300K is shown in Figure 10-9. In molecules with distinguishable nuclei the ratio of g_J and g_0 is unity. In H_2, g_J is 1 if J is

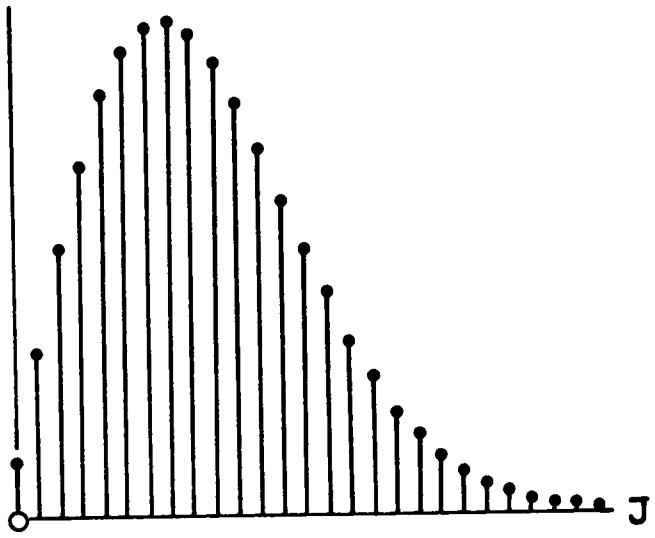


Fig. 10-9. The rotational distribution of CO at T_{rot}= 300K.

even, and 3 if J is odd. In D_2 and N_2, g_J is 6 if J is even, and 3 if J is odd.

Notice that the ortho modification of H_2 has odd rotational quantum numbers, whereas for D_2 the ortho modification has even rotational quantum numbers.

The rotational energies in (10-32) are assumed to be expressed in wavenumbers (cm^{-1}). They were computed using the spectroscopic constants B_e, α_e, and D_e listed in Table 10-6. The conversion between the ortho and para modification of homonuclear diatomic molecules is extremely slow. The expression in (10-32) assumes that the ortho and para modificatons of homonuclear diatomic molecules are at the equilibrium, which corresponds to the rotational temperature T. Let us assume that the sample has been stored at a temperature T_{eq} for an extended period of time prior to the experiment. In this case, the quantities g_J have to be replaced with $g_J p(T_{eq})/p(T)$ if J is even and $g_J(1-p(T_{eq}))/(1-p(T))$ if J is odd, where T is the rotational temperature in the experiment and p is a function

$$p(T)=_{J=0,2,4,\ldots}^{\Sigma} N_J(T)/_{J=0,1,2,\ldots}^{\Sigma} N_J(T) \qquad (10\text{-}33)$$

which has been tabulated in Table 10-9 as a function of the rotational temperature and Θ_r, the "characteristic temperature of rotation."[586] The data in Table 10-9 apply within the rigid rotor approximation.

The characteristic temperature of rotation of N_2 is 2.9K. Even at a temperature of 4K, which is the lowest temperture considered in this work, the expression in (10-32) is adequate for N_2. However, the characteristic temperatures of rotation of H_2 and D_2 are 88K and 44K

TABLE 10-9

NUCLEAR STATISTICS IN HOMONUCLEAR DIATOMIC MOLECULES

$$p=\sum_{J=0,2,\ldots}(2J+1)\exp(-J(J+1)\Theta_r/T)/\sum_{J=0,1,\ldots}(2J+1)\exp(-J(J+1)\Theta_r/T)$$

T/Θ_r	p
0	1
0.3	0.996
0.4	0.980
0.5	0.948
0.6	0.903
0.7	0.853
0.8	0.803
0.9	0.756
1.0	0.714
1.1	0.677
1.2	0.646
1.3	0.619
1.4	0.597
1.5	0.579
1.6	0.564
1.8	0.542
2.0	0.527
2.25	0.516
2.5	0.509
2.75	0.505
3.0	0.503
3.25	0.502
3.5	0.501
∞	0.5

respectively. According to (10-32), H_2 would occupy only the lowest rotational level with J=0 at T=4K. This would actually be the case only if the sample had time to equilibrate at 4K between the ortho and para modification.

For this reason, some of the results for hydrogen will be presented in a manner where the ortho and para modification give rise to separate sets of data.

The averaged cross section from a set of rovibronic transitions $J''_k \rightarrow J'_k$, k=1,2,....,n is

$$\sigma_{ave} = \sum_{k=1}^{n} \bar{N}(J''_k)\sigma(J''_k \rightarrow J'_k) \qquad (10\text{-}34)$$

where the population factors $\bar{N}$ are obtained from the population factors in (10-32) by normalization, such that the sum of the population factors becomes 1. The averaged β values are obtained by taking

$$\beta_{ave} = \left[\sum_{k=1}^{n} \bar{N}(J''_k)\sigma(J''_k \rightarrow J'_k)\beta(J''_k \rightarrow J'_k) \right] / \sigma_{ave} \qquad (10\text{-}35)$$

Here, the doubly primed J_ks refer to the initial state.

In spectra with bound initial and final states, the rotational bands have intensities which are given by relatively simply mathematical expressions which are unique for each possible electronic transition of the system. In vibrational spectra, the initial and the final elecronic state are identical, and the intensities of the rotational bands are given by the well-known Hönl-London formulae.[2]

The uniqueness of the intensity distribution among the rotational subbands of vibronic transitions makes possible an assignment for the transition which is practically unambiguous. There are complications, of course. If an asymmetric rotor is involved, one will have several options for the representation of its wave function. The rotation of the molecule can experience perturbations. For example, so-called "axis-switching" transitions can arise.[587] Although such perturbations themselves often are difficult to interpret, they are not strong enough in most cases to be sufficiently confusing as to prevent an assignment of the electronic transition. Even if the rovibronic bands are not resolved, the contour of the vibronic bands often shows enough structure to make an assignment. For example, Lombardi et al.[588] could confirm some doubtful assignments in benzene by analyzing the rotational contours of its two-photon spectrum.

Band contours can be analyzed through deconvolution. The basic assumption underlying deconvolution algorithms is that the band consists of a convolution of several bands, which are extracted by the deconvolution algorithm. Masri and Fletcher[589] described an algorithm for the deconvolution of Raman bands through matching of experimental and synthesized band contours. Ross[590] reviewed methods for contour analysis in optical spectra, with emphasis on transitions involving asymmetric rotors. The wide variety of reasonable options tends to discredit deconvolution treatments of spectra in some cases.[591] Several reports about deconvolution of photoelectron spectra have appeared in literature.[592-594]

Hubin et al.[592] obtained the spin-orbit coupling constant of CS_2^+ through deconvolution of the photoelectron spectrum of CS_2.

Deconvolution algorithms often assume that there is a global broadening function which is characteristic for the instrument used.[595,596] Allen and Grimm[597] made such an assumption in an algorithm where, from the experimental contour, a new contour is computed in which the effects of instrumental broadening are eliminated. Their algorithm is not a deconvolution algorithm in the usual sense since no attempt is made to extract the individual subbands. A more appropriate name for this method would be "band contour refinement."

Band contours are of considerable interest in connection with intramolecular dynamics. The characteristic Beutler-Fano line shapes associated with preionizations and predissociations have been mentioned in the previous chapter. It turns out that the detailed band contour gives information about the evolution of the excited states created in the transition. This information is provided through the time autocorrelation function. The time autocorrelation function itself, in the case of photoelectron spectra, is simply the fourier transform of the spectrum.[598]

If someone picks up a pebble on the sidewalk, he might expect to learn something about its past by looking at it, or, maybe, about the history of the solar system, or something like that. In spectroscopic measurements, the molecules communicate information about their past and their present, (initial and final state), and, through the band contours, forebodings about their future.

The rotational structure of H_2, HD, and D_2 in photoelectron spectra has been resolved by several research groups.[585,599] The rotational structure in the photoelectron spectrum of H_2 can be resolved only by threshold photoelectron spectroscopy[585] or by using molecular beams.[599]

Let us look at the causes of broadening in photoelectron spectra. The ones considered important are:

(i) Instrumental broadening.

(ii) The width of the photon source.

(iii) Doppler broadening due to the motion of the molecules relative to the photon source.

(iv) Broadening due to the conservation of linear momentum in the photoionization. (Thermal motion.)

(v) Broadening due to the finite lifetime of the final state.

Instrumental broadening is the limiting factor in most cases. The discussion below ignores this limitation.

The broadening resulting from the effect described in (iv) is often referred to as "Doppler broadening."[598,599] The Doppler effect applies to the observation of a wave by an observer in relative motion in respect to the source of the wave. In (iv) we have no wave, such that the term "Doppler broadening" becomes inapplicable.

The width of the photon source can be made very small with a monochromator. In most cases, the natural width of line sources should be sufficiently small to allow the resolution of the rotational structure.

The effects listed in (iii) and (iv) arise from the thermal motion of the molecules. The width due to Doppler broadening of a sample with a Maxwellian velocity distribution is:[600,601]

$$\Delta E=(E_{ph}/c)[8kT\ln(2))/M]^{1/2}=(7.16)10^{-7}E_{ph}[(T/K)(a.m.u./M)]^{1/2} \quad (10\text{-}36)$$

where the full width at half height is given by the quantity ΔE in (10-36), and K stands simply for degrees Kelvin. M is the mass of the molecule being photoionized by photons with energy E_{ph}. Using He(I) radiation, the full width at half height in photoionizations of N_2 or CO at T=300K would be 0.4 cm^{-1}, according to (10-36). Doppler broadening does not prevent the resolution of the rotational structure in the He(I) photoelectron spectra of N_2 and CO. Notice that the photon source itself is broadened through Doppler broadening. Assuming that the emitting He atoms have a translational temperature of 500-1000K, the Doppler broadening of the photon beam would be 3 to 5 times larger than the Doppler broadening due to thermal motion of the target. The Doppler broadening of the source can be suppressed through the use of a monochromator, and the Doppler broadening of the sample can be reduced by using molecular beams. The preparation of a molecular beam requires that the sample be volatile. A high boiling sample can be introduced into a beam of some gas by "seeding" a beam of gas with the high-boiling substance.[602] However, for photoelectron spectra this technique is of limited usefulness because of the continuum absorption by the carrier gas.

Let us now look at (iii). In the photoionization, we have a photon colliding with a molecule. The molecule and the photon both have a linear momentum prior to the absorption. The linear momentum of a photon, such as the photons from a He(I) source, is small in comparison with the linear momentum of a thermal molecule at room temperature. What happens mostly is that the electron picks up an additional velocity component along its path to the detector. This velocity component is given by the direction and speed of the molecule, if, as previously stated, the linear momentum of the photon is ignored.

Assuming that the molecules have velocity components along the path of the electrons, which follow a Maxwellian distribution, the full widths at half height of the broadened peaks would be:[603]

$$\Delta E=5.8[(T/K)(E_e/eV)(a.m.u./M)]^{1/2}cm^{-1} \qquad (10\text{-}37)$$

Carlson gives a similar formula.[604]

The effects of this broadening can be overcome in two ways. Either one lowers the translational temperature along the path of the electrons, or one works at threshold where E_e is close to zero. At T=300K the width of the peaks from N_2 or CO at E_e=1 eV is 19 cm^{-1}, according to (10-37). For H_2, due to its lower mass, the width under the same conditions would be 71 cm^{-1}, which is about as large as B_e of H_2 and roughly twice as large as B_e of H_2^+. One can readily see that, due to the broadening effect in (iii), not even the rotational structure in the photoelectron spectrum of H_2 could be resolved without counter-measures.

The broadening due to the finite lifetimes of the final state can be appreciable, especially for photoionizations from inner shells. Recently, Nordgren et al. measured the natural width of the C1s core hole level of CO_2 as 0.07±0.02 eV.[605] This amounts to roughly 565 cm^{-1}. In this case the natural width alone may prohibit the resolution of some of the vibrational structure.

In optical spectroscopy, there are a number of techniques being used routinely for the preparation of spectra with subnatural line width resolution.[606-608] Zinth et al.[609] have recently reported a technique for subnatural line width Raman spectroscopy based on delayed detection.

No reports of feasable techniques to obtain subnatural line width resolution in photoelectron spectra have appeared in the literature.

It has become apparent that it is rather difficult to obtain a resolution in photoelectron spectra which allows us to examine their rotational structure. One wonders how much is to be gained through the observation of the rotational structure. Unlike in optical spectra, where the rotational subbands have intensity patterns which are characteristic for each transition, photoelectron spectra would not show such characteristic patterns which could be used for assignments. This is due to the fact that the final wave function is composed of partial waves, not all of which have the same symmetry. The relative contributions to the cross sections from the different partial waves not only depend on the rotational initial and final states, but also on the molecule and the energy of the photoelectron. There are selection rules in effect in some cases, such as in homonuclear diatomic

molecules, where $J_f - J_i$ is even for the photoionization of a σ_g orbital, but odd for the photoionization of a σ_u orbital. In most cases, however, it will not be possible to make conclusive assignments in photoelectron spectra based solely on the intensity distribution among rotational subbands.

Shimamura[610] has shown that each initial rotational level has the same total cross section and the same average β value when considering all the possible final rotational states, and making some reasonable assumptions about rotational motion. When taking a given initial rotational level J_k'' in (10-34) and (10-35), according to Shimamura, the same result is obtained for all initial rotational levels represented by J_k''. This means that cross sections and β values do not depend on the rotational temperature of the sample. Let us now look at the assumption made by Shimamura in the derivation of his sum rules:

a. Separability of the rotational wave functions from the vibrational wave functions is assumed.

b. The sudden approximation must be satisfied. For the sudden approximation to be valid, the rotational transition must occur quickly as compared with the rotational period of the molecule.[611]

c. E_e is the same for all rotational subbands in the vibronic transition. The same holds for E_{ph}.

Notice that Shimamura does not assume that the electronic wave function must be written as a single determinantal function. In other words the sum rules apply to CI-induced preionization in the sudden approximation.[611]

Insofar as the three assumptions made by Shimamura are valid, the usually invoked rotational closure applies to the differential cross sections, unless the transition is from a nonlinear to a linear equilibrium configuration. If the transition is from a nonlinear to a linear configuration, the closure of the final states in the three-dimensional angular space is invalidated, and the sum rule does not necessarily apply.[610]

Since the differential cross sections are the same for all initial rotational states, based on the correspondence principle, we conclude that averaging over the rotational states should be equivalent with averaging over all Euler angles, as done by Davenport. In fact, after rotational averaging, (with similar assumptions as Shimamura's), Itikawa obtained the same expression for the differential cross sections as Davenport.

The special case of a transition from a nonlinear to a linear configuration has been mentioned. Let us now ignore this special case and focus our attention on possible additional violations of the sum rules. This will be done by examining the limits of validity of the assumptions made by Shimamura.

In the assumption in "a", the validity of the adiabatic approximation is implied. It has been shown that the adiabatic-nuclei approximation will fail to give an adequate description of some photoionization processes, especially for resonances near the ionization threshold.[254,612-614] Cyanogen shows strong nonadiabatic coupling effects in its photoelectron spectrum.[613] In N_2 and CO, the photoelectron spectra of the inner valence shells are affected by strong nonadiabatic

coupling among several closely lying electronic states.[614] (The inner valence levels of N_2^+ and CO^+ are also strongly predissociating.[615])

The nonadiabatic effects are expected to be connected mostly with vibrational motions, except very close to threshold where rotational autoionization can take place.[657] Nonadiabatic effects have also been observed in the decay of Feshbach resonances.[616]

Very close to threshold, the photoelectrons are "slow" to leave and the sudden approximation breaks down. Also, some rovibronic transitions may have ionization energies larger than the available E_{ph}, i.e., E_{ph} may be in between ionization thresholds of rovibronic bands if the summation is done for E_{ph}=const.[657] Obviously "c" can never hold exactly, i.e., either we change E_e or E_{ph} in the summation. In the absence of rotational autoionization the sum rule would still be valid very close to threshold, if the summation is done for E_e=const.

We conclude that Shimamura's sum rules may break down very close to threshold, due to nonadiabatic effects and due to the energy conservation principle which requires that E_e, and therefore the continuum wave function, depend on J_i and J_f. If the summation is done for E_e=const., E_{ph} will depend on J_i and J_f.

If the photoionization takes place via an autoionizing resonance, the molecule can rotate through an angle of appreciable size before undergoing preionization. This will have a randomizing effect on the angular distribution, making it more isotropic. Read[617] has treated this problem for electron scattering. He looked at a classical rotor, which carries a set of electrons which were promoted into an autoionizing state, and he computed the modified angular distribution arising

from the alteration of the orientation of the rotor after the average lifetime of the resonance. As mentioned previously, the work by Read was intended for electron scattering, but one can readily see that it is applicable also to photoionization. The information needed for such a calculation would be the average lifetime of the autoionizing resonance and the rotational period of the classical rotor at a given temperature. Read evidently assumed that the transition to the autoionizing state would not affect the rotational period of the rotor, as compared to the initial state, i.e. roughly equal increases of J as decreases of J in a quantum mechanical sense. Notice that, through this randomizing effect, only the angular distribution parameter β would be affected, whereas the sum rule for the intensities would still apply.

In long-lived resonances, (with small widths), the initial rotational distribution may also affect the portion of molecules ionizing via preionization, as compared to direct photoionization, due to the different degree of matching between different rovibronic transition energies into the autoionizing resonance, and E_{ph}.

Finally, one will have to consider interference of deexcitation channels, which can effectively compete with preionization. It is a well-known fact that rotational motion can noticeably affect the lifetimes of electronically excited states in respect to conversion processes, nonradiative decay, and collisional deexcitation.[618-629] In internal conversion processes and in collisions, angular momentum constraints are in effect.[629,630] This means that rotational sublevels in the autoionizing state may be depopulated, through processes other

than preionization, to various degrees, which may lead to a breakdown of Shimamura's sum rules.

It has been pointed out that the sum rules break down close to threshold and in the presence of preionization. Since threshold effects and autoionization are neglected by the vast majority of the models currently applied to photoionization processes, the above findings seem to be of little practical importance. However, a breakdown of the sum rules means that the cross sections and β values can become temperature- and possibly pressure-dependent. There is some evidence for such effects. Natalis et al.[631] pointed out that the vibrational branching ratios differ greatly among different sources. They point out the need for well-defined operating conditions.

Ritchie and Tambe[564] stated that the formula in (10-1) can be applied to all linear molecules. This would be the case were it not for the bending vibration of linear polyatomic molecules. The bending vibration of a linear molecule corresponds to the rotation of a slightly bent molecule around the axis of symmetry.[632]

Itikawa writes:[633]

> "....My formulation is based on the assumption that the initial and final wave functions of the molecule can be written as eq. (9) and (11) in my paper,[561] respectively. Thus the resulting formulae, as they stand, cannot be applied to any polyatomic molecule. For linear molecules the bending vibration makes the molecular rotation more complex (like an asymmetric top). ...."

In vibrations with angular momentum, we observe ℓ-type doubling.[634] In linear molecules, the bending mode is the only vibration with angular momentum. In transitions where the bending mode is not activated, no ℓ-type doubling is observed.[635] It may be that for such transitions (10-1) would apply to linear polyatomic molecules.

There are a number of tests which can be done in order to probe the program for errors. If $\Lambda_i=\Lambda_f$, we have

$$(2J_1+1)\sigma(v_fJ_2\leftarrow v_iJ_1)\sim(2J_2+1)\sigma(v_fJ_1\leftarrow v_iJ_2) \tag{10-38}$$

and

$$\beta(v_fJ_1\leftarrow v_iJ_2)\sim\beta(v_fJ_2\leftarrow v_iJ_1) \tag{10-39}$$

These relations are based simply on a commutation rule applied to the third 3-j symbol in (10-1). The above relations hold not exactly because E_e is slightly different for the transitions being compared.

The rotationally averaged differential cross sections according to Itikawa[561] are:

$$\frac{d\sigma}{d\vec{k}}(\gamma_iv_i\Lambda_i\rightarrow\gamma_fv_f\Lambda)\sim W(E_{ph},\varepsilon_i,E_e)\sum_{L=0,2}\begin{pmatrix}1&1&L\\0&0&0\end{pmatrix}P_L(\cos\theta_k)$$

$$\sum_{\ell\bar{\ell}}\sum_{\lambda\bar{\lambda}}\sum_{\mu\bar{\mu}}[(2\ell+1)(2\bar{\ell}+1)]^{1/2}(-1)^{\bar{\mu}-\bar{\lambda}}\begin{pmatrix}\ell&\bar{\ell}&L\\0&0&0\end{pmatrix}\begin{pmatrix}1&1&L\\\mu&-\mu&\lambda-\bar{\lambda}\end{pmatrix}$$

$$\begin{pmatrix}L&\ell&\bar{\ell}\\-\mu-\mu&\lambda&-\bar{\lambda}\end{pmatrix}\langle\langle E_e\ell\lambda\gamma_fv_f\Lambda_f|\hat{a}^{(\mu)}|i\rangle\rangle\langle\langle E_e\bar{\ell}\bar{\lambda}\gamma_fv_f\Lambda_f|\hat{a}^{(\bar{\mu})}|i\rangle\rangle^* \tag{10-40}$$

where the initial state has been abbreviated in the DMAPWs by "i." ($i=\gamma_iv_i\Lambda_i$). The average over the rotational states was taken by Itikawa, assuming that E_e=const. for all rotational subbands of the

vibronic transition, and ignoring the effects of vibration-rotation interaction. As previously stated, the rotationally averaged differential cross sections computed with Itikawa's formula in (10-40) should be identical with the same quantities computed with Davenport's program. There is a trivial difference arising through the different form of the energy conservation principle implemented here. Also, the ionization potential in the present calculation was taken from experiment. Only the factor W will be affected by the above differences, and any disagreement beyond that would be indicative of an error in the program or a misconception otherwise. Assuming that E_e=const. over a vibronic progression, the differential cross section can be vibrationally averaged over the vibronic progression with an initial vibronic level having a vibrational wave function χ_i. The vibrationally averaged cross sections and β values are then:[574]

$$\langle\sigma\rangle=\langle\chi_i\left|\sigma(q)\right|\chi_i\rangle \tag{10-41}$$

and

$$\langle\beta\rangle=\langle\chi_i\left|\sigma(q)\beta(q)\right|\chi_i\rangle/\langle\sigma\rangle \tag{10-42}$$

If the vibrational averaging was done at constant E_e, by using fixed energy electron spectroscopy, the averaging procedure would still not be exact, due to the dependence of the cross section on E_{ph}. However, the factor E_{ph}^{-1} in (10-9) changes slowly and monotonously over the vibronic progression, unless the ionization potential is very small and measurements are done near threshold. It should be pointed out that

Swanson et al.[574] state that E_{ph} changes among the members in the vibronic progression, but only negligibly in general. This is definitely a statement based on the understanding that the vibrational averaging is done at a fixed energy of the photoelectrons. In contrast to this approach, experimental vibrationally averaged quantities are usually reported for summations over vibronic progressions which were measured at fixed E_{ph}.[636] For example, Southworth et al.[637] give vibrationally averaged cross sections of H_2 and D_2 at different energies of the photons.

For hydrogen and its isotopically substituted derivatives, HD and D_2, distinction in the averaging procedure is probably of little importance. However, in the presence of resonances, one should keep in mind that (10-41) and (10-42) apply more directly to an averaging procedure with E_{ph}=const. rather than E_e=const., although the formulae are not exact in either case.

The rotationally averaged cross section shown in (10-40) was implemented in the program, mainly in order to have reasonable assurance that the program works properly in all cases. At any rate, it turns out that the algorithm used to compute (10-40) can readily be modified such that (10-41) and (10-42) are being computed.

In the computation of the rotationally averaged differential cross sections, using (10-40), we have products of DMAPWs which are computed as the expansions shown in (10-17). Let us define the quantities

$$S_n^o(v_i;\beta_o^2)=\langle\chi_i|q^n\exp(-\beta_o^2q^2/2)|\chi_i\rangle \qquad (10\text{-}43)$$

In (10-40), the products of DMAPWs are then expanded as

$$\sum_{nm} \sum_{n'm'} c_{nm}\, c^{*}_{n'm'}\, S^{o}_{n+n'}(v_i;\beta_o^2)(E_e-E_{ref})^{m+m'} \qquad (10\text{-}44)$$

where the coefficients c are still the linear parameters from the least squares approximation of the DMAPWs as shown in (10-15).

If the vibrational averaging is done at constant E_{ph}, the energy of the photoelectron changes over the vibronic progression. Of course, one wonders what E_e, the vibrationally averaged differential cross section, corresponds to, since by keeping E_{ph}=const. the energy of the photoelectron changes in the summation. This dilemma underlies the present investigations of the validity of (10-41) and (10-42) for vibrational averaging of E_{ph}=const. The tests consisted in computing explicitly vibrationally averaged differential cross sections, and comparing these "accurate" results with vibrationally averaged results obtained from (10-41) and (10-42) at different photoelectron energies. The question now arises as to what constitutes an outcome which confirms the validity of (10-41) and (10-42) for vibrational averaging with E_{ph}=const. There are two conditions which should be met by results, which would indicate the validity of the formulae:

(i) The energy of the photoelectron, E_e, at which the total cross section from (10-41) equals the explicitly averaged cross section, should be roughly equal to the E_e at which the β value computed with (10-42) equals the β value from explicit vibrational averaging.

(ii) The energy of the photoelectron, at which the cross section and the β value, computed with (10-41) and (10-42), both match the

respective quantities obtained through explicit averaging, should be located near the energies of the most intense vibronic transitions. (Notice that the maximum of the envelope of the vibronic progression is not exactly at the energy of the vertical transition).[669]

In the computations of the cross sections with Davenport's program, the vertical ionization potentials from the Xα transition states at the considered geometry were used in the factor W. In Davenport's program, the vertical ionization potential used in the computation of the cross sections can be entered, or, the default, which is the energy eigenvalue of the bound orbital, can be used. If an ionization potential is specified on the input, Davenport's program will use it to compute the energy of the photons, E_{ph}. E_{ph} is used in the factor W in the formula for the cross sections. The vertical ionization potentials, at the geometries considered, have been given in Chapter 8. These vertical ionization potentials, $I.P._{vert}(q)$, differ noticeably at widely separated geometries.

The vertical ionization potential at the equilibrium geometry of the molecule being photoionized, $I.P._{vert}(q_e)$, contains energy of nuclear motion. We can use the vertical ionization potential at q_e to compute the energy of the photons. In addition, the purely electronic binding energy, ε_i, occurs in the factor W.

According to the above, the cross sections computed at different geometries can be brought on a "common denominator" by using a scaling factor

$$\left(I.P._{vert}(q)+E_e\right)^3\left[\left(I.P._{vert}(q_e)+E_e\right)\left(\varepsilon_i+E_e\right)^2\right]^{-1} \qquad (10\text{-}45)$$

In the transition corresponding to the adiabatic ionization potential, ΔE_{nucl} is usually relatively small. Therefore, adiabatic ionization potential is a good approximation for ε_i in most cases. If $I.P._{vert}(q_e)$ was specified on the input, the factor

$$(I.P._{vert}(q)+E_e)/(\varepsilon_i+E_e)^2 \qquad (10\text{-}46)$$

is still needed for scaling. This makes sure that ε_i does not change with the geometry. When computing the vibrationally averaged differential cross sections with the formulae in (10-41) and (10-42), the cross sections, $\sigma(q)$, obtained from Davenport's program have to be scaled with the factor shown in (10-45), or in (10-46), before further use.

In the investigations concerning the validity of (10-41) and (10-42), the energy of the photoelectron, E_e, was changed through ΔE_{nucl}.

The exponential factor in (10-15) could be incorporated into the least squares approximation by viewing β_o as a nonlinear least squares parameter. In this work, this exponential factor was not used in this fashion. If the least squares approximation provides an adequate fit insofar as the differential cross sections are concerned, then least squares approximations computed for different values of β_o should give differential cross sections which are in close agreement. Therefore, the exponential factor can be used to determine if the least squares approximations were adequate. A more common approach in this kind of a situation consists in comparing results from least squares approximations with different numbers of terms included. Since we are dealing

with a two-dimensional approximation, the significance of the convergence in respect to the number of terms included might be difficult to assess. At any rate, in Table 10-10, results are shown for H_2. H_2 has DMAPWs which are relatively well-behaved, presumably due to the absence of shape resonances.

The cross sections and β values computed with different β_os and damping parameters clearly show that these quantities are "stable" within three significant figures in respect to reasonable changes of the empirical parameters β_o and η. If, in H_2, the damping parameter were taken as zero, reasonable results would be obtained. In the photoionization of the π level of CO, taking the damping parameter as zero gave a maximum relative error of 7800 percent at the location of the inserted points, indicating strong buckling. Taking η=0.0125 reduced this to 28 percent. The β values changed by as much as 20 percent. If the damping parameter was further increased to 0.025, 0.0375, ... the changes from the results obtained with η=0.0125 did not exceed 1 percent for the β values.

In Table 10-11, the cross sections and β values of N_2 and CO for different rovibronic transitions are given for different β_os and damping parameters, as shown in Table 10-5. The results shown in Table 10-11 were obtained with the r-centroid approximation (RC_{vr}). The r-centroid approximation, as it is being used here, is a probe for the pointwise approximation of the least squares fit.

It has been pointed out previously that the bases used for the computation of the differential cross sections appeared adequate as far as computations with Davenport's program was concerned. It was felt,

TABLE 10-10

LEAST SQUARES APPROXIMATIONS OF THE COMPUTED DIPOLE MOMENT AMPLITUEDS OF HYDROGEN

Maximum Relative Error at the Sampled Points (%)

	$\beta_o=0$	$\beta_o=2\text{Å}^{-2}$	$\beta_o=4\text{Å}^{-2}$	$\beta_o=6\text{Å}^{-2}$
$\eta=0$	1.18	1.21	1.25	1.30
$\eta=0.01$	1.23	1.25	1.27	1.32
$\eta=0.02$	1.25	1.27	1.29	1.34
$\eta=0.03$	1.26	1.28	1.30	1.35
$\eta=0.04$	1.27	1.28	1.30	1.35
$\eta=0.05$	1.28	1.29	1.30	1.36

Maximum Relative Error at the Inserted Points (%)

	$\beta_o=0$	$\beta_o=2\text{Å}^{-2}$	$\beta_o=4\text{Å}^{-2}$	$\beta_o=6\text{Å}^{-2}$
$\eta=0$	6.99	5.82	5.50	4.81
$\eta=0.01$	2.70	2.51	2.51	2.44
$\eta=0.02$	1.80	1.72	1.68	1.74
$\eta=0.03$	1.44	1.39	1.36	1.43
$\eta=0.04$	1.25	1.22	1.20	1.27
$\eta=0.05$	1.15	1.12	1.11	1.17

TABLE 10-10 (CONTINUED)

Average Relative Error at the Sampled Points (%)

	$\beta_o=0$	$\beta_o=2\text{Å}^{-2}$	$\beta_o=4\text{Å}^{-2}$	$\beta_o=6\text{Å}^{-2}$
$\eta=0$	0.25	0.26	0.27	0.29
$\eta=0.01$	0.29	0.30	0.31	0.31
$\eta=0.02$	0.31	0.32	0.32	0.32
$\eta=0.03$	0.32	0.33	0.33	0.33
$\eta=0.04$	0.32	0.33	0.33	0.33
$\eta=0.05$	0.33	0.34	0.34	0.34

Average Relative Error at the Inserted Points (%)

	$\beta_o=0$	$\beta_o=2\text{Å}^{-2}$	$\beta_o=4\text{Å}^{-2}$	$\beta_o=6\text{Å}^{-2}$
$\eta=0$	2.62	2.40	2.12	1.86
$\eta=0.01$	1.11	1.10	1.06	1.00
$\eta=0.02$	0.81	0.81	0.78	0.76
$\eta=0.03$	0.70	0.69	0.67	0.66
$\eta=0.04$	0.64	0.63	0.61	0.60
$\eta=0.05$	0.61	0.59	0.57	0.57

TABLE 10-10 (CONTINUED)

The cross section of the transition with $v_i=v_f=0$ and $J_i=J_f=1$ (in megabarns)

Obtained by "integration" over the nuclear coordinates (RD_{vr})

	$\beta_o=0$	$\beta_o=2\text{Å}^{-2}$	$\beta_o=4\text{Å}^{-2}$	$\beta_o=6\text{Å}^{-2}$
$\eta=0$	0.4175	0.4177	0.4178	0.4179
$\eta=0.01$	0.4180	0.4181	0.4182	0.4183
$\eta=0.02$	0.4181	0.4182	0.4183	0.4184
$\eta=0.03$	0.4182	0.4183	0.4184	0.4185
$\eta=0.04$	0.4182	0.4183	0.4184	0.4186
$\eta=0.05$	0.4182	0.4184	0.4185	0.4186

Computed with the r-centroid approximation (RC_{vr})

	$\beta_o=0$	$\beta_o=2\text{Å}^{-2}$	$\beta_o=4\text{Å}^{-2}$	$\beta_o=6\text{Å}^{-2}$
$\eta=0$	0.4001	0.4004	0.4008	0.4010
$\eta=0.01$	0.4019	0.4020	0.4021	0.4025
$\eta=0.02$	0.4023	0.4024	0.4025	0.4029
$\eta=0.03$	0.4025	0.4026	0.4027	0.4032
$\eta=0.04$	0.4026	0.4027	0.4028	0.4033
$\eta=0.05$	0.4027	0.4028	0.4029	0.4034

TABLE 10-10 (CONTINUED)

The cross section of the transition with $v_i=0$, $v_f=6$ and $J_i=J_f=1$ (in megabarns)

Obtained by "integration" over the nuclear coordinates (RD_{vr})

	$\beta_o=0$	$\beta_o=2\text{Å}^{-2}$	$\beta_o=4\text{Å}^{-2}$	$\beta_o=6\text{Å}^{-2}$
$\eta=0$	0.5548	0.5546	0.5542	0.5539
$\eta=0.01$	0.5535	0.5534	0.5532	0.5528
$\eta=0.02$	0.5533	0.5531	0.5529	0.5525
$\eta=0.03$	0.5532	0.5529	0.5528	0.5524
$\eta=0.04$	0.5531	0.5529	0.5527	0.5522
$\eta=0.05$	0.5530	0.5528	0.5526	0.5522

Computed with the r-centroid approximation (RC_{vr})

	$\beta_o=0$	$\beta_o=2\text{Å}^{-2}$	$\beta_o=4\text{Å}^{-2}$	$\beta_o=6\text{Å}^{-2}$
$\eta=0$	0.5726	0.5723	0.5720	0.5715
$\eta=0.01$	0.5705	0.5707	0.5709	0.5706
$\eta=0.02$	0.5700	0.5703	0.5706	0.5703
$\eta=0.03$	0.5698	0.5701	0.5704	0.5702
$\eta=0.04$	0.5697	0.5700	0.5703	0.5701
$\eta=0.05$	0.5696	0.5699	0.5703	0.5700

TABLE 10-10 (CONTINUED)

The beta values of the transition with $v_i = v_f = 0$ and $J_i = J_f = 1$ (in megabarns)

Obtained by "integration" over the nuclear coordinates (RD_{vr})

	$\beta_o=0$	$\beta_o=2\text{Å}^{-2}$	$\beta_o=4\text{Å}^{-2}$	$\beta_o=6\text{Å}^{-2}$
$\eta=0$	1.8432	1.8433	1.8434	1.8434
$\eta=0.01$	1.8432	1.8432	1.8432	1.8433
$\eta=0.02$	1.8433	0.8432	1.8432	1.8432
$\eta=0.03$	1.8433	1.8432	1.8432	1.8432
$\eta=0.04$	1.8433	1.8433	1.8432	1.8432
$\eta=0.05$	1.8433	1.8433	1.8432	1.8432

Computed with the r-centroid approximation (RC_{vr})

	$\beta_o=0$	$\beta_o=2\text{Å}^{-2}$	$\beta_o=4\text{Å}^{-2}$	$\beta_o=6\text{Å}^{-2}$
$\eta=0$	1.8250	1.8254	1.8258	1.8260
$\eta=0.01$	1.8254	1.8253	1.8253	1.8254
$\eta=0.02$	1.8255	1.8253	1.8252	1.8252
$\eta=0.03$	1.8256	1.8253	1.8251	1.8251
$\eta=0.04$	1.8256	1.8253	1.8251	1.8250
$\eta=0.05$	1.8256	1.8253	1.8251	1.8250

TABLE 10-10 (CONTINUED)

The beta values of the transition with $v_i=0$, $v_f=6$, and $J_i=J_f=1$ (in megabarns)

Obtained by "integration" over the nuclear coordinates (RD_{vr})

	$\beta_o=0$	$\beta_o=2\text{Å}^{-2}$	$\beta_o=4\text{Å}^{-2}$	$\beta_o=6\text{Å}^{-2}$
$\eta=0$	1.9445	1.9444	1.9444	1.9444
$\eta=0.01$	1.9448	1.9449	1.9450	1.9450
$\eta=0.02$	1.9449	1.9450	1.9451	1.9452
$\eta=0.03$	1.9450	1.9451	1.9452	1.9453
$\eta=0.04$	1.9450	1.9452	1.9453	1.9453
$\eta=0.05$	1.9450	1.9452	1.9454	1.9454

Computed with the r-centroid approximation (RC_{vr})

	$\beta_o=0$	$\beta_o=2\text{Å}^{-2}$	$\beta_o=4\text{Å}^{-2}$	$\beta_o=6\text{Å}^{-2}$
$\eta=0$	1.9533	1.9536	1.9539	1.9541
$\eta=0.01$	1.9538	1.9542	1.9544	1.9546
$\eta=0.02$	1.9539	1.9543	1.9546	1.9547
$\eta=0.03$	1.9540	1.9544	1.9547	1.9548
$\eta=0.04$	1.9540	1.9544	1.9547	1.9548
$\eta=0.05$	1.9540	1.9545	1.9548	1.9548

TABLE 10-11

COMPARISON OF CROSS SECTIONS AND BETA VALUES OBTAINED FROM DIFFERENT LEAST SQUARES APPROXIMATIONS[a]

The cross sections and beta values are for the particular branches indicated by $J_f - J_i$ at a temperature of 70K. The unit of the nonlinear parameter β_o is Å^{-2}

Molec.	State of the ion	v_f	$J_f - J_i$	σ(Mb)			β		
				β_o=0	β_o=1	β_o=2	β_o=0	β_o=1	β_o=2
N_2	X	0	0	3.169	3.174	3.178	1.068	1.068	1.067
N_2	X	1	0	0.126	0.127	0.127	1.725	1.725	1.725
N_2	X	2	0	0.007	0.007	0.007	1.712	1.702	1.691
N_2	A	0	0	1.889	1.887	1.887	0.612	0.612	0.612
N_2	A	4	0	0.504	0.504	0.504	0.566	0.567	0.567
N_2	A	8	0	0.012	0.012	0.012	0.526	0.526	0.526
N_2	B	0	-1	0.804	0.804	0.804	1.867	1.867	1.867
N_2	B	1	-1	0.102	0.102	0.102	1.852	1.852	1.852
N_2	B	2	-1	0.002	0.002	0.002	1.822	1.822	1.822
CO	X	0	0	1.954	1.961	1.962	1.263	1.260	1.260
CO	X	1	0	0.030	0.030	0.030	1.345	1.346	1.346
CO	A	0	0	0.432	0.432	0.432	0.979	0.981	0.983
CO	A	6	0	0.451	0.451	0.451	0.525	0.526	0.527
CO	A	12	0	0.008	0.008	0.008	0.493	0.492	0.491
CO	B	0	0	0.172	0.172	0.172	0.768	0.770	0.769
CO	B	2	0	0.018	0.018	0.018	1.620	1.614	1.616
CO	B	4	0	0.001	0.001	0.001	1.823	1.827	1.825

[a]The computations were done in the r-centroid approximation (RC_{vr}).

however, that the bases might prove too small, as far as the effects of rotation are concerned. The reason is that the individual rovibronic transitions draw their intensity from a finite number of partial waves. According to (10-1), and the triangle relations of the 3-j symbols, the following selection rules apply:

$$\begin{aligned} |\Delta J| &\leq \ell_{max}+1 \\ |\Delta \Lambda| &\leq \ell_{max}+1 \end{aligned} \qquad (10\text{-}47)$$

This means that taking a small basis would result in the higher rotational branches being missing. The results in Table 10-12 indicate that the chosen bases should be adequate in most cases. Notice that for the photoionization of the 5σ orbital from CO, the transitions with large ΔJ have relatively large cross sections. This photoionization shows a shape resonance in the region of E_{ph} ~21.2 eV, originating from the ℓ~3 channel, which, according to (10-47), promotes transitions with appreciable changes in J.

The results in Table 10-12 were obtained in the FR approximation. There was no reason to suspect that the different methods, FR, RC, and RD, would give rise to very different outcomes when applying this "convergence" test.

The test results shown in Table 10-11 and in Table 10-12 appear to indicate that the strategy used here leads to reasonable results also for N_2 and CO.

The data for the photoionizations of the valence levels of H_2, N_2, and CO will be presented separately for each photoionization

TABLE 10-12

COMPARISON OF CROSS SECTIONS AND BETA VALUES OF CARBON MONOXIDE OBTAINED WITH DIFFERENT "BASES"

I: $\ell_{out} \leq 5$, $\ell_C \leq 3$, $\ell_O \leq 3$

II: $\ell_{out} \leq 7$, $\ell_C \leq 3$, $\ell_O \leq 3$

III: $\ell_{out} \leq 7$, $\ell_C \leq 5$, $\ell_O \leq 5$

The cross sections and beta values are for $v_i = v_f = J_i = 0$

State of the ion	J_f	σ(Mb)			β		
		I	II	III	I	II	III
X	0	0.9795	0.9819	0.9845	2.0000	2.0000	2.0000
X	1	2.5304	2.5264	2.5511	1.3075	1.3071	1.3056
X	2	2.6974	2.7001	2.7086	0.5441	0.5426	0.5413
X	3	0.8672	0.8659	0.8791	0.2402	0.2401	0.2414
X	4	0.7638	0.7647	0.7733	0.3270	0.3270	0.3269
A	1	0.4977	0.4978	0.4967	0.8043	0.8032	0.8051
A	2	0.1388	0.1387	0.1389	-0.8805	-0.8804	-0.8805
A	3	0.0849	0.0849	0.0847	0.1430	0.1432	0.1435
A	4	0.0008	0.0008	0.0008	0.4826	0.4831	0.4827
A	5	0.0000	0.0000	0.0000	0.3551	0.4399	0.4402
B	0	0.1042	0.1049	0.1052	2.0000	2.0000	2.0000
B	1	0.4168	0.4179	0.4149	1.6776	1.6773	1.6680
B	2	0.2159	0.2157	0.2161	-0.7177	-0.7176	-0.7186
B	3	0.0208	0.0208	0.0201	0.5342	0.5345	0.5382
B	4	0.0037	0.0037	0.0038	0.2805	0.2805	0.2808

process. For N_2 and CO, band contours at different rotational temperatures will be shown. It is assumed here that the widths of the unresolved rovibronic bands is given by the momentum conservation principle, with the momentum of the photon neglected. The formula for the widths of the unresolved bands is shown in (10-37). A sample with a Maxwellian distribution of velocities will give rise to gaussian line shapes, unless the transition is very close to threshold, in which case the line shapes become asymmetrical.[603] The temperature used in (10-37) was taken the same as the rotational temperature, i.e. the sample is considered to be at equilibrium. In molecular beams, we would have to distinguish between a translational temperature along the beam and a perpendicular temperature, which gives rise to the expansion of the beam. These temperatures change along the beam and they do not equal the rotational temperature in general. McClelland et al.[638] gave expressions for the terminal absolute rotational temperature of N_2 and CO in a molecular beam as a function of the nozzle diameter and source pressure, for a temperature of the source of 300K.[639]

B. RESULTS

The results which will be presented were obtained with $\beta_o=0$ in (10-15) and (10-16).

1. The Photoionization of H_2, HD, and D_2

Itikawa[563] gave partial cross sections for several rovibronic transitions of H_2. In Table 10-13, Table 10-14, and Table 10-15, the cross sections and β values of some rovibronic transitions in the photoionization of H_2, HD, and D_2 are shown. Itikawa gave the cross

TABLE 10-13

CROSS SECTIONS AND BETA VALUES FOR PHOTOIONIZATIONS INVOLVING INDIVIDUAL VIBRATIONAL-ROTATIONAL LEVELS OF H_2 AND H_2^+

	σ(Mb)					
$(v_i J_i) \rightarrow (v_f J_f)$	FR	FR_{vr}	RC	RC_{vr}	RD	RD_{vr}
(0,0)→(0,0)	0.623	0.604	0.370	0.359	0.389	0.380
(0,1)→(0,1)	0.656	0.638	0.414	0.403	0.430	0.418
(0,2)→(0,2)	0.644	0.628	0.399	0.390	0.417	0.402
(0,3)→(0,3)	0.638	0.623	0.395	0.385	0.412	0.393
(0,0)→(0,2)	0.085	0.078	0.111	0.101	0.105	0.096
(0,1)→(0,3)	0.051	0.045	0.067	0.059	0.063	0.022
(0,2)→(0,0)	0.016	0.018	0.022	0.023	0.021	0.047
(0,2)→(0,4)	0.044	0.038	0.057	0.049	0.054	0.047
(0,0)→(6,0)	0.391	0.414	0.529	0.560	0.516	0.544
(0,1)→(6,1)	0.410	0.430	0.543	0.570	0.532	0.553
(0,2)→(6,2)	0.402	0.419	0.536	0.558	0.524	0.536
(0,3)→(6,3)	0.398	0.413	0.531	0.551	0.519	0.521
(0,0)→(6,2)	0.051	0.057	0.038	0.042	0.043	0.049
(0,1)→(6,3)	0.031	0.034	0.023	0.025	0.026	0.030
(0,2)→(6,0)	0.010	0.010	0.007	0.007	0.009	0.008
(0,2)→(6,4)	0.026	0.030	0.019	0.022	0.022	0.026

TABLE 10-13 (CONTINUED)

$(v_i J_i) \rightarrow (v_f J_f)$	β					
	FR	FR_{vr}	RC	RC_{vr}	RD	RD_{vr}
(0,0)→(0,0)	2	2	2	2	2	2
(0,1)→(0,1)	1.916	1.916	1.826	1.826	1.844	1.843
(0,2)→(0,2)	1.939	1.939	1.871	1.871	1.885	1.883
(0,3)→(0,3)	1.943	1.943	1.879	1.879	1.892	1.888
(0,0)→(0,2)	0.382	0.382	0.368	0.368	0.383	0.383
(0,1)→(0,3)	0.381	0.381	0.368	0.368	0.383	0.382
(0,2)→(0,0)	0.384	0.384	0.371	0.371	0.386	0.386
(0,2)→(0,4)	0.381	0.381	0.368	0.368	0.383	0.382
(0,0)→(6,0)	2	2	2	2	2	2
(0,1)→(6,1)	1.918	1.918	1.954	1.954	1.946	1.945
(0,2)→(6,2)	1.940	1.940	1.967	1.967	1.961	1.959
(0,3)→(6,3)	1.944	1.944	1.969	1.969	1.964	1.961
(0,0)→(6,2)	0.339	0.339	0.344	0.344	0.330	0.330
(0,1)→(6,3)	0.339	0.339	0.344	0.344	0.330	0.331
(0,2)→(6,0)	0.341	0.341	0.345	0.345	0.332	0.332
(0,2)→(6,4)	0.339	0.339	0.344	0.344	0.330	0.332

FR, RC, and RD, and the subscript "vr" refer to different methods of computation as described in the text.

TABLE 10-14

CROSS SECTIONS AND BETA VALUES FOR PHOTOIONIZATIONS INVOLVING INDIVIDUAL VIBRATIONAL-ROTATIONAL LEVELS OF HD AND HD^+

	σ(Mb)					
$(v_i J_i) \rightarrow (v_f J_f)$	FR	FR_{vr}	RC	RC_{vr}	RD	RD_{vr}
(0,0)→(0,0)	0.405	0.394	0.242	0.235	0.253	0.247
(0,1)→(0,1)	0.427	0.417	0.270	0.264	0.279	0.272
(0,2)→(0,2)	0.419	0.410	0.261	0.255	0.271	0.263
(0,3)→(0,3)	0.416	0.408	0.259	0.253	0.268	0.258
(0,0)→(0,2)	0.055	0.051	0.072	0.067	0.068	0.063
(0,1)→(0,3)	0.033	0.030	0.043	0.039	0.041	0.037
(0,2)→(0,0)	0.011	0.011	0.014	0.015	0.014	0.014
(0,2)→(0,4)	0.029	0.025	0.037	0.033	0.035	0.031
(0,0)→(6,0)	0.512	0.534	0.629	0.656	0.618	0.642
(0,1)→(6,1)	0.538	0.557	0.650	0.673	0.641	0.659
(0,2)→(6,2)	0.529	0.544	0.641	0.660	0.632	0.641
(0,3)→(6,3)	0.524	0.537	0.637	0.652	0.627	0.627
(0,0)→(6,2)	0.067	0.072	0.056	0.060	0.060	0.065
(0,1)→(6,3)	0.040	0.043	0.034	0.036	0.036	0.040
(0,2)→(6,0)	0.013	0.013	0.011	0.011	0.012	0.012
(0,2)→(6,4)	0.035	0.037	0.029	0.031	0.031	0.035

TABLE 10-14 (CONTINUED)

$(v_i J_i) \rightarrow (v_f J_f)$	β					
	FR	FR_{vr}	RC	RC_{vr}	RD	RD_{vr}
(0,0)→(0,0)	2	2	2	2	2	2
(0,1)→(0,1)	1.916	1.916	1.826	1.826	1.842	1.842
(0,2)→(0,2)	1.939	1.939	1.872	1.872	1.884	1.883
(0,3)→(0,3)	1.943	1.943	1.880	1.880	1.891	1.888
(0,0)→(0,2)	0.381	0.381	0.368	0.368	0.381	0.381
(0,1)→(0,3)	0.381	0.381	0.368	0.368	0.381	0.380
(0,2)→(0,0)	0.383	0.383	0.370	0.370	0.383	0.383
(0,2)→(0,4)	0.381	0.381	0.368	0.368	0.381	0.380
(0,0)→(6,0)	2	2	2	2	2	2
(0,1)→(6,1)	1.917	1.917	1.943	1.943	1.938	1.937
(0,2)→(6,2)	1.940	1.940	1.959	1.959	1.955	1.954
(0,3)→(6,3)	1.944	1.944	1.961	1.961	1.958	1.956
(0,0)→(6,2)	0.343	0.343	0.346	0.346	0.339	0.339
(0,1)→(6,3)	0.343	0.343	0.346	0.346	0.339	0.339
(0,2)→(6,0)	0.345	0.345	0.348	0.348	0.340	0.340
(0,2)→(6,4)	0.434	0.343	0.347	0.347	0.339	0.340

FR, RC, and RD, and the subscript "vr" refer to different methods of computation as described in the text.

TABLE 10-15

CROSS SECTIONS AND BETA VALUES FOR PHOTOIONIZATIONS INVOLVING INDIVIDUAL VIBRATIONAL-ROTATIONAL LEVELS OF D_2 AND D_2^+

	σ(Mb)					
$(v_i J_i) \rightarrow (v_f J_f)$	FR	FR_{vr}	RC	RC_{vr}	RD	RD_{vr}
(0,0)→(0,0)	0.229	0.224	0.138	0.135	0.143	0.141
(0,1)→(0,1)	0.241	0.236	0.154	0.151	0.159	0.156
(0,2)→(0,2)	0.237	0.233	0.149	0.147	0.154	0.150
(0,3)→(0,3)	0.236	0.231	0.148	0.146	0.153	0.148
(0,0)→(0,2)	0.031	0.029	0.040	0.038	0.039	0.036
(0,1)→(0,3)	0.019	0.017	0.024	0.022	0.023	0.021
(0,2)→(0,0)	0.006	0.006	0.008	0.008	0.008	0.008
(0,2)→(0,4)	0.016	0.014	0.021	0.019	0.020	0.018
(0,0)→(6,0)	0.652	0.669	0.730	0.749	0.723	0.740
(0,1)→(6,1)	0.686	0.700	0.761	0.777	0.755	0.767
(0,2)→(6,2)	0.674	0.686	0.750	0.763	0.743	0.750
(0,3)→(6,3)	0.670	0.680	0.746	0.756	0.739	0.738
(0,0)→(6,2)	0.086	0.089	0.079	0.082	0.081	0.085
(0,1)→(6,3)	0.052	0.054	0.048	0.049	0.049	0.051
(0,2)→(6,0)	0.017	0.017	0.016	0.016	0.016	0.016
(0,2)→(6,4)	0.044	0.046	0.041	0.042	0.042	0.044

TABLE 10-15 (CONTINUED)

$(v_i J_i) \rightarrow (v_f J_f)$	β					
	FR	FR_{vr}	RC	RC_{vr}	RD	RD_{vr}
(0,0)→(0,0)	2	2	2	2	2	2
(0,1)→(0,1)	1.916	1.916	1.829	1.829	1.842	1.842
(0,2)→(0,2)	1.939	1.939	1.874	1.874	1.884	1.883
(0,3)→(0,3)	1.943	1.943	1.882	1.882	1.891	1.890
(0,0)→(0,2)	0.381	0.381	0.368	0.368	0.379	0.378
(0,1)→(0,3)	0.381	0.381	0.368	0.368	0.378	0.378
(0,2)→(0,0)	0.382	0.382	0.369	0.369	0.380	0.380
(0,2)→(0,4)	0.381	0.381	0.368	0.368	0.378	0.378
(0,0)→(6,0)	2	2	2	2	2	2
(0,1)→(6,1)	1.917	1.917	1.931	1.931	1.929	1.928
(0,2)→(6,2)	1.940	1.940	1.950	1.950	1.949	1.948
(0,3)→(6,3)	1.944	1.944	1.954	1.954	1.952	1.950
(0,0)→(6,2)	0.348	0.348	0.351	0.351	0.347	0.347
(0,1)→(6,3)	0.348	0.348	0.351	0.351	0.347	0.347
(0,2)→(6,0)	0.349	0.349	0.352	0.352	0.348	0.348
(0,2)→(6,4)	0.349	0.349	0.351	0.351	0.347	0.347

FR, RC, and RD, and the subscript "vr" refer to different methods of computation as described in the text.

sections and β values for the ΔJ=0 and $|\Delta J|$=2 branches of H_2 for 58.4 nm and 73.6 nm photons for v_f=0,2, and 8, and v_f=0,1, and 5 respectively. He did separate calculations in which the final wave function was expressed first simply in terms of p waves and then in terms of p and f waves. The β values for the O and S branches differed drastically in the two calculations. The computed cross sections, computed here in the RD approximation, agree very well with the ones computed by Itikawa. However, the β values for the O and S branches were computed here as 0.38 for v_f=0, whereas according to Itikawa, this should be 0.75, and, according to Ritchie and Tambe,[564] β(ΔJ=0) = 1.22 for 58.4 nm photons. According to Pollard et al.[599] this β value is 0.87±0.19. It appears that this β value is very sensitive to the wave function of the photoelectron. According to Pollard et al.,[599] the β value of the O and S branches decreases to 0.08±0.15 if 73.6 nm photons are used. In H_2, the β values for transitions with the same $|\Delta J|$ are nearly equal, with the exception of the Q branch. The rovibronic transitions in the photoionization of σ orbitals with J_i=J_f=0 have β values which are exactly 2.0 regardless of the molecule or E_e. The β values of the O, Q, and S branches increase with increasing energy.[563,564] Judging from the dependence of the β values on v_f, this trend is also indicated by the present data.

The r-centroid method and the "RD" method give very similar results for H_2, HD, and D_2, whereas the results obtained with the Franck-Condon approximation differ considerably from the results obtained with the "RD" method, which represents the highest level of approximation in this work. For high vibrational quantum numbers, v_f,

the cross sections computed with and without vibration-rotation interaction can differ by as much as 10%, whereas the β values differ only by a fraction of a percent.

In Table 10-16, Table 10-17, and Table 10-18, the effects of vibration-rotation interaction on the vibronic cross sections and β values are readily apparent. Let us call the vibronic transitions with the highest intensity the "vertical transitions." In the photoionization of H_2, HD, and D_2, vibronic transitions with vibrational quantum numbers v_f less than the vibrational quantum number of the vertical transition are diminished in intensity through vibration-rotation interaction, whereas the higher members of the vibronic progression have increased intensities, if the effects of vibration-rotation interaction are included in the computations of the vibronic cross sections.

According to Table 10-16, Table 10-17, and Table 10-18, the vertical transitions of H_2, HD, and D_2 have $v_f = 2$, 3, and 4 respectively.

According to Shimamura's sum rules, the vibronic cross sections and β values should not depend on the rotational temperature. In hydrogen, (H_2, HD, and D_2), the effects of vibration-rotation interaction are relatively strong, presumably due to its small reduced mass which gives rise to large amplitude vibrations. In Tables 10-19, 10-20, 10-21, 10-22, 10-23, and 20-24, the cross sections and β values of H_2, HD, and D_2 are given in a form where they can be computed at different temperatures

$$\sigma_{v_f} = \sum_{J_i} N_{J_i} \sigma_{J_i v_f} \qquad (10\text{-}48)$$

TABLE 10-16

VIBRONIC CROSS SECTIONS AND BETA VALUES OF H_2 AT T=300K

	σ(Mb)					
v_f	FR	FR_{vr}	RC	RC_{vr}	RD	RD_{vr}
0	0.706	0.683	0.480	0.462	0.493	0.473
1	1.321	1.322	1.007	1.004	1.022	1.013
2	1.469	1.502	1.255	1.282	1.261	1.276
3	1.275	1.323	1.218	1.264	1.213	1.244
4	0.962	1.008	1.022	1.071	1.012	1.047
5	0.668	0.702	0.783	0.823	0.772	0.803
6	0.440	0.463	0.565	0.594	0.557	0.580
7	0.282	0.296	0.392	0.411	0.388	0.404
8	0.178	0.186	0.267	0.277	0.265	0.275
9	0.112	0.116	0.179	0.185	0.179	0.185
10	0.071	0.073	0.120	0.122	0.120	0.124
11	0.045	0.046	0.080	0.080	0.081	0.083
12	0.029	0.029	0.053	0.053	0.054	0.055
			β			
0	1.805	1.814	1.623	1.638	1.657	1.669
1	1.806	1.813	1.684	1.695	1.707	1.713
2	1.806	1.811	1.739	1.745	1.751	1.752
3	1.806	1.809	1.786	1.788	1.789	1.786
4	1.807	1.806	1.827	1.826	1.821	1.815
5	1.807	1.804	1.861	1.858	1.848	1.840
6	1.808	1.801	1.889	1.885	1.871	1.861
7	1.808	1.798	1.913	1.908	1.890	1.879
8	1.808	1.795	1.932	1.927	1.906	1.894
9	1.808	1.791	1.948	1.943	1.918	1.906
10	1.808	1.788	1.960	1.955	1.929	1.916
11	1.809	1.785	1.969	1.964	1.937	1.924
12	1.809	1.782	1.975	1.971	1.943	1.930

FR, RC, and RD, and the subscript "vr" refer to different methods of computation as described in the text.

TABLE 10-17

VIBRONIC CROSS SECTIONS AND BETA VALUES OF HD AT T=300K

v_f	σ(Mb)					
	FR	FR_{vr}	RC	RC_{vr}	RD	RD_{vr}
0	0.459	0.446	0.313	0.302	0.320	0.309
1	1.014	1.007	0.761	0.754	0.772	0.761
2	1.300	1.312	1.076	1.084	1.083	1.083
3	1.276	1.302	1.162	1.185	1.162	1.175
4	1.070	1.101	1.069	1.099	1.063	1.083
5	0.812	0.839	0.885	0.914	0.877	0.898
6	0.577	0.598	0.683	0.706	0.676	0.694
7	0.394	0.408	0.502	0.519	0.497	0.510
8	0.261	0.270	0.357	0.368	0.354	0.364
9	0.171	0.176	0.249	0.256	0.248	0.254
10	0.111	0.114	0.172	0.175	0.172	0.175
11	0.073	0.074	0.118	0.119	0.118	0.120
12	0.047	0.048	0.081	0.081	0.081	0.082
13	0.031	0.031	0.055	0.055	0.056	0.057
14	0.021	0.021	0.038	0.037	0.039	0.039
15	0.014	0.014	0.026	0.025	0.027	0.027
	β					
0	1.805	1.813	1.624	1.638	1.655	1.664
1	1.806	1.812	1.677	1.686	1.698	1.704
2	1.806	1.811	1.724	1.730	1.738	1.739
3	1.807	1.809	1.767	1.770	1.773	1.771
4	1.807	1.808	1.804	1.804	1.803	1.799
5	1.807	1.806	1.836	1.835	1.830	1.824
6	1.807	1.804	1.864	1.861	1.853	1.846
7	1.808	1.802	1.888	1.884	1.872	1.864
8	1.808	1.800	1.908	1.904	1.889	1.880
9	1.808	1.797	1.925	1.921	1.903	1.894
10	1.808	1.795	1.940	1.935	1.916	1.906
11	1.808	1.792	1.951	1.947	1.926	1.916
12	1.809	1.790	1.961	1.956	1.934	1.924
13	1.809	1.788	1.968	1.964	1.941	1.931
14	1.809	1.785	1.974	1.970	1.947	1.936
15	1.809	1.783	1.978	1.975	1.951	1.941

FR, RC, and RD, and the subscript "vr" refer to different methods of computation as described in the text.

TABLE 10-18

VIBRONIC CROSS SECTIONS AND BETA VALUES OF D_2 AT T=300K

	σ(Mb)					
v_f	FR	FR_{vr}	RC	RC_{vr}	RD	RD_{vr}
0	0.259	0.253	0.178	0.173	0.182	0.176
1	0.694	0.687	0.518	0.511	0.524	0.515
2	1.052	1.051	0.850	0.847	0.856	0.849
3	1.192	1.199	1.043	1.048	1.045	1.044
4	1.130	1.143	1.068	1.081	1.067	1.071
5	0.950	0.966	0.969	0.985	0.965	0.973
6	0.735	0.750	0.806	0.822	0.801	0.811
7	0.537	0.548	0.631	0.644	0.626	0.635
8	0.376	0.384	0.471	0.481	0.468	0.475
9	0.256	0.262	0.341	0.348	0.339	0.344
10	0.171	0.174	0.241	0.245	0.240	0.244
11	0.113	0.115	0.168	0.170	0.168	0.170
12	0.074	0.075	0.116	0.117	0.116	0.117
13	0.049	0.049	0.080	0.080	0.080	0.081
14	0.032	0.032	0.055	0.055	0.055	0.056
15	0.021	0.021	0.038	0.037	0.038	0.038
16	0.014	0.014	0.026	0.026	0.027	0.027
17	0.010	0.010	0.018	0.018	0.019	0.019
18	0.007	0.006	0.013	0.012	0.013	0.013

TABLE 10-18 (CONTINUED)

	β					
v_f	FR	FR_{vr}	RC	RC_{vr}	RD	RD_{vr}
0	1.806	1.812	1.631	1.641	1.655	1.662
1	1.806	1.811	1.674	1.681	1.692	1.697
2	1.806	1.810	1.713	1.719	1.726	1.728
3	1.807	1.809	1.750	1.753	1.757	1.757
4	1.807	1.808	1.782	1.784	1.785	1.783
5	1.807	1.807	1.812	1.812	1.810	1.807
6	1.807	1.806	1.838	1.837	1.833	1.828
7	1.808	1.805	1.862	1.859	1.853	1.847
8	1.808	1.803	1.882	1.879	1.870	1.864
9	1.808	1.802	1.901	1.897	1.886	1.879
10	1.808	1.800	1.917	1.913	1.900	1.892
11	1.808	1.798	1.931	1.927	1.912	1.904
12	1.808	1.797	1.943	1.939	1.922	1.914
13	1.809	1.795	1.953	1.949	1.932	1.923
14	1.809	1.793	1.961	1.958	1.939	1.931
15	1.809	1.791	1.968	1.965	1.946	1.938
16	1.809	1.789	1.974	1.971	1.952	1.944
17	1.809	1.787	1.978	1.976	1.956	1.948
18	1.809	1.785	1.982	1.979	1.960	1.952

FR, RC, and RD, and the subscript "vr" refer to different methods of computation as described in the text.

TABLE 10-19

THE VIBRONIC CROSS SECTIONS OF THE ROTATIONAL LEVELS OF H_2

The cross sections are approximated by $\sigma_{J_i v_f} = \sigma_{0 v_f} (1 - \zeta_1 J_i - \zeta_2 J_i^2)$

	$\sigma_{0 v_f}$ (Mb)					
v_f	FR	FR_{vr}	RC	RC_{vr}	RD	RD_{vr}
0	0.708	0.682	0.481	0.460	0.494	0.476
1	1.326	1.331	1.010	1.010	1.025	1.028
2	1.474	1.521	1.260	1.298	1.265	1.301
3	1.280	1.345	1.223	1.285	1.217	1.273
4	0.966	1.025	1.026	1.089	1.016	1.073
5	0.670	0.714	0.786	0.837	0.775	0.822
6	0.442	0.470	0.567	0.602	0.559	0.593
7	0.283	0.299	0.394	0.415	0.389	0.411
8	0.179	0.187	0.268	0.279	0.266	0.279
9	0.113	0.116	0.180	0.184	0.180	0.187
10	0.071	0.072	0.120	0.121	0.121	0.124
11	0.045	0.045	0.080	0.079	0.081	0.083
12	0.029	0.029	0.053	0.052	0.054	0.055

TABLE 10-19 (CONTINUED)

		$100\,\zeta_k$					
v_f	k	FR	FR_{vr}	RC	RC_{vr}	RD	RD_{vr}
0	1	0.134	-0.470	0.134	-0.546	0.134	0.118
0	2	0.081	0.195	0.081	0.201	0.081	0.251
1	1	0.143	0.340	0.144	0.293	0.143	0.880
1	2	0.087	0.165	0.087	0.170	0.087	0.229
2	1	0.152	0.886	0.153	0.867	0.152	1.386
2	2	0.092	0.132	0.093	0.135	0.092	0.206
3	1	0.161	1.215	0.162	1.213	0.162	1.676
3	2	0.098	0.100	0.098	0.101	0.098	0.186
4	1	0.171	1.360	0.171	1.360	0.171	1.786
4	2	0.104	0.070	0.104	0.070	0.104	0.170
5	1	0.181	1.346	0.179	1.334	0.179	1.745
5	2	0.109	0.041	0.109	0.042	0.109	0.158
6	1	0.190	1.193	0.186	1.155	0.188	1.575
6	2	0.115	0.013	0.113	0.016	0.114	0.150
7	1	0.200	0.922	0.193	0.850	0.195	1.306
7	2	0.121	-0.015	0.118	-0.010	0.119	0.143
8	1	0.209	0.558	0.200	0.443	0.203	0.965
8	2	0.126	-0.044	0.122	-0.037	0.124	0.137
9	1	0.219	0.110	0.206	-0.054	0.210	0.560
9	2	0.132	-0.075	0.126	-0.064	0.128	0.134
10	1	0.228	-0.402	0.212	-0.620	0.217	0.114
10	2	0.137	-0.104	0.130	-0.090	0.132	0.133
11	1	0.237	-0.955	0.218	-1.233	0.223	-0.350
11	2	0.142	-0.128	0.133	-0.110	0.137	0.137
12	1	0.247	-1.529	0.223	-1.875	0.230	-0.808
12	2	0.147	-0.136	0.137	-0.115	0.141	0.153

FR, RC, and RD, and the subscript "vr" refer to different methods of computation as described in the text.

TABLE 10-20

BETA VALUES OF THE ROTATIONAL LEVELS OF H_2 FOR DIFFERENT VIBRATIONAL STATES OF H_2^+

The beta values are approximated by $\beta_{J_i v_f} = \beta_{0 v_f} \left(1 - \tau_1 J_i - \tau_2 J_i^2\right)$

	$\beta_{0 v_f}$					
v_f	FR	FR_{vr}	RC	RC_{vr}	RD	RD_{vr}
0	1.805	1.815	1.623	1.640	1.657	1.675
1	1.806	1.814	1.684	1.697	1.707	1.718
2	1.806	1.812	1.739	1.746	1.751	1.756
3	1.807	1.809	1.786	1.789	1.789	1.789
4	1.806	1.807	1.827	1.826	1.821	1.818
5	1.807	1.803	1.861	1.858	1.848	1.842
6	1.808	1.800	1.889	1.885	1.871	1.863
7	1.808	1.796	1.913	1.907	1.890	1.880
8	1.808	1.792	1.932	1.926	1.906	1.894
9	1.808	1.788	1.948	1.942	1.918	1.906
10	1.808	1.784	1.960	1.954	1.929	1.916
11	1.809	1.779	1.969	1.963	1.937	1.924
12	1.809	1.775	1.975	1.970	1.943	1.930

TABLE 10-20 (CONTINUED)

		$10^4\tau_k$					
v_f	k	FR	FR_{vr}	RC	RC_{vr}	RD	RD_{vr}
0	1	0.039	6.313	-0.020	11.865	0.020	24.800
0	2	0.028	-0.428	-0.034	-0.904	0.004	2.297
1	1	0.038	6.087	0.023	9.709	0.035	19.898
1	2	0.027	-0.534	-0.004	-0.904	0.010	2.274
2	1	0.036	4.707	0.048	6.288	0.047	14.545
2	2	0.026	-0.460	0.020	-0.629	0.021	2.487
3	1	0.034	2.552	0.052	2.828	0.048	9.644
3	2	0.025	-0.264	0.034	-0.285	0.029	2.768
4	1	0.032	-0.142	0.043	-0.115	0.039	5.557
4	2	0.025	0.019	0.037	0.032	0.032	3.042
5	1	0.029	-3.216	0.026	-2.337	0.022	2.343
5	2	0.025	0.364	0.035	0.281	0.029	3.280
6	1	0.026	-6.561	0.009	-3.825	0.001	-0.090
6	2	0.024	0.753	0.029	0.453	0.023	3.476
7	1	0.022	-10.096	-0.006	-4.663	-0.020	-1.870
7	2	0.024	1.174	0.022	0.551	0.014	3.634
8	1	0.017	-13.736	-0.017	-4.972	-0.041	-3.151
8	2	0.023	1.610	0.017	0.588	0.004	3.758
9	1	0.012	-17.502	-0.025	-4.929	-0.058	-4.174
9	2	0.022	2.060	0.012	0.582	-0.005	3.861
10	1	0.007	-21.447	-0.028	-4.686	-0.073	-5.107
10	2	0.021	2.519	0.009	0.551	-0.013	3.951
11	1	0.001	-25.736	-0.029	-4.380	-0.084	-6.095
11	2	0.021	3.000	0.007	0.510	-0.020	4.034
12	1	-0.004	-30.764	-0.029	-4.131	-0.093	-7.262
12	2	0.020	3.532	0.006	0.474	-0.026	4.115

FR, RC, and RD, and the subscript "vr" refer to different methods of computation as described in the text.

TABLE 10-21

THE VIBRONIC CROSS SECTIONS OF THE ROTATIONAL LEVELS OF HD

The cross sections are approximated by $\sigma_{J_i v_f} = \sigma_{0 v_f} \left(1 - \zeta_1 J_i - \zeta_2 J_i^2\right)$

	σ_{0v_f} (Mb)					
v_f	FR	FR_{vr}	RC	RC_{vr}	RD	RD_{vr}
0	0.461	0.445	0.314	0.302	0.321	0.310
1	1.018	1.012	0.764	0.757	0.775	0.770
2	1.304	1.325	1.080	1.094	1.087	1.101
3	1.281	1.319	1.166	1.201	1.166	1.198
4	1.074	1.116	1.073	1.115	1.067	1.106
5	0.815	0.851	0.888	0.927	0.881	0.917
6	0.580	0.606	0.685	0.716	0.678	0.707
7	0.395	0.412	0.504	0.524	0.499	0.520
8	0.263	0.272	0.359	0.371	0.356	0.369
9	0.172	0.177	0.250	0.256	0.249	0.257
10	0.112	0.114	0.173	0.175	0.172	0.177
11	0.073	0.073	0.118	0.118	0.119	0.121
12	0.048	0.047	0.081	0.080	0.082	0.082
13	0.031	0.031	0.056	0.054	0.056	0.056
14	0.021	0.020	0.038	0.036	0.039	0.038
15	0.014	0.013	0.026	0.025	0.027	0.026

TABLE 10-21 (CONTINUED)

		$100\ \zeta_k$					
v_f	k	FR	FR_{vr}	RC	RC_{vr}	RD	RD_{vr}
0	1	0.103	-0.434	0.103	-0.475	0.102	-0.040
0	2	0.063	0.148	0.063	0.150	0.063	0.200
1	1	0.108	0.107	0.109	0.077	0.108	0.473
1	2	0.066	0.132	0.066	0.135	0.066	0.190
2	1	0.114	0.493	0.114	0.477	0.114	0.837
2	2	0.069	0.114	0.070	0.115	0.070	0.178
3	1	0.119	0.748	0.120	0.742	0.120	1.072
3	2	0.073	0.094	0.073	0.095	0.073	0.166
4	1	0.125	0.889	0.126	0.889	0.125	1.194
4	2	0.076	0.074	0.076	0.074	0.076	0.154
5	1	0.131	0.930	0.131	0.929	0.131	1.220
5	2	0.080	0.053	0.080	0.053	0.080	0.143
6	1	0.137	0.884	0.136	0.875	0.136	1.162
6	2	0.083	0.032	0.083	0.033	0.083	0.132
7	1	0.143	0.758	0.140	0.736	0.141	1.032
7	2	0.087	0.010	0.085	0.011	0.086	0.122
8	1	0.149	0.566	0.144	0.526	0.146	0.843
8	2	0.090	-0.013	0.088	-0.011	0.088	0.112
9	1	0.155	0.320	0.148	0.258	0.150	0.610
9	2	0.093	-0.038	0.091	-0.035	0.092	0.101
10	1	0.161	0.023	0.152	-0.063	0.154	0.336
10	2	0.097	-0.066	0.093	-0.061	0.094	0.091
11	1	0.166	-0.314	0.156	-0.425	0.158	0.032
11	2	0.100	-0.094	0.095	-0.089	0.097	0.080
12	1	0.172	-0.679	0.159	-0.817	0.162	-0.290
12	2	0.103	-0.123	0.098	-0.116	0.099	0.071
13	1	0.178	-1.060	0.163	-1.226	0.166	-0.617
13	2	0.106	-0.149	0.100	-0.141	0.102	0.064
14	1	0.183	-1.446	0.166	-1.645	0.170	-0.938
14	2	0.109	-0.167	0.102	-0.158	0.104	0.065
15	1	0.188	-1.831	0.169	-2.070	0.174	-1.243
15	2	0.113	-0.165	0.104	-0.154	0.107	0.080

FR, RC, and RD, and the subscript "vr" refer to different methods of computation as described in the text.

TABLE 10-22

BETA VALUES OF THE ROTATIONAL LEVELS OF HD^+ FOR DIFFERENT VIBRATIONAL STATES OF HD^+

The beta values are approximated by $\beta_{J_i v_f} = \beta_{0 v_f} (1 - \tau_1 J_i - \tau_2 J_i^2)$

	$\beta_{0 v_f}$					
v_f	FR	FR_{vr}	RC	RC_{vr}	RD	RD_{vr}
0	1.805	1.814	1.624	1.639	1.655	1.669
1	1.806	1.813	1.677	1.688	1.699	1.708
2	1.806	1.812	1.724	1.732	1.738	1.743
3	1.807	1.810	1.767	1.771	1.773	1.775
4	1.807	1.808	1.804	1.805	1.803	1.802
5	1.807	1.806	1.836	1.835	1.830	1.826
6	1.807	1.804	1.864	1.861	1.853	1.847
7	1.808	1.801	1.888	1.884	1.872	1.866
8	1.808	1.798	1.908	1.903	1.889	1.881
9	1.808	1.796	1.925	1.920	1.903	1.895
10	1.808	1.793	1.940	1.934	1.916	1.907
11	1.808	1.790	1.951	1.946	1.926	1.917
12	1.809	1.787	1.961	1.956	1.934	1.925
13	1.809	1.784	1.968	1.963	1.941	1.932
14	1.809	1.781	1.974	1.969	1.947	1.937
15	1.809	1.778	1.978	1.974	1.951	1.941

TABLE 10-22 (CONTINUED)

v_f	k	$10^4\tau_k$ FR	FR_{vr}	RC	RC_{vr}	RD	RD_{vr}
0	1	0.030	3.409	-0.012	6.364	0.013	14.697
0	2	0.022	-0.142	-0.023	-0.339	0.002	2.314
1	1	0.029	3.692	0.016	6.014	0.026	12.650
1	2	0.022	-0.253	-0.003	-0.455	0.007	2.176
2	1	0.028	3.272	0.035	4.600	0.035	10.021
2	2	0.021	-0.264	0.014	-0.388	0.016	2.190
3	1	0.027	2.358	0.041	2.839	0.039	7.374
3	2	0.021	-0.204	0.024	-0.245	0.022	2.270
4	1	0.026	1.092	0.037	1.122	0.035	5.000
4	2	0.020	-0.090	0.029	-0.083	0.026	2.372
5	1	0.024	-0.421	0.028	-0.352	0.026	3.017
5	2	0.020	0.063	0.029	0.066	0.026	2.473
6	1	0.022	-2.105	0.017	-1.501	0.014	1.448
6	2	0.020	0.245	0.026	0.187	0.023	2.565
7	1	0.020	-3.900	0.005	-2.312	0.000	0.262
7	2	0.019	0.448	0.021	0.275	0.018	2.643
8	1	0.017	-5.759	-0.005	-2.813	-0.014	-0.586
8	2	0.019	0.665	0.017	0.331	0.012	2.706
9	1	0.014	-7.628	-0.014	-3.047	-0.027	-1.156
9	2	0.018	0.887	0.013	0.357	0.006	2.755
10	1	0.011	-9.502	-0.019	-3.088	-0.038	-1.563
10	2	0.018	1.112	0.009	0.362	0.000	2.795
11	1	0.007	-11.382	-0.023	-2.999	-0.048	-1.884
11	2	0.017	1.335	0.007	0.351	-0.005	2.828
12	1	0.003	-13.301	-0.025	-2.843	-0.055	-2.197
12	2	0.017	1.558	0.005	0.331	-0.010	2.858
13	1	0.000	-15.344	-0.025	-2.673	-0.061	-2.575
13	2	0.016	1.784	0.004	0.308	-0.014	2.888
14	1	-0.004	-17.701	-0.025	-2.540	-0.066	-3.083
14	2	0.015	2.028	0.003	0.288	-0.017	2.920
15	1	-0.007	-20.781	-0.024	-2.496	-0.069	-3.790
15	2	0.015	2.323	0.003	0.277	-0.020	2.956

FR, RC, and RD, and the subscript "vr" refer to different methods of computation as described in the text.

TABLE 10-23

THE VIBRONIC CROSS SECTIONS OF THE ROTATIONAL LEVELS OF D_2

The cross sections are approximated by $\sigma_{J_i v_f} = \sigma_{0 v_f}\left(1-\zeta_1 J_i - \zeta_2 J_i^2\right)$

	σ_{0v_f} (Mb)					
v_f	FR	FR_{vr}	RC	RC_{vr}	RD	RD_{vr}
0	0.260	0.253	0.179	0.173	0.182	0.177
1	0.697	0.690	0.519	0.513	0.526	0.520
2	1.056	1.059	0.853	0.854	0.859	0.861
3	1.196	1.212	1.046	1.059	1.049	1.061
4	1.134	1.156	1.072	1.093	1.071	1.091
5	0.954	0.977	0.973	0.996	0.968	0.991
6	0.738	0.758	0.810	0.831	0.804	0.825
7	0.539	0.553	0.633	0.650	0.629	0.645
8	0.378	0.387	0.473	0.484	0.470	0.482
9	0.257	0.262	0.343	0.349	0.341	0.348
10	0.172	0.174	0.242	0.245	0.241	0.246
11	0.114	0.115	0.169	0.169	0.169	0.171
12	0.075	0.075	0.117	0.116	0.117	0.117
13	0.049	0.049	0.080	0.079	0.081	0.080
14	0.032	0.032	0.055	0.053	0.056	0.055
15	0.021	0.021	0.038	0.036	0.039	0.038
16	0.014	0.014	0.026	0.025	0.027	0.026
17	0.010	0.009	0.018	0.017	0.019	0.018
18	0.007	0.006	0.013	0.012	0.013	0.013

TABLE 10-23 (CONTINUED)

		100ζ					
v_f	k	FR	FR_{vr}	RC	RC_{vr}	RD	RD_{vr}
0		0.066	-0.295	0.066	-0.313	0.066	-0.065
0		0.043	0.108	0.043	0.108	0.043	0.150
1		0.069	0.001	0.070	-0.014	0.069	0.218
1		0.045	0.100	0.045	0.101	0.045	0.147
2		0.072	0.221	0.073	0.211	0.073	0.429
2		0.047	0.090	0.047	0.091	0.047	0.141
3		0.075	0.377	0.076	0.372	0.076	0.575
3		0.049	0.078	0.049	0.079	0.049	0.133
4		0.079	0.474	0.079	0.473	0.079	0.664
4		0.051	0.065	0.051	0.065	0.051	0.125
5		0.082	0.519	0.082	0.519	0.082	0.701
5		0.053	0.051	0.053	0.051	0.053	0.116
6		0.085	0.516	0.085	0.514	0.085	0.691
6		0.055	0.036	0.055	0.036	0.055	0.106
7		0.088	0.468	0.087	0.464	0.088	0.638
7		0.057	0.019	0.057	0.020	0.057	0.096
8		0.092	0.381	0.090	0.370	0.090	0.548
8		0.059	0.001	0.058	0.002	0.059	0.085
9		0.095	0.257	0.092	0.239	0.093	0.425
9		0.061	-0.019	0.060	-0.018	0.060	0.072
10		0.098	0.102	0.095	0.075	0.095	0.275
10		0.063	-0.041	0.061	-0.040	0.062	0.059
11		0.101	-0.083	0.097	-0.120	0.098	0.099
11		0.065	-0.066	0.063	-0.064	0.063	0.044
12		0.105	-0.294	0.099	-0.342	0.100	-0.099
12		0.067	-0.093	0.064	-0.091	0.065	0.028
13		0.108	-0.528	0.101	-0.586	0.102	-0.314
13		0.069	-0.123	0.065	-0.121	0.066	0.010
14		0.111	-0.779	0.102	-0.846	0.104	-0.541
14		0.071	-0.156	0.067	-0.154	0.068	-0.009
15		0.114	-1.042	0.104	-1.119	0.106	-0.776
15		0.072	-0.191	0.068	-0.188	0.069	-0.028
16		0.117	-1.311	0.106	-1.398	0.108	-1.012
16		0.074	-0.277	0.069	-0.224	0.070	-0.047
17		0.120	-1.583	0.108	-1.679	0.110	-1.246
17		0.076	-0.261	0.070	-0.258	0.072	-0.064
18		0.123	-1.852	0.109	-1.959	0.112	-1.472
18		0.078	-0.289	0.071	-0.287	0.073	-0.076

FR, RC, and RD, and the subscript "vr" refer to different methods of computation as described in the text.

TABLE 10-24

BETA VALUES OF THE ROTATIONAL LEVELS OF D_2^+ FOR DIFFERENT VIBRATIONAL STATES OF D_2^+

The beta values are approximated by $\beta_{J_i v_f} = \beta_{0 v_f} (1 - \tau_1 J_i - \tau_2 J_i^2)$

	$\beta_{0 v_f}$					
v_f	FR	FR_{vr}	RC	RC_{vr}	RD	RD_{vr}
0	1.806	1.812	1.631	1.642	1.655	1.666
1	1.806	1.812	1.674	1.682	1.692	1.700
2	1.806	1.811	1.713	1.720	1.726	1.732
3	1.807	1.810	1.750	1.754	1.757	1.760
4	1.807	1.809	1.782	1.784	1.785	1.786
5	1.807	1.807	1.812	1.812	1.810	1.809
6	1.807	1.806	1.838	1.837	1.833	1.830
7	1.808	1.804	1.862	1.859	1.853	1.849
8	1.808	1.803	1.882	1.879	1.870	1.865
9	1.808	1.801	1.901	1.897	1.886	1.880
10	1.808	1.799	1.917	1.912	1.900	1.894
11	1.808	1.797	1.931	1.926	1.912	1.905
12	1.808	1.795	1.943	1.938	1.922	1.916
13	1.809	1.793	1.953	1.948	1.932	1.925
14	1.809	1.791	1.961	1.957	1.939	1.933
15	1.809	1.789	1.968	1.964	1.946	1.940
16	1.809	1.786	1.974	1.970	1.952	1.945
17	1.809	1.784	1.978	1.975	1.956	1.950
18	1.809	1.782	1.982	1.979	1.960	1.954

TABLE 10-24 (CONTINUED)

		$10^4\tau_k$					
v_f	k	FR	FR_{vr}	RC	RC_{vr}	RD	RD_{vr}
0	1	0.020	1.595	-0.005	2.924	0.008	7.447
0	2	0.016	-0.012	-0.012	-0.067	0.002	1.898
1	1	0.019	1.842	0.010	3.026	0.016	6.722
1	2	0.016	-0.082	-0.001	-0.164	0.006	1.780
2	1	0.019	1.770	0.021	2.581	0.022	5.659
2	2	0.016	-0.109	0.009	-0.174	0.011	1.732
3	1	0.018	1.458	0.026	1.877	0.026	4.497
3	2	0.015	-0.102	0.016	-0.136	0.016	1.722
4	1	0.018	0.969	0.027	1.095	0.026	3.383
4	2	0.015	-0.069	0.020	-0.075	0.018	1.732
5	1	0.017	0.348	0.024	0.346	0.023	2.397
5	2	0.015	-0.015	0.021	-0.009	0.020	1.751
6	1	0.016	-0.367	0.019	-0.305	0.018	1.579
6	2	0.015	0.055	0.020	0.054	0.019	1.773
7	1	0.016	-1.144	0.012	-0.828	0.011	0.938
7	2	0.015	0.138	0.018	0.108	0.017	1.794
8	1	0.014	-1.955	0.006	-1.213	0.004	0.469
8	2	0.015	0.231	0.016	0.150	0.014	1.811
9	1	0.013	-2.779	0.000	-1.464	-0.004	0.163
9	2	0.014	0.330	0.013	0.178	0.011	1.824
10	1	0.012	-3.585	-0.005	-1.593	-0.011	-0.001
10	2	0.014	0.432	0.010	0.194	0.007	1.831
11	1	0.010	-4.365	-0.009	-1.624	-0.017	-0.068
11	2	0.014	0.534	0.008	0.200	0.004	1.834
12	1	0.008	-5.104	-0.012	-1.580	-0.023	-0.069
12	2	0.013	0.635	0.006	0.196	0.000	1.832
13	1	0.006	-5.795	-0.014	-1.484	-0.027	-0.039
13	2	0.013	0.733	0.004	0.187	-0.002	1.828
14	1	0.004	-6.439	-0.015	-1.360	-0.031	-0.014
14	2	0.012	0.826	0.003	0.173	-0.005	1.822
15	1	0.002	-7.049	-0.015	-1.226	-0.034	-0.030
15	2	0.012	0.913	0.002	0.157	-0.007	1.817
16	1	0.000	-7.658	-0.014	-1.098	-0.036	-0.121
16	2	0.012	0.997	0.002	0.141	-0.009	1.813
17	1	-0.002	-8.328	-0.013	-0.990	-0.038	-0.312
17	2	0.011	1.081	0.002	0.127	-0.011	1.814
18	1	-0.003	-9.178	-0.012	-0.912	-0.039	-0.624
18	2	0.011	1.173	0.002	0.115	-0.012	1.819

FR, RC, and RD, and the subscript "vr" refer to different methods of computation as described in the text.

The vibronic cross sections of the individual rotational levels themselves were expanded in power series', as shown in the corresponding Tables. These power series' were computed through least squares approximations. The β values of the vibronic bands can be computed from data in these Tables as follows:

$$\beta_{v_f} = \Sigma_{J_i} N_{J_i v_f} \sigma_{J_i v_f} \beta_{J_i v_f} / \sigma_{v_f} \qquad (10\text{-}49)$$

The β values for the individual rotational levels, J_i, are also given as power series' in the corresponding Tables. The least squares approximations were done for $J_i \leq 7$, $J_i \leq 8$, and $J_i \leq 9$ for H_2, HD, and D_2 respectively. The data were reproduced by the approximation to better than 0.2%. The vibrational branching ratios differ measurably with temperature, but the β values of the vibronic bands are barely affected by the rotational temperature.

According to Table 10-19, the normalized cross sections of H_2 at low temperature are, (using RD_{vr}):

37, 79, 100, 98, 82, 63, 46, 32, 21, 14, 10,

for $v_f = 0, 1, \ldots\ldots, 10$. According to Pollard et al.,[599] the normalized cross sections are:

46, 87, 100, 93, 76, 57, 43, 30, 21, 15, 10.

The present data approximate the experimental vibronic cross sections to roughly the same accuracy as Itikawa's results.

The vibronic cross sections computed by O'Neil and Reinhardt[640] agree better with experiment than Itikawa's results and the results reported here. Pollard et al.[599] suggested that the small dipole

moment of HD^+ could affect the cross sections through nonadiabatic coupling between the photoelectron and the vibrating dipole. According to Bishop and Cheung,[560] the dipole moment of HD^+ is very small. (Approx. 0.0003 Debye, depending on v). Nonadiabatic coupling is observed in homonuclear diatomic molecules as well, in which case the coupling originates mostly from the vibrating quadrupole. It is unlikely that the small dipole moment of HD^+ would give rise to noticeable nonadiabatic effects. Due to the symmetry breaking of the electronic structure through nonadiabatic coupling in HD, the P and R branches could - in principle - be observed in the photoelectron spectra of HD. Pollard *et al.*[599] did not observe these branches, but, due to incomplete resolution of the rotational structure, they could not rule out their presence either.

According to Pollard *et al.*,[599] in HD the vibronic band with $v_f=3$ has the largest cross section, whereas, according to the experimental data by Berkowitz and Spohr,[641] the vibronic band with $v_f=2$ has the largest cross section. O'Neil and Reinhard[640] reported data only for H_2 and D_2. The data for HD presented here indicate that the vibronic band with the highest cross section has $v_f=3$, in agreement with the molecular beam experiments by Pollard *et al.*, which are very recent, whereas the data by Berkowitz and Spohr[641] are almost a decade old.

Chiu and Samanta[642] computed the differential cross sections of H_2 using a one-center expansion for the electronic wave functions.

They reviewed much of the experimental and theoretical work done on hydrogen up to last year. O'Neil and Reinhardt[640] used configuration interaction, and they determined the vibrational wave functions

numerically from accurate potential energy surfaces. Obviously, the present data cannot be expected to be as accurate as the data obtained by O'Neil and Reinhardt. If the data obtained with the Franck-Condon approximation and with the "RD" approximation are compared with the experimental data, one finds, nevertheless, that the present approach reproduces nicely the effects of nuclear motion.

The vibronic β values of H_2 increase in the vibronic progression. The highest members in the vibronic progression have β values which are very close to 2.0. According to Kreile and Schweig,[643] the β values in the vibronic progression of H_2 are:

1.76, 1.82, 1.87, 1.88, 1.87, 1.89

for v_f=0,1, ..., 5.

The β values obtained in this work are somewhat lower. For H_2 we obtain β values of:

1.68, 1.72, 1.76, 1.79, 1.82, 1.84

for v_f=0,1, ..., 5. Kreile and Schweig[643] gave the overall β value of H_2 with 58.4 nm photons as 1.86. Southworth et al.[637] gave an overall β value of 1.75 for H_2 using 58.4 nm photons. It may be that the vibronic β values by Kreile and Schweig are too high. The overall β value of H_2 computed in the present work is 1.80 at low temperatures and 1.79 at room temperature. These values are exactly in the middle between the two above experimental values. In Tables 10-25, 10-26, and 10-27, the cross sections and β values are listed for H_2, HD, and D_2 respectively at different temperatures. The overall cross sections at T=4K and T=600K differ by as much as 3 percent, mainly due to vibration-rotation interaction. In Tables 10-28, 10-29, and 10-30, the

TABLE 10-25

THE TOTAL CROSS SECTIONS AND THE AVERAGE BETA VALUES OF H_2 AT DIFFERENT TEMPERATURES

	σ(Mb)					
T(K)	FR	FR_{vr}	RC	RC_{vr}	RD	RD_{vr}
4	7.585	7.838	7.449	7.711	7.443	7.704
70	7.578	7.808	7.441	7.682	7.435	7.657
300	7.557	7.751	7.420	7.627	7.415	7.562
600	7.526	7.684	7.389	7.565	7.383	7.450

	β					
T(K)	FR	FR_{vr}	RC	RC_{vr}	RD	RD_{vr}
4	1.806	1.808	1.797	1.802	1.797	1.798
70	1.806	1.808	1.797	1.801	1.797	1.797
300	1.806	1.808	1.797	1.801	1.797	1.795
600	1.806	1.808	1.797	1.801	1.797	1.793

FR, RC, and RD, and the subscript "vr" refer to different methods of computation as described in the text.

TABLE 10-26

THE TOTAL CROSS SECTIONS AND THE AVERAGE BETA VALUES OF HD AT DIFFERENT TEMPERATURES

	σ(Mb)					
T(K)	FR	FR_{vr}	RC	RC_{vr}	RD	RD_{vr}
4	7.662	7.835	7.575	7.751	7.573	7.755
70	7.657	7.819	7.570	7.736	7.568	7.729
300	7.633	7.761	7.546	7.681	7.544	7.630
600	7.599	7.700	7.513	7.625	7.510	7.525

	β					
T(K)	FR	FR_{vr}	RC	RC_{vr}	RD	RD_{vr}
4	1.807	1.808	1.800	1.803	1.800	1.800
70	1.807	1.808	1.800	1.803	1.800	1.800
300	1.807	1.807	1.800	1.803	1.800	1.798
600	1.807	1.807	1.800	1.803	1.800	1.795

FR, RC, and RD, and the subscript "vr" refer to different methods of computation as described in the text.

TABLE 10-27

THE TOTAL CROSS SECTIONS AND THE AVERAGE BETA VALUES OF D_2 AT DIFFERENT TEMPERATURES

	σ(Mb)					
T(K)	FR	FR_{vr}	RC	RC_{vr}	RD	RD_{vr}
4	7.703	7.802	7.659	7.756	7.660	7.764
70	7.698	7.790	7.655	7.745	7.655	7.743
300	7.673	7.741	7.629	7.700	7.630	7.656
600	7.633	7.682	7.589	7.648	7.589	7.556

	β					
T(K)	FR	FR_{vr}	RC	RC_{vr}	RD	RD_{vr}
4	1.807	1.807	1.802	1.804	1.802	1.802
70	1.807	1.807	1.802	1.804	1.802	1.802
300	1.807	1.807	1.802	1.804	1.802	1.800
600	1.807	1.807	1.802	1.804	1.802	1.798

FR, RC, and RD, and the subscript "vr" refer to different methods of computation as described in the text.

TABLE 10-28

THE TOTAL CROSS SECTIONS AND THE AVERAGE BETA VALUES OF THE ROTATIONAL LEVELS OF H_2

	σ(Mb)					
J_i	FR	FR_{vr}	RC	RC_{vr}	RD	RD_{vr}
0	7.585	7.838	7.449	7.711	7.443	7.704
1	7.568	7.772	7.431	7.647	7.425	7.597
2	7.533	7.684	7.396	7.564	7.390	7.453
3	7.482	7.581	7.344	7.468	7.339	7.278
4	7.415	7.462	7.277	7.358	7.271	7.073
5	7.333	7.329	7.195	7.237	7.189	6.841
6	7.239	7.184	7.100	7.106	7.094	6.587
7	7.134	7.028	6.994	6.967	6.988	6.313

	β					
J_i	FR	FR_{vr}	RC	RC_{vr}	RD	RD_{vr}
0	1.806	1.808	1.797	1.802	1.797	1.790
1	1.806	1.807	1.797	1.801	1.797	1.796
2	1.806	1.807	1.797	1.801	1.797	1.793
3	1.806	1.807	1.797	1.801	1.797	1.789
4	1.806	1.807	1.797	1.801	1.797	1.784
5	1.806	1.807	1.796	1.802	1.797	1.778
6	1.806	1.807	1.796	1.802	1.796	1.771
7	1.806	1.807	1.796	1.803	1.796	1.762

FR, RC, and RD, and the subscript "vr" refer to different methods of computation as described in the text.

TABLE 10-29

THE TOTAL CROSS SECTIONS AND THE AVERAGE BETA VALUES OF THE ROTATIONAL LEVELS OF HD

	σ(Mb)					
J_i	FR	FR_{vr}	RC	RC_{vr}	RD	RD_{vr}
0	7.662	7.835	7.575	7.751	7.573	7.755
1	7.648	7.790	7.562	7.708	7.560	7.681
2	7.622	7.730	7.535	7.651	7.533	7.579
3	7.582	7.656	7.495	7.584	7.493	7.450
4	7.531	7.571	7.443	7.506	7.441	7.297
5	7.467	7.474	7.379	7.419	7.377	7.120
6	7.393	7.366	7.305	7.323	7.302	6.922
7	7.310	7.249	7.220	7.219	7.218	6.706
8	7.217	7.124	7.127	7.110	7.124	6.473

	β					
J_i	FR	FR_{vr}	RC	RC_{vr}	RD	RD_{vr}
0	1.807	1.808	1.800	1.803	1.800	1.800
1	1.807	1.807	1.800	1.802	1.800	1.799
2	1.807	1.807	1.800	1.803	1.800	1.797
3	1.807	1.807	1.800	1.803	1.800	1.794
4	1.807	1.807	1.800	1.803	1.799	1.790
5	1.807	1.807	1.800	1.803	1.799	1.785
6	1.807	1.807	1.799	1.804	1.799	1.780
7	1.807	1.807	1.799	1.804	1.799	1.774
8	1.806	1.806	1.799	1.805	1.799	1.766

FR, RC, and RD, and the subscript "vr" refer to different methods of computation as described in the text.

TABLE 10-30

THE TOTAL CROSS SECTIONS AND THE AVERAGE BETA VALUES OF THE ROTATIONAL LEVELS OF D_2

	σ(Mb)					
J_i	FR	FR_{vr}	RC	RC_{vr}	RD	RD_{vr}
0	7.703	7.802	7.659	7.756	7.660	7.764
1	7.694	7.776	7.650	7.732	7.651	7.721
2	7.676	7.740	7.632	7.700	7.633	7.658
3	7.649	7.696	7.605	7.660	7.606	7.576
4	7.614	7.642	7.570	7.614	7.570	7.476
5	7.571	7.581	7.526	7.560	7.526	7.358
6	7.520	7.512	7.474	7.501	7.474	7.224
7	7.461	7.435	7.415	7.437	7.415	7.074
8	7.395	7.352	7.348	7.367	7.348	6.911
9	7.323	7.263	7.275	7.293	7.276	6.735

	β					
J_i	FR	FR_{vr}	RC	RC_{vr}	RD	RD_{vr}
0	1.807	1.807	1.802	1.804	1.802	1.802
1	1.807	1.807	1.802	1.804	1.802	1.801
2	1.807	1.807	1.802	1.804	1.802	1.800
3	1.807	1.807	1.802	1.804	1.802	1.798
4	1.807	1.807	1.802	1.804	1.802	1.796
5	1.807	1.807	1.802	1.805	1.802	1.793
6	1.807	1.807	1.802	1.805	1.802	1.789
7	1.807	1.807	1.802	1.806	1.802	1.785
8	1.807	1.807	1.802	1.806	1.802	1.780
9	1.807	1.806	1.802	1.807	1.801	1.774

FR, RC, and RD, and the subscript "vr" refer to different methods of computation as described in the text.

total cross sections of the initial rotational levels, (summed over v_f and J_f), are given for H_2, HD, and D_2 respectively. From these and the average β values, which are also given, the overall cross sections and the average β values can be computed for any rotational temperature, using (10-48) and (10-49).

The β values computed in this work, for the O and S branches, appear to be too small by approximately a factor of 2. If only p waves had been used to represent the photoelectron, the β values of the O and S branches would be 1/5.[561] Itikawa[563] has shown that the β values of the O and S branches are strongly affected by the interference of p and f waves. The rotational structure of vibronic bands, in general, is expected to be a sensitive probe of minute details in the continuum wave function. Since the partial waves contribute differently to the rovibronic cross sections, the resolution of the rotational structure can, in a sense, be regarded as an "experimental partial wave analysis." The ratios of the cross sections $\sigma(J \leftarrow J)/\sigma(J+\Delta J \leftarrow J)$ computed here agree qualitatively with the ratios obtained with the cross sections computed by Itikawa. Itikawa obtained similar cross sections for calculations with p and f waves and with p waves alone. This wasn't the case for the β values. It appears that the DMAPWs computed with the Xα method could give reliable results for vibronic cross sections.

According to Pollard et al.,[599] the ratio of the intensity of the Q and the S branch of n-H_2 in the vibronic band, with $v_f=0$, should be 10.26. Assuming that, in the molecular beam, the ortho and para modification are in their respective ground states of $J_i=1$ and $J_i=0$,

this ratio, according to Itikawa's cross sections, would be 6.4. The present results give a value of 10.1 for this ratio, which agrees with the experimental value by Pollard et al. within experimental accuracy. The cross sections used for this computation were taken from Table 10-13 for the RD_{vr} approximation, and it was assumed that the sample of n-hydrogen consisted originally of 75 percent ortho hydrogen and 25 percent para hydrogen.

O'Neil and Reinhardt[640] studied also the dissociative photoionization of H_2. The $^1\Sigma_u^+$ resonance Rydberg state undergoes autoionization into the vibrational continuum of the $^2\Sigma_g^+$ state of H_2^+, producing energetic H^+ ions.[645] The cross section for the production of H^+ shows oscillatory behaviour.[645,646]

2. The $3\sigma_g$ Photoionization of N_2

The photoelectron spectra of N_2 are more or less affected by shape resonances. In Table 10-31, the cross sections and β values for the $3\sigma_g$ photoionization are shown for energies E_e of interest in connection with 58.4 nm photons, and at different internuclear separations. One can readily see that a shape resonance is present at internuclear separations slightly larger than r_e of N_2. This shape resonance should affect the higher members of the vibronic progression, and possibly also the rovibronic transitions with $v_f=0$.

In Tables 10-32 and 10-33, the scaled rovibronic cross sections and the β values are given for the $3\sigma_g$ photoionization of N_2. In Tables 10-32 and 10-33, the symbol ΔJ stands for J_f-J_i. This notation applies throughout.

TABLE 10-31

PHOTOIONIZATION CROSS SECTIONS AND BETA VALUES OF N_2

$N_2(X^1\Sigma_g^+) \rightarrow N_2^+(X^2\Sigma_g^+) + e^-$

σ (Mb)

Channel	$r_{NN}(a_o)$	E_e=0.37 Ryd	E_e=0.39 Ryd	E_e=0.41 Ryd	E_e=0.43 Ryd
$3\sigma_g \rightarrow k\sigma_u$	1.9	2.11	2.16	2.21	2.26
	2.05	3.35	3.56	3.81	4.10
	2.2	15.13	18.85	23.24	27.45
	2.35	2.40	1.85	1.46	1.19
	2.5	0.16	0.16	0.16	0.16
$3\sigma_g \rightarrow k\pi_u$	1.9	1.89	1.87	1.86	1.84
	2.05	1.64	1.64	1.66	1.67
	2.2	1.53	1.57	1.62	1.66
	2.35	1.61	1.68	1.76	1.83
	2.5	1.86	1.96	2.05	2.15

β

$r_{NN}(a_o)$	E_e=0.37 Ryd	E_e=0.39 Ryd	E_e=0.41 Ryd	E_e=0.43 Ryd
1.9	1.20	1.76	1.58	1.41
2.05	0.81	0.79	0.78	0.77
2.2	0.37	0.38	0.39	0.41
2.35	0.34	0.36	0.37	0.38
2.5	0.39	0.39	0.39	0.39

TABLE 10-32

SCALED PHOTOIONIZATION CROSS SECTIONS FOR

$N_2(X^1\Sigma_g^+) \rightarrow N_2^+(X^2\Sigma_g^+) + e^-$ (hν=21.2 eV)

v_f	J_i	ΔJ= -6	ΔJ= -4	ΔJ= -2	ΔJ=0	ΔJ=2	ΔJ=4	ΔJ=6
0	0				422	1445	389	0
0	1				1000	1040	216	0
0	2			289	946	844	176	0
0	3			446	878	773	158	0
0	4		43	470	861	735	148	0
0	5		59	493	853	711	141	0
0	6	0	69	510	849	695	136	0
0	12	0	91	558	843	653	122	0
0	24	0	105	592	848	637	117	0
1	0				882	888	195	0
1	1				991	621	108	0
1	2			177	976	509	88	0
1	3			266	965	467	79	0
1	4		22	282	963	445	73	0
1	5		30	297	962	431	69	0
1	6	0	35	308	962	422	66	0
1	12	0	47	338	969	401	58	0
1	24	0	55	368	1000	410	53	0
2	0				42	1316	2028	0
2	1				570	1691	1125	0
2	2			264	1000	1202	918	0
2	3			729	763	1069	823	0
2	4		227	673	714	1003	766	0
2	5		310	688	693	963	729	0
2	6	0	358	704	682	936	702	0
2	12	0	469	761	663	861	623	0
2	24	0	527	799	653	809	565	0

TABLE 10-33

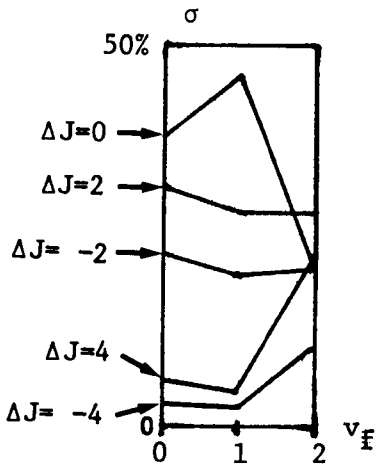
BETA VALUES FOR $N_2(X^1\Sigma_g^+) \rightarrow N_2^+(X^2\Sigma_g^+) + e^-$ ($h\nu$=21.2 eV)

v_f	J_i	ΔJ= −6	ΔJ= −4	ΔJ= −2	ΔJ=0	ΔJ=2	ΔJ=4	ΔJ=6
0	0				2.00	0.26	0.31	0.37
0	1				1.00	0.27	0.31	0.37
0	2			0.26	1.04	0.27	0.31	0.37
0	3			0.27	1.10	0.27	0.31	0.37
0	4		0.31	0.27	1.12	0.27	0.31	0.37
0	5		0.31	0.27	1.13	0.27	0.31	0.37
0	6	0.37	0.31	0.27	1.13	0.27	0.31	0.37
0	12	0.37	0.31	0.27	1.13	0.26	0.31	0.37
0	24	0.37	0.31	0.27	1.13	0.26	0.31	0.37
1	0				2.00	0.31	0.27	0.36
1	1				1.24	0.30	0.27	0.36
1	2			0.31	1.30	0.30	0.27	0.36
1	3			0.30	1.35	0.30	0.27	0.36
1	4		0.27	0.30	1.37	0.30	0.27	0.36
1	5		0.27	0.30	1.37	0.30	0.27	0.36
1	6	0.36	0.27	0.30	1.38	0.30	0.27	0.36
1	12	0.37	0.27	0.31	1.38	0.30	0.27	0.36
1	24	0.37	0.28	0.31	1.38	0.31	0.27	0.36
2	0				2.00	−0.10	0.31	0.37
2	1				0.06	0.12	0.31	0.37
2	2			−0.10	0.23	0.08	0.31	0.37
2	3			0.12	0.22	0.07	0.31	0.37
2	4		0.31	0.08	0.21	0.07	0.31	0.37
2	5		0.31	0.07	0.21	0.07	0.31	0.37
2	6	0.37	0.31	0.07	0.21	0.06	0.31	0.37
2	12	0.37	0.31	0.07	0.21	0.06	0.31	0.37
2	24	0.37	0.31	0.07	0.21	0.06	0.31	0.37

In the photoionization of hydrogen, the β values of all rovibronic transitions of a branch with $\Delta J \neq 0$ usually had almost identical β values. This is the case for the photoionization of σ orbitals of N_2 and CO as well, if shape resonances do not interfere. In Table 10-33, the effect of the σ-σ shape resonance, which is apparent in Table 10-31, can be seen for the O and the S branch. The shape resonance evidently increases the cross sections of the $|\Delta J|=4$ branches as can be seen in Figure 10-10. In the first few members of the branches, the cross sections and sometimes the β values change strongly, but seem to approach asymptotically a limiting value for large quantum members J. Shimamura[644] has proven theoretically that the partial cross sections of branches with $\pm\Delta J$ approach a common limiting value as J becomes large. In one of the branches, the limiting cross section is approached from above; in the branch with opposite sign of ΔJ the limiting cross section is approached from below. The same applies to the product $\beta\sigma_{tot}$.[644]

In Tables 10-34, 10-35, and 10-36, the relative intensities and the average β values of the branches are given for different temperatures and for different approximations. One can readily see that the r-centroid approximation, which worked fine for H_2, breaks down completely for $v_f=1$ and $v_f=2$. It is to be expected that the r-centroid approximation will fail practically always in the presence of shape resonances.

In Table 10-37, the vibronic cross sections are shown for different rotational temperatures and the different methods of computation. The results obtained with the Franck-Condon approximation and with the



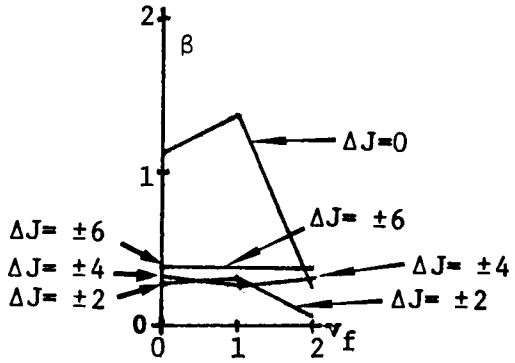


Fig. 10-10. The cross sections of the branches in the $(3\sigma_g)^{-1}$ photoionization of N_2, expressed in % of the vibronic cross sections, and their average β values.

The results shown here were obtained in the RD_{vr} approximation at T_{rot}=300K.

TABLE 10-34

RELATIVE INTENSITIES AND AVERAGE BETA VALUES OF THE BRANCHES IN THE PHOTOIONIZATION OF THE $3\sigma_g$ LEVEL OF N_2 FOR $v_f=0$

Rel. Intensities (% of the Intensity of the Vibronic Band)

	T=4K		T=60K		T=300K			
ΔJ	FR_{vr}	RD_{vr}	FR_{vr}	RD_{vr}	FR_{vr}	RC_{vr}	RD	RD_{vr}
0	31	26	43	38	42	36	38	38
-2	1	1	16	16	22	22	22	22
2	61	58	37	37	31	31	31	31
-4			1	1	1	3	3	3
4	7	15	4	8	3	7	6	6

Average Beta Values of the Branches

	T=4K		T=60K		T=300K			
ΔJ	FR_{vr}	RD_{vr}	FR_{vr}	RD_{vr}	FR_{vr}	RC_{vr}	RD	RD_{vr}
0	1.57	1.50	1.23	1.11	1.24	1.08	1.13	1.13
-2	0.30	0.26	0.30	0.27	0.30	0.27	0.27	0.27
2	0.30	0.26	0.30	0.27	0.30	0.27	0.27	0.26
-4	0.28	0.31	0.28	0.31	0.28	0.31	0.31	0.31
4	0.28	0.31	0.28	0.31	0.28	0.31	0.31	0.31
-6	0.35	0.37	0.35	0.37	0.35		0.37	0.37
6	0.35	0.37	0.35	0.37	0.35		0.37	0.37

TABLE 10-35

RELATIVE INTENSITIES AND AVERAGE BETA VALUES OF THE BRANCHES IN THE PHOTOIONIZATION OF THE $3\sigma_g$ LEVEL OF N_2 FOR $v_f=1$

Rel. Intensities (% of the Intensity of the Vibronic Band)

	T=4K		T=60K		T=300K			
ΔJ	FR_{vr}	RD_{vr}	FR_{vr}	RD_{vr}	FR_{vr}	RC_{vr}	RD	RD_{vr}
0	33	36	44	46	44	66	46	46
-2	1	1	16	14	21	14	20	20
2	60	53	36	33	31	20	28	28
-4				1	1		2	2
4	6	11	3	6	2		4	4

Average Beta Values of the Branches

	T=4K		T=60K		T=300K			
ΔJ	FR_{vr}	RD_{vr}	FR_{vr}	RD_{vr}	FR_{vr}	RC_{vr}	RD	RD_{vr}
0	1.59	1.68	1.26	1.36	1.27	1.73	1.38	1.37
-2	0.26	0.31	0.26	0.30	0.26	0.45	0.31	0.31
2	0.26	0.31	0.26	0.30	0.26	0.45	0.30	0.30
-4	0.28	0.27	0.28	0.27	0.28	0.31	0.27	0.27
4	0.28	0.27	0.28	0.27	0.28	0.32	0.27	0.27
-6	0.35	0.36	0.35	0.37	0.35		0.36	0.37
6	0.35	0.36	0.35	0.36	0.35		0.36	0.36

TABLE 10-36

RELATIVE INTENSITIES AND AVERAGE BETA VALUES OF THE BRANCHES IN THE PHOTOIONIZATION OF THE $3\sigma_g$ LEVEL OF N_2 FOR $v_f=2$

Rel. Intensities (% of the Intensity of the Vibronic Band)

	T=4K		T=60K		T=300K			
ΔJ	FR_{vr}	RD_{vr}	FR_{vr}	RD_{vr}	FR_{vr}	RC_{vr}	RD	RD_{vr}
0	36	7	46	21	46	61	20	20
-2	1		15	15	21	9	20	20
2	59	41	35	33	31	13	28	28
-4				4	1	6	10	11
4	5	52	3	27	2	13	21	21

Average Beta Values of the Branches

	T=4K		T=60K		T=300K			
ΔJ	FR_{vr}	RD_{vr}	FR_{vr}	RD_{vr}	FR_{vr}	RC_{vr}	RD	RD_{vr}
0	1.62	0.35	1.30	0.21	1.31	1.72	0.21	0.21
-2	0.21	-0.09	0.21	0.06	0.21	0.03	0.07	0.07
2	0.21	-0.02	0.21	0.07	0.21	0.03	0.06	0.06
-4	0.27	0.31	0.27	0.31	0.27	0.32	0.31	0.31
4	0.27	0.31	0.27	0.31	0.27	0.32	0.31	0.31
-6		0.37		0.37			0.37	0.37
6		0.37		0.37			0.37	0.37

TABLE 10-37

VIBRONIC INTENSITIES AND BETA VALUES FOR THE PHOTOIONIZATION OF THE $3\sigma_g$ LEVEL OF N_2 AT DIFFERENT ROTATIONAL TEMPERATURES

σ(Mb)

	T=4K			T=60K			T=300K			
v_f	FR_{vr}	RD	RD_{vr}	FR_{vr}	RD	RD_{vr}	FR_{vr}	RC_{vr}	RD	RD_{vr}
0	4.95609	7.26125	7.26256	4.95582	7.26135	7.26742	4.95273	8.61479	7.25830	7.28402
1	0.39111	0.36180	0.36231	0.39123	0.36184	0.36289	0.39162	0.19066	0.36185	0.36536
2	0.02162	0.13064	0.13067	0.02165	0.13065	0.13060	0.02174	0.01171	0.13068	0.13037

β

	T=4K			T=60K			T=300K			
v_f	FR_{vr}	RD	RD_{vr}	FR_{vr}	RD	RD_{vr}	FR_{vr}	RC_{vr}	RD	RD_{vr}
0	0.695	0.595	0.595	0.695	0.595	0.595	0.695	0.565	0.595	0.594
1	0.703	0.792	0.792	0.703	0.792	0.792	0.703	1.293	0.792	0.792
2	0.713	0.173	0.173	0.713	0.173	0.173	0.713	1.110	0.174	0.173

FR, RC, and RD, and the subscript "vr" refer to different methods of computation as described in the text.

RD method differ greatly. The β values computed with the r-centroid method for v_f=1 and v_f=2 are very different from the results obtained with the RD method.

Kreile and Schweig[643] give a β value of 0.66 for the vibronic band with v_f=0. This result is reasonably well reproduced in this work. However, for the vibronic band with v_f=1, Kreile and Schweig measured a β value of 1.55 which is very much higher than the value of 0.79 computed in the present work. Nevertheless, it has to be said that the computations presented here predict correctly that the β value of the vibronic band with v_f=1 is larger than the β value of the vibronic band with v_f=0. Kreile and Schweig compared their results with a massive number of experimental results from the previous literature. Six references reported β values for the vibronic band with v_f=1, ranging from 1.35 to 1.50, i.e., all experimental results cited by Kreile and Schweig showed β values much higher than the present result.

Parr et al.[647] measured the vibronic cross sections and β values of the bands with v_f=2 and v_f=3, but at lower photon energies than 21.2 eV. They could correlate structures observed in the vibronic cross sections and β values to two members of the Hopfield series of N_2. Carlson et al.[521] gave some experimental values for v_f=2, but not in the neighbourhood of 21.2 eV photon energy. Mintz and Kuppermann[648] measured a β value of 1.3 for the vibronic band with v_f=2, but previously a lower value of 0.73 had been reported.[648] Carlson et al.[649] gave, for the intensity ratio I(10°)/I(90°) for the v_f=2 band, a value of approximately 3.3, using unpolarized 21.2 eV radiation. This

would give a β value of 1.86. Mintz and Kuppermann found that there is a great variation of the β values of the v_f=1 and the v_f=2 vibronic band above 20.09 eV energy of the photons. The threshold for the dissociation of N_2 into $N(^4S_o)$ and $N(^4P)$ is 20.09 eV. Mintz and Kuppermann argue that autoionization might be responsible for the observed anomalies, apparently through a transition into a dissociative state whose rate of autoionization exceeds the rate of separation of the dissociation products. However, autoionization processes tend to lower the β values in magnitude in most cases,[650] i.e., autoionization cannot serve as a plausible explanation for the disagreement of the β values computed here with the experimental β values. Williams and Langhoff noted that there are strong effects of configuration mixing in the photoelectron spectra of N_2.[651]

The results reported here demonstrate that the β values of different vibronic bands differ greatly, due to the presence of a shape resonance in the σ-σ channel. The experimental results confirm this prediction, but the quantitative agreement of the computed vibronic β values with the experimental values is poor. It is unlikely that the disagreement is caused by an incorrect position of the shape resonance only. Effects not considered in this work may play important roles in an accurate description of the photoionization processes in N_2.

According to Gardner and Samson,[15] the relative vibronic intensities are 100, 6.9, and 0.3 for v_f=0,1, and 2 respectively. In the RD_{vr} approximation, the relative vibronic cross sections are 100, 5.0, and 1.8 for v_f=0,1, and 2 respectively. Comparisons with results obtained in the Franck-Condon and in the r-centroid approximation

indicate that the effects of nuclear motion are reproduced correctly by the RD approximation as far as vibrational branching ratios are concerned.

The differential photoionization cross sections can be separated into an isotropic component, σ_{tot}, and an anisotropic component, $\beta\sigma_{tot}$. In Figure 10-11 and in Figure 10-12, the band contours of the isotropic and the anisotropic component of the vibronic band with $v_f=v_i=0$ are drawn. At high temperatures, the structure in the vibronic bands is due to different branches. In Figure 10-11 and in Figure 10-12, the contours of the individual branches are shown. The overall contour of the vibronic band is a superposition of the contours of the branches without further scaling. The whole thing, of course, is a superposition of a large number of rovibronic bands. These rovibronic bands were assumed to have Gaussian band contours, with widths given by the conservation of linear momentum, (see (10-37)), where it has been assumed that the translational and the rotational temperature of the sample are identical. Notice that the branches with $\Delta J>0$ have larger cross sections than the branches with identical values of $|\Delta J|$, but with $\Delta J<0$. If B_e doesn't change greatly, the photoionized molecules will always have a higher rotational temperature than the original sample.

In Figure 10-13 and in Figure 10-14, the band contours of the isotropic and anisotropic component of the three vibronic bands with $v_f=0,1,2$ are drawn for different temperatures. The vibronic band with $v_f=2$ shows relatively large contributions from branches with large values of $|\Delta J|$, as can be seen in Table 10-36. This is apparently

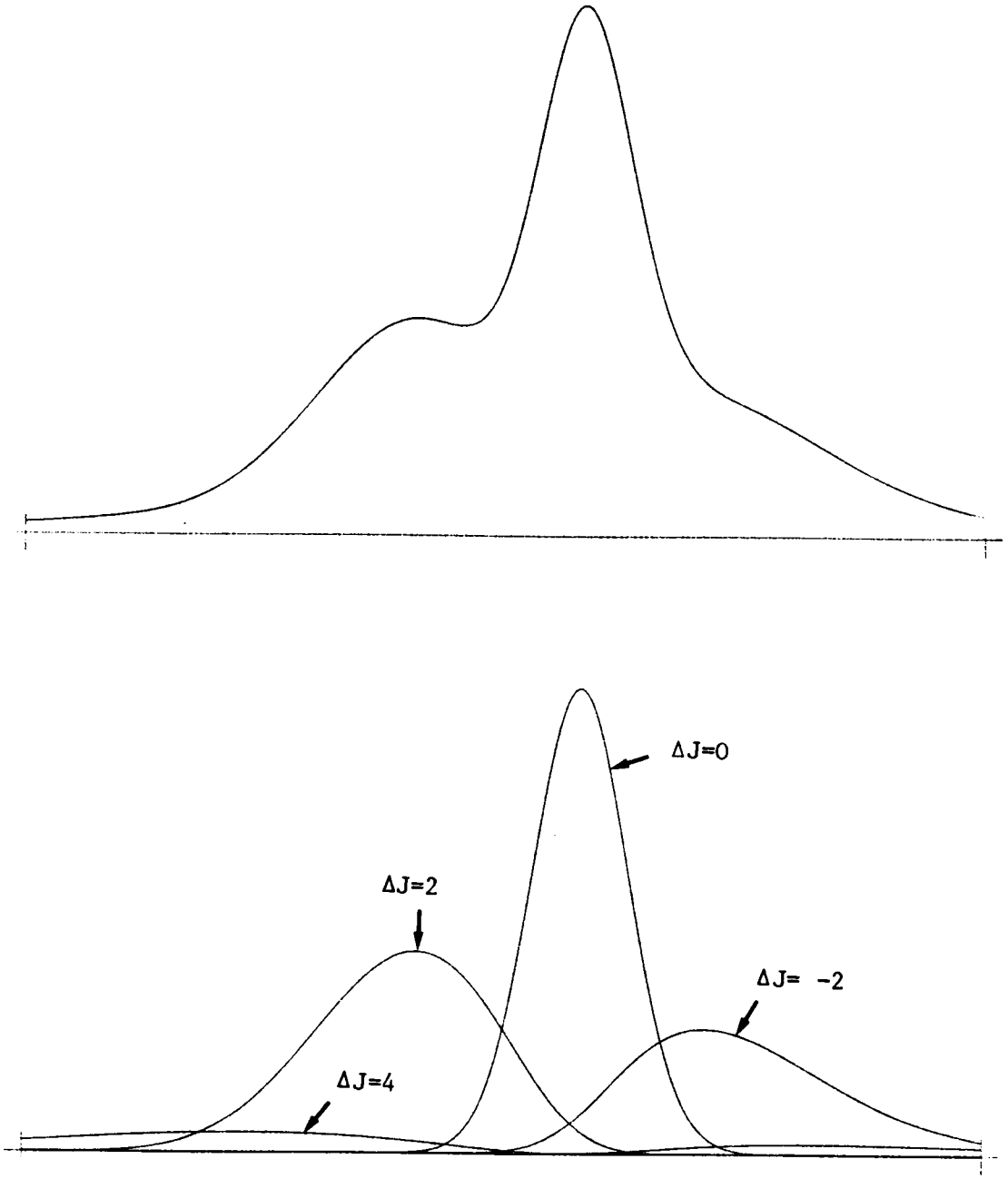


Fig. 10-11. The isotropic component of the vibronic band with $v_f = 0$ and its individual branches in the $(3\sigma_g)^{-1}$ photoionization of N_2 at T = 300K.

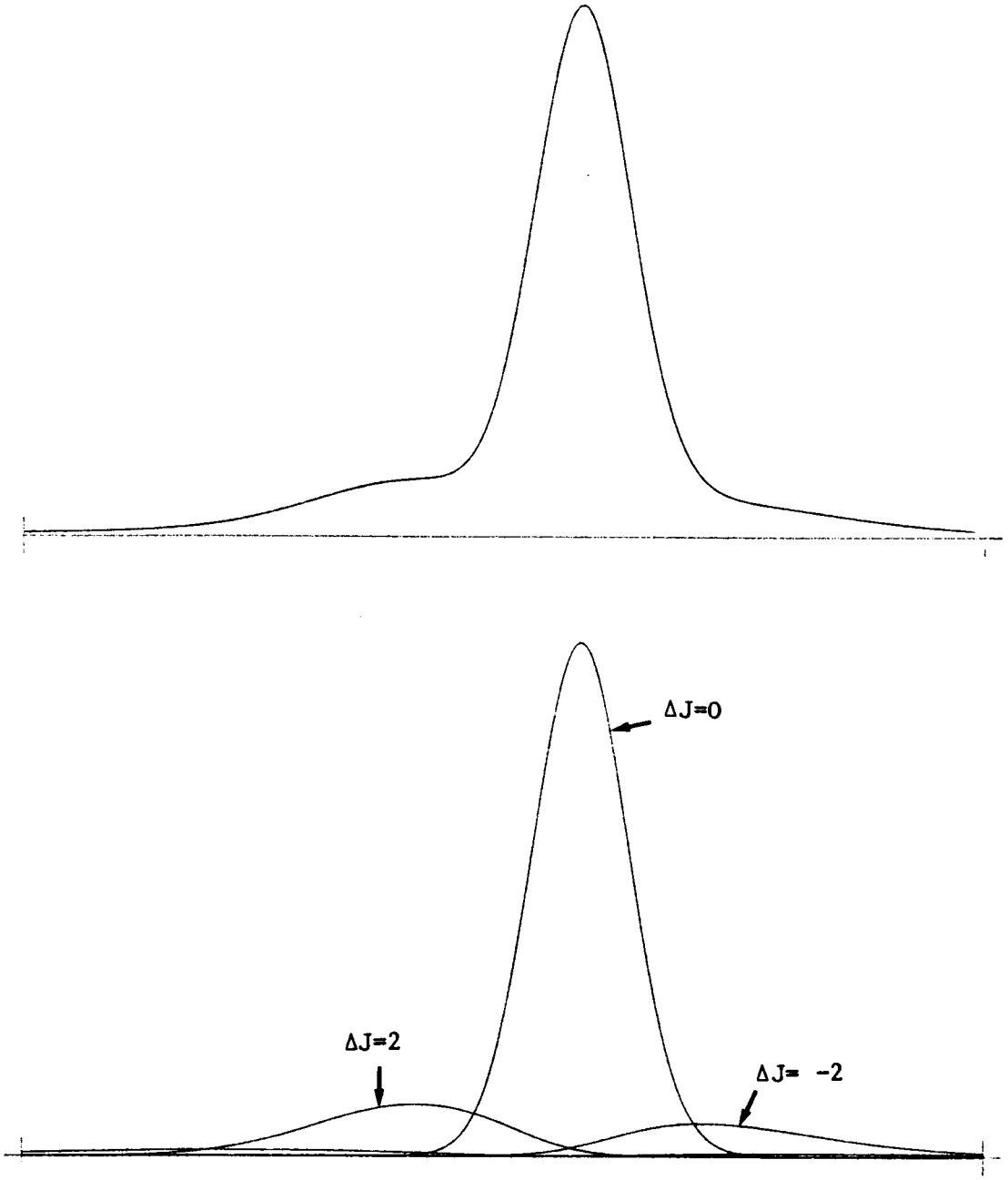


Fig. 10-12. The anisotropic component of the vibronic band with $v_f=0$ and its individual branches in the $(3\sigma_g)^{-1}$ photoionization of N_2 at T = 300K.

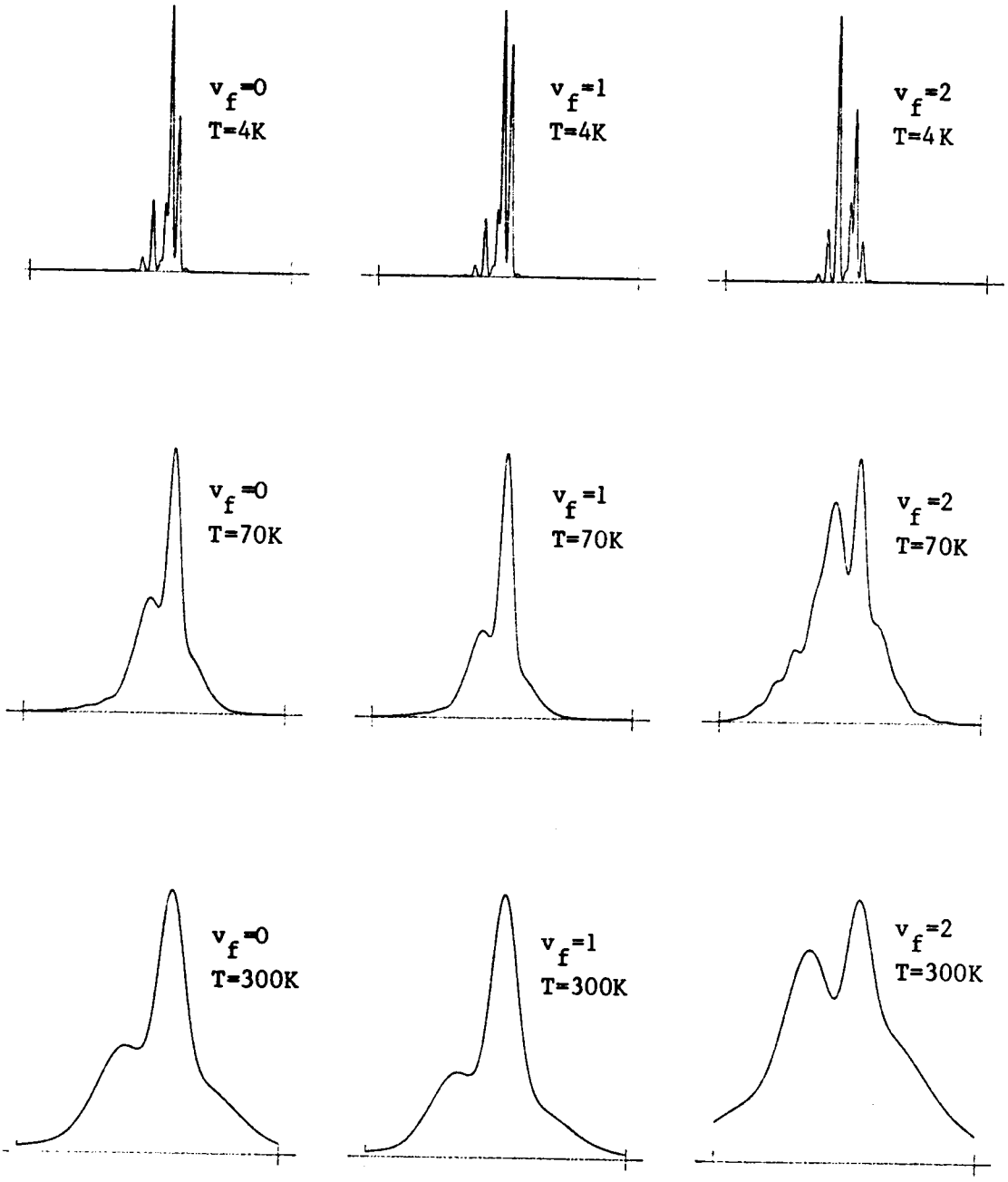


Fig. 10-13. Vibronic band contours in the $(3\sigma_g)^{-1}$ photoionization of N_2 at different temperatures.

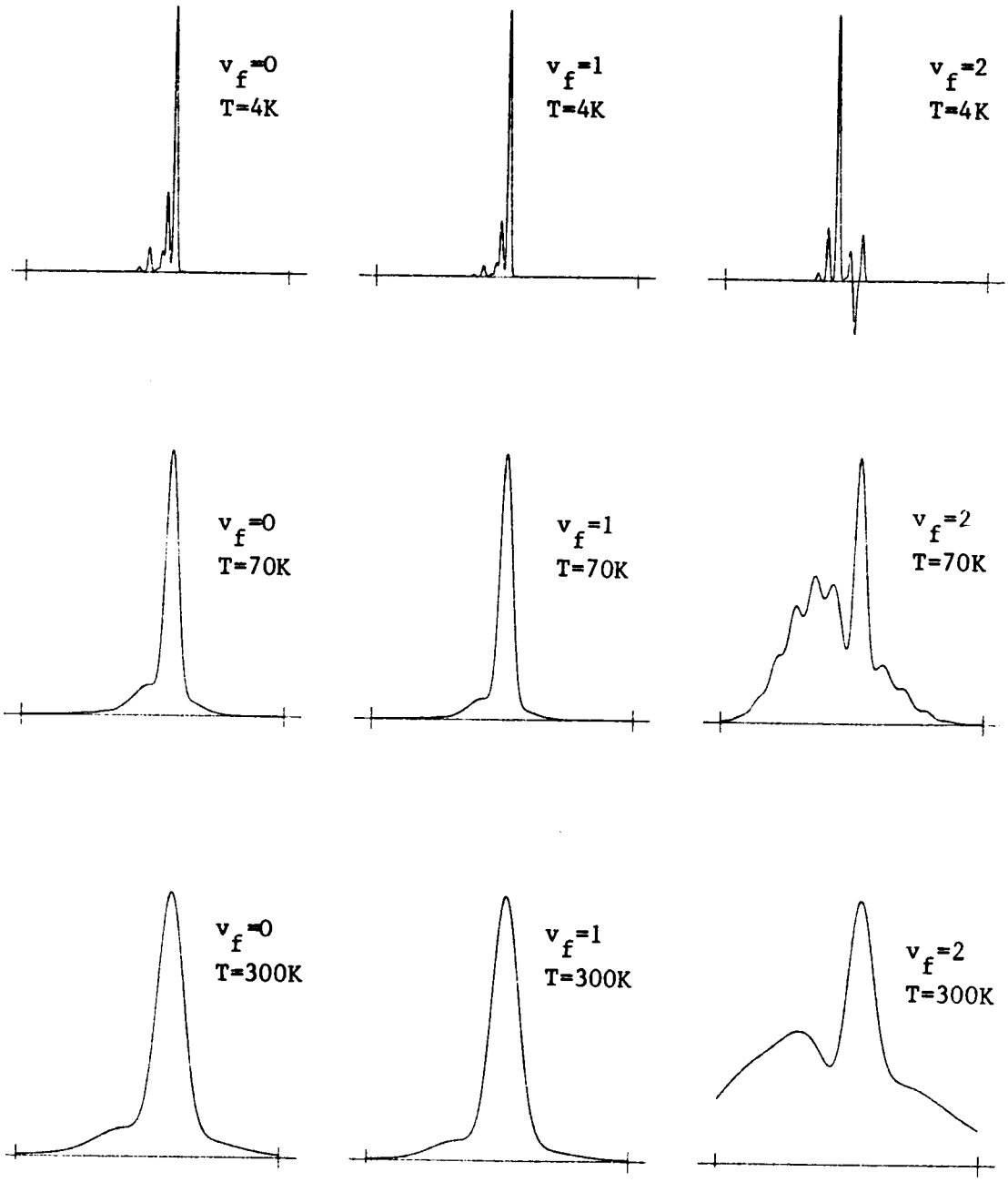


Fig. 10-14. Contours of the anisotropic component of the vibronic bands in the $(3\sigma_g)^{-1}$ photoionization of N_2 at different temperatures.

caused by the shape resonance. The contour of this vibronic band has a rather odd shape.

All graphs of contours cover an energy range of 400 cm^{-1}. The I.U.P.A.C. recommendation that ionization potentials should increase from right to left was followed in all cases.[652] Let the range of the graphs be expressed in terms of the change in energy of nuclear motion, ΔE_{nucl}, (see (10-10)). The lengths of the graphs are then given by:

$$-250\ cm^{-1} \leq \Delta E_{nucl} \leq 150\ cm^{-1} \text{ for } v_f=0$$

$$1900\ cm^{-1} \leq \Delta E_{nucl} \leq 2300\ cm^{-1} \text{ for } v_f=1$$

$$4050\ cm^{-1} \leq \Delta E_{nucl} \leq 4450\ cm^{-1} \text{ for } v_f=2$$

where ΔE_{nucl} decreases from left to right in the graphs.

In Table 10-32, the relative cross sections of the rovibronic transitions are given. In order to obtain the cross sections in megabarns, the relative cross sections in Table 10-32 have to be divided by 3.11 (10^2), 4.21 (10^3), or 2.59 (10^4) if v_f=0,1, or 2 respectively.

The rovibronic cross sections for the photoionization of hydrogen were affected noticeably by vibration-rotation interaction. In the photoelectron spectra of N_2 and CO, vibration-rotation interaction plays only a minor role.

For the graphing of vibronic band contours, results obtained in the RD_{vr} approximation were used throughout.

In Table 10-32 and in Table 10-33, the rovibronic cross sections and β values were computed in the RD_{vr} approximation. This is the method used in all cases where the method of computation is not mentioned explicitly in this text. Specifically, all data used for the preparation of band contours were obtained with the RD_{vr} method.

3. The $1\pi_u$ Photoionization of N_2

There are no resonances apparent in the photoionization of the $1\pi_u$ level of N_2, judging from the cross sections and β values shown in Table 10-38 for different internuclear separations and energies of the photoelectron.

The relative cross sections and the β values of individual rovibronic bands are shown in Table 10-39 and in Table 10-40. The relative cross sections and β values of rotational transitions $J+\Delta J \leftarrow J$, for different vibronic transitions, change gradually with v_f. In order to convert the relative cross sections in Table 10-39 into cross sections expressed in megabarns, the relative cross sections have to be divided by 9.65 (10^2), 3.80 (10^3), and 1.46 (10^5) for v_f=0,4, and 8 respectively. According to Kreile and Schweig, the β values decrease in the vibronic progression. Their β values for the vibronic bands are:

0.39, 0.34, 0.26, 0.26, 0.23, 0.20

for v_f=0,1, ..., 5 respectively. The cross sections and β values computed in this work are shown in Table 10-41 and in Table 10-42. The β values computed here fall off much more slowly than the experimental values. In the RD_{vr} approximations, the β values of the vibronic bands are:

TABLE 10-38

PHOTOIONIZATION CROSS SECTIONS AND BETA VALUES OF N_2

$N_2(X^1\Sigma_g^+) \rightarrow N_2^+(A^2\Pi_{ui}) + e^-$

σ (Mb)

Channel	$r_{NN}(a_o)$	E_e=0.19 Ryd	E_e=0.23 Ryd	E_e=0.27 Ryd	E_e=0.31 Ryd
$1\pi_u \rightarrow k\sigma_g$	1.9	3.79	3.52	3.28	3.05
	2.05	3.54	3.26	3.00	2.77
	2.2	3.22	2.95	2.70	2.48
	2.35	2.93	2.67	2.43	2.23
	2.5	2.68	2.43	2.22	2.03
$1\pi_u \rightarrow k\pi_g$	1.9	0.01	0.01	0.02	0.03
	2.05	0.08	0.10	0.11	0.12
	2.2	0.20	0.22	0.23	0.25
	2.35	0.33	0.35	0.36	0.37
	2.5	0.46	0.47	0.48	0.49
$1\pi_u \rightarrow k\delta_g$	1.9	18.36	17.55	16.62	15.63
	2.05	17.93	17.05	16.07	15.07
	2.2	17.35	16.42	15.43	14.42
	2.35	16.69	15.75	14.74	13.75
	2.5	15.95	15.00	14.03	13.08

β

$r_{NN}(a_o)$	E_e=0.19 Ryd	E_e=0.23 Ryd	E_e=0.27 Ryd	E_e=0.31 Ryd
1.9	0.26	0.34	0.41	0.47
2.05	0.18	0.26	0.33	0.39
2.2	0.14	0.22	0.29	0.35
2.35	0.12	0.20	0.26	0.32
2.5	0.12	0.19	0.26	0.31

TABLE 10-39

SCALED PHOTOIONIZATION CROSS SECTIONS FOR $N_2(X^1\Sigma_g^+) \rightarrow N_2^+(A^2\Pi_{ui}) + e^-$ ($h\nu$=21.2 eV)

v_f	J_i	$\Delta J=-4$	$\Delta J=-3$	$\Delta J=-2$	$\Delta J=-1$	$\Delta J=0$	$\Delta J=1$	$\Delta J=2$	$\Delta J=3$	$\Delta J=4$
0	0						1809	318	338	0
0	1					1000	1086	197	181	0
0	2				334	976	838	172	145	0
0	3			100	357	971	747	161	128	0
0	4		24	108	392	970	698	155	118	0
0	5	0	37	112	416	969	667	151	111	0
0	6	0	44	116	433	968	646	148	107	0
0	12	0	63	124	481	964	590	139	93	0
0	24	0	71	127	502	952	554	133	84	0
4	0						1820	302	369	0
4	1					1000	1101	192	198	0
4	2				335	984	844	169	158	0
4	3			104	354	981	752	159	140	0
4	4		26	111	388	980	702	154	130	0
4	5	0	40	115	412	979	672	150	123	0
4	6	0	48	118	430	979	651	148	118	0
4	12	0	67	124	478	979	598	142	104	0
4	24	0	75	126	503	980	573	140	98	0
8	0						1797	292	395	
8	1					985	1098	189	212	
8	2				334	975	838	168	170	
8	3			109	348	974	746	159	151	
8	4		28	114	381	974	697	154	140	
8	5		42	118	405	974	667	151	133	
8	6		51	120	422	975	646	150	128	
8	12		71	126	471	980	598	146	115	
8	24		79	128	502	1000	587	148	112	

TABLE 10-40

BETA VALUES FOR $N_2(X^1\Sigma_g^+) \rightarrow N_2^+(A^2\Pi_{ui}) + e^-$ ($h\nu$=21.2 eV)

v_f	J_i	ΔJ= -4	ΔJ= -3	ΔJ= -2	ΔJ= -1	ΔJ=0	ΔJ=1	ΔJ=2	ΔJ=3	ΔJ=4
0	0						0.67	-1.00	0.19	-1.00
0	1					0.51	0.53	-0.83	0.19	-0.80
0	2				0.11	0.61	0.51	-0.75	0.19	-0.68
0	3			-0.13	0.23	0.62	0.50	-0.70	0.19	-0.61
0	4		0.19	-0.25	0.29	0.63	0.48	-0.67	0.19	-0.56
0	5	0.22	0.19	-0.32	0.32	0.63	0.47	-0.65	0.19	-0.52
0	6	0.11	0.19	-0.36	0.34	0.63	0.47	-0.63	0.19	-0.50
0	12	-0.12	0.19	-0.45	0.38	0.64	0.45	-0.59	0.19	-0.41
0	24	-0.21	0.19	-0.49	0.40	0.64	0.43	-0.56	0.19	-0.36
4	0						0.60	-1.00	0.25	-1.00
4	1					0.46	0.49	-0.80	0.25	-0.77
4	2				0.10	0.55	0.47	-0.71	0.25	-0.65
4	3			-0.06	0.21	0.57	0.45	-0.66	0.25	-0.57
4	4		0.25	-0.18	0.26	0.57	0.44	-0.62	0.25	-0.52
4	5	0.22	0.25	-0.25	0.29	0.57	0.43	-0.60	0.25	-0.48
4	6	0.12	0.25	-0.29	0.30	0.58	0.42	-0.58	0.25	-0.45
4	12	-0.08	0.25	-0.38	0.34	0.58	0.40	-0.53	0.25	-0.37
4	24	-0.17	0.25	-0.42	0.36	0.58	0.39	-0.50	0.25	-0.31
8	0						0.55	-1.00	0.25	
8	1					0.41	0.44	-0.78	0.25	
8	2				0.08	0.50	0.42	-0.68	0.25	
8	3			-0.03	0.17	0.51	0.40	-0.63	0.25	
8	4		0.25	-0.15	0.22	0.52	0.39	-0.59	0.25	
8	5		0.25	-0.21	0.24	0.52	0.38	-0.57	0.25	
8	6		0.25	-0.25	0.26	0.52	0.37	-0.55	0.25	
8	12		0.25	-0.35	0.30	0.52	0.35	-0.50	0.25	
8	24		0.25	-0.39	0.32	0.53	0.34	-0.47	0.25	

0.39, 0.38, 0.37, 0.37, 0.36, 0.35

for v_f=0,1, ..., 5 respectively. It turns out that the Franck-Condon approximation would give vibronic β values in better agreement with experiment than the RD approximation. Since there seem to be no effects from a resonance, one would expect the r-centroid approximation to give results in close agreement with the results obained from the RD method. According to Table 10-41 and Table 10-42, this is the case.

According to Gardner and Samson,[15] the relative vibronic cross sections are:

87.1, 100, 76.3, 43.5, 19.1, 7.1, 2.5, 1.7, 0.4

for v_f=0,1, ..., 8 respectively. In the RD_{vr} approximation, the relative vibronic cross sections were computed to be:

77.9, 100, 73.8, 41.6, 20.1, 8.8, 3.6, 1.4, 0.5

for v_f=0,1, ..., 8 respectively. The transition with v_f=0 gave a relative cross section which is roughly 10 percent lower than the experimental value. However, for v_f>0, the effects of nuclear motion on the vibrational branching ratios are reproduced quite well.

In the photoionization of σ orbitals, rovibronic transitions with the same v_f and the same $|\Delta J|$ have usually almost the same β values, unless ΔJ=0. This is not the case in the photoionization of π orbitals, in most cases. However, in the $1\pi_u$ photoionization, according to Table 10-40, the members of the branches with $|\Delta J|$=3 have almost identical β values. The rovibronic transitions with J_i=0, and with ΔJ a positive, even number seem to have β values of exactly 1.0, regardless of the energy of the photoelectron. Notice that, in the present notation, $J \geq \Lambda$. This means that $J_f \geq 1$ in the photoionization of a π orbital from a Σ ground state.

TABLE 10-41

VIBRONIC INTENSITIES FOR THE PHOTOIONIZATION OF THE $1\pi_u$ LEVEL OF N_2 AT DIFFERENT ROTATIONAL TEMPERATURES

	σ(Mb)									
	T=4K			T=60K			T=300K			
v_f	FR_{vr}	RD	RD_{vr}	FR_{vr}	RD	RD_{vr}	FR_{vr}	RC_{vr}	RD	RD_{vr}
0	5.63051	5.10994	5.10681	5.62795	5.10921	5.10399	5.61395	5.04325	5.10349	5.08926
1	6.95825	6.54846	6.54980	6.95581	6.54741	6.54661	6.94354	6.48716	6.53978	6.53140
2	4.90071	4.82759	4.83093	4.89983	4.82678	4.82915	4.89527	4.84214	4.82093	4.82090
3	2.60703	2.72042	2.72284	2.60718	2.71994	2.72231	2.60714	2.77086	2.71650	2.71946
4	1.17209	1.31100	1.31214	1.17250	1.31075	1.31216	1.17363	1.35105	1.30907	1.31177
5	0.47272	0.57203	0.57242	0.47304	0.57191	0.57258	0.47398	0.59109	0.57118	0.57290
6	0.17736	0.23336	0.23342	0.17754	0.23331	0.23357	0.17809	0.23889	0.23300	0.23392
7	0.06341	0.09070	0.09070	0.06351	0.09068	0.09077	0.06378	0.09085	0.09057	0.09102
8	0.02197	0.03399	0.03397	0.02201	0.03398	0.03401	0.02213	0.03296	0.03393	0.03414

FR, RC, and RD, and the subscript "vr" refer to different methods of computation as described in the text.

TABLE 10-42

AVERAGE BETA VALUES FOR THE PHOTOIONIZATION OF THE $1\pi_u$ LEVEL OF N_2 FOR DIFFERENT VIBRONIC BANDS AND AT DIFFERENT ROTATIONAL TEMPERATURES

	σ(Mb)									
	T=4K			T=60K			T=300K			
v_f	FR_{vr}	RD	RD_{vr}	FR_{vr}	RD	RD_{vr}	FR_{vr}	RC_{vr}	RD	RD_{vr}
0	0.410	0.389	0.389	0.410	0.389	0.389	0.411	0.386	0.389	0.389
1	0.389	0.380	0.380	0.389	0.380	0.380	0.389	0.379	0.380	0.380
2	0.366	0.372	0.372	0.366	0.372	0.372	0.366	0.374	0.373	0.372
3	0.341	0.365	0.365	0.341	0.365	0.365	0.341	0.368	0.365	0.365
4	0.314	0.357	0.357	0.314	0.357	0.357	0.315	0.363	0.358	0.357
5	0.287	0.349	0.349	0.287	0.349	0.349	0.287	0.357	0.350	0.349
6	0.258	0.340	0.340	0.258	0.340	0.340	0.258	0.351	0.341	0.340
7	0.228	0.330	0.329	0.228	0.330	0.329	0.228	0.343	0.330	0.329
8	0.197	0.318	0.317	0.197	0.318	0.318	0.198	0.335	0.318	0.318

FR, RC, and RD, and the subscript "vr" refer to different methods of computation as described in the text.

In Tables 10-43, 10-44, and 10-45, the relative intensities and the average β values of the branches of three vibronic bands with v_f=0, v_f=4, and v_f=8 are given. In Figure 10-15, the relative cross sections and the average β values of the branches, obtained in the RD_{vr} approximation at T=300K, are graphed. One would expect the contours of the vibronic bands to change only slightly with v_f. In the photoionization of π orbitals, the rovibronic bands are split by spin-orbit interaction. This splitting, which is observable in the band contours shown in Figures 10-16, 10-17, 10-18, and 10-19, was introduced as described at the beginning of this chapter. (See (10-7)).

In the photoionization of a σ orbital of a homonuclear diatomic molecule, the selection rule ΔJ=even or ΔJ=odd applies for σ_g and σ_u orbitals respectively. In the photoionization of π orbitals from homonuclear diatomic molecules, all possible rovibronic transitions are allowed.

In Figures 10-16, 10-17, 10-18, and 10-19, the ranges of the graphs expressed in terms of ΔE_{nucl} are:

$$-450 \text{ cm}^{-1} \leq \Delta E_{nucl} \leq -50 \text{ cm}^{-1} \text{ for } v_f=0$$

$$6850 \text{ cm}^{-1} \leq \Delta E_{nucl} \leq 7250 \text{ cm}^{-1} \text{ for } v_f=4$$

$$13700 \text{ cm}^{-1} \leq \Delta E_{nucl} \leq 14100 \text{ cm}^{-1} \text{ for } v_f=8$$

where ΔE_{nucl} decreases from left to right in the graphs.

4. The $2\sigma_u$ Photoionization of N_2

Marr et al.[526,653] measured β values for the $2\sigma_u$ photoionization of N_2 which were near 1.0 for photon energies in the range of 20-40

TABLE 10-43

RELATIVE INTENSITIES AND AVERAGE BETA VALUES OF THE BRANCHES IN THE PHOTOIONIZATION OF THE $1\pi_u$ LEVEL OF N_2 FOR $v_f=0$

Rel. Intensities (% of the Intensity of the Vibronic Band)

	T=4K		T=60K		T=300K			
ΔJ	FR_{vr}	RD_{vr}	FR_{vr}	RD_{vr}	FR_{vr}	RC_{vr}	RD	RD_{vr}
0	12	12	37	37	39	39	39	39
-1	1	1	13	13	17	18	17	18
1	64	64	33	33	27	27	27	27
-2			3	3	4	4	4	4
2	11	11	7	7	6	6	6	6
-3			1	1	2	2	2	2
3	12	12	6	6	5	4	4	4

Average Beta Values of the Branches

	T=4K		T=60K		T=300K			
ΔJ	FR_{vr}	RD_{vr}	FR_{vr}	RD_{vr}	FR_{vr}	RC_{vr}	RD	RD_{vr}
0	0.55	0.53	0.64	0.61	0.65	0.63	0.63	0.63
-1	0.13	0.11	0.28	0.26	0.37	0.34	0.35	0.35
1	0.66	0.64	0.54	0.52	0.50	0.47	0.47	0.47
-2	-0.11	-0.13	-0.26	-0.28	-0.37	-0.39	-0.39	-0.39
2	-0.96	-0.96	-0.72	-0.74	-0.62	-0.64	-0.64	-0.64
-3	0.21	0.19	0.21	0.19	0.21	0.19	0.19	0.19
3	0.21	0.19	0.21	0.19	0.21	0.19	0.19	0.19
-4	0.23	0.22	0.12	0.11	-0.02	-0.04	-0.04	-0.04
4	-0.95	-0.95	-0.64	-0.65	-0.48	-0.50	-0.50	-0.50
-5	0.42	0.42	0.42	0.42	0.42	0.42	0.42	0.42
5	0.42	0.42	0.42	0.42	0.42	0.42	0.42	0.42

TABLE 10-44

RELATIVE INTENSITIES AND AVERAGE BETA VALUES OF THE BRANCHES IN THE PHOTOIONIZATION OF THE $1\pi_u$ LEVEL OF N_2 FOR $v_f=4$

Rel. Intensities (% of the Intensity of the Vibronic Band)

	T=4K		T=60K		T=300K			
ΔJ	FR_{vr}	RD_{vr}	FR_{vr}	RD_{vr}	FR_{vr}	RC_{vr}	RD	RD_{vr}
0	12	12	37	37	39	39	39	39
-1	1	1	13	13	17	17	17	17
1	64	64	34	33	27	27	27	27
-2			3	3	4	4	4	4
2	11	11	7	7	6	6	6	6
-3			1	1	2	2	2	2
3	12	13	6	6	5	5	5	5

Average Beta Values of the Branches

	T=4K		T=60K		T=300K			
ΔJ	FR_{vr}	RD_{vr}	FR_{vr}	RD_{vr}	FR_{vr}	RC_{vr}	RD	RD_{vr}
0	0.43	0.47	0.51	0.56	0.53	0.58	0.57	0.57
-1	0.06	0.11	0.18	0.23	0.26	0.32	0.31	0.31
1	0.54	0.58	0.43	0.47	0.38	0.43	0.43	0.43
-2	-0.11	-0.06	-0.26	-0.21	-0.37	-0.32	-0.32	-0.32
2	-0.96	-0.96	-0.73	-0.70	-0.63	-0.59	-0.59	-0.59
-3	0.22	0.25	0.22	0.25	0.22	0.24	0.25	0.25
3	0.22	0.25	0.22	0.25	0.22	0.24	0.25	0.25
-4	0.20	0.22	0.09	0.12	-0.05	-0.02	-0.01	-0.01
4	-0.96	-0.95	-0.66	-0.61	-0.51	-0.47	-0.46	-0.46
-5	0.41	0.39	0.41	0.39	0.41	0.40	0.39	0.39
5	0.41	0.39	0.41	0.39	0.41	0.40	0.39	0.39

TABLE 10-45

RELATIVE INTENSITIES AND AVERAGE BETA VALUES OF THE BRANCHES IN THE PHOTOIONIZATION OF THE $1\pi_u$ LEVEL OF N_2 FOR v_f=8

Rel. Intensities (% of the Intensity of the Vibronic Band)

	T=4K		T=60K		T=300K			
ΔJ	FR_{vr}	RD_{vr}	FR_{vr}	RD_{vr}	FR_{vr}	RC_{vr}	RD	RD_{vr}
0	12	12	37	37	39	39	39	39
-1	1	1	13	13	17	17	17	17
1	64	63	34	33	27	27	26	27
-2			3	3	4	4	5	4
2	11	10	7	7	6	6	6	6
-3			1	1	2	2	2	2
3	12	14	6	7	4	5	5	5

Average Beta Values of the Branches

	T=4K		T=60K		T=300K			
ΔJ	FR_{vr}	RD_{vr}	FR_{vr}	RD_{vr}	FR_{vr}	RC_{vr}	RD	RD_{vr}
0	0.28	0.42	0.36	0.50	0.38	0.54	0.52	0.52
-1	-0.03	0.08	0.07	0.19	0.13	0.29	0.27	0.27
1	0.38	0.52	0.28	0.42	0.24	0.40	0.38	0.38
-2	-0.11	-0.04	-0.27	-0.18	-0.38	-0.28	-0.29	-0.29
2	-0.96	-0.95	-0.73	-0.67	-0.63	-0.55	-0.56	-0.56
-3	0.23	0.25	0.23	0.25	0.23	0.26	0.25	0.25
3	0.23	0.25	0.23	0.25	0.23	0.26	0.25	0.25
-4						-0.03		
4						-0.48		
-5						0.41		
5		0.42		0.42		0.41		0.42

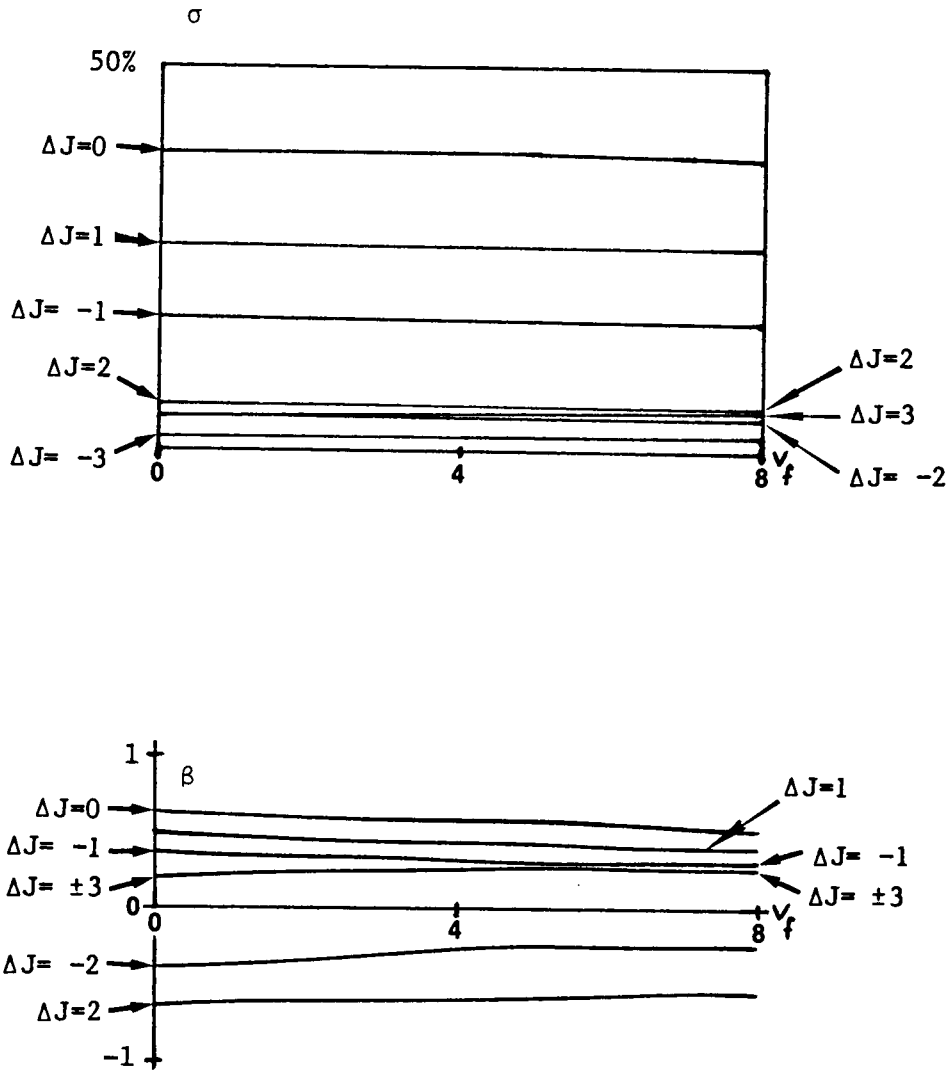


Fig. 10-15. The cross sections of the branches in the $(1\pi_u)^{-1}$ photoionization of N_2, expressed in % of the vibronic cross sections, and their average β values.

The results shown here were obtained in the RD_{vr} approximation at T_{rot} = 300K.

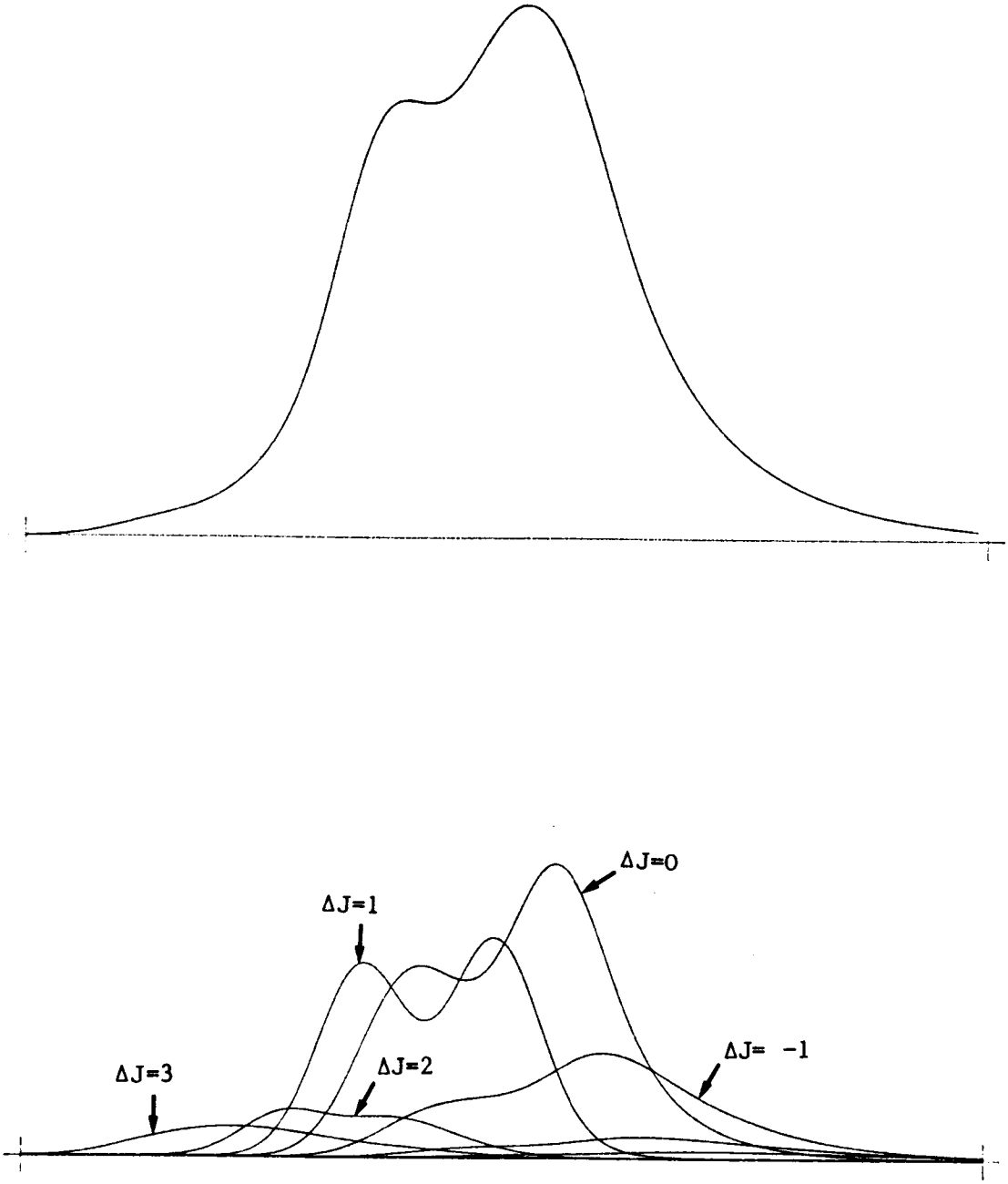


Fig. 10-16. The isotropic component of the vibronic band with $v_f = 0$ and its individual branches in the $(1\pi_u)^{-1}$ photoionization of N_2 at T = 300K.

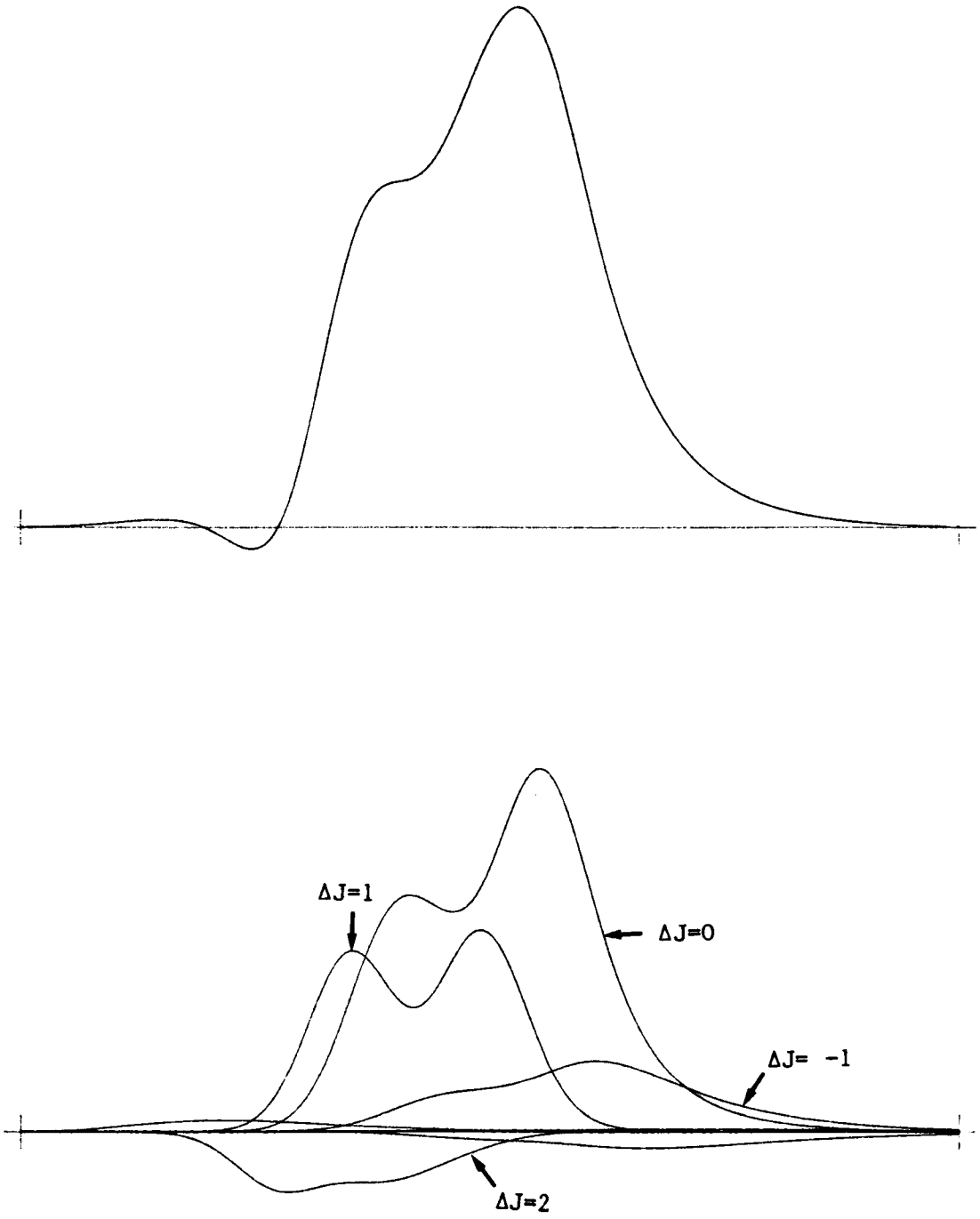


Fig. 10-17. The anisotropic component of the vibronic band with $v_f = 0$ and its individual branches in the $(1\pi_u)^{-1}$ photoionization of N_2 at T = 300K.

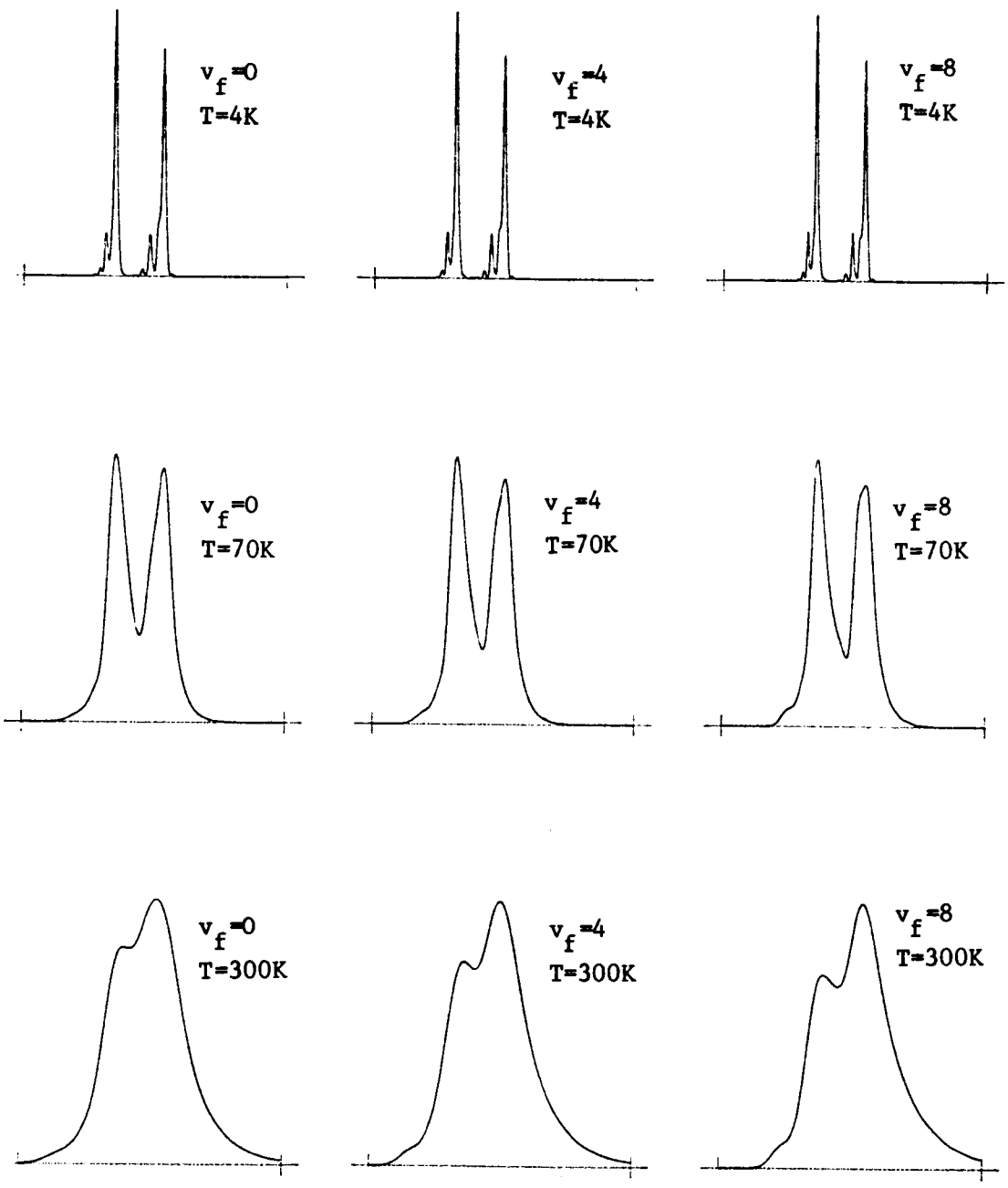


Fig. 10-18. Vibronic band contours in the $(1\pi_u)^{-1}$ photoionization of N_2 at different temperatures.

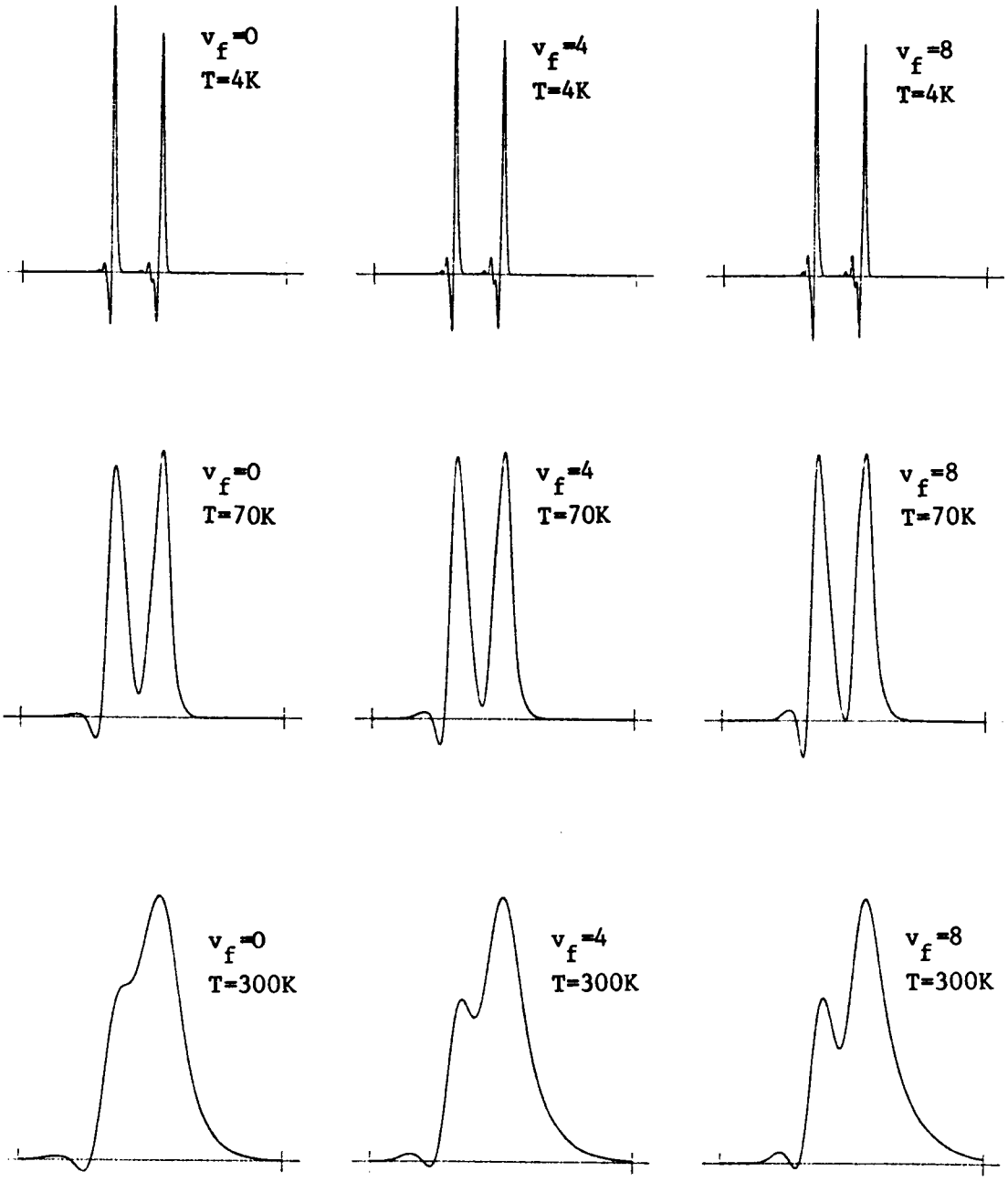


Fig. 10-19 Contours of the anisotropic component of three vibronic bands in the $(1\pi_u)^{-1}$ photoionization of N_2 at different temperatures.

eV. The β values computed with the Xα method are substantially higher than the experimental values.[523]

The selection rule for the rovibronic transitions is ΔJ=odd. The cross sections for the σ-σ channel depend strongly on the internuclear separation, according to Table 10-46, but there is no evidence of a shape resonance. (See also Figure 10-2).

The vibronic bands consist mostly of a P and an R branch. The relative rovibronic cross sections and β values for v_f=0,1, and 2 are shown in Table 10-47 and in Table 10-48. In order to obtain the rovibronic cross sections, expressed in megabarns, the relative rovibronic cross sections, in Table 10-47, have to be divided by 5.25 (10^2), 4.01 (10^3), and 2.27 (10^5) for members of the vibronic bands with v_f=0,1, and 2 respectively.

The Franck-Condon and the r-centroid approximation, and the RD method give vibrational branching ratios and vibronic β values which are in close agreement. (See Table 10-49). Gardner and Samson[15] did not measure the relative cross sections with 58.4 nm photons. The vibronic β value for v_f=0, according to Kreile and Schweig,[643] is 1.16, and β=1.15 for the vibronic band with v_f=1.

The vibronic β values shown in Table 10-49 are considerably higher than the experimental values.

The branches with $|\Delta J|>1$ have much lower β values than the P and R branches. The P and R branches have combined cross sections which represent 94-99 percent of the intensities of the respective vibronic bands. If the contribution of the P and R branches to the vibronic cross sections were reduced by some scheme, such as configuration

TABLE 10-46

PHOTOIONIZATION CROSS SECTIONS AND BETA VALUES OF N_2

$N_2(X^1\Sigma_g^+) \rightarrow N_2^+(B^2\Sigma_u^+) + e^-$

σ (Mb)

Channel	$r_{NN}(a_o)$	E_e=0.14 Ryd	E_e=0.16 Ryd	E_e=0.18 Ryd	E_e=0.20 Ryd
$2\sigma_u \rightarrow k\sigma_g$	1.9	2.20	2.19	2.17	2.15
	2.05	1.76	1.75	1.74	1.72
	2.2	1.39	1.39	1.38	1.37
	2.35	1.11	1.11	1.10	1.10
	2.5	0.89	0.89	0.89	0.89
$2\sigma_u \rightarrow k\pi_g$	1.9	0.62	0.65	0.68	0.71
	2.05	0.69	0.71	0.74	0.77
	2.2	0.71	0.74	0.77	0.79
	2.35	0.72	0.75	0.77	0.80
	2.5	0.71	0.74	0.76	0.79

β

$r_{NN}(a_o)$	E_e=0.14 Ryd	E_e=0.16 Ryd	E_e=0.18 Ryd	E_e=0.20 Ryd
1.9	1.73	1.75	1.76	1.77
2.05	1.77	1.79	1.80	1.82
2.2	1.79	1.81	1.83	1.84
2.35	1.81	1.82	1.84	1.85
2.5	1.81	1.83	1.84	1.86

TABLE 10-47

SCALED PHOTOIONIZATION CROSS SECTIONS FOR

$N_2(X^1\Sigma_g^+) \rightarrow N_2^+(B^2\Sigma_u^+) + e^-$ (hν=21.2 eV)

v_f	J_i	ΔJ= -5	ΔJ= -3	ΔJ= -1	ΔJ=1	ΔJ=3	ΔJ=5
0	0				1000	77	0
0	1			333	700	44	0
0	2			420	621	37	0
0	3		11	443	590	34	0
0	4		15	458	573	32	0
0	5	0	17	468	562	30	0
0	6	0	18	475	555	30	0
0	12	0	21	493	536	27	0
0	24	0	22	503	527	26	0
1	0				1000	48	0
1	1			334	687	27	0
1	2			413	612	23	0
1	3		7	439	582	21	0
1	4		9	454	565	20	0
1	5	0	11	464	554	19	0
1	6	0	11	471	546	18	0
1	12	0	13	491	525	16	0
1	24	0	14	500	509	15	0
2					1000	20	
2	1			335	674	11	
2	2			407	603	9	
2	3		3	436	573	8	
2	4		4	452	556	8	
2	5		4	463	544	7	
2	6		5	470	536	7	
2	12		6	490	507	6	
2	24		6	492	467	5	

TABLE 10-48

BETA VALUES FOR $N_2(X^1\Sigma_g^+) \rightarrow N_2^+(B^2\Sigma_u^+) + e^-$ ($h\nu$=21.2 eV)

v_f	J_i	$\Delta J = -5$	$\Delta J = -3$	$\Delta J = -1$	$\Delta J = 1$	$\Delta J = 3$	$\Delta J = 5$
0	0				1.92	0.40	0.33
0	1			1.92	1.84	0.40	0.33
0	2			1.84	1.87	0.40	0.33
0	3		0.40	1.87	1.87	0.40	0.33
0	4		0.40	1.87	1.87	0.40	0.33
0	5	0.33	0.40	1.87	1.87	0.40	0.33
0	6	0.33	0.40	1.87	1.87	0.40	0.33
0	12	0.33	0.40	1.87	1.87	0.40	0.33
0	24	0.33	0.41	1.87	1.87	0.40	0.34
1	0				1.88	0.49	0.34
1	1			1.88	1.84	0.49	0.34
1	2			1.84	1.85	0.49	0.34
1	3		0.49	1.85	1.85	0.49	0.34
1	4		0.49	1.85	1.85	0.49	0.34
1	5	0.34	0.49	1.85	1.85	0.49	0.34
1	6	0.34	0.49	1.85	1.85	0.49	0.34
1	12	0.34	0.49	1.85	1.85	0.49	0.35
1	24	0.34	0.49	1.85	1.85	0.49	0.35
2	0				1.80	0.74	
2	1			1.80	1.78	0.74	
2	2			1.78	1.79	0.74	
2	3		0.74	1.79	1.79	0.74	
2	4		0.74	1.79	1.79	0.74	
2	5		0.74	1.79	1.79	0.74	
2	6		0.74	1.79	1.79	0.74	
2	12		0.74	1.79	1.79	0.74	
2	24		0.74	1.79	1.78	0.73	

TABLE 10-49

VIBRONIC INTENSITIES AND BETA VALUES FOR THE PHOTOIONIZATION OF THE $2\sigma_u$ LEVEL OF N_2 AT DIFFERENT ROTATIONAL TEMPERATURES

σ(Mb)

	T=4K			T=60K			T=300K			
v_f	FR_{vr}	RD	RD_{vr}	FR_{vr}	RD	RD_{vr}	FR_{vr}	RC_{vr}	RD	RD_{vr}
0	2.05260	2.05303	2.05364	2.05263	2.05305	2.05362	2.05194	2.05916	2.05224	2.05286
1	0.26262	0.26121	0.26119	0.26256	0.26122	0.26109	0.26211	0.25579	0.26111	0.26061
2	0.00480	0.00452	0.00448	0.00480	0.00451	0.00448	0.00477	0.00423	0.00451	0.00445

β

	T=4K			T=60K			T=300K			
v_f	FR_{vr}	RD	RD_{vr}	FR_{vr}	RD	RD_{vr}	FR_{vr}	RC_{vr}	RD	RD_{vr}
0	1.810	1.807	1.807	1.810	1.807	1.807	1.810	1.807	1.807	1.807
1	1.795	1.814	1.814	1.796	1.814	1.814	1.795	1.816	1.814	1.814
2	1.778	1.774	1.776	1.777	1.776	1.775	1.778	1.810	1.776	1.775

FR, RC, and RD, and the subscript "vr" refer to different methods of computation as described in the text.

mixing, to roughly 80 percent, the computed β vlues would be in agreement with experiment. The contributions of the branches to the vibronic cross sections and the average β values of the branches of the vibronic bands with v_f=0,1, and 2 are shown in Tables 10-50, 10-51, and 10-52. Results obtained in the RD_{vr} approximation are also graphed in Figure 10-20.

In Figures 10-21, 10-22, 10-23, and 10-24, the contours are shown for the vibronic bands with v_f=0,1, and 2 at different temperatures. The contours do not show drastic differences among vibronic bands with v_f=0,1, and 2.

The ranges of the graphs, expressed in terms of the change of energy of nuclear motion, ΔE_{nucl}, are given by:

$$-200 \text{ cm}^{-1} \leq \Delta E_{nucl} \leq 200 \text{ cm}^{-1} \text{ for } v_f=0$$

$$2200 \text{ cm}^{-1} \leq \Delta E_{nucl} \leq 2600 \text{ cm}^{-1} \text{ for } v_f=1$$

$$4550 \text{ cm}^{-1} \leq \Delta E_{nucl} \leq 4950 \text{ cm}^{-1} \text{ for } v_f=2$$

As usual, the length of the graphs is 400 cm^{-1}, and ΔE_{nucl} decreases from left to right.

In the photoionization of the $2\sigma_u$ level of N_2, only the branches with odd values of ΔJ are allowed if symmetry breaking is ignored. Hurley[707] has determined that the "critical" internuclear separation of H_2^+, at which a broken-symmetry solution becomes energetically favourable, is roughly 3.6 a_o. This internuclear separation is too far removed from the Franck-Condon region to activate measurably "forbidden" rotational branches in the photoionization of H_2.

TABLE 10-50

RELATIVE INTENSITIES AND AVERAGE BETA VALUES OF THE BRANCHES IN THE PHOTOIONIZATION OF THE $2\sigma_u$ LEVEL OF N_2 FOR $v_f=0$

Rel. Intensities (% of the Intensity of the Vibronic Band)

	T=4K		T=60K		T=300K			
ΔJ	FR_{vr}	RD_{vr}	FR_{vr}	RD_{vr}	FR_{vr}	RC_{vr}	RD	RD_{vr}
1	10	10	38	38	44	44	44	44
1	84	84	58	57	52	52	52	52
-3			1	1	2	2	2	2
3	6	6	3	3	3	3	3	3

Average Beta Values of the Branches

	T=4K		T=60K		T=300K			
ΔJ	FR_{vr}	RD_{vr}	FR_{vr}	RD_{vr}	FR_{vr}	RC_{vr}	RD	RD_{vr}
1	1.90	1.90	1.87	1.87	1.87	1.87	1.87	1.87
1	1.90	1.90	1.87	1.87	1.87	1.87	1.87	1.87
-3	0.41	0.40	0.41	0.40	0.41	0.40	0.40	0.40
3	0.41	0.40	0.41	0.40	0.41	0.40	0.40	0.40
-5	0.33	0.33	0.33	0.33	0.33	0.33	0.33	0.33
5	0.33	0.33	0.33	0.33	0.33	0.33	0.33	0.33

TABLE 10-51

RELATIVE INTENSITIES AND AVERAGE BETA VALUES OF THE BRANCHES IN THE PHOTOIONIZATION OF THE $2\sigma_u$ LEVEL OF N_2 FOR $v_f=1$

Rel. Intensities (% of the Intensity of the Vibronic Band)

	T=4K		T=60K		T=300K			
ΔJ	FR_{vr}	RD_{vr}	FR_{vr}	RD_{vr}	FR_{vr}	RC_{vr}	RD	RD_{vr}
-1	10	10	38	39	44	45	44	45
1	84	86	57	58	52	53	53	53
-3			1	1	2	1	1	1
3	6	4	3	2	3	2	2	2

Average Beta Values of the Branches

	T=4K		T=60K		T=300K			
ΔJ	FR_{vr}	RD_{vr}	FR_{vr}	RD_{vr}	FR_{vr}	RC_{vr}	RD	RD_{vr}
-1	1.89	1.87	1.85	1.85	1.86	1.85	1.85	1.85
1	1.89	1.87	1.86	1.85	1.86	1.85	1.85	1.85
-3	0.40	0.49	0.40	0.49	0.40	0.49	0.49	0.49
3	0.40	0.49	0.40	0.49	0.40	0.49	0.49	0.49
-5	0.34	0.34	0.34	0.34	0.34	0.34	0.34	0.34
5	0.34	0.34	0.34	0.34	0.34	0.34	0.34	0.34

TABLE 10-52

RELATIVE INTENSITIES AND AVERAGE BETA VALUES OF THE BRANCHES IN THE PHOTOIONIZATION OF THE $2\sigma_u$ LEVEL OF N_2 FOR $v_f=2$

Rel. Intensities (% of the Intensity of the Vibronic Band)

	T=4K		T=60K		T=300K			
ΔJ	FR_{vr}	RD_{vr}	FR_{vr}	RD_{vr}	FR_{vr}	RC_{vr}	RD	RD_{vr}
-1	10	10	39	40	44	46	45	46
1	84	88	57	59	51	53	54	53
-3			1		2			
3	6	2	3	1	3	1	1	1

Average Beta Values of the Branches

	T=4K		T=60K		T=300K			
ΔJ	FR_{vr}	RD_{vr}	FR_{vr}	RD_{vr}	FR_{vr}	RC_{vr}	RD	RD_{vr}
-1	1.87	1.79	1.84	1.79	1.84	1.82	1.79	1.79
1	1.87	1.79	1.84	1.79	1.84	1.82	1.79	1.79
-3	0.39	0.74	0.39	0.74	0.39	0.76	0.74	0.74
3	0.39	0.74	0.39	0.74	0.39	0.76	0.73	0.74
-5						0.41		
5						0.41		

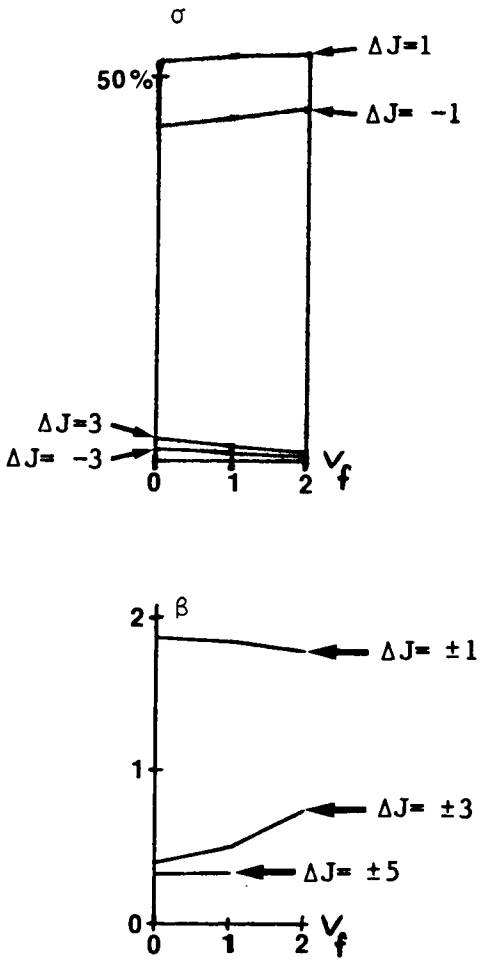


Fig. 10-20. The cross sections of the branches in the $(2\sigma_u)^{-1}$ photoionization of N_2, expressed in % of the vibronic cross sections, and their average β values.

The results shown here were obtained in the RD_{vr} approximation at T_{rot}=300K.

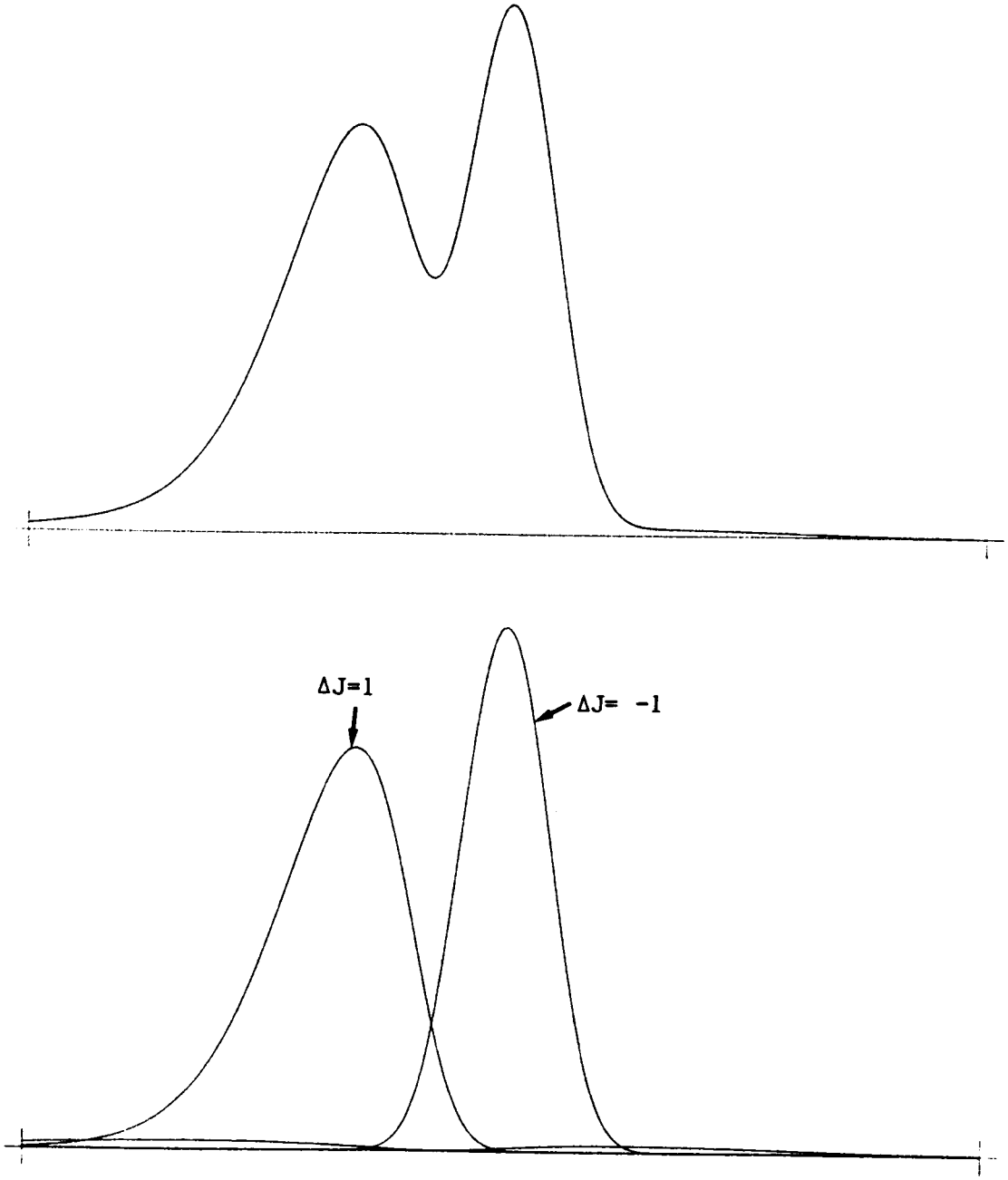


Fig. 10-21. The isotropic component of the vibronic band with $v_f = 0$ and its individual branches in the $(2\sigma_u)^{-1}$ photoionization of N_2 at T = 300K.

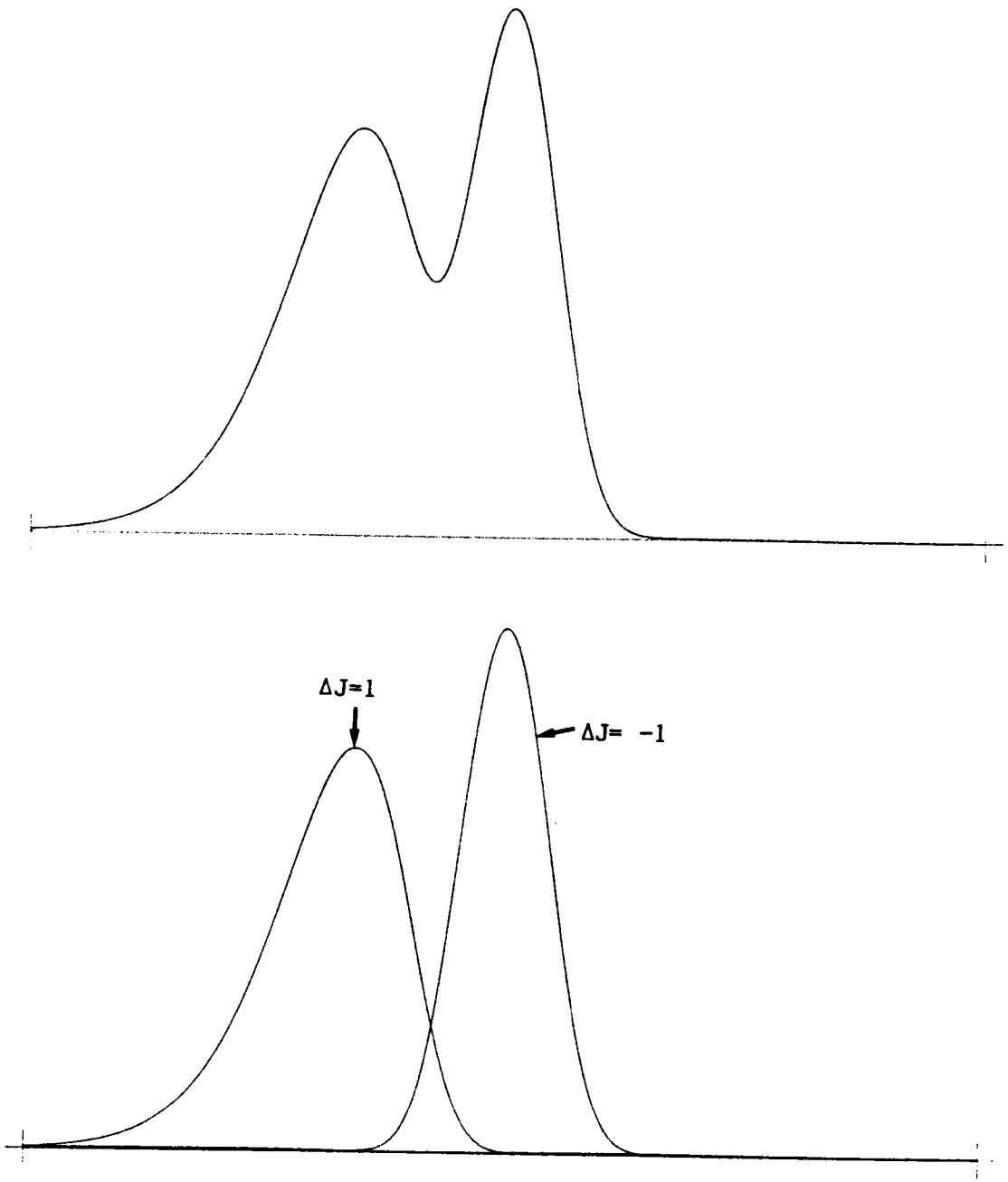


Fig. 10-22. The anisotropic component of the vibronic band with $v_f=0$ and its individual branches in the $(2\sigma_u)^{-1}$ photoionization of N_2 at T = 300K.

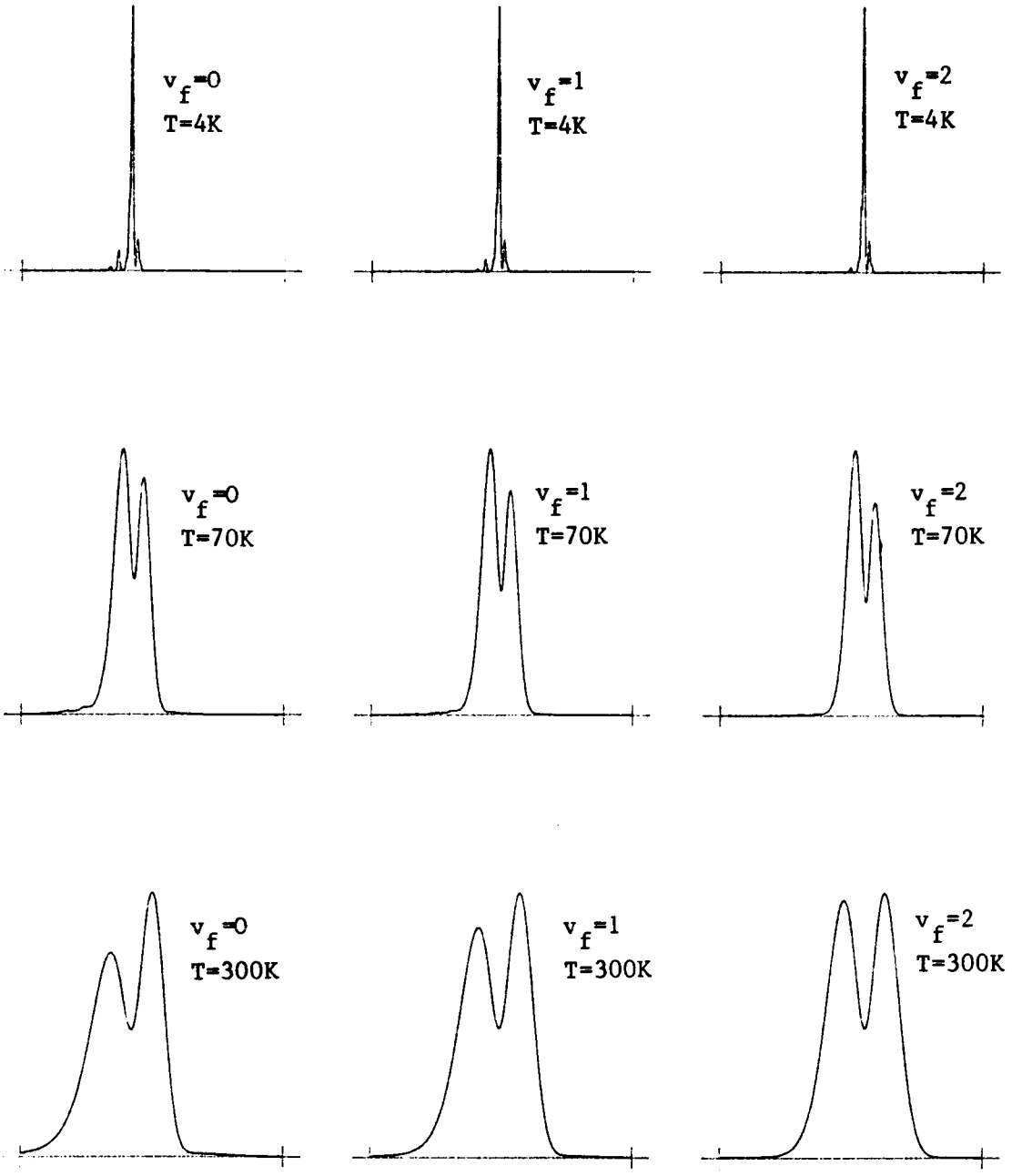


Fig. 10-23. Vibronic band contours in the $(2\sigma_u)^{-1}$ photoionization of N_2 at different temperatures.

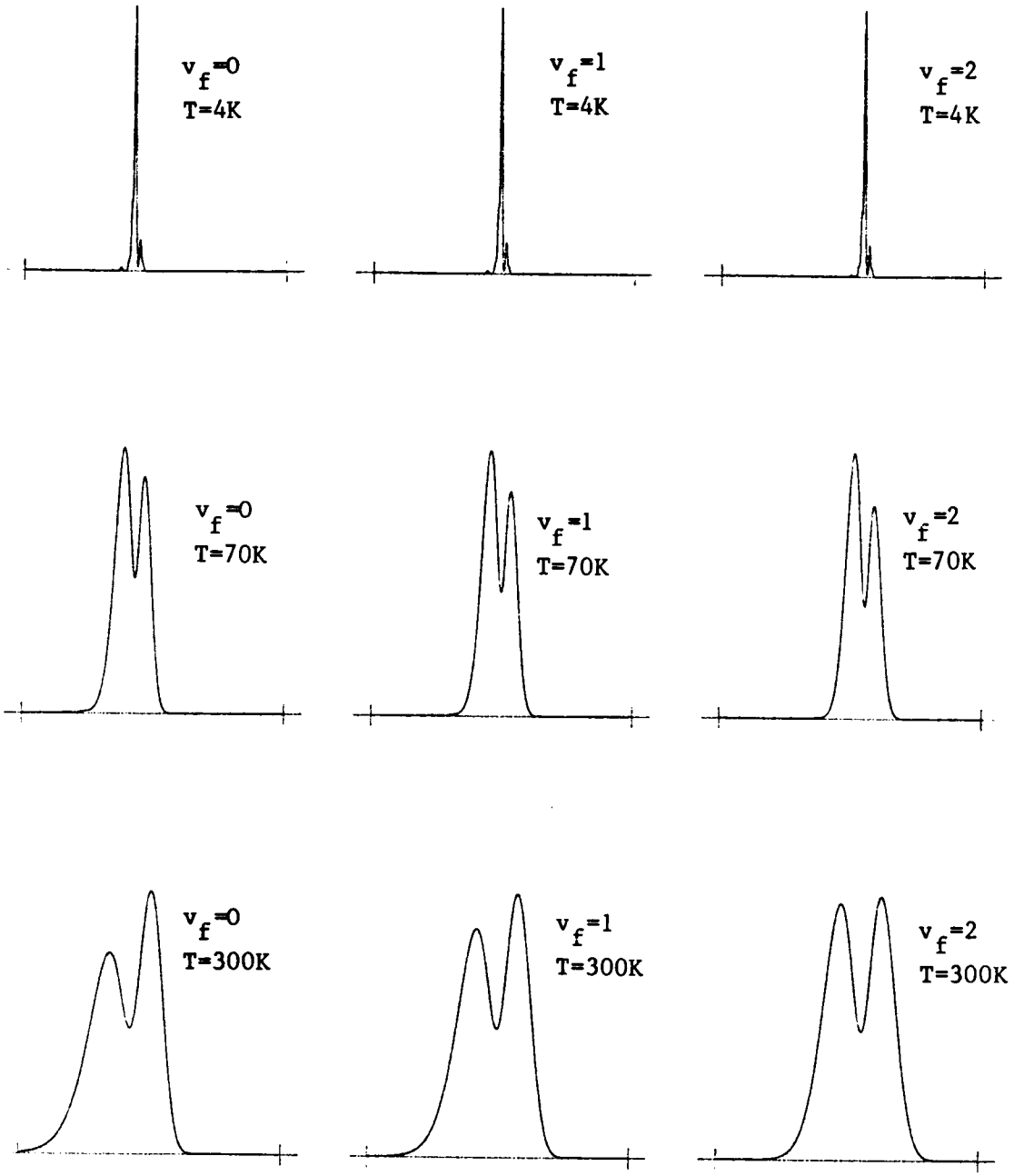


Fig. 10-24. Contours of the anisotropic component of the vibronic bands in the $(2\sigma_u)^{-1}$ photoionization of N_2 at different temperatures.

If there are any effects of symmetry breaking in N_2, they would be expected to be strongest in the photoionization of the $2\sigma_u$ level, when compared with the photoionization of the other valence levels. Shimamura's sum rules remain valid in the presence of symmetry breaking processes, unless strong nonadiabatic effcts are associated with these processes.

Nonadiabatic coupling is defined as[708] $\langle\psi_j|\nabla|\psi_k\rangle$, where ψ_j and ψ_k represent wave functions of different electronic states. Nonadiabatic coupling is governed by selection rules. In the presence of symmetry breaking these selection rules are violated, and "forbidden" conversion pathways become accessible for conformations of the nuclear framework for which a broken-symmetry solution is energetically favourble.

5. The 5σ Photoionization of Carbon Monoxide

According to Cole et al.,[468] the 5σ photoelectron spectra, obtained with photons of energies greater than 21 eV, can be assumed to be affected mainly by a shape resonance centered at approximately 24 eV. Below 21 eV, autoionization is responsible for anomalies observed in the vibrational branching ratios and the vibronic β values.[468]

In Table 10-53, a shape resonance is apparent in the σ-σ channel. This shape resonance is also clearly visible in Figure 10-4 (p 243). In Table 10-54 and in Table 10-55, the rotational structure of the different vibronic bands can be seen to differ greatly. In Tables 10-56, 10-57, and 10-58, the relative cross sections and the average β values of the branches with v_f=0,1, and 2 respectively are shown. The r-centroid for v_f=2 was located outside the range of sampled internuclear separations. However, the breakdown of the

TABLE 10-53

PHOTOIONIZATION CROSS SECTIONS AND BETA VALUES OF CARBON MONOXIDE

$CO(X^1\Sigma^+) \rightarrow CO^+(X^2\Sigma^+) + e^-$

σ (Mb)

Channel	$r_{CO}(a_o)$	E_e=0.49 Ryd	E_e=0.51 Ryd	E_e=0.53 Ryd	E_e=0.55 Ryd
$5\sigma \rightarrow k\sigma$	1.9	2.82	2.82	2.83	2.84
	2.13	6.47	6.75	7.01	7.20
	2.2	9.70	9.58	9.23	8.68
	2.35	2.10	1.75	1.48	1.27
	2.5	0.39	0.36	0.34	0.33
$5\sigma \rightarrow k\pi$	1.9	2.19	2.18	2.17	2.16
	2.13	2.17	2.19	2.20	2.22
	2.2	2.19	2.21	2.24	2.26
	2.35	2.30	2.34	2.39	2.43
	2.5	2.52	2.58	2.64	2.71

β

$r_{CO}(a_o)$	E_e=0.49 Ryd	E_e=0.51 Ryd	E_e=0.53 Ryd	E_e=0.55 Ryd
1.9	1.44	1.43	1.43	1.42
2.13	0.97	0.94	0.91	0.89
2.2	0.67	0.64	0.60	0.57
2.35	0.25	0.28	0.32	0.35
2.5	0.52	0.55	0.58	0.60

TABLE 10-54

SCALED PHOTOIONIZATION CROSS SECTIONS FOR $CO(X^1\Sigma^+) \rightarrow CO^+(X^2\Sigma^+) + e^-$ ($h\nu$=21.2 eV)

v_f	J_i	$\Delta J = -4$	$\Delta J = -3$	$\Delta J = -2$	$\Delta J = -1$	$\Delta J = 0$	$\Delta J = 1$	$\Delta J = 2$	$\Delta J = 3$	$\Delta J = 4$
0	0					484	1260	1291	480	469
0	1				420	1000	1045	983	274	261
0	2			258	627	987	884	786	229	213
0	3		69	421	631	913	832	718	208	191
0	4	52	91	436	646	895	805	682	196	178
0	5	71	104	456	658	887	789	659	188	170
0	6	82	112	471	666	882	778	643	182	164
0	12	107	131	511	689	873	748	601	167	147
0	24	119	140	528	695	866	728	577	159	138
1	0					163	1562	969	926	1956
1	1				521	551	1439	1451	529	1086
1	2			194	864	1000	1184	1006	440	888
1	3		133	624	847	778	1109	890	400	796
1	4	218	177	562	864	732	1071	833	376	743
1	5	298	202	570	878	713	1048	799	361	708
1	6	344	217	582	889	702	1032	776	350	682
1	12	450	257	623	920	683	991	715	319	613
1	24	511	279	645	939	670	969	674	301	580
2	0					56	2277	1090	762	2211
2	1				759	491	1844	1638	435	1227
2	2			217	1106	1000	1569	1135	362	1002
2	3		109	702	1120	749	1478	1005	329	898
2	4	247	145	630	1149	697	1431	942	310	837
2	5	337	165	639	1170	675	1401	904	297	797
2	6	389	178	651	1186	664	1381	878	288	767
2	12	506	209	693	1225	643	1325	812	262	683
2	24	562	223	711	1235	632	1283	771	244	625

TABLE 10-55

BETA VALUES FOR $CO(X^1\Sigma^+) \rightarrow CO^+(X^2\Sigma^+) + e^-$ ($h\nu$=21.2 eV)

v_f	J_i	ΔJ= −4	ΔJ= −3	ΔJ= −2	ΔJ= −1	ΔJ=0	ΔJ=1	ΔJ=2	ΔJ=3	ΔJ=4
0	0					2.00	1.18	0.53	0.24	0.33
0	1				1.18	1.24	1.00	0.49	0.24	0.33
0	2			0.53	1.00	1.22	1.05	0.50	0.24	0.33
0	3		0.24	0.49	1.05	1.29	1.06	0.50	0.24	0.33
0	4	0.33	0.24	0.50	1.06	1.31	1.06	0.50	0.24	0.33
0	5	0.33	0.24	0.50	1.06	1.32	1.06	0.50	0.24	0.33
0	6	0.33	0.24	0.50	1.06	1.32	1.06	0.50	0.24	0.33
0	12	0.34	0.24	0.50	1.06	1.33	1.06	0.50	0.24	0.33
0	24	0.34	0.24	0.50	1.05	1.33	1.05	0.50	0.24	0.34
1	0					2.00	0.12	0.21	0.22	0.35
1	1				0.12	0.74	0.15	0.30	0.22	0.35
1	2			0.21	0.15	0.58	0.14	0.28	0.22	0.35
1	3		0.22	0.30	0.14	0.65	0.14	0.28	0.22	0.35
1	4	0.35	0.22	0.28	0.14	0.67	0.14	0.28	0.22	0.35
1	5	0.35	0.22	0.28	0.14	0.68	0.14	0.28	0.22	0.35
1	6	0.35	0.22	0.28	0.14	0.68	0.14	0.28	0.22	0.35
1	12	0.36	0.22	0.28	0.13	0.69	0.13	0.27	0.22	0.35
1	24	0.36	0.22	0.27	0.11	0.68	0.11	0.27	0.22	0.35
2	0					2.00	0.70	0.51	0.30	0.32
2	1				0.70	0.68	0.63	0.40	0.30	0.32
2	2			0.52	0.63	0.47	0.65	0.41	0.30	0.32
2	3		0.30	0.40	0.65	0.52	0.65	0.42	0.30	0.32
2	4	0.32	0.30	0.42	0.65	0.53	0.65	0.42	0.30	0.32
2	5	0.32	0.30	0.42	0.65	0.54	0.65	0.42	0.30	0.32
2	6	0.32	0.30	0.42	0.65	0.54	0.65	0.42	0.30	0.32
2	12	0.32	0.30	0.43	0.65	0.55	0.65	0.42	0.30	0.32
2	24	0.32	0.30	0.43	0.65	0.56	0.66	0.42	0.30	0.32

TABLE 10-56

RELATIVE INTENSITIES AND AVERAGE BETA VALUES OF THE BRANCHES IN THE PHOTOIONIZATION OF THE 5σ LEVEL OF CO FOR v_f=0

Rel. Intensities (% of the Intensity of the Vibronic Band)

	T=4K		T=60K		T=300K			
ΔJ	FR_{vr}	RD_{vr}	FR_{vr}	RD_{vr}	FR_{vr}	RC_{vr}	RD	RD_{vr}
0	19	18	23	23	23	21	22	22
-1	5	5	15	15	17	17	17	17
1	29	29	22	22	20	20	20	20
-2			9	9	12	12	12	12
2	30	29	20	19	17	16	16	16
-3			1	2	3	3	3	3
3	9	10	5	6	4	5	5	5
-4			1	1	2	2	2	2
4	8	9	4	5	3	4	4	4

Average Beta Values of the Branches

	T=4K		T=60K		T=300K			
ΔJ	FR_{vr}	RD_{vr}	FR_{vr}	RD_{vr}	FR_{vr}	RC_{vr}	RD	RD_{vr}
0	1.51	1.52	1.31	1.30	1.33	1.28	1.32	1.32
-1	1.28	1.16	1.17	1.06	1.18	1.05	1.06	1.06
1	1.23	1.11	1.17	1.06	1.18	1.05	1.06	1.06
-2	0.54	0.53	0.52	0.50	0.52	0.50	0.50	0.50
2	0.53	0.51	0.52	0.50	0.52	0.50	0.50	0.50
-3	0.24	0.24	0.24	0.24	0.24	0.24	0.24	0.24
3	0.24	0.24	0.24	0.24	0.24	0.24	0.24	0.24
-4	0.33	0.33	0.33	0.33	0.33	0.33	0.33	0.34
4	0.33	0.33	0.33	0.33	0.33	0.33	0.33	0.33
-5	0.48	0.49	0.48	0.49	0.48	0.45	0.49	0.49
5	0.48	0.49	0.47	0.49	0.47	0.44	0.49	0.49

TABLE 10-57

RELATIVE INTENSITIES AND AVERAGE BETA VALUES OF THE BRANCHES IN THE PHOTOIONIZATION OF THE 5σ LEVEL OF CO FOR v_f=1

Rel. Intensities (% of the Intensity of the Vibronic Band)

	T=4K		T=60K		T=300K			
ΔJ	FR_{vr}	RD_{vr}	FR_{vr}	RD_{vr}	FR_{vr}	RC_{vr}	RD	RD_{vr}
0	19	6	24	13	23	26	13	13
-1	5	5	15	14	17	10	16	16
1	30	27	22	21	20	11	19	19
-2			9	8	12	10	10	10
2	29	21	19	17	16	14	14	14
-3			1	2	3	3	4	4
3	9	13	5	8	4	5	6	6
-4			1	3	2	7	6	6
4	7	28	4	15	3	14	12	12

Average Beta Values of the Branches

	T=4K		T=60K		T=300K			
ΔJ	FR_{vr}	RD_{vr}	FR_{vr}	RD_{vr}	FR_{vr}	RC_{vr}	RD	RD_{vr}
0	1.53	1.03	1.33	0.67	1.35	1.36	0.68	0.68
-1	1.32	0.12	1.22	0.14	1.22	-0.57	0.14	0.13
1	1.27	0.13	1.22	0.14	1.22	-0.57	0.14	0.13
-2	0.52	0.22	0.50	0.28	0.50	0.30	0.28	0.28
2	0.51	0.26	0.50	0.28	0.50	0.30	0.28	0.28
-3	0.24	0.22	0.24	0.22	0.24	0.11	0.22	0.22
3	0.24	0.22	0.24	0.22	0.24	0.11	0.22	0.22
-4	0.32	0.35	0.32	0.35	0.32	0.39	0.35	0.36
4	0.32	0.35	0.32	0.35	0.32	0.39	0.35	0.35
-5	0.46	0.46	0.46	0.46	0.46	0.46	0.46	0.46
5	0.46	0.46	0.46	0.46	0.46	0.46	0.46	0.46

TABLE 10-58

RELATIVE INTENSITIES AND AVERAGE BETA VALUES OF THE BRANCHES IN THE PHOTOIONIZATION OF THE 5σ LEVEL OF CO FOR $v_f=2$

Rel. Intensities (% of the Intensity of the Vibronic Band)

	T=4K		T=60K		T=300K		
ΔJ	FR_{vr}	RD_{vr}	FR_{vr}	RD_{vr}	FR_{vr}	RD	RD_{vr}
0	20	4	25	11	24	10	10
-1	5	6	16	16	18	18	18
1	31	32	23	24	20	22	22
-2			9	7	12	10	10
2	29	21	18	17	15	14	14
-3			1	2	3	3	3
3	8	10	5	6	4	5	5
-4			1	3	2	6	6
4	6	27	3	15	2	12	12

Average Beta Values of the Branches

	T=4K		T=60K		T=300K		
ΔJ	FR_{vr}	RD_{vr}	FR_{vr}	RD_{vr}	FR_{vr}	RD	RD_{vr}
0	1.55	0.80	1.36	0.54	1.38	0.54	0.54
-1	1.36	0.69	1.26	0.65	1.26	0.65	0.65
1	1.31	0.67	1.26	0.65	1.26	0.65	0.65
-2	0.49	0.51	0.48	0.42	0.48	0.42	0.42
2	0.48	0.45	0.48	0.42	0.48	0.42	0.42
-3	0.24	0.30	0.24	0.30	0.24	0.30	0.30
3	0.24	0.30	0.24	0.30	0.24	0.30	0.30
-4	0.32	0.32	0.32	0.32	0.32	0.32	0.32
4	0.32	0.32	0.32	0.32	0.32	0.32	0.32
-5		0.35		0.35		0.35	0.35
5		0.35		0.35		0.35	0.35

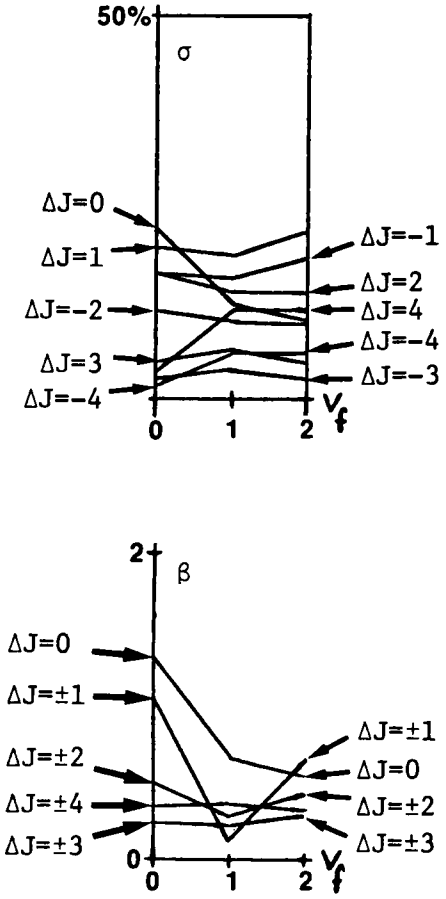
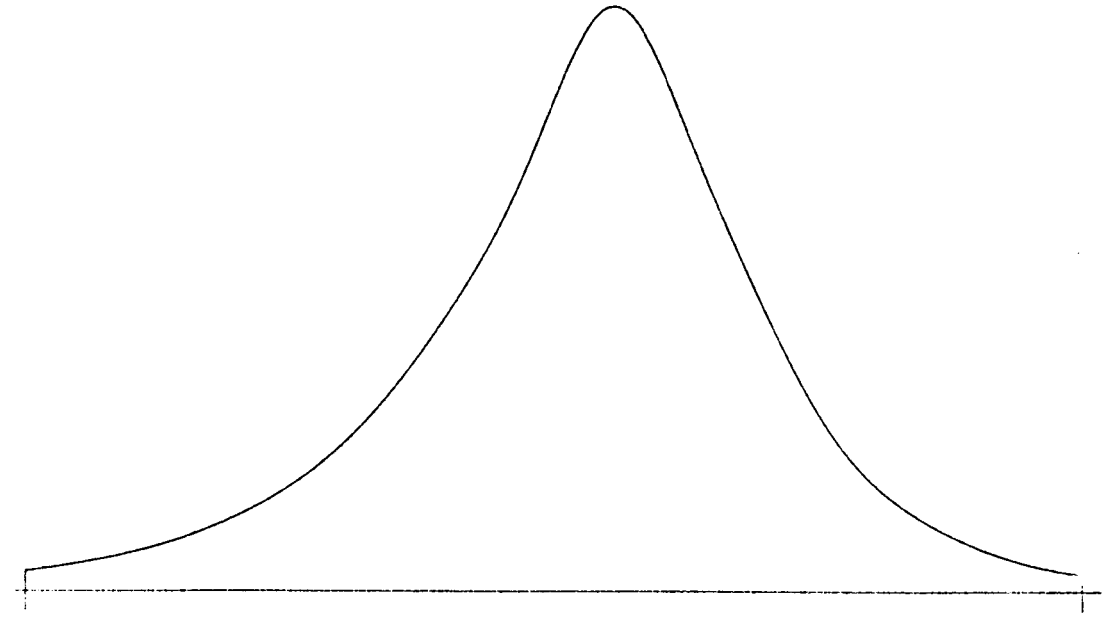


Fig. 10-25. The cross sections of the branches in the $(5\sigma)^{-1}$ photoionization of CO, expressed in % of the vibronic cross sections, and their average β values.

The results shown here were obtained in the RD_{VR} approximation at T_{rot}=300K.



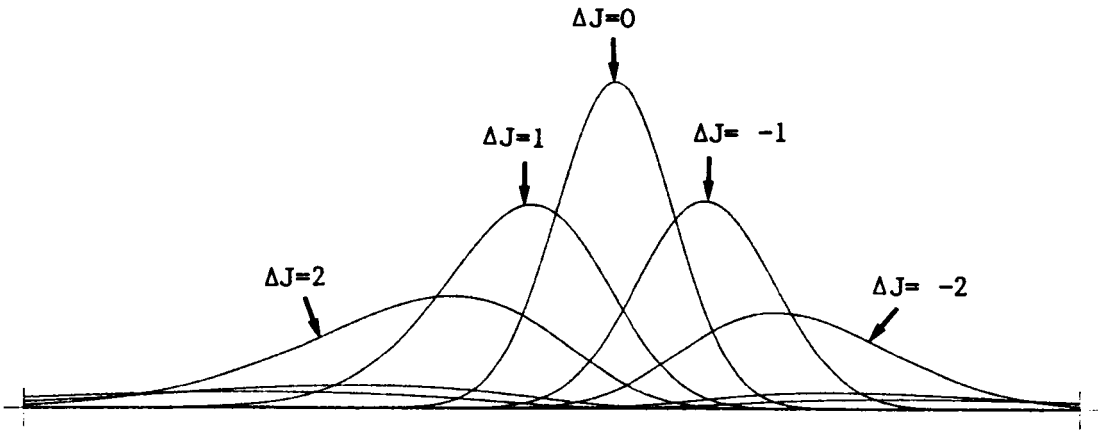


Fig. 10-26. The isotropic component of the vibronic band with $v_f=0$ and its individual branches in the $(5\sigma)^{-1}$ photoionization of CO at T = 300K.

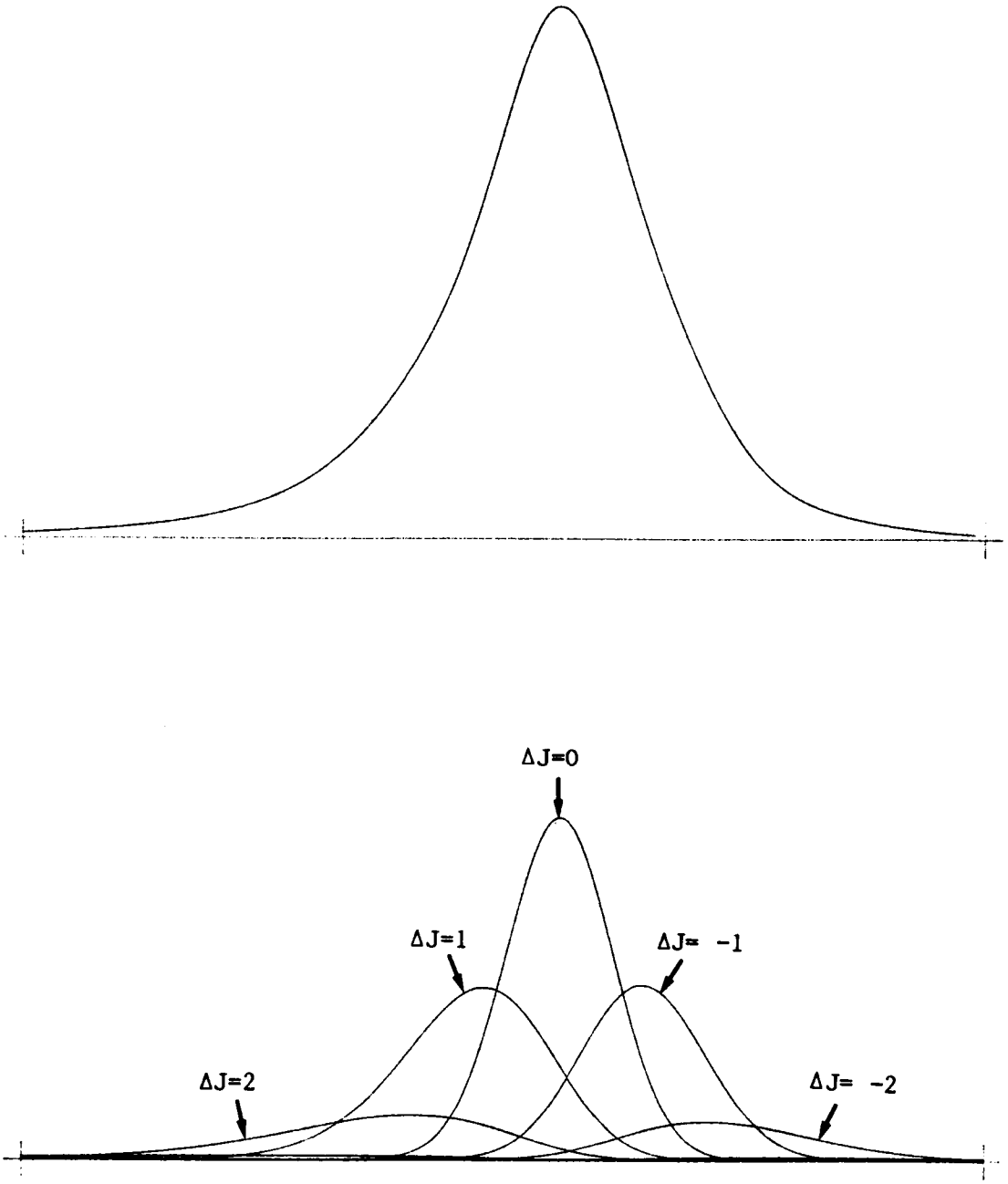


Fig. 10-27. The anisotropic component of the vibronic band with $v_f=0$ and its individual branches in the $(5\sigma)^{-1}$ photoionization of CO at T = 300K.

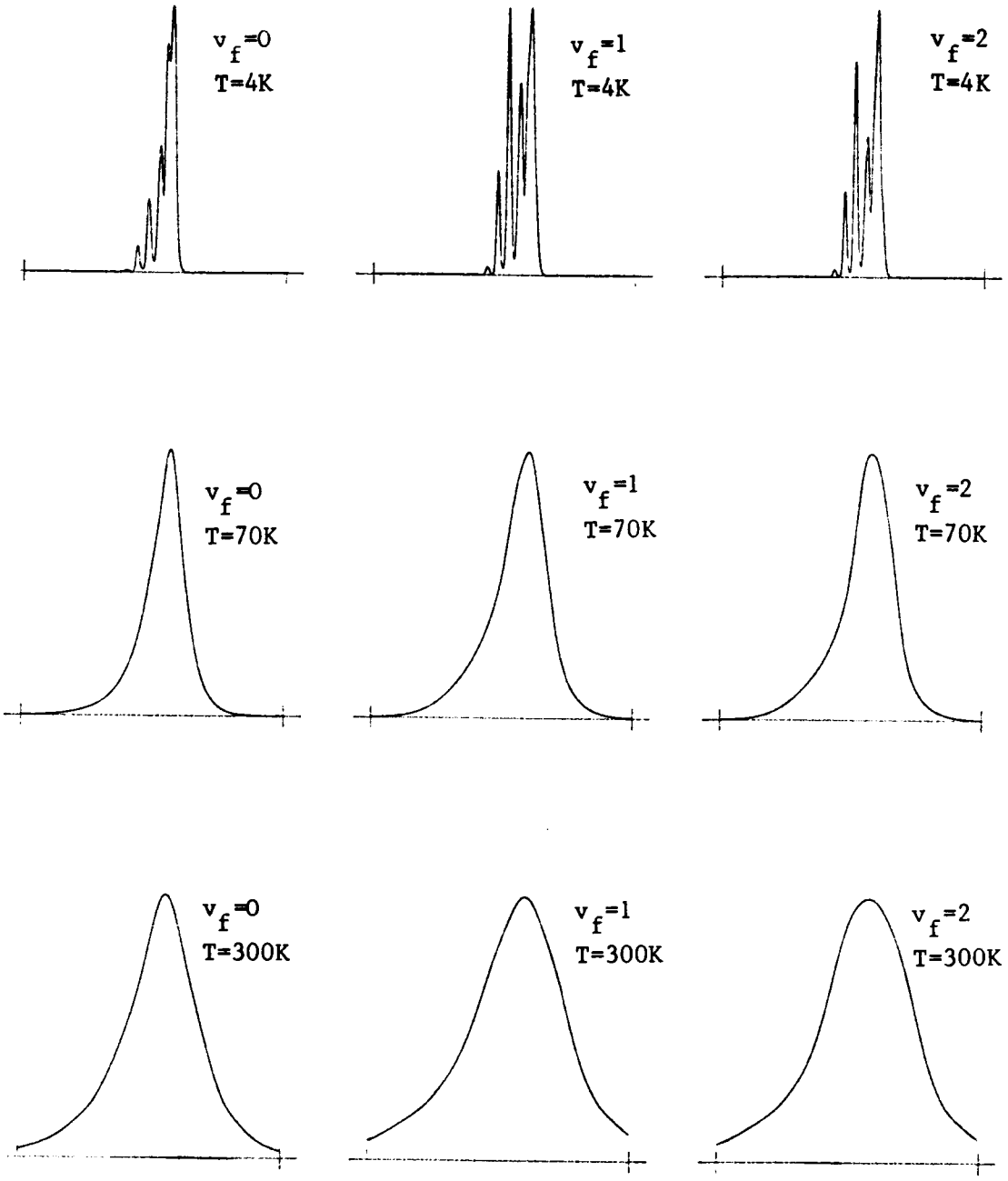


Fig. 10-28. Vibronic band contours in the $(5\sigma)^{-1}$ photoionization of CO at different temperatures.

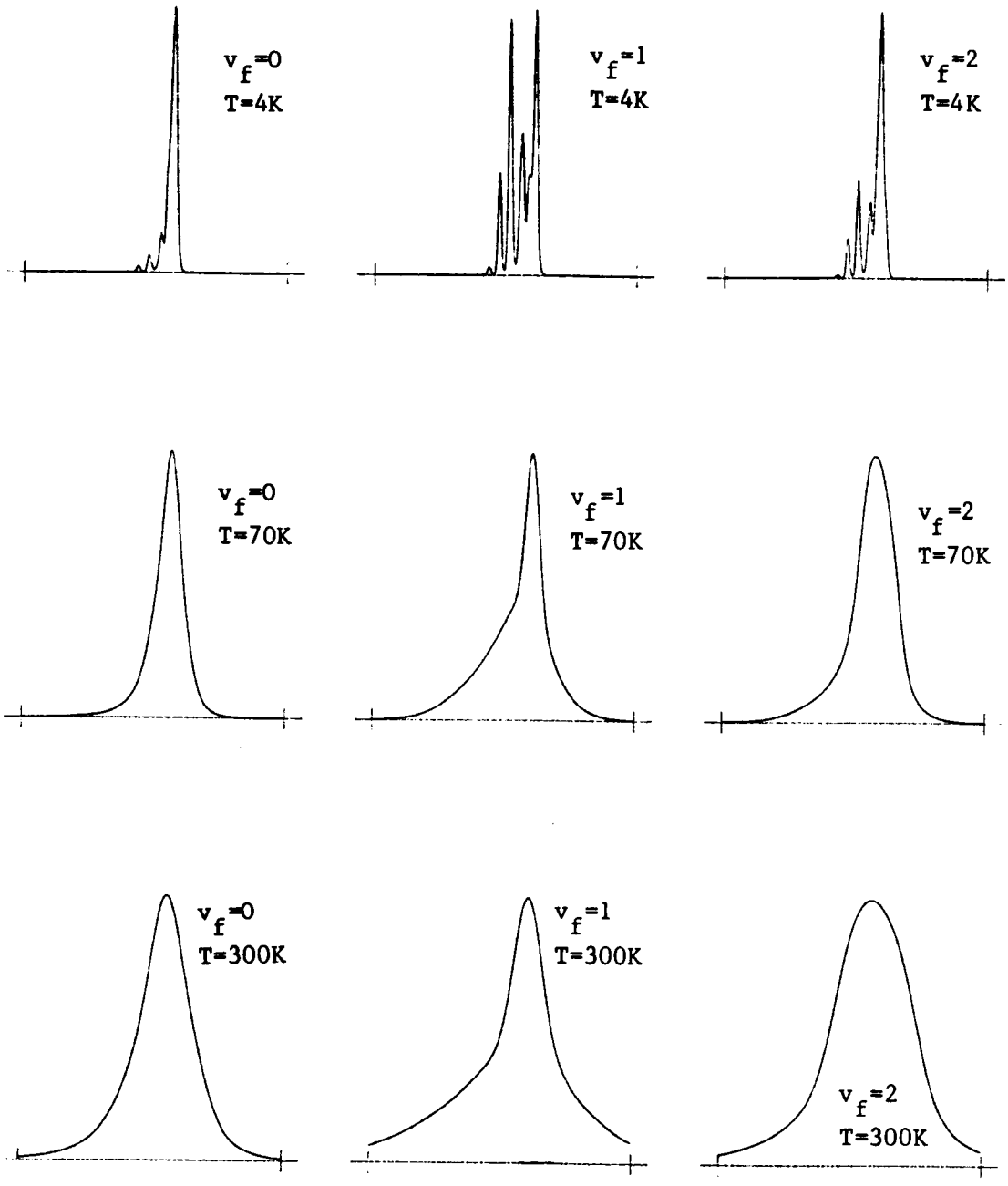


Fig. 10-29. Contours of the anisotropic component of the vibronic bands in the $(5\sigma)^{-1}$ photoionization of CO at different temperatures.

r-centroid approximation is clearly evident from Table 10-57, which contains data for the vibronic band with v_f=1. The relative cross sections of the branches and their β values, computed with the RD_{vr} method, are shown in Figure 10-25. Due to the presence of a shape resonance, the band contours of the different vibronic bands are expected to differ considerably. The shape resonance causes the branches with large values of $|\Delta J|$ to gain in intensity. The band contours are shown in Figures 10-26, 10-27, 10-28, and 10-29. The ranges of the graphs, expressed in terms of ΔE_{nucl}, are given by:

$$-150 \text{ cm}^{-1} \leq \Delta E_{nucl} \leq 250 \text{ cm}^{-1} \text{ for } v_f=0$$

$$2050 \text{ cm}^{-1} \leq \Delta E_{nucl} \leq 2450 \text{ cm}^{-1} \text{ for } v_f=1$$

$$4200 \text{ cm}^{-1} \leq \Delta E_{nucl} \leq 4600 \text{ cm}^{-1} \text{ for } v_f=2$$

In Table 10-54, the scaling factors 4.9 (10^2), 1.5 (10^4), and 6.78 (10^4) were applied to obtain the relative cross sections from the cross sections expressed in megabarns.

Gardner and Samson[15] gave, for the vibronic cross sections of the bands with v_f=0 and v_f=1, relative cross sections of 100 and 3.5 respectively. According to Gardner and Samson, the vibrational branching ratio would be about the same as predicted by the Franck-Condon factors. However, in the RD approximation, the band with v_f=1 is predicted to have enhanced intensity due to the presence of the shape resonance. The relative cross sections obtained here are 100, 6.6, and 1.2 for v_f=0,1, and 2 respectively. Sell *et al.*[518] give vibronic β

values of 0.95, 0.60, and 0.73 for v_f=0,1, and 2 respectively. The β values given by Kreile and Schweig agree with the ones given by Sell *et al.* within experimental error, but they give no value for the vibronic band with v_f=2. In Table 10-59, the vibronic β values are shown. In the RD approximation, the vibronic β values come out as 0.855 for v_f=0, 0.287 for v_f=1, and 0.499 for v_f=2. The ordering of the β values for the different vibronic bands is correct, but all three of the computed β values are too low.

6. The Photoionization of the 1π Level of Carbon Monoxide

In the photoelectron spectra of the 1π level of CO, we again have effects of spin-orbit interaction. These effects have been implemented artifically in a manner described at the beginning of this chapter.

In Table 10-60, the channel contributions to the cross sections and the β values are shown for internuclear separations and photoelectron energies of interest in connection with the photoelectron spectrum of the 1π level of CO, using 58.4 nm photons.

The π-σ channel shows a depression in the cross section at internuclear separations slightly greater than r_e of CO, and the β values show a relatively flat maximum in this region. The same can be observed in Figure 10-6 (p 245).

The experimental vibronic β values show a sharp dip at v_f=8 and v_f=9, where the β values become negative.[518] In Table 10-61 and in Table 10-62, vibronic cross sections and β values are shown. The β values computed in the RD approximation show a minimum at v_f=7, but the minimum isn't nearly as sharp and deep as the minimum observed experimentally. The β values for the vibronic progression, according to Sell *et al.*,[518] are:

TABLE 10-59

VIBRONIC INTENSITIES AND BETA VALUES FOR THE PHOTOIONIZATION OF THE 5σ LEVEL OF CO AT DIFFERENT ROTATIONAL TEMPERATURES

σ(Mb)

	T=4K			T=60K			T=300K			
v_f	FR_{vr}	RD	RD_{vr}	FR_{vr}	RD	RD_{vr}	FR_{vr}	RC_{vr}	RD	RD_{vr}
0	7.89954	8.02121	8.02366	7.89927	8.02137	8.02162	7.89402	8.98554	8.01720	8.00774
1	0.28578	0.53011	0.52952	0.28572	0.53011	0.52946	0.28536	0.11325	0.52984	0.52904
2	0.00078	0.09422	0.09430	0.00079	0.09421	0.09418	0.00079		0.09417	0.09388

β

	T=4K			T=60K			T=300K			
v_f	FR_{vr}	RD	RD_{vr}	FR_{vr}	RD	RD_{vr}	FR_{vr}	RC_{vr}	RD	RD_{vr}
0	0.916	0.857	0.857	0.916	0.857	0.856	0.916	0.836	0.857	0.855
1	0.945	0.289	0.289	0.945	0.289	0.288	0.945	0.406	0.289	0.287
2	0.975	0.498	0.499	0.976	0.498	0.499	0.975		0.498	0.499

FR, RC, and RD, and the subscript "vr" refer to different methods of computation as described in the text.

TABLE 10-60

PHOTOIONIZATION CROSS SECTIONS AND BETA VALUES OF CARBON MONOXIDE

$CO(X^1\Sigma^+) \rightarrow CO^+(A^2\Pi_i) + e^-$

σ(Mb)

Channel	$r_{CO}(a_o)$	E_e=0.17 Ryd	E_e=0.23 Ryd	E_e=0.29 Ryd	E_e=0.35 Ryd
$1\pi \rightarrow k\sigma$	1.9	3.25	2.88	2.56	2.27
	2.05	2.88	2.48	2.13	1.84
	2.2	2.30	1.88	1.54	1.30
	2.35	1.35	1.32	2.10	2.67
	2.5	3.55	3.21	2.76	2.37
$1\pi \rightarrow k\pi$	1.9	0.55	0.49	0.44	0.40
	2.05	0.46	0.42	0.38	0.35
	2.2	0.40	0.38	0.36	0.35
	2.35	0.38	0.37	0.37	0.38
	2.5	0.39	0.40	0.43	0.46
$1\pi \rightarrow k\delta$	1.9	16.34	15.33	14.10	12.81
	2.05	15.66	14.57	13.32	12.07
	2.2	14.90	13.78	12.54	11.33
	2.35	14.12	12.99	11.80	10.65
	2.5	13.36	12.24	11.10	10.02

β

$r_{CO}(a_o)$	E_e=0.17 Ryd	E_e=0.23 Ryd	E_e=0.29 Ryd	E_e=0.35 Ryd
1.9	0.24	0.35	0.43	0.50
2.05	0.17	0.28	0.36	0.43
2.2	0.14	0.25	0.34	0.43
2.35	0.25	0.46	0.62	0.64
2.5	0.31	0.34	0.38	0.43

TABLE 10-61

VIBRONIC INTENSITIES FOR THE PHOTOIONIZATION OF THE 1π LEVEL OF CO AT DIFFERENT ROTATIONAL TEMPERATURES

σ(Mb)

	T=4K			T=60K			T=300K			
v_f	FR_{vr}	RD	RD_{vr}	FR_{vr}	RD	RD_{vr}	FR_{vr}	RC_{vr}	RD	RD_{vr}
0	1.43814	1.25270	1.25097	1.43673	1.25249	1.24959	1.42938	1.23790	1.25078	1.24254
1	3.25389	2.92551	2.92398	3.25118	2.92493	2.92104	3.23781	2.89803	2.92070	2.90679
2	4.04965	3.79409	3.79458	4.04965	3.79324	3.79130	4.03487	3.77923	3.78739	3.77599
3	3.68256	3.62619	3.62835	3.68116	3.62532	3.62590	3.67433	3.63040	3.61940	3.61468
4	2.74327	2.85598	2.85854	2.74301	2.85524	2.85732	2.74129	2.86523	2.85035	2.85151
5	1.78011	1.96338	1.96544	1.78050	1.96286	1.96521	1.78174	1.96598	1.95937	1.96364
6	1.04515	1.21857	1.21988	1.04576	1.21821	1.22017	1.04791	1.21436	1.21603	1.22090
7	0.56963	0.69810	0.69877	0.57019	0.69790	0.69924	0.57216	0.69224	0.69663	0.70074
8	0.29350	0.37528	0.37558	0.29392	0.37519	0.37598	0.29537	0.37128	0.37449	0.37739
9	0.14493	0.19193	0.19201	0.14518	0.19186	0.19230	0.14613	0.19028	0.19151	0.19336
10	0.06929	0.09447	0.09448	0.06945	0.09446	0.09467	0.07001	0.09433	0.09429	0.09534
11	0.03235	0.04526	0.04522	0.03244	0.04523	0.04534	0.03275	0.04567	0.04514	0.04573
12	0.01484	0.02127	0.02123	0.01489	0.02127	0.02130	0.01506	0.02175	0.02123	0.02153

FR, RC, and RD, and the subscript "vr" refer to different methods of computation as described in the text.

TABLE 10-62

AVERAGE BETA VALUES FOR THE PHOTOIONIZATION OF THE 1π LEVEL OF CO FOR DIFFERENT VIBRONIC BANDS AND AT DIFFERENT ROTATIONAL TEMPERATURES

σ(Mb)

	T=4K			T=60K			T=300K			
v_f	FR_{vr}	RD	RD_{vr}	FR_{vr}	RD	RD_{vr}	FR_{vr}	RC_{vr}	RD	RD_{vr}
0	0.403	0.531	0.532	0.403	0.531	0.532	0.403	0.540	0.532	0.533
1	0.388	0.481	0.481	0.388	0.481	0.481	0.388	0.476	0.481	0.482
2	0.372	0.423	0.423	0.372	0.423	0.424	0.372	0.413	0.424	0.425
3	0.355	0.369	0.369	0.356	0.369	0.369	0.356	0.362	0.369	0.370
4	0.339	0.324	0.324	0.339	0.324	0.324	0.339	0.328	0.325	0.325
5	0.322	0.294	0.294	0.322	0.294	0.294	0.322	0.311	0.294	0.294
6	0.304	0.278	0.278	0.304	0.278	0.278	0.305	0.306	0.278	0.278
7	0.286	0.276	0.275	0.286	0.276	0.275	0.287	0.309	0.276	0.275
8	0.267	0.283	0.283	0.268	0.283	0.283	0.268	0.314	0.284	0.282
9	0.248	0.296	0.296	0.248	0.296	0.296	0.249	0.317	0.297	0.295
10	0.228	0.310	0.309	0.228	0.310	0.309	0.229	0.315	0.310	0.309
11	0.208	0.319	0.318	0.208	0.319	0.318	0.209	0.308	0.319	0.318
12	0.187	0.318	0.318	0.187	0.318	0.318	0.188	0.296	0.320	0.318

FR, RC, and RD, and the subscript "vr" refer to different methods of computation as described in the text.

0.47, 0.32, 0.29, 0.25, 0.10, 0.27, 0.24, 0.22, -0.07, -0.02, 0.32

for v_f=0,1,2, ..., 10 respectively. Notice that there is a further irregularity for the vibronic band with v_f=4, which has a low β value of 0.10. The Franck-Condon and the r-centroid approximation predict a monotone decrease of the β values in the vibronic progression.

Gardner and Samson[15] give relative vibronic cross sections of

39, 83, 100, 87, 68, 50, 24, 15, 8, 5, 3, 1

for the vibronic bands with v_f=0,1, ..., 11.

These are reasonably well reproduced by data obtained in the RD approximation, which are shown in Table 10-61. The computed relative vibronic cross sections are:

33, 77, 100, 96, 76, 52, 32, 19, 10, 5, 3, 1

for vibronic bands with v_f=0,1, ..., 11 respectively.

In Table 10-63 and in Table 10-64, the cross sections of individual rovibronic bands are shown. In Tables 10-65, 10-66, 10-67, and 10-68, we have the usual decomposition into branches. The relative cross sections of the branches and their β values, computed with the RD_{vr} method for a rotational temperature of 300 degrees Kelvin, are shown in Figure 10-30.

In Figures 10-31, 10-32, 10-33, and 10-34, the contours of the vibronic bands and of individual branches are shown. The limits of the graphs, indicated by tic marks, expressed in terms of ΔE_{nucl}, are given by:

TABLE 10-63

SCALED PHOTOIONIZATION CROSS SECTIONS FOR $CO(X^1\Sigma^+) \rightarrow CO^+(A^2\Pi_i) + e^-$ ($h\nu$=21.2 eV)

v_f	J_i	ΔJ= −4	ΔJ= −3	ΔJ= −2	ΔJ= −1	ΔJ=0	ΔJ=1	ΔJ=2	ΔJ=3	ΔJ=4
0	0						1670	549	245	13
0	1					1000	1020	319	132	7
0	2				374	912	815	264	106	5
0	3			101	403	895	738	240	94	5
0	4		20	119	434	888	697	226	86	4
0	5	1	29	130	456	885	670	217	82	4
0	6	1	34	138	471	883	652	210	78	4
0	12	2	47	156	511	874	601	192	68	3
0	24	3	53	163	522	850	560	176	60	3
6	0						1776	375	317	0
6	1					100	1072	227	170	0
6	2				344	960	834	195	136	0
6	3			100	368	953	747	181	121	0
6	4		23	110	401	951	700	173	112	0
6	5	0	34	116	424	950	671	168	106	0
6	6	0	41	120	441	949	652	165	101	0
6	12	0	58	131	488	949	602	156	90	0
6	24	0	65	136	514	953	582	154	85	0
12	0						1744	369	311	1
12	1					982	1053	223	168	0
12	2				337	942	820	193	135	0
12	3			97	361	937	736	179	120	0
12	4		22	107	393	935	691	172	111	0
12	5	0	33	114	417	935	664	167	105	0
12	6	0	40	118	434	936	646	164	101	0
12	12	0	56	128	483	948	607	158	92	0
12	24	0	65	136	528	1000	618	164	94	0

TABLE 10-64

BETA VALUES FOR $CO(X^1\Sigma^+) \rightarrow CO^+(A\Pi_i) + e^-$ ($h\nu$=21.2 eV)

v_f	J_i	ΔJ= -4	ΔJ= -3	ΔJ= -2	ΔJ= -1	ΔJ=0	ΔJ=1	ΔJ=2	ΔJ=3	ΔJ=4
0	0						1.06	-0.86	0.07	0.35
0	1					0.74	0.80	-0.78	0.07	0.35
0	2				0.10	0.94	0.75	-0.76	0.07	0.35
0	3			-0.36	0.29	0.97	0.72	-0.74	0.08	0.35
0	4		0.10	-0.48	0.38	0.99	0.70	-0.73	0.08	0.35
0	5	0.35	0.09	-0.53	0.42	1.00	0.68	-0.72	0.08	0.35
0	6	0.35	0.09	-0.56	0.45	1.00	0.67	-0.71	0.08	0.35
0	12	0.34	0.08	-0.61	0.52	1.01	0.63	-0.69	0.08	0.34
0	24	0.34	0.08	-0.64	0.56	1.02	0.61	-0.67	0.07	0.34
6	0						0.53	-0.85	0.21	0.46
6	1					0.37	0.41	-0.73	0.21	0.46
6	2				0.03	0.47	0.39	-0.66	0.21	0.46
6	3			-0.13	0.12	0.49	0.37	-0.63	0.21	0.46
6	4		0.21	-0.25	0.17	0.50	0.35	-0.60	0.21	0.46
6	5	0.45	0.21	-0.31	0.20	0.50	0.34	-0.59	0.21	0.47
6	6	0.46	0.21	-0.34	0.21	0.50	0.34	-0.57	0.21	0.47
6	12	0.47	0.21	-0.42	0.25	0.51	0.32	-0.54	0.21	0.48
6	24	0.50	0.20	-0.46	0.27	0.51	0.30	-0.52	0.20	0.53
12	0						0.57	-0.84	0.26	0.32
12	1					0.42	0.46	-0.71	0.26	0.32
12	2				0.06	0.52	0.43	-0.65	0.26	0.32
12	3			-0.10	0.16	0.54	0.41	-0.61	0.26	0.32
12	4		0.26	-0.22	0.21	0.54	0.39	-0.58	0.26	0.32
12	5	0.32	0.26	-0.28	0.24	0.55	0.38	-0.57	0.26	0.32
12	6	0.32	0.26	-0.31	0.25	0.55	0.38	-0.55	0.26	0.32
12	12	0.32	0.26	-0.39	0.29	0.55	0.36	-0.51	0.26	0.32
12	24	0.32	0.26	-0.43	0.31	0.55	0.34	-0.49	0.25	0.31

TABLE 10-65

RELATIVE INTENSITIES AND AVERAGE BETA VALUES OF THE BRANCHES IN THE PHOTOIONIZATION OF THE 1π LEVEL OF CO FOR $v_f=0$

Rel. Intensities (% of the Intensity of the Vibronic Band)

	T=4K		T=60K		T=300K			
ΔJ	FR_{vr}	RD_{vr}	FR_{vr}	RD_{vr}	FR_{vr}	RC_{vr}	RD	RD_{vr}
0	18	18	36	35	37	35	36	36
-1	1	1	14	14	18	19	19	19
1	56	55	32	32	27	27	27	27
-2			3	3	5	6	5	5
2	16	18	9	10	8	9	9	9
-3			1	1	2	1	1	1
3	9	8	5	4	4	3	3	3

Average Beta Values of the Branches

	T=4K		T=60K		T=300K			
ΔJ	FR_{vr}	RD_{vr}	FR_{vr}	RD_{vr}	FR_{vr}	RC_{vr}	RD	RD_{vr}
0	0.58	0.76	0.72	0.94	0.75	1.02	0.99	0.99
-1	0.05	0.11	0.24	0.34	0.34	0.47	0.47	0.47
1	0.74	0.97	0.57	0.75	0.51	0.69	0.67	0.67
-2	-0.26	-0.36	-0.40	-0.49	-0.50	-0.59	-0.58	-0.58
2	-0.85	-0.84	-0.73	-0.75	-0.67	-0.71	-0.71	-0.71
-3	0.15	0.10	0.15	0.09	0.15	0.06	0.08	0.08
3	0.14	0.07	0.14	0.07	0.14	0.05	0.08	0.08
-4	0.48	0.35	0.48	0.35	0.48	0.35	0.34	0.34
4	0.48	0.35	0.48	0.35	0.48	0.35	0.35	0.34
-5	0.44	0.42	0.44	0.42	0.44	0.41	0.42	0.42
5	0.44	0.42	0.44	0.42	0.44	0.41	0.42	0.42

TABLE 10-66

RELATIVE INTENSITIES AND AVERAGE BETA VALUES OF THE BRANCHES IN THE PHOTOIONIZATION OF THE 1π LEVEL OF CO FOR $v_f=4$

Rel. Intensities (% of the Intensity of the Vibronic Band)

	T=4K		T=60K		T=300K			
ΔJ	FR_{vr}	RD_{vr}	FR_{vr}	RD_{vr}	FR_{vr}	RC_{vr}	RD	RD_{vr}
0	18	18	36	36	37	37	37	37
-1	1	1	14	14	18	18	18	18
1	57	57	33	33	27	27	27	27
-2			3	3	5	5	5	5
2	15	14	9	9	8	7	7	7
-3			1	1	2	2	2	2
3	9	9	5	5	4	4	4	4

Average Beta Values of the Branches

	T=4K		T=60K		T=300K			
ΔJ	FR_{vr}	RD_{vr}	FR_{vr}	RD_{vr}	FR_{vr}	RC_{vr}	RD	RD_{vr}
0	0.49	0.46	0.61	0.59	0.64	0.62	0.61	0.62
-1	0.02	0.02	0.19	0.18	0.28	0.27	0.26	0.26
1	0.63	0.60	0.49	0.46	0.43	0.41	0.41	0.41
-2	-0.24	-0.22	-0.38	-0.35	-0.48	-0.45	-0.46	-0.46
2	-0.85	-0.84	-0.72	-0.71	-0.66	-0.64	-0.64	-0.65
-3	0.17	0.18	0.17	0.18	0.17	0.18	0.17	0.17
3	0.17	0.17	0.17	0.17	0.17	0.18	0.17	0.17
-4	0.48	0.50	0.48	0.51	0.48	0.52	0.51	0.51
4	0.48	0.51	0.48	0.51	0.48	0.52	0.51	0.51
-5	0.43	0.43	0.43	0.43	0.43	0.43	0.43	0.43
5	0.43	0.43	0.43	0.43	0.43	0.43	0.43	0.43

TABLE 10-67

RELATIVE INTENSITIES AND AVERAGE BETA VALUES OF THE BRANCHES IN THE PHOTOIONIZATION OF THE 1π LEVEL OF CO FOR $v_f=8$

Rel. Intensities (% of the Intensity of the Vibronic Band)

	T=4K		T=60K		T=300K			
ΔJ	FR_{vr}	RD_{vr}	FR_{vr}	RD_{vr}	FR_{vr}	RC_{vr}	RD	RD_{vr}
0	18	18	36	37	37	38	39	39
-1	1	1	14	13	18	18	18	18
1	58	59	33	33	27	27	27	27
-2			3	3	5	5	4	4
2	14	11	9	7	7	7	6	6
-3			1	1	2	2	2	2
3	9	10	5	5	4	4	4	4

Average Beta Values of the Branches

	T=4K		T=60K		T=300K			
ΔJ	FR_{vr}	RD_{vr}	FR_{vr}	RD_{vr}	FR_{vr}	RC_{vr}	RD	RD_{vr}
0	0.39	0.38	0.51	0.46	0.53	0.54	0.48	0.48
-1	-0.01	0.05	0.12	0.17	0.20	0.26	0.23	0.23
1	0.52	0.47	0.39	0.38	0.34	0.38	0.34	0.34
-2	-0.22	-0.09	-0.36	-0.22	-0.46	-0.36	-0.33	-0.33
2	-0.83	-0.79	-0.71	-0.62	-0.65	-0.58	-0.54	-0.54
-3	0.19	0.23	0.19	0.23	0.19	0.23	0.23	0.23
3	0.19	0.23	0.19	0.23	0.19	0.23	0.23	0.23
-4	0.47	0.18	0.47	0.17	0.47	0.13	0.16	0.16
4	0.47	0.15	0.47	0.15	0.47	0.09	0.15	0.16
-5	0.41	0.40	0.41	0.40	0.42	0.41	0.40	0.40
5	0.41	0.40	0.41	0.40	0.41	0.41	0.40	0.40

TABLE 10-68

RELATIVE INTENSITIES AND AVERAGE BETA VALUES OF THE BRANCHES IN THE PHOTOIONIZATION OF THE 1π LEVEL OF CO FOR v_f=12

Rel. Intensities (% of the Intensity of the Vibronic Band)

	T=4K		T=60K		T=300K			
ΔJ	FR_{vr}	RD_{vr}	FR_{vr}	RD_{vr}	FR_{vr}	RC_{vr}	RD	RD_{vr}
0	18	18	37	37	37	38	38	38
-1	1	1	14	13	18	18	18	18
1	58	59	33	33	27	27	27	27
-2			3	3	5	5	5	5
2	14	12	9	8	7	7	7	7
-3			1	1	1	2	2	2
3	9	10	5	5	4	4	7	4

Average Beta Values of the Branches

	T=4K		T=60K		T=300K			
ΔJ	FR_{vr}	RD_{vr}	FR_{vr}	RD_{vr}	FR_{vr}	RC_{vr}	RD	RD_{vr}
0	0.28	0.43	0.39	0.52	0.42	0.51	0.55	0.55
-1	-0.06	0.07	0.05	0.19	0.12	0.24	0.26	0.26
1	0.40	0.53	0.29	0.43	0.24	0.35	0.38	0.38
-2	-0.20	-0.10	-0.34	-0.24	-0.44	-0.32	-0.34	-0.34
2	-0.81	-0.79	-0.69	-0.63	-0.63	-0.53	-0.56	-0.55
-3	0.20	0.26	0.20	0.26	0.20	0.25	0.26	0.26
3	0.20	0.26	0.20	0.26	0.20	0.25	0.26	0.26
-4	0.45	0.32	0.45	0.32	0.45	0.36	0.32	0.32
4	0.45	0.32	0.45	0.32	0.45	0.36	0.32	0.32
-5						0.40		
5						0.39		

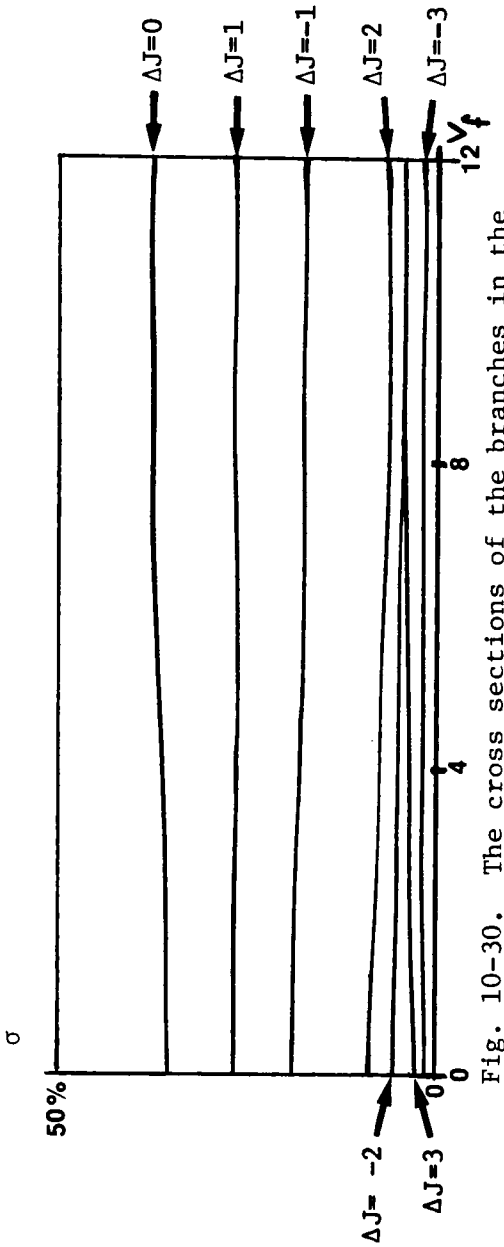


Fig. 10-30. The cross sections of the branches in the $(1\pi)^{-1}$ photoionization of CO, expressed in % of the vibronic cross sections, and their average β values.

The results shown here were obtained in the RD_{vr} approximation at Trot=300K.

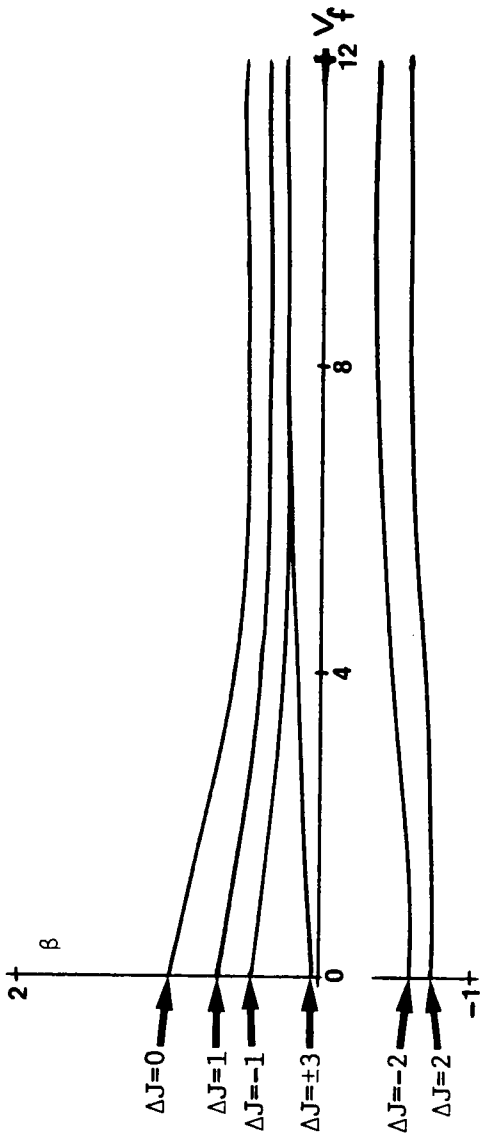


Fig. 10-30. (Continued).

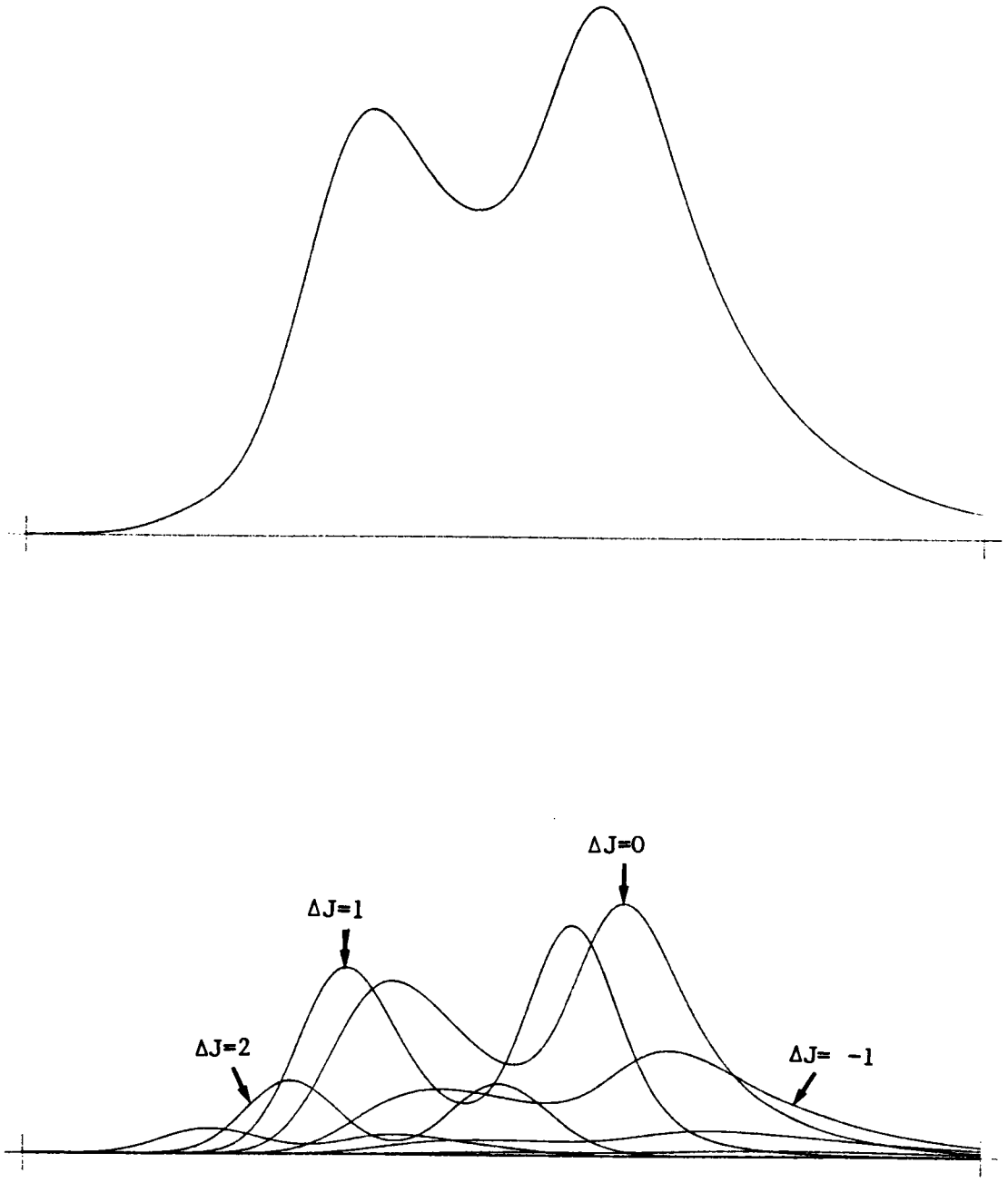


Fig. 10-31. The isotropic component of the vibronic band with v_f=0 and its individual branches in the $(1\pi)^{-1}$ photoionization of CO at T = 300K.

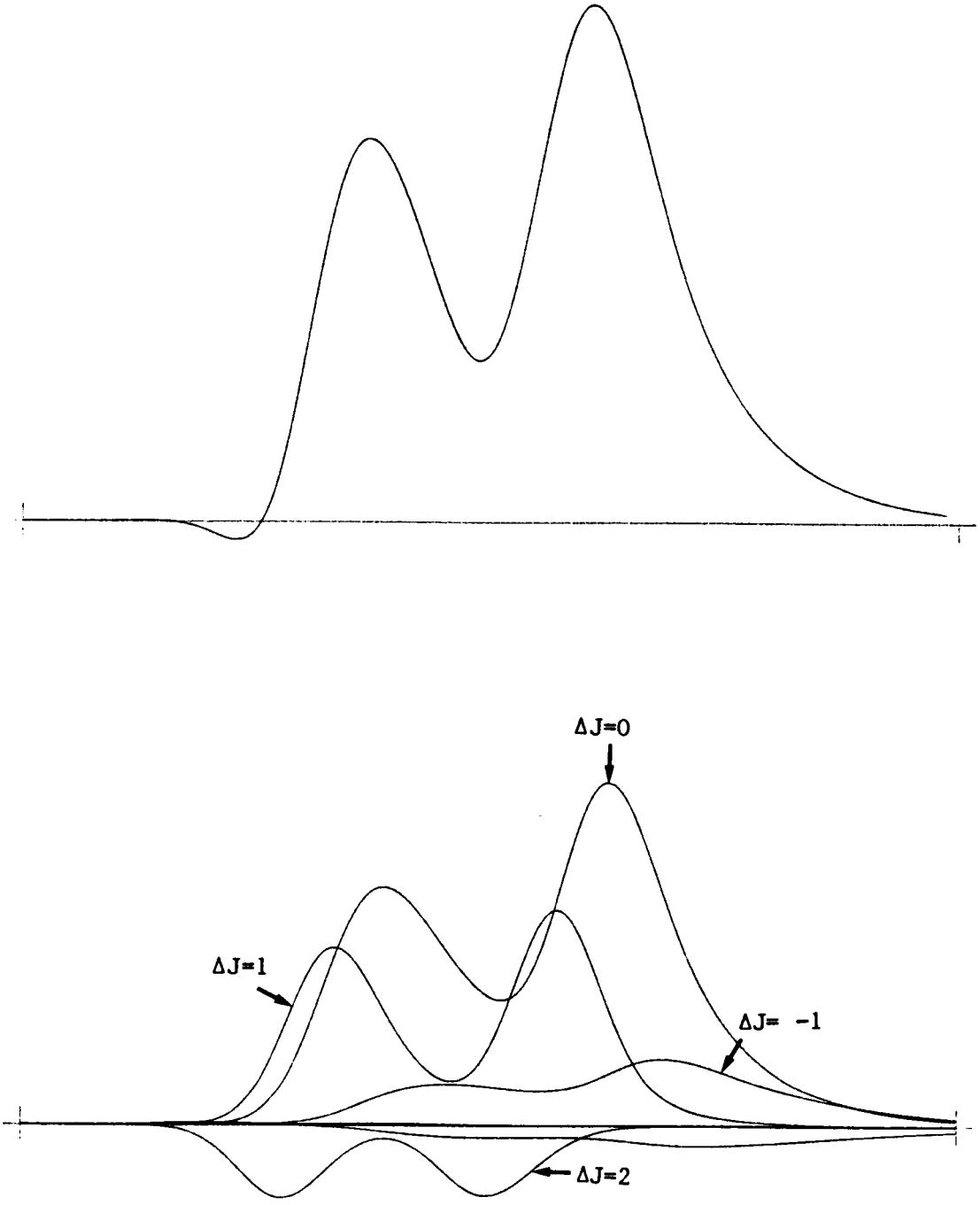


Fig. 10-32. The anisotropic component of the vibronic band with v_f=0 and its individual branches in the $(1\pi)^{-1}$ photoionization of CO at T = 300K.

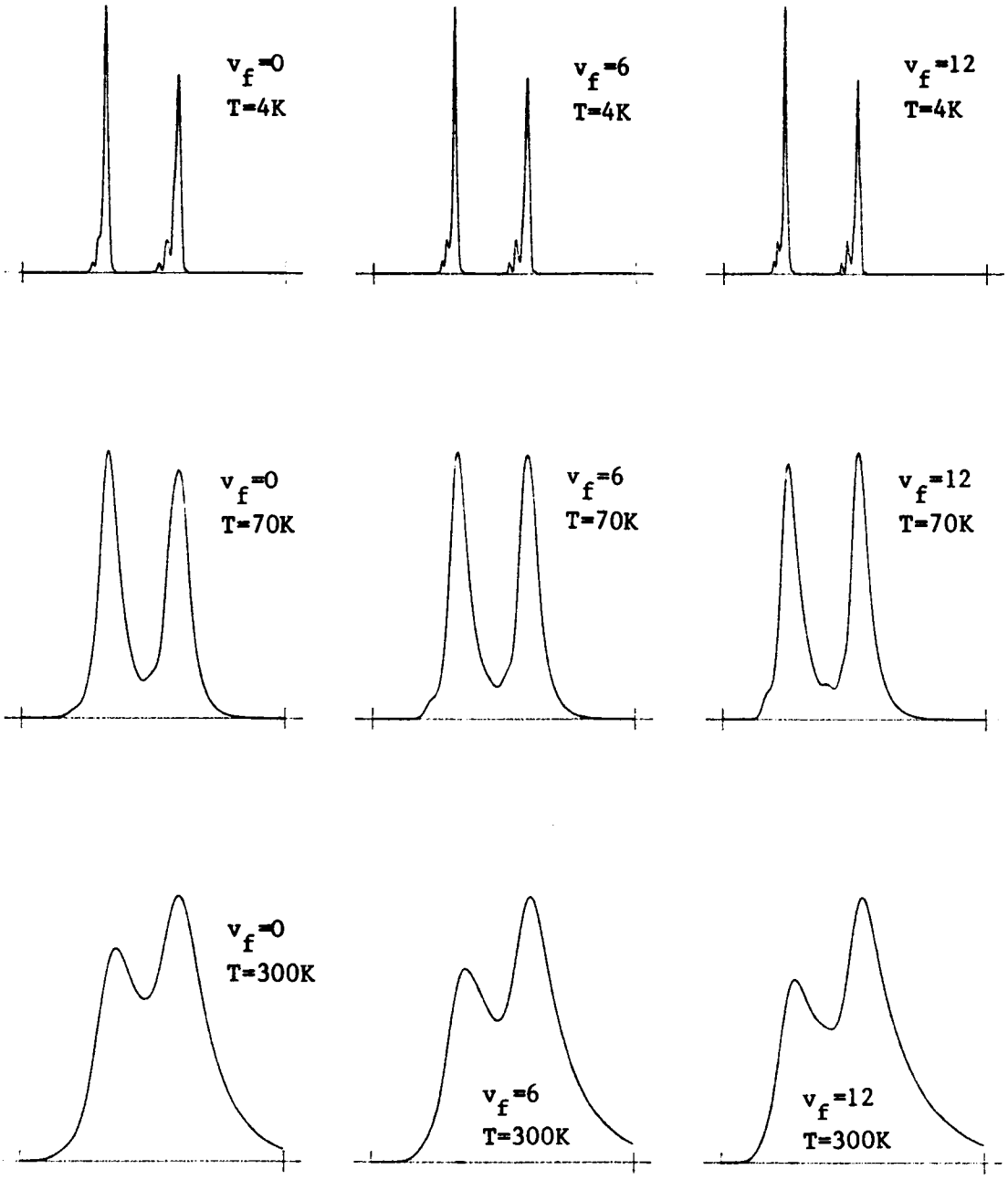


Fig. 10-33. Vibronic band contours in the $(1\pi)^{-1}$ photoionization of CO at different temperatures.

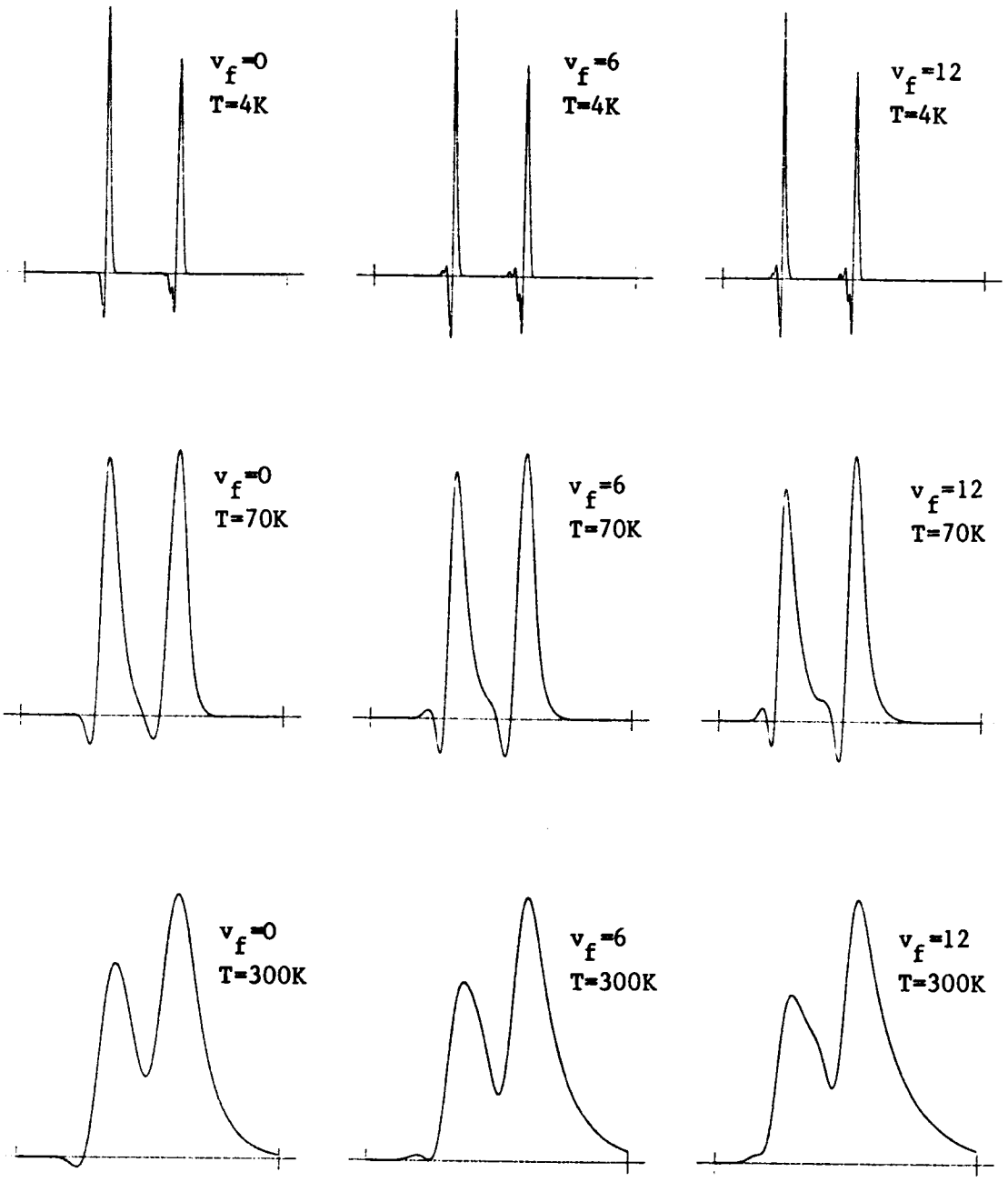


Fig. 10-34. Contours of the anisotropic component of three vibronic bands in the $(1\pi)^{-1}$ photoionization of CO at different temperatures.

$$-520\ cm^{-1} \leq \Delta E_{nucl} \leq -120\ cm^{-1} \text{ for } v_f=0$$

$$8280\ cm^{-1} \leq \Delta E_{nucl} \leq 8680\ cm^{-1} \text{ for } v_f=6$$

$$16080\ cm^{-1} \leq \Delta E_{nucl} \leq 16480\ cm^{-1} \text{ for } v_f=12$$

The relative cross sections of the rovibronic bands shown in Table 10-63 were obtained from cross sections expressed in megabarns by applying scaling factors of 3.96 (10^3), 4.05 (10^3), and 2.28 (10^5), for members of the vibronic bands with v_f=0,6, and 12 respectively.

7. The Photoionization of the 4σ Level of Carbon Monoxide

The ionization potential of the vibronic band with v_f=0 is roughly 19.7 eV.[16] The photoelectrons emitted by 58.4 nm photons will be rather close to threshold, where the cross sections and β values change strongly with the internuclear separation. In Table 10-69, the cross sections and β values can be seen to be strongly affected by r_{CO}.

The experimental β value of the vibronic band, with v_f=0, is given as 0.41 by Sell et al.,[518] and as 0.35 by Kreile and Schweig.[643] The β values of the higher members of the vibronic progressions differ drastically among different sources in the literature. Kreile and Schweig gave β values for the vibronic bands with v_f>0 which did not differ much from the β value of the first vibronic band in the vibronic progression. They measured, for the vibronic bands with v_f=1 and v_f=2, β values of 0.31 and 0.50 respectively.

However, Sell et al.[518] gave β values of 0.54, 1.03, 0.63, and 1.22 for the vibronic bands with v_f=1,2,3, and 4 respectively.

TABLE 10-69

PHOTOIONIZATION CROSS SECTIONS AND BETA VALUES OF CARBON MONOXIDE

$CO(X^1\Sigma^+) \rightarrow CO^+(B^2\Sigma^+) + e^-$

σ (Mb)

Channel	$r_{CO}(a_o)$	E_e=0.05 Ryd	E_e=0.07 Ryd	E_e=0.09 Ryd	E_e=0.11 Ryd
$4\sigma \rightarrow k\sigma$	1.9	1.13	1.14	1.14	1.14
	2.05	0.90	0.90	0.90	0.90
	2.2	0.69	0.69	0.70	0.71
	2.35	0.66	0.74	0.85	0.10
	2.5	4.16	5.16	5.73	5.73
$4\sigma \rightarrow k\pi$	1.9	0.62	0.62	0.62	0.62
	2.05	0.42	0.43	0.44	0.45
	2.2	0.32	0.34	0.36	0.38
	2.35	0.32	0.35	0.38	0.41
	2.5	0.41	0.44	0.48	0.52

β

$r_{CO}(a_o)$	E_e=0.05 Ryd	E_e=0.07 Ryd	E_e=0.09 Ryd	E_e=0.11 Ryd
1.9	1.45	1.46	1.46	1.46
2.05	1.31	1.29	1.27	1.24
2.2	0.93	0.86	0.79	0.71
2.35	0.25	0.10	0.00	-0.07
2.5	0.82	0.89	0.98	1.08

There also seems to be little agreement, among different sources, regarding the relative cross sections of the vibronic bands. Sell et al. gave relative cross sections, which were uncorrected for detection efficiency:

100, 43, 17, 10, 10, 9, 9

for vibronic bands with v_f=0,1 ..., 6 respectively. Gardner and Samson apparently observed only the vibronic bands with v_f=0,1, and 2, having relative cross sections of 100, 35, and 8 respectively. From the data shown in Table 10-70, we obtain relative vibronic cross sections, computed with the RD method, which are:

100, 41, 13, 3, 0.5

Since the higher members of the vibronic progression reach pretty close to threshold, one can expect autoionization to play a prominent role. Autoionization is expected to lower the observed β values of these vibronic bands.

In Table 10-71 and in Table 10-72, the relative cross sections and the β values of individual rovibronic bands are shown. The relative cross sections were obtained from cross sections which were expressed in megabarns, by applying the scaling factors 4.99 (10^3), 5.89 (10^4), and 1.01 (10^6) for members of the vibronic bands with v_f=0,2, and 4 respectively.

In Tables 10-73, 10-74, 10-75, 10-76, and 10-77, the relative cross sections and β values of individual branches of all five vibronic bands are shown.

In Figure 10-35, some of these data have been graphed.

TABLE 10-70

VIBRONIC INTENSITIES AND BETA VALUES FOR THE PHOTOIONIZATION OF THE 4σ LEVEL OF CO AT DIFFERENT ROTATIONAL TEMPERATURES

σ(Mb)

	T=4K			T=60K			T=300K			
v_f	FR_{vr}	RD	RD_{vr}	FR_{vr}	RD	RD_{vr}	FR_{vr}	RC_{vr}	RD	RD_{vr}
0	0.76008	0.71294	0.71287	0.75972	0.71294	0.71249	0.75771	0.70985	0.71258	0.71054
1	0.26904	0.28856	0.28888	0.26914	0.28854	0.28882	0.26970	0.30574	0.28834	0.28868
2	0.05556	0.09145	0.09155	0.05565	0.09146	0.09159	0.05604	0.07283	0.09141	0.09176
3	0.00924	0.02381	0.02382	0.00927	0.02381	0.02389	0.00937	0.01301	0.02378	0.02415
4	0.00147	0.00363	0.00363	0.00148	0.00364	0.00366	0.00150	0.00235	0.00364	0.00375

β

	T=4K			T=60K			T=300K			
v_f	FR_{vr}	RD	RD_{vr}	FR_{vr}	RD	RD_{vr}	FR_{vr}	RC_{vr}	RD	RD_{vr}
0	0.999	0.561	0.561	0.999	0.561	0.560	0.998	0.458	0.561	0.554
1	1.038	1.221	1.220	1.039	1.221	1.219	1.038	1.353	1.221	1.211
2	1.074	1.661	1.660	1.073	1.661	1.660	1.073	1.461	1.661	1.659
3	1.105	1.638	1.636	1.105	1.637	1.636	1.105	1.380	1.638	1.637
4	1.133	1.629	1.629	1.133	1.628	1.625	1.133	1.498	1.629	1.627

FR, RC, and RD, and the subscript "vr" refer to different methods of computation as described in the text.

TABLE 10-71

SCALED PHOTOIONIZATION CROSS SECTIONS FOR $CO(X^1\Sigma^+) \rightarrow CO^+(B^2\Sigma^+) + e^-$ ($h\nu$=21.2 eV)

v_f	J_i	$\Delta J = -4$	$\Delta J = -3$	$\Delta J = -2$	$\Delta J = -1$	$\Delta J = 0$	$\Delta J = 1$	$\Delta J = 2$	$\Delta J = 3$	$\Delta J = 4$
0	0					464	1660	1338	32	63
0	1				553	1000	1120	831	18	35
0	2			268	672	865	1004	704	15	29
0	3		5	357	717	833	955	650	14	26
0	4	7	6	393	743	822	928	620	13	24
0	5	10	7	416	759	817	910	600	13	23
0	6	11	7	432	771	814	898	586	12	22
0	12	15	8	475	797	807	861	549	11	20
0	24	18	8	504	795	797	825	529	9	19
2	0					825	3562	438	523	46
2	1				1186	1000	2600	284	299	25
2	2			87	1558	963	2279	238	249	21
2	3		75	121	1625	950	2161	220	227	18
2	4	5	99	131	1677	947	2098	210	214	17
2	5	7	113	138	1711	945	2059	204	205	16
2	6	8	122	143	1736	944	2033	200	199	16
2	12	11	142	157	1805	946	1970	191	182	13
2	24	11	150	168	1854	960	1960	197	172	11
4	0					904	2006	239	465	37
4	1				667	1000	1539	160	267	21
4	2			48	919	984	1334	134	224	17
4	3		66	68	946	976	1266	123	205	15
4	4	4	87	73	975	975	1232	118	194	15
4	5	5	99	77	996	975	1214	115	188	14
4	6	6	107	80	1013	976	1204	113	184	14
4	12	9	127	88	1082	991	1216	110	179	14
4	24	13	149	98	1254	1051	1397	120	202	19

TABLE 10-72

BETA VALUES FOR $CO(X^1\Sigma^+) \rightarrow CO^+(B^2\Sigma^+) + e^-$ ($h\nu$=21.2 eV)

v_f	J_i	$\Delta J = -4$	$\Delta J = -3$	$\Delta J = -2$	$\Delta J = -1$	$\Delta J = 0$	$\Delta J = 1$	$\Delta J = 2$	$\Delta J = 3$	$\Delta J = 4$
0	0					2.00	1.26	−0.80	0.89	0.30
0	1				1.26	0.50	1.25	−0.76	0.88	0.30
0	2			−0.80	1.25	0.73	1.26	−0.77	0.88	0.30
0	3		0.89	−0.76	1.25	0.78	1.26	−0.77	0.88	0.30
0	4	0.30	0.89	−0.77	1.25	0.79	1.25	−0.78	0.88	0.30
0	5	0.30	0.89	−0.77	1.25	0.80	1.25	−0.78	0.88	0.30
0	6	0.30	0.89	−0.77	1.25	0.81	1.25	−0.78	0.88	0.30
0	12	0.30	0.91	−0.77	1.24	0.81	1.25	−0.78	0.89	0.30
0	24	0.30	0.97	−0.77	1.21	0.79	1.22	−0.78	0.93	0.30
2	0					2.00	2.00	0.01	0.33	0.37
2	1				2.00	1.65	1.85	0.03	0.33	0.37
2	2			0.01	1.85	1.72	1.89	0.02	0.33	0.37
2	3		0.33	0.04	1.89	1.74	1.90	0.02	0.33	0.37
2	4	0.37	0.33	0.04	1.90	1.75	1.91	0.02	0.33	0.37
2	5	0.37	0.33	0.04	1.91	1.75	1.91	0.01	0.33	0.37
2	6	0.37	0.33	0.04	1.91	1.75	1.91	0.01	0.33	0.37
2	12	0.37	0.33	0.03	1.91	1.75	1.91	−0.02	0.33	0.37
2	24	0.37	0.33	0.00	1.91	1.74	1.91	−0.10	0.33	0.38
4	0					2.00	1.94	0.39	0.30	0.36
4	1				1.94	1.85	1.73	0.38	0.30	0.36
4	2			0.39	1.73	1.87	1.79	0.38	0.30	0.36
4	3		0.30	0.39	1.79	1.88	1.80	0.38	0.30	0.36
4	4	0.36	0.30	0.39	1.80	1.89	1.80	0.39	0.30	0.36
4	5	0.36	0.30	0.40	1.80	1.89	1.80	0.39	0.30	0.36
4	6	0.36	0.30	0.40	1.80	1.89	1.80	0.39	0.30	0.36
4	12	0.36	0.30	0.44	1.80	1.89	1.81	0.42	0.30	0.36
4	24	0.36	0.30	0.58	1.79	1.90	1.80	0.53	0.30	0.36

TABLE 10-73

RELATIVE INTENSITIES AND AVERAGE BETA VALUES OF THE BRANCHES IN THE PHOTOIONIZATION OF THE 4σ LEVEL OF CO FOR v_f=0

Rel. Intensities (% of the Intensity of the Vibronic Band)

	T=4K		T=60K		T=300K			
ΔJ	FR_{vr}	RD_{vr}	FR_{vr}	RD_{vr}	FR_{vr}	RC_{vr}	RD	RD_{vr}
0	19	20	22	23	21	24	23	23
-1	8	7	23	19	25	21	21	21
1	47	40	33	28	30	25	26	25
-2			7	9	9	12	12	12
2	23	31	14	19	12	17	17	17
-3					1			
3	2	1	1		1			
4		1		1		1	1	1

Average Beta Values of the Branches

	T=4K		T=60K		T=300K			
ΔJ	FR_{vr}	RD_{vr}	FR_{vr}	RD_{vr}	FR_{vr}	RC_{vr}	RD	RD_{vr}
0	1.28	1.05	1.03	0.77	1.06	0.80	0.80	0.80
-1	1.66	1.26	1.65	1.25	1.65	1.09	1.25	1.25
1	1.66	1.26	1.65	1.25	1.65	1.10	1.26	1.25
-2	-0.72	-0.80	-0.71	-0.77	-0.71	-0.80	-0.77	-0.77
2	-0.71	-0.79	-0.71	-0.78	-0.71	-0.81	-0.78	-0.78
-3	0.54	0.89	0.54	0.89	0.54	1.00	0.90	0.91
3	0.54	0.88	0.54	0.88	0.54	0.97	0.88	0.89
-4	0.28	0.30	0.28	0.30	0.28	0.30	0.30	0.30
4	0.28	0.30	0.28	0.30	0.28	0.30	0.30	0.30
-5	0.31	0.31	0.31	0.31	0.31	0.31	0.31	0.31
5	0.31	0.31	0.31	0.31	0.31	0.31	0.31	0.31

TABLE 10-74

RELATIVE INTENSITIES AND AVERAGE BETA VALUES OF THE BRANCHES IN THE PHOTOIONIZATION OF THE 4σ LEVEL OF CO FOR $v_f=1$

Rel. Intensities (% of the Intensity of the Vibronic Band)

	T=4K		T=60K		T=300K			
ΔJ	FR_{vr}	RD_{vr}	FR_{vr}	RD_{vr}	FR_{vr}	RC_{vr}	RD	RD_{vr}
0	19	20	22	22	22	20	22	22
-1	9	9	23	24	26	29	27	27
1	48	50	34	36	31	34	32	32
-2			6	5	8	6	7	7
2	21	17	13	11	12	8	9	9
-3				1	1	1	1	1
3	2	3	1	2	1	2	2	2

Average Beta Values of the Branches

	T=4K		T=60K		T=300K			
ΔJ	FR_{vr}	RD_{vr}	FR_{vr}	RD_{vr}	FR_{vr}	RC_{vr}	RD	RD_{vr}
0	1.34	1.49	1.10	1.29	1.13	1.36	1.32	1.31
-1	1.66	1.76	1.64	1.73	1.64	1.83	1.73	1.73
1	1.65	1.75	1.64	1.73	1.64	1.83	1.73	1.72
-2	-0.77	-0.73	-0.76	-0.73	-0.76	-0.60	-0.73	-0.73
2	-0.76	-0.73	-0.76	-0.73	-0.76	-0.60	-0.73	-0.74
-3	0.51	0.46	0.51	0.46	0.52	0.40	0.46	0.46
3	0.51	0.46	0.51	0.46	0.51	0.40	0.46	0.46
-4	0.29	0.25	0.29	0.25	0.29	0.42	0.25	0.25
4	0.29	0.25	0.29	0.25	0.29	0.42	0.25	0.26
-5	0.32	0.31	0.32	0.31	0.32	0.32	0.31	0.31
5	0.32	0.32	0.32	0.32	0.32	0.33	0.32	0.32

TABLE 10-75

RELATIVE INTENSITIES AND AVERAGE BETA VALUES OF THE BRANCHES IN THE PHOTOIONIZATION OF THE 4σ LEVEL OF CO FOR v_f=2

Rel. Intensities (% of the Intensity of the Vibronic Band)

	T=4K		T=60K		T=300K			
ΔJ	FR_{vr}	RD_{vr}	FR_{vr}	RD_{vr}	FR_{vr}	RC_{vr}	RD	RD_{vr}
0	20	17	22	18	22	25	17	18
-1	9	10	23	28	26	27	32	32
1	48	58	34	42	32	33	38	38
-2			5	2	7	4	3	3
2	20	7	12	4	11	6	4	4
-3				1	1	2	2	2
3	3	8	2	4	1	3	4	4
4		1						

Average Beta Values of the Branches

	T=4K		T=60K		T=300K			
ΔJ	FR_{vr}	RD_{vr}	FR_{vr}	RD_{vr}	FR_{vr}	RC_{vr}	RD	RD_{vr}
0	1.39	1.83	1.17	1.74	1.20	1.63	1.75	1.75
-1	1.66	1.98	1.64	1.90	1.64	1.82	1.91	1.91
1	1.65	1.94	1.64	1.90	1.64	1.82	1.91	1.91
-2	-0.81	0.02	-0.80	0.03	-0.80	-0.54	0.04	0.03
2	-0.81	0.02	-0.80	0.02	-0.80	-0.55	0.02	0.00
-3	0.50	0.33	0.50	0.33	0.50	0.36	0.33	0.33
3	0.50	0.33	0.49	0.33	0.49	0.36	0.33	0.33
-4	0.30	0.37	0.30	0.37	0.30	0.43	0.37	0.37
4	0.30	0.37	0.30	0.37	0.30	0.43	0.37	0.37
-5						0.33		
5		0.39		0.38		0.33	0.39	0.38

TABLE 10-76

RELATIVE INTENSITIES AND AVERAGE BETA VALUES OF THE BRANCHES IN THE PHOTOIONIZATION OF THE 4σ LEVEL OF CO FOR v_f=3

Rel. Intensities (% of the Intensity of the Vibronic Band)

	T=4K		T=60K		T=300K			
ΔJ	FR_{vr}	RD_{vr}	FR_{vr}	RD_{vr}	FR_{vr}	RC_{vr}	RD	RD_{vr}
0	20	17	22	18	22	32	18	18
-1	9	10	24	28	27	24	31	31
1	49	56	35	41	32	29	37	37
-2			5	1	7	4	2	2
2	18	5	11	3	10	6	3	3
-3				2	1	2	3	3
3	3	10	2	6	1	3	5	5
4		2		1			1	1

Average Beta Values of the Branches

	T=4K		T=60K		T=300K			
ΔJ	FR_{vr}	RD_{vr}	FR_{vr}	RD_{vr}	FR_{vr}	RC_{vr}	RD	RD_{vr}
0	1.45	1.93	1.23	1.87	1.26	1.72	1.88	1.88
-1	1.65	1.90	1.63	1.80	1.63	1.65	1.80	1.80
1	1.64	1.85	1.63	1.80	1.63	1.65	1.81	1.81
-2	-0.84	0.85	-0.84	0.79	-0.84	-0.68	0.79	0.80
2	-0.84	0.81	-0.84	0.77	-0.84	-0.68	0.77	0.76
-3	0.48	0.30	0.48	0.30	0.48	0.35	0.30	0.30
3	0.48	0.30	0.48	0.30	0.48	0.35	0.30	0.30
-4	0.31	0.35	0.31	0.35	0.31	0.30	0.35	0.35
4	0.31	0.35	0.31	0.35	0.31	0.30	0.35	0.35
-5						0.34		
5						0.34		

TABLE 10-77

RELATIVE INTENSITIES AND AVERAGE BETA VALUES OF THE BRANCHES IN THE PHOTOIONIZATION OF THE 4σ LEVEL OF CO FOR v_f=4

Rel. Intensities (% of the Intensity of the Vibronic Band)

	T=4K		T=60K		T=300K			
ΔJ	FR_{vr}	RD_{vr}	FR_{vr}	RD_{vr}	FR_{vr}	RC_{vr}	RD	RD_{vr}
0	21	26	23	27	23	34	27	26
-1	9	9	24	24	27	23	27	27
1	50	49	36	36	33	29	32	33
-2			5	2	6	3	2	2
2	17	6	11	4	9	4	3	3
-3			1	2	1	2	3	3
3	3	10	2	6	2	4	5	5
4		1		1				

Average Beta Values of the Branches

	T=4K		T=60K		T=300K			
ΔJ	FR_{vr}	RD_{vr}	FR_{vr}	RD_{vr}	FR_{vr}	RC_{vr}	RD	RD_{vr}
0	1.50	1.93	1.30	1.88	1.32	1.83	1.89	1.89
-1	1.64	1.91	1.61	1.80	1.61	1.68	1.80	1.80
1	1.62	1.86	1.61	1.80	1.61	1.68	1.80	1.80
-2	-0.87	0.39	-0.87	0.39	-0.86	-0.33	0.39	0.43
2	-0.87	0.38	-0.87	0.39	-0.87	-0.34	0.37	0.41
-3	0.47	0.30	0.47	0.30	0.47	0.32	0.30	0.30
3	0.46	0.30	0.46	0.30	0.46	0.32	0.30	0.30
-4	0.32	0.36	0.32	0.36	0.32	0.39	0.36	0.36
4	0.32	0.36	0.32	0.36	0.32	0.39	0.36	0.36
-5						0.35		
5						0.35		

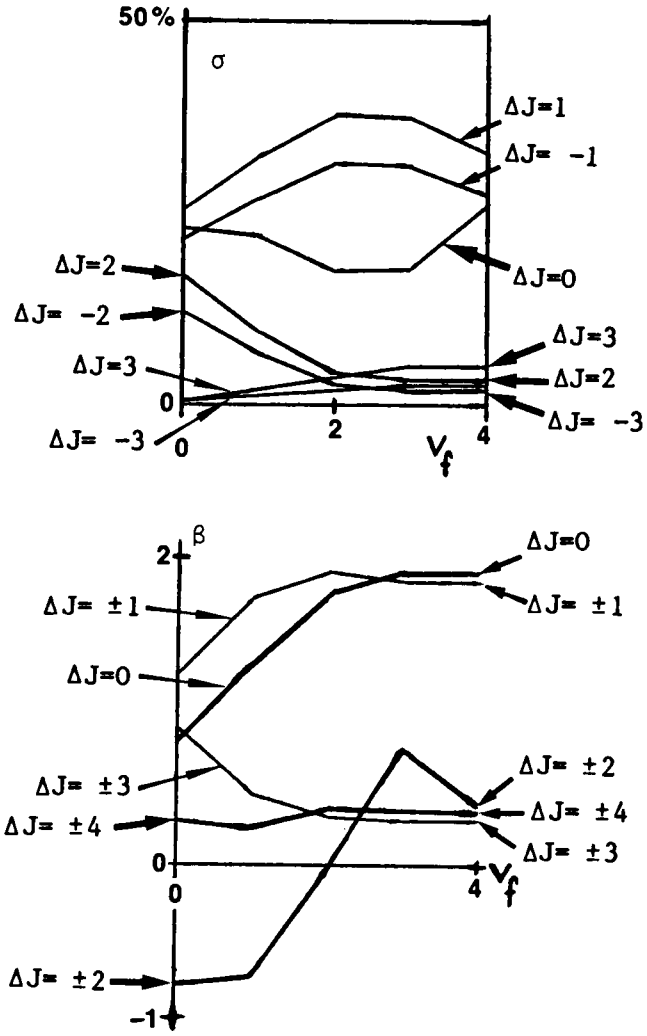


Fig. 10-35. The cross sections of the branches in the $(4\sigma)^{-1}$ photoionization of CO, expressed in % of the vibronic cross sections, and their average β values.

The results shown here were obtained in the RD_{vr} approximation at T_{rot}=300K.

In the photoionization of the 5σ level, the Q branch had the highest cross section. Here we find that the R branch has the highest cross section in all five vibronic bands. Even at room temperature, (T=300K), branches with the same $|\Delta J|$ have cross sections which differ considerably. Because of this, the vibronic bands are expected to have highly asymmetrical band contours. The lengths of the graphs with the band contours shown in Figures 10-36, 10-37, 10-38, and 10-39, expressed in terms of ΔE_{nucl}, are:

$$-400 \text{ cm}^{-1} \leq \Delta E_{nucl} \leq 0 \qquad \text{if } v_f=0$$

$$2900 \text{ cm}^{-1} \leq \Delta E_{nucl} \leq 3300 \text{ cm}^{-1} \qquad \text{if } v_f=2$$

$$5950 \text{ cm}^{-1} \leq \Delta E_{nucl} \leq 6350 \text{ cm}^{-1} \qquad \text{if } v_f=4$$

where ΔE_{nucl} decreases from left to right.

8. Vibrationally Averaged Cross Sections and β Values

In order to compute the vibrationally averaged cross sections and β values from the vibronic cross sections and β values, one can make use of the formulae shown in (10-34) and (10-35).

However, according to Swanson, Dill, and Dehmer,[574] the vibrationally averaged cross sections and β values can be obtained without computing these two quantities for each vibronic band in the vibronic progression. Earlier in this chapter, it has been pointed out that the formulae by Swanson et al.[574] represent approximate relationships. Swanson et al. are well aware of this fact, and they point out the approximation involved in the derivation of their formulae. These

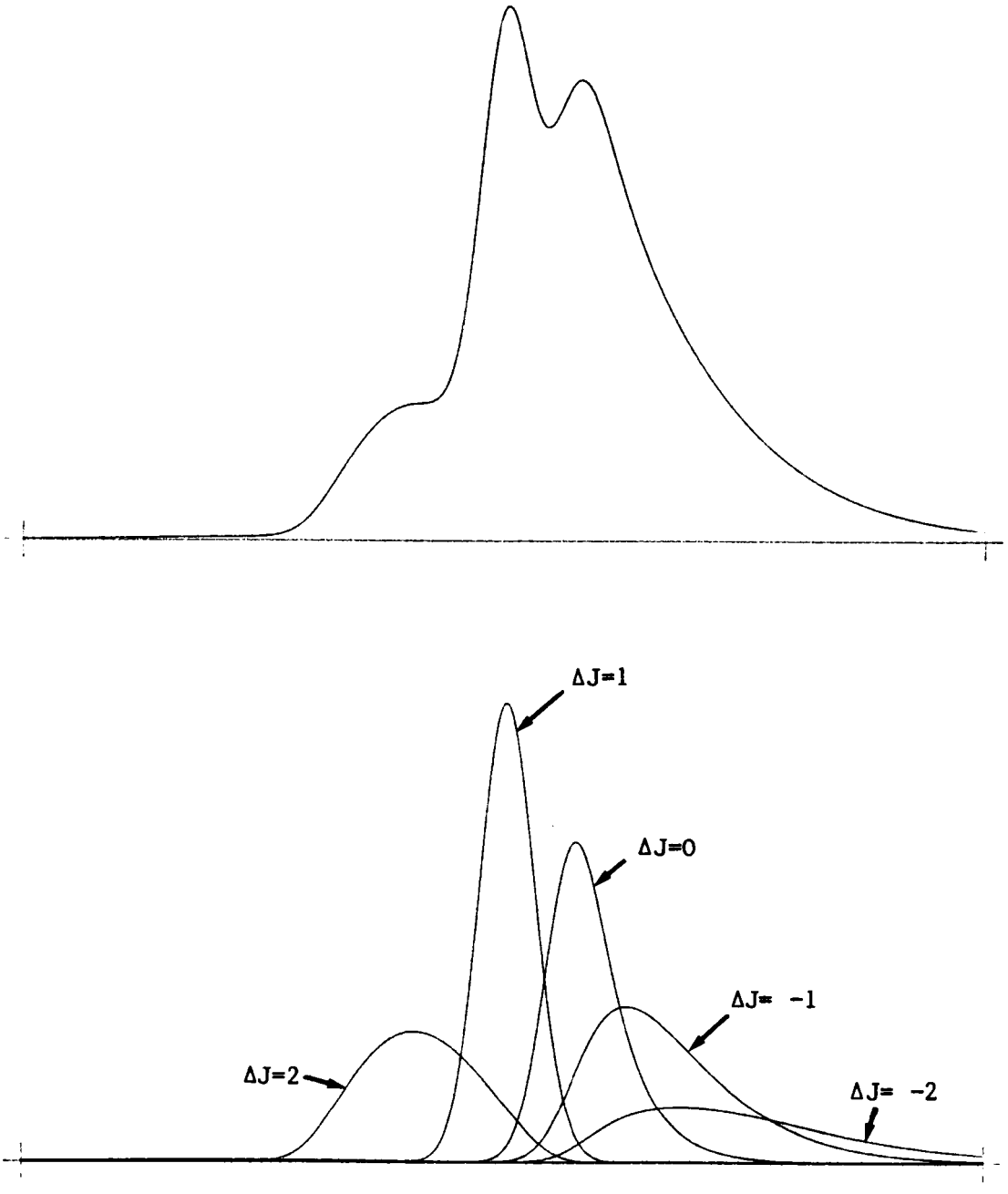


Fig. 10-36. The isotropic component of the vibronic band with v_f=0 and its individual branches in the $(4\sigma)^{-1}$ photoionization of CO at T = 300K.

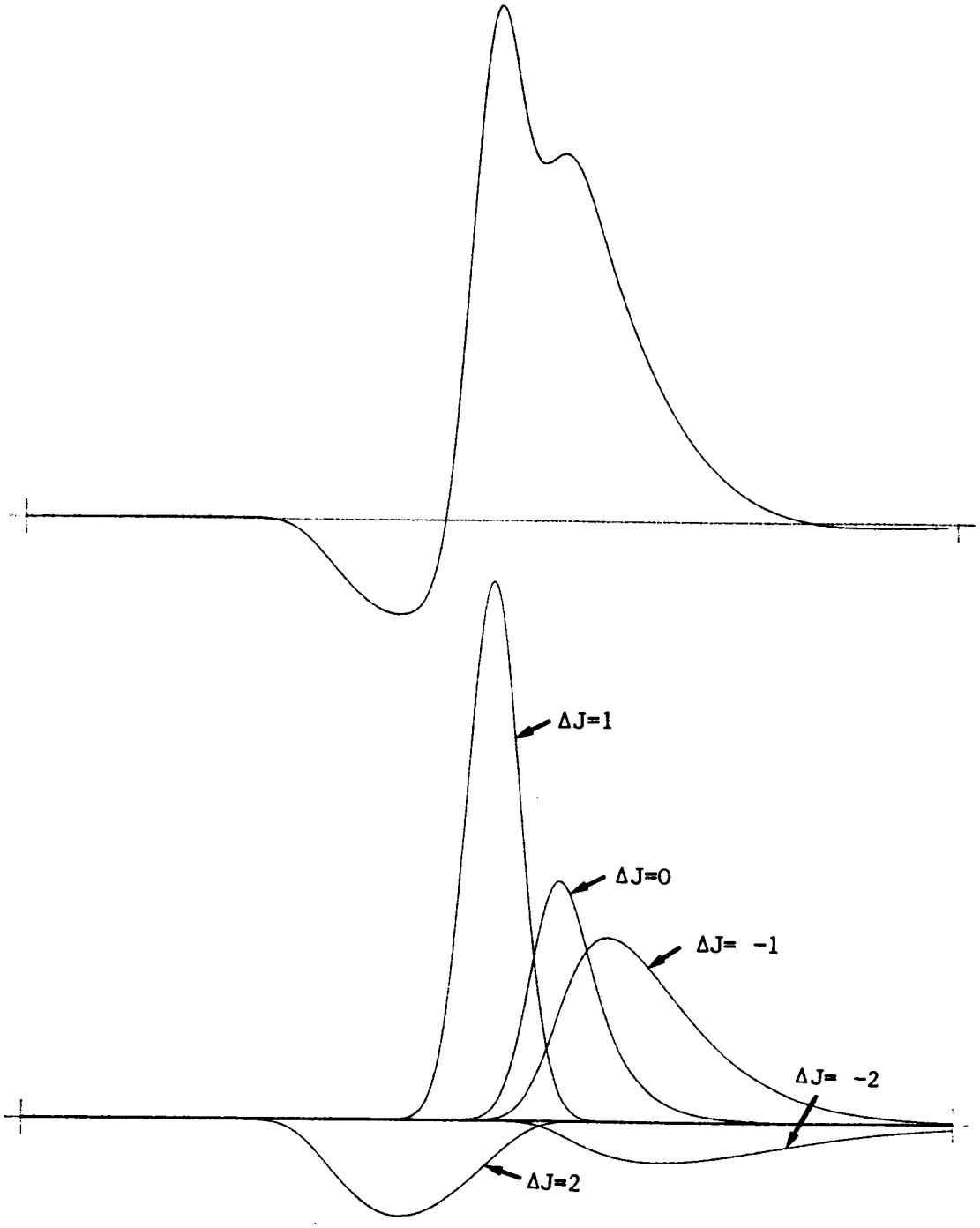


Fig. 10-37. The anisotropic component of the vibronic band with $v_f=0$ and its individual branches in the $(4\sigma)^{-1}$ photoionization of CO at T = 300K.

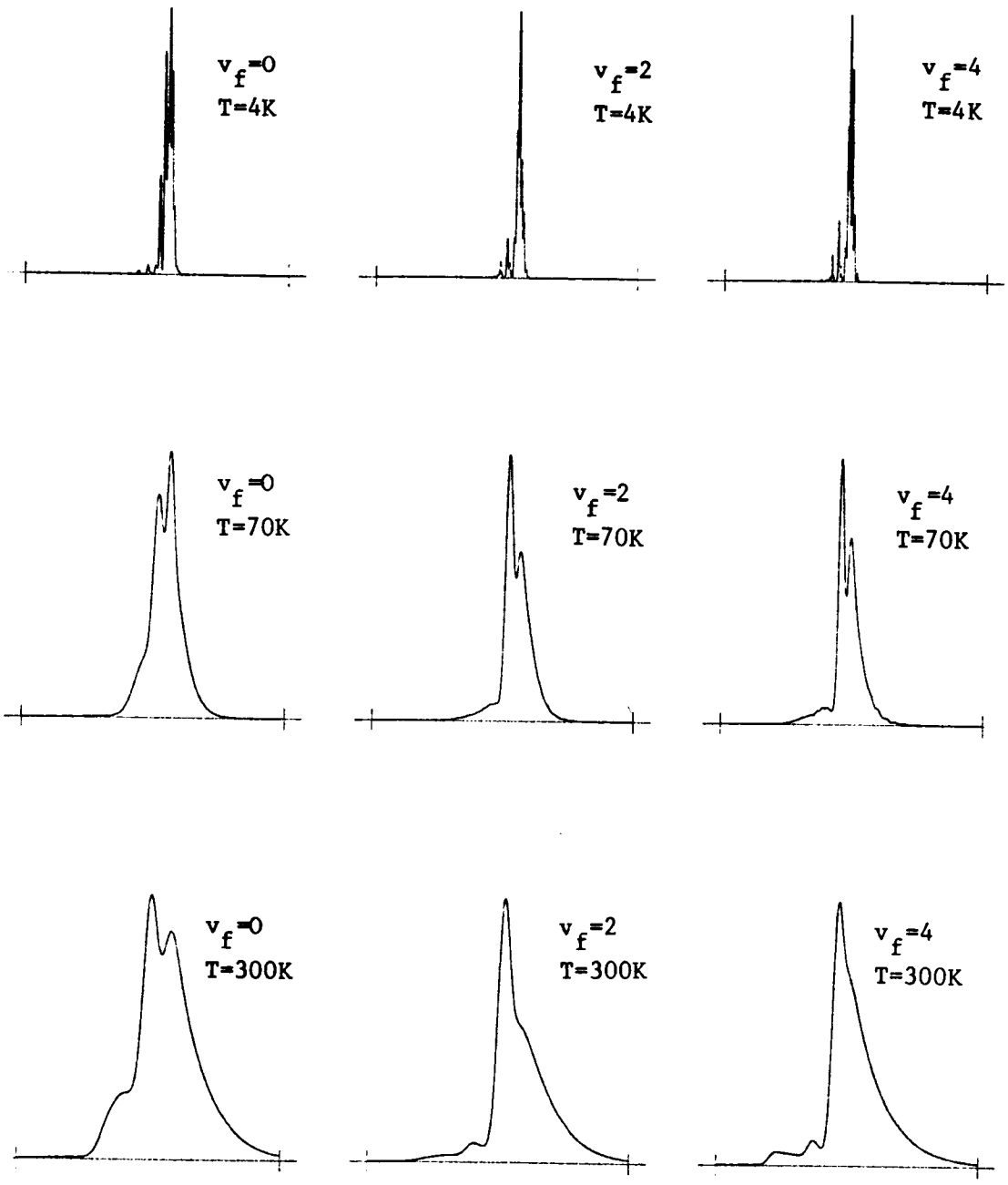


Fig. 10-38. Vibronic band contours in the $(4\sigma)^{-1}$ photoionization of CO at different temperatures.

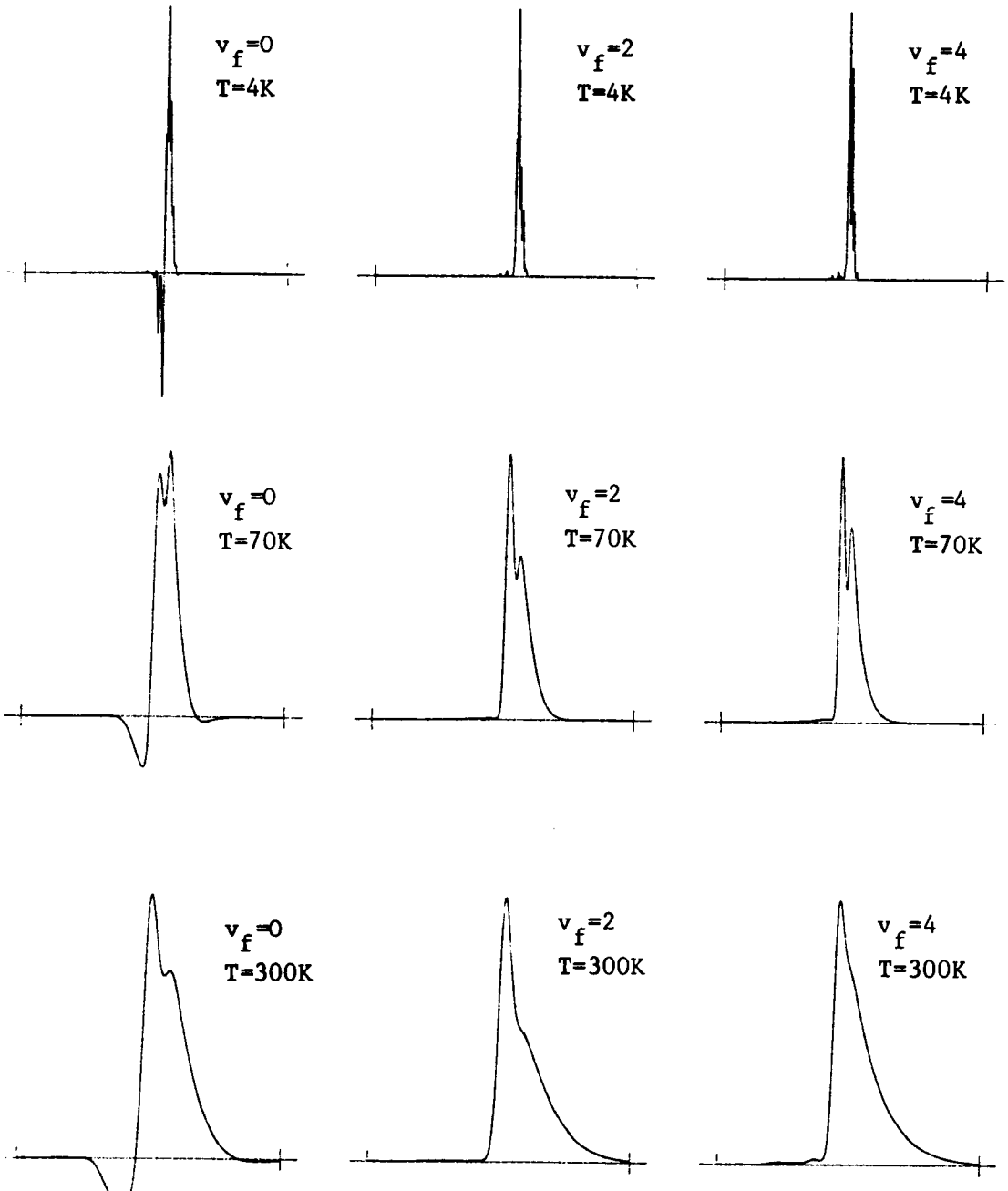


Fig. 10-39. Contours of the anisotropic component of three vibronic bands in the $(4\sigma)^{-1}$ photoionization of CO at different temperatures.

authors apparently considered an averaging procedure in which E_e is kept constant and the vibronic progression is measured by sweeping E_{ph}. Here, we probe the validity of the averaging formulae when applied to the more common experimental apporoach, where the vibronic progression is observed at a fixed energy of the photons. It has been mentioned that a severe disagreement of the formulae for vibrational averaging with values obtained by explicit vibrational averaging would be expected mainly for long vibronic progressions in the presence of a shape resonance.

There is also some uncertainty about the relationship between E_e and E_{ph}, when using the formulae for vibrational averaging for long vibronic progressions, since, at a fixed E_{ph}, the energy of the photoelectron is different for each vibronic band. E_e can differ considerably between the first and the last members of the vibronic progression.

In Tables 10-78, 10-79, and 10-80, the vibrationally averaged cross sections and β values are shown for H_2, HD, and D_2. The results obtained with (10-41) and (10-42) are said to have been obtained by "closure" in these Tables.

For H_2, the results obtained by using (10-41) and (10-42) agree with values obtained by explicit averaging between an energy of the photoelectrons located between the values E_e of the vibronic bands with v_f=2 and v_f=3. According to Table 10-16, these bands are also the two members of the vibronic progression having the largest cross sections.

In HD, according to Table 10-17 (p 309), the vibronic band with v_f=3 has the largest cross section. The explicitly and "implicitly"

TABLE 10-78

VIBRATIONALLY AVERAGED CROSS SECTIONS AND BETA VALUES OF H_2

v_f^a	$\langle\sigma\rangle$ (Mb)	$\langle\beta\rangle$	Method of computation
0	6.886	1.796	closure
1	7.105	1.796	closure
2	7.320	1.797	closure
3	7.530	1.797	closure
4	7.733	1.797	closure
5	7.928	1.798	closure
6	8.114	1.798	closure
7	8.289	1.798	closure
8	8.452	1.798	closure
9	8.600	1.798	closure
10	8.734	1.799	closure
11	8.852	1.799	closure
12	8.953	1.799	closure
	7.443	1.797	explicit averaging[b]

[a] v_f indicates the energy of the photoelectron and the energy of nuclear motion of the ion.

[b] The total cross section and the average beta value of $J_i=0$ obtained with the method RD

TABLE 10-79

VIBRATIONALLY AVERAGED CROSS SECTIONS AND BETA VALUES OF HD

v_f[a]	$\langle\sigma\rangle$ (Mb)	$\langle\beta\rangle$	Method of computation
0	6.920	1.797	closure
1	7.112	1.798	closure
2	7.301	1.798	closure
3	7.486	1.798	closure
4	7.668	1.799	closure
5	7.843	1.799	closure
6	8.013	1.799	closure
7	8.175	1.799	closure
8	8.329	1.799	closure
9	8.473	1.800	closure
10	8.607	1.800	closure
11	8.730	1.800	closure
12	8.842	1.800	closure
13	8.941	1.800	closure
14	9.027	1.800	closure
15	9.100	1.800	closure
	7.573	1.800	explicit averaging[b]

[a] v_f indicates the energy of the photoelectron and the energy of nuclear motion of the ion.

[b] The total cross section and the average beta value of $J_i=0$ obtained with the method RD.

TABLE 10-80

VIBRATIONALLY AVERAGED CROSS SECTIONS AND BETA VALUES OF D_2

v_f[a]	$\langle\sigma\rangle$ (Mb)	$\langle\beta\rangle$	Method of computation
0	6.957	1.798	closure
1	7.116	1.799	closure
2	7.274	1.799	closure
3	7.429	1.799	closure
4	7.581	1.800	closure
5	7.731	1.800	closure
6	7.877	1.800	closure
7	8.019	1.800	closure
8	8.156	1.801	closure
9	8.288	1.801	closure
10	8.414	1.801	closure
11	8.533	1.801	closure
12	8.646	1.801	closure
13	8.752	1.801	closure
14	8.850	1.801	closure
15	8.939	1.801	closure
16	9.020	1.801	closure
17	9.093	1.801	closure
18	9.157	1.802	closure
	7.660	1.802	explicit averaging[b]

[a] v_f indicates the energy of the photoelectron and the energy of nuclear motion of the ion.

[b] The total cross section and the average beta value of $J_i=0$ obtained with the method RD.

averaged results, shown in Table 10-79, agree for a value of E_e near the E_e of the vibronic band with v_f=3.

In D_2, according to Table 10-18 (p 310), the vibronic bands with v_f=3 and v_f=4 have the highest cross sections, but agreement between the two methods, for the computation of vibrationally averaged cross sections, is obtained for a value of E_e located between the energies of the photoelectrons from the vibronic lands with v_f=4 and v_f=5. The β values obtained through vibrational averaging change slowly with E_e, such that a matching of the β values would be unreliable in finding the value of E_e to be used in the vibrational averaging procedure with (10-41) and (10-42).

In the photoionizations of σ levels from N_2 and CO, the vibronic band with v_f=0 has always by far the highest cross section. Since the photoionizations of the σ levels often show strong effects of shape resonances, they would constitute a sensitive probe of the validity of the vibrational averaging procedure by Swanson et al., if, in addition, they would consist of long vibronic progressions. The latter, however, is not the case. At any rate, the results in Tables 10-81 and 10-82 show a match of the vibrationally averaged cross sections near the energy of the photoelectrons from the vibronic band with v_f=0 in all cases.

In the photoionization of the π levels from N_2 and CO, the vibrationally averaged β values obtained with (10-41) and (10-42) vary sufficiently to make a "match" for the cross sections, and for the β values, separately.

TABLE 10-81

VIBRATIONALLY AVERAGED CROSS SECTIONS AND BETA VALUES OF N_2

State of the ion	v_f^a	$\langle\sigma\rangle$(Mb)	$\langle\beta\rangle$	averaging procedure
X	0	7.95	0.59	closure
X	1	7.22	0.59	closure
X	2	6.48	0.60	closure
X		7.78	0.60	explicit averaging
A	0	20.78	0.41	closure
A	1	21.21	0.39	closure
A	2	21.65	0.37	closure
A	3	22.07	0.34	closure
A	4	22.48	0.32	closure
A	5	22.88	0.29	closure
A	6	23.25	0.26	closure
A	7	23.59	0.23	closure
A	8	23.90	0.20	closure
A		21.40	0.38	explicit averaging
B	0	2.32	1.81	closure
B	1	2.28	1.79	closure
B	2	2.23	1.78	closure
B		2.32	1.81	explicit averaging

[a] v_f indicates the amount of energy which has been converted to energy of nuclear motion.

TABLE 10-82

VIBRATIONALLY AVERAGED CROSS SECTIONS AND BETA VALUES OF CO

State of the ion	v_f^a	$\langle\sigma\rangle$(Mb)	$\langle\beta\rangle$	averaging procedure
X	0	8.66	0.82	closure
X	1	8.55	0.84	closure
X	2	8.41	0.86	closure
X		8.63	0.82	explicit averaging
A	0	17.90	0.43	closure
A	1	18.19	0.42	closure
A	2	18.47	0.41	closure
A	3	18.75	0.39	closure
A	4	19.04	0.37	closure
A	5	19.33	0.35	closure
A	6	19.62	0.33	closure
A	7	19.92	0.31	closure
A	8	20.22	0.29	closure
A	9	20.52	0.26	closure
A	10	20.80	0.24	closure
A	11	21.07	0.22	closure
A	12	21.32	0.19	closure
A		19.01	0.38	explicit averaging
B	0	1.14	0.85	closure
B	1	1.11	0.91	closure
B	2	1.08	0.96	closure
B	3	1.05	1.00	closure
B	4	1.02	1.04	closure
B		1.12	0.84	explicit averaging

[a] v_f indicates the amount of energy which has been converted to energy of nuclear motion.

In the photoionization of the π_u level in N_2, the "match" occurs between the photoelectron energies of the vibronic bands with v_f=1 and v_f=2, for both, the vibrationally averaged cross sections and the vibrationally averaged β values. However, according to Table 10-41, the two vibronic bands with the highest cross sections are the ones with v_f=0 and v_f=1.

In the photoionization of the π level of CO, the "match" occurs for an energy of the photoelectron located between the energies of the photoelectrons from the vibronic bands with v_f=3 and v_f=4, but, according to Table 10-61, the vibronic bands with the highest cross sections have v_f=2 and v_f=3.

The investigation undertaken here has shown that vibrationally averaged cross sections and β values obtained with the formulae by Swanson *et al.*[574] tend to agree fairly well with results obtained through explicit averaging, if the energy E_e, at which the DMAPWs are computed, is taken as the energy of the photoelectrons from the vibronic band with the highest cross section. A more plausible choice for the "average" energy, $\bar{E}_e$, might be obtained by a weighted average:

$$\bar{E}_e = \sum_{v_f} \sigma(v_f \leftarrow v_i) E_e(v_f \leftarrow v_i) / \sum_{v_f} \sigma(v_f \leftarrow v_i) \qquad (10\text{-}50)$$

There are still some reservations about the validity of the formulae by Swanson *et al.*, if one is dealing with a long vibronic progression in the presence of a shape resonance.

The data used in this discussion have not been generated specifically for the purpose of testing the validity of these formulae.

In order to compute the vibrationally averaged cross sections and β values, the expectation values shown in (10-43) have to be computed. These expectation values become very small for large values of n. For example, for H_2, taking β_o=0, we obtain for S_n^o: 1.0000, 0.0221, 0.0084, 0.0007, and 0.0002 for n=0,1,2,3, and 4 respectively. For N_2, the maximum n for which S_n^o was computed was n=11, and for CO the highest n considered was 13. The remaining expectation values were set to zero. If the maximum of n was reduced by one, the results changed by a small fraction of a percent. For H_2 and its isotopically substituted derivatives, all expectation values were computed.

For the spin-orbit split band, the vibrationally averaged results were obtained with one calculation only, by taking the spin-orbit coupling constant as zero.

In the explicit vibrational averaging procedure, one is dealing - in principle - with a sum of an infinite number of terms. It seems that the neglected terms would change the sums by very little in all cases which have been examined in this work.

According to the above, experimental vibrationally averaged cross sections and β values have to be compared with cross sections and β values computed at an average energy, E_e, of the vibronic progression.

Notice that there is also an expected breakdown of the averaging procedure at threshold, simply because the "average" E_e of the vibronic progression becomes zero before the threshold of the lowest few members of the vibronic progression has been passed.

C. SUMMARY AND DISCUSSION

The vibrational branching ratios represent sensitive probes for the presence of resonances. In the case of shape resonances, anomalous, non-Franck-Condon branching ratios are observed due to the dependence of the dipole moment amplitudes on the molecular geometry.

Eland[481] has shown that the non-Franck-Condon behaviour of the vibrational branching ratios of O_2, near autoionizing resonance absorptions, does not signify a breakdown of the Franck-Condon approximation, in contrast to the case of the shape resonances.

An outcome of major importance of this work is that the sum rules for rotation turned out to be satisfied when considering vibration-rotation interaction, even in the presence of strong shape resonances. This is indicated by the fact that the cross sections and β values are nearly independent of the rotational temperature. Some minor effects of vibration-rotation interaction have been observed in the photoelectron spectra of H_2, HD, and D_2. Vibration-rotation interaction is expected to play only a minor role in the photoionization of most rigid molecules. Strong effects of vibration-rotation interaction cannot be ruled out in the presence of vibrational and/or rotational autoionization, even for rigid molecules.

The rotational sum rules are expected to break down at threshold, i.e., rotation has to be taken into account explicitly at threshold. This is expected to be the case because rotational autoionization takes place at threshold.

At threshold, we also expect a special set of rotational selection rules to go into effect. Consider an electron which has been

promoted to exactly the threshold. If the electron wishes to depart as a partial wave with $\ell>0$, it will have to overcome a "centrifugal" barrier. Being a "threshold" electron, it can do so only by tunneling with a correspondingly low probability of departure. If the electrons are being forced, in this manner, to depart almost exclusively as s waves, some rotational transitions become "forbidden." Schulz et al.[656] observed rotational structure in the threshold photodetachment of OH^- and OD^- with a tunable laser. The rotational selection rules, observed by Schulz et al., indicate that the electrons departed as s-waves.

In the photoionization of a σ_g level from a homonuclear diatomic molecule, the transitions into s-waves are not allowed. This fact, i.e., the "trapping" of the "threshold" electrons, may be responsible for the strong rotational autoionization of H_2 at threshold.[657]

At threshold, processes take place which have only recently been observed. In the extended fine structure in core ionization continued, (EXAFS, EXELFS),[658,659] oscillations are observed, which are related to the short-range order around the core-ionized atom. Recently, Raman resonance scattering involving electronic transitions has been observed across the K x-ray absorption edge.[660]

It has been mentioned that the rotational temperature of the sample could affect the angular distribution of the photoelectrons in the presence of longlived autoionizing resonances, and in the presence of competing nonradiative decay processes. Experimental evidence of competing channels of decay of autoionizing resonances have been observed on numerous occasions.[661] Baer and Guyon[662] observed fluorescent channels competing with autoionization. Since radiative decay

probabilities are not strongly affected by the rotational states, (in the absence of competing nonradiative decay processes), the presence of competing radiative decay channels may leave the angular distribution of photoelectrons independent of the rotational temperature. However, in most nonradiative conversion processes, total angular momentum constraints are in effect which may selectively depopulate rotational levels in the autoionizing resonance - which would invalidate rotational closure.

There have been studies of the temperature dependence of the photoelectron spectra of solids, some of which show strong temperature dependence,[663] but, for gases, temperature dependence of the photoelectron spectra is much more difficult to study experimentally, because the gases are leaked into the source volume in most cases. The expansion of the gases associated with this technique causes uncertainties about the actual temperatures of the gaseous samples. In "large," nonrigid molecules, temperature dependence of the photoelectron spectra is not necessarily caused by rotational motion alone. For example, all photoelectron spectra of molecules, in temperature dependent conformational equilibria, are expected to be more or less temperature dependent.

It has been shown that, in the presence of a shape resonance, the rotational structure, and therefore also the band contours, of the vibronic bands change strongly over the vibronic progression. The strong effect of shape resonances on the experimental vibrational branching ratios and on the vibronic β values has also been observed in the present data, but quantitative agreement with experiment is poor.

In this work, the validity of the Born-Oppenheimer approximation has been assumed, and the potential energy curves were approximated by Morse functions. The different methods for computing Franck-Condon factors of diatomic molecules have been reviewed by Chakraborty and Pan.[664] The Morse potentials used here were obtained from experimental spectroscopic constants. Chong et al.[665] investigated various methods of ab initio computation of potential energy curves involved in photoionizations. According to Chong et al., it is essential that the potential energy curve of the final state be most accurate in the "Franck-Condon region," which is roughly equivalent to the classical region of the initial vibrational level. It is possible that the ranges of internuclear separations considered in this work were excessive in most cases.

In the presence of several closely lying electronic states, we can expect strong nonadiabatic couplings. The same situation also gives rise to many-body effects. This means that severe breakdowns of the one-particle picture of the photoionization process should give rise to simultaneous breakdowns of the Born-Oppenheimer approximation. Nonadiabatic coupling exists often on a single-particle level of approximation, but, according to Köppel et al.,[666] in some cases nonadiabatic coupling arises only by virtue of strong electron correlation effects. In non-degenerate electronic bands, excitation of degenerate vibrations can be observed experimentally.[26] These vibronic bands borrow intensity from nearly degenerate electronic states via a pseudo-Jahn-Teller interaction.[668]

The spectroscopic constants B_e of H_2, H_2^+, HD, HD^+, D_2, and D_2^+ range from 15 to 61 cm^{-1}. The spectroscopic constants B_e of N_2 and CO, and their ions are between 1.6 and 2 cm^{-1}. The rotational spacings in the photoelectron spectra of N_2 and CO are therefore expected to be an order of magnitude smaller than the rotational spacings in the photoelectron spectra of H_2 and its isotopically substituted deruvatives. Pollard et al.[599] barely managed to resolve the rotational structure in the photoelectron spectra of H_2, HD, and D_2, using molecular beams. The resolution achieved by Pollard et al. might be sufficient to show some sharp features which have been predicted in the contours of N_2 and CO for some of the vibronic bands.

The values of B_e should not be less than about half of the value of B_e of H_2 for most hydrides, AH, and their ions, AH^+. This means that Pollard et al. have recently acquired the capability to resolve the rotational structure of these hydrides, or will be able to do so pending only minor improvements.

In this work, complex spherical harmonics have been used with Condon-Shortley phase conventions. However, James Davenport used real spherical harmonics.[667] This problem of incompatability was not solved by switching to real spherical harmonics. Instead, from the DMAPWs computed with real spherical harmonics, the DMAPWs, which would have been obtained with complex spherical harmonics, are computed. This is possible only for linear molecules. This procedure, and its justification, are shown in Appendix 9.

CHAPTER 11

AN OUTLOOK ON POLYATOMIC MOLECULES

In the absence of strong Fermi resonances, the vibronic energy levels of a polyatomic molecule can be expressed as a power series of the vibrational quantum numbers[670]

$$E_{v_1,v_2,\ldots}=X_0+\sum_{j=1}^{n}\left[X_j(v_j+1/2)+\sum_{k=1}^{j}X_{jk}(v_j+1/2)(v_k+1/2)\right] \qquad (11\text{-}1)$$

where n is the number of nondegenerate normal modes.

The Hamiltonian of nuclear motion can be written as[671,677]

$$\hat{\mathcal{H}} = \Sigma_{jk}\left(-\frac{\hbar^2}{2}G_{jk}\frac{\partial^2}{\partial q_j \partial q_k}\right)+V(\vec{q}) \qquad (11\text{-}2)$$

where, in this chapter, $\vec{q}$ represents internal coordinates and G_{jk} are the elements of the G-Matrix.[672,673] In (11-2), the kinetic energy terms with $j\neq k$ are called kinematic anharmonicities.[674-676] One can always find a set of coordinates such that the kinematic anharmonicities are removed.[676]

Wallace developed the so-called method of partial oscillators.[678] In this model, the kinematic anharmonicities are neglected and the potential energy term is expressed in terms of the internal coordinates as

$$V(\vec{q})=\Sigma_k U(q_k) \qquad (11\text{-}3)$$

where the Us are Morse potentials for stretching coordinates, (bond

lengths), and harmonic potentials for bending coordinates, (bond angles). One can readily see that, with Wallace's model, the interaction terms with $j \neq k$ will have to be neglected, and for the bending modes we require $X_{jj}=0$. Wallace[679] later developed a model for triatomic molecules in which the separation of variables gives rise to effective potentials which embody interaction terms among the vibrations.

Wallace's model of partial Morse oscillators rests on the local mode representation of vibrational motion. Some authors have claimed that the normal mode picture of vibrational motion decreases in quality with increasing energy content of the system, and that a local mode description becomes more realistic.[680,681] However, there are some misconceptions about the reason why the local mode picture becomes more appropriate at high energies. For example, Henry[682] states that a local mode description would realistically predict the rupture of a single CH bond in benzene, rather than a simultaneous cleavage of six CH bonds, as predicted by a dissociation along the totally symmetric stretching mode. However, it is questionable that symmetry breaking of this nature is purely a matter of choosing "proper" coordinates. When using local mode coordinates, one will have to symmetrize the wave functions of such systems as benzene.[683] Local mode coordinates may be more suitable to represent cleavage processes in classical and semiclassical descriptions, but on a purely quantum mechanical basis one will have to make allowance for symmetry breaking in such processes, regardless of the choice of coordinates.

In this chapter, an opportunistic point of view will be taken regarding the choice of the coordinate systems. Specifically, the coordinates giving rise to the least mathematical complexity are considered the best choice of coordinates.

It can be shown that the kinematic anharmonicities can be removed by transforming into an appropriate coordinate system consisting of linear combinations of the internal coordinates.[223]

Let us now look at a reasonable procedure to find the anharmonic eigenfunctions of vibrational motion of polyatomic molecules.

We plan to make use of Morse potentials (MPs), but also Pöschl-Teller potentials (PTPs) will be used in this work. The procedure consists of four steps:

Step A: Find a coordinate system, $\vec{Q}$, in which the kinematic anharmonicities vanish. In terms of these coordinates, (11-2) becomes

$$\hat{\mathcal{H}} = \Sigma_j\left(-\frac{\hbar^2}{2}\mu_j^{-1}\frac{\partial^2}{\partial Q_j^2}\right)+V(\vec{Q}) \qquad (11\text{-}4)$$

Step B: Express the potential energy surface of the polyatomic molecule as a sum of one-dimensional MPs and PTPs in terms of the coordinates $\vec{Q}$, plus a perturbation

$$V(\vec{Q})=\Sigma_j U_j(Q_j)+V_{pert}(\vec{Q}) \qquad (11\text{-}5)$$

where U_j stands for the appropriate one-dimensional

anharmonic potentials. Were it not for the perturbation, the vibrational wave function of the polyatomic molecule could be written as a product

$$\psi(\vec{Q})=\Pi_j \psi_j(Q_j) \tag{11-6}$$

and the total energy would be a sum of eigen energies of the one-dimensional anharmonic potentials

$$E_{tot}=\Sigma_j \epsilon_j \tag{11-7}$$

The energy eigenvalues of the MPs and the PTPs are of the form

$$\epsilon_j=A_j+X_j(v_j+1/2)+X_{jj}(v_j+1/2)^2 \tag{11-8}$$

and the total energy of vibration is then of the form

$$E_{tot}=\langle\psi|\hat{\mathcal{H}}|\psi\rangle=X_o+\Sigma_j X_j(v_j+1/2)+X_{jj}(v_j+1/2)^2 \tag{11-9}$$

which is the same as (11-1), except that the interaction terms with $j\neq k$ are missing in (11-9). At any rate, term-by-term comparison of (11-9) and (11-1) serves to determine the parameters of the anharmonic potentials, where the interaction terms in (11-1) are being ignored in this step.

Step C: In this step, we introduce interaction terms of the form

$$V_{pert}(\vec{Q})=\Sigma_j\Sigma_k C_{jk}u_j(Q_j)u_k(Q_k),\ k<j \tag{11-10}$$

where

$$u_j(Q_j)=1-\exp(-\beta_j Q_j) \tag{11-11}$$

if U_j was a Morse potential and

$$u_j(Q_j)=\tanh^2(\alpha_j Q_j) \tag{11-12}$$

if U_j was a PTP. According to (6-7) and (7-22) the first order correction to the energy can then be expressed as

$$\langle\psi|V_{pert}|\psi\rangle=C_o+\Sigma_j\Sigma_k X_{jk}(v_j+1/2)(v_k+1/2),\ k<j \tag{11-13}$$

In this step, we adjust the expansion coefficients C_{jk} in (11-10) such that (11-9) and (11-13) combined are identical with the expression in (11-1).

Step D: In the previous steps, the hamiltonian has been constructed. In this step, the eigenfunctions of this hamiltonian have to be determined.

In the absence of Fermi resonances, perturbation theory would be appropriate; but in the presence of strong Fermi resonances, more elaborate procedures are called for.

Let us now discuss some of the details in the individual steps. First we introduce the quantities:

$$\overset{\star}{p} = \{\frac{\partial}{\partial q_1}, \frac{\partial}{\partial q_2}, \ldots\ldots \}$$

$$\overset{\star}{P} = \{\frac{\partial}{\partial Q_1}, \frac{\partial}{\partial Q_2}, \ldots\ldots \} \qquad (11\text{-}14)$$

Let us write the transformation in matrix form

$$\vec{Q} = \underset{\sim}{U}\vec{q} \qquad (11\text{-}15)$$

We want U to be a unitary matrix

$$\underset{\sim}{U}^{\dagger}\underset{\sim}{U} = \underset{\sim}{1} \qquad (11\text{-}16)$$

The kinetic energy, in terms of the cordinates $\vec{Q}$, is shown in (11-4). Using the internal coordinates, the kinetic energy can be written in matrix notation as

$$\hat{T} = -(1/2)\hbar^2(\overset{\star}{p})^{\dagger}\underset{\sim}{G}\overset{\star}{p} \qquad (11\text{-}17)$$

where $\underset{\sim}{G}$ is the G-matrix.[672,673] From (11-14) and (11-15), using the chain rule of differentiation, we obtain

$$\overset{\star}{P} = \underset{\sim}{U}\overset{\star}{p} \qquad (11\text{-}18)$$

From (11-17) and (11-18), we obtain

$$\hat{T} = -(1/2)\hbar^2(\overset{\star}{p})^{\dagger}\underset{\sim}{U}^{\dagger}\underset{\sim\sim}{UGU}^{\dagger}\underset{\sim}{U}\overset{\star}{p} = -(1/2)\hbar^2(\overset{\star}{P})^{\dagger}\underset{\sim\sim}{UGU}^{\dagger}\overset{\star}{P} \qquad (11\text{-}19)$$

where the right hand side of (11-19) is of the same form as the kinetic energy term in (11-4), if U diagonalizes the G-matrix; i.e.,

$$\underset{\sim}{U}\underset{\sim}{G}\underset{\sim}{U}^{\dagger} = \underset{\sim}{K} \tag{11-20}$$

where $\underset{\sim}{K}$ is a diagonal matrix. This determines the transformation in (11-15). The elements of $\underset{\sim}{K}$ are

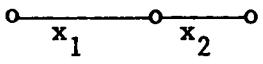
$$k_{ij} = \delta_{ij}/\mu_j \tag{11-21}$$

where μ_j is the "reduced mass" of the j-th vibrational mode. One can readily see from (11-20) and (11-15) that the coordinates Q are the normal mode coordinates which would be obtained with Wilson's GF method, if we replace the force constant matrix by a unit matrix.

The second step, (step B), is basically an exercise in elementary algebra, except for the choice between MPs and PTPs. As previously indicated, the coordinates $\vec{Q}$ represent normal mode coordinates. If the molecule has no symmetry, one might want to take Morse potentials in all cases. However, if the molecule has some symmetry, symmetry considerations will dictate the use of PTPs in some cases. Let us examine the molecule CO_2 as an example. We consider here the linear configuration of the ground state of CO_2. Let us first look at the symmetric stretching mode. For this mode, a Morse potential is definitely appropriate. For the bending mode we would use a PTP. The relevant characteristic of PTPs is that

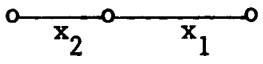
$$V(x) = V(-x) \tag{11-22}$$

In the asymmetric stretching mode, displacements in opposite directions have the same potential energy. The configuration



(11-23)

has the same potential energy as a configuration which is its mirror image



(11-24)

It becomes apparent that, for molecules with symmetries, Morse potentials are used only for the totally symmetric normal modes.

When dealing with Morse oscillators, we have a dissociation limit as $Q \to +\infty$. A Morse potential was used for the symmetric stretching mode of CO_2. In this case, it was quite obvious what displacement, $+\infty$ or $-\infty$, the dissociation limit would be assigned to. However, when dealing with complicated vibrational motions, we might become "disoriented" in this respect. Suzuki[685] has addressed this problem.

In the last step, the hamiltonian constructed in the previous steps is being solved. Since perturbation theory has been used in the construction of the hamiltonian, one might want to find the eigenfunctions by perturbation theory as well. This attitude is based on the rationale that it does not make sense to determine the wave functions beyond the accuracy of first order perturbation theory, if the hamiltonian itself is not determined with an accuracy beyond that of first order perturbation theory. However, in the presence of strong Fermi resonances, i.e., near-degeneracies, first order perturbation

theory breaks down. One might expect that the hamiltonian also would become inaccurate in the presence of such near-degeneracies. Spectroscopists introduce in (11-1) additional parameters which are effective only for the energy levels which are affected by Fermi resonances.[2] The spectroscopic constants which are used for this model could be obtained from the energy levels, which are unaffected by Fermi resonances. On the other hand, the Fermi resonances which are observed should be reproduced by the hamiltonians obtained with the present approach, if an appropriate method of solution is being used. An "appropriate" method would be a variational scheme.[690] There exist also schemes which are hybrids between perturbation and variational techniques, which can deal effectively with degenerate or near-degenerate levels.[686] Recently, selfconsistent field methods have been applied for coupled vibrational modes.[687-689]

The additional spectroscopic constants, which the spectroscopists use to deal with Fermi resonances, are redundant in our model. For this reason, the accuracy with which this model reproduces the effects of Fermi resonances would be a sensitive test of the accuracy of the potential energy hypersurfaces which are obtained.

Let us assume that we have an initial and a final electronic state which have different potential energy surfaces and therefore also different equilibrium geometries. This means that the G-matrices will be different for the initial and the final state, which in turn means that we are dealing with a Duschinsky effect in most cases. This would require that we compute multidimensional integrals for all the modes which show Duschinsky mixing. One could use the same transformation

matrix to construct the coordinates Q for both states. The transformation matrix could, for example, be obtained by the diagonalization of one of the two G-matrices or by diagonalizing the G-matrix of the "average geometry." When using the same transformation matrix for both levels, one will have some residual kinematic anharmonicities left in at least one of the two hamiltonians, unless there is no Duschinsky mixing of the modes. These kinematic anharmonicities have to be retained in the computation of the wave functions.

Analytical formulae have appeared in the literature for the computation of matrix elements of harmonic oscillators with Duschinsky mixing.[699-701] It is unlikely that such formulae can be found for the anharmonic oscillators used in this work.

Duschinsky rotation of the frames has been shown to affect considerably the vibronic intensities in the fluorescence spectra of pyridine[702] and pyrazine.[421] For this reason, one can't just ignore the Duschinsky effect. The method proposed here deals with this effect by transforming both frames onto a common set of coordinates.

The diagonal elements for the kinematic anharmonicities are zero for Morse Oscillators. The necessary matrix elements have been expressed analytically, by the author, for Morse oscillators.[691] Wallace[678] gave also some formulae for matrix elements for Morse oscillators. Efremov and Zhirnov[692] pointed out some errors in Wallace's formulae. Several additional authors have also given formulae for matrix elements of Morse oscillators.[693-697] Laursen and Mita[698] have published some formulae for integrals relating to the diagonal elements of the Pöschl-Teller oscillator (PTO). However, no

extensive study appears to have been done on the matrix elements of the PTO. The eigenfunctions of the Morse oscillator and the PTO belong to a class of functions known as hypergeometric functions. Exton compiled extensive tables of formulae for integrals involving hypergeometric functions.[655] He also presented algorithms and computer programs for the numerical computation of such integrals.

The wave functions for degenerate vibrations have to be properly symmetrized.[684]

The elements of the G-matrix depend on the molecular geometry. In this work, this dependence has been ignored. For large amplitude vibrations, such as ring-puckering motions, the effect of the geometry on the reduced mass may be considerable.[471,503] This effect has been neglected in this work.

In many molecules, one or more of the normal modes have to be represented by double-potentials. Several mathematical forms of such double-minimum potentials have been used.[703-706] The Manning potential,[706] which is related to the PTO, has been used by Fletcher and Brown[525] in a one-dimensional treatment of the inversion mode of some cyanamides.

Nonadiabatic effects in polyatomic molecules have recently attracted considerable attention. In "large" molecules, conic intersections of potential energy surfaces constitute a widespread phenomenon.[573,654] The nonadiabatic effects connected with such intersections, and with avoided crossings, have two important consequences:

(i) The concept of potential energy surfaces is no longer applicable.

(ii) The nonadiabatic coupling terms promote extremely fast non-radiative transitions such that, on the time scale of many processes, the molecule spends time in more than one electronic state.

The present model can obviously be refined to include some of the effects which have been neglected in the present work.

LIST OF REFERENCES

LIST OF REFERENCES

1. Gerhard Herzberg, "Molecular Spectra and Structure. I. Spectra of Diatomic Molecules," (Van Nostrand, 1950).

2. Gerhard Herzberg, "Molecular Spectra and Structure. II. Infrared and Raman Spectra of Polyatomic Molecules," (Van Nostrand, 1945).

3. Milton Abramowitz and Irene A. Stegun, "Handbook of Mathematical Functions. With Formulas, Graphs, and Mathematical Tables," (Dover,Ninth Edition,1970).

4. J.B. Coon, Texas A&M College; private communication.

5. H. Sponer and E. Teller, Revs. Mod. Phys. 13(2),(1941)75-170.

6. F. Duschinsky, Acta Physicochim. U.R.S.S. 7(1937)551-566.

7. Donald T. Greenwood, "Classical Dynamics," (Prentice Hall,1977) p.229.

8. J.B. Coon, R.E. DeWames, and C.M. Loyd, J. Molec. Spectrosc. 8(4), (1962)285-299.

9. H. Yersin, H. Otto, Jeffrey I. Zink, and G. Gliedmann, J. Am. Chem. Soc. 102(3),(1980)951-955.

10. M. Wagner, Z. Naturforsch. 14A(1),(1959)81-91.

11. F. Ansbacher, Z. Naturforsch. 14A(10),(1959)889-892.

12. S. Koide, Z. Naturforsch. 15A(2),(1960)123-128.

13. J.R. Henderson, M. Muramoto, R.A. Willett, J. Chem. Phys. 41(2), (1964)580-581.

14. Peter Senn, Dept. of Chemistry, Univ. of Tennessee, Knoxville, Technical Report No. 1. (Unpublished work).

15. J. L. Gardner and James A. R. Samson, J. Electron Spectrosc. Relat. Phenom. 13(1),(1978)7-15.

16. K.P. Huber and Gerhard Herzberg, "Molecular Spectra and Molecular Structure Constants of Diatomic Molecules," (Van Nostrand,1979).

17. James A.R. Samson, Univ. of Nebraska at Omaha, Private comm., Nov. 27, 1978.

18. J.M. Hollas and T.A. Sutherley, Mol. Phys. 24(5),(1972)1123-1131; These authers used the rule attributed to them as a criterion. They did not make any claim about its general validity as proposed here.

19. S. Bell, R.D. McKenzie, and J.B. Coon, J. Molec. Spectrosc. 20(2), (1966)217-225.

20. Thomas B. Ake, Astrophys. J. 234(2,pt.1),(1979)538-547.

21. J.A.C. Gallas, R.E. Francke, H.P. Grieneisen, and B.P. Chakraborty, Astrophys. J. 234(2,pt. 1),(1979)851-855.

22. S. Schoonveld and S. Sundaram, Astrophys. J. 192(1,pt.1),(1974) 207-211.

23. I.S. Gradshteyn and I.W. Ryzhik, "Table of Integrals, Series and Products," (Acad. Press,Fourth Edition,N.Y.,1965), sect. 7.374, formula No. 8.

24. Same as ref. 23, but formula No. 9.

25. Thomas R. Faulkner and F.S. Richardson, J. Chem. Phys. 70(3), (1979)1201-1213.

26. P.M. Dehmer, J.L. Dehmer, and W.A. Chupka, J. Chem. Phys. 73(1), (1980)126-133.

27. Same as ref. 23, but sect. 7.375, formula No. 2.

28. Enrico Fermi, "Notes on Quantum Mechanics," (The Univ. of Chicago Press & The Univ. of Toronto Press,1961).

29. P.A. Fraser, Can. J. Phys. 32(8),(1954)515-521.

30. Joel Tellinghuisen, J. Quant. Spectrosc. Radiat. Transfer, 19(2), (1978)149-161; J. Molec. Spectrosc. 44(1),(1972)194-196; Computer Phys. Comm. 6(5),(1973)221-228.

31. A. Schadee, J. Quant. Spectrosc. Radiat. Transfer 19(4),(1978) 451-453.

32. Henry A. Bent, J. Chem. Educ. 57(6),(1980)395-405.

33. A.C.G. Mitchell and M.W. Zemansky, "Resonance Radiation and Excited Atoms," (The University Press, Cambridge, 1934).

34. M.A. El'yashevich, Soviet Phys. (Usp.),(Engl.) 22(7),(1979)555-575.

35. Allan Laslett Smith, J. Molec. Spectrosc. 28(2),(1968)269-271.

36. S.M. Yazykova and E.V. Butyrskaya, J. Phys. B: Atom. Molec. Phys. 13(17),(1980)3361-3367.

37. P. Halevi, Proc. Phys. Soc. (Lond.) 86(553),(1965)1051-1054.

38. R.E.W. Jansson and B.E. Cunio, J. Quant. Spectrosc. Radiat. Transfer 8(11),(1968)1747-1762.

39. R.W. Nicholls, Spectrosc. Lett. 9(1),(1976)23-29.

40. Kate Kirby Docken, Chem. Phys. Lett. 30(2),(1975)334-336.

41. R.E. Francke, J.A.C. Gallas, H.P. Grieneisen, J. Schifino, and B.P. Chakraborty, J. Chem. Phys. 72(3),(1980)1476-1481.

42. R.W. Nicholls, "Transition Probabilities of Molecular Band Systems," Scientific Report No. 3, Contract AF 19(122)-470(1952).

43. R.W. Nicholls and W.R. Jarmain, Proc. Phys. Soc. (Lond.) A69(1956) 253-264.

44. R.W. Nicholls, Final Report, Contract AF 19(122)-470(1956).

45. R.W. Nicholls, J. Quant. Spectrosc. Radiat. Transfer 14(3),(1974) 233-237.

46. R.W. Nicholls and W.R. Jarmain, J. Chem. Phys. 23(8),(1955) p. 1561; Proc. Phys. Soc. (Lond.) 74(1959)133-136.

47. R.W. Nicholls, Proc. Phys. Soc. (Lond.) 85(1965)159-162 and Proc. Phys. Soc. (Lond.) 89(563),(1966)181-183.

48. R.W. Nicholls, Chem. Phys. Lett. 17(2),(1972)252-255 and Chem. Phys. Lett. 20(3),(1973)261-264.

49. Allan Laslett Smith, Drexel University, Private communication.

50. Richard N. Sileo and Terrill A. Cool, J. Chem. Phys. 65(1),(1976) 117-133.

51. R.G. Turner and R.W. Nicholls, Can. J. Phys. 32(7),(1954)468-474 and 475-479.

52. Allister Vallance Jones, "Aurora," (Reidel,1974).

53. W.R. Jarmain and R.W. Nicholls, Can. J. Phys. 32(2),(1954)201-204.

54. D.L. Yaeger and V. McKoy, J. Chem. Phys. 67(6),(1977)2473-2477.

55. B.E. Cunio and R.E. Jansson, J. Quant. Spectrosc. Radiat. Transfer 8(11),(1968)1763-1771.

56. Granino A. Korn and Theresa M. Korn, "Mathematical Handbook for Scientists and Engineers," (McGraw-Hill,N.Y.,1961), sections (18.4-1) to (18.4-12).

57. A.V. Hazi and H.S. Taylor, Phys. Rev. A1(4),(1970)1109-1120.

58. Joachim Römelt and Ralf Runau, Theoret. Chim. Acta (Berl.) 54(2), (1980)171-177 and refs. therein.

59. C.L. Pekeris, Phys. Rev. 45(2),(1934)98-103.

60. D.T. Birtwistle, Chem. Phys. Lett. 63(3),(1979)523-524.

61. Byung Chan Eu, J. Chem. Phys. 73(5),(1980)2405-2411.

62. Derek Steele, Ellis R. Lippincott, and Joseph T. Vanderslice, Revs. Mod. Phys. 34(2),(1962)239-251.

63. Linus Pauling and E. Bright Wilson, "Introduction to Quantum Mechanics," (McGraw-Hill,N.Y.,1935).

64. N. Sreedhara Murthy and L. Siddarama Gowda, J. Phys. B: Atom. Molec. Phys. 10(3),(1977)491-494.

65. R. Tripathi and S.B. Rai, Indian J. Pure Appl. Phys. 18(5),(1980) 372-374.

66. J.B. Schumaker, J. Quant. Spectrosc. Radiat. Transfer 9(1),(1969) 153-156.

67. Ş. Erkoç, J.N. Murrell, and D.C. Clary, Chem. Phys. Lett. 72(2), (1980)264-268.

68. L.A. Rahn, R.L. Farrow, M.L. Koszykowski, and P.L. Mattern, Phys. Rev. Lett. 45(8),(1980)620-623.

69. "Handbook of Physics," edited by E.U. Condon and Hugh Odishaw, (McGraw-Hill,1967), part 7, chapter 1, section 8.

70. J.N. Huffaker, J. Chem. Phys. 64(11),(1980)4564-4570 and J. Chem. Phys. 64(8),(1980)3175-3181.

71. Parmesh H. Dwivedi and J.N. Huffaker, J. Chem. Phys. 64(4),(1977) 1726-1735.

72. J.N. Huffaker and Parmesh H. Dwivedi, J. Chem. Phys. 68(3),(1978) 1303-1305.

73. J.N. Huffaker, J. Chem. Phys. 72(4),(1980)2601-2605 and J. Chem. Phys. 74(2),(1981)1217-1220.

74. J.N. Huffaker and Parmesh H. Dwivedi, J. Math. Phys. 16(4),(1975) 862-867.

75. Same as ref. 23, but sect. 7.414, formula No. 3.

76. A. Requena, R. Peña, and A. Serna, Int. J. Quant. Chem. 17(5), (1980)931-942.

77. Same as ref. 23, but sect. 7.622, formula No. 3.

78. H. Grosse and A. Martin, Phys. Reports 60(6),(1980)341-392.

79. L. Montanet, G.C. Rossi, and G. Veneziano, Phys. Reports 63(3), (1980)149-222.

80. Ran B. Singh and D.K. Rai, Indian J. Pure Appl. Phys. 4(3),(1966) 102-105.

81. António J.C. Varandas, J. Chem. Soc., Farad. Trans. II 76(2), (1980)129-135.

82. S. Noor Mohammad, Physica 96C(3),(1979)410-421.

83. M. Berrando and A. Palma, J. Phys. A: Math. Gen. 13(3),(1980)773-780.

84. Siegfried Flügge, "Practical Quantum Mechanics," (Springer,Berl., 1971). A translation of "Rechenmethoden der Quantentheorie."

85. Same as ref. 23, but sect. 7.313. Multiply out a factor of (1+x) to obtain the desired formula.

86. Florian Cajori, "A History of Physics," (Mac Millan Co.,1899,1929) p.334.

87. Friedrich Hund, "The History of Quantum Theory," (Harper and Row, 1967).

88. A. Einstein, Ann. Phys. 17(6),(1905)132-148; Ann. Phys. 20(6), (1906)199-206; Ann. Phys. 47(15),(1915)879-885.

89. A. Einstein, Z. Phys. 31(1925)784-785.

90. M.A. El'yashevich, Sov. Phys. (Usp.), (Engl.) 20(8),(1977)656-682.

91. A.J. Fennelly in "Encyclopedia of Physics," eds. Rita G. Lerner and George L. Trigg, (Addison-Wesley,1981)749-750.

92. John G. Jenkin, J. Electron Spectrosc. Relat. Phenom. 23(2,3), (1981)187-273.

93. W. von Niessen, L.S. Cederbaum, W. Domcke, and J. Schirmer in "Computational Methods in Chemistry," ed. Joachim Bargon, (Plenum Press,1980)65-102.

94. Heinrich Hora, "Physics of Laser Driven Plasmas," (Wiley,1981), section 9.4.

95. G. Vitrant, J.M. Raimond, M. Gross, and S. Haroche, J. Phys. B: Atom. Molec. Phys. 15(2),(1982)L49-L55.

96. R.J. Bickerton, Phil. Trans. Roy. Soc. (Lond.) A300(1456),(1981) 475-488.

97. P.S. Ganas, J. Chem. Phys. 75(7),(1981)3641-3643.

98. Kenneth Davies, "Ionospheric Radio Propagation," NBS Monograph 80, (National Bureau of Standards,1965).

99. Peter N. Saveskie, "Radio Propagation Handbook," (Tab Books Inc., 1980), chapter 2.

100. M.P.M. Hall, "Effects of the Troposphere on Radio Communication," (Institute of Electrical Engineers,1979).

101. J. Eberhart, Sci. News 121(2),(1982)22-23.

102. J.V. Evans, Science 216(4545),(1982)467-474.

103. Ralph Markson in "Solar-Terrestrial Influences on Weather and Climate," eds. Billy M. McCormac and Thomas A. Seliga, (D. Reidel,1979)215-232.

104. Václav Bucha, J. Geomag. Geoelectr. 32(4),(1980)217-264.

105. J. William McGowan, Ralph H. Kummler, and Forrest R. Gilmore, Adv. Chem. Phys. 28(1975)379-422.

106. George C. Reid in "Advances in Atomic and Molecular Physics," eds. D.R. Bates and Benjamin Bederson, (Acad. Press,1976), vol. 12.

107. Julian Heicklen, "Atmospheric Chemistry," (Acad. Press,1976).

108. Thomas H. Maugh II, Science 206(4423),(1979)1167-1168 and Science 207(4429),(1980)394-395.

109. G.R.A. Johnson and J.M. Warman, Farad. Discuss. Chem. Soc. (Lond.) 37(1964)87-95.

110. William B. Scott, Aviation Week and Space Technology 116(11), (1982)71-74.

111. Janet Rudolf, Sci. News 119(19),(1981)300-302.

112. W.T. Huntress, Jr., J. Chem. Educ. 53(4),(1976)204-208.

113. Siegfried J. Bauer, "Physics of Planetary Ionospheres," (Springer, 1973).

114. Joseph W. Chamberlain, "Theory of Planetary Atmospheres: An Introduction to their Physics and Chemistry," (Acad. Press,1978).

115. F.E. Roach in "Atmospheric Emissions," eds. Billy M. McCormac and Anders Omholt,(Van Nostrand,1969)439-447.

116. Robert A. Helliwell, "Whistlers and Related Ionospheric Phenomena," (Stanford Univ. Press,1965).

117. G. Herendel, R. Lüst, E. Rieger, and H. Völk in "Atmospheric Emissions," eds. Billy M. McCormac and Anders Omholt, (Van Nostrand,1969)293-303.

118. O. Harang in "Atmospheric Emissions," eds. Billy M. McCormac and Anders Omholt, (Van Nostrand,1969)489-499.

119. J.S. Lee, J.P. Doering, T.A. Potemra, and L.H. Brace, Planet. Space Sci. 28(10),(1980)947-972 and 973-996.

120. Harry L.F. Houpis and D.A. Mendis, Astrophys. J. 243(3,pt.1), (1981)1088-1102.

121. A.H. Delsemme, Appl. Opt. 19(23),(1980)4007-4014.

122. "X-Ray Astronomy," NATO Adv. Study Institute, Sicily, July 1979, eds. Riccardo Giacconi and Giancarlo Setti, (D. Reidel,Holland).

123. Marijke Burger, Astron. Astrophys. 94(1),(1981)199-200.

124. Joseph Patterson, Glew Williams, and W.A. Hiltner, Astrophys. J. 245(2,pt.1),(1981)618-623.

125. N.E. White, Astrophys. J. 244(2,pt.2),(1981)L85-L88.

126. D.E. Thomsen, Sci. News 121(4),(1982)p. 52.

127. Gerrit L. Verschuur, "The Invisible Universe: The Story of Radio Astronomy," (English Universities Press,Springer,1974).

128. James Lequeux, La Recherche 12(119),(1981)240-241.

129. Steven Detweiler, Am. J. Phys. 49(5),(1981)394-400.

130. B. Carter and J.P. Luminet, Nature 296(5854),(1982)211-214.

131. P.W. Guilbert and A.C. Fabian, Nature 296(5854),(1982)226-228.

132. James C. Kemp, Mark S. Barbour, and Richard E. McBirney, Astrophys. J. 244(2,pt.2),(1981)L73-L77.

133. S.W. Hawking, Nature 248(5442),(1974)30-31.

134. J. Higbie, Am. J. Phys. 49(7),(1981)652-655.

135. Frederic H. Chaffee, Jr., Sci. American 243(5),(1980)70-78.

136. C. Lloyd, Nature 294(5854),(1981)727-728.

137. D.E. Thomsen, Sci. News 120(21),(1981)p. 325.

138. R.W. Porcas, Nature 294(5836),(1981)47-49.

139. K.S. Thorne, Sci. American 231(6),(1974)32-43.

140. Harri L. Shipman, "Black Holes, Quasars and the Universe," (Houghton Mifflin,1980).

141. Fred Hoyle and Jayant Narlikar, "The Physics-Astronomy Frontier," (Freeman,1980).

142. S.W. Hawking, Commun. Math. Phys. 80(3),(1981)421-442.

143. A.D. Dolgov, Sov. Phys. JETP (Engl.) 52(2),(1980)169-175.

144. D.E. Thomsen, Sci. News 121(1),(1982)p.4.

145. Wallace H. Tucker, "Radiation Processes in Astrophysics," (MIT Press,1975), chapter 7.

146. Paul S. Sapiro and John N. Bahcall, Astrophys. J. 241(1,pt.1), (1980)1-24.

147. J. Michael Schull, Appl. Opt. 19(23),(1980)4002-4006.

148. Leo Blitz, Sci. American 246(4),(1982)84-94.

149. J.E. Dyson and D.A. Williams, "Physics of the Interstellar Medium," (Wiley,1980), chapter 5.

150. Neil R. Erickson, Ronald L. Snell, Robert B. Loren, Lee Mundy, and Richard L. Plambeck, Astrophys. J. 245(2,pt.2),(1981)L83-L86.

151. S.M. Varnavskikh, Opt. Spectrosc. (Engl.) 49(6),(1980)644-645.

152. Toshio Masuoka and James A.R. Samson, J. Chem. Phys. 75(10), (1981)4946-4948.

153. P. Eisenberger and L.C. Feldman, Science 214(4518),(1981)300-305.

154. Bertram M. Schwarzschild, Phys. Today 34(3),(1981)19-21.

155. G. Beamson, H.Q. Porter, and D.W. Turner, Nature 290(5807),(1981) 556-561.

156. David F. Gray, "The Observation and Analysis of Stellar Photospheres," (Wiley,1976)75-84.

157. Vincent B. Stein and Rajner S. Narang, Anal. Chem. 54(6),(1982) 991-992.

158. U. Boesl, H.J. Neusser, and E.W. Schlag, Chem. Phys. 55(2),(1981) 193-204.

159. T. Hayashi, S. Iwata, M. Sasanuma, E. Ishiguro, Y. Morioka, Y. Iida, and M. Nakamura, J. Phys. B: Atom. Molec. Phys. 15(1), (1982)79-92.

160. Charles T. Rettner and John H. Brophy, Chem. Phys. 56(1),(1981) 53-61.

161. Jeffre W. Hudgens, Mark Seaver, and J.J. De Corpo, J. Phys. Chem. 85(7),(1981)761-762.

162. Samuel Leutwyler, André Herrmann, Ludger Wöste, and Ernst Schumacher, Chem. Phys. 48(2),(1980)253-267.

163. Thomas W. Scott, C.L. Braun, and A.C. Albrecht, J. Chem. Phys. 76(11),(1982)5195-5202.

164. R.D. Birkhoff, J.M. Heller, Jr., L.R. Painter, J.C. Ashley, and H.H. Hubbell, Jr., J. Chem. Phys. 76(11),(1982)5208-5213.

165. T.N. Chang, J. Phys. B: Atom. Molec. Phys. 15(3),(1982)L81-L85.

166. G.J. Pert, Phil. Trans. Roy. Soc. (Lond.) A300(1456),(1981)631-640.

167. Michael A. Duguay in "Laser Induced Fusion and X-Ray Laser Studies," eds. Stephen F. Jacobs, Marlan O. Scully, Murray Sargent III, and Cyrus D. Cantrell, (Addison-Wesley,1976).

168. G.J. Pert, Phys. Bull. 33(3),(1982)92-94.

169. Cleanthes A. Nicholaides and Yannis Komninos, Chem. Phys. Lett. 80(3),(1981)463-468.

170. Peter Knight, Nature 292(5819),(1981)p. 108.

171. Clarence A. Robinson, Jr., Aviation Week and Space Technology 114(8),(1981)25-27.

172. G.S. Hurst, M.H. Nayfeh, and J.P. Young, Appl. Phys. Lett. 30(5), (1977)229-231.

173. V.S. Letokhov, Comments At. Mol. Phys. 7(3,4),(1977)93-107 and 107-116; Comments At. Mol. Phys. 10(6),(1981)257-266; Optics and Laser Techn. 13(3),(1981)131-139.

174. V.I. Balykin, G.I. Bekov, V.S. Letokhov, and V.I. Mishin, Sov. Phys. (Usp.), (Engl.) 23(10),(1980)651-678.

175. B.S. Schneider and A.L. Smith in "Electron Spectroscopy," ed. D.A. Shirley, (North-Holland,1972)335-343.

176. C.E. Brio, K.H. Tan, M.J. Van der Wiel, and Ph.E. Van der Leeuv, J. Electron Spectrosc. Relat. Phenom. 17(2),(1979)101-119.

177. B. Brehm, J.H.D. Eland, R. Frey, and A. Küstler, Int. J. Mass Spectrom. Ion Phys. 12(3),(1973)213-224.

178. Keith Johnson, I. Powis, and C.J. Danby, Chem. Phys. 63(1,2), (1981)1-11.

179. P.W. Langhoff, N. Padial, G. Csanak, T.N. Rescigno, and B.V. McKoy, Int. J. Quant. Chem. Symp. 14(1980)285-304.

180. Javed Husain, Ind. J. Phys. 53B(6),(1979) and Proc. Ind. Assoc. for the Cultivation of Science 62B(6),(1979)263-265.

181. H. Klar, J. Phys. B: Atom. Molec. Phys. 13(10),(1980)2037-2049.

182. E.D. Poliakoff, J.L. Dehmer, Dan Dill, A.C. Parr, K.H. Jackson, and R.N. Zare, Phys. Rev. Lett. 46(14),(1981)907-910.

183. U. Heinzmann, Appl. Opt. 19(23),(1980)4087-4091.

184. N.A. Cherepkov, J. Phys. B: Atom. Molec. Phys. 14(3),(1981)L73-L77; J. Phys. B: Atom. Molec. Phys. 14(13),(1981)2165-2177.

185. Keh-Ning Huang, Phys. Lett. 77A(2,3),(1980)133-136.

186. H. Klar and H. Kleinhoppen, J. Phys. B: Atom. Molec. Phys. 15(6), (1982)933-950.

187. J. Kessler, Comments At. Mol. Phys. 10(2,3),(1981)47-56.

188. H.S.W. Massey, Endeavour 35(125),(1976)58-65.

189. R. Cayrel in "The Solar Spectrum," ed. C. DeJager, (Reidel,1965) 106-109.

190. P.C. Engelking, R.R. Corderman, J.J. Wendoloski, G.B. Ellison, S.V. ONeill, and W.C. Linenberger, J. Chem. Phys. 74(10),(1981) 5460-5473.

191. Bruce H. Mahan and Anthony O'Keefe, J. Chem. Phys. 74(10),(1981) 5606-5612.

192. Gregory I. Gellene, Brian Wesley Williams, and Richard F. Porter, J. Chem. Phys. 74(10),(1981)5636-5642.

193. F. Breyer, P. Frey, and H. Hotop, Z. Phys. A: Atoms and Nuclei 300(1),(1981)7-24.

194. Eric Herbst, Nature 289(5799),(1981)656-657.

195. John C. Slater, Adv. Quant. Chem. 1(1964)35-58.

196. Keith H. Johnson, Adv. Quant. Chem. 7(1973)143-185.

197. Keith H. Johnson in "Computers in Chemical Research and Education," vol. 2, Union of the Chem. Soc. SFR, Yugoslavia, Ljubljana/Zagreb, 1973, (Elsevier,1973)4/39-4/69.

198. J.W. Mintmire, Int. J. Quant. Chem. Symp. 13(1979)163-168.

199. B.J. Dunlap and H.I. Yu, Chem. Phys. Lett. 73(3),(1980)525-529.

200. Hideo Sambe, Chem. Phys. 59(3),(1981)315-327.

201. Hideo Sambe and R.H. Felton, Chem. Phys. 59(3),(1981)329-339.

202. Levente Szasz, Z. Naturforsch. 35A(6),(1980)628-636.

203. Shinichi Katsuki and Hiroshi Taketa, Int. J. Quant. Chem. (Proc. Third Internat. Congress) 18(1),(1980)25-29.

204. Hideo Sambe, Int. J. Quant. Chem. Symp. 9(1975)95-104.

205. Karlheinz Schwarz, Phys. Rev. B5(7),(1972)2466-2468; Theoret. Chim. Acta (Berl.) 34(3),(1974)225-231.

206. M.S. Gopinatham, M.A. Whitehead, and R. Bogdanović, Phys. Rev. A14(1),(1976)1-10.

207. E.A. Kmetko, Phys. Rev. A1(1),(1970)37-38.

208. P. Rennert, Acta Phys. Acad. Scient. Hung. 37(3),(1974)219-252.

209. M.P. Das, Int. J. Quant. Chem. Symp. 14(1980)67-70.

210. John C. Slater, Int. J. Quant. Symp. 9(1975)7-21.

211. Rafael Benguria, Haim Brezis, and Elliott H. Lieb, Commun. Math. Phys. 79(2),(1981)167-180.

212. Ref. 63, section 32c.

213. Gary Kemister and Sture Nordholm, J. Chem. Phys. 76(10),(1982) 5043-5050.

214. H. Weinstein, P. Politzer, and S. Srebrenik, Theoret. Chim. Acta (Berl.) 38(2),(1975)159-163.

215. Giancarlo deAlti, Piero Decleva, and Adriana Lisini, Chem. Phys. 66(3),(1982)425-433.

216. John W. Mintmire and J.R. Sabin, Chem. Phys. 50(1),(1980)91-103.

217. T. Koopmans, Physica 1(1934)104-113.

218. B. Duke in "Theoretical Chemistry: A Review of the Recent Literature," vol. 2, eds. R.N. Dixon and C. Thomson, (Chem. Soc., Burlington,Lond.,1975)159-202.

219. Nobuhiro Kosugi, Haruo Kurado, and Suehiro Iwata, Chem. Phys. 58(2),(1981)267-273.

220. W. von Niessen, G. Bieri, J. Schirmer, and L.S. Cederbaum, Chem. Phys. 65(2),(1982)157-176.

221. Charles E. Mortimer, "Chemistry: A Conceptual Approach," (Van Nostrand,Second Ed.,1971), sect. 4.4.

222. Juergen Hinze, Adv. Chem. Phys. 26(1974)213-263.

223. Joseph O. Hirschfelder, Charles F. Curtis, and R. Byron Bird, "Molecular Theory of Gases and Liquids," (Wiley,1954), chapt. 13.

224. J.B. Danese, Chem. Phys. Lett. 45(1),(1977)150-154.

225. S.J. Niemczyk and C.F. Melius, Chem. Phys. Lett. 46(2),(1981)236-241.

226. Richard W. Jothan, J. Chem. Educ. 52(6),(1975)377-378.

227. E. Teller and H.L. Sahlin in "Physical Chemistry: An Advanced Treatise," ed. Henry Eyring, (Acad. Press,1970)1-34.

228. E. Teller, J. Phys. Chem. 41(1),(1937)109-116.

229. Gerhard Herzberg and H.C. Longuet-Higgins, Farad. Discuss. Chem. Soc. (Lond.) 35(1963)77-82.

230. Jacob Katriel and Ernest R. Davidson, Chem. Phys. Lett. 76(2), (1980)259-262.

231. Tucker Carrington, Acc. Chem. Res. 7(1),(1974)20-25.

232. R.L. Day, R.J. Anderson, and F.A. Sharpton, J. Chem. Phys. 71(9), (1979)3683-3688.

233. L. Wolniewicz and K. Dressler, J. Molec. Spectrosc. 77(2),(1979) 286-297.

234. Stephen V. Oneil and Henry F. Schaefer III, J. Chem. Phys. 53(10), (1970)3994-4004.

235. David J. Nesbitt and Stephen R. Leone, Chem. Phys. Lett. 87(2), (1982)123-127.

236. S. Manoli and M.A. Whitehead, Phys. Rev. A23(5),(1981)2150-2155.

237. Jeppe Olsen, Poul Jørgsen, and Danny L. Yaeger, J. Chem. Phys. 76(1),(1982)527-542.

238. Andoni Garritz, José Luis Gázquez, Miguel Castro, and Jaime Keller, Int. J. Quant. Chem. 15(6),(1979)731-744.

239. R. Roberge and D.R. Salahub, J. Chem. Phys. 70(3),(1979)1177-1186.

240. D.R. Salahub, S.H. Lamson, and R.P. Messmer, Chem. Phys. Lett. 85(4),(1982)430-433.

241. P. Hohenberg and W. Kohn, Phys. Rev. B136(3),(1964)864-871.

242. W. Kohn and L.J. Sham, Phys. Rev. A140(4),(1965)1133-1138.

243. Michael Schlüter and Lu Jeu Sham, Phys. Today 35(2),(1982)36-43.

244. Eugene S. Kryachko, Int. J. Quant. Chem. 18(4),(1980)1029-1035.

245. P.-O. Löwdin, Advan. Chem. Phys. 2(1959)207-365.

246. S.R. La Paglia, "Introduction to Quantum Chemistry," (Harper and Row,1971), section 4.10.

247. Walter Thiel, J. Am. Chem. Soc. 103(6),(1981)1413-1420.

248. John Mitchem, The Two-Year College Mathematics Journal 12(2), (1981)108-116.

249. K.D. Sen, Chem. Phys. Lett. 74(1),(1980)201-202.

250. D.B. Cook, Molec. Phys. 42(1),(1981)235-238.

251. Reidar Arneberg, Jiri Müller, and Rolf Manne, Chem. Phys. 64(2), (1982)249-258.

252. Stephen R. Langhoff and Delano P. Chong, Chem. Phys. 55(3),(1981) 355-360.

253. L.S. Cederbaum, G. Hohlneicher, and W. von Niessen, Chem. Phys. Lett. 18(4),(1973)503-508; Molec. Phys. 26(6),(1973)1405-1424.

254. L.S. Cederbaum and W. Domcke, Adv. Chem. Phys. 36(1977)205-344.

255. W. von Niessen, L.S. Cederbaum, W. Domcke, and G.H.F. Diercksen, Chem. Phys. 56(1),(1981)43-52.

256. I. Hubač and M. Urban, Theoret. Chim. Acta (Berl.) 45(3),(1977) 185-195.

257. D.P. Chong, F.G. Herring, and D. Mc.Williams, J. Chem. Phys. 61(1),(1974)78-84; J. Chem. Phys. 61(3),(1974)958-962; J. Chem. Phys. 61(9),(1974)3567-3570; Chem. Phys. Lett. 25(4),(1974)568-570.

258. D.P. Chong and S.R. Langhoff, Chem. Phys. 67(2),(1982)153-159.

259. Stephen R. Langhoff and Delano P. Chong, Chem. Phys. Lett. 86(5, 6),(1982)487-490.

260. Dietmar Saddei, Hans-Joachim Freund, and Georg Hohlneicher, Chem. Phys. 55(3),(1981) 339-354.

261. Michael C. Böhm and Rolf Gleitner, Theoret. Chim. Acta (Berl.) 57(4),(1980)315-321.

262. Michael C. Böhm, Ber. Buns. Ges. Phys. Chem. 86(1),(1982)56-63.

263. F.S. Levin, Int. J. Quant. Chem. Symp. 12(1978)109-130.

264. J.C. Slater, "The Self Consistent Field for Molecules and Solids," vol. 6, (McGraw-Hill,New York,1974).

265. J.W.D. Connolly, "Modern Theoretical Chemistry," vol. 7, ed. G.A. Segal, (Plenum Press,New York,1976),p.105.

266. John C. Slater, "The Calculation of Molecular Orbitals," (Wiley, 1979), chapter 7.

267. Karlheinz Schwarz, Chem. Phys. 7(1),(1975)100-107.

268. Nelson H.F. Beebe, Chem. Phys. Lett. 19(2),(1981)290-294.

269. Kali D. Sen, Peter C. Schmidt, and Aldrich Weiss, Theoret. Chim. Acta (Berl.) 58(1),(1980)69-71.

270. G.L. Gutsev and A.I. Boldyrev, Chem. Phys. 56(3),(1981)277-283.

271. Du Li, Ji-Kang Zhu, Junqing Li, and Yuh-Kang Pan, Chem. Phys. Lett. 87(5),(1982)463-466.

272. Giancarlo De Alti and Piero Decleva, Chem. Phys. Lett. 77(2), (1981)413-418.

273. K.D. Sen, P.C. Schmidt, and Aldrich Weiss, J. Chem. Phys. 75(2), (1981)1037-1038.

274. L.J. Bartoletti, S.R. Gadre, and R.G. Parr, J. Am. Chem. Soc. 102(9),(1980)2945-2948.

275. K.D. Sen, J. Phys. B: Atom. Molec. Phys. 11(19),(1978)L577-L578.

276. K.D. Sen, J. Chem. Phys. 71(2),(1979)1035-1036.

277. Arthur R. Williams, Robert A. de Groot, and Charles B. Sommers, J. Chem. Phys. 63(2),(1975)628-631.

278. D.P. Chong, Chem. Phys. Lett. 73(1),(1980)181-185.

279. H.S. Brandi, M.M. De Matos, and R. Ferreira, Chem. Phys. Lett. 73(3),(1980)597-601.

280. Tom Ziegler and Arvi Rauk, Theoret. Chimia Acta (Berl.) 46(1), (1977)1-10.

281. M.S. Gopinathan, J. Phys. B: Atom. Molec. Phys. 12(4),(1979)521-529.

282. P. Corrêa de Mello, M. Hohenberger, and M.C. Zerner, Int. J. Quant. Chem. 21(1),(1982)251-257.

283. Luiz G. Ferreira, J. Comp. Phys. 36(2),(1980)198-208.

284. David A. Case and Cary Y. Yang, Int. J. Quant. Chem. 18(4),(1980) 1091-1099.

285. A.V. Lyaptsev, A.M. Petrunkin, and A.A. Kiselev, Opt. Spectrosc. (Engl.) 49(3),(1980)268-272.

286. A. Rosén and D.E. Ellis, Chem. Phys. Lett. 27(4),(1974)595-599.

287. Bo G. Cartling and Douglas M. Whitmore, Int. J. Quant. Chem. 10(3),(1976)393-410.

288. Annik Goursot and Henry Chermette, Chem. Phys. 69(3),(1982)329-334.

289. V.M. Machado and G. Ferreira, Chem. Phys. Lett. 37(1),(1976)51-54.

290. C.Y. Yang, K.H. Johnson, and J.A. Horsley, J. Chem. Phys. 68(3), (1978)1001-1005.

291. J.H. Wood, Michael Boring, and Susan Beatty Woodruff, J. Chem. Phys. 74(9),(1981)5225-5233.

292. S.G. Gagarin and A.P. Kovtun, J. Struct. Chem. (Engl.) 21(4), (1980)420-426.

293. Pekka Pyykkö, Adv. Quant. Chem. 11(1978)353-409.

294. P. Murilo Oliveira and B. Maffeo, Int. J. Quant. Chem. 20(5), (1981)1127-1139.

295. L. Scheire and P. Phariseau, Chem. Phys. Lett. 26(2),(1974)149-151.

296. Frank Herman, Arthur R. Williams, and Keith Johnson, J. Chem. Phys. 61(9),(1974)3508-3522.

297. D.R. Salahub, R.P. Messmer, and K.H. Johnson, Mol. Phys. 31(2), (1976)529-534.

298. Aniko E. Foti, Vedene H. Smith, and M.A. Whitehead, Mol. Phys. 45(2),(1982)385-396.

299. Cary Y. Yang and K.H. Johnson, Int. J. Quant. Chem. Symp. 10(1976)159-165.

300. M. Costas and A. Garritz, Int. J. Quant. Chem. Symp. 13(1979) 141-162.

301. Jaime Keller, Int. J. Quant. Chem. 9(4),(1975)583-604.

302. L. Scheire and P. Phariseau, Int. J. Quant. Chem. 9(5),(1975) 887-900.

303. V.C. Rakhecha and N.S. Satya Murthy, J. Phys. C: Solid State Phys. 14(13),(1981)1809-1820.

304. L. Scheire, Physica A81(4),(1975)613-622.

305. S.A. Titov, Opt. Spectrosc. (Engl.) 51(3),(1981)219-220.

306. J.B. Danese, J. Chem. Phys. 61(8),(1974)3071-3080 and ref. 224.

307. R. Latter, Phys. Rev. 99(2),(1955)510-519.

308. S.F. Ruzankin and V.I. Avdeev, J. Struct. Chem. (Engl.) 20(5), (1980)818-820.

309. E. Hartman and R. Szargan, Chem. Phys. Lett. 68(1),(1979)175-178.

310. Joe G. Norman, Jr., J. Chem. Phys. 61(11),(1974)4630-4635.

311. M. Born, W. Heisenberg, and P. Jordan, Z. Phys. 35(8,9),(1925) 557-615.

312. S. Antoci, L. Mihich, and G.F. Nardelli, J. Chem. Phys. 61(3), (1974)1245-1246.

313. Ulla Mitzdorf, Theoret. Chim. Acta (Berl.) 37(2),(1975)129-145.

314. I.A. Topol and A.I. Dementev, J. Struct. Chem. (Engl.) 21(2), (1980)131-134.

315. H.H. Michels, R.H. Hobbs, L.A. Wright, and J.W. Connolly, Int. J. Quant. Chem. 13(2),(1978)169-187.

316. Marcy E. Rosenkrantz and Daniel D. Konowalow, Int. J. Quant. Chem. 12(4),(1977)707-719; Int. J. Quant. Chem. 16(6),(1979) 1301-1305.

317. Daniel D. Konowalow and Marcy E. Rosenkrantz, Chem. Phys. Lett. 44(2),(1976)321-324; Chem. Phys. Lett. 49(1),(1977)54-58.

318. Mark H. Mc Adon and Daniel D. Konowalow, J. Chem. Phys. 71(7), (1979)3089-3098.

319. Peter Senn, Research Proposal, Dept. of Chemistry, The University of Tennessee at Knoxville, June 5, 1979.

320. W.L. Barrow, Hideo Sambe, and R.H. Felton, Chem. Phys. Lett. 68(1),(1979)170-174.

321. J.C. Slater, J. Chem. Phys. 41(10),(1964)3199-3204.

322. F.C. Smith, Jr. and K.H. Johnson, Phys. Rev. Lett. 22(22),(1969), 1168-1171.

323. K.H. Johnson and F.C. Smith, Jr., Phys. Rev. B5(3),(1972)831-843.

324. Shinicho Katsuki, Mariusz Klobukowski, and Paucracio Palting, Comp. Phys. Comm. 25(1),(1982)39-55.

325. D.A. Liberman and I.P. Batra, "Multiple Scattering Program Descriptions," (IBM, San Jose Division, 1973) IBM Research Report RJ1224.

326. W. Kolos and L. Wolniewicz, J. Chem. Phys. 43(7),(1965)2429-2441.

327. H. Wind, J. Chem. Phys. 42(7),(1965)2371-2373.

328. Ira N. Levine, "Physical Chemistry," (McGraw-Hill,1978), section 19.7.

329. Lee A. Collins, David C. Cartwright, and Willard R. Wadt, J. Phys. B: Atom. Molec. Phys. 13(20),(1980)L613-L616.

330. Nobumitsu Honjou and Fukashi Sasaki, Mol. Phys. 37(5),(1979) 1593-1604.

331. Ran B. Singh and D. Kai Rai, J. Mol. Spectrosc. 19(4),(1966)424-434.

332. O. Gunnarsson, J. Harris, and R.O. Jones, Int. J. Quant. Chem. Symp. 11(1977)71-74.

333. Giannoula Theodorakopoulos, S.D. Peyerimhoff, and Robert J. Bunker, Chem. Phys. Lett. 81(3),(1981)413-420.

334. Michael Cook and Martin Karplus, J. Chem. Phys. 72(1),(1980)7-19.

335. David A. Case and Martin Karplus, Chem. Phys. Lett. 39(1),(1976) 33-38.

336. David A. Case, Michael Cook, and Martin Karplus, J. Chem. Phys. 73(7),(1980)3294-3313.

337. C.H. Li, Int. J. Quant. Chem. Symp. 10(1976)193-202.

338. A.S. Chesnyi, I.A. Topol, and N.G. Rambidi, Chem. Phys. 49(1), (1980)107-115.

339. A.S. Chesnyi, I.A. Topol, and S.L. Bazhenov, Theoret. Exp. Chem. (Engl.) 16(2),(1980)125-134.

340. I.A. Topol, A.S. Chesnyi, V.M. Kovba, and N.F. Stepanov, Chem. Phys. 53(1,2),(1980)63-69.

341. Sven Larsson, Michael Hehenberger, and Paulo Corrêa de Mello, Int. J. Quant. Chem. 18(5),(1980)1271-1278.

342. Diana Guenzburger, Bruno Maffeo, and Sven Larsson, Int. J. Quant. Chem. 12(2),(1977)383-396.

343. Hans-Georg Bartel, Theoret. Chim. Acta (Berl.) 58(1),(1980)41-44.

344. Michael Cook and Martin Karplus, Chem. Phys. Lett. 84(3),(1981) 565-570.

345. Al Schenk, "Calculus and Analytic Geometry," (Goodyear,1977).

346. Michael Roche and Dennis R. Salahub, J. Electron Spectrosc. Relat. Phenom. 19(3),(1980)273-284.

347. J.C. Lorquet and M. Desouter, Chem. Phys. Lett. 16(1),(1972)136-140.

348. A.L. Roche and H. Lefebvre-Brion, Chem. Phys. Lett. 32(1),(1975) 155-158.

349. Robert S. Mulliken, Int. J. Quant. Chem. 8(5),(1974)817-821.

350. Roman F. Nalewajski, Int. J. Quant. Chem. Symp. 12(1978)87-102.

351. C.N. Yang, Phys. Rev. 74(7),(1948)764-772.

352. F.A. Grimm in "Electron Spectroscopy," ed. D.A. Shirley, (North-Holland,1972)199-206.

353. R. Parzynski, Acta Phys. Pol. A54(4),(1978)479-492; Acta Phys. Pol. A57(1),(1980)49-57 and 59-71.

354. Burke Ritchie, Phys. Rev. A13(4),(1976)1411-1415; Phys. Rev. A14(1),(1976)359-362.

355. J.F. Nicoud and H.B. Kahn, Israel J. Chem. 15(1,2),(1976,1977)78-81.

356. P.T. Pickup and D.W. Sabo, Theoret. Chim. Acta (Berl.) 58(1),(1980)1-8.

357. Z.I. Kuplyauskis, Opt. Spectrosc. (Engl.) 48(2),(1980)119-120.

358. K. Ya. Burshtein and P.P. Shorygin, Russ. J. Phys. Chem. 54(4),(1980)488-494.

359. W. Gordon, Ann. Phys. 2(5),(1929)1031-1056.

360. M. Stobbe, Ann. Phys. 7(6),(1930)661-715.

361. V.D. Kondratovich and V.N. Ostrovskii, Sov. Phys. (JETP), (Engl.) 52(2),(1980)198-205.

362. S.M. Kara and M.R.C. McDowell, J. Phys. B: Atom. Molec. Phys. 14(11),(1981)1719-1739.

363. E. Karule, J. Phys. B: Atom. Molec. Phys. 11(3),(1978)441-447.

364. S. Klarsfield and A. Maquet, J. Phys. B: Atom. Molec. Phys. 12(18),(1979)L553-L556.

365. Y. Gontier, M. Poirier, and M. Trahin, J. Phys. B: Atom. Molec. Phys. 13(7),(1980)1381-1387.

366. D.R. Bates, U. Öpik, and G. Poots, Proc. Phys. Soc. (Lond.) A66(1953)1113-1123.

367. D.R. Bates and U. Öpik, Proc. Phys. Soc. (Lond.), Ser. 2, At. Mol. Phys. 1(4),(1968)543-547.

368. H.D. Cohen and U. Fano, Phys. Rev. 150(1),(1966)30-33.

369. A.D. Nadezhin, Opt. Spectrosc. (Engl.) 47(2),(1979)143-145.

370. V.E. Semenov, Opt. Spectrosc. (Engl.) 48(4),(1980)398-401.

371. John R. Rumble, Jr., Donald G. Truhlar, and Michael A. Morrison, J. Phys. B: Atom. Molec. Phys. 14(8),(1981)L301-L305.

372. J. Wayne Rabalais and Tom P. Debies, J. Electron Spectrosc. Relat. Phenom. 5(1974)847-880.

373. Lawrence L. Lohr, Jr. in "Electron Spectroscopy," ed. D.A. Shirley, (North-Holland,1972)245-258.

374. Takashi Fujikawa, Toshiaki Ohta, and Haruo Kuroda, J. Electron Spectrosc. Relat. Phenom. 16(4),(1979)285-299.

375. Manoj Mishra and Yngve Öhrn, Int. J. Quant. Chem. Symp. 14(1980) 335-348.

376. D. Dill and J.L. Dehmer, J. Chem. Phys. 61(2),(1974)692-699.

377. J. Siegel, D. Dill, and J.L. Dehmer, J. Chem. Phys. 64(8),(1976) 3204-3206.

378. J.L. Dehmer and Dan Dill, J. Chem. Phys. 65(12),(1977)5327-5334.

379. S. Wallace, D. Dill, and J.L. Dehmer, Phys. Rev. B17(4),(1978) 2004-2010.

380. J.L. Dehmer and Dan Dill in "Electron-Molecule and Photon-Molecule Collisions," eds. Thomas Reseigno, Vincent McKoy, and Berry Schneider, (Plenum,1979)225-265.

381. John C. Tully, R. Stephen Berry, and Bryan J. Dalton, Phys. Rev. 176(1),(1968)95-105.

382. Joseph Cipriani and Bernard Silvi, Mol. Phys. 45(2),(1982)259-272.

383. M.J. Seaton, J. Phys. B: Atom. Molec. Phys. 14(20),(1981)3827-3834.

384. Albert Messiah, "Quantum Mechanics," vol. 1, (North-Holland,1961), chapter 5, section 19.

385. H.P. Kelly, Chem. Phys. Lett. 20(6),(1973)547-550.

386. Maurice Cohen, Chem. Phys. Lett. 81(3),(1981)513-518.

387. Walter Thiel, Chem. Phys. 57(1,2),(1981)227-243.

388. L. Noodleman, J. Chem. Phys. 64(6),(1976)2343-2349.

389. J.B. Diamond, Chem. Phys. Lett. 20(1),(1973)63-66.

390. F.A. Grimm, Thomas A. Carlson, W.B. Dess, Paul Agron, J.O. Thomson, and James W. Davenport, J. Chem. Phys. 72(5),(1980) 3041-3048.

391. Thomas A. Carlson, Manfred O. Krause, Frederick A. Grimm, John D. Allen, Jr., David Mehaffy, Paul R. Keller, and James W. Taylor, J. Chem. Phys. 75(7),(1981)3288-3292.

392. David Mehaffy, Paul R. Keller, James W. Taylor, Thomas A. Carlson, Manfred O. Krause, Frederick A. Grimm, and John D. Allen,Jr., J. Electron Spectrosc. Relat. Phenom. 26(3),(1982)213-221.

393. Ref. 422, equation (2.2.21) and text following this equation.

394. Dan Dill and J.L. Dehmer, J. Chem. Phys. 75(9),(1981)4546-4552.

395. Walter Thiel, Chem. Phys. Lett. 87(3),(1982)249-253.

396. Hugh P. Kelly in "Atomic Inner-Shell Processes," ed. B. Craseman, (Acad. Press,1975)331-352.

397. Geor D. Purvis and Ingve Öhrn, J. Chem. Phys.62(6),(1975)2045-2049.

398. L.S. Cederbaum, J. Schirmer, and W. Domcke, Int. J. Quant. Chem. 14(5),(1978)593-601.

399. J. Schirmer, L.S. Cederbaum, and W. von Niessen, Chem. Phys. 56(3),(1981)285-302.

400. G. Wendin, "Breakdown of the One-Electron Pictures in Photoelectron Spectra," in "Structure and Bonding," vol. 45, (Springer,1981).

401. M. Ya. Amusia, Comments At. Mol. Phys. 10(4),(1981)155-170.

402. Manuel Braga and Sven Larsson, Int. J. Quant. Chem. Symp. 11(1977)61-69.

403. John S. Tse, J. Chem. Phys. 73(11),(1980)5734-5737; Chem. Phys. Lett. 77(2),(1981)373-376.

404. D.K. Creber, J.S. Tse, and G.M. Bancroft, J. Chem. Phys. 72(8), (1980)4291-4299.

405. J.S. Tse, G.M. Bancroft, and D.K. Creber, J. Chem. Phys.74(4), (1981)2097-2107.

406. John S. Tse and G. Loubriel, J. Chem. Phys. 74(9),(1981)5190-5196.

407. Abha Gupta and J.A. Tossell, J. Electron Spectrosc. Relat. Phenom. 26(3),(1982)223-234.

408. U. Gelius and K. Siegbahn, Farad. Discuss. Chem. Soc. (Lond.) 54(1972)257-268.

409. P.R. Hilton, S. Nordholm, and N.S. Hush, J. Electron Spectrosc. Relat. Phenom. 18(1,2),(1980)101-119.

410. I.G. Kaplan and V.N. Smutnyi, Opt. Spectrosc. (Engl.) 49(4), (1980)361-364.

411. V.G. Yarzhemsky, V.I. Nefedov, M.Ya. Amusia, N.A. Cherepkov, and L.V. Chernysheva, J. Electron Spectrosc. Relat. Phenom. 23(2,3),(1981)175-186 and refs. therein.

412. F.A. Grimm, Chem. Phys. 53(1,2),(1980)71-75.

413. T.A. Carlson, M.O. Krause, F.A. Grimm, P.R. Keller, and J.W. Taylor, Chem. Phys. Lett. 87(6),(1982)552-555.

414. J.H.D. Eland, "Photoelectron Spectroscopy," (Butterworths,1974), chapter 6.

415. H. Köppel, E. Haller, L.S. Cederbaum, and W. Domcke, Mol. Phys. 41(3),(1980)669-677.

416. Thomas A. Carlson and R.M. White, Farad. Discuss. Chem. Soc. (Lond.) 54(1972)285-291.

417. R.E. Ballard, Appl. Spectrosc. Reviews 7(2),(1973)183-213.

418. Takashi Fujikawa and Haruo Kuroda, Int. J. Quant. Chem. (Proc. Third Internat. Congress), 18(1),(1980)251-256.

419. Takashi Fujikawa, J. Phys. Soc. Japan 50(4),(1981)1321-1329.

420. Steven Trent Manson, J. Electron Spectrosc. Relat. Phenom. 1(5), (1973)413-438; J. Electron Spectrosc. Relat. Phenom. 2(5),(1973) 482-484.

421. Daniel B. Donald and Stuart A. Rice, J. Chem. Phys. 74(9),(1981) 4893-4906.

422. James Whitman Davenport, Ph.D. Diss., Dept. of Physics, The University of Pennsylvania, 1976.

423. M.S. Banna, R.J. Key, C.S. Ewig, J. Electron Spectrosc. Relat. Phenom. 26(3),(1982)259-266.

424. Charlotte E. Moore, "Atomic Energy Levels," National Bureau of Standards, 1949.

425. Donald L. Miller and Anthony F. Starace, J. Phys. B: Atom. Molec. Phys. 13(17),(1980)L525-L529.

426. Paul Rehmus and R. Stephen Berry, Phys. Rev. A23(2),(1981)416-426.

427. Ref. 422, equations (2.2.12) and (2.2.13).

428. Ref. 422, equations (2.2.18) and (2.2.20).

429. M.C. Artru, C. Jamar, D. Petrini, and F. Praderie, Astron. Astrophys. 96(1,2),(1981)380-392.

430. F. Albert Cotton and Geoffrey Wilkinson, "Advanced Inorganic Chemistry: A Comprehensive Text," (Wiley&Sons,1966).

431. Robert S. Mulliken, J. Chem. Phys. 2(7),(1934)400-402.

432. Hans-Joachim Werner, Mol. Phys. 44(1),(1981)111-123.

433. J.O. Clayton and W.F. Giauque, J. Am. Chem. Soc. 54(7),(1932) 2610-2626.

434. D. Nicholls, Coord. Chem. Rev. 1(3),(1966)379-414.

435. Albert B. Rives and Richard F. Fenske, J. Chem. Phys. 75(3), (1981)1293-1302.

436. S.Å. Lindgren, J. Paul, and L. Walldén, Chem. Phys. Lett. 84(3), (1981)487-490.

437. K.H. Johnson and U. Wahlgren, Int. J. Quant. Chem. Symp. 6(1972) 243-255.

438. S. Larsson and M. Braga, Int. J. Quant. Chem. 15(1),(1979)1-5.

439. J.W. Davenport, Chem. Phys. Lett. 77(1),(1981)45-48.

440. Joseph Haggin, Chem. & Eng. News 59(8),(1981)39-47.

441. Cheryl K. Rofer-De Poorter, Chem. Rev. 81(5),(1981)447-474.

442. K. Kugeler, H.F. Niessen, M. Röth-Kamat, D. Böcker, B. Rüter, and K.A. Theis, Nucl. Engineering and Design 34(1),(1975)65-72.

443. Th. Dittrich, H.W. Buschmann, and W. Vielstich, Ber. Buns. Ges. Phys. Chem. 85(4),(1981)289-297.

444. D.P. Vercauteren, J.G. Fripiat, and J.M. André, Int. J. Quant. Chem. Symp. 15(1981)219-224.

445. Eugene B. Bradley and K.A. Arunkumar, Spectrosc. Lett. 15(2), (1982)113-124.

446. Henry Nichols and Robert M. Hexter, J. Chem. Phys. 76(11),(1982) 5595-5598.

447. M.R. McClellan, M. Trenary, N.D. Shinn, M.J. Sayers, K.L. D'Amico, Edward I. Solomon, and F.R. McFeely, J. Chem. Phys. 74(8),(1981)4726-4731.

448. Gloria B. Lubkin, Phys. Today 33(11),(1980)17-18.

449. Michael L. Knotek, Nature 291(5815),(1981)452-453.

450. Yukikazu Itikawa, J. Electron Spectrosc. Relat. Phenom. 2(2), (1973)125-142.

451. H. Tai and M.R. Flannery, Phys. Rev. A16(3),(1977)1124-1135.

452. Arthur A. Williams, Int. J. Quant. Chem. Symp. 8(1974)89-108.

453. A.D. Becke, J. Chem. Phys. 76(12),(1982)6037-6045.

454. O.K. Anderson and R.G. Woolley, Mol. Phys. 26(4),(1973)905-927.

455. O. Gunnarson, J. Harris, and R.O. Jones, J. Chem. Phys. 67(9), (1977)3970-3979.

456. Hideo Sambe and Ronald H. Felton, J. Chem. Phys. 62(3),(1975) 1122-1126.

457. Nadia Magnenat and Jacques Weber, Chem. Phys. Lett. 47(3),(1977) 490-494.

458. B.I. Dunlap, J.W.D. Connolly, and J.R. Sabin, J. Chem. Phys. 71(8),(1979)3396-3402; J. Chem. Phys. 71(12),(1979)4993-4999.

459. D.E. Ellis and G.S. Painter, Phys. Rev. B2(8),(1970)2887-2896.

460. E.J. Baerends, D.E. Ellis, and P. Ros, Chem. Phys. 2(1),(1973) 41-51.

461. E.J. Baerends and P. Ros, Chem. Phys. 2(1),(1973)52-59; Chem. Phys. 8(3),(1975)412-418.

462. W. Heijser, A.Th. Van Kessel, and E.J. Baerends, Chem. Phys. 16(4),(1976)371-379.

463. G.L. Gutsev and A.A. Levin, J. Struct. Chem. (Engl.) 20(5), (1979)655-662 and 663-665.

464. F.A. Grimm, John D. Allen, Thomas A. Carlson, Manfred O. Krause, David Mehaffy, Paul R. Keller, and James W. Taylor, J. Chem. Phys. 75(1),(1981)92-98.

465. J.L. Dehmer, Dan Dill, and Scott Wallace, Phys. Rev. Lett. 43(14),(1979)1005-1008.

466. D.L. Ederer, Roger Stockbauer, and J.L. Dehmer, J. Phys. B: Atom. Molec. Phys. 13(3),(1980)L105-L108.

467. Roger Stockbauer, B.E. Cole, D.L. Ederer, John B. West, Albert C. Parr, and J.L. Dehmer, Phys. Rev. Lett. 43(11),(1979)757-761.

468. B.E. Cole, D.L. Ederer, Roger Stockbauer, Keith Codling, Albert C. Parr, John B. West, E.D. Poliakoff, and J.L. Dehmer, J. Chem. Phys. 72(11),(1980)6308-6310.

469. J.B. West, Appl. Optics 19(23),(1980)4063-4067.

470. A.C. Parr, D.L. Ederer, J.B. West, D.M.P. Holland, and J.L. Dehmer, J. Chem. Phys. 76(9),(1982)4349-4355.

471. W.D. Gwinn and A.S. Gaylord, "Spectroscopic Studies of Ring-Puckering Motions," Int. Rev. of Science, Phys. Chem., Series 2, vol. 3, Spectroscopy, (Butterworths,Lond.,1976)205-262.

472. John R. Swanson, Dan Dill, and J.L. Dehmer, J. Chem. Phys. 75(2), (1981)619-624.

473. T. Gustafsson, Chem. Phys. Lett. 78(1),(1981)28-31.

474. V. Čermák, J. Electron Spectrosc. Relat. Phenom. 6(2),(1975)135-144.

475. Hidekazu Takagi and Hiroki Nakamura, J. Chem. Phys. 74(10), (1981)5808-5813.

476. P.M. Dehmer and W.A. Chupka, J. Chem. Phys. 65(6),(1976)2243-2273.

477. R.S. Berry, J. Chem. Phys. 45(4),(1966)1228-1245.

478. Dan Dill in "Electron Spectroscopy," ed. D.A. Shirley, (North-Holland,1972)277-282.

479. M. Raoult and Ch. Jungen, J. Chem. Phys. 74(6),(1981)3388-3399.

480. Paul-Marie Guyon and Irene Nenner, Appl. Optics 19(23),(1980) 4068-4078.

481. J.H.D. Eland, J. Chem. Phys. 72(11),(1980)6015-6019.

482. Goran Wendin, Int. J. Quant. Chem. Symp. 13(1979)659-670.

483. L. Åsbrink, C. Fridh, and E. Lindholm, Chem. Phys. 27(2),(1978) 159-168.

484. H. Harvey Michels, Adv. Chem. Phys. 45(1981)225-340.

485. J. Mazeau, C. Schermann, and G. Joyez, J. Electron Spectrosc. Relat. Phenom. 7(3),(1975)269-279.

486. Robert S. Mulliken, Acc. Chem. Res. 9(1),(1976)7-12.

487. J.H. Fock, P. Gürtler, and E.E. Koch, Chem. Phys. 47(1),(1980) 87-93.

488. E.M. Eleveth and A. Sevin, J. Am. Chem. Soc. 103(25),(1981)7414-7422.

489. Hiroki Nakamura, Chem. Phys. Lett. 28(4),(1974)534-539; Chem. Phys. 10(2,3),(1975)271-283, Chem. Phys. Lett. 33(1),(1975)151-155.

490. H. Okabe, J. Am. Chem. Soc. 93(25),(1971)7095-7096.

491. Phaedon Avouris, William M. Gelbart, and A. El-Sayed, Chem. Rev. 77(6),(1977)793-833.

492. G.R. Wight, M.J. Van der Wiel, and C.E. Brion, J. Phys. B: Atom. Molec. Phys. 9(4),(1976)675-689.

493. James A.R. Samson, T. Masuoka, and W.T. Huntress, Geophys. Res. Lett. 8(4),(1981)405-408.

494. Toshio Masuoka and James A.R. Samson, J. Chem. Phys. 74(2),(1981) 1093-1097.

495. A.P. Hitchcock, C.E. Brion, and M.J. Van der Wiel, Chem. Phys. 45(3),(1980)461-478.

496. Henry A. Kurtz and Yngve Öhrn, Phys. Rev. A19(1),(1979)43-48.

497. Young Soon Kim, Akiva Ron, R.H. Pratt, B.R. Tambe, and Steven T. Manson, Phys. Rev. Lett. 46(20),(1981)1326-1329.

498. T.M. Luke, J. Phys. B: Atom. Molec. Phys. 11(14),(1978)2457-2466.

499. T.M. Luke and S. Phillips, J. Phys. B: Atom. Molec. Phys. 14(14), (1981)2337-2343.

500. U. Fano, Phys. Rev. 124(6),(1961)1866-1878.

501. G. Herzberg in "Topics in Modern Physics," (Colorado Assoc. Univ. Press,1971)191-197.

502. André Bandrauk and Jean Pierre Laplante, J. Chem. Phys. 65(7), (1979)2602-2608.

503. F.L. Boschke (ed.), "Large Amplitude Motion in Molecules I and II," (Topics in Current Chemistry-Fortschritte der Chemischen Forschung), vols. 81 and 82, (Springer,Berlin,Heidelberg,N.Y., 1979).

504. T.M. Luke, J. Phys. B: Atom. Molec. Phys. 15(8),(1982)1217-1228.

505. P.E. Coleman and P.L. Knight, J. Phys. B: Atom. Molec. Phys. 15(7),(1982)L235-L241.

506. E.B. Aleksandrov, N.I. Kaliteevskii, and M.P. Chaika, Sov. Phys. (Usp.), (Engl.) 22(9),(1979)760-767.

507. W. Mehlhorn and K. Taulberg, J. Phys. B: Atom. Molec. Phys. 13(3),(1980)445-451.

508. P.L. Knight, Optics Comm. 32(2),(1980)261-265.

509. J. Chaiken, M. Gurnick, and J.D. McDonald,J. Chem. Phys. 74(1), (1981)106-116, 117-122, and 123-126.

510. E.M. Rowe, Phys. Today 34(5),(1981)28-37.

511. Hermann Winick, George Brown, Klaus Halbach, and John Harris, Phys. Today 34(5),(1981)50-63.

512. "Synchrotron Radiation Research," eds. Hermann Winick and S. Donach, (Plenum,N.Y.,1980).

513. J.N. Elgin, Phys. Bull. 33(3),(1982)90-92.

514. T.I. Smith and J.M.J. Madey, Appl. Phys. B27(4),(1982)195-199.

515. P. Sprangle, R.A. Smith, and V.L. Granatstein, Naval Res. Lab. Memorandum Rep. 3911(Dec. 8,1978).

516. P. Sprangle and R.A. Smith, Naval Res. Lab. Memorandum Rep. 4033(Sept. 18,1979).

517. P. Sprangle, Cha-Mei Tang, and W.M. Manheimer, Naval Res. Memorandum Rep. 4034(Sept. 28,1979).

518. Jeffrey A. Sell, Aaron Kuppermann, and Donald M. Mintz, J. Electron Spectrosc. Relat. Phenom. 16(3),(1979)127-145.

519. N.M. Kabachnik and I.P. Sazhina, J. Phys. B: Atom. Molec. Phys. 9(10),(1976)1681-1697.

520. J. Kreile, A. Schweig, and W. Thiel, Chem. Phys. Lett. 79(3), (1981)547-552.

521. Thomas A. Carlson, M.O. Krause, D. Mehaffy, J.W. Taylor, F.A. Grimm, and J.D. Allen, Jr., J. Chem. Phys. 73(12),(1980)6056-6058.

522. J.L. Dehmer and Dan Dill, Phys. Rev. Lett. 35(4),(1975)213-215; J. Chem. Phys. 65(12),(1976)5327-5334.

523. Scott Wallace, Dan Dill, and J.L. Dehmer, J. Phys. B: Atom. Molec. Phys. 12(14),(1979)L417-L420.

524. James W. Davenport, Phys. Rev. Lett. 36(16),(1976)945-949.

525. William H. Fletcher and Farrell B. Brown, J. Chem. Phys. 39(10), (1963)2478-2490.

526. G.V. Marr, J.M. Morton, R.M. Holmes, and D.G. McCoy, J. Phys. B: Atom. Molec. Phys. 12(1),(1979)43-52.

527. D.K. Bulgin, J.M. Dyke, and Alan Morris, J. Chem. Soc. (Lond.), Farad. Trans. II 73(7),(1977)983-990.

528. M. Wu and T.P. Fehlner, Chem. Phys. Lett. 36(1),(1975)114-116.

529. T.V. Ramakrishna Rao and V.J. Lakshman, Ind. J. Pure Appl. Phys. 4(7),(1966)259-262.

530. S. Sützer, S.-T. Lee, and D.A. Shirley, J. Chem. Phys. 65(1), (1976)412-417.

531. N. Jonathan, A. Morris, M. Okuda, K.J. Ross, and D.J. Smith, Chem. Soc. (Lond.), Farad. Discuss. 54(1972)48-55.

532. E.A. Colbourn, J.M. Dyke, E.P.F. Lee, A. Morris, and I.R. Trickle, Mol. Phys. 35(3),(1978)873-882.

533. M.G. White, R.A. Rosenberg, S.-T. Lee, and D.A. Shirley, J. Electron Spectrosc. Relat. Phenom. 17(5),(1979)323-344.

534. M. Wu and T.P. Fehlner, J. Am. Chem. Soc. 98(24),(1976)7578-7585.

535. J.M. Dyke, A. Morris, A.M.A. Ridha, and J.G. Snijder, Chem. Phys. 67(3),(1982)245-253.

536. D.L. Hildebrand, Int. J. Mass Spectrom. Ion Phys. 7(3),(1971)255-260.

537. R.K. Nesbet, J. Chem. Phys. 43(12),(1965)4403-4409.

538. J.B. West, K. Codling, A.C. Parr, D.L. Ederer, B.E. Cole, R. Stockbauer, and J.L. Dehmer, J. Phys. B: Atom. Molec. Phys. 14(11),(1981)1791-1801.

539. W.B. Lewis and W.R. Wadt, Chem. Phys. Lett. 78(2),(1981)266-269.

540. W. Kolos and L. Wolniewicz, J. Chem. Phys. 50(8),(1969)3228-3240.

541. Paul J.A. Ruttnik and Joop H. Lenthe, J. Chem. Phys. 74(10), (1981)5785-5793.

542. N. Moiseyev, J. Katriel, and C. Trindle, Int. J. Quant. Chem. 12(4),(1977)759-763.

543. Chris L. Smith, New Scientist 92(1274),(1981)94-97.

544. Nicholas Rescher in "The Encyclopedia of Philosophy," ed. Paul Edwards, (Macmillan,1967), under "Buridan."

545. J. Brickman, Ber. Buns. Ges. Phys. Chem. 85(2),(1981)106-112.

546. F.V. Kurmartsev and É.I. Rashba, JETP Lett. 33(3),(1981)155-158.

547. A.E. Fischer, J.E. Marsden, and Vincent Moncriet in "Essays in General Relativity," ed. Frank J. Tipler, (Acad. Press,1980), chapter 7.

548. R. Broer and W.C. Nieuwpoort, Chem. Phys. 54(3),(1981)291-303.

549. Hans Ågren, Lennart Selander, Joseph Nordgren, Carl Nordling, Kai Siegbahn, and Jiri Muller, Chem. Phys. 37(2),(1979)161-171.

550. Jiri Müller, Hans Ågren, and Osvaldo Goscinki, Chem. Phys. 38(3), (1979)349-359.

551. M.Ya. Amusia, Appl. Opt. 19(23),(1980)4042-4050.

552. G.L. Gutsev and A.E. Smoljar, Chem. Phys. 56(2),(1981)189-194.

553. B.I. Dunlap, P.A. Mills, and D.E. Ramaker, J. Chem. Phys. 75(1), (1981)300-305.

554. Dan Dill, Scott Wallace, Jon Siegel, and J.L. Dehmer, Phys. Rev. Lett. 41(18),(1978)1230-1233; Phys. Rev. Lett. 42(6),(1979) p. 411.

555. Shunsuke Hara, J. Phys. Soc. Japan 22(3),(1967)710-718.

556. J.A. Stephens, Dan Dill, and J.L. Dehmer, J. Phys. B: Atom. Molec. Phys. 14(20),(1981)3911-3918.

557. L. Noodleman, D. Post, and E.J. Baerends, Chem. Phys. 64(1), (1982)159-166.

558. P. Anthony Cox, Marc Bénard, and Alain Veillard, Chem. Phys. Lett. 87(2),(1982)159-161.

559. James W. Davenport, Brookhaven National Laboratory, private comm., Feb. 17, 1982.

560. David M. Bishop and Lap M. Cheung, Mol. Phys. 36(2),(1978)501-507.

561. Yukikazu Itikawa, Chem. Phys. 28(3),(1978)461-471.

562. Yukikazu Itikawa, Chem. Phys. 30(1),(1978)109-117.

563. Yukikazu Itikawa, Chem. Phys. 37(3),(1979)401-410.

564. Burke Ritchie and B.R. Tambe, J. Chem. Phys. 68(2),(1978)755-761.

565. F.A. Jenkins, J. Opt. Soc. Am. 43(5),(1953)425-426.

566. Report of the Joint Commission for Spectrosc. of the Internat. Astronom. Union and the Internat. Union of Pure and Appl. Phys., J. Chem. Phys. 23(1),(1955)1997-2011.

567. R.E. Ballard, "Photoelectron Spectroscopy and Molecular Orbital Theory," (Wiley,1978), section 43.

568. A.E. Douglas, Astrophys. J. 117(3),(1953)380-386.

569. K. Narahari Rao, Astrophys. J. 111(2),(1950)306-313.

570. Masataka Mizushima, "The Theory of Rotating Molecules," (Wiley, 1975), Table 6-6a.

571. A.R. Edmonds, "Angular Momentum in Quantum Mechanics," in "Investigations in Physics," vol. 4, (Princeton U. Press,1957).

572. M.E. Rose, "Elementary Theory of Angular Momentum," (Wiley,1957).

573. L.S. Cederbaum, H. Köppel, and W. Domcke, Int. J. Quant. Chem. Symp. 15(1981)251-267.

574. J.R. Swanson, Dan Dill, and J.L. Dehmer, J. Phys. B: Atom. Molec. Phys. 13(8),(1980)L231-L234; J. Phys. B: Atom. Molec. Phys. 14(6),(1981)L207-L211.

575. S.T. Manson and A.F. Starace, Revs. Mod. Phys. 54(2),(1982)389-405.

576. V. Špirko and P. Čársky, J. Molec. Spectrosc. 87(2),(1981)584-586.

577. Manuel Rotenberg, R. Bivins, N. Metropolis, and John K. Wooten, Jr., "The 3-j and 6-j Symbols," (The Technology Press,M.I.T., Cambridge,Mass.,1959).

578. M.P. Varma and B.L. Jha, J. Quant. Spectrosc. Radiat. Transf. 26(1),(1981)49-52.

579. W.E. Blass, Appl. Spectrosc. Lett. 11(1),(1976)57-123.

580. John H.D. Eland, J. Chem. Phys. 72(4),(1980)2878-2880.

581. Jacques Delwiche, Marie-Jeanne Hubin-Franskin, Paul-Marie Guyon, and Irène Nenner, J. Chem. Phys. 74(8),(1981)4219-4227.

582. Peter Senn and Dawn Crosby, "YODEL," Dept. of Chemistry, The University of Tennessee, 1982.

583. K. Schulten and R.G. Gordon, J. Math. Phys. 16(10),(1975)1961-1970 and 1971-1988; Comp. Phys. Comm. 11(2),(1976)269-278. These authors give recursion formulas for the 3-j, (and 6-j) symbols for j_3 and m_3 in (10-8). The recursion of the 3-j symbols for different j_3s is referred to in this text.

584. Robert C. Weast and Melvin J. Astle, "CRC Handbook of Chemistry and Physics," (CRC Press,59-th Edition,1978).

585. L. Åsbrink, Chem. Phys. Lett. 7(5),(1970)549-552.

586. Donald A. McQuarrie, "Statistical Thermodynamics," (Harper and Row,1973), sections 6-4 and 6-5.

587. M.R. Aliev, Opt. Spectrosc. 51(3),(1981)309-310.

588. J.R. Lombardi, R. Wallenstein, T.W. Hänsch, and D.M. Friedrich, J. Chem. Phys. 65(6),(1976)2357-2366.

589. Frederick N. Masri and William H. Fletcher, J. Chem. Phys. 52(11),(1970)5759-5766; J. Raman Spectrosc. 1(3),(1973)221-241.

590. Ian G. Ross, Adv. Chem. Phys. 20(1971)341-391.

591. R.P. Vasquez, J.D. Klein, J.J. Barton, and F.J. Grunthaner, J. Electron Spectrosc. Relat. Phenom. 23(1),(1981)63-81.

592. M.-J. Hubin-Franskin, J. Delwiche, P. Natalis, and G. Caprace, J. Electron Spectrosc. Relat. Phenom. 18(4),(1980)295-308.

593. Albert F. Carley and Richard W. Joyner, J. Electron Spectrosc. Relat. Phenom. 16(1,2),(1979)1-23.

594. N. Gurker, J. Electron Spectrosc. Relat. Phenom. 14(1),(1978)1-18.

595. William E. Blass and George W. Halsey, "Deconvolution of Absorption Spectra," (Acad. Press,1981).

596. S. Gouraud and R. Abouaf, Int. J. Mass Spectrom. Ion Phys. 40(3),(1981)351-359.

597. John D. Allen, Jr. and Frederick A. Grimm, Chem. Phys. Lett. 66(1),(1979)72-78.

598. A.J. Lorquet, J.C. Lorquet, J. Delwiche, and M.J. Hubin-Franskin, J. Chem. Phys. 76(10),(1982)4692-4699.

599. J.E. Pollard, D.J. Trevor, J.E. Reutt, Y.T. Lee, and D.A. Shirley, Chem. Phys. Lett. 88(4),(1982)434-438; J. Chem. Phys. 77(1),(1982)34-46 and refs. therein.

600. Larry A. Pugh and K. Narahari Rao in "Molecular Spectroscopy: Modern Research," vol. 2, ed. K. Narahari Rao, (Acad.Press,1976), 165-227.

601. S.O. Kastner, J. Opt. Soc. Am. 70(11),(1980)1371-1372.

602. G.J. Fisanick, A. Gedanken, T.S. Eichelberger IV, N.A. Kuebler, and M.B. Robin, J. Chem. Phys. 75(11),(1981)5215-5225.

603. Peter Senn, "Intramolecular Dynamics," unpublished.

604. Thomas A. Carlson, "Photoelectron and Auger Spectroscopy," (Plenum,1975), chapter 3, section 2.

605. J. Nordgren, L. Pettersson, L. Selander, C. Nordling, K. Siegbahn, and H. Ågren, J. Phys. B: Atom. Molec. Phys. 15(5), (1982)L153-L155.

606. P.L. Knight and P.E. Coleman, J. Phys. B: Atom. Molec. Phys. 13(22),(1980)4345-4352.

607. P.L. Knight, Comments At. Molec. Phys. 10(6),(1981)241-255.

608. Harold Metcalf and William Phillips, Opt. Lett. 5(12),(1980)540-542.

609. W. Zinth, M.C. Nuss, and W. Kaiser, Chem. Phys. Lett. 88(3), (1982)257-261.

610. Isao Shimamura, Phys. Rev. A23(6),(1981)3350-3353; J. Phys. B: Atom. Molec. Phys. 15(1),(1982)93-100.

611. Isao Shimamura, The Institute of Space and Astronautical Science, Tokyo 153, Japan, private comm., June 22, 1982.

612. R. Unwin, I. Khan, N.V. Richardson, A.M. Bradshaw, L.S. Cederbaum, and W. Domcke, Chem. Phys. Lett. 77(2),(1981)242-245.

613. L.S. Cederbaum, W. Domcke, J. Schirmer, and H. Köppel, J. Chem. Phys. 72(2),(1980)1348-1358.

614. L.S. Cederbaum and H. Koppel, Chem. Phys. Lett. 87(1),(1982)14-17.

615. R. Locht and J.M. Dürer, Chem. Phys. Lett. 34(3),(1975)508-512 and refs. therein.

616. F. Gresteau, R.I. Hall, A. Huetz, D. Vichon, and J. Mazeau, J. Phys. B: Atom. Molec. Phys. 12(17),(1979)2937-2945.

617. F.H. Read, Proc. Phys. Soc. Lond., Ser. 2, Atom. Molec. Phys. 1(6),(1968)1056-1060.

618. Gerard ter Horst and Jan Kommander, J. Chem. Phys. 76(1),(1982) 137-142.

619. Ray L. Day and Richard J. Anderson, J. Chem. Phys. 69(12),(1978) 5518-5520.

620. P.M. Guyon, J. Breton, and M. Glass-Maujean, Chem. Phys. Lett. 68(2,3),(1979)314-319.

621. M. Glass-Maujean, Chem. Phys. Lett. 68(2,3),(1979)320-323.

622. R.A. Sutherland and R.A. Anderson, J. Chem. Phys. 58(3),(1973) 1226-1234.

623. A.L. Roche and Joel Tellinghuisen, Mol. Phys. 38(1),(1979)129-143.

624. Paul S. Julienne, J. Molec. Spectrosc. 63(1),(1976)60-79.

625. J.E. Frederick and R.D. Hudson, J. Molec. Spectrosc. 74(2), (1979)247-258.

626. James C. Weisshaar and C. Bradley Moore, J. Chem. Phys. 70(11), (1979)5135-5146.

627. I. Arnold, F.J. Comes, and G.K. Moortgat, Chem. Phys. 24(2), (1977)211-217.

628. A. Metropoulos and Ying-Nan Chiu, Chem. Phys. 42(1,2),(1979)61-72; J. Chem. Phys. 68(12),(1978)5607-5614; J. Chem. Phys. 69(4), (1978)1336-1341.

629. Ivan Powis, Chem. Phys. 68(3),(1982)251-254.

630. Frank A. Novak and Stuart A. Rice, J. Chem. Phys. 71(11),(1979) 4680-4687.

631. P. Natalis, J. Delwiche, G. Caprace, J.E. Collin, M.-J. Hubin, and M.-Th. Praet, J. Electron Spectrosc. Relat. Phenom. 10(2), (1977)93-102.

632. P.A. Braun and T.K. Rebane, Opt. Spectrosc. 51(1),(1981)51-55.

633. Yukikazu Itikawa, Excerpt from a private comm., June 6, 1981.

634. C.C. Costain in "Physical Chemistry: An Advanced Treatise," ed. Douglas Henderson, (Acad. Press.1970)19-66.

635. Lawrence S. Bernstein, J. Quant. Spectrosc. Radiat. Transfer 23(2),(1980)157-167.

636. C.M. Truesdale, Lawrence Berkeley Laboratory, private comm., March 11, 1982.

637. S. Southworth, W.D. Brewer, C.M. Truesdale, P.H. Korbin, D.W. Lindle, and D.A. Shirley, J. Electron Spectrosc. Relat. Phenom. 26(1),(1982)43-51.

638. G.M. McClelland, K.L. Saenger, J.J. Valentini, and D.R. Herschbach, J. Phys. Chem. 83(8),(1979)947-959.

639. Kathy Saenger, Massachusetts Institute of Technology, Research Laboratory for Electronics, private comm., Aug. 5, 1981.

640. S.V. O'Neil and W.P. Reinhart, J. Chem. Phys. 69(5),(1978)2126-2142.

641. J. Berkowitz and R. Spohr, J. Electron Spectrosc. Relat. Phenom. 2(2),(1973)143-152.

642. Lue-Yung Chow Chiu and Swadesh Samanta, J. Quant. Spectrosc. Radiat. Transfer 25(3),(1981)253-264.

643. J. Kreile and A. Schweig, J. Electron Spectrosc. Relat. Phenom. 20(3),(1980)191-211.

644. Isao Shimamura, "Partial-Sum Rules for and Asymmetry between Rotational Transitions $J^{\pm} \Delta J \leftarrow J$," to be published.

645. K. Kirby, T. Utzer, A.C. Allison, and A. Dalgarno, J. Chem. Phys. 75(6),(1981)2820-2825.

646. C.E. Brion and A. Hammett, Adv. Chem. Phys. 45(1981)2-80.

647. A.C. Parr, D.L. Ederer, B.E. Cole, J.B. West, Roger Stockbauer, Keith Codling, and J.L. Dehmer, Phys. Rev. Lett. 46(1),(1981)22-25.

648. Donald M. Mintz and Aaron Kuppermann, J. Chem. Phys. 69(9),(1978) 3953-3966.

649. T.A. Carlson, G.E. McGuire, A.E. Jonas, K.L. Cheng, C.P. Anderson, C.C. Lu, and B.P. Pullen in "Electron Spectroscopy," ed. D.A. Shirley, (North-Holland,1972)207-231.

650. T.A. Carlson, Chem. Phys. Lett. 9(1),(1971)23-26.

651. Geoffrey R.J. Williams and Peter W. Langhoff, Chem. Phys. Lett. 78(1),(1981)21-27.

652. Dennis L. Lichtenberger and John L. Hubbard, J. Electron Spectrosc. Relat. Phenom. 16(1,2),(1979), p. 123.

653. R.M. Holmes and G.V. Marr, J. Phys. B: Atom. Molec. Phys. 13(5), (1980)945-950.

654. H. Köppel, L.S. Cederbaum, and W. Domcke, J. Chem. Phys. 77(4), (1982)2014-2022.

655. Harold Exton, "Handbook of Hypergeometric Integrals: Theory, Applications, Computer Programs," (Ellis,Horwood,1978).

656. P.A. Schulz, Rou D. Mead, P.L. Jones, and W.C. Lindenberger, J. Chem. Phys. 77(3),(1982)1153-1165.

657. Dan Dill, Phys. Rev. A6(1),(1972)160-172 and ref. 478.

658. A.P. Hitchcock, J. Electron Spectrosc. Relat. Phenom. 25(2,3), (1982)245-275.

659. T.I. Morrison, A.H. Reis, Jr., E. Gebert, L.E. Iton, G.D. Stucky, and S.L. Suib, J. Chem. Phys. 72(11),(1980)6276-6282.

660. J. Tulkki and T. Åberg, J. Phys. B: Atom. Molec. Phys. 15(13), (1982)L435-L440.

661. A.C. Parr, D.L. Ederer, J.L. Dehmer, and D.M.P. Holland, J. Chem. Phys. 77(1),(1982)111-117.

662. T. Baer, Private comm. to the authors of ref. 661. (See ref. 36 in ref. 661).

663. R.S. Bauer and W.E. Spicer in "Electron Spectroscopy," ed. D.A. Shirley, (North-Holland,1972)569-574.

664. B. Chakraborty and Y.K. Pan, Appl. Spectrosc. Rev. 7(2),(1973) 283-311.

665. D.P. Chong, F.G. Herring, and D. McWilliams, J. Electron Spectrosc. Relat. Phenom. 7(6),(1975)429-443.

666. H. Köppel, L.S. Cederbaum, and W. Domcke, Chem. Phys. 69(1,2), (1982)175-183.

667. James W. Davenport, Brookhaven National Laboratory, private comm., Jan. 4, 1982.

668. E. Haller, H. Köppel, L.S. Cederbaum, G. Bieri, and W. von Niessen, Chem. Phys. Lett. 85(1),(1982)12-16.

669. William C. Trogler, J. Molec. Struct. 85(1,2),(1981)1-8.

670. E. Bright Wilson, Jr., J.C. Decius, and Paul C. Cross, "Molecular Vibrations. The Theory of Infrared and Raman Vibrational Spectra," (McGraw-Hill,1955), section 8-6.

671. Paul R. Stannard, Mark L. Elert, and William M. Gelbart, J. Chem. Phys. 74(11),(1981)6050-6062.

672. Same as ref. 670, but section 4-3.

673. D.F. McIntosh and K.H. Michaelian, Can. J. Spectrosc. 24(1), (1979)1-10; Can. J. Spectrosc. 24(2),(1979)35-43; Can. J. Spectrosc. 24(3),(1979)65-74.

674. L.A. Gribov, A.I. Pavlyuchko, and G.V. Khorin, Opt. Spectrosc. (Engl.) 47(3),(1979)265-267.

675. Yu. I. Ponomarev and A.I. Pavlyuchko, Opt. Spectrosc. (Engl.) 44(6),(1978)703-704.

676. L.A. Gribov and N.I. Prokofeva, Opt. Spectrosc. 44(5),(1978)605-607.

677. M. Ali Mohammadi, Chem. Phys. 66(1,2),(1982)153-159.

678. R. Wallace, Chem. Phys. 11(1),(1975)189-199; Chem. Phys. Lett. 37(1),(1976)115-118.

679. R. Wallace, Chem. Phys. 37(1),(1979)93-102.

680. Charles Jaffé and Paul Brumer, J. Chem. Phys. 73(11),(1980)5646-5658.

681. D.W. Noid, M.L. Koszykowski, and R.A. Marcus, J. Chem. Educ. 57(9),(1980)624-626.

682. Bryan R. Henry, Acc. Chem. Res. 10(6),(1977)207-213.

683. Yu. S. Efremov and N.I. Zhirnov, Opt. Spectrosc. 49(5),(1980) 479-483.

684. E.V. Doktorov, I.A. Malkin, and V.I. Man'ko, J. Phys. B: Atom. Molec. Phys. 9(3),(1976)507-514.

685. Isao Suzuki, J. Molec. Spectrosc. 80(1),(1980)12-22; Bull. Chem. Soc. Japan 48(12),(1975)3565-3572; Bull. Chem. Soc. Japan 52(6), (1979)1606-1613.

686. Joseph O. Hirschfelder, W. Byers Brown, and Sault T. Epstein, Adv. Quant. Chem. 1(1964)255-347.

687. T.C. Thompson and D.G. Truhlar, Chem. Phys. Lett. 75(1),(1980) 87-90.

688. Mark A. Ratner, V. Buch, and R.B. Gerber, Chem. Phys. 53(3), (1980)345-356.

689. Kurt M. Christoffel and Joel M. Bowman, J. Chem. Phys. 74(9), (1981)5057-5075.

690. S. Maluendes, G. Arteca, F.M. Fernández, and E.A. Castro, Mol. Phys. 45(2),(1982)511-520.

691. Peter Senn, unpublished work.

692. Yu. S. Efremov and N.I. Zhirnov, Opt. Spectrosc. (Engl.) 46(2),(1979)222-224; Opt. Spectrosc. (Engl.) 49(6),(1980)612-614.

693. Martin L. Sage, Chem. Phys. 35(3),(1978)375-380.

694. I.A. Watson, B.R. Henry, and I.G. Ross, Spectrochimica Acta 37A(10),(1981)857-865.

695. J.N. Huffaker and Loc Binh Tran, J. Chem. Phys. 76(7),(1982) 3838-3839.

696. Francisco M. Fernández and Eduardo A. Castro, J. Molec. Spectrosc. 94(1),(1982)28-37.

697. C. Chackerian, Jr. and R.H. Tipping, J. Molec. Spectrosc. 93(1), (1982)237-244.

698. M.L. Laursen and Katsunori Mita, J. Phys. A: Math. Gen. 14(5), (1981)1065-1068.

699. E.V. Doktorov, L.A. Malkin, and V.I. Man'ko, J. Molec. Spectrosc. 56(1),(1975)1-20; J. Molec. Spectrosc. 64(2),(1977)302-326.

700. F. Metz, M.J. Robey, E.W. Schlag, and F. Dörr, Chem. Phys. Lett. 51(1),(1977)8-12.

701. V.I. Baranov and L.A. Gribov, Opt. Spectrosc. (Engl.) 49(1), (1980)108-109.

702. Yoko Mochizuki, Koji Kaya, and Mitsuo Ito, Chem. Phys. 54(3), (1981)375-382.

703. J.B. Coon, F.A. Cesani, and C.M. Loyd, Chem. Soc. (Lond.), Farad. Discuss. 35(1963)118-123.

704. N.I. Zhirnov and A.V. Turev, Opt. Spectrosc. (Engl.) 47(5), (1979)480-484.

705. A.G. Robiette, T.R. Borgers, and H.L. Strauss, Mol. Phys. 42(6), (1981)1519-1524.

706. Millard F. Manning, J. Chem. Phys. 3(3),(1935)136-138.

707. A.C. Hurley, Int. J. Quant. Chem. 22(2),(1982)241-251.

708. John C. Tully, Adv. Chem. Phys. 42(1980)63-112.

709. R.E. Sherrod and F.A. Grimm, U. of Tennessee. (Unpubl. work).

APPENDICES

APPENDIX 1

HARMONIC FRANCK-CONDON FACTORS

This Appendix contains input instructions for a computer program to calculate Franck-Condon factors for two displaced harmonic oscillators with the restriction v"=0.

First Card: NINIT, NFIN

Format (2i5)

NINIT and NFIN denote initial and final v'

$$v' = NINIT,\ NINIT + 1,\ \ldots\ldots\ldots\ldots,\ NFIN \qquad (A1\text{-}1)$$

Second Card: ND, DINIT, DD

Format (i5, 2f 10.0)

For each v' the program computes ND·NDEL Franck-Condon factors using

$$\alpha''\delta_i = D_i = DINIT+(i-1)\cdot DD,\ i = 1,2,\ \ldots\ldots\ldots,\ ND \qquad (A1\text{-}2)$$

and

$$(\omega_e''/\omega_e')^{1/2} = DELINI + (j-1)\cdot DDEL,\ j = 1,2\ \ldots\ldots,\ NDEL \qquad (A1\text{-}3)$$

where the quantities DELINI and DDEL will be explained on the next card.

Third Card: NDEL, DELINI, DDEL

Format (i5, 2f10.0)

This card defines the range the ratio of the square roots of ω_es can take and the increment DDEL used.

One can place any number of sets of three cards as shown above in the input consecutively. Proper termination of the program requires an additional "first card" with NINIT<0 at the end of the input.

```
      IMPLICIT REAL*8 (A-H,O-Z)
      REAL*8 FOCTS(40)
      COMMON /FACTO/FOCTS
      DO 1 J=1,40
    1 FOCTS(J)=DLGAMA(DFLOAT(J))
    2 READ (5,4) NINIT,NFIN
      IF (NINIT.LT.0) STOP
      READ (5,5) ND,DINIT,DD,NDEL,DELINI,DDEL
      NINIT=NINIT+1
      NFIN=NFIN+1
      DO 3 JN=NINIT,NFIN
      N=JN-1
      DO 3 JDEL=1,NDEL
      DEL=DELINI+DDEL*DFLOAT(JDEL-1)
      DO 3 JD=1,ND
      D=DINIT+DD*DFLOAT(JD-1)
      A=FCO(D,DEL,N)
      DUL=DEL*DEL
    3 WRITE (6,6) N,DUL,D,A
      GO TO 2
    4 FORMAT (2I5)
    5 FORMAT (I5,2F10.0/I5,2F10.0)
    6 FORMAT (35X,17HFC(V',V",W"/W',D),1X,1H=,1X,3HFC(,I2,3H,0,,F8.5,
     #1H,,F6.3,1H),1X,1H=,F13.10)
      END

      REAL FUNCTION FCO*8 (D,DEL,N)
      IMPLICIT REAL*8 (A-H,O-Z)
      REAL*8 FOCTS(40)
      LOGICAL*1 LOPS
      COMMON /IMAG/LOPS/FACTO/FOCTS
      DLAG(XYZ)=DLOG(DABS(XYZ+1.0D-70))
      A1=1.0D0
      A2=A1/DEL
      IF (DABS(A1-A2).LT.1.0D-4) A2=A1
      DELT=D/A1
      FCT=A1*A2
      AST=A2
      A1=A1*A1
      A2=A2*A2
      LOPS=A2.GT.A1
      IF (A2.EQ.A1) GO TO 2
      FCO=HERM(A1*AST*(DELT/DSQRT(DABS(A1*A1-A2*A2))),N)
      FCO=SEXP(DLAG((FCT+FCT)/(A1+A2))+2.0D0*DLAG(FCO)-(A1*A2*DELT*
     #DELT/(A1+A2))-FOCTS(N+1)+DFLOAT(N)*DLAG(((A1-A2)*0.5D0)/
     #(A1+A2)))
    1 RETURN
    2 IF (DELT.EQ.0.0D0) GO TO 3
      FCO=SEXP(DFLOAT(N+1)*6.931471805599453D-01+DFLOAT(N+N+1)*
     #(DLOG(AST)-DLOG(A1+A2))+DFLOAT(4*N+1)*0.5D0*DLOG(A1)+DFLOAT(N+N)*
     #DLOG(DELT)-(A1*A2*DELT*DELT/(A1+A2))-FOCTS(N+1))
      GO TO 1
    3 FCO=1.0D0
      IF (N.NE.0) FCO=0.0D0
      GO TO 1
      END

      REAL FUNCTION HERM*8 (X,N)
      IMPLICIT REAL*8 (A-H,O-Z)
      LOGICAL*1 LOPS
      COMMON /IMAG/LOPS
      HM=1.0D0
      IF (N.EQ.0) GO TO 3
      HERM=X+X
      IF (N.EQ.1) GO TO 2
      X2=HERM
      ISG=1
      IF (LOPS) ISG=-ISG
      NP=N+N-2
      DO 1 J=2,NP,2
```

```
      HST=HERM
      HERM=X2*HERM-HM*DFLOAT(ISG*J)
    1 HM=HST
    2 RETURN
    3 HERM=HM
      GO TO 2
      END

      REAL FUNCTION SEXP*8 (X)
      IMPLICIT REAL*8 (A-H,O-Z)
      IF (X.LT.-150.0D0) GO TO 2
      SEXP=DEXP(X)
    1 RETURN
    2 SEXP=0.0D0
      GO TO 1
      END
```

APPENDIX 2

GEOMETRY OF THE EXCITED STATE FROM EXPERIMENTAL TRANSITION PROBABILITIES

This Appendix contains an input description of a program which computes the possible dislocations of a pair of harmonic oscillators from given ωs and two observed intensities.

$$k \longleftarrow 0 \quad , \ Int_k$$

$$j \longleftarrow 0 \quad , \ Int_j \qquad \text{(A2-1)}$$

with the restriction v" = 0.

First Card: Format (10a8)

This card is simply a title card.

Second Card: NINT, NDS, DSTART, DEND

Format (2i5, 2f10.0)

The above parameters, with the exception of NDS, control the preliminary pedestrian search for the location of roots on a finite interval. NINT is the number of segments in the interval to be searched. The storage limitations in the program in its present form are such that it is required NINT $\leqslant$ 1024. NDS is an output parameter. If NDS$\neq$0 the computed values of the function are being listed. In this case every NDS-th value calculated appears on the printed output. This output could be helpful in uncovering the presence of near double roots or near multiple roots in general. DSTART and DEND define the beginning and the end of the search for D=α"δ to be searched for roots.

If k and j are both odd integers, the program will attempt to locate a physically meaningless root at D=0. This will in general result in premature termination of the computer run due to overflow/underflow conditions. To remedy this situation one takes in general DSTART $>$ 0, where DSTART can be very close to zero.

Third Card: K, J, SK, SJ, WK, WJ

Format (2i5, 4f10.0)

K and J are quantum numbers of the final vibrational level, i.e. v'. SK and SJ are the transition probabilities of the transitions shown in (A2-1). SK refers to the transition K $\leftarrow$ 0 and SJ refers to the transition J $\leftarrow$ 0. WK is ω_e'' where v"=0 and WJ is ω_e'.

From the calculated roots D the displacement in terms of normal mode coordinates is

$$\delta = D[\hbar/(2\pi c\omega_e'')]^{1/2} = (0.236615)\ D\ [10^3 cm^{-1}/\omega_e'']^{1/2}\ 10^{-20} g^{1/2}\ cm$$

$$= (5.80656)\ D\ (a.m.u./(\omega_e''\ cm))^{1/2}\ \text{Å} \qquad \text{(A2-2)}$$

where ω_e'' is the ω_e of the state with v"=0 and its units are cm^{-1}.

Any number of cards called "third card" can be placed in the input consecutively. The computer run is being terminated properly by placing a blank card (with v'=v"=0) at the end of the input.

```
      IMPLICIT REAL*8 (A-H,O-Z)
      REAL*8 RT(1025),IU
      INTEGER*2 ITRIP,ITROP,IJISS
      LOGICAL*1 LOGO,L2
      DATA ITRIP,ITROP/'0 ',' '/
      READ (5,5) (RT(J),J=1,10)
      WRITE (6,6) (RT(J),J=1,10)
      READ (5,7) NINT,NDS,DSTART,DEND
      WRITE (6,8) NINT,DSTART,DEND
      L2=NDS.EQ.0
      DST=(DEND-DSTART)/DFLOAT(NINT)
      NINT=NINT+1
      IF (NINT.GT.1025) GO TO 3
   16 READ (5,9) K,J,SK,SJ,WK,WJ
      IF ((K.EQ.0).AND.(J.EQ.0)) GO TO 4
      WRITE (6,10) K,J,K,SK,J,SJ,WK,WJ
      IU=(WK-WJ)/(WK+WJ)
      SU=0.5D0*DSQRT((1.0D0-IU*IU)/DABS(IU))
      AKJ=-DSQRT((SK/SJ)*(DGAMMA(DFLOAT(K+1))/DGAMMA(DFLOAT(J+1)))*
     #((2.0D0/DABS(IU))**(K-J)))
      LOGO=IU.GE.0.0D0
      NS=0
      DO 2 JSX=1,2
      AKJ=-AKJ
      RT(1)=F(DSTART,SU,AKJ,K,J,LOGO)
      DO 1 JCX=2,NINT
      RT(JCX)=F(DSTART+DST*DFLOAT(JCX-1),SU,AKJ,K,J,LOGO)
      IF (RT(JCX)*RT(JCX-1).GT.0.0D0) GO TO 1
      NS=NS+1
      CALL NEWT(DSTART,DST,SU,AKJ,K,J,JCX,NS,LOGO)
    1 CONTINUE
      WRITE (6,15)
      IF (L2) GO TO 2
      WRITE (6,11) (RT(JCX),JCX=1,NINT,NDS)
      IJISS=ITRIP
      JJ=((NINT-1)/NDS)+1
      IF (11*(JJ/11).EQ.JJ) IJISS=ITROP
      WRITE (6,12) IJISS
    2 IF ((NS.EQ.0).AND.(JSX.EQ.2)) WRITE (6,13)
      GO TO 16
    3 WRITE (6,14)
    4 STOP
    5 FORMAT (10A8)
    6 FORMAT (1H-/1H-,19X,10A8)
    7 FORMAT (2I5,2F10.0)
    8 FORMAT (1HO,9X,6HNUMBER,1X,2HOF,1X,9HINTERVALS,1X,1H=,I5,7X,1H(,
     #F10.5,1X,1H,,F10.5,1X,1H)/1HO)
    9 FORMAT (2I5,4F10.0)
   10 FORMAT (1HO,9X,1HK,1X,1H=,I2,3X,1HJ,1X,1H=,I2,2(5X,1HI,I1,1X,1H=,
     #F12.6),6X,3HWE',1X,1H=,F12.4,6X,3HWE',1X,1H=,F12.4)
   11 FORMAT (1HO,1X,128(1H=)//200(5X,11(D11.2)/))
   12 FORMAT (A2,128(1H=)/1X)
   13 FORMAT (1HO,9X,2HNO,1X,4HREAL,1X,5HROOTS,1X,7HLOCATED/1X)
   14 FORMAT (1HO,9X,3HTOO,1X,4HMANY,1X,9HINTERVALS,1X,10HSPECIFIED./
     #10X,9HEXECUTION,1X,11HTERMINATED.,10(/1HO,9X,19(1X,5HSORRY))/1H-/
     #1H-/1H-)
   15 FORMAT (1X)
      END

      SUBROUTINE NEWT(DX,DST,SU,AKJ,K,J,JCX,NS,LOGO)
      IMPLICIT REAL*8 (A-H,O-Z)
      LOGICAL*1 LOGO
      D=DX+DST*DFLOAT(JCX-1)
      DO 1 JJ=1,40
      TERM=FP(D,SU,AKJ,K,J,LOGO)/SU
      IF (DABS(TERM/D).LT.1.0D-12) GO TO 2
    1 D=D-TERM
      WRITE (6,4)
      GO TO 3
    2 D=D-TERM
    3 WRITE (6,5) NS,D
```

```
      RETURN
    4 FORMAT (1HO,9X,6HNEWTON,1X,10HITERATIONS,1X,3HNOT,1X,9HCONVERGED/
     #1X)
    5 FORMAT (10X,1H(,I2,1H),3X,1HD,1X,1H=,F7.4)
      END

      REAL FUNCTION FP*8 (D,SU,AKJ,K,J,LOGO)
      IMPLICIT REAL*8 (A-H,O-Z)
      LOGICAL*1 LOGO
      X=SU*D
      FP=AKJ*HP(HJ,X,J,LOGO)+HP(HK,X,K,LOGO)
      FP=(AKJ*HJ+HK)/FP
      RETURN
      END

      REAL FUNCTION F*8 (D,SU,AKJ,K,J,LOGO)
      IMPLICIT REAL*8 (A-H,O-Z)
      LOGICAL*1 LOGO
      X=SU*D
      F=AKJ*H(X,J,LOGO)+H(X,K,LOGO)
      RETURN
      END

      REAL FUNCTION H*8 (X,N,LOGO)
      IMPLICIT REAL*8 (A-H,O-Z)
      LOGICAL*1 LOGO
      HM=1.0D0
      IF (N.EQ.0) GO TO 3
      H=X+X
      IF (N.EQ.1) GO TO 2
      ISG=1
      IF (.NOT.LOGO) ISG=-ISG
      NP=N-1
      DO 1 J=1,NP
      HST=H
      H=X*H-HM*DFLOAT(ISG*J)
      H=H+H
    1 HM=HST
    2 RETURN
    3 H=HM
      GO TO 2
      END

      REAL FUNCTION HP*8 (H,X,N,LOGO)
      IMPLICIT REAL*8 (A-H,O-Z)
      LOGICAL*1 LOGO
      HPM=0.0D0
      HM=1.0D0
      IF (N.EQ.0) GO TO 3
      HP=2.0D0
      H=X+X
      IF (N.EQ.1) GO TO 2
      ISG=1
      IF (.NOT.LOGO) ISG=-ISG
      NP=N-1
      DO 1 J=1,NP
      HST=H
      HPST=HP
      ISGJ=J*ISG
      HP=H+X*HP-HPM*DFLOAT(ISGJ)
      H=X*H-HM*DFLOAT(ISGJ)
      H=H+H
      HP=HP+HP
      HM=HST
    1 HPM=HPST
    2 RETURN
    3 H=HM
      HP=HPM
      GO TO 2
      END
```

APPENDIX 3

EXCITED STATE GEOMETRY FOR TWO MODES WITH DUSCHINSKY MIXING

This Appendix contains a listing and input instructions for the program which computes normal mode coordinate displacements of two harmonic oscillators with Duschinsky mixing from a pair of intensity ratios.

One can do any number of computations successively with this program.

First Card: A title card (maximum, 80 characters).

If this card contains the word "STOP" starting in the first column the run is terminated. In other words the last input card must contain the word "STOP".

Second Card: α_1'', α_1', δ_1, α_2'', α_2', δ_2

Format (6f10.0)

The doubly primed quantities refer here to the ground state where we have the restriction $v_1'' = v_2'' = 0$.

Third and Fourth Card: These cards contain the Duschinsky matrix. On the third card we enter ℓ_{11} and ℓ_{12} with format (2f20.0), and on the fourth card ℓ_{21} and ℓ_{22} with format (2f20.0).

Fifth Card: This card contains the quantum numbers and the observed intensities involved in the first intensity ratio Int_1/Int_2.

$(v_1')_1$ $(v_2')_1$ Int_1 $(v_1')_2$ $(v_2')_2$ Int_2

with the format (2i5, f20.0, 2i5, f20.0).

Sixth Card: This card contains the quantum numbers and observed intensities Int_3/Int_4 and the maximum number of Newton iterations is specified by JITMAX. If JITMAX is left blank the program takes JITMAX=60. In general much less iterations should be required. According to the above the sixth card contains

$(v_1')_3$ $(v_2')_3$ Int_3 $(v_1')_4$ $(v_2')_4$ Int_4 JITMAX

The format used is (2i5, f20.0, 2i5, f20.0, 15x, i5). The last digit of JITMAX has to be in column 80 according to this format.

Let us demonstrate the use of this program on a practical example. We used the data published by Coon et al on the 3700 Å system of sulfur dioxide.[8] We express his dislocations evaluated in the parallel frame approximation in "harmonic oscillator units" which we abbreviate (h.o.u.) and define as follows:

$$cm(g^{1/2}) = (0.77603)10^{20}(a.m.u.)^{1/2}\ \text{Å} = (0.77603)10^{20}(h.o.u.)$$

We obtain $\delta_1 = 0.280$ (h.o.u.) which was calculated by Coon et al from the intensity ratio $Int(v_1', v_2')_1/Int(v_1', v_2')_2 = Int\ (1,0)/Int\ (0,0) = 1.323$, and $\delta_2 = 0.406$ (h.o.u.) obtained from the intensity ratio $Int(0,1)/Int(0,0) = 1.223$. The qunatum number v_1 refers to the S-O symmetric stretching mode of the molecule.

From the frequency measurements given by Coon et al we obtain

$$\alpha_1'' = 5.845(h.o.u.)^{-1} \qquad \alpha_2'' = 3.919(h.o.u.)^{-1}$$
$$\alpha_1' = 5.185(h.o.u.)^{-1} \qquad \alpha_2' = 3.272(h.o.u.)^{-1} \qquad \text{(A3-2)}$$

We take the Duschinsky matrix as an orthonormal matrix. Such a matrix can be specified by an angle of rotation, i.e. $\ell_{11}=\ell_{22}=\cos\Theta$ and $\ell_{12}=-\ell_{21}=\sin\Theta$. If $\Theta=0$ the Duschinsky matrix is a unit matrix and we should recover the δs computed in the parallel frame approximation. (If the Duschinsky matrix is exactly a unit matrix the program encounters an overflow condiiton). We use the same intensities as the ones used to

compute the above δs in the parallel frame approximation using

$$Int_1/Int_2 = Int(0,1)/Int(0,0)$$

$$Int_3/Int_4 = Int(1,0)/Int(0,0)$$

and we obtain

$\delta_1 = 0.156$(h.o.u.) and $\delta_2 = 0.529$(h.o.u.) if $\Theta = -20°$

$\delta_1 = 0.222$(h.o.u.) and $\delta_2 = 0.474$(h.o.u.) if $\Theta = -10°$

$\delta_1 = 0.251$(h.o.u.) and $\delta_2 = 0.442$(h.o.u.) if $\Theta = -5°$

$\delta_1 = 0.307$(h.o.u.) and $\delta_2 = 0.366$(h.o.u.) if $\Theta = 5°$

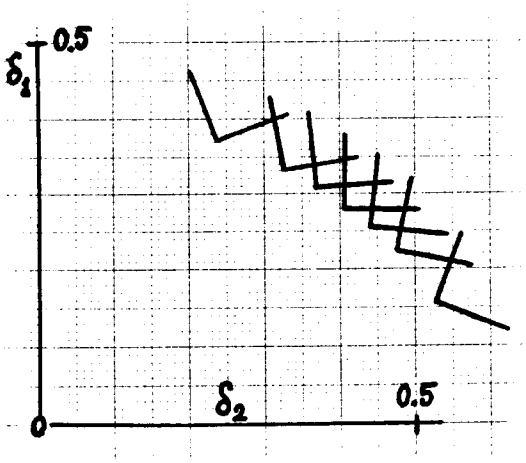
$\delta_1 = 0.331$(h.o.u.) and $\delta_2 = 0.325$(h.o.u.) if $\Theta = 10°$

$\delta_1 = 0.371$(h.o.u.) and $\delta_2 = 0.234$(h.o.u.) if $\Theta = 20°$

One can readily see that the excited state geometry is quite sensitive to the Duschinsky mixing of the two modes.

In the input the δs and αs can be expressed in any suitable units as long as both units are compatible, i.e. the units for α should be the reciprocal of the units of δ.

The Duschinsky-transformed coordinate systems are sketched below.



```
      IMPLICIT REAL*8 (A-H,O-Z)
      REAL*8 A(10),I1,I2,I3,I4,L11,L12,L21,L22
      COMMON /DUSCHE/L11,L12,L21,L22/NEWT/JITMAX
      DATA IONE,I10,BB/1,10,'STOP    '/
    1 READ (5,3) (A(J),J=IONE,I10)
      IF (A(IONE).EQ.BB) STOP
      WRITE (6,4) (A(J),J=IONE,I10)
      READ (5,5) A1,B1,D1,A2,B2,D2,L11,L12,L21,L22,M1,N1,I1,M2,N2,I2,
     #M3,N3,I3,M4,N4,I4,JITMAX
      IF (JITMAX.EQ.0) JITMAX=60
      D1ST=D1
      D2ST=D2
      A12=-(I1/I2)
      A34=-(I3/I4)
      CALL NEWTON(A12,A34,A1,A2,B1,B2,D1,D2,N1,N2,N3,N4,M1,M2,M3,M4)
      WRITE (6,2) A1,B1,A2,B2,D1ST,D2ST,D1,D2,L11,L12,L21,L22,M1,N1,
     #I1,M2,N2,I2,M3,N3,I3,M4,N4,I4
      GO TO 1
    2 FORMAT (1HO,10X,5HALFA1,1X,1H=,F13.6,5X,5HBETA1,1X,1H=,F13.6,5X,
     #5HALFA2,1X,1H=,F13.6,5X,5HBETA2,1X,1H=,F13.6/11X,7HINITIAL,1X,
     #12HDISLOCATIONS,1X,1H:,4X,2HD1,1X,1H=,F10.6,5X,2HD2,1X,1H=,F10.6/
     #11X,5HFINAL,1X,12HDISLOCATIONS,3X,1H:,4X,2HD1,1X,1H=,F10.6,5X,
     #2HD2,1X,1H=,F10.6/1HO,59X,1H+,29X,1H+/60X,1H!,F12.5,F15.5,2X,1H!/
     #32X,3HTHE,1X,10HDUSCHINSKY,1X,6HMATRIX,2X,1H:,4X,1H!,29X,1H!/
     #60X,1H!,F12.5,F15.5,2X,1H!/60X,1H+,29X,1H+/1HO,10X,2H#1,
     #1X,1H:,2X,2HV1,1X,1H=,I2,4X,2HV2,1X,1H=,I2,4X,2HI1,1X,1H=,F10.6,
     #3X,1H,,3X,2H#2,1X,1H:,2X,2HV1,1X,1H=,I2,4X,2HV2,1X,1H=,I2,4X,
     #2HI2,1X,1H=,F10.6/11X,2H#3,1X,1H:,2X,2HV1,1X,1H=,I2,4X,2HV2,1X,
     #1H=,I2,4X,2HI3,1X,1H=,F10.6,3X,1H,,3X,2H#4,1X,1H:,2X,2HV1,1X,1H=,
     #I2,4X,2HV2,1X,1H=,I2,4X,2HI4,1X,1H=,F10.6/1H-)
    3 FORMAT (10A8)
    4 FORMAT (1H-,24X,10A8)
    5 FORMAT (6F10.0,2(/2F20.0)/2(2I5,F20.0)/2(2I5,F20.0),15X,I5)
      END

      SUBROUTINE NEWTON (A12,A34,A1,A2,B1,B2,D1,D2,N1,N2,N3,N4,M1,
     #M2,M3,M4)
      IMPLICIT REAL*8 (A-H,O-Z)
      DATA TOL/1.0D-6/
      COMMON /NEWT/JITMAX
      DO 1 JIT=1,JITMAX
      CALL VALS(G1,G1X,G1Y,A1,A2,B1,B2,D1,D2,N1,M1)
      CALL VALS(G2,G2X,G2Y,A1,A2,B1,B2,D1,D2,N2,M2)
      G1=A12*G2+G1
      G1X=A12*G2X+G1X
      G1Y=A12*G2Y+G1Y
      CALL VALS(G3,G3X,G3Y,A1,A2,B1,B2,D1,D2,N3,M3)
      CALL VALS(G2,G2X,G2Y,A1,A2,B1,B2,D1,D2,N4,M4)
      G2=A34*G2+G3
      G2X=A34*G2X+G3X
      G2Y=A34*G2Y+G3Y
      ACOB=G1X*G2Y-G2X*G1Y
      DX=(G1*G2Y-G2*G1Y)/ACOB
      DY=(G2*G1X-G1*G2X)/ACOB
      IF ((DABS(DX/D1)+DABS(DY/D2)).LT.TOL) GO TO 3
      D1=D1-DX
    1 D2=D2-DY
      WRITE (6,4)
    2 RETURN
    3 D1=D1-DX
      D2=D2-DY
      GO TO 2
    4 FORMAT (1HO,10X,35(1H*)/11X,1H*,1X,6HNEWTON,1X,10HITERATIONS,1X,
     #3HNOT,1X,9HCONVERGED,1X,1H*/11X,35(1H*))
      END

      SUBROUTINE VALS(G,GX,GY,A1,A2,B1,B2,D1,D2,N,M)
      IMPLICIT REAL*8 (A-H,O-Z)
      DATA DXY/0.001D0/
      DDX=DXY*DABS(D1)
```

```
      DDY=DXY*DABS(D2)
      G=FC(A1,A2,B1,B2,D1,D2,N,M)
      GX=(FC(A1,A2,B1,B2,D1+DDX,D2,N,M)-G)/DDX
      GY=(FC(A1,A2,B1,B2,D1,D2+DDY,N,M)-G)/DDY
      RETURN
      END

      REAL FUNCTION FC*8 (A1,A2,B1,B2,D1,D2,N,M)
      IMPLICIT REAL*8 (A-H,O-Z)
      REAL*8 BX(51),FACT(41),AT(25),L11,L12,L21,L22,KAT,NAP
      LOGICAL*1 LFACT,LOGO
      COMMON /DUSCHE/L11,L12,L21,L22
      DATA LFACT/.FALSE./,ZERO,HALF,ONE,DL2/0.0D0,0.5D0,1.0D0,
     #6.931471805599453D-1/
      A1SQ=A1*A1
      A2SQ=A2*A2
      B1SQ=B1*B1
      ASQ=A1SQ*L11*L11+A2SQ*L21*L21+B1SQ
      SO=A1SQ*L11*D1+A2SQ*L21*D2
      SO=HALF*(A1SQ*D1*D1+A2SQ*D2*D2-((SO*SO)/ASQ))
      S1=HALF*(A1SQ*D1*L12+A2SQ*D2*L22-((A1SQ*L11*D1+A2SQ*L21*D2)/ASQ)*
     #(A1SQ*L11*L12+A2SQ*L21*L22))
      S2SQ=A1SQ*L11*L12+A2SQ*L21*L22
      S2SQ=HALF*(A1SQ*L12*L12+A2SQ*L22*L22+B2*B2-((S2SQ*S2SQ)/ASQ))
      NAP=ONE-((B1SQ+B1SQ)/ASQ)
      POW=ONE
      IF (NAP.LT.ZERO) POW=-POW
      NAP=-ASQ*DSQRT(DABS(NAP))/B1
      KAT=(A1SQ*L11*L12+A2SQ*L21*L22)/(NAP*B2)
      NAP=(A1SQ*D1*L11+A2SQ*D2*L21)/NAP
      IF (LFACT) GO TO 2
      LFACT=.TRUE.
      DO 1 JJ=1,41
    1 FACT(JJ)=DLGAMA(DFLOAT(JJ))
    2 IF (M.GT.0) GO TO 3
      AT(1)=ONE
      GO TO 5
    3 JJ=M+1
      AT(JJ)=KAT**M
      AT(M)=-DFLOAT(M+M)*NAP*AT(JJ)/KAT
      IF (M.EQ.1) GO TO 5
      JSM=M-1
      DO 4 JJ=1,JSM
      K=M-JJ
    4 AT(K)=(DFLOAT(K+K)*(KAT*NAP*AT(K+1)-(KAT*KAT-POW)*DFLOAT(K+1)*
     #AT(K+2)))/(KAT*KAT*DFLOAT(K-M-1))
    5 FC=ZERO
      CH=ONE-B2*B2/S2SQ
      LOGO=CH.GE.ZERO
      IF (.NOT.LOGO) CH=-CH
      XX=(S1*B2/S2SQ)/DSQRT(CH)
      CHL=DLOG(CH)
      BX(1)=ONE
      BX(2)=XX+XX
      ISG=1
      IF (.NOT.LOGO) ISG=-ISG
      K=N+M-1
      IF (K.LT.1) GO TO 7
      DO 6 J=1,K
      JJ=J+2
      BX(JJ)=XX*BX(J+1)-BX(J)*DFLOAT(ISG*J)
    6 BX(JJ)=BX(JJ)+BX(JJ)
    7 JSM=M+1
      DO 9 KK=1,JSM
      K=KK-1
      SUM=ZERO
      JEND=MINO(K,N)+1
      DO 8 JJ=1,JEND
      J=JJ-1
    8 SUM=SUM+DEXP(DL2*DFLOAT(J)+FACT(KK)-FACT(KK-J)+FACT(N+1)-FACT(JJ)-
```

```
     #FACT(N-J+1)+HALF*DFLOAT(K+N-J-J)*CHL)*EX(KK+N-J-J)
   9 FC=FC+AT(KK)*SUM
     FC=FC*DEXP(((S1*S1)/S2SQ)-SO)
     FC=((FC*FC*A1*A2*B1*B2)/(ASQ*S2SQ))*DEXP(DFLOAT(M)*
     #DLOG(DABS(ONE-(((B1+B1)*B1)/ASQ)))-DFLOAT(N+M-1)*DL2-FACT(N+1)-
     #FACT(M+1))
     RETURN
     END
```

APPENDIX 4

TRANSITION MOMENT WEIGHTED FRANCK-CONDON FACTORS OF TWO DISPLACED ONE-DIMENSIONAL HARMONIC OSCILLATORS

The program listed in this Appendix calculates Franck-Condon factors between two displaced harmonic oscillators including the normal mode coordinate dependence of the transition moment. This normal mode coordinate dependence of the transition moment is expressed in form of a power series expansion

$$M(q) = [M_o + M_1 q + M_2 q^2 + ...] \exp\ (-(1/2)\alpha_o{}^2 q^2) \qquad \text{(A4-1)}$$

The input consists of sets of seven or more cards.

First Card: MINIT, MFIN, NINIT, NFIN

Format (4i5)

The above parameters define the range for each quantum number v' and v". We have

$$\text{MINIT} \leqslant v'' \leqslant \text{MFIN}$$

$$\text{NINIT} \leqslant v' \leqslant \text{NFIN} \qquad \text{(A4-2)}$$

Second Card: ND, DINIT, DD

Format (i5, 2f10.0)

The above parameters define the range covered by the dimensionless displacement parameter D

$$D = \text{DINIT} + (j - 1)\text{DD} \quad , j = 1,2,....., \text{ND} \qquad \text{(A4-3)}$$

where $D = \alpha''\delta$.

Third Card: NAU, AUINIT, DAU

Format (5i, 2f10.0)

The above parameters define the range covered by α_o^2.

$$\alpha_o^2 = \text{AUINIT} + (j - 1)\cdot\text{DAU} \quad , j = 1,2,\ldots\ldots, \text{NAU} \tag{A4-4}$$

Fourth Card: NA1, A1INIT, DA1

Format (i5, 2f10.0)

The above parameters define the range covered by α''

$$\alpha'' = \text{A1INIT} + (j - 1)\ \text{DA1} \quad , j = 1,2,\ldots\ldots, \text{NA1} \tag{A4-5}$$

Fifth Card: NA2, A2INIT, DA2

Format (i5, 2f10.0)

This card is the same as the previous card, but referring to α'

$$\alpha' = \text{A2INIT} + (j - 1)\ \text{DA2} \quad , j = 1,2,\ldots\ldots, \text{NA2} \tag{A4-6}$$

Sixth Card: NAW

Format (i5)

NAW is the number of terms in the expansion of the transition moment. We require NAW $>$ 0 and due to storage limitations NAW $\leqslant$ 31.

Seventh Card: AW(j), j = 1, NAW

Format (8f10.0)

On this card the expansion coefficients in (A4-1), M_o, M_1,..... are entered. If more than eight terms are included in the expansion, additional cards will be read.

After one calculation has been completed execution returns to the beginning of the program and input for an additional run is entered unless on the first card MINIT $<$ 0.

The array initialized with a DATA statement in the subroutine WTOVLP contains the logarithmic gamma function of the positive integers.

If one is dealing with non-weighted Franck-Condon factors one specifies

$$\alpha_0 = 0,\ M_o = 1, \text{ and } M_1, M_2,\ldots\ldots = 0 \tag{A4-7}$$

In the notation used here the expansion center of the transition moment is the final (singly primed) state.

In CGS units the αs and the Ms have units

$$\alpha = \ldots\ldots\ldots (g^{1/2}cm)^{-1}$$

$$M_k = \ldots\ldots\ldots (g^{1/2}cm)^{-k} \qquad \text{(A4-8)}$$

In general, the formats used in the programs shown here are not suitable for working in CGS units. It is recommended that one use for the normal mode coordinates the units

$$(a.m.u.)^{1/2}\ \text{Å} = (1.288616)10^{-20}\ g^{1/2}\ cm \qquad \text{(A4-9)}$$

```
      IMPLICIT REAL*8 (A-H,O-Z)
      REAL*8 AW(31)
    1 READ (5,5) MINIT,MFIN,NINIT,NFIN
      IF (MINIT.LT.0) GO TO 3
      READ (5,6) ND,DINIT,DD,NAU,AUINIT,DAU,NA1,A1INIT,DA1,NA2,A2INIT,
     #DA2,NAW
      IF (NAW.GT.31) GO TO 4
      READ (5,8) (AW(JA1),JA1=1,NAW)
      K=NAW-1
      MINIT=MINIT+1
      MFIN=MFIN+1
      NINIT=NINIT+1
      NFIN=NFIN+1
      DO 2 JAU=1,NAU
      AU=AUINIT+DAU*DFLOAT(JAU-1)
      WRITE (6,7) AU,(AW(JA1),JA1=1,NAW)
      WRITE (6,9)
      DO 2 JA1=1,NA1
      A1=A1INIT+DA1*DFLOAT(JA1-1)
      DO 2 JA2=1,NA2
      A2=A2INIT+DA2*DFLOAT(JA2-1)
      DO 2 JD=1,ND
      D=DINIT+DD*DFLOAT(JD-1)
      DO 2 JM=MINIT,MFIN
      M=JM-1
      DO 2 JN=NINIT,NFIN
      N=JN-1
      A=WTOVLP(AW,D,AU,A1,A2,K,M,N,ISIG)
      AA=A*A
    2 WRITE (6,10) D,M,A1,N,A2,AA,A,ISIG
      WRITE (6,9)
      GO TO 1
    3 WRITE (6,9)
      STOP
    4 WRITE (6,11) NAW
      GO TO 3
    5 FORMAT (4I5)
    6 FORMAT (I5,2F10.0/I5,2F10.0/I5,2F10.0/I5,2F10.0/I5)
    7 FORMAT (1H-,10X,5HAO*AO,1X,1H=,F6.3/11X,2HAW,2X,1H:,2X,10F10.5,
     #4(/18X,10F10.5))
    8 FORMAT (8F10.0)
    9 FORMAT (1X)
   10 FORMAT (6X,1HD,1X,1H=,F6.3,4X,2HV",1X,1H=,I2,3X,6HALPHA1,1X,
     #1H=,D11.4,5X,2HV',1X,1H=,I2,3X,6HALPHA2,1X,1H=,D11.4,5X,3HFCF,1X,
     #1H=,F10.6,5X,7HOVERLAP,1X,1H=,F10.6,3X,1H(,I2,1H))
   11 FORMAT (1H-,10X,3HNAW,1X,1H=,I3,1X,1H>,1X,2H31/1H-)
      END

      REAL FUNCTION WTOVLP*8 (AW,D,AU,A1,A2,KK,M,N,ISIG)
      IMPLICIT REAL*8 (A-H,O-Z)
      REAL*8 B(121),C(121),FCT(121),SS1(45),SS2(45),SS3(31),AW(31),A(31)
     #,OW(31)
      REAL*4 SNGL,ALOG10
      EQUIVALENCE (SS1(1),FCT(1)),(SS2(1),FCT(46)),(SS3(1),FCT(91)),
     #(SUM2,S2),(SUM3,D2)
      DATA SS1 /Z0000000000000000,Z0000000000000000,Z40B17217F7D1CF7B,
     #          Z411CAB0BFA2A2002,Z4132D94EF92459F1,Z414C9990F111E724,
     #          Z4169449CEB3C0727,Z4188670F996E6184,Z41A9AC7417E5B868,
     #          Z41CCD4490D3FBE7E,Z41F1ABAC84AA68A4,Z421180973F3A8D73,
     #          Z4213FCBA16D50143,Z42168D5A9C3B32CD,Z421930F3DF162A42,
     #          Z421EE636A63FD347,Z421EABFF061F1A84,Z4221814C7E5E6A73,
     #          Z4224653BE5ABDCA4,Z42275702A66C7309,Z422A55EAF5DAEF7B,
     #          Z422D6150C868E551,Z4230789F57509E0C,Z42339B4F170AD489,
     #          Z4236C8E4069D1A27,Z423A00EC459ACBCE,Z423D42FEE2F8CF27,
     #          Z42408EBAD9F93FB9,Z4243E3C634CC08FE,Z424741CD4E45C8C2,
     #          Z424AA8822D674394,Z424E179BF6796902,Z42518ED66E50820F,
     #          Z42550DF18CEB3928,Z425894B11D225AE5,Z425C22DC67845960,
     #          Z425FB83DE6C99D60,Z426354A30490F657,Z4266F7DBDD495E8C,
     #          Z426AA1BB0A5A6048,Z426E521571C0AE89,Z427208C21A728412,
     #          Z4275C59A04F84BB8,Z4279887807BAE939,Z427D5138AE9A73C2/
      DATA SS2 /Z42811FBA1D6EECF9,Z4284F3DBF520F546,Z4288CD7F3B13135D,
```

```
     #          Z428CAC86429D2ACB,Z429090D498637614,Z42947A4EEF58F98B,
     #          Z429868DB0F4319AB,Z429C5C5FC498EED3,Z42A054C4D19D3668,
     #          Z42A451F2E09578CB,Z42A853D377043888,Z42AC5A50E9CED39A,
     #          Z42B06556523A3A32,Z42B474CF85ABCBC6,Z42B888A9021D9622,
     #          Z42BCA0CFF936E2C4,Z42C0BD3233FB7DC8,Z42C4DDBE15057502,
     #          Z42C902628F3E3B0D,Z42CD2B0F1F0D25E6,Z42D157B3C3F23047,
     #          Z42D58840FA84B92C,Z42D9BCA7B6CEBD7B,Z42DDF4D95EFDB10A,
     #          Z42E230C7C662B7B5,Z42E6706528BC8800,Z42EAB3A425C5BDB2,
     #          Z42EEFA77BD02D382,Z42F344D349CB5F7B,Z42F792AA7F8A8A40,
     #          Z42FBE3F166330C19,Z43100389C56E3462,Z43104909FF8B652A,
     #          Z43108EBF13DBF263,Z4310D4A85602B129,Z43111AC51DF8932A,
     #          Z43116114C7E34737,Z4311A796B3EDE1AB,Z4311EE4A46236D3E,
     #          Z4312352EE64B46D5,Z43127C43FFC72961,Z4312C3890172D057,
     #          Z43130AFD5D851956,Z431352A089728F1C,Z43139A71FDD14947/
      DATA SS3 /Z4313E271363E0DF7,Z43142A9DB142A36B,Z431472F6F03D410D,
     #          Z4314BB7C77491066,Z4315042DCD27AF64,Z43154D0A7B2BA658,
     #          Z431596120D23C4EC,Z4315DF4411475A1C,Z431628A018233BED,
     #          Z43167225B4879462,Z4316BBD47B7669B6,Z431705AC0412D89F,
     #          Z43174FABE790F7BE,Z431799D3C1265C0E,Z4317E4232DFB367E,
     #          Z43182E99CD1C0368,Z431879373F6BC4FE,Z4318C3FB2796C21B,
     #          Z4319OEE52A05C35F,Z431959F4ECD1C8B3,Z4319A52A17B831CB,
     #          Z4319F084540F545E,Z431A3C034CBB7B2C,Z431A87A6AE24493A,
     #          Z431AD36E262A7CC0,Z431B1F59641E0DB4,Z431B6B6818B4A3EB,
     #          Z431BB799F600610A,Z431C03EEAF66FACD,Z431C5065F9992225,
     #          Z431C9CFF8A8A340D/,I0,I1,I2,ZERO,HALF,ONE,AL2/0,1,2,
     #          0.0D0,0.5D0,1.0D0,6.9314718055994530D-1/
      B1=DSQRT(HALF*(AU+A1*A1+A2*A2))
      B0=(HALF*D*A1)/B1
      G1=ONE/B1
      G0=B0/B1
      S1=A1/B1
      S2=A2/B1
      D1=A1*G0-D
      D2=A2*G0
      KP1=KK+I1
      MP1=M+I1
      NP1=N+I1
      DO 6 JK=I1,KP1
      OW(JK)=ZERO
      IF (AW(JK).EQ.ZERO) GO TO 6
      K=JK-I1
      IF (K.GT.I0) GO TO 1
      A(I1)=ONE
      GO TO 4
    1 IF (K.GT.I1) GO TO 2
      A(I1)=G0
      A(I2)=HALF*G1
      GO TO 4
    2 JEND=K-I1
      S1D1=HALF*G1
      A(K)=S1D1**JEND
      A(JK)=S1D1*A(K)
      A(K)=G0*DFLOAT(K)*A(K)
      DO 3 J1S=I1,JEND
      J1=JK-J1S
      JM=J1-I1
    3 A(JM)=(DFLOAT(JM+JM)/DFLOAT(J1S+I1))*(DFLOAT(J1)*A(J1+I1)+B0*
     #A(J1))
    4 DO 5 J1S=I1,JK
    5 OW(J1S)=OW(J1S)+A(J1S)*AW(JK)
    6 CONTINUE
      IF (M.GT.I0) GO TO 7
      B(I1)=ONE
      GO TO 10
    7 IF (M.GT.I1) GO TO 8
      B(I1)=D1+D1
      B(I2)=S1
      GO TO 10
    8 B(M)=S1**(M-I1)
      B(MP1)=S1*B(M)
```

```
      B(M)=DFLOAT(M+M)*D1*B(M)
      JEND=M-I1
      S1SQ=S1*S1
      TERM=ONE-S1SQ
      S1D1=S1*D1
      DO 9 J2S=I1,JEND
      J2=M-J2S
      J2P=J2+I1
    9 B(J2)=(DFLOAT(J2+J2)/(S1SQ*DFLOAT(MP1-J2)))*(S1D1*B(J2P)-
     #DFLOAT(J2P)*TERM*B(J2+I2))
   10 IF (N.GT.IO) GO TO 11
      C(I1)=ONE
      GO TO 14
   11 IF (N.GT.I1) GO TO 12
      C(I1)=D2+D2
      C(I2)=S2
      GO TO 14
   12 JEND=N-I1
      C(N)=S2**JEND
      C(NP1)=S2*C(N)
      C(N)=DFLOAT(N+N)*D2*C(N)
      S1SQ=S2*S2
      TERM=ONE-S1SQ
      S1D1=S2*D2
      DO 13 J3S=I1,JEND
      J3=N-J3S
      J3P=J3+I1
   13 C(J3)=(DFLOAT(J3+J3)/(S1SQ*DFLOAT(NP1-J3)))*(S1D1*C(J3P)-
     #DFLOAT(J3P)*TERM*C(J3+I2))
   14 WTOVLP=ZERO
      TMAX=ZERO
      DO 17 J1=I1,KP1
      SUM2=ZERO
      S1SQ=OW(J1)
      DO 16 J2=I1,MP1
      SUM3=ZERO
      S1D1=B(J2)*S1SQ
      DO 15 J3=I1,NP1
      J3S=J1+J2+J3-3
      IS=J3S/I2
      IF ((IS+IS).NE.J3S) GO TO 15
      IIS=IS+I2
      IS1=IIS-J1
      IF (IS1.LT.I1) GO TO 15
      IS2=IIS-J2
      IF (IS2.LT.I1) GO TO 15
      IS3=IIS-J3
      IF (IS3.LT.I1) GO TO 15
      TERM=C(J3)*DEXP(AL2*DFLOAT(IS)+FCT(J1)+FCT(J2)+FCT(J3)-FCT(IS1)-
     #FCT(IS2)-FCT(IS3))
      TERS=DABS(TERM*S1D1)
      IF (TERS.GT.TMAX) TMAX=TERS
      SUM3=SUM3+TERM
   15 CONTINUE
   16 SUM2=SUM2+B(J2)*SUM3
   17 WTOVLP=WTOVLP+OW(J1)*SUM2
      IF (WTOVLP.EQ.ZERO) GO TO 19
      ISIG=15-IFIX(ALOG10(SNGL(TMAX/DABS(WTOVLP))))
      WTOVLP=(WTOVLP/B1)*(DSQRT(A1*A2)/DEXP(HALF*(AL2*DFLOAT(M+N)+
     #FCT(MP1)+FCT(NP1)+D*D)-BO*BO))
   18 RETURN
   19 ISIG=15
      GO TO 18
      END
```

APPENDIX 5

GEOMETRY OF THE EXCITED STATE FROM EXPERIMENTAL TRANSITION PROBABILITIES WITH VIBRONIC COUPLING TERMS INCLUDED

The program described here calculates the possible dislocations of a pair of harmonic oscillators from given ωs and two observed transition probabilities

$$v_1' \quad v_1'' \quad , \mathrm{Int}_1$$
$$v_2' \quad v_2'' \quad , \mathrm{Int}_2 \qquad \text{(A5-1)}$$

with a transition moment of the form

$$M(q) = (M_o + M_1 q + \ldots.) \exp\left(-(1/2)\alpha_o{}^2 q^2\right) \qquad \text{(A5-2)}$$

A normal mode analysis will yield the excited state geometry from the computed displacements if the ground state geometry was known.

The input consists of sets of six cards and two cards at the beginning (first and second card).

First Card: This is simply a title card (maximum 80 characters).

Second Card: NINT, NDS, DSTART, DEND

Format (2i5, 2f10.0)

The above parameters, with the exception of NDS, control the preliminary pedestrian search for the location of the roots on the finite interval DSTART $\leqslant$ D $\leqslant$ DEND, where D is the dimensionless displacement parameter $D=\alpha''\delta$. The computed values are being stored in an array. NINT indicates the number of intervals in the search for the roots. The storage limitations in the program are such that we require NINT $\leqslant$ 1024. NDS is an output parameter. If NDS$\neq$0 every NDS-th calculated value of the function whose roots have to be located will appear on the printed output.

Third Card: KDP, KP, SK, ALFK1, ALFK2

Format (2:5, 3f10.0)

The quantities above mean the following

KDP ..... v_1''

KP .,... v_1'

SK ..... trans. $prob._1$

ALFK1 ... α_1''

ALFK2 ... α_1'

Notice that the transition probability is not the same as the intensity. In optical spectra the transition probability can be obtained from the intensities readily, simply by multiplying the latter with appropriate integer powers of the wavelengths.

Fourth Card: JDP, JP, SJ, ALFJ1, ALFJ2

Format (2i5, 3f10.0)

The quantities above denote the following

JDP ..... v_2'

JP ..... v_2''

SJ ..... trans. $prob._2$

ALFJ1 ... α_2''

ALFJ2 ... α_2'

Fifth Card: KTRM1, AU1

Format (i5, f10.0)

KTRM1 denotes the number of terms in the transition moment in (A5-1) for the first transition (third card). AU1 is the parameter of the exponential factor in the transition moment of the first transition

$$AU1 = \alpha_o^2 \qquad \text{(A5-3)}$$

If KTRM1 < 0 the current calculation is the last one. The program replaces a negative KTRM1 by its absolute value. Due to storage limitations we require $|KTRM1| \leq 31$

Sixth Card: the expansion coefficients for the transition moment of the first transition (third card)

$M_o, M_1, \ldots\ldots, M_k$, $k = KTRM1 - 1$

Format (8f10.0)

Seventh Card: same as the fifth card, but for the second transition (fourth card).

Eighth Card: same as the sixth card, but for the second transition.

If one the fifth card we had KTRM1 > 0 additional calculations are implicitly requested. In this case an additional data set is entered starting however with the third card (cards No. 3-8). An unlimited number of such sets of six cards can be entered consecutively. In general the transition moments of both transitions will be identical.

In the listing of the program the subroutine WTOVLP has been omitted. It is the same as the one shown in Appendix 4.

```
      IMPLICIT REAL*8 (A-H,O-Z)
      REAL*8 RT(1025),AW(31),OW(31)
      INTEGER*2 ITRIP,ITROP,IJISS
      LOGICAL*1 L2,LUS
      COMMON /PARS/AW,OW,AKJ,AU1,AU2,ALFK1,ALFK2,ALFJ1,ALFJ2,KSRM1,
     #KSRM2,KDP,KP,JDP,JP
      DATA ITRIP,ITROP/'O ',' '/
      READ (5,6) (RT(J),J=1,10)
      WRITE (6,7) (RT(J),J=1,10)
      READ (5,8) NINT,NDS,DSTART,DEND
      WRITE (6,9) NINT,DSTART,DEND
      L2=NDS.EQ.0
      DST=(DEND-DSTART)/DFLOAT(NINT)
      NINT=NINT+1
      IF (NINT.GT.1025) GO TO 5
    1 READ (5,8) KDP,KP,SK,ALFK1,ALFK2,JDP,JP,SJ,ALFJ1,ALFJ2,KTRM1,AU1
      LUS=KTRM1.LE.0
      IF (LUS) KTRM1=-KTRM1
      READ (5,10) (AW(J),J=1,KTRM1)
      READ (5,11) KTRM2,AU2
      READ (5,10) (OW(J),J=1,KTRM2)
      KSRM1=KTRM1-1
      KSRM2=KTRM2-1
      WRITE (6,12) KDP,KP,SK,ALFK1,ALFK2,JDP,JP,SJ,ALFJ1,ALFJ2,KTRM1,
     #AU1,(AW(J),J=1,KTRM1)
      WRITE (6,13) KTRM2,AU2,(OW(J),J=1,KTRM2)
      AKJ=-DSQRT(SJ/SK)
      NS=0
      DO 3 JSX=1,2
      AKJ=-AKJ
      RT(1)=F(DSTART)
      DO 2 JCX=2,NINT
      RT(JCX)=F(DSTART+DST*DFLOAT(JCX-1))
      IF (RT(JCX)*RT(JCX-1).GT.0.0D0) GO TO 2
      NS=NS+1
      CALL FALSI(DSTART+DST*DFLOAT(JCX-2),DSTART+DST*DFLOAT(JCX-1),
     #RT(JCX-1),RT(JCX),NS)
    2 CONTINUE
      WRITE (6,14)
      IF (L2) GO TO 3
      WRITE (6,15) (RT(JCX),JCX=1,NINT,NDS)
      IJISS=ITRIP
      JJ=((NINT-1)/NDS)+1
      IF (11*(JJ/11).EQ.JJ) IJISS=ITROP
      WRITE (6,16) IJISS
    3 CONTINUE
      IF (NS.EQ.0) WRITE (6,17)
      IF (.NOT.LUS) GO TO 1
    4 STOP
    5 WRITE (6,18) NINT
      GO TO 4
    6 FORMAT (10A8)
    7 FORMAT (28X,10A8)
    8 FORMAT (2I5,3F10.0/2I5,3F10.0/I5,F10.0)
    9 FORMAT (1HO,9X,6HNUMBER,1X,2HOF,1X,9HINTERVALS,1X,1H=,I5,7X,1H(,
     #F10.5,1X,1H,,F10.5,1X,1H)/1HO)
   10 FORMAT (8F10.0)
   11 FORMAT (I5,F10.0)
   12 FORMAT (1HO,5X,5HFIRST,1X,10HTRANSITION,3X,1H:,4X,2HV",1X,1H=,I2,
     #3X,2HV',1X,1H=,I2,5X,4HREL.,1X,9HINTENSITY,1X,1H=,F7.3,5X,6HALPHA"
     #,1X,1H=,D15.7,3X,6HALPHA',1X,1H=,D15.7/6X,6HSECOND,1X,
     #10HTRANSITION,2X,1H:,4X,2HV",1X,1H=,I2,3X,2HV',1X,1H=,I2,5X,
     #4HREL.,1X,9HINTENSITY,1X,1H=,F7.3,5X,6HALPHA",1X,1H=,D15.7,3X,
     #6HALPHA',1X,1H=,D15.7/6X,9HEXPANSION,1X,2HOF,1X,3HTHE,1X,
     #10HTRANSITION,1X,6HMOMENT,2X,1H:/6X,5HFIRST,1X,10HTRANSITION,3X,
     #1H:,I7,1X,5HTERMS,3X,1H,,3X,2HAU,1X,1H=,F10.6,3(/6X,12F10.6))
   13 FORMAT (6X,6HSECOND,1X,10HTRANSITION,2X,1H:,I7,1X,5HTERMS,3X,1H,,
     #3X,2HAU,1X,1H=,F10.6,3(/6X,12F10.6))
   14 FORMAT (1X)
   15 FORMAT (1HO,1X,128(1H=)//200(5X,11(D11.2)/))
```

```
16 FORMAT (A2,128(1H=)/1X)
17 FORMAT (1HO,5X,2HNO,1X,4HREAL,1X,5HROOTS,1X,7HLOCATED/1X)
18 FORMAT (1HO,5X,4HNINT,1X,1H=,I5,2X,1H:,5X,3HTOO,1X,4HMANY,1X,
  #9HINTERVALS,1X,10HSPECIFIED./6X,9HEXECUTION,1X,11HTERMINATED.,
  #10(/1HO,9X,19(1X,5HSORRY))/1H-/1H-/1H-)
   END

   REAL FUNCTION F*8 (D)
   IMPLICIT REAL*8 (A-H,O-Z)
   REAL*8 AW(31),OW(31)
   COMMON /PARS/AW,OW,AKJ,AU1,AU2,ALFK1,ALFK2,ALFJ1,ALFJ2,KSRM1,
  #KSRM2,KDP,KP,JDP,JP/ZAP/ISIG
   F=AKJ*WTOVLP(AW,D,AU1,ALFK1,ALFK2,KSRM1,KDP,KP,ISIG)+WTOVLP(OW,D,
  #AU2,ALFJ1,ALFJ2,KSRM2,JDP,JP,ISIG)
   RETURN
   END

   SUBROUTINE FALSI(DO,D1,FO,F1,NS)
   IMPLICIT REAL*8 (A-H,O-Z)
   COMMON /ZAP/ISIG
   D=DO-FO*((D1-DO)/(F1-FO))
   IF (DABS(F1/FO).GT.1.0D0) GO TO 1
   DM=D1
   FM=F1
   GO TO 2
 1 DM=DO
   FM=FO
 2 FX=F(D)
   DO 5 N=1,45
   W=(FM*D-FX*DM)/(FM-FX)
   FW=F(W)
   IF (FX*FW.GT.0.0D0) GO TO 3
   DSX=W-DM
   DM=W
   FM=FW
   GO TO 4
 3 DSX=W-D
   D=W
   FX=FW
 4 IF (DABS(DSX).LT.1.0D-7) GO TO 6
 5 CONTINUE
   WRITE (6,8)
   GO TO 7
 6 WRITE (6,9) NS,W,ISIG
 7 RETURN
 8 FORMAT (1HO,9X,6HREGULA,1X,5HFALSI,1X,10HITERATIONS,1X,3HNOT,1X,
  #9HCONVERGED/1X)
 9 FORMAT (10X,1H(,I2,1H),3X,1HD,1X,1H=,F7.4,16X,1H(,I2,1X,4HSIG.,1X,
  #8HFIGURES))
   END
```

APPENDIX 6

CALCULATION OF THE TRANSITION MOMENT FUNCTION FROM EXPERIMENTAL VIBRONIC TRANSITION PROBABILITIES

This Appendix contains input instructions for the FORTRAN program which computes the linear coefficients of an expansion for the transition moment function from experimental vibronic transition probabilities. The quantities in this Appendix have the same meaning as in Chapter 4.

The initial card with Format (i5) contains simply the number of desired runs. Then for each run a set of cards is read as follows:

First Card: IEND, JEND, JSOURC, IFRAN, IRC.

Format (5i5)

(i) IEND is the number of title cards to be entered (and printed).

(ii) If the printed output is to start on a new page, we take JEND=1, otherwise JEND=0. Notice that taking JEND=1 and/or ISX=1 (see third card!) can give rise to the occurrence of blank pages on the printed output.

(iii) JSOURC indicates the input where the expectation values are to be read. For example JSOURC=5 in general would indicate that the expectation values will be read from cards. If JSOURC=0 the expectation values are computed internally in the harmonic oscillator approximation. If JSOURC=99999 the expectation values from a previous run will be retained. If JSOURC $<$ 0 the format used for entering the expectation values will be read from cards, otherwise the default format (8f10.0) will be used. The program replaces a negative JSOURC by its absolute value. If JSOURC=99999, the transitions have to be left in the same order as in the previous run. One can leave out the last few transitions by decreasing

NINT (see third card!), but there is no way to remove cards in between, except removing them artificially by taking their weighting factors as zero.

(iv) IFRAN and IRC refer to the r-centroid analysis of the residues. In this analysis, the residues (difference between experimental and computed weighted overlaps) are plotted against the ratio of expectation values $\langle v'|q|v''\rangle / \langle v'|v''\rangle$ in the harmonic oscillator approximation. If IFRAN≠0, instead of taking $\langle v'|v''\rangle$ in the harmonic oscillator approximation the IFRAN-th expectation value will be used in the above ratio. Similarly, if IRC≠0 the expectation value $\langle v'|q|v''\rangle$ in the harmonic oscillator approximation will be replaced by the IRC-th expectation value in $\langle v'|q|v''\rangle / \langle v'|v''\rangle$.

Second Card: Title cards, where # of title cards=IEND. If IEND=0, these title cards are missing of course.

Third Card: NINT, NTRMST, MTRMFN, MTRMD, ND, NAU, NSIGN, JSQ, ISX, JECT, I, MPROG, NSNIFF, JS, JD, JE

Format (16i5)

(i) NINT is the number of transitions. If NINT $>$ 0 the experimental intensities are being entered later (twelfth card). If NINT $<$ 0 the experimental weighted Franck-Condon amplitudes (with proper signs!) are being read later. The program replaces a negative NINT by its absolute value. (See also ninth and twelfth card.)

(II) NTRMST, NTRMFN, and NTRMD refer to the number of terms to be included in the expansion of the transition moment. The number of terms included will be

# of terms = NTRMST, NTRMST + NTRMD, ..., NTRMFN

According to the above, NTRMD is an increment in the number of terms and

NTRMST $\ll$ # of terms $\ll$ NTRMFN.

If NTRMST is left blank, the program takes NTRMST=1. The same holds for NTRMD.

(iii) ND denotes the number of dislocations of the normal mode coordinate frames to be considered. (See the quantities DSTAR and DEND on the fourth card.) If ND is left blank, the program takes ND=1.

(iv) NAU is the number of nonlinear parameters α_o^2 for which computations have to be done. (See the quantities AUSTAR and AUEND on the fourth card). If NAU is left blank the program takes NAU=1.

(v) NSIGN is the maximum number of self-consistent signs iterations permitted for each run. In general, taking NSIGN=6 should be plenty. The program will indicate on the printed output that the self-consistent signs iterations did not converge if NSIGN was taken too small. If NSIGN is left blank, the program takes NSIGN=1.

(vi) JSQ is the number of the vibronic progression whose intensities constitute the dependent variable. Only if MPROG $>$ 1 can the dependent variable be declared. Otherwise the intensities will constitute the dependent variable. If JSQ is left blank and MPROG $>$ 1, the intensities of the first vibronic progress will constitute the dependent variable, i.e., taking JSQ=0 amounts to the same as taking JSQ=1. The vibronic progressions are counted starting from one. If JSQ $<$ 0, the program will replace JSQ by its absolute value and the JSQ-th term of the transition

moment function constitutes the dependent variable. The program will not check whether the transition moment expansion has a sufficient number of terms for this case, i.e. if NTRMST $\geqslant$ JSQ.

(vii) If an r-centroid analysis of the residues is requested, the graph with the residues will be omitted if ISX $<$ 0, and it will start on a new page if ISX=1. The points on the graph are represented by stars. If points coincide the graph will not indicate that.

(viii) JECT indicates the number of points to be left out in the graph of residues (see eighth card).

(ix) "I" determines three options:

1 - Scale the final transition moment such that $\mathcal{M}_0 = 1$.

2 - Multiply the transition moment with a factor TSCALE (see sixth card).

3 - Multiply all experimental intensities by a factor ISCALE, where ISCALE is a real constant. (See sixth card.)

The following truth table indicates which options are in effect:

I	(1)	(2)	(3)	X
0	F	F	F	F
1	T	F	F	F
2	F	F	T	T
3	F	T	F	T
4	F	T	T	T
5	T	F	T	T

where the quantity X indicates whether the fifth card is to be included in the input.

(x) MPROG is the number of vibronic progressions. If the entire spectrum consists of one vibronic progression, one can also take MPROG=0. In some cases one knows the relative population factors through some other considerations. One can take MPROG=1 (or 0) in this case if the quantities on the twelfth card are scaled accordingly.

Any group of transitions with a common initial state or equivalently the same initial population, can be considered a vibronic progression. Rotational sublevels of the initial state can be viewed as giving rise to distinct vibronic progressions if rotational resolution is possible.

(xi) NSNIFF is the number of Gauss-Seidel iterations allowed to solve the linear systems. If the solution has to be found by Gauss-Seidel iterations alone, many hundreds of such iterations are required. If the Gauss-Seidel iterations are used for iterative improvement, only a few iterations are necessary, even for large systems. The latter is the recommended option regarding the solution of the linear systems.

(xii) JS serves as a logical parameter. If JS=0, the initial solution of the linear system will be computed by Gaussian elimination. This solution is then refined by Gauss-Seidel iterations. If JS≠0, and NSNIFF $>$ 0 the program will attempt to find the solution from scratch by Gauss-Seidel iterations with $\mathcal{M}_k = Gs_{v'} = 0$ as the starting solution. If JS≠0, and NSNIFF=0 the linear system will be solved by Gaussian elimination.

(xiii) If the experimental intensities or, depending on the sign of NINT, the weighted Franck-Condon amplitudes of the previous run have to be retained, but some of the weighting factors have to be changed,

then JD≠0, and JD=# of weighting factors to be changed. (See fifth card.)

(xiv) JE≠0 indicates that the experimental intensities or weighed Franck-Condon amplitudes of the previous run have to be kept and are being used in the current run, unless there was no previous run.

The following three output options are determined by the third card:

1- Print the expectation values used in the r-centroid analysis of the residues. This option is activated by taking NTRMST (columns 6-10) negative. The program replaces a negative NTRMST by its absolute value.

2- Perform the r-centroid analysis of the residues. This option can be suppressed by taking NTRMFN (columns 11-15) negative. The program replaces a negative NTRMFN by its absolute value.

3- Print the computed weighted Franck-Condon amplitudes together with the difference between the experimental and the computed values for each computed transition moment function. This option can be suppressed by taking NSIGN (columns 31-35) negative. The program replaces a negative NSIGN by its absolute value.

Fourth Card: DSTAR, DEND, AUSTAR, AUEND, A1, A2, TOLERA

Format (6f10.0, f20.0)

(i) DSTAR and DEND refer to the range of the dimensionless parameter $D=\alpha''\delta$ in the run. ND equidistant values in the interval

$$DSTAR \leqslant D \leqslant DEND$$

are being treated. If ND=1, the program takes D=DSTAR.

(ii) AUSTAR and AUEND refer to the range of values α_o^2 will take in the computations. NAU equidistant values in the interval

$$\text{AUSTAR} \leqslant \alpha_o^2 \leqslant \text{AUEND}$$

are considered. If NAU=1 the program takes α_o^2=AUSTAR.

(iii) A1 = α''

A2 = α'

The singly primed and the doubly primed cases can be interchanged as long as one is consistent.

(iv) TOLERA is the convergence threshold for the Gauss-Seidel iterations. The iterations are considered as having converged if norm infinity of the difference of two consecutive solution vectors $\underset{\sim}{x}$ of the linear system is less than TOLERA

$$\|\underset{\sim}{x}_{j+1} - \underset{\sim}{x}_j\|_\infty < \text{TOLERA}$$

Since the convergence of the Gauss-Seidel iterations for large systems is very slow, the uncertainity for norm infinity of $\underset{\sim}{x}$ can be 100 for 1000 times larger than TOLERA.

Fifth Card: This card is missing if JD=0 or JE=0, or if one is dealing with the initial run. Otherwise this card contains the numbers of the transitions and the corresponding modified weighting factors:

(# of transition, weighting factor), j = 1, JD

with the format (8(i5, f5.0)). For example, if the weighting factors of the third and fifth transition have to be taken as 1/2 and 1/4 respectively, one would take

3 0.5 5 0.25

More than one card will be required for this entry if JD > 8.

Sixth Card: This card is missing if I $\leq$ 1. Otherwise it contains ISCALE and TSCALE with format (2f10.0). ISCALE is a scaling factor for the experimental intensities or weighted Franck-Condon amplitudes. The use of ISCALE can be useful if one wants to avoid having to punch decimal points for the experimental intensities or weighted Franck-Condon amplitudes. TSCALE is the scaling factor which has to be applied to the final transition moment. Notice that only if I=4 are both of these quantities actually being used in the calculations. If I=2,3 or 5 one can leave blank the quantity which is not needed.

Seventh Card: NLOC (j), j=1, MPROG

Format (25i3)

This card is missing if MPROG $\leq$ 1. The quantities in NLOC indicate the number of transitions in each vibronic progression in the same sequence as they are being entered. (See twelfth card.) For example, having two vibronic progressions:

(1) $v' = 0,\ v'' = 0,\ 1,\ 2,\ 3$

(2) $v' = 1,\ v'' = 1,\ 2,\ 3,\ 4,\ 5$

would require the two numbers

4 5

More than one card will be required for this entry if MPROG $>$ 25.

Eigth Card: This card is missing of JECT=0. Due to near breakdowns of the r-centroid approximation, some points can be greatly displaced in the graph of residues. This might make attempts to identify a pattern rather difficult. The transitions that are troublemakers in this respect can be omitted from the graph. On this card the transitions to be excluded from the graph are being listed. The number of omitted transitions is equal

to JECT (see third card, item (viii)). The format used is the same as the one of the seventh card (25i3).

Ninth Card: This card is missing if initially NINT < 0, otherwise it contains the quantity IPOW, (format (i5)) which is used to make the initial assignment of signs to the experimental weighted Franck-Condon amplitudes. Taking k=IPOW we have

$$\mathcal{W}_{v'v''} = \text{sgn} \left(\langle v' | \mathcal{M}_k | v'' \rangle \right)$$

in the harmonic oscillator approximation. If IPOW < 0 the program replaces IPOW by its absolute value and the signs are assigned using the IPOW-th expectation value instead of $\langle v' | \mathcal{M}_k | v'' \rangle$.
It is not advisable to make the initial assignments of signs using the harmonic oscillator approximation if the expectation values are based on a more elaborate model. The reason is that the notation of the eigenfunctions may differ in the two cases.

Tenth Card: This card contains the sequence of the terms in the transition moment expansion in the harmonic oscillator approximation. For example if the transition moment function is to be expanded as

$$M(q) = \mathcal{M}_0 \, \mathcal{M}_0 + \mathcal{M}_1 \, \mathcal{M}_1 + \mathcal{M}_2 \, \mathcal{M}_2$$

the sequence of numbers 0 1 2 would have to be entered here.
If M was assumed to be of the form

$$M(q) = \mathcal{M}_1 \, \mathcal{M}_1 + \mathcal{M}_3 \, \mathcal{M}_3$$

the sequence 1 3
would indicate that. The number of integers in the sequence has to be at least as large as the maximum number of terms considered in the expansion for the transition moment function. The format is the same as the one of

the seventh card (25i3). This card has to be included in the input, even if the expectation values are entered via an input device.

Eleventh Card: This card is missing if initially JSOURC $\geqslant 0$, otherwise it contains the input format for the expectation values; for example: (10A8).

Twelfth Card: These cards (NINT cards!) are missing if this is not the initial run and on the third card JE$\neq$0, otherwise for each transition a card with

$$v', v'', \text{Int}_{v'v''}, \text{ and } W_{v'v''}$$

or

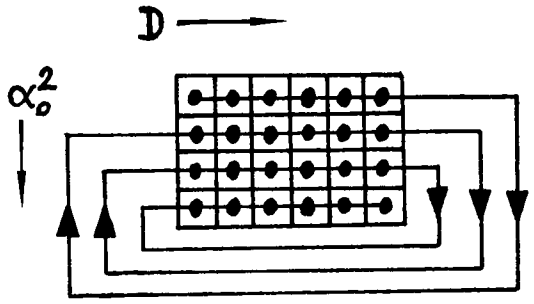
$$v', v'', \text{I0}_{v'v''} \text{Int}^{1/2}_{v'v''}, \text{ and } W_{v'v''}$$

will be entered. The first case applies if initially NINT $>$ 0 and the second case applies if NINT $<$ 0. The Ws denote weighting factors for the transitions indicated by the subscripts. If a weighting factor is left blank (or entered as 0.0) the program takes $W_{v'v''}$=1. The format used is (2i5, 2f10.0). According to the above leaving all weighting factors blank will result in a non-weighted least squares fit. To obtain $W_{v'v''}$=0 one has to enter a negative number for this weighting factor, which will be converted to a zero by the program.

Thirteenth Card: These cards (NINT cards, or a multiple of NINT cards) are missing if JSOURC$\neq\pm$5. If JSOURC$\neq$0, JSOURC$\neq$99999, and JSOURC$\neq\pm$5 these cards would be read from an input device other than cards, designated by JSOURC. If JSOURC=0 or JSOURC=99999 these cards would be missing altogether. If the eleventh card is missing, i.e. if initially JSOURC $>$ 0 the default format will be used for reading the expectation values. This default format is (8f10.0). If an "eleventh" card was

entered the corresponding format would be used here. A sufficient number of expectation values have to be supplied to cover the maximum number of terms used in the expansion of the transition moment in the run, i.e. the number of expectation values for each transition should be at least NTRMFN.

If NAU $>$ 1 or ND $>$ 1, or both, the program will read from the input unit indicated by JSOURC the required NAU·ND sets of NINT·NTRMFN expectation values. The program computes the transition moment functions in the sequence indicated by the arrows below



for the case NAU=4 and ND=6. If the basis set $\mathcal{H}$ used in the entered expectation values is not of the form

$$\mathcal{H}_k = \exp\,(-(1/2)\alpha_o{}^2 q^2)\; q^k$$

the labelling of the transition moment on the printed output will be incorrect. One should have little trouble to interpret the output even in these cases, however. In photoelectron spectra the transition moment function is a function of the normal mode coordinate and of the energy of the ejected electron, which itself depends on the energies of nuclear motion of the parent species and the ion. One can take into account this kind of dependence with this program in connection with the input option for the expectation values. Let us assume that we have a "transition moment function" M which gives

$$\langle v'|M(q, E_e)|v''\rangle = \mathcal{K}_0 \langle v'|v''\rangle + \mathcal{K}_1 \langle v'|q|v''\rangle$$

$$+ \mathcal{K}_3 \langle v'|v''\rangle E_e(v', v'') + \mathcal{K}_4 \langle v'|q|v''\rangle$$

$$\cdot E_e(v', v'')$$

where $E_e(v', v'')$ is the kinetic energy of the ejected electron. In this case one can prepare a list of the expectation values $\langle v'|v''\rangle$ and $\langle v'|q|v''\rangle$. One can obtain from these the expectation values $\langle v'|v''\rangle$ $E_e(v', v'')$ and $\langle v'|q|v''\rangle$ $E_e(v', v'')$ simply by multiplying with $E_e(v', v'')$. Transition moment functions of the above kind have never been extracted from experimental data to the best of my knowledge. No actual run of the above type has ever been performed with the program, due mainly to the lack of experimental data.

A word of caution is in order at this point. Experimental evidence of autoionization processes has shown up in almost all photoelectron spectra which have been studied extensively and at high resolution. These autoionization processes cannot be incorporated in the present model in a straightforward manner. For this reason results obtained with the above technique might be suspect.

The subroutine POWER is practically identical with the subroutine WTOVLP which computes harmonic expectation values $\langle v'|M|v''\rangle$. POWER computes expectation values of the form $\langle v'|q^m|v''\rangle$.

The storage limitations of the program are such that

(i) # of transitions $\leqslant 501$

(ii) (# of expansion terms) + (# of vibronic progressions) $\leqslant 30$

The increase of these storage limitations represents not a straightforward task, due to the presence of EQUIVALENCE statements and some output features.

```
      IMPLICIT REAL*8 (A-H,O-Z)
      REAL*8 STORE(501,31),A(31,31),AST(31,31),SCHNUG(1002),INT(501),
     #WT(501),CREB(501),B(31),IA(31),CHOOSE(6),SLASH(3),MSIGN,ISCALE
      REAL*4 SNGL
      INTEGER NVDP(501),NVP(501),KS(31),REJECT(25),NLOC(25)
      INTEGER*2 LIMS(1004),SELFS(31),SMASH(30),IFM(25),IPLUS,IBLANK,IMI,
     #ZAR
      LOGICAL*1 GRAPH(62,128),NSIG(501),ISIGN(8),JULIE,RIPA,JILL,SNAZ,
     #LJECT,SNAPPY,SNORR,LSNIFF,LEX,LUV,BABY,BLIM,BLAM,BLUM,DEEDEE,SUE,
     #NANCY,GRAB,RAM,JET,DOG,FIGHT,SLIM
      COMMON /BANDS/NINT/NORM/WAX,SERR,RIPA/WORK/LIMS/LEAST/LSQ,NANCY
      EQUIVALENCE (A,SCHNUG,GRAPH),(MSIGN,LSIGN),(SAU,DEND),(DX,AXMAX),
     #(DY,AYMAX),(CREB(1),SCHNUG(502))
      DATA IO,I1,I2,ZERO,DD,DAU,ONE/0,1,2,3*0.0D0,1.0D0/,
     #ISIS,IPLUS,IBLANK/' IA(',' +','  '/,ISIR/'*Q*Q'/,IMI,ZAR/' -',
     #' <'/,MSIGN,ICLAM,I3,I51,I125,I126,I501/'+-! *   ',' ( ',3,51,
     #125,126,501/,I4,I5/4,5/,CHOOSE/'FRANCK-C','ONDON AM','PLITUDE ',
     #' FRANCK-','CONDON F','ACTOR   '/,ISLAN/' NO.'/,DEEDEE/.FALSE./,
     #DA,ANU,PERCY/'+------+','! NO. ! ','! %  ! '/,IFM/' (','01','(2',
     #'X)',',A','7,',',30','(4','H-','—','-)',',2','H-','+/','01','(2',
     #'X)',',A','7,',',30','I4',',1','X,','1H',',!)'/,I10,I30/10,30/,I7/7/
      DATA SMASH/'01','02','03','04','05','06','07','08','09','10','11',
     #'12','13','14','15','16','17','18','19','20','21','22','23','24',
     #'25','26','27','28','29','30'/,SLASH/' THE DEP','ENDENT V',
     #'ARIABLE '/,SLUSH,CRAMM/'(8F10.0)','        '/
      READ (5,6) NTIMES
      DO 5 JECK=I1,NTIMES
      READ (5,6) IEND,JEND,JSOURC,IFRAN,IRC
      IF (IEND.EQ.IO) GO TO 65
      IEND=IEND*I10
      READ (5,7) (SCHNUG(J),J=I1,IEND)
      WRITE (6,8) JEND
      WRITE (6,46) (SCHNUG(J),J=I1,IEND)
   65 READ (5,6) NINT,NTRMST,NTRMFN,NTRMD,ND,NAU,NSIGN,JSQ,ISX,JECT,I,
     #MPROG,NSNIFF,JS,JD,JE,DSTAR,DEND,AUSTAR,AUEND,A1,A2,TOLERA
      LEX=.TRUE.
      BLIM=(JE.NE.IO).AND.(JECK.GT.I1)
      RAM=JSOURC.NE.IO
      IF (RAM) SLIM=JSOURC.EQ.99999
      JET=JSOURC.LT.IO
      DOG=IFRAN.NE.IO
      FIGHT=IRC.NE.IO
      SUE=NTRMST.GT.IO
      SNAZ=NTRMFN.GT.IO
      LJECT=JECT.NE.IO
      JILL=NSIGN.LT.I1
      JULIE=NINT.GT.IO
      LSNIFF=NSNIFF.GE.I1
      SNORR=MPROG.LE.I1
      IF (JSQ.EQ.IO) JSQ=I1
      NANCY=(JSQ.NE.I1).AND.(.NOT.SNORR)
      GRAB=(NTRMD.GT.IO).AND.(JSQ.GE.I1).AND.(.NOT.SNORR)
      BABY=JS.EQ.IO
      SNAPPY=(I.EQ.I1).OR.(I.EQ.I5)
      BLAM=(I.EQ.I2).OR.(I.EQ.I4).OR.(I.EQ.I5)
      BLUM=(I.EQ.I3).OR.(I.EQ.I4)
      IF ((JD.EQ.IO).OR.(.NOT.BLIM)) GO TO 64
      LEX=.FALSE.
      READ (5,80) (REJECT(J),SCHNUG(J),J=I1,JD)
      DO 63 J=I1,JD
      I=REJECT(J)
   63 WT(I)=SCHNUG(J)
   64 IF (JILL) NSIGN=-NSIGN
      IF (JET) JSOURC=-JSOURC
      IF (.NOT.JULIE) NINT=-NINT
      IF (.NOT.SUE) NTRMST=-NTRMST
      IF (.NOT.SNAZ) NTRMFN=-NTRMFN
      IF (NTRMD.LT.IO) NTRMD=-NTRMD
      IF (NTRMD.EQ.IO) NTRMD=I1
      IF (NTRMST.EQ.IO) NTRMST=I1
```

```
      IF (ND.EQ.IO) ND=I1
      IF (NAU.EQ.IO) NAU=I1
      IF (NSIGN.EQ.IO) NSIGN=I1
      IF (SNORR) MPROG=I1
      IF (SNORR) NLOC(I1)=NINT
      IF (BLAM.OR.BLUM) READ (5,62) ISCALE,TSCALE
      IF (JSQ.LT.IO) LSQ=-JSQ
      IF (SNORR) GO TO 52
      READ (5,45) (NLOC(I),I=I1,MPROG)
      DO 51 I=I2,MPROG
   51 NLOC(I)=NLOC(I)+NLOC(I-I1)
      NINT=NLOC(MPROG)
   52 IF (LJECT) READ (5,45) (REJECT(J),J=I1,JECT)
      IF (JULIE) READ (5,6) IPOW
      WRITE (6,9) A1,A2
      IF (LEX) GO TO 92
      WRITE (6,90)
      IEND=(NINT+I3)/I4
      DO 91 I=I1,IEND
      JSTART=I4*(I-I1)+I1
      JEND=I4*I
      IF (JEND.GT.NINT) JEND=NINT
   91 WRITE (6,55) (ISLAN,J,WT(J),J=JSTART,JEND)
   92 READ (5,10) (KS(J),J=I1,NTRMFN)
      IF (JULIE.AND.(IPOW.GE.IO).AND.(NAU.EQ.I1).AND.(AUSTAR.EQ.
     #ZERO)) WRITE (6,86) IPOW
      IA(I1)=SLUSH
      DO 98 J=I1,I30
   98 IA(J+I1)=CRAMM
      IF (JET) READ (5,7) (IA(J),J=I1,I10)
      WAX=ZERO
      LUV=JILL
      IF (MPROG.GT.I1) JILL=.TRUE.
      IF (JILL.AND.JULIE.AND.(.NOT.BLIM)) WRITE (6,15) (CHOOSE(I),
     #I=I4,6)
      IF (JILL.AND.((.NOT.JULIE).OR.BLIM)) WRITE (6,15) (CHOOSE(I),
     #I=I1,I3)
      DO 1 I=I1,MPROG
      JS=I1
      IF (I.GT.I1) JS=NLOC(I-I1)+I1
      JE=NLOC(I)
      DO 1 J=JS,JE
      IF (.NOT.BLIM) READ (5,11) NVDP(J),NVP(J),INT(J),WT(J)
      IF (BLAM) INT(J)=ISCALE*INT(J)
      IF (WT(J).EQ.ZERO) WT(J)=ONE
      IF (WT(J).LT.ZERO) WT(J)=ZERO
      WAX=WAX+WT(J)
      IF (JILL) WRITE (6,12) J,I,NVP(J),NVDP(J),INT(J),WT(J)
    1 IF (JULIE.AND.(.NOT.BLIM)) INT(J)=DSQRT(INT(J))
      IF (JILL) WRITE (6,16)
      JILL=LUV
      WAX=WAX-ONE
      IF (.NOT.JULIE) CALL SIGRET(INT,NSIG)
      IF (ND.GT.I1) DD=(DEND-DSTAR)/DFLOAT(ND-I1)
      IF (NAU.GT.I1) DAU=(AUEND-AUSTAR)/DFLOAT(NAU-I1)
      DO 5 JAU=I1,NAU
      AU=AUSTAR+DAU*DFLOAT(JAU-I1)
      SAU=-0.5DO*AU
      DO 5 JD=I1,ND
      D=DSTAR+DD*DFLOAT(JD-I1)
      NTRM=(NTRMFN-NTRMST)/NTRMD
      NTRMFN=NTRMST+NTRM*NTRMD
      IF (SLIM.OR.(.NOT.RAM)) GO TO 100
      DO 99 J=I1,NINT
   99 READ (JSOURC,IA) (STORE(J,I),I=I1,NTRMFN)
  100 DO 5 NTRM=NTRMST,NTRMFN,NTRMD
      IF (JSQ.GT.I1) LSQ=JSQ+NTRM-I1
      NDIM=NTRM+MPROG-I1
      IF (.NOT.JULIE) CALL REFILL(INT,NSIG)
      IF (NTRM.EQ.NTRMST) CALL INIT(STORE,AST,WT,D,AU,A1,A2,NVDP,NVP,
```

```
     #KS,NTRMFN,RAM)
      J=-IPOW
      IF (JULIE.AND.(IPOW.LT.IO)) WRITE (6,101) J
      IF (JULIE.AND.(IPOW.GE.IO).AND.(SAU.NE.ZERO)) WRITE (6,102) IPOW,
     #SAU,ISIR
      IF (JULIE) CALL HARPER(STORE,INT,D,AU,A1,A2,NVDP,NVP,IPOW)
      DO 4 JSIG=I1,NSIGN
      RIPA=JSIG.EQ.NSIGN
      IF (.NOT.BABY) GO TO 59
      LUV=.FALSE.
      LEX=.FALSE.
      DO 58 IEND=I1,I2
      DO 57 J=I1,NTRM
      DO 56 I=J,NTRM
      A(I,J)=AST(I,J)
   56 IF (J.NE.I) A(J,I)=A(I,J)
   57 B(J)=SKFILL(STORE,INT,WT,I1,NLOC(I1),J)
      IF (.NOT.SNORR) CALL SAVAGE(STORE,A,INT,WT,B,NLOC,MPROG,NTRM)
      IF (IEND.EQ.I1) CALL GAUSS(A,B,IA,31,NDIM)
      IF (NSNIFF.EQ.IO) GO TO 60
   58 IF (IEND.EQ.I2) CALL SNIFF(A,B,IA,TOLERA,31,NDIM,NSNIFF,LEX,LUV,
     #BABY)
      IF ((.NOT.LEX).AND.(.NOT.LUV)) GO TO 60
   59 DO 3 J=I1,NTRM
      DO 2 I=J,NTRM
      A(I,J)=AST(I,J)
    2 IF (J.NE.I) A(J,I)=A(I,J)
    3 B(J)=SKFILL(STORE,INT,WT,I1,NLOC(I1),J)
      LUV=.FALSE.
      LEX=.FALSE.
      IF (.NOT.SNORR) CALL SAVAGE (STORE,A,INT,WT,B,NLOC,MPROG,NTRM)
      IF (ISNIFF) CALL SNIFF(A,B,IA,TOLERA,31,NDIM,NSNIFF,LEX,LUV,
     #DEEDEE)
      IF ((.NOT.ISNIFF).OR.LEX) CALL GAUSS(A,B,IA,31,NDIM)
      IF ((.NOT.ISNIFF).OR.LEX.OR.(.NOT.LUV)) GO TO 49
      DO 48 J=I1,NTRM
      B(J)=SKFILL(STORE,INT,WT,I1,NLOC(I1),J)
      DO 48 I=J,NTRM
      A(I,J)=AST(I,J)
   48 IF (I.NE.J) A(J,I)=A(I,J)
      IF (.NOT.SNORR) CALL SAVAGE (STORE,A,INT,WT,B,NLOC,MPROG,NTRM)
      CALL GAUSS(A,B,IA,31,NDIM)
   49 IF (LEX.OR.LUV) WRITE (6,50)
   60 IF (.NOT.NANCY) GO TO 77
      IF (LSQ.LE.NTRM) GO TO 87
      WRITE (6,82) JSQ,(SLASH(J),J=I1,I3)
      GO TO 88
   87 WRITE (6,83) LSQ,(SLASH(J),J=I1,I3)
   88 AUEND=IA(NDIM)
      JE=LSQ+NDIM
      DO 81 I=LSQ,NDIM
      J=JE-I
   81 IA(J+I1)=IA(J)
      IA(LSQ)=ONE
      DO 78 J=I1,NDIM
   78 IA(J)=IA(J)/AUEND
      GO TO 79
   77 IF (.NOT.SNORR) WRITE (6,82) I1,(SLASH(J),J=I1,I3)
   79 IF (.NOT.GRAB) GO TO 97
      IF (JSQ.EQ.I1) JS=I1
      IF (JSQ.GT.I1) JS=NLOC(JSQ-I1)+I1
      JE=NLOC(JSQ)
      AUEND=ZERO
      DO 93 J=JS,JE
   93 AUEND=AUEND+WT(J)*INT(J)*INT(J)
      AXMAX=ZERO
      DO 94 J=I1,NTRM
   94 AXMAX=AXMAX+IA(J)*SKFILL(STORE,INT,WT,JS,JE,J)
      IF (JSQ.EQ.I1) GO TO 95
      IA(LSQ)=AXMAX/AUEND
```

```
      GO TO 97
   95 AXMAX=AXMAX/AUEND
      DO 96 J=I1,NDIM
   96 IA(J)=IA(J)/AXMAX
   97 WRITE (6,13) JSIG,D,SAU,ISIR,(ISIS,KS(J),IA(J),J=I1,NTRM)
      CALL COMPAR(STORE,INT,WT,CREB,IA,NLOC,MPROG,NTRM,NSWITC)
      IF (NSWITC.EQ.IO) GO TO 20
    4 CONTINUE
   20 IF (MPROG.LE.I1) GO TO 22
      JE=MPROG+I1
      SCHNUG(JE)=ZERO
      AYMAX=ZERO
      SCHNUG(I1)=ZERO
      IF (.NOT.JILL) WRITE (6,17)
      JEND=NLOC(I1)
      DO 21 J=I1,JEND
      AUEND=CREB(J)+INT(J)
      SCHNUG(I1)=SCHNUG(I1)+WT(J)*CREB(J)*CREB(J)
      SCHNUG(JE)=SCHNUG(JE)+INT(J)*INT(J)
      AYMAX=AYMAX+WT(J)*INT(J)*INT(J)
   21 IF (.NOT.JILL) WRITE (6,18) J,NVP(J),NVDP(J),INT(J),AUEND,CREB(J),
     #WT(J)
      IF (MPROG.LE.I1) GO TO 68
      DO 67 I=I2,MPROG
      SCHNUG(I)=ZERO
      SCHNUG(MPROG+I)=ZERO
      JSTART=NLOC(I-I1)+I1
      JEND=NLOC(I)
      DO 67 J=JSTART,JEND
      AYMIN=IA(NTRM+I-I1)*INT(J)
      AUEND=CREB(J)+AYMIN
      SCHNUG(I)=SCHNUG(I)+WT(J)*CREB(J)*CREB(J)
      SCHNUG(MPROG+I)=SCHNUG(MPROG+I)+AYMIN*AYMIN
      AYMAX=AYMAX+WT(J)*AYMIN*AYMIN
   67 IF (.NOT.JILL) WRITE (6,18) J,NVP(J),NVDP(J),AYMIN,AUEND,CREB(J),
     #WT(J)
   68 IF (.NOT.JILL) WRITE (6,19)
      IF (.NOT.JILL) WRITE (6,85)
      LUV=.FALSE.
      DO 75 JE=I1,I2
      LUV=.NOT.LUV
      AUEND=ZERO
      DO 73 J=I1,MPROG
      I=J+(JE-I1)*MPROG
   73 AUEND=AUEND+SCHNUG(I)
      DO 74 J=I1,MPROG
      I=J+(JE-I1)*MPROG
   74 LIMS(J)=IFIX(100.0*SNGL(SCHNUG(I)/AUEND)+0.5)
      JS=(MPROG+29)/I30
      IF (LUV) WRITE (6,76)
      IF (.NOT.LUV) WRITE (6,89)
      DO 75 J=I1,JS
      JSTART=I30*(J-I1)+I1
      JEND=J*I30
      IF (MPROG.LT.JEND) JEND=MPROG
      IFM(I2)=SMASH(I30+JSTART-JEND)
      IFM(I7)=SMASH(JEND-JSTART+I1)
      IFM(15)=IFM(I2)
      IFM(20)=IFM(I7)
      WRITE (6,IFM) DA,ANU,(I,I=JSTART,JEND)
      WRITE (6,IFM) DA,PERCY,(LIMS(I),I=JSTART,JEND)
   75 WRITE (6,IFM) DA
      SERR=100.0D0*SERR*DSQRT(WAX/AYMAX)
      WRITE (6,84) AUEND,SERR
   22 IF (NSWITC.NE.IO) GO TO 30
      DO 23 J=I1,NTRM
      IF (SNAPPY.AND.(J.GT.I1)) IA(J)=IA(J)/IA(I1)
      IF (BUM) IA(J)=TSCALE*IA(J)
      SELFS(J)=IPLUS
      IF (J.EQ.NTRM) GO TO 23
```

```
      IF (IA(J+I1).LT.ZERO) SELFS(J)=IMI
   23 IF (J.NE.I1) IA(J)=DABS(IA(J))
      IF (SNAPPY) IA(I1)=ONE
      SELFS(NTRM)=IBLANK
      WRITE (6,14) SAU,ISIR,(IA(J),KS(J),SELFS(J),J=I1,NTRM)
      IF (NDIM.IE.NTRM) GO TO 30
      IA(NTRM)=ONE
      DO 53 J=NTRM,NDIM
      IEND=J-NTRM+I1
      IF (IA(J).LT.ZERO) WRITE (6,61) IEND,IO
      IA(J)=ONE/(IA(J)*IA(J))
   53 SELFS(J)=IEND
      WRITE (6,54)
      SELFS(NTRM)=I1
      IEND=(MPROG+I3)/I4
      DO 66 I=I1,IEND
      JSTART=I4*(I-I1)+NTRM
      JEND=I4*I+NTRM-I1
      IF (JEND.GT.NDIM) JEND=NDIM
   66 WRITE (6,55) (ISLAN,SELFS(J),IA(J),J=JSTART,JEND)
   30 IF (SUE.OR.(NTRM.NE.NTRMFN)) GO TO 24
      DO 69 J=I1,NINT
      IF (DOG) CREB(J)=STORE(J,IFRAN)
   69 IF (.NOT.DOG) CREB(J)=POWER(D,ZERO,A1,A2,IO,NVDP(J),NVP(J))
      WRITE (6,71)
      IEND=(NINT+I4)/I5
      DO 70 I=I1,IEND
      JSTART=I5*(I-I1)+I1
      JEND=I5*I
      IF (JEND.GT.NINT) JEND=NINT
   70 WRITE (6,72) (ZAR,NVP(J),NVDP(J),CREB(J),J=JSTART,JEND)
      WRITE (6,29)
      DO 25 J=I1,NINT
      IF (FIGHT) CREB(J)=STORE(J,IRC)
   25 IF (.NOT.FIGHT) CREB(J)=POWER(D,ZERO,A1,A2,I1,NVDP(J),NVP(J))
      WRITE (6,27)
      IEND=(NINT+I4)/I5
      DO 26 I=I1,IEND
      JSTART=I5*(I-I1)+I1
      JEND=I5*I
      IF (JEND.GT.NINT) JEND=NINT
   26 WRITE (6,28) (ZAR,NVP(J),NVDP(J),CREB(J),J=JSTART,JEND)
      WRITE (6,29)
   24 IF (.NOT.SNAZ) GO TO 5
      WRITE (6,38)
      DO 31 J=I1,NINT
      IF (DOG) SCHNUG(J)=STORE(J,IFRAN)
      IF (.NOT.DOG) SCHNUG(J)=POWER(D,ZERO,A1,A2,IO,NVDP(J),NVP(J))
      CREB(J)=CREB(J)/SCHNUG(J)
      IF (FIGHT) SCHNUG(J)=STORE(J,IRC)/SCHNUG(J)
   31 IF (.NOT.FIGHT) SCHNUG(J)=POWER(D,ZERO,A1,A2,I1,NVDP(J),NVP(J))/
     #SCHNUG(J)
      IEND=(NINT+I4)/I5
      DO 47 I=I1,IEND
      JSTART=I5*(I-I1)+I1
      JEND=I5*I
      IF (JEND.GT.NINT) JEND=NINT
   47 WRITE (6;39) (ICLAM,SCHNUG(J),CREB(J),J=JSTART,JEND)
      WRITE (6,40)
      IF (ISX.LT.IO) GO TO 5
      AXMAX=-1.OD50
      AXMIN=-AXMAX
      AYMAX=AXMAX
      AYMIN=AXMIN
      DO 32 J=I1,NINT
      IF (.NOT.LJECT) GO TO 44
      DO 43 I=I1,JECT
      IF (J.EQ.REJECT(I)) GO TO 32
   43 CONTINUE
   44 AUEND=SCHNUG(J)
```

```
      XZ=CREB(J)
      IF (AXMAX.LT.AUEND) AXMAX=AUEND
      IF (AXMIN.GT.AUEND) AXMIN=AUEND
      IF (AYMAX.LT.XZ) AYMAX=XZ
      IF (AYMIN.GT.XZ) AYMIN=XZ
   32 CONTINUE
      DX=(AXMAX-AXMIN)/125.0D0
      DY=(AYMAX-AYMIN)/50.0D0
      DO 33 J=I1,NINT
      LIMS(J)=IFIX(0.5+SNGL((SCHNUG(J)-AXMIN)/DX))+I1
   33 LIMS(J+I501)=IFIX(0.5+SNGL((CREB(J)-AYMIN)/DY))+I1
      DO 34 J=I2,50
      GRAPH(J,I1)=LSIGN(I3)
      GRAPH(J,I126)=LSIGN(I3)
      DO 34 I=I2,I125
   34 GRAPH(J,I)=LSIGN(I4)
      DO 35 I=I2,I125
      GRAPH(I1,I)=LSIGN(I2)
   35 GRAPH(I51,I)=LSIGN(I2)
      GRAPH(I1,I1)=LSIGN(I1)
      GRAPH(I51,I1)=LSIGN(I1)
      GRAPH(I1,I126)=LSIGN(I1)
      GRAPH(I51,I126)=LSIGN(I1)
      DO 36 J=I1,NINT
      IEND=LIMS(J)
      JEND=LIMS(J+I501)
      IF ((JEND.GT.I51).OR.(IEND.GT.I126)) GO TO 36
      GRAPH(JEND,IEND)=LSIGN(I5)
   36 CONTINUE
      WRITE (6,41) ISX
      DO 37 J=I1,I51
   37 WRITE (6,42) (GRAPH(J,I),I=I1,I126)
      IF ((JECK.NE.NTIMES).OR.(JD.NE.ND).OR.(JAU.NE.NAU).OR.(NTRM.NE.
     #NTRMFN)) WRITE (6,41) ISX
    5 CONTINUE
      STOP
    6 FORMAT (16I5/6F10.0,F20.0)
    7 FORMAT (10A8)
    8 FORMAT (I1/1HO)
    9 FORMAT (1HO,10X,6HALPHA",1X,1H=,F12.7,5X,6HALPHA',1X,1H=,F12.7)
   10 FORMAT (26I3)
   11 FORMAT (2I5,2F10.0)
   12 FORMAT (16X,1H!,I4,1X,1H!,10X,I3,10X,1H!,2(I3,1X,1H!),2(F18.8,9X,
     #1H!))
   13 FORMAT (1H-,10X,9HITERATION,1X,3HNO.,I3,1X,1H:,5X,3HTHE,
     #1X,13HDIMENSIONLESS,1X,9HPARAMETER,1X,2HOF,1X,12HDISPLACEMENT,
     #2X,1HD,1X,1H=,1X,12HALPHA"*DELTA,1X,1H=,F9.5/11X,3HTHE,1X,
     #11HEXPONENTIAL,1X,6HFACTOR,1X,2HOF,1X,3HTHE,1X,10HTRANSITION,
     #1X,6HMOMENT,2X,1H:,4X,4HEXP(,F7.3,A4,1H)/11X,3HTHE,1X,6HLINEAR,
     #1X,12HCOEFFICIENTS,1X,3HARE,2X,1H:,25(/10X,4(A4,I2,1H),1X,
     #1H=,F12.6,6X)))
   14 FORMAT (1HO,10X,3HTHE,1X,5HFINAL,1X,10HTRANSITION,1X,6HMOMENT,
     #2X,1H:,4X,4HEXP(,F7.3,A4,1H)/11X,3HTHE,1X,6HLINEAR,1X,
     #12HCOEFFICIENTS,1X,3HARE,2X,1H:,7(/11X,5(F12.6,6H*(Q**(,I2,
     #2H)),A2)))
   15 FORMAT (2(1HO/),16X,1H+,5(1H-),1H+,23(1H-),1H+,2(4(1H-),1H+),
     #2(27(1H-),1H+)/16X,1H!,5X,1H!,23X,1H!,2(4X,1H!),2(27X,1H!)/16X,
     #1H!,1X,3HNO.,1X,1H!,2X,3HNO.,1X,2HOF,1X,6HENERGY,1X,5HLEVEL,2X,
     #1H!,1X,2HV',1X,1H!,1X,2HV",1X,1H!,2X,3A8,1X,1H!,5X,9HWEIGHTING,
     #1X,6HFACTOR,6X,1H!/16X,1H!,5X,1H!,23X,1H!,2(4X,1H!),2(27X,1H!)/
     #16X,1H+,5(1H-),1H+,23(1H-),1H+,2(4(1H-),1H+),2(27(1H-),1H+)/16X,
     #1H!,5X,1H!,23X,1H!,2(4X,1H!),2(27X,1H!))
   16 FORMAT (16X,1H!,5X,1H!,23X,1H!,2(4X,1H!),2(27X,1H!)/16X,1H+,
     #5(1H-),1H+,23(1H-),1H+,2(4(1H-),1H+),2(27(1H-),1H+)/1HO)
   17 FORMAT (1H-,2X,1H+,3(5(1H-),1H+),4(26(1H-),1H+)/3X,1H!,3(5X,1H!),
     #4(26X,1H!)/3X,1H!,1X,3HNO.,1X,1H!,2X,2HV',1X,1H!,2X,2HV",1X,1H!,
     #2X,4HEXP.,1X,13HFRANCK-CONDON,1X,4HAMP.,1X,1H!,1X,5HCALC.,1X,
     #13HFRANCK-CONDON,1X,4HAMP.,1X,1H!,8X,10HDIFFERENCE,8X,1H!,
     #5X,9HWEIGHTING,1X,6HFACTOR,5X,1H!/3X,1H!,3(5X,1H!),4(26X,1H!)/
     #3X,1H+,3(5(1H-),1H+),4(26(1H-),1H+)/3X,1H!,3(5X,1H!),4(26X,1H!))
```

```
 18 FORMAT (3X,1H!,3(I4,1X,1H!),4(F18.7,8X,1H!))
 19 FORMAT (3X,1H!,3(5X,1H!),4(26X,1H!)/3X,1H+,3(5(1H-),1H+),4(26(1H-)
   #,1H+)/1X)
 27 FORMAT (1HO,60X,9H<V'!Q!V">/3X,1H+,125(1H-),1H+)
 28 FORMAT (T130,1H!,T4,1H!,4X,5(A2,I2,3H!Q!,I2,1H>,1X,1H=,F9.5,3X))
 29 FORMAT (3X,1H+,125(1H-),1H+)
 38 FORMAT (1H-/45X,10HR-CENTROID,1X,8HANALYSIS,1X,2HOF,1X,8HRESIDUES,
   #2X,1H:/1X)
 39 FORMAT (2X,5(A3,F10.5,1H,,F10.5,1H)))
 40 FORMAT (1HO,26X,3HTHE,1X,10HQUANTITIES,1X,5HABOVE,1X,3HARE,2X,
   #38H(<V'!Q!V">/<V'!V">,DIFFERENCE/<V'!V">))
 41 FORMAT (I1/1H-)
 42 FORMAT (3X,126A1)
 45 FORMAT (25I3)
 46 FORMAT (25X,10A8)
 50 FORMAT (1HO,10X,3HTHE,1X,6HLINEAR,1X,6HSYSTEM,1X,3HWAS,1X,
   #6HSOLVED,1X,2HBY,1X,8HGAUSSIAN,1X,11HELIMINATION)
 54 FORMAT (1H-,10X,8HRELATIVE,1X,10HPOPULATION,1X,2HOF,1X,3HTHE,1X,
   #6HENERGY,1X,6HLEVELS,2X,1H:/1X)
 55 FORMAT (10X,4(A4,I3,F12.5,8X))
 61 FORMAT (1H-,10X,36(1H*),3X,6HENERGY,1X,5HLEVEL,1X,3HNO.,I3,1X,1H:,
   #3X,7HSQRT(N),1X,1H<,I2,3X,36(1H*))
 62 FORMAT (8F10.0)
 71 FORMAT (1H-,61X,7H<V'!V">/3X,1H+,125(1H-),1H+)
 72 FORMAT (T130,1H!,T4,1H!,4X,5(A2,I2,1H!,I2,1H>,1X,1H=,F11.6,3X))
 76 FORMAT (1HO,29X,12HDISTRIBUTION,1X,2HOF,1X,3HTHE,1X,4HSUMS,1X,
   #1X,2HOF,1X,5HERROR,1X,5HTERMS,1X,5HAMONG,1X,3HTHE,1X,8HVIBRONIC,
   #1X,12HPROGRESSIONS/1X)
 80 FORMAT (8(I5,F5.0))
 82 FORMAT (1HO,10X,3HTHE,1X,11HINTENSITIES,1X,2HOF,1X,3HTHE,1X,
   #8HVIBRONIC,1X,11HPROGRESSION,1X,3HNO.,I2,1X,10HCONSTITUTE,3A8)
 83 FORMAT (1HO,10X,4HTERM,1X,3HNO.,I2,1X,2HOF,1X,3HTHE,1X,
   #10HTRANSITION,1X,6HMOMENT,1X,9HEXPANSION,1X,2HIS,3A8)
 84 FORMAT (43X,5HTOTAL,1X,9HINTENSITY,1X,2HOF,1X,3HTHE,1X,
   #8HSPECTRUM,2X,1H:,F13.6/43X,8HRELATIVE,1X,5HERROR,19X,1H:,F11.4,
   #1X,1H%)
 85 FORMAT (23X,2HIN,1X,3HTHE,1X,5HABOVE,1X,5HTABLE,1X,3HTHE,1X,
   #14H"EXPERIMENTAL",1X,13HFRANCK-CONDON,1X,10HAMPLITUDES,1X,3HARE,
   #1X,3HTHE,1X,12HEXPERIMENTAL/25X,10HTRANSITION,1X,
   #1X,13HPROBABILITIES,1X,7HDIVIDED,1X,2HBY,1X,3HTHE,1X,
   #10HCALCULATED,1X,8HRELATIVE,1X,10HPOPULATION,1X,7HFACTORS/1X)
 86 FORMAT (1HO,10X,3HTHE,1X,7HINITIAL,1X,5HSIGNS,1X,2HOF,1X,3HTHE,
   #1X,12HEXPERIMENTAL,1X,13HFRANCK-CONDON,1X,10HAMPLITUDES/11X,4HWERE
   #,1X,5HTAKEN,1X,4HSUCH,1X,4HTHAT,2X,17HSGN(<V'!M(Q)!V">),1X,1H=,1X,
   #12HSGN(<V'!Q**(,I1,7H)!V">).)
 89 FORMAT (1HO,36X,12HDISTRIBUTION,1X,2HOF,1X,11HINTENSITIES,1X,
   #5HAMONG,1X,3HTHE,1X,8HVIBRONIC,1X,12HPROGRESSIONS/46X,6H(USING,1X,
   #3HTHE,1X,10HCALCULATED,1X,10HPOPULATION,1X,8HFACTORS)/1X)
 90 FORMAT (1HO,10X,3HTHE,1X,8HMODIFIED,1X,9HWEIGHTING,1X,7HFACTORS,
   #1X,3HARE,2X,1H:/1X)
101 FORMAT (1HO,10X,3HTHE,1X,7HINITIAL,1X,5HSIGNS,1X,2HOF,1X,3HTHE,1X,
   #12HEXPERIMANTAL,1X,13HFRANCK-CONDON,1X,10HAMPLITUDES,1X,4HWERE/
   #11X,5HTAKEN,1X,4HSUCH,1X,4HTHAT,2X,17HSGN(<V'!M(Q)!V">),1X,1H=,
   #1X,15HSGN(EXPECTATION,1X,5HVALUE,1X,3HNO.,I2,2H).)
102 FORMAT (1HO,10X,3HTHE,1X,7HINITIAL,1X,5HSIGNS,1X,2HOF,1X,3HTHE,1X,
   #12HEXPERIMANTAL,1X,13HFRANCK-CONDON,1X,10HAMPLITUDES,1X,4HWERE,
   #1X,5HTAKEN/11X,4HSUCH,1X,4HTHAT,2X,17HSGN(<V'!M(Q)!V">),1X,1H=,
   #1X,12HSGN(<V'!Q**(,I1,6H)*EXP(,F7.3,A4,7H)!V">).)
    END

    SUBROUTINE SIGRET(INT,NSIG)
    REAL*8 INT(501)
    LOGICAL*1 NSIG(501)
    COMMON /BANDS/NINT
    DO 1 J=1,NINT
  1 NSIG(J)=INT(J).GT.0.0D0
    RETURN
    END
```

```
      SUBROUTINE REFILL(INT,NSIG)
      REAL*8 INT(501),STO,DABS
      LOGICAL*1 NSIG(501)
      COMMON /BANDS/NINT
      DO 1 J=1,NINT
      STO=DABS(INT(J))
      IF (.NOT.NSIG(J)) STO=-STO
    1 INT(J)=STO
      RETURN
      END

      SUBROUTINE INIT(S,AST,WT,D,AU,A1,A2,NVDP,NVP,KS,NTRM,RAM)
      IMPLICIT REAL*8 (A-H,O-Z)
      REAL*8 S(501,31),AST(31,31),WT(501)
      INTEGER NVDP(501),NVP(501),KS(31)
      LOGICAL*1 RAM
      COMMON /BANDS/NINT
      DATA I1/1/
      IF (RAM) GO TO 4
      DO 1 J=I1,NTRM
      DO 1 I=I1,NINT
    1 S(I,J)=POWER(D,AU,A1,A2,KS(J),NVDP(I),NVP(I))
    4 DO 3 I=I1,NTRM
      DO 3 J=I,NTRM
      SUM=0.0D0
      DO 2 K=I1,NINT
    2 SUM=SUM+WT(K)*S(K,I)*S(K,J)
      AST(I,J)=SUM
    3 IF (I.NE.J) AST(J,I)=SUM
      RETURN
      END

      SUBROUTINE HARPER (S,INT,D,AU,A1,A2,NVDP,NVP,IPOW)
      IMPLICIT REAL*8 (A-H,O-Z)
      REAL*8 S(501,31),INT(501)
      INTEGER NVDP(501),NVP(501)
      COMMON /BANDS/NINT
      DATA I1,ZERO/1,0.0D0/
      IF (IPOW.LT.0) GO TO 3
      DO 1 J=I1,NINT
    1 IF (INT(J)*POWER(D,AU,A1,A2,IPOW,NVDP(J),NVP(J)).LT.ZERO) INT(J)=
     #-INT(J)
    2 RETURN
    3 N=-IPOW
      DO 4 J=I1,NINT
    4 IF (INT(J)*S(J,N).LT.ZERO) INT(J)=-INT(J)
      GO TO 2
      END

      REAL FUNCTION SKFILL*8 (S,INT,W,JS,JE,N)
      REAL*8 S(501,31),INT(501),W(501)
      SKFILL=0.0D0
      DO 1 I=JS,JE
    1 SKFILL=SKFILL+W(I)*S(I,N)*INT(I)
      RETURN
      END

      SUBROUTINE COMPAR(S,INT,W,CREB,IA,NLOC,MPROG,NTRM,NSWITC)
      IMPLICIT REAL*8 (A-H,O-Z)
      REAL*8 S(501,31),INT(501),W(501),CREB(501),IA(31)
      INTEGER LU(502),NLOC(25)
      LOGICAL*1 LES,RIPA,SOB,MEGA
      COMMON /NORM/WAX,SNOOP,RIPA/WORK/LU
      DATA IO,I1,ZERO/0,1,0.0D0/
      MEGA=.FALSE.
      NSWITC=IO
      SNOOP=ZERO
      DO 2 JSP=I1,MPROG
      SOB=JSP.EQ.I1
```

```
      IF (SOB) GO TO 10
      K=JSP-I1
      JS=NLOC(K)+I1
      GO TO 11
   10 JS=I1
   11 JE=NLOC(JSP)
      DO 2 J=JS,JE
      SUM=ZERO
      DO 1 I=I1,NTRM
    1 SUM=SUM+IA(I)*S(J,I)
      LES=INT(J)*SUM.GT.ZERO
      IF (SOB) SUM=SUM-INT(J)
      IF (.NOT.SOB) SUM=SUM-INT(J)*IA(NTRM+K)
      IF (RIPA) CREB(J)=SUM
      IF ((.NOT.LES).AND.RIPA) MEGA=.TRUE.
      IF (LES.OR.RIPA) GO TO 2
      NSWITC=NSWITC+I1
      LU(NSWITC)=J
      INT(J)=-INT(J)
    2 SNOOP=SNOOP+SUM*SUM*W(J)
      SNOOP=DSQRT(SNOOP/WAX)
      LES=NSWITC.EQ.IO
      IF (.NOT.LES) WRITE (6,7) (LU(J),J=I1,NSWITC)
      IF (LES) WRITE (6,8)
      WRITE (6,9) SNOOP
      IF (MEGA) WRITE (6,14)
      IF (LES.AND.(.NOT.RIPA)) GO TO 4
    3 RETURN
    4 DO 6 JSP=I1,MPROG
      SOB=JSP.EQ.I1
      IF (SOB) GO TO 12
      K=JSP-I1
      JS=NLOC(K)+I1
      GO TO 13
   12 JS=I1
   13 JE=NLOC(JSP)
      DO 6 J=JS,JE
      SUM=ZERO
      DO 5 I=I1,NTRM
    5 SUM=SUM+IA(I)*S(J,I)
      IF (SOB) CREB(J)=SUM-INT(J)
    6 IF (.NOT.SOB) CREB(J)=SUM-INT(J)*IA(NTRM+K)
      GO TO 3
    7 FORMAT (1HO,10X,3HTHE,1X,5HSIGNS,1X,2HOF,1X,3HTHE,1X,9HFOLLOWING,
     #1X,13HFRANCK-CONDON,1X,10HAMPLITUDES,1X,4HHAVE,1X,4HBEEN,1X,
     #7HCHANGED,2X,1H:,19(/10X,27I4))
    8 FORMAT (1X)
    9 FORMAT (11X,8HSTANDARD,1X,5HERROR,1X,2HOF,1X,8HESTIMATE,1X,1H=,
     #F11.5)
   14 FORMAT (1HO/39X,26(2H**)/39X,1H*,2X,15HSELF-CONSISTENT,1X,5HSIGNS,
     #1X,10HITERATIONS,1X,3HNOT,1X,9HCONVERGED,2X,1H*/39X,26(2H**)/1X)
      END

      SUBROUTINE GAUSS(A,B,X,ND,N)
      IMPLICIT REAL*8 (A-H,O-Z)
      REAL*8 A(ND,ND),B(ND),X(ND)
      EQUIVALENCE (EXC,FACTOR)
      DATA I1/1/
      IF (N.EQ.I1) GO TO 9
      NP1=N+I1
      NM1=N-I1
      DO 5 J=I1,NM1
      JP1=J+I1
      IK=J
      XX=DABS(A(J,J))
      DO 1 K=JP1,N
      IF (DABS(A(K,J)).LT.XX) GO TO 1
      XX=DABS(A(K,J))
      IK=K
    1 CONTINUE
```

```
      IF (IK.EQ.J) GO TO 3
      DO 2 K=J,N
      EXC=A(J,K)
      A(J,K)=A(IK,K)
    2 A(IK,K)=EXC
      EXC=B(J)
      B(J)=B(IK)
      B(IK)=EXC
    3 XX=A(J,J)
      DO 5 K=JP1,N
      FACTOR=A(K,J)/XX
      DO 4 I=JP1,N
    4 A(K,I)=A(K,I)-FACTOR*A(J,I)
    5 B(K)=B(K)-FACTOR*B(J)
      X(N)=B(N)/A(N,N)
      DO 7 J=I1,NM1
      IJ=N-J
      JP1=IJ+I1
      XX=B(IJ)
      DO 6 I=JP1,N
    6 XX=XX-A(IJ,I)*X(I)
    7 X(IJ)=XX/A(IJ,IJ)
    8 RETURN
    9 X(I1)=B(I1)/A(I1,I1)
      GO TO 8
      END

      SUBROUTINE SNIFF (A,B,X,TOLERA,ND,N,NIT,LEX,MOSSAD,DEEDEE)
      IMPLICIT REAL*8 (A-H,O-Z)
      REAL*8 A(ND,ND),B(ND),X(ND)
      LOGICAL*1 LEX,MOSSAD,DEEDEE
      DATA IO,I1,ISB,IBB,ZERO/0,1,'S   ','    ',0.0D0/
      LEX=.FALSE.
      MOSSAD=.FALSE.
      JX=IO
      DO 2 I=I1,N
      DIV=A(I,I)
      IF (DIV.EQ.ZERO) GO TO 7
      IF (.NOT.DEEDEE) X(I)=ZERO
      DO 1 J=I1,N
    1 A(I,J)=-A(I,J)/DIV
      A(I,I)=ZERO
      JX=I
    2 B(I)=B(I)/DIV
      DO 5 JX=I1,NIT
      JIF=JX
      ERR=ZERO
      DO 4 I=I1,N
      SUM=ZERO
      DO 3 J=I1,N
    3 IF (I.NE.J) SUM=SUM+A(I,J)*X(J)
      SUM=SUM+B(I)
      IF (SUM.NE.ZERO) DIV=DABS((X(I)-SUM)/SUM)
      IF (DIV.GT.ERR) ERR=DIV
    4 X(I)=SUM
      IF (ERR.LT.TOLERA) GO TO 9
    5 CONTINUE
      WRITE (6,10)
      MOSSAD=.TRUE.
    6 RETURN
    7 WRITE (6,11)
      LEX=.TRUE.
      IF (JX.EQ.IO) GO TO 6
      DO 8 I=I1,JX
    8 A(I,I)=1.0D0
      GO TO 6
    9 JX=ISB
      IF (JIF.EQ.I1) JX=IBB
      WRITE (6,12) JIF,JX
      GO TO 6
```

```
10 FORMAT (1HO,10X,10(1H*),2X,12HGAUSS-SEIDEL,1X,10HITERATIONS,1X,
  #3HNOT,1X,9HCONVERGED,2X,10(1H*))
11 FORMAT (1HO,10X,10(1H*),2X,3HTHE,1X,6HLINEAR,1X,6HSYSTEM,1X,2HIS,
  #1X,3HNOT,1X,8HSUITABLE,1X,3HFOR,1X,8HSOLUTION,1X,2HBY,1X,
  #12HGAUSS-SEIDEL,1X,10HITERATIONS,2X,10(1H*))
12 FORMAT (1HO,8X,I5,1X,12HGAUSS-SEIDEL,1X,9HITERATION,A4)
   END

   SUBROUTINE SAVAGE (STORE,A,INT,WT,B,NLOC,MPROG,NTRM)
   IMPLICIT REAL*8 (A-H,O-Z)
   REAL*8 STORE(501,31),A(31,31),INT(501),WT(501),B(31)
   INTEGER NLOC(25)
   LOGICAL*1 TIT
   COMMON /LEAST/LSQ,TIT
   DATA I1,I2,ZERO/1,2,0.0D0/
   DO 1 JS=I2,MPROG
   JSTART=NLOC(JS-I1)+I1
   JEND=NLOC(JS)
   DO 1 J=I1,NTRM
   I=NTRM+JS-I1
   SUM=-SKFILL(STORE,INT,WT,JSTART,JEND,J)
   A(J,I)=SUM
 1 A(I,J)=SUM
   JEND=NTRM-I1
   DO 2 J=I2,MPROG
   JS=JEND+J
   DO 2 I=I2,MPROG
   JQ=JEND+I
 2 A(JS,JQ)=ZERO
   DO 4 JS=I2,MPROG
   SUM=ZERO
   J=NLOC(JS)
   JSTART=NLOC(JS-I1)+I1
   JQ=JEND+JS
   B(JQ)=ZERO
   DO 3 I=JSTART,J
 3 SUM=SUM+WT(I)*INT(I)*INT(I)
 4 A(JQ,JQ)=SUM
   IF (TIT) GO TO 6
 5 RETURN
 6 SUM=ZERO
   JEND=NLOC(I1)
   DO 7 J=I1,JEND
 7 SUM=SUM+WT(J)*INT(J)*INT(J)
   JEND=NTRM+MPROG-I1
   JQ=MPROG+NTRM
   DO 8 I=I1,JEND
   A(I,JQ)=-B(I)
 8 A(JQ,I)=-B(I)
   A(JQ,JQ)=SUM
   DO 9 J=I1,LSQ
 9 B(J)=-A(LSQ,J)
   DO 10 J=LSQ,JEND
10 B(J)=-A(LSQ,J+I1)
   DO 11 J=LSQ,JEND
   DO 11 I=I1,JQ
11 A(J,I)=A(J+I1,I)
   DO 12 J=I1,JEND
   DO 12 I=LSQ,JEND
12 A(J,I)=A(J,I+I1)
   GO TO 5
   END

   REAL FUNCTION POWER*8 (D,AU,A1,A2,K,M,N)
   IMPLICIT REAL*8 (A-H,O-Z)
   REAL*8 B(130),C(121),FCT(121),SS1(45),SS2(45),SS3(31),OW(31),A(31)
   REAL*4 SNGL,ALOG10
   COMMON /WORK/B,C
   EQUIVALENCE (SS1(1),FCT(1)),(SS2(1),FCT(46)),(SS3(1),FCT(91)),
  #(SUM2,S2),(SUM3,D2)
```

```
      DATA SS1 /Z0000000000000000,Z0000000000000000,Z40B17217F7D1CF7B,
     #          Z411CABOBFA2A2002,Z4132D94EF92459F1,Z414C9990F111E724,
     #          Z4169449CEB3C0727,Z4188670F996E6184,Z41A9AC7417E5B868,
     #          Z41CCD4490D3FBE7E,Z41F1ABAC84AA68A4,Z4211809973F3A8D73,
     #          Z4213FCBA16D50143,Z42168D5A9C3B32CD,Z4219130F3DF162A42,
     #          Z421BE636A63FD347,Z421EABFF061F1A84,Z4221814C7E5E6A73,
     #          Z4224653BE5ABDCA4,Z42275702A66C7309,Z422A55EAF5DAEF7B,
     #          Z422D6150C868E551,Z4230789F57509E0C,Z42339B4F170AD489,
     #          Z4236C8E4069D1A27,Z423AC0EC459ACBCE,Z423D42FEE2F8CF27,
     #          Z42408EBAD9F93FB9,Z4243E3C634CC03FE,Z424741CD4E45C8C2,
     #          Z424AA8822D674394,Z424E179BF6796902,Z42518ED66E50820F,
     #          Z42550DF18CEB3928,Z425894B11D225AE5,Z425C22DC67845960,
     #          Z425FB83DE6C99D60,Z426354A30490F657,Z4266F7DBDD495E8C,
     #          Z426AA1BB0A5A6048,Z426E521571C0AE89,Z427208C21A728412,
     #          Z4275C59A04F84BB8,Z4279887807BAE939,Z427D5138AE9A73C2/
      DATA SS2 /Z42811FBA1D6EECF9,Z4284F3DBF520F546,Z4288CD7F3B13135D,
     #          Z428CAC86429D2ACB,Z429090D498637614,Z42947A4EEF58F98B,
     #          Z429868DB0F4319AB,Z429C5C5FC498EED3,Z42A054C4D19D3668,
     #          Z42A451F2B09578CB,Z42A853D377043888,Z42AC5A50E9CED39A,
     #          Z42B06556523A3A32,Z42B474CF83ABCBC6,Z42B888A9021D9622,
     #          Z42BCA0CFF936E2C4,Z42C0BD3233FB7DC8,Z42C4DDBE15057502,
     #          Z42C902628F3E3B0D,Z42CD2B0F1F0D25E6,Z42D157B3C3F23047,
     #          Z42D5884OFA84B92C,Z42D9BCA7B6CEBD7B,Z42DDF4D95EFDB10A,
     #          Z42E230C7C662B7B5,Z42E6706528BC8800,Z42EAB3A425C5BDB2,
     #          Z42EEFA77BD02D382,Z42F344D349CB5F7B,Z42F792AA7F8A8A40,
     #          Z42FBE3F166330C19,Z43100389C56E3462,Z43104909FF8B652A,
     #          Z43108EBF13DBF263,Z4310D4A85502B129,Z43111AC51DF8932A,
     #          Z43116114C7E34737,Z4311A796B3EDE1AB,Z4311EE4A45236D3E,
     #          Z4312352EE64B46D5,Z43127C43FFC72961,Z4312C3890172D057,
     #          Z43130AFD5D851956,Z431352A089728F1C,Z43139A71FDD14947/
      DATA SS3 /Z4313E271363E0DF7,Z43142A9DB142A36B,Z431472F6F03D410D,
     #          Z4314BB7C77491066,Z4315042DCD27AF64,Z43154D0A7B2BA658,
     #          Z431596120D23C4EC,Z4315DF4411475A1C,Z431628A018233BED,
     #          Z43167225B4379462,Z4316BBD47B7669B6,Z431705AC0412D89F,
     #          Z43174FABE790F7BE,Z4317991D3C1265C0E,Z4317E4232DFB367E,
     #          Z43182E99CD1C0368,Z4318793173F6BC4FE,Z4318C3FB2796C21B,
     #          Z4319OEE52A05C35F,Z431959F4ECD1C8B3,Z4319A52A17B831CB,
     #          Z4319F084540F545E,Z431A3C034CBB7B2C,Z431A87A6AE24493A,
     #          Z431AD36E262A7CC0,Z431B1F59641E0DB4,Z431B6B6818B4A3EB,
     #          Z431BB799F600610A,Z431C03EEAF66FACD,Z431C5065F9992225,
     #          Z431C9CFF8A8A340D/,I0,I1,I2,ZERO,HALF,ONE,AL2/0,1,2,
     #          0.0D0,0.5D0,1.0D0,6.9314718055994530D-1/
      B1=DSQRT(HALF*(AU+A1*A1+A2*A2))
      B0=(HALF*D*A1)/B1
      G1=ONE/B1
      G0=B0/B1
      S1=A1/B1
      S2=A2/B1
      D1=A1*G0-D
      D2=A2*G0
      JK=K+I1
      MP1=M+I1
      NP1=N+I1
      DO 6 J1S=I1,JK
    6 OW(J1S)=ZERO
      IF (K.GT.I0) GO TO 1
      A(I1)=ONE
      GO TO 4
    1 IF (K.GT.I1) GO TO 2
      A(I1)=G0
      A(I2)=HALF*G1
      GO TO 4
    2 JEND=K-I1
      S1D1=HALF*G1
      A(K)=S1D1**JEND
      A(JK)=S1D1*A(K)
      A(K)=G0*DFLOAT(K)*A(K)
      DO 3 J1S=I1,JEND
      J1=JK-J1S
      JM=J1-I1
```

```
    3 A(JM)=(DFLOAT(JM+JM)/DFLOAT(J1S+I1))*(DFLOAT(J1)*A(J1+I1)+BO*
     #A(J1))
    4 DO 5 J1S=I1,JK
    5 OW(J1S)=OW(J1S)+A(J1S)
      IF (M.GT.IO) GO TO 7
      B(I1)=ONE
      GO TO 10
    7 IF (M.GT.I1) GO TO 8
      B(I1)=D1+D1
      B(I2)=S1
      GO TO 10
    8 B(M)=S1**(M-I1)
      B(MP1)=S1*B(M)
      B(M)=DFLOAT(M+M)*D1*B(M)
      JEND=M-I1
      S1SQ=S1*S1
      TERM=ONE-S1SQ
      S1D1=S1*D1
      DO 9 J2S=I1,JEND
      J2=M-J2S
      J2P=J2+I1
    9 B(J2)=(DFLOAT(J2+J2)/(S1SQ*DFLOAT(MP1-J2)))*(S1D1*B(J2P)-
     #DFLOAT(J2P)*TERM*B(J2+I2))
   10 IF (N.GT.IO) GO TO 11
      C(I1)=ONE
      GO TO 14
   11 IF (N.GT.I1) GO TO 12
      C(I1)=D2+D2
      C(I2)=S2
      GO TO 14
   12 JEND=N-I1
      C(N)=S2**JEND
      C(NP1)=S2*C(N)
      C(N)=DFLOAT(N+N)*D2*C(N)
      S1SQ=S2*S2
      TERM=ONE-S1SQ
      S1D1=S2*D2
      DO 13 J3S=I1,JEND
      J3=N-J3S
      J3P=J3+I1
   13 C(J3)=(DFLOAT(J3+J3)/(S1SQ*DFLOAT(NP1-J3)))*(S1D1*C(J3P)-
     #DFLOAT(J3P)*TERM*C(J3+I2))
   14 POWER=ZERO
      DO 17 J1=I1,JK
      SUM2=ZERO
      DO 16 J2=I1,MP1
      SUM3=ZERO
      DO 15 J3=I1,NP1
      J3S=J1+J2+J3-3
      IS=J3S/I2
      IF ((IS+IS).NE.J3S) GO TO 15
      IIS=IS+I2
      IS1=IIS-J1
      IF (IS1.LT.I1) GO TO 15
      IS2=IIS-J2
      IF (IS2.LT.I1) GO TO 15
      IS3=IIS-J3
      IF (IS3.LT.I1) GO TO 15
      TERM=C(J3)*DEXP(AL2*DFLOAT(IS)+FCT(J1)+FCT(J2)+FCT(J3)-FCT(IS1)-
     #FCT(IS2)-FCT(IS3))
      SUM3=SUM3+TERM
   15 CONTINJE
   16 SUM2=SUM2+B(J2)*SUM3
   17 POWER=POWER+OW(J1)*SUM2
      POWER=(POWER/B1)*(DSQRT(A1*A2)/DEXP(HALF*(AL2*DFLOAT(M+N)+
     #FCT(MP1)+FCT(NP1)+D*D)-BO*BO))
      RETURN
      END
```

APPENDIX 7

WEIGHTED FRANCK-CONDON FACTORS BETWEEN MORSE OSCILLATORS

This Appendix gives input instructions for the computer program which computes the weighted overlap between two displaced Morse oscillators with the rotational term partially included.

The initial card contains the integer NFG which indicates the number of desired runs. The format used is

Format (i5)

After this NFG sets of cards as shown below will be entered.

First Card: This is simply a title card.

Second Card: LOP, NTIMES

Format (L1, I4)

LOP is a logical parameter. If LOP is read as "T", the weighted overlap in the range of the integration interval will be tabulated in the printed output, otherwise this information will be left out. This can be useful in cases where there is some doubt whether the integration limits were chosen properly. NTIMES is the number of weighted Franck-Condon factors to be computed for a given pair of Morse oscillators.

Third Card: MU, BETAO

Format (2f20.0)

MU is the reduced mass of the oscillator and BETAO is the parameter β_o in the exponential factor of the transition moment

$$M(\rho') = \exp\left(-(1/2)\ \beta_o(\rho')^2\right) \oint(\rho') \qquad \text{(A7-1)}$$

where $\rho' = r - r_e'$. The singly primed state represents here always the Morse oscillator No. 1, and the doubly primed state refers to the Morse

oscillator No. 2. MU is expressed in atomic mass units.

Fourth Card: On this card we have ω_e', $\omega_e x_e'$, and r_e' in the format (3f20.0). The spectroscopic constants are in cm^{-1} and the internuclear equilibrium distance r_e' is in Å.

Fifth Card: NG, IO, IB

Format (3i5)

NG denotes the number of expansions terms in the transition moment function. If NG is left blank, the program takes NG=1. IO indicates the input unit where the eighth card (NTIMES cards) wil be read. Leaving IO blank has the same effect as taking IO=5. IB indicates the output unit where

a - the energy of the transition (based on the Morse oscillator model)

b - the computed weighted Franck-Condon factor

c - the computed weighted Franck-Condon amplitude

for each transition will be punched with the format (3A8). The computed energy of the transition (in cm^{-1}) is simply the difference in energies measured from the bottoms of the wells; in other words, the energy of the transition shifted by T_e. If IB is left blank, this constant will be omitted. If NG $\geqslant$ 0 the expansion of the transition moment function in (A7-1) will be of the form

$$f(\rho') = \Sigma_k \mathcal{A}_k (\rho')^k \qquad \text{(A7-2)}$$

otherwise

$$f(\rho') = \Sigma_k \mathcal{A}_k ((2b')e^{-\beta'\rho'})^k \qquad \text{(A7-3)}$$

The program replaces a negative NG by its absolute value.

Seventh Card: The expansion coefficeints $\mathscr{M}$ in the transition moment function. Notice that the coordinates used here are not normal mode coordinates. The units are

$$\begin{aligned} r_e &\ldots\ldots\ldots\ldots \text{Å} \\ \beta_o &\ldots\ldots\ldots\ldots \text{Å}^{-1} \\ \mathscr{M}_k &\ldots\ldots\ldots\ldots \text{Å}^{-k} \end{aligned} \qquad \text{(A7-4)}$$

If the transition moment function was given in normal mode coordinates, the quantities above have to be scaled by appropriate half-integer powers of the reduced mass. The expansions coefficients are entered in the order

$$\mathscr{M}_o, \quad \mathscr{M}_1, \quad \mathscr{M}_2, \ldots\ldots\ldots \qquad \text{(A7-5)}$$

with the format (4f20.0).

Eighth Card: L1, L2, NINT, V1, V2, J1, J2, DELTA1, DELTA2

Format (2L1, i8, 4i5, 2f10.0)

(i) L1 is a logical constant. If L1 is "F", then for the first Morse potential, the rotational term will be included with the restriction $\alpha_o=0$ in effect, otherwise $\alpha_o\neq 0$. The choice of L1 is irrelevant if J'=0. L2 is the same as L1, but referring to the Morse potential No. 2. This is the Morse potential with the doubly primed parameters.

(ii) NINT is the number of integration intervals in the Simpson integration.

(iii) V1, V2, J1, and J2 are quantum numbers

$$\begin{aligned} \text{V1} &= v' \quad , \quad \text{J1} = J' \\ \text{V2} &= v'' \quad , \quad \text{J2}=J'' \end{aligned} \qquad \text{(A7-6)}$$

(iv) DELTA1 and DELTA2 are parameters which partially define the limits of integration. Denoting the classical turning points as $r_{min.}$ and $r_{max.}$ respectively the integration interval is taken

$$\min(r'_{min}, r''_{min}) - \text{DELTA1} \leq r \leq \max(r'_{max}, r''_{max}) + \text{DELTA2} \quad \text{(A7-7)}$$

DELTA1 and DELTA2 are expressed in Å. A large number of test calculations were done for photoionizations of diatomic molecules for which Gardner and Samson published relative intensities and theoretical Franck-Condon factors.[15] In these cases, taking DELTA1=0.1 Å (at the steep end!) and DELTA2=0.25 Å turned out to be appropriate. NTIMES such cards will be read. If IO≠0, and IO≠5 on the sixth card, these NINT cards will be read from an input unit other than the card reader. The number of this input unit is designated by IO.

```
      IMPLICIT REAL*8 (A-H,O-Z)
      REAL*8 G(60),MU
      INTEGER V1,V2
      INTEGER*2 AS,BS,CS
      LOGICAL*1 L1,L2,LOP,LUP,SMACK,GROSS,BABY
      COMMON /REDM/MU/CONTR/IB,BABY,LUP,LOP/GAUSS/BETAO,SMACK
      DATA AS,BS,CS/'#1','#2','G('/,ANG/1.0D8/,L/1/,I10/10/,IO/0/,
     #AP,BP/'(SINGLY ','(DOUBLY '/
C     THE REDUCED MASS IS IN ATOMIC WEIGHT UNITS, THE INTERNUCLEAR DISTANC
C     ARE IN ANGSTROMS, AND ALL SPECTROSCOPIC CONSTANTS ARE IN WAVENUMBERS
      CALL ERRSET(207,500,-1,1,0,217)
      READ (5,10) NFG
      IF (NFG.EQ.IO) NFG=L
      DO 1 NFH=L,NFG
      READ (5,8) (G(I),I=L,I10)
      WRITE (6,9) (G(I),I=L,I10)
      READ (5,2) LOP,NTIMES,MU,BETAO,WE1,WEXE1,RE1,WE2,WEXE2,RE2,NG,
     #IO,IB
      IF (NTIMES.EQ.IO) NTIMES=L
      IF (IO.EQ.IO) IO=5
      IF (NG.EQ.IO) NG=L
      BABY=IB.NE.IO
      SMACK=NG.LT.IO
      IF (SMACK) NG=-NG
      IF (SMACK) WRITE (6,12)
      LUP=.FALSE.
      READ (5,3) (G(I),I=L,NG)
      WRITE (6,4) MU,AS,WE1,WEXE1,RE1,AP,BS,WE2,WEXE2,RE2,BP,
     #(CS,I,G(I),I=L,NG)
      DELTA1=-0.5DO*BETAO
      IF (BETAO.NE.0.0DO) WRITE (6,11) DELTA1
      MU=MU/6.022169D23
      RE1=RE1/ANG
      RE2=RE2/ANG
      WRITE (6,7)
      DO 1 J=L,NTIMES
      READ (IO,5) L1,L2,NINT,V1,V2,J1,J2,DELTA1,DELTA2
      F=FC(G,WE1,WE2,WEXE1,WEXE2,RE1,RE2,DELTA1,DELTA2,V1,V2,J1,J2,NINT,
     #NG,L1,L2)
      FF=F*F
      GROSS=(F.LT.-9.0DO).OR.(F.GT.99.0DO).OR.(FF.GT.99.0DO)
      IF (.NOT.GROSS) WRITE (6,6) V1,J1,V2,J2,FF,F,L1,L2
    1 IF (GROSS) WRITE (6,13) V1,J1,V2,J2,FF,F,L1,L2
      WRITE (6,7)
      STOP
    2 FORMAT (L1,I4/2F20.0/2(3F20.0/),3I5)
    3 FORMAT (4F20.0)
    4 FORMAT (1H-,5X,3HTHE,1X,7HREDUCED,1X,4HMASS,1X,2HIS,1X,1H:,F10.4,
     #1X,6HA.W.U./2(1HO,5X,A2,1X,1H:,5X,2HWE,1X,1H=,F10.4,1X,8HCM**(-1),
     #4X,4HWEXE,1X,1H=,F10.4,1X,8HCM**(-1),4X,2HRE,1X,1H=,F10.5,1X,
     #9HANGSTROMS,4X,A8,7HPRIMED)/)/20(1HO,5X,3(A2,I2,1H),1X,1H=,
     #D24.16,4X)/)/1HO)
    5 FORMAT (2L1,I8,4I5,2F10.0)
    6 FORMAT (6X,2HV',1X,1H=,I3,3X,2HJ',1X,1H=,I3,4X,2HV",1X,1H=,
     #I3,3X,2HJ",1X,1H=,I3,4X,13HFRANCK-CONDON,1X,6HFACTOR,1X,1H=,F10.7,
     #4X,13HFRANCK-CONDON,1X,9HAMPLITUDE,1X,1H=,F10.7,3X,1H(,L1,1H,,L1,
     #1H)/)
    7 FORMAT (1H-/1H-/1H-)
    8 FORMAT (10A8)
    9 FORMAT (1H-/1H-,5X,10A8/1H-)
   10 FORMAT (I5)
   11 FORMAT (1HO,5X,3HTHE,1X,8HGAUSSIAN,1X,6HFACTOR,1X,2HIN,1X,3HTHE,
     #1X,10HTRANSITION,1X,6HMOMENT,2X,1H:,3X,4HEXP(,F10.5,5H*R*R))
   12 FORMAT (1HO,5X,3HTHE,1X,10HTRANSITION,1X,6HMOMENT,1X,2HIS,1X,
     #8HEXPANDED,1X,2HIN,1X,11HEXPONENTIAL,1X,9HFUNCTIONS)
   13 FORMAT (6X,2HV',1X,1H=,I3,3X,2HJ',1X,1H=,I3,4X,2HV",1X,1H=,
     #I3,3X,2HJ",1X,1H=,I3,4X,3HF-C,1X,6HFACTOR,1X,1H=,D22.13,4X,
     #3HF-C,1X,9HAMPLITUDE,1X,1H=,D22.13,3X,1H(,L1,1H,,L1,1H)/)
      END
```

```
      REAL FUNCTION FC*8 (G,WE1,WE2,WEXE1,WEXE2,RE1,RE2,DELTA1,DELTA2,
     #V1,V2,J1,J2,NONT,NG,LOGS1,LOGS2)
      IMPLICIT REAL*8 (A-H,O-Z)
      REAL*8 G(60),N1,N2
      REAL*4 AN(500),SNGL
      INTEGER FMRT(2),V1,V2,IB
      LOGICAL*1 LULU(60),LAG(60),LOGS1,LOGS2,LOP,LUP,BABY
      COMMON /DISS/D,GAMMA,ALFAO/CONTR/IB,BABY,LUP,LOP/SNORT/BETAS,LAG
      EQUIVALENCE (RMIN,ZMAX),(RMAX,ZMIN),(FMRT,SUCK)
      DATA HALF,ONE/0.5D0,1.0D0/,ANG/1.0D8/,FOUR,ERGEV,ERGCM/4.0D0,
     #6.242D11,Z4E11E26A2CD0353C/,ZERO/0.0D0/,SUCK/'(10A8)  '/
      NINT=NONT
      CALL JULIE (WE1,WEXE1,RE1,V1,J1,N1,A1,B1,BETA1,T,S,LOGS1)
      D1=D+ALFAO
      GAMMA1=GAMMA*FOUR
      CALL JULIE (WE2,WEXE2,RE2,V2,J2,N2,A2,B2,BETA2,SU,ST,LOGS2)
      RMIN=T
      IF (SU.LT.RMIN) RMIN=SU
      RMAX=S
      IF (ST.GT.RMAX) RMAX=ST
      RMIN=RMIN-DELTA1
      RMAX=RMAX+DELTA2
      FJ=BETA1/ANG
      FK=BETA2/ANG
      WRITE (6,8) T,S,SU,ST,RMIN,RMAX,FJ,FK
      RMIN=RMIN/ANG
      RMAX=RMAX/ANG
      SU=B1+B1
      BETAS=ANG/BETA1
      PU=DLOG(SU)
      ZMIN=DSQRT(SU*DEXP(BETA1*(RE1-RMAX)))
      ZMAX=DSQRT(SU*DEXP(BETA1*(RE1-RMIN)))
      T=BETA2/BETA1
      S=(B2+B2)/DEXP(T*(DLOG(B1+B1)+BETA1*(RE1-RE2)))
      SU=DLOG(S)
      FJ=DFLOAT(V1+1)
      FJ=HALF*DLGAMA(A1+FJ)-DLGAMA(FJ)-DLGAMA(A1+ONE)
      FK=DFLOAT(V2+1)
      FK=HALF*DLGAMA(A2+FK)-DLGAMA(FK)-DLGAMA(A2+ONE)
      FACT=HALF*(A2*SU+DLOG(T)-N1-N2)+FJ+FK
      IF (LUP) GO TO 2
      DO 1 I=1,NG
      LULU(I)=G(I).LT.ZERO
      LAG(I)=G(I).EQ.ZERO
      IF (LAG(I)) GO TO 1
      G(I)=DLOG(DABS(G(I)))
    1 CONTINUE
      LUP=.TRUE.
    2 FC=ZERO
      SU=HALF*(A1+A2*T)
      NINT=NINT/10
      DIFF=(ZMAX-ZMIN)/DFLOAT(10*NINT)
      D6=DIFF/6.0D0
      FA=HARP(G,FACT,A1,A2,S,SU,PU,T,ZMIN,V1,V2,NG,LULU)
      DO 4 N=1,NINT
      FCD=ZERO
      DO 3 NJ=1,10
      Z=ZMIN+DIFF*DFLOAT(NJ+10*N-10)
      ZAB=Z-HALF*DIFF
      FB=HARP(G,FACT,A1,A2,S,SU,PU,T,Z,V1,V2,NG,LULU)
      FAB=HARP(G,FACT,A1,A2,S,SU,PU,T,ZAB,V1,V2,NG,LULU)
      FCD=FCD+D6*(FA+FOUR*FAB+FB)
    3 FA=FB
      FC=FC+FCD
    4 IF (LOP) AN(N)=SNGL(FCD)
      IF (.NOT.LOP) GO TO 10
      WRITE (6,6)
      WRITE (6,7) (AN(N),N=1,NINT)
      WRITE (6,6)
```

```
10 SU=D1*ERGEV
   ST=D*ERGEV
   S=(D1-((A1*A1)/GAMMA1))*ERGCM
   T=(D+ALFAO-((A2*A2)/(FOUR*GAMMA)))*ERGCM
   WRITE (6,5) S,SU,T,ST
   IF (.NOT.BABY) GO TO 9
   S=S-T
   T=FC*FC
   WRITE (IB,FMRT) S,T,FC
 9 RETURN
 5 FORMAT (2(6X,6HENERGY,1X,4HFROM,1X,3HTHE,1X,6HBOTTOM,1X,2HOF,1X,
  #3HTHE,1X,9HPOTENTIAL,1X,4HWELL,2X,1H:,F12.3,1X,8HCM**(-1),4X,1H,,
  #4X,12HDISSOCIATION,1X,5HLIMIT,2X,1H:,F6.2,1X,13HELECTRONVOLTS/))
 6 FORMAT (1HO,15X,101('=')/)
 7 FORMAT (15X,10F10.6)
 8 FORMAT (1H-,5X,9HCLASSICAL,1X,7HREGIONS,1X,2HIN,1X,9HANGSTROMS,3X,
  #1H:,12X,2(1H(,F8.4,1X,1H,,F8.4,1X,1H),10X)/6X,11HINTEGRATION,
  #1X,6HLIMITS,1X,2HIN,1X,9HANGSTROMS,2X,1H:,5X,F13.4,1X,1H<,1X,1HR,
  #1X,1H<,F8.4,4X,1H,,4X,4HBETA,2X,1H:,F9.4,1X,1H,,F8.4,1X,
  #14HANGSTROM**(-1))
   END

   SUBROUTINE JULIE (WE,WEXE,RE,NV,J,N,A,B,BETA,RMIN,RMAX,LOGS)
   IMPLICIT REAL*8 (A-H,O-Z)
   REAL*8 N,MU
   LOGICAL*1 LOGS
   COMMON /REDM/MU/DISS/D,GAMMA,ALFAO
   DATA C,H,HBAR,PI/2.997925D10,6.626196D-27,1.0545919D-27,
  #3.14159265358979 3D0/,HALF,ONE,THREE/0.5D0,1.0D0,3.0D0/,ANG/1.0D8/,
  #I/1/
   BETA=DSQRT((C+C)*H*MU*WEXE)/HBAR
   GAMMA=HBAR*BETA
   GAMMA=(MU+MU)/(GAMMA*GAMMA)
   Q=HALF*DFLOAT(J*(J+I))*HBAR*HBAR/MU
   N=RE*RE
   IF (LOGS) GO TO 1
   ALFAO=BETA*RE
   ALFA1=(Q+Q)*(ALFAO-ONE)/(N*ALFAO)
   ALFA2=-Q*(ALFAO-2.0D0)/(N*ALFAO)
   ALFAO=0.0D0
   GO TO 2
 1 ALFAO=ONE/(BETA*RE)
   B=ALFAO*ALFAO
   ALFA1=(Q+Q)*(ALFAO+ALFAO-THREE*B)/N
   ALFA2=Q*(THREE*B-ALFAO)/N
   ALFAO=Q*(ONE-THREE*(ALFAO-B))/N
 2 D=(C+C)*PI*(WE/BETA)
   D=D*D*MU*HALF
   A=(D+D-ALFA1)*DSQRT(GAMMA/(D+ALFA2))-DFLOAT(NV+NV+1)
   B=DSQRT(GAMMA*(D+ALFA2))
   N=-DLOG(A)-DLGAMA(DFLOAT(NV+I))
   RMIN=HALF*A
   RMIN=DSQRT(ONE-(RMIN*(RMIN/(GAMMA*D))))
   RMAX=RE-(DLOG(ONE-RMIN)/BETA)
   RMIN=RE-(DLOG(ONE+RMIN)/BETA)
   RMIN=RMIN*ANG
   RMAX=RMAX*ANG
   RETURN
   END

   REAL FUNCTION HARP*8 (G,FACT,A1,A2,S,SU,PU,T,U,NV1,NV2,NG,LULU)
   IMPLICIT REAL*8 (A-H,O-Z)
   REAL*8 G(60)
   LOGICAL*1 LULU(60),LAG(60),SMACK
   COMMON /SNORT/BETAS,LAG/GAUSS/BETAO,SMACK
   DATA ONE/1.0D0/,AMIN,AMAX/Z2417FD974D372E44,Z5DAABBCDCC279F5A/,
  #ZERO,HALF,I80/0.0D0,0.5D0,80/
   X=U+U
   Z=U*U
   HARP=ZERO
```

```
      ZULU=DLOG(Z)
      ST=S*DEXP(T*ZULU)
      TERM1=ALAG(A1,Z,NV1,I1)*ALAG(A2,ST,NV2,I2)
      IF (DABS(TERM1).GT.AMIN) GO TO 1
      TERM1=TERM1*AMAX
      I2=I2-I80
    1 IF (DABS(TERM1).LT.AMAX) GO TO 2
      TERM1=TERM1*AMIN
      I2=I2+I80
    2 FICT=FACT+DFLOAT(I1+I2)-HALF*(Z+ST)+(SU-ONE)*ZULU
      RHO=BETAS*(PU-ZULU)
      RHO2=HALF*BETAO*RHO*RHO
      ST=DLOG(DABS(TERM1))
      POW=ONE
      IF (SMACK) POW=ZERO
      DO 5 I=1,NG
      IF (LAG(I)) GO TO 10
      TERM=FICT+G(I)
      IF ((TERM+ST).LT.-160.0D0) GO TO 3
      IF (SMACK) GO TO 9
      TERM=TERM1*X*POW*DEXP(TERM-RHO2)
      GO TO 4
    9 TERM=TERM1*X*DEXP(TERM+POW-RHO2)
      GO TO 4
    3 TERM=ZERO
    4 IF (LULU(I)) TERM=-TERM
      HARP=HARP+TERM
   10 IF (I.EQ.NG) GO TO 5
      IF (SMACK) GO TO 8
      POW=POW*RHO
      GO TO 5
    8 POW=POW+ZULU
    5 CONTINUE
      RETURN
      END

      REAL FUNCTION ALAG*8 (A,X,N,IC)
      IMPLICIT REAL*8 (A-H,O-Z)
      DATA ONE/1.0D0/,AMIN,AMAX/Z2417FD974D372E44,Z5DAABBCDCC279F5A/,
     #I/1/,I80/80/
      IC=0
      IF (N.EQ.0) GO TO 4
      C=A+ONE
      PHIN=ONE-(X/C)
      IF (N.EQ.I) GO TO 5
      AS=C-X
      PHINM1=ONE
      NM1=N-I
      DO 2 J=I,NM1
      D=DFLOAT(J)
      ALAG=((AS+DFLOAT(J+J))*PHIN-D*PHINM1)/(C+D)
      PHINM1=PHIN
      IF (DABS(ALAG).LT.AMAX) GO TO 1
      ALAG=ALAG*AMIN
      PHINM1=PHINM1*AMIN
      IC=IC+I80
    1 IF (DABS(ALAG).GT.AMIN) GO TO 2
      ALAG=ALAG*AMAX
      PHINM1=PHINM1*AMAX
      IC=IC-I80
    2 PHIN=ALAG
    3 RETURN
    4 ALAG=ONE
      GO TO 3
    5 ALAG=PHIN
      GO TO 3
      END
```

APPENDIX 8

THE PÖSCHL-TELLER OSCILLATOR

This Appendix gives instructions for using the FORTRAN program which calculates the wave functions and expectation values of the form

$$\langle v' | \Sigma_k c_k \tanh^k (\gamma x) | v'' \rangle \tag{A8-1}$$

and

$$\langle v' | \Sigma_k c_k x^k \exp(-(1/2)\gamma x^2) | v'' \rangle \tag{A8-2}$$

of the Pöschl-Teller oscillator.

The quantities in this Appendix have the same meaning as in Chapter 7.

First Card: NTIMES, NT, NINT, J, FCT, GAM

Format (4i5, 2f10.0)

(i) NTIMES is the number of expectation values to be computed for a given potential.

(ii) NT is the number of terms in the transition moment. For example, if the expansion coefficients c_o, c_1, and c_3 are included, we would take NT=3. If NT is left blank, the program takes NT=1.

(iii) NINT is the number of intervals in the Simpson integration. If NINT is left blank, the program takes NINT=120.

(iv) If J=0, expectation values of the form shown in (A8-2) will be computed, otherwise expectation values of the form shown in (A8-1) will be computed.

(v) FCT determines the integration limit in terms of the classical turning points x_1 and x_2

$$x_{max} = \pm \text{FCT} \cdot \max\ (x_1, x_2) \qquad \text{(A8-3)}$$

If FCT is left blank, the program takes FCT=3.

(vi) GAM stands for γ. If GAM is left blank in the case J≠0, the program takes GAM=1.

Second Card: CO1, AL1, CO2, AL2

Format (4f20.0)

CO1 is the c_o of the first potential and AL1 is the α of the first potential. Similarly CO2 and AL2 are the parameters c_o and α of the second potential. The coefficients c_o have to be negative. The program replaces a positive c_o by $-|c_o|$. Any α left blank will be taken as α=1.

Third Card: This card is missing if NT=0. It can extend over several cards if NT > 4. It contains the expansion coefficients of the transition moment function. These coefficients are entered as follows

(IPOW (j), TRA (j), j = 1, NT)

with the format (4(i5, f15.0)). In the above statement, IPOW (j) defines the k of the j-th term and TRA (j) denotes the corresponding c_k. If for NT=2, one takes

0 1.0 2 0.5

the program would compute NTIMES expectation values of the form

$$\langle v' | 1 - (1/2)\ \tanh^2\ (\gamma\ x) | v'' \rangle$$

where we have assumed that on the first card we had J=0.

Fourth Card: (N1 (j), N2 (j), j=1, NTIMES)

Format (16i5)

There is more than one such card if NTIMES $>$ 8. The N1s are the quantum numbers of potential No. 1 and the N2s are quantum numbers of potential No. 2.

Integrands with odd parity should give vanishing expectation values because the integration limits are symmetrical. However, the program computes the expectation values as follows

$$\langle \psi_n | M | \psi_m \rangle = 2 \int_0^1 \psi_n M \psi_m dx \qquad \text{(A8-4)}$$

This means that these terms are not set equal to zero. The program does recognize these odd parity terms and it will print a warning if such terms are included in the transition moment function. In general, one would not expect that this condition would arise.

```
      IMPLICIT REAL*8 (A-H,O-Z)
      REAL*8 TRU(125),TRA(50),DOOBEY(4)
      INTEGER IPOW(50)
      INTEGER*2 N1(500),N2(500),ITT,IBL,IMI
      LOGICAL*1 TYPE,SOUP,JILL
      COMMON /EXPA/DOOBEY,AL1,AL2,NV1,NV2/TRANSY/TRA,GAM,SAM,IPOW,
     #NT,TYPE,SOUP
      EQUIVALENCE (TRU,N2)
      DATA IO,I1,I2,ITT,IBL,IMI,ZERO,ONE/0,1,2,' +',' ',' -',0.0D0,
     #1.0D0/
      CALL ERRSET(207,500,-1,1,0,217)
    1 READ (5,4) NTIMES,NT,NINT,J,FCT,GAM
      IF ((NTIMES.EQ.IO).OR.(NT.GT.50).OR.(NTIMES.GT.500)) STOP
      TYPE=J.EQ.IO
      SOUP=TYPE.AND.(GAM.NE.ZERO)
      IF (SOUP) SAM=-0.5D0*GAM
      IF (NT.EQ.IO) NT=I1
      IF (NINT.EQ.IO) NINT=120
      READ (5,5) CO1,AL1,CO2,AL2
      IF (NT.NE.IO) READ (5,6) (IPOW(J),TRA(J),J=I1,NT)
      IF (FCT.EQ.ZERO) FCT=3.0D0
      IF ((.NOT.TYPE).AND.(GAM.EQ.ZERO)) GAM=ONE
      IF (CO1.GT.ZERO) CO1=-CO1
      IF (CO2.GT.ZERO) CO2=-CO2
      IF (AL1.EQ.ZERO) AL1=ONE
      IF (AL2.EQ.ZERO) AL2=ONE
      WRITE (6,3) I1,CO1,AL1,I2,CO2,AL2,NINT,FCT
      IF (NT.EQ.IO) GO TO 13
      DO 12 J=I1,NT
      TRU(J)=DABS(TRA(J))
      N1(J)=ITT
   12 IF (TRA(J).LT.ZERO) N1(J)=IMI
      IF (TRA(I1).GT.ZERO) N1(I1)=IBL
      IF (.NOT.TYPE) WRITE (6,8) (N1(J),TRU(J),GAM,IPOW(J),J=I1,NT)
      IF (.NOT.TYPE) GO TO 13
      JILL=(NT.EQ.I1).AND.(IPOW(I1).EQ.IO).AND.(TRA(I1).EQ.ONE)
      IF (SOUP) WRITE (6,14) SAM
      IF ((.NOT.JILL).AND.(.NOT.SOUP)) WRITE (6,16)
      IF (.NOT.JILL) WRITE (6,15) (N1(J),TRU(J),IPOW(J),J=I1,NT)
   13 WRITE (6,9)
      READ (5,7) (N1(J),N2(J),J=I1,NTIMES)
      DO 2 J=I1,NTIMES
      NV1=N1(J)
      NV2=N2(J)
      A=HONPO(CO1,CO2,FCT,NINT)
      AA=A*A
      WRITE (6,10) NV1,NV2,A,AA
    2 CALL COMPAR(IPOW,NV1,NV2,NT)
      WRITE (6,11)
      GO TO 1
    3 FORMAT (1H-,5X,2(9HPOTENTIAL,1X,3HNO.,I2,2X,1H:,F13.4,
     #7H/(COSH(,F13.7,7H*X)**2),4X)/1HO,5X,6HNUMBER,1X,2HOF,
     #1X,11HINTEGRATION,1X,9HINTERVALS,1X,1H=,I4,3X,1H,,3X,6HFACTOR,
     #1X,3HFOR,1X,11HINTEGRATION,1X,5HLIMIT,1X,1H=,F5.2)
    4 FORMAT (4I5,2F10.0)
    5 FORMAT(4F20.0)
    6 FORMAT (4(I5,F15.0))
    7 FORMAT (16I5)
    8 FORMAT (1H-,50X,3HTHE,1X,10HTRANSITION,1X,6HMOMENT,1X,2HIS,2X,1H:/
     #20(/6X,3(A2,F10.5,7H*(TANH(,F10.5,3H*X),1X,2H**,I2,1H))))
    9 FORMAT (1H-,29X,1H+,2(6(1H-),1H+),2(27(1H-),1H+)/30X,1H!,2(6X,
     #1H!),2(27X,1H!)/30X,1H!,2X,2HV1,2X,1H!,2X,2HV2,2X,1H!,2X,
     #13HFRANCK-CONDON,1X,9HAMPLITUDE,2X,1H!,4X,13HFRANCK-CONDON,
     #1X,6HFACTOR,3X,1H!/30X,1H!,2(6X,1H!),2(27X,1H!)/30X,1H+,
     #2(6(1H-),1H+),2(27(1H-),1H+)/30X,1H!,2(6X,1H!),2(27X,1H!))
   10 FORMAT (30X,1H!,2(I4,2X,1H!),2(F18.7,9X,1H!))
   11 FORMAT (30X,1H!,2(6X,1H!),2(27X,1H!)/30X,1H+,2(6(1H-),1H+),
     #2(27(1H-),1H+))
   14 FORMAT (1H-,5X,3HTHE,1X,11HEXPONENTIAL,1X,6HFACTOR,1X,2HIN,1X,
     #3HTHE,1X,10HTRANSITION,1X,6HMOMENT,2X,1H:,4X,4HEXP(,F10.4,5H*X*X))
```

```
15 FORMAT (6X,3HTHE,1X,5HPOWER,1X,6HSERIES,1X,3HFOR,1X,3HTHE,1X,
  #10HTRANSITION,1X,6HMOMENT,7X,1H:/20(/33X,3(A2,F10.5,3H*(X,1X,2H**,
  #I2,1H))))
16 FORMAT (1HO)
   END

   REAL FUNCTION HONPO*8(CO1,CO2,FCTCS,NINT)
   IMPLICIT REAL*8 (A-H,O-Z)
   REAL*8 NORMA
   COMMON /EXPA/AN1,AN2,A1,A2,AL1,AL2,N1,N2
   DATA ZERO,QUART,HALFE,ONENO/0.0D0,0.25D0,0.5D0,1.0D0/
   NORMA(A,N)=DEXP(1.1447298858494D0+(1.0D0-A-A)*6.931471805599453D-1
  #+DLGAMA(A+A+DFLOAT(N))-DLGAMA(DFLOAT(N+1))-2.0D0*DLGAMA(A))/
  #(A-0.5D0)
   X1=DSQRT(-CO1)/(DSQRT(QUART-CO1)-DFLOAT(N1)-HALFE)
   X2=DSQRT(-CO2)/(DSQRT(QUART-CO2)-DFLOAT(N2)-HALFE)
   XEND1=DLOG(X1+DSQRT(X1*X1-ONENO))/AL1
   XEND2=DLOG(X2+DSQRT(X2*X2-ONENO))/AL2
   XEND=XEND1
   IF (XEND2.GT.XEND) XEND=XEND2
   DIFF=(FCTCS*XEND)/DFLOAT(NINT)
   DIFF=DIFF+DIFF
   EN1=CO1/(X1*X1)
   EN2=CO2/(X2*X2)
   A1=HALFE+DSQRT(-EN1)
   A2=HALFE+DSQRT(-EN2)
   AN1=DSQRT(NORMA(A1,N1)/AL1)
   AN2=DSQRT(NORMA(A2,N2)/AL2)
   SUM=ZERO
   FM=FY(ZERO)
   DO 1 J=1,NINT
   X=DIFF*DFLOAT(J)
   XM=X-HALFE*DIFF
   F=FY(X)
   SUM=SUM+((FM+4.0D0*FY(XM)+F)/6.0D0)*DIFF
 1 FM=F
   HONPO=SUM+SUM
   RETURN
   END

   REAL FUNCTION FY*8 (X)
   IMPLICIT REAL*8 (A-H,O-Z)
   REAL*8 TRA(50)
   INTEGER IPOW(50)
   LOGICAL*1 TYPE,SILLY
   COMMON /EXPA/AN1,AN2,A1,A2,AL1,AL2,N1,N2/TRANSY/TRA,GAM,SAM,IPOW,
  #NT,TYPE,SILLY
   DATA IO,I1/0,1/
   IF (NT.EQ.IO) GO TO 4
   FY=0.0D0
   DO 2 J=I1,NT
   IF (IPOW(J).EQ.IO) GO TO 1
   K=IPOW(J)
   IF (TYPE) W=X
   IF (.NOT.TYPE) W=DTANH(GAM*X)
   IF (K.NE.I1) W=W**K
   FY=FY+W*TRA(J)
   GO TO 2
 1 FY=FY+TRA(J)
 2 CONTINUE
   FY=FY*FX(AN1,A1,AL1,X,N1)*FX(AN2,A2,AL2,X,N2)
 3 IF (SILLY) FY=FY*DEXP(SAM*X)
   RETURN
 4 FY=FX(AN1,A1,AL1,X,N1)*FX(AN2,A2,AL2,X,N2)
   GO TO 3
   END
```

```
      REAL FUNCTION FX*8 (AN,A,AL,X,N)
      IMPLICIT REAL*8 (A-H,O-Z)
      FX=ULTRA(AN,A,DTANH(AL*X),N)*DEXP((0.5DO-A)*DLOG(DCOSH(AL*X)))
      RETURN
      END

      REAL FUNCTION ULTRA*8 (AN,A,X,N)
      IMPLICIT REAL*8 (A-H,O-Z)
      DATA L/1/
      ULM=1.0DO
      IF (N.EQ.0) GO TO 3
      UL=(A+A)*X
      IF (N.EQ.L) GO TO 2
      JT=N-L
      DO 1 J=L,JT
      ULE=UL
      UL=((X+X)*(DFLOAT(J)+A)*ULE-(DFLOAT(J-L)+A+A)*ULM)/DFLOAT(J+L)
    1 ULM=ULE
    2 ULTRA=UL/AN
      RETURN
    3 UL=ULM
      GO TO 2
      END

      SUBROUTINE COMPAR(IPOW,N1,N2,NT)
      INTEGER IPOW(50)
      DATA IO,I1,I2/0,1,2/
      NTIM=IO
      IF (NT.EQ.IO) GO TO 3
      DO 1 J=I1,NT
      N=IPOW(J)+N1+N2
    1 IF (I2*(N/I2).NE.N) NTIM=NTIM+I1
      IF (NTIM.GT.I1) WRITE (6,5)
    2 IF (NTIM.EQ.I1) WRITE (6,4)
      RETURN
    3 N=N1+N2
      IF (I2*(N/I2).NE.N) NTIM=I1
      GO TO 2
    4 FORMAT (30X,1H!,20X,28(1H*),21X,1H!/30X,1H!,20X,1H*,1X,3HODD,1X,
     #6HPARITY,1X,4HTERM,1X,8HINCLUDED,1X,1H*,21X,1H!/30X,1H!,20X,
     #28(1H*),21X,1H!/30X,1H!,69X,1H!)
    5 FORMAT (30X,1H!,20X,29(1H*),20X,1H!/30X,1H!,20X,1H*,1X,3HODD,
     #1X,6HPARITY,1X,5HTERMS,1X,8HINCLUDED,1X,1H*,20X,1H!/30X,1H!,20X,
     #29(1H*),20X,1H!/30X,1H!,69X,1H!)
      END
```

APPENDIX 9

THE USE OF REAL SPHERICAL HARMONICS

The Xα wave functions in the Xα program are expressed in terms of real spherical harmonics.

Let $Y_{\ell m}$ denote the usual complex spherical harmonics. The spherical harmonics can be formulated as products of ϕ-dependent and θ-dependent parts. The real spherical harmonics are denoted by $y_{\ell m}$

$$Y_{\ell m}(\theta,\phi)=(-1)^m(2\pi)^{-1/2}X_m(\phi)Z_{\ell m}(\theta) \qquad \text{(A-9-1)}$$

$$y_{\ell m}(\theta,\phi)=(-1)^m(\pi(1+\delta_{m0}))^{-1/2}x_m(\phi)Z_{\ell m}(\theta) \qquad \text{(1-9-2)}$$

where

$$Z_{\ell m}(\theta)=[(2\ell+1)(\ell-|m|)!/(2(\ell+|m|)!)]^{1/2}P_\ell^{|m|}(\cos\theta) \qquad \text{(A-9-3)}$$

and P_ℓ^m represents associated Legendre polynomials.[3] The ϕ-dependent parts are:

$$X_m(\phi) = \begin{cases} \exp(im\phi) & \text{if } m\geq 0 \\ (-1)^m\exp(im\phi) & \text{if } m<0 \end{cases} \qquad \text{(A-9-4)}$$

and

$$x_m(\phi) = \begin{cases} \cos(m\phi) & \text{if } m\geq 0 \\ \sin(-m\phi) & \text{if } m<0 \end{cases} \qquad \text{(A-9-5)}$$

Davenport[422] had the option of either converting the Xα program to the usual complex spherical harmonics or to adopt conventions

established in the Xα program. He chose the latter option. He had to convert the Gaunt integrals

$$I(\alpha,\alpha',\alpha'')=\int Y_{\alpha}^{*}Y_{\alpha'}Y_{\alpha''}d\theta d\phi \qquad \text{(A-9-6)}$$

to "real" Gaunt integrals

$$I_{R}(\alpha,\alpha',\alpha'')=\int y_{\alpha}y_{\alpha'}y_{\alpha''}d\theta d\phi \qquad \text{(A-9-7)}$$

where the αs represent pairs of quantum numbers ℓ and m.

In the present work, the Gaunt integrals are expressed by 3-j symbols in Edmonds' notation.[571] Davenport followed Rose's notation.[572] Besides 3-j symbols, the present work deals also with 6-j symbols. A conversion to real spherical harmonics might be difficult. For this reason, the possibility of converting the dipole moment amplitudes of partial waves (DMAPWs), obtained from Davenport's program, to DMAPWs, which would have been obtained had Davenport used complex spherical harmonics, was investigated. Such a conversion is possible for linear molecules, (and atoms).

The dipole moment operator in the molecular frame is

$$\hat{A} = \sum_{\mu}\hat{a}^{(\mu)} \qquad \text{(A-9-8)}$$

where

$$\hat{a}^{(\mu)}=(4\pi/3)^{1/2}(-1)^{\mu}\hat{O}(\vec{r})Y_{1\mu}(\vec{r})D_{0\mu}^{(1)}(\vec{A}) \qquad \text{(A-9-9)}$$

In (A-9-9), $\vec{A}$ represents the molecular orientation and $\hat{O}$ is an operator which will depend on the representation chosen for the dipole

moment operator. If we are dealing with linear molecules, the initial wave function can be chosen such that it contains spherical harmonics of a fixed projection quantum number, either in terms of real spherical harmonics or in terms of complex spherical harmonics. A "fixed" projection quantum number means that we don't take linear combinations of $Y_{\ell m}$ and $Y_{\ell,-m}$.

The essential features of bound Xα wave functions are reproduced in the expression below:

$$\psi''_{\lambda''}(\vec{r}) = \sum_{\ell''s} c''_{\ell''\lambda''s}\, G_{\ell''}(r_s) Y_{\ell''\lambda''}(\vec{r}_s) \qquad \text{(A-9-10)}$$

where s is the index of summation over the sites. If, in (A-9-10), real spherical harmonics had been used instead of Y, the expansion coefficients c" would remain the same for linear molecules.

In Davenport's notation, an individual partial wave of the continuum wave function becomes

$$|E_e \ell\lambda\rangle = \sum_{\ell'\lambda' s} c''_{\ell\lambda\ell'\lambda' s}\, F_{\ell'}(r_s) Y^*_{\ell\lambda}(\vec{k}) Y_{\ell'\lambda'}(\vec{r}_s) \qquad \text{(A-9-11)}$$

where $\vec{k}$ is the propagation vector of the free electron.

According to Davenport[393] we can write the secular equations as

$$\sum_{j\alpha'} G^{ij}_{\alpha\alpha'} C_{\alpha'} = 0 \qquad \text{(A-9-12)}$$

where it has been assumed that the initial state is a bound state.

The quantities G^{ij} are structure constants between pairs of sites i and j.[389] They can be formulated as[427]

$$G^{ij}_{a'a}=4\pi\sum_{\alpha''} i^{\ell+\ell''-\ell'} I(\alpha,\alpha',\alpha'')z_{\ell''}(kR_{ij})Y_{\alpha''}(\hat{R}_{ij}),\ i\neq j \qquad \text{(A-9-13)}$$

where the functions z are spherical Bessel functions of different types, depending on whether the outer sphere is involved in the pair of sites.

Notice that α" does not refer to the initial state in (A-9-13), but simply serves as a summation index.

Davenport has written his dissertation as though he had used the usual complex spherical harmonics. If i=j, the structure constants contain a factor[428]

$$\delta_{\ell,\ell'}\,\delta_{\lambda,\lambda'} \qquad \text{(A-9-14)}$$

For a linear molecule, $\hat{R}_{ij}$ lies along the z-axis, such that we have λ"=0.[559] In this case, the Gaunt integrals of the complex spherical harmonics are nonzero only if λ=λ'. When using real spherical harmonics, the Gaunt integrals would be nonzero only if λ=±λ'.

It becomes apparent that, in the nonzero DMAPWs, the integral over ϕ can be factored out. For real spherical harmonics we can write

$$\langle E_e \ell\lambda \left|\hat{a}^{(\mu)}\right|\psi''_{\lambda''}\rangle=[(1+\delta_{\lambda,0})(1+\delta_{\mu,0})(1+\delta_{\lambda'',0})/8]^{1/2}$$
$$\int x_\lambda x_\mu x_{\lambda''}d\phi\langle....\rangle \qquad \text{(A-9-15)}$$

and for complex spherical harmonics

$$\langle E_e \ell\lambda \left|\hat{a}^{(\mu)}\right|\psi''_{\lambda''}\rangle=\int X_\lambda X_\mu X_{\lambda''}d\phi\langle....\rangle \qquad \text{(A-9-16)}$$

where <....> in (A-9-15) and (A-9-16) are identical. The integration in (A-9-16) can be readily performed analytically

$$\int_0^{2\pi} \exp(i(\lambda"+\mu-\lambda)\phi)d\phi=2\pi\delta_{\lambda,\lambda"+\mu} \qquad \text{(A-9-17)}$$

which gives the selection rule

$$\lambda = \lambda" + \mu \qquad \text{(A-9-18)}$$

Besides the integral shown in (A-9-17), the integral in (A-9-16) also contains a factor of

$$(-1)^{(\lambda"S_{\lambda"}+\mu S_{\mu}-\lambda S_{-\lambda})+\lambda} \qquad \text{(A-9-19)}$$

where S represents a modal quantity

$$S_n = \begin{cases} 0 \text{ if } n\geq 0 \\ 1 \text{ if } n<0 \end{cases} \qquad \text{(A-9-20)}$$

If real spherical harmonics are used, the integration over ϕ gives a factor

$$[8/((1+\delta_{\lambda,0})(1+\delta_{\mu,0})(1+\delta_{\lambda",0}))]^{1/2}\int_0^{2\pi} \begin{matrix}\sin\\\cos\end{matrix}(|\lambda|\phi)\begin{matrix}\sin\\\cos\end{matrix}(|\mu|\phi) \begin{matrix}\sin\\\cos\end{matrix}(|\lambda|"\phi)d\phi \qquad \text{(A-9-21)}$$

where the choice of sine or cosine depends on the "S_ns" of λ, μ, and $\lambda"$.

The selection rule obtained from (A-9-21) is different from the selection rule shown in (A-9-18).

If the integrand is not an even function in (A-9-2), the integral vanishes. This gives

$$\mathrm{sgn}(\lambda)\ \mathrm{sgn}(\mu)\ \mathrm{sgn}(\lambda'') > 0 \qquad \text{(A-9-22)}$$

If one of the projection quantum numbers is zero, the following relations apply

$$\int_0^{2\pi} \sin(n\phi)\sin(n'\phi)d\phi=\delta_{n,n'}\pi(1-\delta_{n,0})$$

$$\int_0^{2\pi} \cos(n\phi)\cos(n'\phi)d\phi=\delta_{n,n'}\pi(1+\delta_{n,0}) \qquad \text{(A-9-23)}$$

From (A-9-23) we obtain:

(i) if $\lambda'' = 0$ then $\lambda = \mu$

(ii) if $\mu = 0$ then $\lambda = \lambda''$

(iii) if $\lambda = 0$ then $\mu = \lambda''$ (A-9-24)

The selection rule, obtained when using real spherical harmonics, becomes

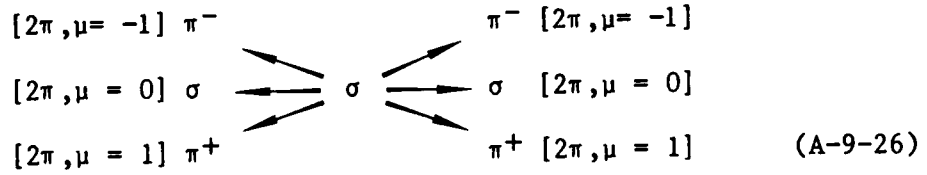
$$\lambda=\pm\lambda''\pm\mu, \text{ except } \lambda\neq-\lambda'' \text{ if } \lambda''\neq 0 \qquad \text{(A-9-25)}$$

Let us use the following notation:

For an initial orbital with the quantum number λ'', we draw arrows to the possible symmetries of the partial waves of the final states. The arrows pointing to the right indicate the accessible partial waves, when expressing them in terms of real spherical harmonics, and arrows pointing to the left indicate the accessible partial waves, when expressing them in terms of complex spherical harmonics. In addition, we also indicate in square brackets the values of the DMAPWs, excluding the quantity denoted <....> in (A-9-15),

and (A-9-16). Finally, the components μ of the nonzero DMAPWs will also be indicated.

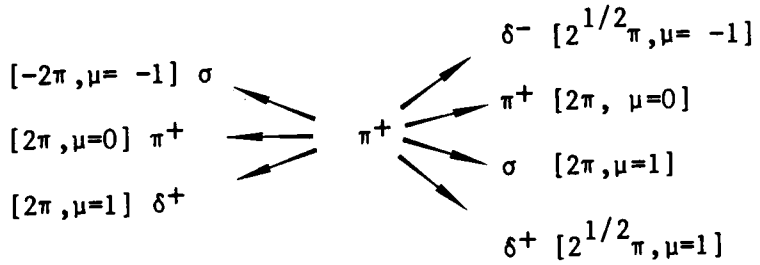
Using the above notation, we obtain the following scheme for the photoionization of a σ orbital:



(A-9-26)

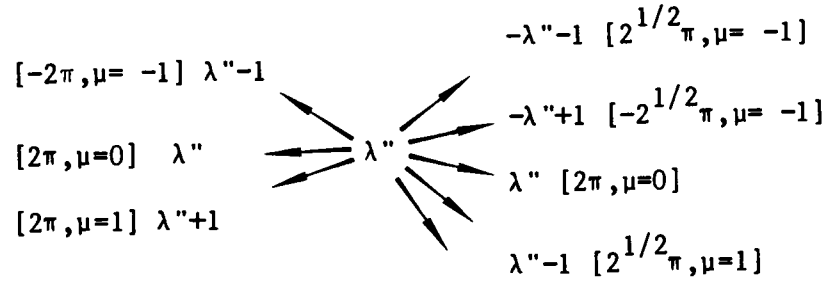
According to the above, it just so happens that the DMAPWs obtained in the photoionizations of σ orbitals are the same when using real or complex spherical harmonics.

For the photoionization of a π^+, orbital we obtain the following scheme:



(A-9-27)

For the photoionization of orbitals with $|\lambda''| \geq 2$, the following scheme arises:



(A-9-28)

From (A-9-27) and (A-9-28), one can construct conversion rules for the conversion of DMAPWs obtained with real spherical harmonics ($DMAPW_R$) to DMAPWs which would have been obtained with complex spherical harmonics ($DMAPW_C$).

The following set of operations applies to the photoionization of a π^+ orbital:

$$\begin{aligned} DMAPW_C(\sigma\leftarrow\pi^+,\mu=-1) &= -DMAPW_R(\sigma\leftarrow\pi^+,\mu=1) \\ DMAPW_C(\pi^+\leftarrow\pi^+,\mu=0) &= DMAPW_R(\pi^+\leftarrow\pi^+,\mu=0) \\ DMAPW_C(\delta^+\leftarrow\pi^+,\mu=1) &= 2^{1/2}DMAPW_R(\delta^+\leftarrow\pi^+,\mu=1) \end{aligned} \qquad \text{(A-9-29)}$$

This means that, in the conversion of the DMAPWs for the $\sigma\leftarrow\pi^+$ transition, for example, we would have to change the signs of the DMAPWs and also switch the sign of μ. For the transition $\delta^+\leftarrow\pi^+$, simply a scaling factor of $2^{1/2}$ is needed. At the end of such conversions the $DMAPW_R$s which do not occur on the right hand side of (A-9-29) have to be set zero. This would affect the DMAPWs of the $\delta^-\leftarrow\pi^+$ transition in the above case. Obviously, in the conversions, such as the one shown in (A-9-29), the DMAPWs have to have the same value of ℓ on both sides of each equation. Without any further explanations, let us present the conversion scheme for the photoionization of orbitals with $|\lambda"|\geq 2$:

$$\begin{aligned} DMAPW_C(\lambda"-1\leftarrow\lambda",\mu=-1) &= -2^{1/2}DMAPW_R(\lambda"-1\leftarrow\lambda",\mu=1) \\ DMAPW_C(\lambda"\leftarrow\lambda",\mu=0) &= DMAPW_R(\lambda"\leftarrow\lambda",\mu=0) \\ DMAPW_C(\lambda"+1\leftarrow\lambda",\mu=1) &= 2^{1/2}DMAPW_R(\lambda"+1\leftarrow\lambda",\mu=1) \end{aligned} \qquad \text{(A-9-30)}$$

VITA

Peter Senn was born on April 2, 1950 in Switzerland. He emigrated to Canada in 1973. He was awarded a B. Sc. degree in Chemistry from the University of Alberta in 1975 and a Master of Science degree in 1978. In 1978 he emigrated to the United States of America where he studied at the University of Tennessee at Knoxville towards a Ph. D. degree from 1978 to 1982.